POCUS in Critical Care, Anesthesia and Emergency Medicine

Noreddine Bouarroudj
Peňafrancia C. Cano
Shahridan bin Mohd Fathil
Habiba Hemamid
Editors

Springer

ALGrawany

POCUS in Critical Care, Anesthesia and Emergency Medicine

Noreddine Bouarroudj
Peňafrancia C. Cano
Shahridan bin Mohd Fathil
Habiba Hemamid
Editors

POCUS in Critical Care, Anesthesia and Emergency Medicine

Springer

ALGrawany

Editors
Noreddine Bouarroudj
Department of Anesthesiology
and Critical Care
Clinique Maissalyne
Constantine, Algeria

Peñafrancia C. Cano
Department of Anesthesiology
University of the Phillipines-Philippine
General Hospital
Manila, Philippines

Shahridan bin Mohd Fathil
Anesthesiology
Gleneagles Medini Hospital Johor
Iskandar Puteri, Malaysia

Habiba Hemamid
Intensive Care Unit
CHU Saadna Abdenour de Sétif
Sétif, Algeria

ISBN 978-3-031-43720-5 ISBN 978-3-031-43721-2 (eBook)
https://doi.org/10.1007/978-3-031-43721-2

© The Editor(s) (if applicable) and The Author(s), under exclusive license to Springer Nature Switzerland AG 2024
This work is subject to copyright. All rights are solely and exclusively licensed by the Publisher, whether the whole or part of the material is concerned, specifically the rights of translation, reprinting, reuse of illustrations, recitation, broadcasting, reproduction on microfilms or in any other physical way, and transmission or information storage and retrieval, electronic adaptation, computer software, or by similar or dissimilar methodology now known or hereafter developed. The use of general descriptive names, registered names, trademarks, service marks, etc. in this publication does not imply, even in the absence of a specific statement, that such names are exempt from the relevant protective laws and regulations and therefore free for general use.
The publisher, the authors, and the editors are safe to assume that the advice and information in this book are believed to be true and accurate at the date of publication. Neither the publisher nor the authors or the editors give a warranty, expressed or implied, with respect to the material contained herein or for any errors or omissions that may have been made. The publisher remains neutral with regard to jurisdictional claims in published maps and institutional affiliations.

This Springer imprint is published by the registered company Springer Nature Switzerland AG
The registered company address is: Gewerbestrasse 11, 6330 Cham, Switzerland

Paper in this product is recyclable.

Foreword

"Wherever the art of Medicine is loved, there is also a love of Humanity."

—Hippocrates

Healthcare landscape is rapidly evolving. The ability to rapidly and accurately assess patients in different clinical contexts is critical to delivering optimal care and improve their outcomes. Point-of-care ultrasound (POCUS) has emerged as a powerful tool in the hands of healthcare professionals across various specialties. POCUS has revolutionized the way we diagnose, monitor, and treat patients. This transformative technology is an indispensable asset in the armamentarium of healthcare providers.

This book is a step-by-step guide to physicians and healthcare providers across the globe on the utility of POCUS in different specialties. As we embark on this educational journey, it is essential to acknowledge the authors who contributed their collective knowledge and experiences to create this invaluable resource. The chapters within this book provide an in-depth examination of POCUS in diverse clinical scenarios, covering its use in cardiovascular assessment, pulmonary care, trauma management, and all ultrasound techniques in anesthesia practice (i.e., gastric ultrasound, airway ultrasound, and ultrasound-guided vascular access). Each chapter has clear explanations, detailed images, and case studies. Readers will gain invaluable insights into the practical application of POCUS in real-world medical settings.

Point-of-care ultrasound empowers clinicians to make rapid, informed decisions at the bedside. It grants us the ability to visualize the internal workings of the human body in real-time, transcending the limitations of traditional physical examinations. The pages of this book are a treasure trove of insights, protocols, and clinical wisdom, aimed at demystifying the complexities of POCUS and enabling healthcare practitioners to harness its potential for the benefit of their patients.

The applications of POCUS are vast and encompass critical care, anesthesia, and emergency medicine, making it an essential skill for professionals in these fields. From assessing the hemodynamic status of a critically ill patient to guiding invasive procedures with precision, POCUS has revolutionized our ability to provide timely, targeted care. The narratives contained within these pages demonstrate the profound impact POCUS has on patient outcomes and the satisfaction of the clinicians who wield this powerful tool.

As POCUS continues to evolve, this book acts as a beacon of knowledge, illuminating the path to mastery. Whether you are a novice eager to learn the fundamentals or an experienced practitioner seeking to refine your skills, the chapters herein cater to a wide range of expertise. The detailed illustrations, case studies, and step-by-step instructions offer a comprehensive guide to incorporating POCUS into your daily practice.

In the modern healthcare environment, where time is often of the essence, and accurate diagnosis and intervention can make the difference between life and death, POCUS is not just a technological marvel but a humanitarian imperative. This book is a testament to the dedication of healthcare providers and their unwavering commitment to improving patient care.

As you delve into the pages of this book, you embark on a journey of discovery and enlightenment. It is our hope that, through this collective effort, you will gain the knowledge and confidence to wield POCUS as a powerful instrument of healing and compassion. May this book serve as an enduring resource, enabling you to provide the best care for your patients, even in the most challenging and time-critical situations.

The practice of medicine in critical care, anesthesia, and emergency medicine demands a profound understanding of human physiology, rapid decision-making, and precise interventions. POCUS is a game-changer in these disciplines, providing clinicians with real-time, non-invasive, and highly informative imaging at the patient's bedside. With its ability to assess cardiac function, detect fluid accumulation, identify pathology, guide procedures, and monitor patient response to treatment, POCUS empowers healthcare providers to deliver more efficient, safer, and patient-centered care.

This book, crafted by a team of esteemed experts, represents a comprehensive exploration of POCUS in the context of critical care, anesthesia, and emergency medicine. It delves into the principles, techniques, and clinical applications of POCUS, offering a wealth of knowledge to both novices and seasoned practitioners. It serves as a guide for those who seek to harness the full potential of this technology to enhance patient care.

Furthermore, the integration of POCUS into educational curricula is explored, underscoring its role in shaping the future of medical training and continuing education.

As we navigate the complex terrain of modern healthcare, our responsibility as healthcare providers is to continuously adapt and embrace innovative solutions that advance the well-being of our patients. POCUS is a tool that exemplifies this commitment to progress. It is a means of improving patient outcomes, enhancing safety, and increasing diagnostic accuracy. This book is an essential resource for anyone who is passionate about delivering exceptional care in critical moments.

I commend the authors for their dedication to advancing our understanding of POCUS in critical care, anesthesia, and emergency medicine. I trust that their expertise and insights will inspire readers to embrace this powerful technology, ensuring that the benefits of POCUS continue to reshape and enhance the delivery of healthcare across the globe.

A L G r a w a n y

In closing, I invite you to embark on a journey through the pages of this book, to explore the world of POCUS and to envision its limitless potential in the noble pursuit of saving and improving lives. It is my hope that this book will empower and inspire healthcare providers, educators, and learners alike to embrace the future of medicine, one where POCUS is an indispensable ally in the quest for better patient care.

Clinical Operations, Department of Anesthesiology Nabil Elkassabany
University of Virginia
Charlottesville, VA, USA

Contents

Part I Basic Ultrasound in Critical Care, Anesthesia and Emergency

1 Principle of Ultrasound 3
Shahridan bin Mohd Fathil, Yeoh Jie Cong, Lee Kee Choon, Lim See Choo, Sultan Haji Ahmad Shah Ahmad Suhailan Mohamed, Muhazan Mazlan, Nurul Shaliza Shamsudin, and Muhamad Rasydan Abd Ghani

1.1 Introduction 3
1.1.1 History and Evolution of Medical Ultrasound. 3
1.1.2 Evolution of POCUS in Critical Care, Anesthesiology, and Emergency Medicine 4
1.1.3 Lung Ultrasound 4
1.1.4 Echocardiography 4
1.1.5 Abdominal Ultrasound for Trauma 4
1.1.6 Ultrasound Guidance for Vascular Cannulation. 4
1.1.7 Ultrasound-Guided Regional Anesthesia. 5
1.1.8 Advancement of POCUS from the Past Decade 5
1.1.9 Machine Learning and Artificial Intelligence in POCUS (AI and ML). 5
1.1.10 Newer Applications in Handheld Portable Devices. 5
1.2 Ultrasound Physics. 6
1.2.1 Piezoelectric Crystal and Effect [*32*, *33*] 6
1.2.2 Basic Physics Definitions [*32*, *34–37*]. 6
1.2.3 Ultrasound Wave Interaction with Tissues [*32*, *34*] 7
1.2.4 Resolution [*32*, *34*]. 9
1.2.5 Scanning Modes [*32*, *34*, *35*, *37*, *38*] 10
1.3 Transducers, Image Optimization, and Artifacts 14
1.3.1 Transducer 14
1.3.2 Ultrasound Image Optimization. 15
1.3.3 Artifacts 19
1.3.4 Ergonomics in Point-of-Care Ultrasound 21
References. 25

2 Basic Transthoracic of Echocardiography 29
Noreddine Bouarroudj and Cherif Bouzid
2.1 The Motion Mode (M Mode). 29
2.2 The 2D Mode or B Mode or Brightness Mode 30
2.3 The Doppler Effect. 30
2.3.1 Flow Doppler 30
2.3.2 Tissue Doppler Imaging (TDI) 31
2.4 Three-Dimensional Imaging 31
2.4.1 Data Acquisition. 31
2.4.2 Data Acquisition Modes. 32
2.4.3 3DE Display. 33

3 Preparation, Equipment, and Techniques 35
Noreddine Bouarroudj and Cherif Bouzid
3.1 Preparation 35
3.2 Equipment and Techniques 35
3.2.1 2D Mode 35
3.2.2 M-Mode 36
3.2.3 Doppler Imaging 36

4 Windows. 39
Noreddine Bouarroudj and Cherif Bouzid

5 Sonoanatomy of Standard Views. 41
Noreddine Bouarroudj and Cherif Bouzid
5.1 Parasternal Long-Axis (PLAX) View 41
5.1.1 Introduction 41
5.1.2 Technique. 41
5.1.3 Assessments and Measurements 42
5.2 Parasternal Short Axis (PSAX) View. 42
5.2.1 Introduction 42
5.2.2 Technique. 42
5.2.3 Assessments and Measurements 44
5.3 Apical Four Chamber (A4C) View 44
5.3.1 Introduction 44
5.3.2 Technique. 44
5.3.3 Assessment and Measurements (Fig. 5.9) 45
5.4 Apical Five-Chamber (A5C) View. 45
5.4.1 Technique. 45
5.4.2 Assessment and Measurements 45
5.5 Apical Two-Chamber (A2C) View (Fig. 5.9). 46
5.5.1 Technique. 46
5.5.2 Assessment and Measurements 46
5.6 Apical Three-Chamber (A3C) View (Fig. 5.9) 47
5.6.1 Technique. 47
5.6.2 Assessment and Measurements 47
5.7 Sub-costal Views 47
5.7.1 Sub-costal Four-Chamber View. 47
5.7.2 Inferior Vena Cava (IVC) View 48
5.7.3 Sub-costal Short-Axis View. 48

ALGrawany

5.7.4 Supra-sternal Long Axis View 49
5.7.5 Supra-sternal Short-Axis View 49

6 Aorta, Vena Cava, and Heart Chambers 51
Noreddine Bouarroudj and Cherif Bouzid
6.1 LV Systolic Function 51
6.1.1 Introduction 51
6.1.2 Approaches to Estimate EF 51
6.2 LV Diastolic Function 54
6.2.1 Introduction 54
6.2.2 Pertinence of LV Diastolic Function Evaluation 55
6.2.3 Standard Cardiology Assessment of LV Diastolic Function 55
6.3 Left and Right Atria 57
6.3.1 Left Atrium. 57
6.3.2 Right Atrium 58
6.4 Thoracic Aorta 59
6.4.1 Introduction 59
6.4.2 Thoracic Aorta Anatomy 59
6.4.3 Technique. 59
6.4.4 Pathologic Finding 60
6.4.5 Complications Diagnosis 60
6.5 Inferior Vena Cava 61
6.5.1 Introduction 61
6.5.2 Physiology 61
6.5.3 Technique. 61
6.5.4 Clinical Applications 61
References. 62

Part II Adults and Pediatrics Diseases

7 Adult Heart Diseases. 65
Noreddine Bouarroudj and Cherif Bouzid
7.1 Coronary Artery Disease 65
7.1.1 Introduction 65
7.1.2 Regional Wall Motion Abnormality. 65
7.1.3 Mechanical Complications of Acute Myocardial Infarction 65
7.2 Right Heart Diseases 66
7.2.1 Introduction 66
7.2.2 Assessment of the RV in the Different Standard Views. 66
7.2.3 The Interpretation of Pathological Finding 67
7.3 Pulmonary Hypertension(PHT) 67
7.3.1 Introduction 67
7.3.2 Pertinence of Measurement of Pulmonary Pressure 68
7.3.3 Technique of Measurement 68

7.4 Pericardial Effusion and Tamponade 69
7.4.1 Introduction 69
7.4.2 Positive Diagnosis of Pericardial Effusion 69
7.4.3 Differential Diagnosis 69
7.4.4 Pathological Finding 70
7.5 Heart Valve Disease 70
7.5.1 Introduction 70
7.5.2 The Technique of the Echocardiographic Exam 71
7.5.3 Pathologic Findings 71
7.6 Cardiomyopathies 72
7.6.1 Hypertrophic Cardiomyopathy 72
7.6.2 Dilated Cardiomyopathy 73
7.6.3 Restrictive Cardiomyopathy 74
7.7 Acute Fibrillation and Other Arrhythmias 74
7.7.1 Atrial Fibrillation 74
7.7.2 Other Arrhythmia 74
7.8 Prosthetic Valves 75
7.8.1 Introduction 75
7.8.2 2D and TM Features of Replacement Valves 75
7.8.3 Doppler Features of Replacement Valves 75
7.8.4 Pathologic Findings 76
7.9 Endocarditis 76
7.9.1 Introduction 76
7.9.2 Vegetations 76
7.9.3 Destructive Lesions 77
7.9.4 Hemodynamic Consequences 77
7.10 Advanced Cardiac Life Support (Cardiac Arrest) 77
7.10.1 Introduction 77
7.10.2 Diagnostic Approach 77
7.10.3 Prognostic 78
7.10.4 Technique 78
7.11 Pericardiocentesis 78
7.11.1 Introduction 78
7.11.2 Contraindications 78
7.11.3 Ultrasound Technique 79
7.11.4 Complications 79
References 79

8 Pediatric and Congenital Heart Disease 81
Noreddine Bouarroudj and Cherif Bouzid
8.1 Patent Foramen Ovale 81
8.1.1 Introduction 81
8.1.2 Diagnosis of PFO 81
8.2 Atrial Septal Defects 81
8.2.1 Introduction 81
8.2.2 Anatomic Classification 81
8.2.3 Technique 82
8.2.4 Echographic Finding 82

8.3 Ventricular Septal Defect 83
8.3.1 Introduction 83
8.3.2 Pathophysiology 83
8.3.3 Anatomy and Imaging 83
8.3.4 Steps of Echocardiography Exam 84
8.4 Patent Ductus Arteriosus 84
8.4.1 Introduction 84
8.4.2 Steps of Echocardiography Exam 85
8.5 Tetralogy of Fallot 85
8.5.1 Introduction 85
8.5.2 Objective of the Echographic Exam: Fig. 8.3 86
8.5.3 Echography Imaging of the Main Lesions 86
8.6 Transposition of the Great Arteries (Complete TGA or D-TGA) 86
8.6.1 Introduction 86
8.6.2 Pathophysiology 87
8.6.3 Objective of the Echographic Assessment 87
8.6.4 2D-Imaging Mode 87
8.6.5 Doppler Imaging 87
8.7 Atrioventricular Septal Defects 88
8.7.1 Introduction 88
8.7.2 2D-Imaging Mode 88
8.7.3 Doppler Finding 89
8.8 Other Anomalies 89
8.8.1 Pulmonary Stenosis 89
8.8.2 Coarctation of the Aorta: Fig. 8.5 89
8.8.3 Aortic Aneurysm Can Lead to Dissection or Rupture 90
References 90

9 Tips and Tricks 91
Noreddine Bouarroudj and Cherif Bouzid

Part III US in Different Settings

10 Lung Ultrasound in Acute Care 95
Lim Teng Cheow, Nur Hafiza Yezid, and Shahridan bin Mohd Fathil
10.1 Introduction 95
10.2 Principles 95
10.3 Technical Considerations 95
10.4 Technique of Examination 96
10.5 Sonography of Normal Lung 98
10.6 Sonography of Lung Pathologies 99
10.6.1 Interstitial Syndrome 99
10.6.2 Pleural Effusion 100
10.6.3 Pneumothorax 100
10.6.4 Alveolar Syndrome 102
10.7 Conclusion 102
References 102

ALGrawany

11 Ultrasound-Guided Vascular Access 105
Noreddine Bouarroudj and Cherif Bouzid
11.1 Introduction 105
11.2 General Considerations 105
11.2.1 Blood Vessel Identification 105
11.2.2 Approaches for Vascular Cannulation 107
11.2.3 Transducer and Imaging Mode 108
11.2.4 Preparation 108
11.3 Ultrasound-Guided Internal Jugular Vein Cannulation 109
11.3.1 Anatomic and Sonoanatomic Considerations 109
11.3.2 Cannulation Technique 109
11.3.3 Complications 110
11.4 Ultrasound-Guided Subclavian Vein Cannulation 110
11.4.1 Anatomic and Sonoanatomic Considerations 111
11.4.2 Cannulation Technique 111
11.4.3 Complications 113
11.5 Femoral Vein Cannulation 113
11.5.1 Anatomic and Sonoanatomic Considerations 113
11.5.2 Cannulation Technique 113
11.6 Peripherally Inserted Central Catheter Lines 114
11.6.1 Definition 114
11.6.2 Indications 114
11.6.3 Contraindications 114
11.6.4 Technique 114
11.6.5 Complications 116
11.7 Ultrasound-Guided Arterial Cannulation 116
11.7.1 Technique 116
11.7.2 Arteries Cannulation Sites Particularities 116
11.8 Ultrasound-Guided Peripheral Venous Cannulation 117
11.8.1 Indications 118
11.8.2 Technique 118
11.8.3 Complication 119
11.9 Pediatric Considerations 119
11.9.1 Central Venous Access 119
11.9.2 Peripheral Venous Cannulation 119
11.9.3 Arterial Cannulation 120
References 120

12 E-FAST and Abdominal Ultrasound 121
Divesh Arora, Hetal Vadera, and Amrita Rath
12.1 Introduction 121
12.2 Preparation Equipment and Technique 122
12.2.1 Transducer Selection 122
12.2.2 Orientation Marker 122
12.2.3 Patient Position 123
12.2.4 E-FAST Sequence 123
12.3 Anatomy 124

12.4 Sonoanatomy E-FAST Views . . . 124
12.4.1 Right Upper Quadrant View . . . 124
12.4.2 Subcostal View . . . 125
12.4.3 Left Upper Quadrant View . . . 126
12.4.4 Pelvic View (Long and Short Axis) . . . 126
12.4.5 Rectovesical Pouch in Males . . . 127
12.4.6 Rectouterine Pouch in Females . . . 127
12.4.7 E-FAST Thoracic View . . . 128
12.5 Other Abdominal Views . . . 129
12.5.1 Liver Ultrasound . . . 129
12.5.2 Liver Pathology . . . 129
12.5.3 Gall Bladder and Common Bile Duct Ultrasound . . . 129
12.6 Gall Bladder and CBD Pathology . . . 130
12.6.1 Cholelithiasis . . . 130
12.6.2 Cholecystitis . . . 130
12.6.3 Choledocholithiasis . . . 131
12.6.4 Appendicitis . . . 131
12.7 Pathology . . . 132
12.7.1 Hemoperitoneum in the Hepatorenal Space . . . 132
12.7.2 Haemothorax in the Right and Left Pleural Space . . . 132
12.7.3 Haemoperitoneum in the Splenorenal Space . . . 132
12.7.4 Haemoperitoneum in the Rectovesical and Rectouterine Excavation . . . 133
12.7.5 Haemopericardium . . . 133
12.7.6 Detecting Pneumothorax . . . 134
12.7.7 Abdominocentesis . . . 134
12.8 Advantages of E-FAST . . . 135
12.9 Tips and Tricks . . . 135
12.10 E-FAST Examination in Medical Decision-Making . . . 137
12.11 Conclusion . . . 138
References . . . 138

13 Point-of-Care Gastric Ultrasound . . . 139
Noreddine Bouarroudj
13.1 Introduction . . . 139
13.1.1 Gastric Ultrasound: An Emerging Technique . . . 139
13.1.2 Gastric Ultrasound to Prevent Perioperative Pulmonary Aspiration . . . 139
13.2 Principles . . . 140
13.3 Assessment of Gastric Content vs. Schrödinger's Cat Thought Experiment . . . 141
13.3.1 Teaching Schrödinger's Cat to Evaluate the Clinical State of Superposition? . . . 141
13.4 Anatomy and Physiology . . . 142
13.4.1 Applied Anatomy . . . 142
13.4.2 Gastric Wall Histology . . . 144
13.4.3 Gastric Motor Function Physiology and Pathophysiology . . . 144

13.5 Indications . . . 145
13.5.1 Confirm Gastric Emptiness in Superposition of Clinical States . . . 145
13.5.2 Other Clinical Applications . . . 146
13.6 Preparation, Equipment, and Techniques . . . 146
13.6.1 Preparation . . . 146
13.6.2 Position . . . 146
13.7 Sonoanatomy . . . 148
13.7.1 Sonographic Appearance of Gastric Wall Layers . . . 149
13.7.2 Sonographic Appearance of Gastric Content . . . 149
13.7.3 Sonographic Appearance of Antrum . . . 150
13.8 Ultrasonographic Measurement of Antral Area . . . 151
13.8.1 Qualitative Assessment of Gastric Volume . . . 151
13.8.2 Quantitative Assessment of Gastric Volume . . . 152
13.9 Interpretation and Scores . . . 153
13.9.1 Medical Decision-Making . . . 153
13.10 Specific Patients . . . 155
13.10.1 Point-of-Care Gastric Ultrasound in Adults . . . 155
13.10.2 Point-of-Care Gastric Ultrasound in Pregnancy . . . 155
13.10.3 Point-of-Care Gastric Ultrasound in Pediatrics . . . 157
13.10.4 Point-of-Care Gastric Ultrasound in Obese Patients . . . 158
13.10.5 Point-of-Care Gastric Ultrasound for Critically Ill Patients . . . 160
13.11 Tips and Tricks . . . 160
References . . . 160

14 Vascular Ultrasound . . . 161
Fatima Zohra Ouichen and Lydia Nekmouche
14.1 Introduction . . . 161
14.2 Techniques . . . 161
14.3 Assessment of Upper Limb Vessels . . . 162
14.3.1 Anatomy . . . 162
14.3.2 Sonoanatomy . . . 163
14.3.3 Pathology . . . 168
14.4 Neck Vessels . . . 169
14.5 Assessment of Lower Limb Vessels . . . 173
14.5.1 Assessment of Lower Limb Artery . . . 173
14.5.2 Assessment of Lower Limb Venous . . . 179
14.6 Abdominal Aorta . . . 182
14.7 Arteriovenous Fistula . . . 185
14.8 Fistula Complication . . . 186
References . . . 187

15 Role of Ultrasound in Airway Management . . . 189
Peñafrancia C. Cano
15.1 Introduction . . . 189

ALGrawany

15.2 Sonoanatomy of the Airway . . . 189
15.3 Functions of Ultrasound in the Airway . . . 192
15.3.1 Cricothyroidotomy . . . 192
15.3.2 Confirmation of Endotracheal Tube (ETT) Placement . . . 192
15.3.3 Prediction of Difficult Laryngoscopy . . . 193
15.3.4 Prediction of Endotracheal Tube Size . . . 193
15.3.5 Prediction of Postextubation Stridor . . . 194
15.4 Conclusion . . . 194
References . . . 195

16 Echocardiographic Evaluation of Shock . . . 197
Habiba Hemamid
16.1 Introduction . . . 197
16.1.1 Value of Echocardiography in Shock State . . . 198
16.1.2 When and How to Use Echocardiography in Shock . . . 198
16.2 Mechanisms of Shock . . . 199
16.2.1 Obvious Cardiac Abnormalities . . . 199
16.2.2 Hyperkinetic State . . . 200
16.2.3 Hypokinetic State . . . 201
16.2.4 Normokinetic State . . . 201
16.3 Haemodynamic Profile of Shock . . . 202
16.3.1 Left Ventricular Systolic Function . . . 202
16.3.2 Cardiac Output Assessment . . . 203
16.3.3 Fluid Requirement . . . 203
16.3.4 Vasoplegia . . . 204
16.3.5 Right Ventricular Function . . . 204
16.4 Haemodynamic Monitoring Using Repeated Echocardiography . . . 205
16.5 Management of Shock . . . 206
16.5.1 Therapeutic Impact . . . 207
16.5.2 Assessment of Efficacy and Tolerance Therapy . . . 207
16.6 Limitation of Echocardiography . . . 207
16.7 Conclusion . . . 208
References . . . 208

17 Transcranial Doppler Sonography . . . 211
Lamine Abdennour, Alice Jacquens, and Vincent Degos
17.1 Introduction . . . 211
17.2 The Main Acoustic Windows . . . 211
17.2.1 Transtemporal Window (Picture 17.1) . . . 211
17.2.2 Transforaminal Window (Picture 17.2) . . . 212
17.2.3 Transorbital Window (Picture 17.3) . . . 212
17.2.4 Submandibular Window (Picture 17.4) . . . 213
17.3 Anatomical Landmarks . . . 213
17.4 The Main Cerebral Arteries . . . 215
17.4.1 Carotid Circulation . . . 215

17.4.2 Posterior Circulation (Vertebro-basilar Circulation) . . . 217
17.4.3 The Characteristics of the Circle of Willis . . . 220
17.5 Different Velocities Measurement and Index Calculation . . . 221
17.5.1 Normal Velocities . . . 221
17.5.2 Pulsatility Index (Gosling Index): PI . . . 222
17.5.3 Resistance Index (Pourcelot Index): RI . . . 223
17.5.4 Lindegaard or Aaslid Index (LI or AI): LI . . . 223
17.6 Exploration of Vascular Reactivity . . . 224
17.6.1 Vascular Reactivity to Arterial Pressure: *Cerebral Pressure Autoregulation* . . . 224
17.6.2 Cerebrovascular Reactivity to Au CO_2 . . . 225
17.7 Pathological Situations . . . 227
17.7.1 Hypoperfusion Situation . . . 227
17.7.2 Hyperaemia and Hyperaemia Syndrome . . . 228
17.7.3 Vasospasm . . . 228
17.7.4 Brain Death . . . 228
17.8 Other Situations . . . 230
17.8.1 Patent Foramen Ovale . . . 230
17.8.2 Carotid Artery Dissection . . . 230
17.8.3 Vertebral Artery Dissection . . . 232
17.8.4 Carotidcavernous Fistula . . . 233
17.8.5 Venous Sinus Thrombosis . . . 233
17.9 Conclusions . . . 235
References . . . 235

18 Renal Ultrasound . . . 237
Nurul Shaliza Shamsudin, Muhammad Faiz Baherin, and Nurul Liana Roslan
18.1 Introduction . . . 237
18.2 Sonoanatomy of the Kidney . . . 237
18.3 Clinical Indications . . . 238
18.4 Preparation, Equipment, and Scanning Techniques . . . 239
18.4.1 Patient and Machine Positioning . . . 239
18.4.2 Transducer Selection and Machine Setting . . . 239
18.4.3 Scanning Technique . . . 239
18.5 Normal Sonographic Findings of Kidney, Ureter, and Bladder . . . 240
18.5.1 Renal Ultrasound Landmark Summary . . . 241
18.6 Renal Ultrasound Pathology . . . 245
18.6.1 Hydronephrosis . . . 245
18.6.2 Direct Visualization of Kidney Stone . . . 247
18.6.3 Hydronephrosis of Affected Kidney . . . 248
18.6.4 Absence of Ureteral Jets . . . 248
18.6.5 Twinkling Artifact . . . 248
18.6.6 Renal Cysts . . . 248
18.6.7 Renal Masses . . . 249

18.6.8 Urinary Tract Infection 250
18.7 Bladder Volume Calculation 254
18.7.1 Steps to Perform Urinary Bladder Ultrasound 255
18.8 Renal Hemodynamics 256
18.8.1 Renal Venous Congestion 256
18.8.2 Renal Resistive Index (RI) 257
References 259

19 Obstetric and Gynaecological Ultrasound 263
Mohammad Fadhly Yahya, Mohd Hafis Mohamed Sakan, and Nor Hanisah Mohd Said
19.1 Introduction 263
19.2 Principles 264
19.3 Normal Anatomy 265
19.3.1 Pelvic Cavity 265
19.3.2 Anterior Cul-de-Sac 266
19.3.3 Posterior Cul-de-Sac 266
19.3.4 Uterine Anatomy 266
19.3.5 Relations and Position 267
19.3.6 Ovarian Anatomy 267
19.4 Preparation, Equipment and Techniques 267
19.4.1 Preparation 267
19.4.2 Equipment 268
19.4.3 Technique 268
19.5 Sonoanatomy 269
19.5.1 Transabdominal Sagittal Plane (Fig. 19.7) 269
19.5.2 Transabdominal Transverse Plane (Figs. 19.8, 19.9, and 19.10) 270
19.6 POCUS in First Trimester Pregnancy Sonography of Important Pathology 271
19.6.1 Ectopic Pregnancy 271
19.6.2 Molar Pregnancy 271
19.6.3 Missed/Incomplete Abortion 272
19.7 POCUS in Antenatal (Second and Third Trimester Pregnancy) Sonography of Important Pathology 274
19.7.1 Placental Abruption (Abruptio Placentae) 274
19.7.2 Placenta Previa 274
19.7.3 Uterine Rupture 275
19.7.4 Fetal Demise 275
19.7.5 Retained Placenta 275
19.8 POCUS in the Non-Pregnant with Lower Abdominal Pain Sonography of Important Pathology 276
19.8.1 Ovarian Cysts Accident (Ruptured, Twisted, Haemorrhage) 276
19.8.2 Tubo-Ovarian Abscess 277
19.8.3 Pelvic Inflammatory Disease 278
References 279

ALGrawany

Contributors

Lamine Abdennour Neuro-Réanimation Chirurgicale, Département d'Anesthésie-Réanimation, Groupe Hospitalier Pitié-Salpêtrière, APHP-Sorbonne Université, Paris, France

Divesh Arora Department of Anaesthesia and OT Services, Asian Hospital, Faridabad, Haryana, India

Muhammad Faiz Baherin Emergency and Trauma Department, Hospital Tuanku Ja'afar, Seremban, Negeri Sembilan, Malaysia

Noreddine Bouarroudj Department of Anesthesiology and Critical Care, Clinique Maissalyne, Constantine, Algeria

Department of Anaesthesia and Critical Care, Maissalyne Hospital, Constantine, Algeria

Cherif Bouzid Department of Anaesthesia and Critical Care, El Afia Hospital, Mila, Algeria

Peňafrancia C. Cano Division of Regional Anesthesia, Department of Anesthesiology, University of the Philippines-Philippine General Hospital, Manila, Philippines

Lim Teng Cheow Department of Anaesthesia and Intensive Care, Malacca General Hospital, Melaka, Malaysia

Lim See Choo Emergency and Trauma Department, Hospital Sultan Haji Ahmad Shah, Temerloh, Malaysia

Lee Kee Choon Emergency and Trauma Department, Hospital Sultan Haji Ahmad Shah, Temerloh, Malaysia

Yeoh Jie Cong Department of Anaesthesiology and Intensive Care, Hospital Kuala Lumpur, Kuala Lumpur, Malaysia

Vincent Degos Neuro-Réanimation Chirurgicale, Département d'Anesthésie-Réanimation, Groupe Hospitalier Pitié-Salpêtrière, APHP-Sorbonne Université, Paris, France

Shahridan bin Mohd Fathil Department of Anaesthesia, Gleneagles Medini Hospital Johor, Iskandar Puteri, Malaysia

Muhamad Rasydan Abd Ghani Department of Anaesthesiology and Intensive Care, Kulliyyah of Medicine, Bandar Indera Mahkota Campus, International Islamic University, Kuantan, Malaysia

Department of Anaesthesiology and Intensive Care, Sultan Ahmad Shah Medical Centre @ IIUM, International Islamic University, Kuantan, Malaysia

Habiba Hemamid Medical Faculty, Intensive Care Unit, Critical Care Department, University Hospital of Sadna Mohamed Abdennour, University of Elbaz, Sétif, Algeria

Alice Jacquens Neuro-Réanimation Chirurgicale, Département d'Anesthésie-Réanimation, Groupe Hospitalier Pitié-Salpêtrière, APHP-Sorbonne Université, Paris, France

Muhazan Mazlan Emergency and Trauma Department, Hospital Sungai Buloh, Sungai Buloh, Malaysia

Sultan Haji Ahmad Shah Ahmad Suhailan Mohamed Emergency Department, National Heart Institute, Kuala Lumpur, Malaysia

Lydia Nekmouche EPH Laghouat, Laghouat, Algeria

Fatima Zohra Ouichen Clinique Chifa, Algiers, Algeria

Amrita Rath Department of Anaesthesia, IMS, BHU, Varanasi, UP, India

Nurul Liana Roslan Emergency and Trauma Department, Hospital Kuala Lumpur, Kuala Lumpur, Malaysia

Nor Hanisah Mohd Said Hospital Pantai Ayer Keroh, Melaka, Malaysia

Mohd Hafis Mohamed Sakan Emergency and Trauma Department, Melaka General Hospital, Melaka, Malaysia

Nurul Shaliza Shamsudin Emergency and Trauma Department, Hospital Serdang, Kajang, Malaysia

Emergency and Trauma Department, Hospital Sultan Idris Shah, Serdang, Selangor, Malaysia

Hetal Vadera Department of Anaesthesia, Sterling Hospital, Rajkot, Gujarat, India

Mohammad Fadhly Yahya Emergency and Trauma Department, Melaka General Hospital, Melaka, Malaysia

Nur Hafiza Yezid Department of Emergency Medicine, Hospital Sultanah Bahiyah, Alor Setar, Malaysia

ALGrawany

Part I

Basic Ultrasound in Critical Care, Anesthesia and Emergency

Principle of Ultrasound

1

Shahridan bin Mohd Fathil, Yeoh Jie Cong, Lee Kee Choon, Lim See Choo, Sultan Haji Ahmad Shah Ahmad Suhailan Mohamed Muhazan Mazlan, Nurul Shaliza Shamsudin, and Muhamad Rasydan Abd Ghani

1.1 Introduction

1.1.1 History and Evolution of Medical Ultrasound

The discovery of ultrasound waves dates back to 1793, when Lazzaro Spallanzani, an Italian biologist, observed the echolocation ability of bats in navigation [1]. Later on, in 1915, Pierre and Jacques Curie observed the phenomenon of piezoelectric effect, which refers to the generation of electric charges by specific crystals under mechanical pressure thereby generating pressure waves upon application of electricity. This significant finding led to the development of ultrasound transducers capable of emitting and receiving such waves.

The medical application potential was realized by John Wild, an English-born surgeon in 1950 through his research papers that highlighted how ultrasonic imaging could effectively differentiate between normal tissue and those invaded by tumors, setting the foundation for future advancements in this field [2].

In 1953, Inge Edler, a Swedish physician, together with Carl Hertz, a German physicist, pioneered the initial usage of echocardiography using M mode recording using a sophisticated ultrasonic reflectoscope, which is a tool employed for examining the inner regions of solid compo-

S. M. Fathil (✉)
Department of Anaesthesia, Gleneagles Medini Hospital Johor, Iskandar Puteri, Malaysia

Y. J. Cong
Department of Anaesthesiology and Intensive Care, Hospital Kuala Lumpur, Kuala Lumpur, Malaysia

L. K. Choon · L. S. Choo
Emergency and Trauma Department, Hospital Sultan Haji Ahmad Shah, Temerloh, Malaysia

S. H. A. S. A. S. Mohamed
Emergency Department, National Heart Institute, Kuala Lumpur, Malaysia
e-mail: drsuhailan@ijn.com

M. Mazlan
Emergency and Trauma Department, Hospital Sungai Buloh, Sungai Buloh, Malaysia

N. S. Shamsudin
Emergency and Trauma Department, Hospital Serdang, Kajang, Malaysia

M. R. A. Ghani
Department of Anaesthesiology and Intensive Care, Kulliyyah of Medicine, Bandar Indera Mahkota Campus, International Islamic University, Kuantan, Malaysia

Department of Anaesthesiology and Intensive Care, Sultan Ahmad Shah Medical Centre @ IIUM, International Islamic University, Kuantan, Malaysia
e-mail: rasydan@iium.edu.my

© The Author(s), under exclusive license to Springer Nature Switzerland AG 2024
N. Bouarroudj et al. (eds.), *POCUS in Critical Care, Anesthesia and Emergency Medicine*,
https://doi.org/10.1007/978-3-031-43721-2_1

ALGrawany

nents to identify imperfections [3]. During the same period, medical doppler imaging was also developed by a Japanese physicist, Shigeo Satumura, to measure blood flow and velocity non-invasively. [4] Medical ultrasound technology has continued to progress in the 1990s with harmonic imaging and the advancement of imaging technology was marked by the adoption of three-dimensional (3D) and four-dimensional (4D) ultrasound, which significantly improved image resolution and quality. [5]

1.1.2 Evolution of POCUS in Critical Care, Anesthesiology, and Emergency Medicine

In 1993, a French intensivist, Daniel Liechtenstein, was the first to describe the use of diagnostic and procedural guidance with ultrasound for the abdomen, lung, and major veins in the intensive care setting [6].

1.1.3 Lung Ultrasound

Lung ultrasound was initially viewed with skepticism due to its inability to assess the parenchyma of the aerated lung properly. The first mention of thoracic ultrasound was from André Dénier, the father of medical ultrasound. However, it was Daniel Lichtenstein who improved on the concept and understanding of lung ultrasound, redefining its uses and debunking many criticisms. [7]

1.1.4 Echocardiography

As described above, in 1953, Inge Edler and Carl Hertz succeeded in capturing the initial dynamic visual depiction of cardiac movement [8]. In 1976, Leon Frazin and colleagues first described transesophageal echocardiography using a rounded transducer that was swallowed by the patients themselves. [9] In 1980, Eugene DiMagno introduced a side-viewing gastroscope that integrated an ultrasound probe within its tip. This innovation facilitated the examination of the upper gastrointestinal tract using endoscopy and enabled ultrasonic imaging of internal organs like the heart. [10]

1.1.5 Abdominal Ultrasound for Trauma

In 1970, American radiologists, Barry Goldberg and colleagues instilled fluid into cadavers and patients to assess the capacity of A mode ultrasound for identifying “free fluid.” [11] In 1971, JK Kristensen and colleagues from Germany published the primary case report detailing the application of ultrasound in assessing blunt abdominal trauma. [12] In 1976, Michael Asher and colleagues conducted a preliminary study on the use of ultrasound for screening purposes in a cohort of 70 patients who exhibited blunt abdominal trauma and were suspected to have sustained splenic injury. [13] In 1992, Paul Tso and colleagues compared the usefulness of ultrasound with diagnostic peritoneal lavage (DPL) and computed tomography scan on 163 blunt abdominal traumas. Overall, ultrasound had high specificity and sensitivity. [14] The currently accepted nomenclature Focused Assessment with Sonography for Trauma (FAST) was standardized in 1996 to describe the ultrasound scanning for free fluid in abdominal trauma. [15]

1.1.6 Ultrasound Guidance for Vascular Cannulation

James Ullman and Robert Stoelting reported the use of an ultrasound doppler pencil-shaped flow probe to improve the rate of successful cannulation of the internal jugular vein [16]. A decade later, in 1986, Akitomo Yonnei and colleagues described the first real-time ultrasound-guided cannulation of the internal jugular vein. [17] Today, ultrasound guidance is the standard of practice for central and peripheral venous and arterial cannulations across all medical disciplines. [18–21]

1.1.7 Ultrasound-Guided Regional Anesthesia

The first ultrasound guidance for a regional block was performed by P Ting and V Sivagnanaratnam in 1989 in Singapore. The authors documented the before and after local anesthetic administration ultrasound images of the axilla for axillary brachial plexus blocks in ten patients. [22] In 1994, Stephan Kapral and colleagues from Austria, documented the first case series of real-time ultrasound-guided supraclavicular blocks in 40 patients [23]. Since then, ultrasound-guided regional anesthesia and pain blocks has evolved into a mainstream anesthesia sub-specialty. [24–26]

1.1.8 Advancement of POCUS from the Past Decade

The implementation of point-of-care ultrasound (POCUS) guidance has resulted in improved outcomes and reduced complications for a range of medical procedures, such as central and peripheral vascular access, thoracocentesis, and regional anesthesia. It appears that acquiring proficiency in using POCUS for these procedures requires less time than other techniques; however, there is currently no widely accepted method to determine competence. Clinicians who master the use of POCUS can also apply this tool to monitor clinical conditions that may escalate quickly, leading to earlier interventions with potentially favorable patient outcomes.

Point-of-care ultrasonography has emerged as an efficient and cost-effective alternative to traditional ultrasonography. It has led to reduced referrals, improved diagnosis accuracy, and effective management of various clinical conditions. However, it requires appropriate training and quality assurance since indiscriminate use may lead to unnecessary testing or interventions. Despite the potential benefits of POCUS on patient outcomes, studying its impact is challenging due to factors such as patient diversity, lack of standardization in protocols used by clinicians alongside confounding variables that include concurrent therapeutic measures, variation in clinician skills level, as well as difficulty finding unbiased professionals toward using POCUS techniques. [27, 28]

1.1.9 Machine Learning and Artificial Intelligence in POCUS (AI and ML)

In today's world, AI and ML in POCUS have garnered tremendous attention, especially in the realm of medical imaging. Point-of-care ultrasound is an area where these technologies are finding their feet while computed tomography and radiography already bear witness to their efficacy [29]. Using AI/ML to sift through massive amounts of data and formulate algorithms can equip clinicians with invaluable support for quick decision-making, error detection tools, and techniques for image optimization [30]. Despite this progress though, it remains crucial that further research be conducted on safety concerns as well as ethical dilemmas and legal implications that may arise before we can fully rely on AI/ML in clinical applications.

1.1.10 Newer Applications in Handheld Portable Devices

Handheld portable ultrasound devices have been available for over a decade, evolving from laptop to pocket size and now wirelessly connected to tablets or smartphones. The more affordable capacitive micromachined ultrasound transducer (CMUT) can replace the piezoelectric crystal, allowing for analysis of a wide range of frequencies and enhancing portability. Longer battery life, better heat dissipation, and ergonomic probe design are attractive features for users. These smaller, durable, pocket-sized devices have also improved tele-ultrasound services, especially in remote areas where POCUS expertise is required. The utilization of technology has been significantly influenced and molded by worldwide pandemics, including the recent COVID-19 pandemic. [31]

1.2 Ultrasound Physics

1. Describe ultrasound as a mechanical wave
2. Elaborate piezoelectric crystal and effect
3. Basic physics definitions
   (a) Frequency
   (b) Velocity
   (c) Wavelength
   (d) Amplitude
   (e) Intensity
   (f) Power
      (i) Mechanical index
      (ii) Thermal index

Ultrasound is a mechanical wave that travels through the body and interacts with the tissues along the penetration. A sound wave can be a moving longitudinal or transverse waveform in the medium. The propagation of the longitudinal soundwave is parallel to the displacement of the medium. Therefore, only longitudinal soundwaves are important in medical ultrasonography. Medical ultrasound commonly ranges from 1 to 15 MHz (1 MHz = 1 million hertz). Meanwhile, normal human hearing ranges from 20 to 20,000 Hz; anything above the human hearing range is considered *ultrasound* [32].

1.2.1 Piezoelectric Crystal and Effect [32, 33]

The ultrasound source is the piezoelectric (piezo is a Greek word piezein—to squeeze/press) crystal. When electrical current is present, the piezoelectric crystals' vibration will generate sound waves. This elastic property of the crystal is known as the piezoelectric effect. Inversely, the crystals can convert the waves to electrical energy, and the data will be processed as anatomic images. Current ultrasound transducers commonly use lead zirconate titanate (PZT) ceramics. PZT is preferred due to its ability to produce a wide range of frequencies.

1.2.2 Basic Physics Definitions [32, 34–37]

1.2.2.1 Frequency and Wavelength

In soundwave, frequency represents the number of cycles per second (Hertz). One hertz (Hz) is equivalent to one wave per second. It is an essential property of waves as it determines their wavelength and energy. Higher frequency waves exhibit a shorter wavelength, while lower frequency waves exhibit a longer wavelength. Long-wavelength sound waves can travel into deeper tissues than short wavelengths; however, they produce a lower resolution.

1.2.2.2 Velocity

Velocity is the speed at which an ultrasound wave passes through a medium. It is the product of wavelength and frequency [v = wavelength (λ) × frequency (f)]. Different mediums will produce different velocities (shown in Table 1.1). The velocities of sound waves change when passing through a different mediums. Changes in the medium cause a certain amount of energy loss. For example, the sound velocity through the water and soft tissue is 1430 m/s and 1540 m/s, respectively. Due to minor differences, no significant amount of energy was lost. However, when the low velocity of the sound wave passes through the air (331 m/s), it results in a significant loss of signal, thus making it a poor acoustic window.

Table 1.1 The reported velocity of soundwaves in human soft tissues

Media	Velocity (m/s)
Air	330
Water	1480
Fat	1450
Blood	1570
Kidney	1560
Liver	1550
Muscle	1580
Bone	4080

A L G r a w a n y

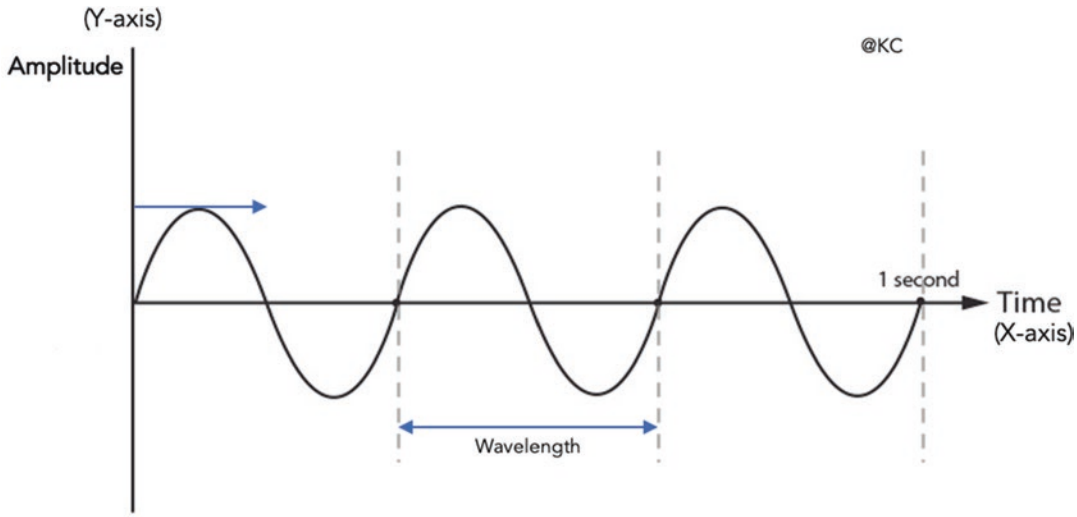

1.2.2.3 Amplitude

Amplitude is related to the loudness or size of the wave. It refers to the maximum displacement (from baseline to top of the wave) or distance of the particles in the medium which the soundwave traveled. The amplitude of a sound wave can affect its ability to penetrate tissue. A higher voltage applied to the piezoelectric crystal will increase the vibration, thus making the image brighter.

1.2.2.4 Intensity

Intensity is defined as the energy concentration in the cross section of the soundwave. It is the product of power divided by the cross-sectional area of the sound wave [I = Power (Watts)/ Area (cm^2)]. It is directly proportional to power. Theoretically, high intensity ultrasound can cause tissue damage.

1.2.2.5 Power

It is the rate of energy (joules) transferred over a certain amount of time (watts). Although power is not visible in ultrasound, the two variables are indirectly related. The first is the mechanical index, which represents the risk of cavitation (the formation of small gas bubbles within the scanning area). The second is the thermal index (TI), which is related to the tissue temperature increment in the region of interest. TI is calculated from the acoustic power of the source divided by the power required to raise the tissue temperature by 1 °C. Although there are no known biological effects of ultrasound, it is recommended that total exposure time and intensity be kept as low as reasonably achievable – also known as the ALARA principle.

1. Ultrasound interaction with tissues
   (a) Reflection
   (b) Attenuation
      (i) Absorption
      (ii) Scattering
      (iii) Refraction

1.2.3 Ultrasound Wave Interaction with Tissues [32, 34]

1.2.3.1 Reflection

Ultrasound waves transmitted through tissues and different mediums are reflected to the transducer and displayed as ultrasound images. The greater the reflection, the brighter the images are displayed on the ultrasound machine. The intensity of the reflection determines the image brightness display and the descriptions are as follows:

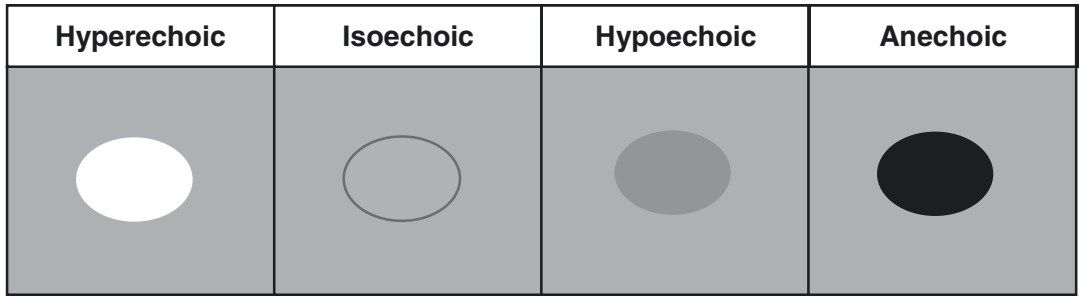

Fig. 1.1 Different echogenicity with the surrounding tissue

Hyperechoic: An area that generates a bright signal due to intense reflection.
Isoechoic: Same echogenicity with surrounding tissue.
Hypoechoic: Darker signal at the area that does not reflect as much.
Anechoic: Completely black area with no sound waves reflected (Fig. 1.1).

The reflection of the soundwave is determined by the acoustic impedance difference of the two mediums, the angle of incidence and the ultrasound wave frequency.

The acoustic impedance of a medium describes its ability to transmit ultrasound waves. It also measures the material's resistance to the transmission of soundwaves. It is calculated from the density of the material and the speed of sound in the material.

$$Z = \rho \times v$$

Z (acoustic impedance); ρ (density of the medium); v (velocity).

Mediums with high acoustic impedance, such as bone, offer greater resistance to the transmission of acoustic waves compared to mediums with low acoustic impedance, such as soft tissue. As the difference in acoustic impedance between two mediums increases and the mismatch grows, it leads to reflection of sound waves back to the transducer, causing an artifact phenomenon known as acoustic shadowing (Table 1.2) (Fig. 1.2).

Table 1.2 Impedance of different mediums

Medium	Acoustic Impedance (Rayls)
Air	0.00043
Fat	1.3×10^6
Water	1.48×10^6
Muscle	1.6×10^6
Liver	1.6×10^6
Blood	1.6×10^6
Kidney	1.7×10^6
Bone	$6.5–8.0 \times 10^6$

Fig. 1.2 Ultrasound of aorta—the acoustic impedance (AI) difference between surrounding tissues and vertebrae bone is high, which results in acoustic shadowing of the vertebrae body

1.2.3.2 Attenuation

As the ultrasound wave propagates through different mediums, attenuation occurs in which there is a gradual reduction in the intensity of the ultrasound wave. A portion of the wave returns to the probe to be displayed as an image on the ultrasound machine results of the reflection of the ultrasound wave.

However, the rest of the sound wave loses energy in three ways: absorption, scattering, and refraction.

(a) ***Absorption***—the soundwave energy is absorbed by the medium and converted to heat energy.
(b) ***Scattering***—the ultrasound wave is redirected in different directions when it encounters small structures or irregularities within the medium.
(c) ***Refraction***—when the ultrasound wave is transmitted through two media with different acoustic impedances (e.g., a soft tissue and a bone), the direction of the ultrasound wave is bent or altered due to a change in its velocity and direction. This process leads to some of the energy being lost in the process.

The degree of attenuation is also determined by the soundwave frequency and the density of the medium. Higher frequency sound waves attenuated more, resulting in less penetration; conversely, lower frequency sound waves have lesser attenuation, better penetration, resulting in better visualization of deep structures (Fig. 1.3).

1. Resolution
   (a) Spatial
      (i) Axial
      (ii) Lateral
   (b) Temporal

1.2.4 Resolution [32, 34]

It is the ability to accurately distinguish between two subjects that are nearby at a particular distance. In addition to distance or space (Spatial), resolution can also be defined by time (Temporal) or color (Contrast). There are two types of spatial resolution. Axial and lateral resolution (Fig. 1.4).

1.2.4.1 Axial Resolution

Axial resolution is the ability to distinguish between two objects at different distances from the transducer along the axis of the ultrasound beam. A short pulse is better for distinguishing between two objects that are very close to each other. Therefore, the higher the frequency setting, the higher the resolution (Fig. 1.5).

1.2.4.2 Lateral Resolution

Lateral resolution is the ability to distinguish between two objects that are aligned to the ultrasound beam. Lateral resolution is highest in the

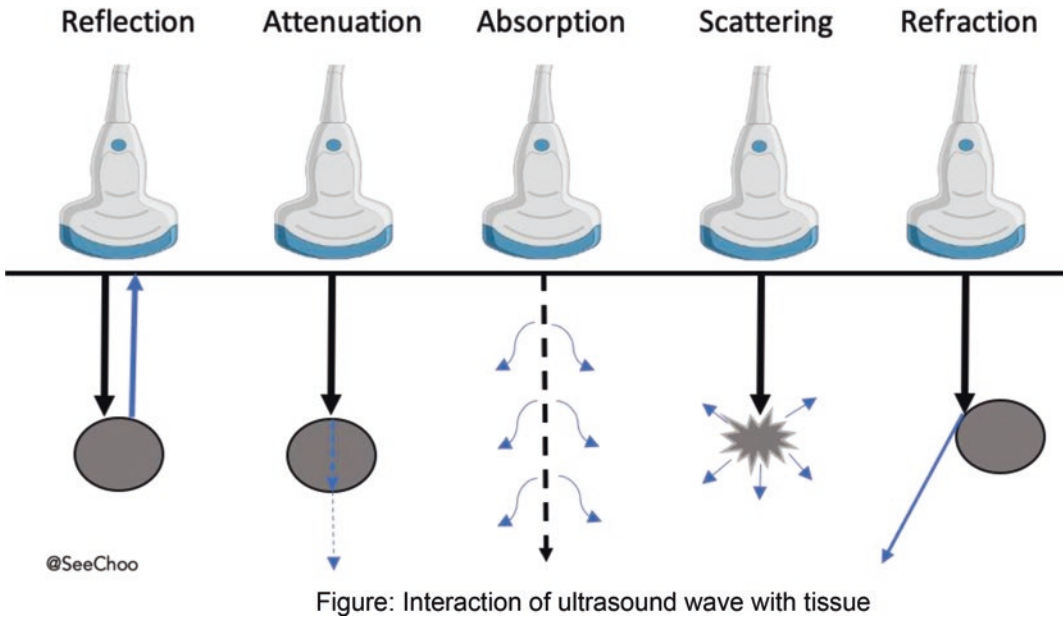

Fig. 1.3 Interaction of ultrasound wave with tissue

A L G r a w a n y

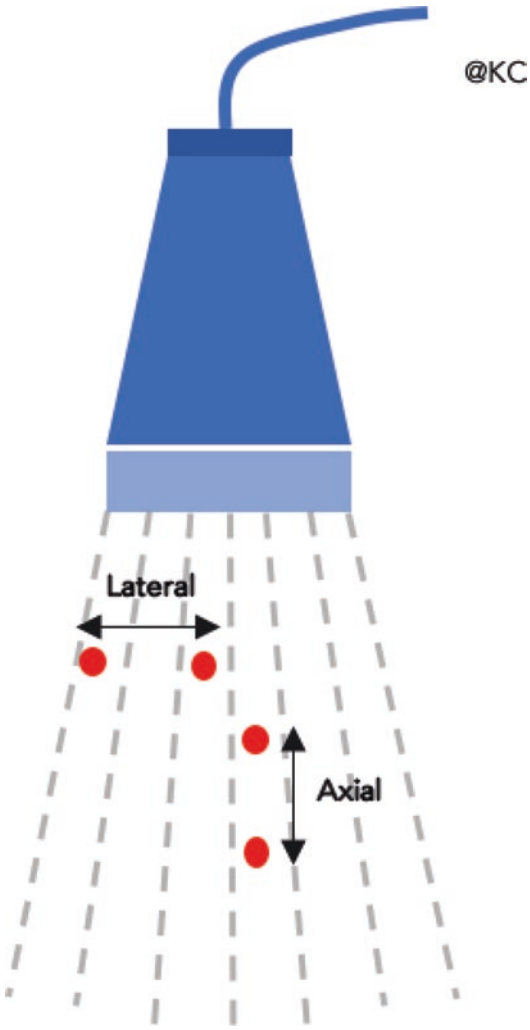

Fig. 1.4 Diagram shows the difference between axial and lateral resolution

narrowest part of the beam and decreases with distance (Fig. 1.6).

1.2.4.3 Temporal Resolution

This is the ability of an ultrasound machine to accurately detect and display changes of moving tissue over time. Higher temporal resolution allows the machine to capture images quickly, producing sharper images of dynamic structures like the heart and blood vessels. However, there are several factors such as ultrasound transducer frequency, frame rate, and computer system processing power that affect resolution.

1. Scanning modes
   (a) A-mode
   (b) B-mode
   (c) M-mode
   (d) Doppler
      (i) Define Doppler effect/shift
      (ii) Describe different types of Doppler mode
         - Pulsed wave
         - Continuous wave
         - Color

1.2.5 Scanning Modes [32, 34, 35, 37, 38]

1.2.5.1 A-Mode

This mode represents the amplitude mode of medical ultrasound. It displays the intensity or amplitude of each returning echo and plots it on the display as a vertical line representing the depth at which the echo was received. The image produced looks like a series of peaks or spikes. Higher peaks indicate stronger echoes and deeper structures. A-mode is commonly used in ophthalmic sonography to measure the axial length of the eyeball and retina. This is important for intraocular lens implantation.

1.2.5.2 M-Mode

M mode stands for motion mode. Images displayed in M-mode represent the movement of tissue or structures (y-axis) over time (x-axis). It is advantageous as it allows for accurate measurement of size and distance, as well as providing high temporal resolution. M-mode in echocardiography has several common uses. For instance, it is used to measure left ventricular wall thickness in the parasternal short-axis view, calculate diastolic and systolic diameters to determine LV fractional shortening, and estimate LV function by measuring systolic excursion of the mitral annulus plane (Fig. 1.7). Additionally, M-mode

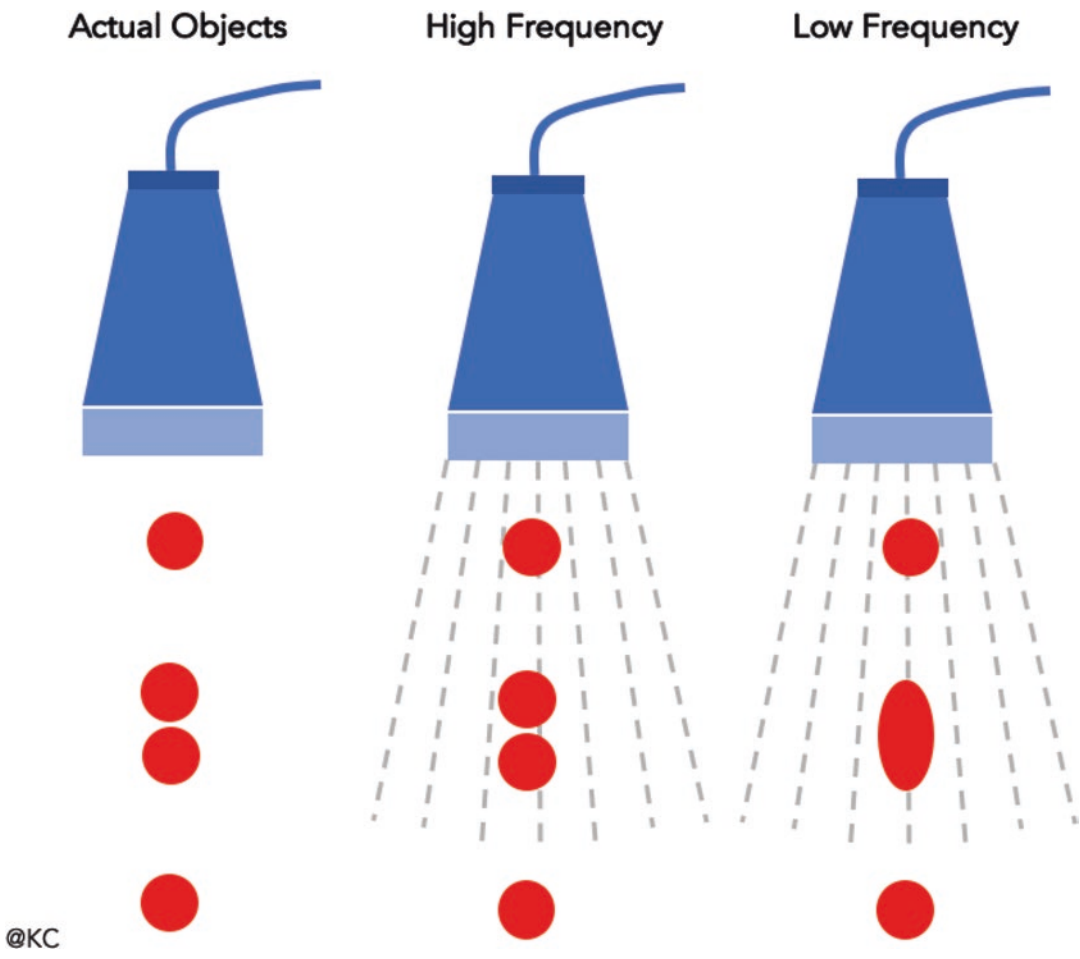

Fig. 1.5 Axial resolution. The red dots on the left side indicate the actual subjects. The middle transducer has a shorter wavelength, while the right transducer has a longer wavelength

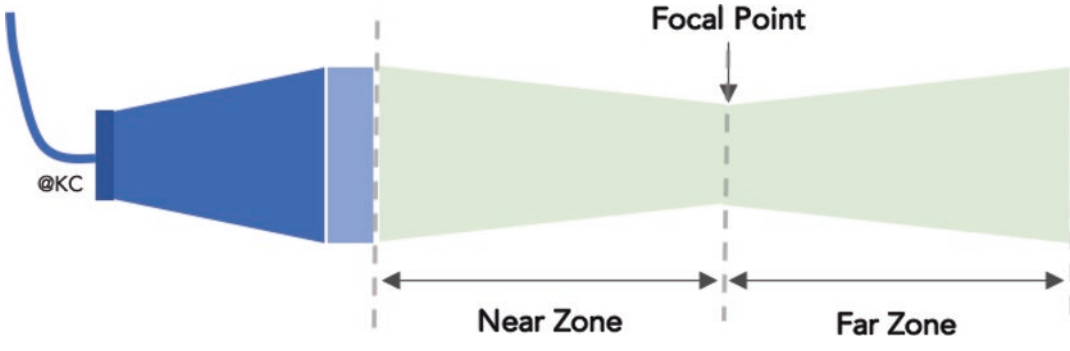

Fig. 1.6 Diagram shows the anatomy of the ultrasound beam. The best image resolution is at the focal point

A L G r a w a n y

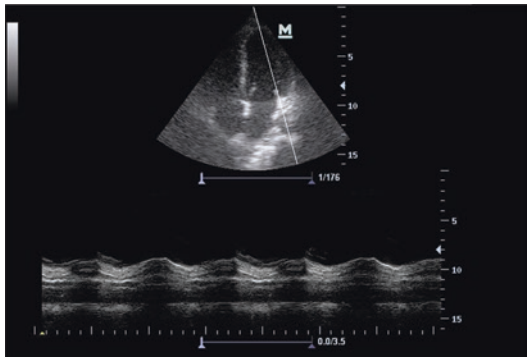

Fig. 1.7 The image shows the usage of M-mode to measure the mitral annulus plane systolic excursion (MAPSE)

facilitates in demonstration of systolic anterior motion of the mitral valves.

1.2.5.3 B-Mode

In B-mode, the transducer sends sound waves into the body, which are later reflected by tissue and returned to the transducer as echoes. These echoes are interpreted and processed by the ultrasound machine to create a two-dimensional image of the internal structures. Different echo intensities or amplitudes result in different brightness in the image. Strong reflections appear as bright white dots and vice versa.

1.2.5.4 Doppler Mode

Doppler is named after Austrian physicist Christian Doppler, who first described the principle of the Doppler effect. The Doppler effect (or Doppler shift) is a phenomenon that occurs when there is relative motion between a sound source and an observer. The classic example is the change of siren pitch of an approaching or receding ambulance. As the ambulance moves closer, the pitch appears to increase; while it recedes, the pitch appears to decrease.

Doppler shift was the basis for all Doppler modes. This depends on three factors involved in the Doppler shift equation.

1. ***The velocity of the moving tissues***. The higher the velocity of the moving tissues, the greater the Doppler shift.
2. ***The frequency of the soundwave.*** The higher the frequency of the ultrasound beam, the greater the Doppler shift. However, higher frequency ultrasound has the trade-off of less penetration.
3. ***The incident or angle of the ultrasound beam***. If the Cosine of an angle is 0 (Cosine 90° = 0), zero Doppler shift will be recorded. The optimum angle of incidence is between 0° and 60°.

$$\text{Doppler shift} = \frac{2 \text{ x } F \text{ x } V \text{ x } \cos\theta}{C}$$

where F = frequency of the transmitted beam, V = velocity of moving tissue, C = speed of sound in soft tissue, θ = angle of incidence between ultrasound beam and flow direction

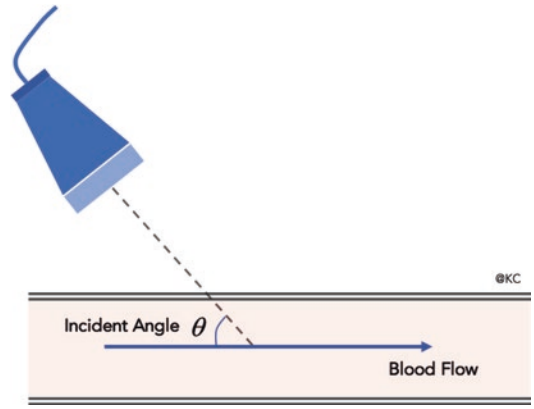

There are several examples of Doppler mode used in clinical ultrasound.

1. Color Doppler
2. Spectral Doppler
   (a) Pulsed-wave Doppler
   (b) Continuous-wave Doppler
   (c) Tissue Doppler Imaging

Color Doppler

It is called "color" because it displays the blood flow as a color image superimposed on the B-mode image. The Doppler effect allows us to analyze the return waves from the ultrasound device and determine the speed and direction of moving cells. The color indicator is to determine the direction towards or away from the transducer. Typically, red indicates blood flowing

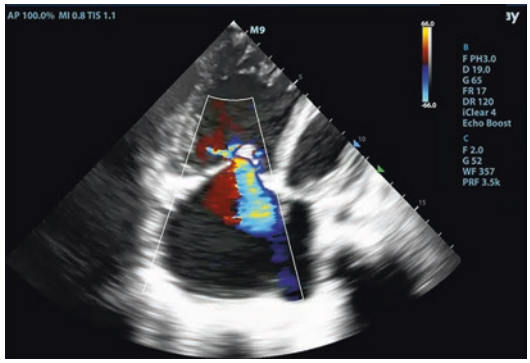

Fig. 1.8 The echocardiography image of the apical four-chamber view shows a mosaic pattern at the mitral valve area which suggests turbulent flow (white arrow – TF) likely due to underlying valve pathology such as mitral regurgitation

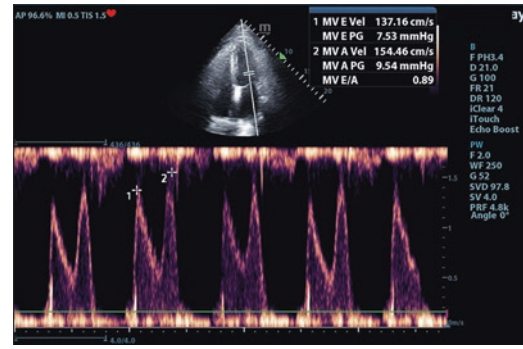

Fig. 1.9 This image shows forward flow to the probe shown above the baseline. PW mode is used to measure peak velocities in passive (E) and active (A) diastole and to estimate the E/A ratio for diastolic function

toward the transducer, and blue indicates blood flowing away from the transducer. The brightness of the color indicates the speed of blood flow, and the brighter the color, the higher the velocity of the blood flow. If blood flows in different directions and varies velocities, this can create turbulence which can be observed as mosaic or speckled patterns in color images. This occurs due to a mixture of red and blue colors, creating superimposed yellow and green colors. Turbulent flow is commonly associated with irregularities in the vessels, valvular stenosis, and regurgitation (Fig. 1.8).

Spectral Doppler

Pulsed-Wave Doppler

PW Doppler samples velocity at specific points determined by the sample volume of the ultrasound beam. Ultrasound transducers alternately emit sound waves and receive returning echoes (Fig. 1.9).

Most transducers use *pulsed echo mode* whereby the piezoelectric crystal spends a small amount of time generating a burst of sound waves while most of the time receiving the returning impulses. The number of transmit and receive cycles generated per second is called the pulse repetition frequency (PRF). If the Doppler shift frequency is greater than half the PRF (Nyquist limit), the signal will appear on the opposite side of the baseline and the velocity assessment will be inaccurate. This condition is called an aliasing artifact. Aliasing can be avoided by a few adjustments: (1) decreasing the transducer-sampling volume distance, (2) adjusting the baseline to a wider range of velocities, (3) increasing the PRF, (4) changing to continuous-wave mode, or (5) using a lower frequency transducer (Fig. 1.10).

Continuous-Wave Doppler

In contrast to PW Doppler, this mode functions by sending and receiving soundwave continuously. It is not possible to both send and receive signals with a single piezoelectric crystal. Therefore, two separate crystals are needed in the transducer to apply CW Doppler mode. The signals displayed represent all of the motion detected along the entire ultrasound beam. Because of the continuous wave, the machine is unable to pinpoint the origin of the velocity shown in the wave signal. Despite the poor depth discrimination, CW Doppler is ideal for measuring high velocities since it is not necessary to localize the precise source of a signal along the line of interrogation. In clinical applications, this mode is very useful to estimate pressure gradients across a pathological valve such as tricuspid regurgitation and mitral stenosis.

Tissue Doppler [38]

Tissue Doppler mode essentially applies the same principle as Doppler shift to measure high-amplitude, low-velocity signals of tissue motion. Previously, TDI was primarily used in Doppler

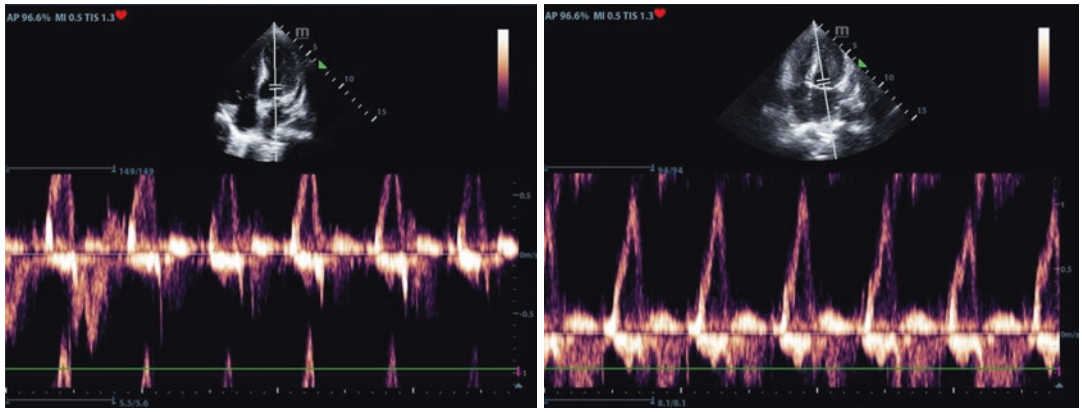

Fig. 1.10 Images on the left panel show the signal of the PW Doppler signal appearing on the opposite side of the baseline as the result of aliasing. Images on the right panel show the result of baseline adjustment to avoid the aliasing artifact, thus allowing correct measurement

echocardiography, but recent applications include measuring diaphragmatic velocity to predict successful weaning from the ventilator. TDI only estimates motion vectors parallel to the direction of the sound beam. Common clinical application of TDI includes assessment of left ventricle (LV) systolic and diastolic function by measuring the myocardial velocity at the lateral mitral annulus.

1.3 Transducers, Image Optimization, and Artifacts

1.3.1 Transducer

The ultrasound transducer consists of a probe with one or more piezoelectric crystals that produce sound waves when an electrical current passes through them. These crystals also act as receivers, converting sound waves back into electrical signals, which are then processed by the ultrasound system to create images of the body part being examined.

There are several types of ultrasound transducers in different footprints, sizes, and frequencies. The choice of transducer depends on the region of the body being examined and the specific imaging that is required. The footprint of the transducer affects the field of view, while the frequency of the emitted sound waves from the transducer affects the resolution of the image and the depth of penetration [39].

The common types of transducers are listed below:

- **Linear array transducer**: Linear transducer has a long, narrow, rectangular transducer face and is often referred to as "vascular" or "high frequency" transducers [40]. The transducer emits a linear ultrasound array and creates a rectangular image. Its frequency range is of 5–13 MHz and therefore has low penetration. Higher frequencies produce better image resolution and are preferred for superficial procedures requiring high accuracy. It is commonly used to image surface structures such as the breast, thyroid, pleura, blood vessels, and the musculoskeletal system.
- **Curvilinear array transducer**: The curvilinear transducer emits an array of curved ultrasound beams and produces a curved image. Curvilinear transducers can be small (microconvex) or large, with a frequency range of 1–5 MHz [40]. Due to the low frequency, the image resolution is grainy and inferior to the resolution of a linear transducer [39]. However, it creates a wider image area and greater depth. Thus, this transducer is commonly used for

A L G r a w a n y

imaging deeper structures such as the abdominal and obstetrics organs.

- **Phased array transducer:** The phased array probe has a small and almost square footprint with a frequency range of 1–5 MHz. Similar to a curvilinear transducer, a phased array transducer is used to image deeper structures. Its small footprint allows it to fit between the rib spaces and is the probe of choice for cardiac imaging [39].
- **Endocavity transducer:** The endocavity transducer is typically a micro-convex curvilinear transducer at the end of the transducer. It has a frequency range of 4–10 MHz and is used for transvaginal and transrectal [39].
- **3D/4D transducer:** Typically, it is used for three-dimensional (3D) and four-dimensional (4D) imaging, which allows for the visualization of the fetus or other structures in three dimensions and in real-time. It can be either linear or curvilinear in shape.
- **Transesophageal echocardiography (TEE) transducer**: This transducer is designed for insertion into the esophagus to image the heart. It produces high-quality images and is commonly used for cardiac imaging in critically ill patients (Figs. 1.11 and 1.12).

The transducer should be held as if it were a pen. The operator should grasp the side of the transducer close to the transducer face, with the thumb, index finger, and middle finger. The ring and little fingers on the side of the hand can be used to anchor the patient for added stability. This technique allows the operator to use the small muscles of the hand and wrist, thereby increasing precise control of the transducer and proper anchoring to prevent slipping out of the small acoustic window [41] (Fig. 1.13).

Proper maintenance and care of the transducer are essential to protect the sensitive piezoelectric crystal elements. Clean the transducer after each use with a mild detergent or disinfectant solution. Handle the transducer carefully to avoid dropping or colliding with a hard surface. Do not drive over the cable with the machine's wheels as this may damage the cable and affect image quality. Hook or wind the cable to the ultrasound machine properly, being careful not to overtwist the probe cable too tightly.

Fig. 1.11 Most common ultrasound transducers with different frequencies

1.3.2 Ultrasound Image Optimization

The utility of point-of-care ultrasound in critical care and emergency setting has grown significantly over the past few decades and continues to evolve as technology advances. Despite the increased complexity and capabilities of point-of-care devices over time, the basic principles of

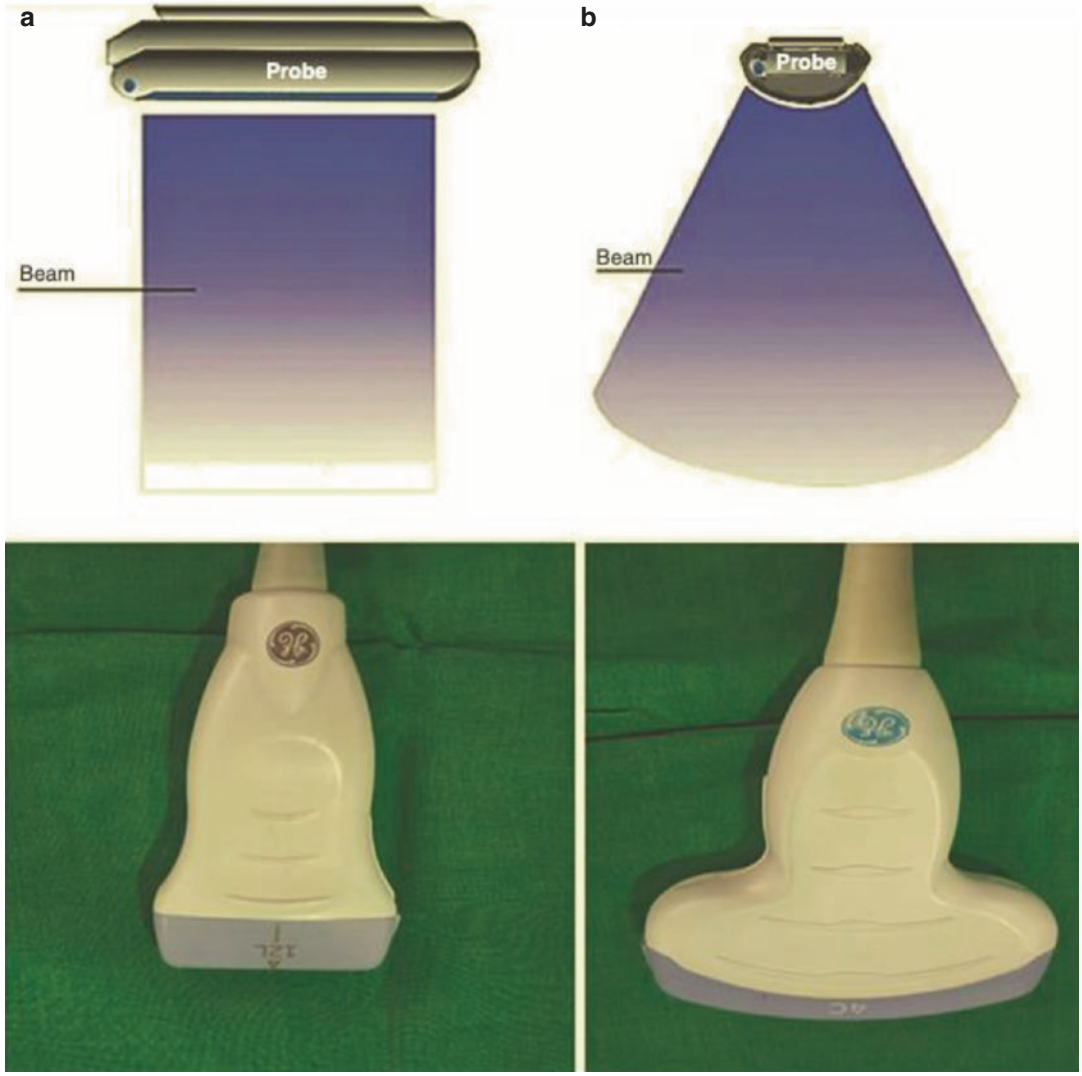

Fig. 1.12 Linear (**a**) and curvilinear (**b**) transducers with their ultrasound beam pattern. Chakraborty, A., & Ashokka, B. (Eds.). (2022). A Practical Guide to Point of Care Ultrasound (POCUS). ISBN 978-981-16-7686-4

ultrasound knobology remain the same. To achieve an optimal ultrasound image, the following scanning steps should be kept in mind [35, 42, 43]:

1. Select the right transducer frequency.
2. Select the right application preset.
3. Adjust the depth to center the area of interest.
4. Optimize the overall gain for the best image contrast.
5. Adjust the time-gain compensation (TGC) to achieve the best image resolution at the depth of the area of interest.
6. Adjust the focus or focal zone to the same level or slightly below the area of interest.
7. Decrease the sector width to allow appropriate interrogation of the image.
8. Application of zoom and freeze/cine.

Frequency of transducer: Once the ultrasound machine is switched on, the right ultrasound transducer with optimal frequency range is selected. The transducer selection is often based on the region of the body being examined, structural representation, depth penetration, and field of view [7]. The high frequency transducer is

Fig. 1.13 Tripod grip. Díaz-Gómez, J. L., Nikravan, S., & Conlon, T. (Eds.). (2020). Comprehensive Critical Care Ultrasound Second Edition. Society of Critical Care Medicine

used to visualize superficial structures providing higher image resolution. Conversely, using a low frequency transducer will result in lower image resolution, therefore it is used to scan deep structures.

Application preset: The next step is to select the correct application preset for a certain examination type. This gives an ultrasound operator a great starting point for scanning and further fine-tuning the image with other knobs and controls. The modern ultrasound machine has a wide range of application presets which include abdomen, cardiac, lung, obstetrics and gynecology, vascular, and other small-part examination such as musculoskeletal imaging. Selecting the right application preset will automatically adjust the basic settings for the selected exam including transducer frequency, overall gain, depth, dynamic range, and other related settings.

The gel is generously applied to the area to be scanned to avoid air pockets between the transducer and the skin. This permits all crystals to transmit and receive sound waves and consequently an adequate image acquisition. The probe is placed on the patient according to external landmarks and ultrasound orientations. If you see a suboptimal image, use a tripod grip to stabilize the transducer and a small and slow transducer manipulation in other planes may improve the image visualization. The structure of interest is typically scanned in at least two orthogonal planes to understand the structure of interest in detail [43].

Depth: When visualizing an optimal ultrasound image, the image depth should be adjusted to perfectly center the area of interest. Sufficient depth is necessary to center the area of interest and wasted depth can be avoided as this will reduce the temporal resolutions. The optimal depth should be at least a few centimeters deeper than the depth of the target image to ensure that other anatomical structures in the vicinity of the target image are also visualized (Fig. 1.14). This is important to avoid missing pathologies beyond the field view. Excessive depth setting reveals a small ultrasound image and fewer details of the structures can be appreciated and vice versa (Fig. 1.15).

Gain: The gain knob allows the operator to adjust the image brightness. An optimal gain can be adjusted manually by two function knobs using the overall gain and a time-gain compensation (TGC). Optimal gain adjustment results in obtaining the best possible contrast between tis-

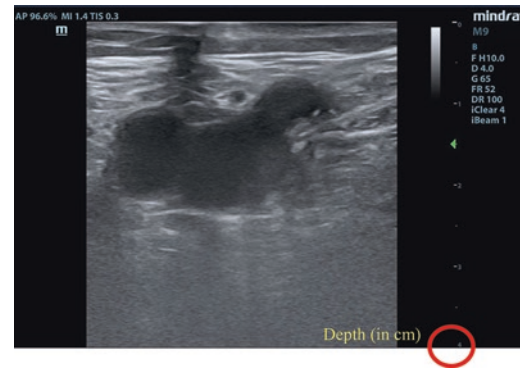

Fig. 1.14 Optimal depth settings center the area of interest, and the target image occupies about two-thirds of the field view

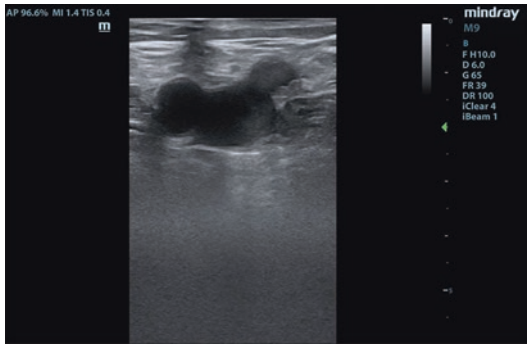

Fig. 1.15 Excessive depth setting produces a small ultrasound image, occupying only less than half of the field view

Fig. 1.17 Optimal gain settings allow better resolution of the ultrasound image

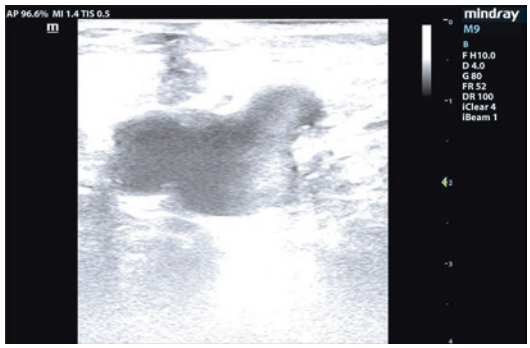

Fig. 1.16 Excessive gain setting produces brighter structures and causes blurring of tissue boundaries

Fig. 1.18 Overall gain and time gain compensation (TGC) knobs on a standard ultrasound machine

sues of varying acoustic impedance, neither too bright nor too dark (Figs. 1.16 and 1.17). In addition, the optimal overall gain works well with the TGC knob to achieve the best image possible. It is typically controlled by a series of slider knobs, with each slider knob controlling the gain for a specific depth on the screen (Fig. 1.18).

Focus: After depth and gain settings are optimized, focus can be adjusted to fine-tune the ultrasound image (Fig. 1.19). In clinical practice, focus or focal zone is adjusted at the same level or slightly below the target image. On the ultrasound machines, the focus knob is indicated by a small arrow on the depth markings. The image resolution frequently decreases dramatically deep to the focal zone, where beyond the focus point, the image quality begins to degrade.

Sector width: The choice of sector width is always a compromise between the field of view on the one hand and frame rate and image resolution on the other. The sector width should be as narrow as possible to increase the frame rate and temporal resolution.

Zoom: The zoom function magnifies specific structures to create a larger image on the screen.

The image is magnified within the region of interest (box). This is the most useful knob when the operator wants to visualize the deeper structures. It is important to note that the zoom function only magnifies the structures, but the resolution remains the same.

Freeze, save, and cine loop: These control knobs are essential for capturing and storing still images and video clips from the ultrasound examination. The cine loop function allows the operator to scroll through the captured frames to locate the best possible representative image. This is useful when making measurements.

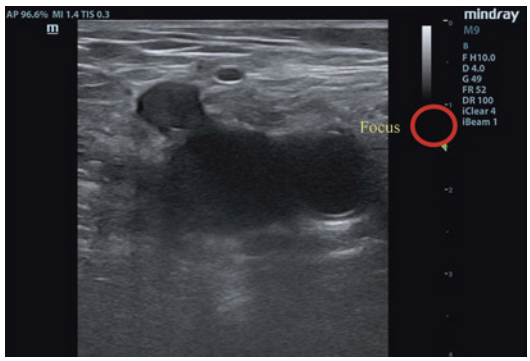

Fig. 1.19 Optimal focus setting on the area of interest indicated by the arrow on the depth markings

1.3.3 Artifacts

1.3.3.1 Acoustic Shadowing Artifact

The acoustic shadowing artifact occurs when the sound beam is attenuated by a strong reflector (e.g., stone, bone), and it reflects the entire sound beam to the transducer. This results in a hyperechoic structure with an anechoic shadow distal to the strong reflector structure. Stones and bones create clean shadows, whereas air creates dirty shadows.

This artifact helps diagnose gallbladder and kidney stones; however, it hinders the visualization of deeper organs.

Examples: Gallbladder stone, ribs, vertebrae body, foreign body, air (Fig. 1.20)

1.3.3.2 Edge Artifact

This type of ultrasound artifact occurs when a sound wave is refracted at the curved fluid-filled structure and does not return to the transducer. Thus, the missing sound wave is registered as an anechoic stripe which can obscure the underlying structures and interfere with interpretation. This artifact can be easily misinterpreted as acoustic shadowing. To differentiate between the two artifacts, the ultrasound transducer should be posi-

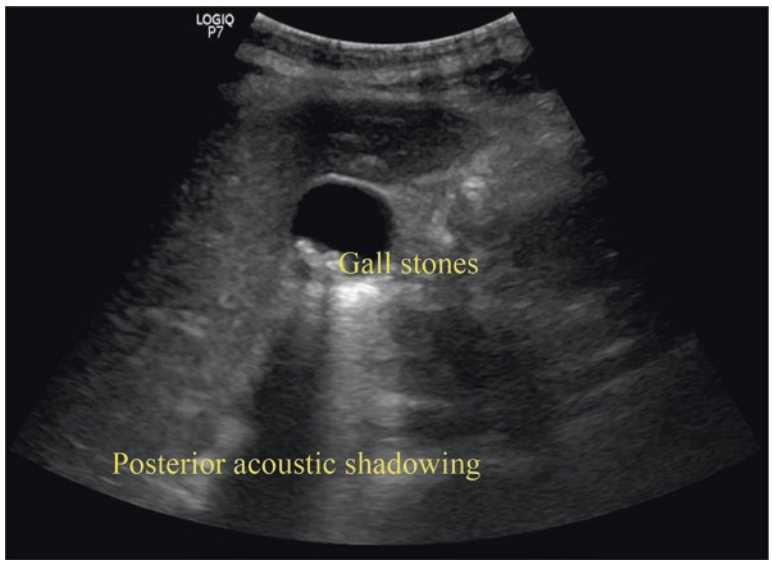

Fig. 1.20 Posterior acoustic shadowing artifact

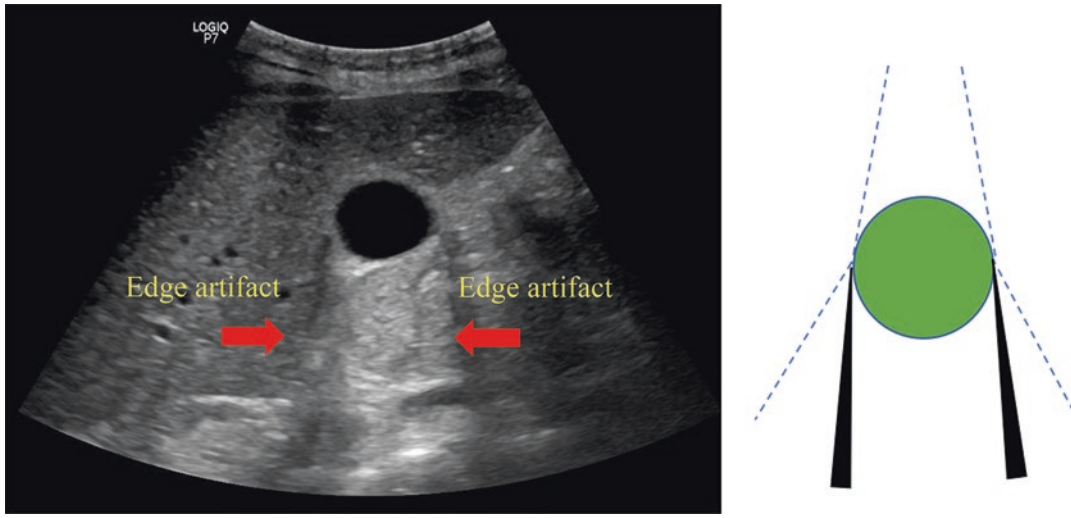

Fig. 1.21 Edge artifact

tioned and angled carefully to optimize the angle of insonation at the tissue boundary.

Examples: Gallbladder, fluid-filled cyst, bladder, eye, large vessels

Clinical Importance: Do not mistake this as gallstone's posterior acoustic shadowing.

Sonographic Pearls: By changing the angle of insonation, edge artifacts can be differentiated from acoustic shadowing because of stones (Fig. 1.21).

1.3.3.3 Side Lobe Artifact

It is formed by multiple low-amplitude sound waves that project radially from the main beam axis at the probe footprint. Strong reflectors along the path of these off-axis beams can produce echoes that are detectable by the transducer, translating these structures as if they originated from the main beam.

Examples: Aortic flap, sludge in gallbladder (Fig. 1.22)

1.3.3.4 Reverberation Artifact

If two parallel highly reflective mediums with different densities are present, the ultrasound waves will be reflected and bounce back and forth from the same structure. An ultrasound machine displays these reflections as bright, parallel lines at uniform intervals deeper to the reflective structures.

Examples: A-lines in the lung ultrasound of the pleural surface. This reverberation artifact is created by multiple reflections between the pleural surface and the skin-transducer interface.

Clinical Importance: A-lines are seen in lungs filled with air, which hinders the visualization of deeper structures (Fig. 1.23).

1.3.3.5 Mirror Image Artifact

This artifact occurs in the presence of highly reflective structure along the path of the ultrasound beam. The sound wave is reflected off at a different angle before returning to the transducer. This creates image duplication of the true structure but normally weaker and deeper than the true structure.

Example: A reflection of the liver above the diaphragm (reflective structure) may be misinterpreted as consolidation of the lung. This can be particularly problematic in the case of imaging metallic or gas-containing objects, such as prosthetic heart valves or bowel gas.

Sonographic Pearls: Change the angle of insonation or slide the transducer cephalad to directly visualize the lower lobe of the lung, to differentiate the mirror image of the liver or spleen from lung consolidation (Fig. 1.24).

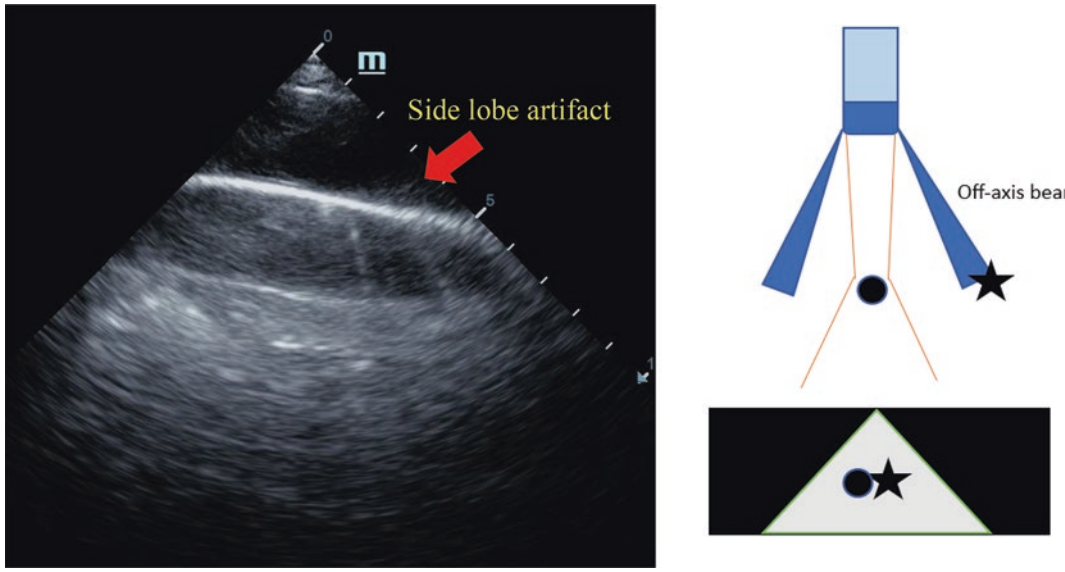

Fig. 1.22 Side lobe artifact

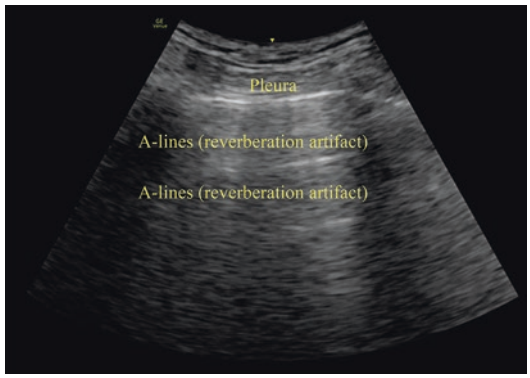

Fig. 1.23 Reverberation artifact

1.3.3.6 Acoustic Enhancement Artifact

This artifact is often seen posterior to the fluid-filled structures such as the urinary bladder and the gallbladder. It occurs when an ultrasound wave is transmitted through a structure with low acoustic impedance and excess energy reflects from the tissues deeper into the fluid-filled structure. This creates a brighter area or increased enhancement behind the attenuating structure.

This artifact can be minimized by reducing the far-field gain to decrease the brightness of the deeper structure for better visualization.

Examples: Urinary bladder, gallbladder (Fig. 1.25)

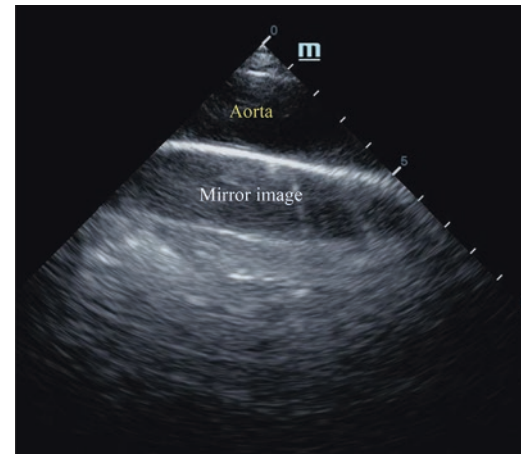

Fig. 1.24 Transesophageal echocardiography of the aorta with mirror image artifact

1.3.4 Ergonomics in Point-of-Care Ultrasound

1.3.4.1 Ergonomics Definition

Work is where ergonomics got its start; the Greek term ergon means "work". Workplace ergonomics is the study and practice of improving productivity and worker safety via the optimal layout of facilities, tools, and personnel. [44]

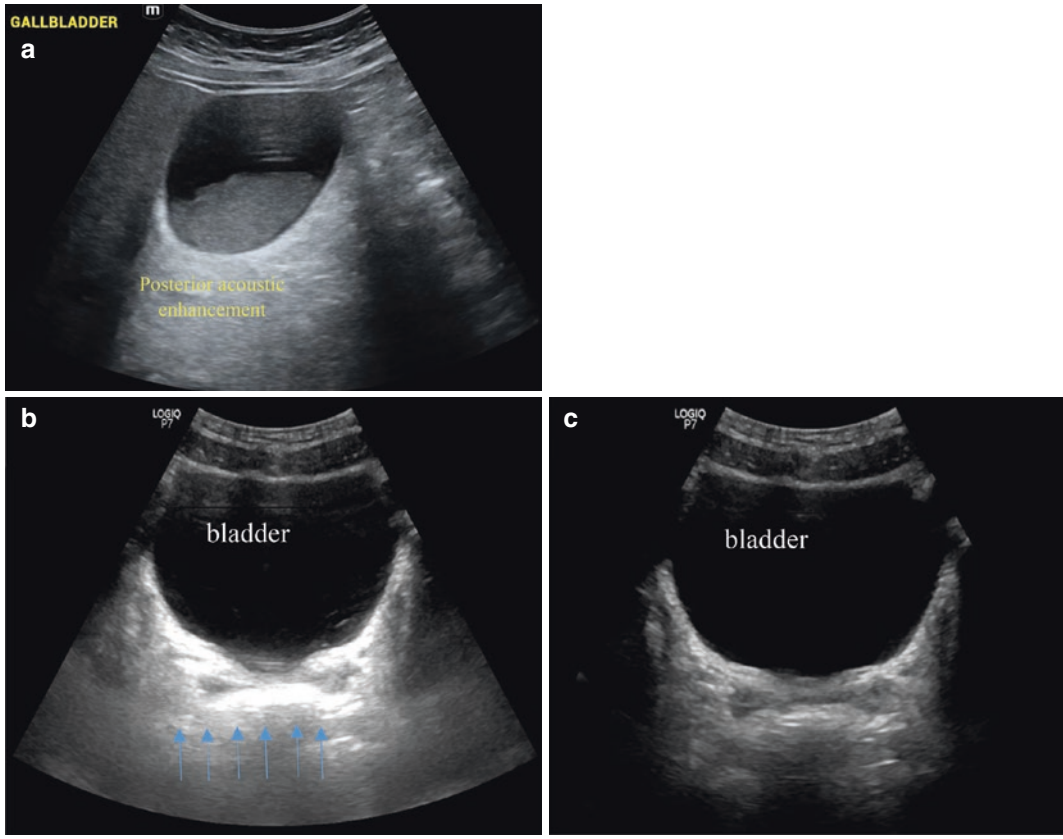

Fig. 1.25 Acoustic enhancement artifact (**a**), posterior acoustic enhancement (blue arrows) (**b**), adjustment of gain to reduce amplitude at the far field of the image to improve visualization (**c**)

Work-related musculoskeletal disorders (WRMSD) may develop from poor ultrasound ergonomics. We use the words "musculoskeletal strain injuries" and "work-related musculoskeletal disorders" to describe ailments that arise from or are made worse by one's job. Many people, including physicians and ultrasound technicians, suffer from these agonizing illnesses, which affect the muscles, nerves, ligaments, and tendons [45].

WRMSDs, on the other hand, develop gradually over time owing to recurring exposure to several risk factors; they may be uncomfortable at work; and they are among the most often reported reasons of limited or missed work time [45].

1.3.4.2 Ergonomics to Reduce WRMSD

Echocardiography and other point-of-care ultrasound (POCUS) modalities require the following ergonomic positions:

The monitor should be placed at hand level in front of the operator to facilitate look-down gazing and the alignment of the visual axes [46, 47]. The monitor's tilt angle should also be less than 20° [46]. Placing the monitor at eye level and precisely in front of the operator so that he or she can observe it with 15°–20° of neck flexion (ideally, articulating and vertically adjustable monitors) [46, 47]. These are the most important adjustments to make prior to scanning [45–47] (Fig. 1.26a, b).

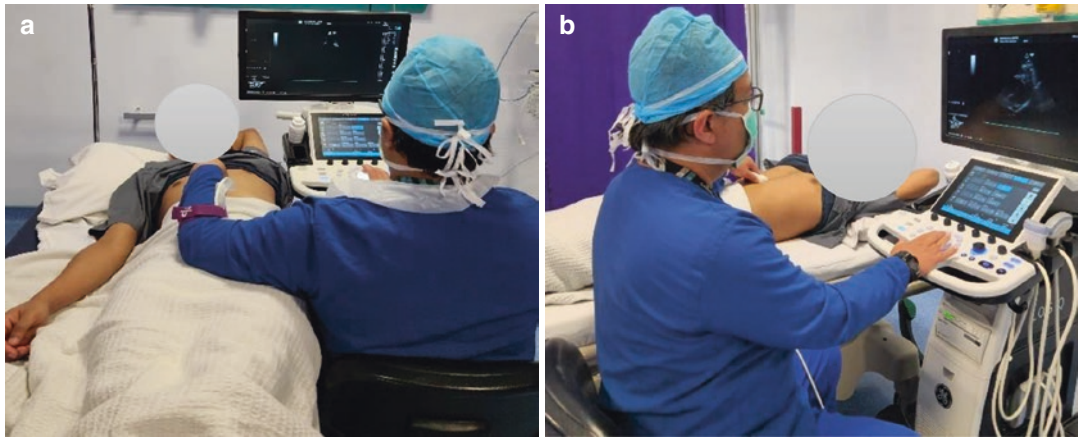

Fig. 1.26 (**a**) At the level of the hands, vertically adjustable articulating monitors permit look-down viewing and alignment of the visual axis. (**b**) The ultrasound monitor is situated directly in front so that the operator can see it with a modest 15°–20° neck flexion

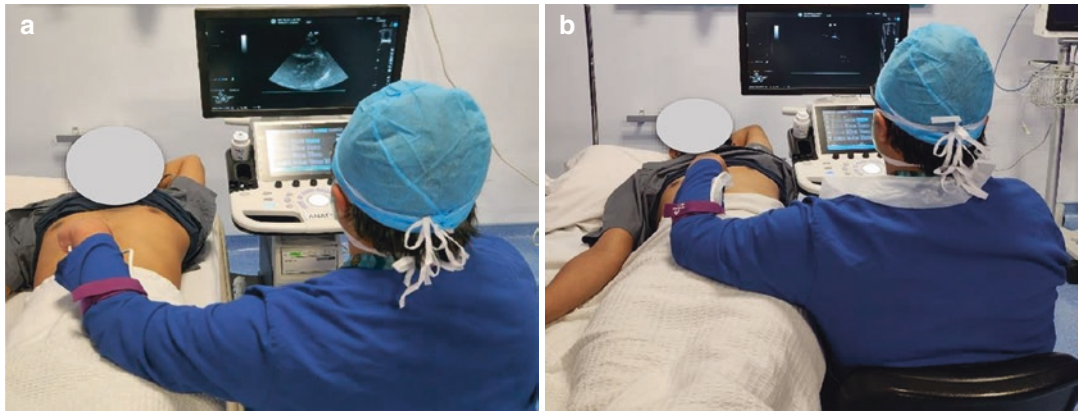

Fig. 1.27 (**a**) Wrong position: The patient bit far away from the operator, and the arm is abducted >30°. (**b**) Correct position: The patient is moved closer to the operator, and the arm is abducted <30°

Equilibrium in either a seated or standing position, with the operator's center of gravity at the middle of their body [46–48]. The next stage is to bring the patient into closer proximity to the doctor or operator [47, 48] (Fig. 1.27a, b).

Next necessary steps are to avoid the following non-neutral postures: sustained reach; trunk bending and twisting; excessive neck flexion, extension, protraction, and rotation; irregular weight distribution while sitting down or standing up; bending of the wrist or extension; and deviation pinching grasp. [46–49] Ultrasound operators should keep away also from incorrect postures: Arm abduction, that is defined as a torso-upper extremity angle greater than 30°, and overextending necessitate the operator to utilize muscles of the shoulder [46–49]. Any procedure tray should be set on the operator's dominant hand or the non-scanning hand side. This is done to prevent reaching across and beyond [48, 49].

These non-neutral or incorrect postures can lead to tendonitis, tenosynovitis, or bursitis that may result when a muscle is unable to satisfy the demands of a particular endeavor. Shoulder injury sometimes occurs due to the combination of repeated abduction of the transducer that exerts pressure on the scanning arm, which stimulates the muscles statically. This results in

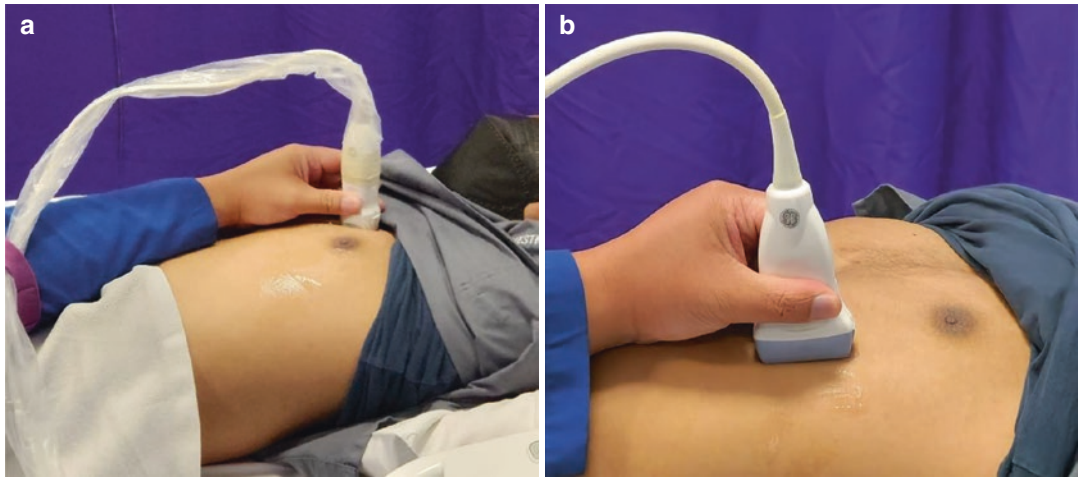

Fig. 1.28 (**a**) Incorrect: Pincer grip for phased array probe. (**b**) Incorrect: Pincer grip for linear probe

impingement of the rotator cuff against the bony parts of the girdle of the shoulder, decreased flow of blood to the muscles and tendons, and microtrauma to the muscle fibers [50–52].

Adopt a neutral forearm position while supporting the ultrasound instrument on the individual's body or using the patient's skin layer as support to properly hold the ultrasound probe. Palmar hold is more stable and less tiring [46–49] (Fig. 1.28a, b).

A neutral wrist position should be maintained for scanning and non-scanning hands [46–49]. Arm abduction is kept at less than 30° [47–49]. Overreaching of the control panel should be avoided. [46–49] Reduce grip force and transducer pressure. Avoid misunderstanding; excessive pressure on the probe improves the quality of the image. Image optimization, such as frequency and harmonics, is more practical. [49] Use a tourniquet or adjustable strap to properly fasten the ultrasound probe cable to the operator's hand to avoid dangling cable [46, 47].

Keeping a neutral forearm position for both the scanning and non-scanning hands are another important aspect [46, 47]. Try to avoid excessive use of the control interface on the ultrasound machine by straining the joints and muscles [47–49]. One of the pertinent steps in using the power of the scanning hand is to reduce grasp force and pressure on the transducer. There is a lot of misconception and misunderstanding that intense pressure on the probe improves image quality. It is more advisable and practicable to optimize an image using frequency and harmonics [47]. Add on the use of a tourniquet or an adjustable harness to secure the ultrasound probe cable to the operator's hand for the purpose of preventing cable dangling is another simple tip for optimizing ergonomics [46, 47] (Fig. 1.29).

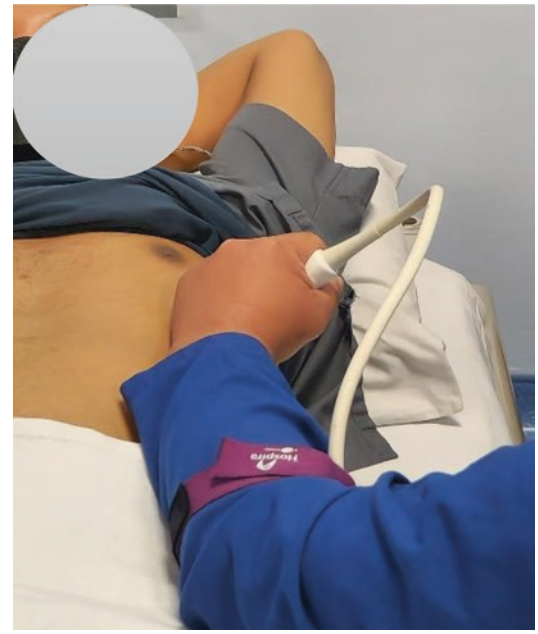

Fig. 1.29 The use of a strap to secure the probe cable with the forearm improves ergonomics

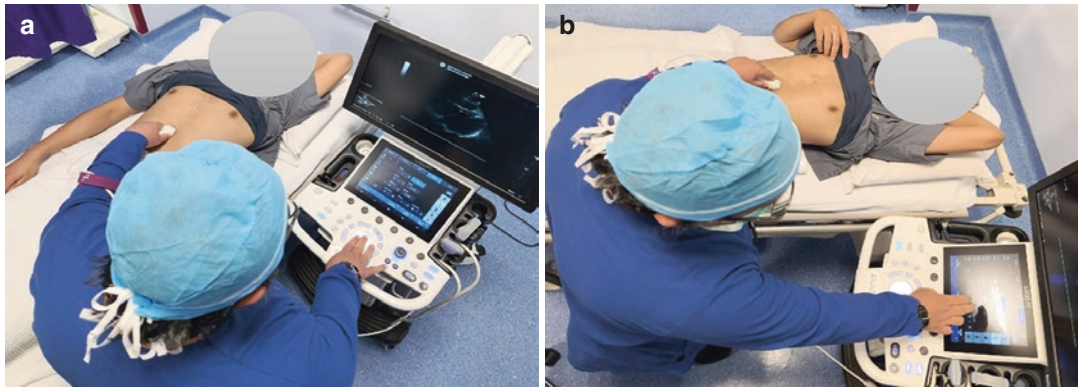

Fig. 1.30 (**a**) Stand up to scan subcostals and other bits from far away view (avoiding overstretching). (**b**) Keep the body in straight alignment—no bending/twisting of the back or neck. Stand with weight evenly distributed

Other useful important aspects for sonographers in practice are to take the time to plan (especially in confined spaces) the placement of the ultrasound machine and visualize the most ergonomic position for the operator's body and handedness when performing the scan [46–48]. Having an ergonomic chair that has adjustable height and capable of supporting both limbs, patient on a bed or trolley that is adjustable (especially for height) are part of ergonomic workstations. The operator can utilize a support pad, such as a towel, sheet, or block cushion to properly position the patient, for example, for slight left lateral position [49]. Given the variety of body types and sizes, sometimes positioning cushions precisely can be difficult and extra hands for assistance should be nearby [49] (Fig. 1.30a, b).

The operator can choose to sit or stand, but the weight of the body should be evenly distributed on both feet. For some scanning, for example, of subcostal view, the operator should stand up. By standing up, arching or twisting the back or neck must be avoided. Our main priority is to scan the patient from the adjacent side and not from the opposite side [52–54].

After capturing an image, relax your hand periodically by relieving pressure on the probe's handle [53, 54]. If feasible, take micro-breaks and execute dynamic muscle movements during the scan [53, 54]. Dynamic movements such as performing wrist and forearms, neck, shoulders, and upper back stretching for about 15 s each greatly helps in preventing WRMDS [55].

The physiotherapist should be available to provide brief exercise courses with stretching and strengthening modules for the physicians and operators [53–55]. Risk management, stretching, and strengthening exercises are the future for all physicians and sonographers [53–55].

References

1. Kaproth-Joslin KA, Nicola R, Dogra VS. The history of US: from bats and boats to the bedside and beyond: RSNA centennial article. RadioGraphics. 2015;35(3):960–70.
2. Dietrich CF, Bolondi L, Duck F, Evans DH, Ewertsen C, Fraser AG, et al. History of ultrasound in medicine from its birth to date (2022), on occasion of the 50 Years Anniversary of EFSUMB. A publication of the European Federation of Societies for Ultrasound in Medicine and Biology (EFSUMB), designed to record the historical development of medical ultrasound. Med Ultrasonogr. 2022;24(4):434.
3. Edler I, Hertz CH. The use of ultrasonic reflectoscope for the continuous recording of the movements of heart walls. Clin Physiol Funct Imaging. 2004;24(3):118–36.
4. Coman IM, Popescu BA. Shigeo Satomura: 60 years of Doppler ultrasound in medicine. Cardiovasc Ultrasound. 2015;13(1)
5. Campbell S. A short history of sonography in obstetrics and gynaecology. Facts, Views Vision in ObGyn [Internet]. 2013;5(3):213–29. https://www.ncbi.nlm.nih.gov/pmc/articles/PMC3987368/
6. Lichtenstein D, Axler O. Intensive use of general ultrasound in the intensive care unit. Intensive Care Med. 1993;19(6):353–5.
7. Lichtenstein D. Lung ultrasound in the critically ill. Curr Opin Crit Care. 2014;20(3):315–22.

8. Singh S, Goyal A. The origin of echocardiography: a tribute to Inge Edler. Texas Heart Inst J. 2007;34(4):431–8.
9. Frazin L, Talano JV, Stephanides L, Loeb HS, Kopel L, Gunnar RM. Esophageal echocardiography. Circulation. 1976;54(1):102–8.
10. DiMagno EP, Buxton JL, Regan PT, Hattery RR, Wilson DA, Suarez JR, et al. Ultrasonic endoscope. Lancet (London, England). 1980;1(8169):629–31.
11. Goldberg BB, Goodman GR, Clearfield HR. Evaluation of ascites by ultrasound. Radiology. 1970;96(1):15–22.
12. Kristensen JK, Buemann B, Kühl E. Ultrasonic scanning in the diagnosis of splenic haematomas. Acta Chir Scand. 1971;137(7):653–7.
13. Michael Asher W, Parvin S, Virgilio RW, Haber K. Echographic evaluation of splenic injury after blunt trauma. Radiology. 1976;118(2):411–5.
14. Tso P, Rodriguez A, Cooper C, Militello P, Mirvis S, Badellino MM, Boulanger BR, Foss FA Jr, Hinson DM, Mighty HE, Nasrallah DV, Raimonde AJ, Yates WD, Yuschak JV. Sonography in blunt abdominal trauma: a preliminary progress report. J Trauma 33(1):p 39–44, July 1992.
15. Scalea TM, Rodriguez A, Chiu WC, Brenneman FD, Fallon WF Jr, Kato K, McKenney MG, Nerlich ML, Ochsner MG, Yoshii H. Focused assessment with sonography for trauma (FAST): results from an international consensus conference. J Trauma. 1999 Mar;46(3):466–72.
16. Ullman JI, Stoelting RK. Internal jugular vein location with the ultrasound Doppler blood flow detector. Anesth Analg. 1978;57(1):118.
17. Yonei A, Nonoue T, Sari A. Real-time ultrasonic guidance for percutaneous puncture of the internal jugular vein. Anesthesiology. 1986;64(6):830–1.
18. Lamperti M, Bodenham AR, Pittiruti M, Blaivas M, Augoustides JG, Elbarbary M, et al. International evidence-based recommendations on ultrasound-guided vascular access. Intensive Care Med. 2012;38(7):1105–17.
19. Practice Guidelines for Central Venous Access 2020. Anesthesiology. 2020;132(1):8–43.
20. Guidance | Guidance on the use of ultrasound locating devices for placing central venous catheters | Guidance | NICE [Internet]. Nice.org.uk. NICE; 2002. https://www.nice.org.uk/guidance/ta49/chapter/1-guidance
21. Bodenham Chair A, Babu S, Bennett J, Binks R, Fee P, Fox B, et al. Association of anaesthetists of Great Britain and Ireland: safe vascular access 2016. Anaesthesia [Internet]. 2016;71(5):573–85. https://www.ncbi.nlm.nih.gov/pmc/articles/PMC5067617/
22. Ting PL, Sivagnanaratnam V. Ultrasonographic study of the spread of local anaesthetic during axillary brachial plexus block. Br J Anaesth. 1989;63(3):326–9.
23. Kapral S, Krafft P, Eibenberger K, Fitzgerald R, Gosch M, Weinstabl C. Ultrasound-guided supraclavicular approach for regional anesthesia of the brachial plexus. Anesth Analg [Internet]. 1994;78(3):507–13. [cited 2022 Mar 31] https://pubmed.ncbi.nlm.nih.gov/8109769/
24. Neal JM, Brull R, Horn JL, Liu SS, McCartney CJL, Perlas A, et al. The second american society of regional anesthesia and pain medicine evidence-based medicine assessment of ultrasound-guided regional anesthesia. Reg Anesth Pain Med. 2016;41(2):181–94.
25. Narouze SN, Provenzano D, Peng P, Eichenberger U, Lee SC, Nicholls B, et al. The American Society of Regional Anesthesia and Pain Medicine, the European Society of Regional Anaesthesia and Pain Therapy, and the Asian Australasian Federation of Pain Societies Joint Committee Recommendations for Education and Training in Ultrasound-Guided Interventional Pain Procedures. Reg Anesth Pain Med. 2012;37(6):657–64.
26. Turbitt LR, Mariano ER, El-Boghdadly K. Future directions in regional anaesthesia: not just for the cognoscenti. Anaesthesia. 2019;75(3):293–7.
27. Moore CL, Copel JA. Point-of-care ultrasonography. N Engl J Med. 2011;364(8):749–57.
28. Díaz-Gómez JL, Mayo PH, Koenig SJ. Point-of-Care Ultrasonography. Ingelfinger JR, editor. N Engl J Med. 2021;385(17):1593–602.
29. Sonko ML, Arnold C. Machine learning in point of care ultrasound. POCUS J. 2022;07:78; Kidney.
30. Shokoohi H, LeSaux MA, Roohani YH, Liteplo A, Huang C, Blaivas M. Enhanced point-of-care ultrasound applications by integrating automated feature-learning systems using deep learning. J Ultrasound Med. 2018;38(7):1887–97.
31. Recker F, Höhne E, Damjanovic D, Schäfer VS. Ultrasound in telemedicine: a brief overview. Appl Sci. 2022;12(3):958.
32. Shriki J. Ultrasound physics. Crit Care Clin. 2014;30(1):1–24. https://doi.org/10.1016/j.ccc.2013.08.004.
33. Meng Y, Chen G, Huang M. Piezoelectric materials: properties, advancements, and design strategies for high-temperature applications. Nanomaterials. 2022;12(7) https://doi.org/10.3390/nano12071171.
34. Lawrence JP. Physics and instrumentation of ultrasound. Crit Care Med. 2007;35(8 Suppl) https://doi.org/10.1097/01.CCM.0000270241.33075.60.
35. Enriquez JL, Wu TS. An introduction to ultrasound equipment and knobology. Crit Care Clin. 2014;30(1):25–45. https://doi.org/10.1016/j.ccc.2013.08.006.
36. Lopez-Haro SA, Vera A, Leija L. Evaluation of an ultrasonic propagation speed measurement system in the temperature range from 20°C to 45°C. In: Pan American Health Care Exchanges, PAHCE 2010; 2010, pp. 85–89. doi: https://doi.org/10.1109/PAHCE.2010.5474594
37. Docker MM, Duck FA, British Institute of Radiology (1958), British Medical Ultrasound Society. The safe use of diagnostic ultrasound. British Institute of Radiology; 1991

38. Ho CY, Solomon SD. A clinician's guide to tissue doppler imaging. Circulation. 2006;113(10) https://doi.org/10.1161/CIRCULATIONAHA.105.579268.
39. Chakraborty A, Ashokka B, editors. A practical guide to point of care ultrasound (POCUS); 2022. ISBN: 978-981-16-7686-4.
40. Brown SM, Blaivas M, Hirshberg EL, Kasal J, Pustavoitau A, editors. Comprehensive critical care ultrasound. Society of Critical Care Medicine; 2015. ISBN: 9781620750322.
41. Díaz-Gómez JL, Nikravan S, Conlon T, editors. Comprehensive Critical Care Ultrasound. 2nd ed. Society of Critical Care Medicine; 2020.
42. Zander D, Hüske S, Hoffmann B, Cui XW, Dong Y, Lim A, Jenssen C, Löwe A, Koch JBH, Dietrich CF. Ultrasound image optimization ("Knobology"): B-mode. Ultrasound Int Open. 2020;6(1):E14–24.
43. Amo Wiafe Y, Badu-Peprah A. The influence of ultrasound equipment knobology in abdominal sonography [Internet]. Essentials of Abdominal Ultrasound. Intech Open; 2019. doi: https://doi.org/10.5772/intechopen.83713.
44. What Is Ergonomics (HFE)? | The International Ergonomics Association is a global federation of human factors/ergonomics societies, registered as a non-profit organization in Geneva, Switzerland. What Is Ergonomics (HFE)? | The International Ergonomics Association Is a Global Federation of Human Factors/Ergonomics Societies, Registered as a Nonprofit Organization in Geneva, Switzerland n.d. https://iea.cc/what-is-ergonomics/. Accessed 1 May 2023.
45. Ergonomics—Overview | Occupational Safety and Health Administration. Ergonomics—Overview | Occupational Safety and Health Administration; n.d. https://www.osha.gov/SLTC/ergonomics/. Accessed 30 April 2023.
46. Baker JP, Coffin CT. The importance of an ergonomic workstation to practicing sonographers. J Ultrasound Med. 2013;32:1363–75. https://doi.org/10.7863/ultra.32.8.1363.
47. Coffin C. Work-related musculoskeletal disorders in sonographers: a review of causes and types of injury and best practices for reducing injury risk. Rep Med Imaging. 2014:15. https://doi.org/10.2147/rmi.s34724.
48. Murphy C. Brief ergonomic review cardiac ultrasound [Internet]. 2012 [cited 2023 Apr 28]. https://www.hsabc.org/sites/default/files/uploads/ohs%20sono%20Cardiac_ultrasonographers__Debrief_June_14_amended_2012.pdf
49. Deb S, Venkateshvaran A. Essential ergonomics to minimise work-related musculoskeletal disorders in echocardiography. J Indian Acad Echocardiogr Cardiovasc Imaging. 2018;2:49–52.
50. Evans K, Roll S, Baker J. Work-related musculoskeletal disorders (WRMSD) among registered diagnostic medical sonographers and Vascular Technologists. J Diagn Med Sonogr. 2009;25(6):287–99.
51. Murphey S. Work-related musculoskeletal disorders in Sonography. J Diagn Med Sonogr. 2017;33(5):354–69.
52. Sommerich CM, Lavender SA, Evans K, Sanders E, Joines S, Lamar S, et al. Collaborating with cardiac sonographers to develop work-related musculoskeletal disorder interventions. Ergonomics. 2016;59(9):1193–204.
53. Work-related Musculoskeletal Disorders (WMSDs). CCOHS: Work-Related Musculoskeletal Disorders (WMSDs) 2023. https://www.ccohs.ca/oshanswers/diseases/rmirsi.html. Accessed 30 April 2023.
54. Village J, Trask C. Ergonomic analysis of postural and muscular loads to diagnostic sonographers. Int J Industr Ergon. 2007;37:781–9. https://doi.org/10.1016/j.ergon.2007.06.005.
55. Cursaro M, Rich J, Alvaro V, Bradley J, Shirazi M, Edwards S. Ergonomics-taking care of yourself. J Am Soc Echocardiogr [Internet]. 2014;27(3):A36–7. https://doi.org/10.1016/j.echo.2014.01.008.

2 Basic Transthoracic of Echocardiography

Noreddine Bouarroudj and Cherif Bouzid

Echocardiography has become one of the techniques of choice used by physicians in the evaluation of the hemodynamic status of patients, notably in the context of critical care, emergency, and perioperative medicine. This extensive use is the result of multiple factors: nonharmful and repetitive technique, reproducibility in the same and between operators, and short time consumption to get impactful information; furthermore, the recent scientific advances in information technology and data treatment allow the use of the newest modality of imaging and Doppler like 3D (three dimensional), tissue Doppler imaging (TDI), strain, and strain rate. However, the learning curve and ultrasound machine availability are the two factors that limit the overspread of the technique.

The point-of-care ultrasounds (POCUS) is a concept specifically designed to overcome these two limits; by allowing an increasing number of physicians with adapted training, equipped with adapted ultrasound machines. These physicians are aiming to accomplish a bedside-oriented examination in order to provide a specific solution to a diagnostic problem, or to monitor a diagnostic and therapeutic procedures. Cardiac point-of-care ultrasound (CPOCUS) is the application of point of care protocol to the heart; this chapter is mainly focused on the latter with an overlapping view on the advanced critical care echocardiography concept.

2.1 The Motion Mode (M Mode)

The M mode displays the movement relative to the time of all structures along one scan line. The result is a plot of all structures crossed by the cursor M mode over time as shown on Fig. 2.1. The technology of M mode relies on a single crystal which emits and receives simultaneously; it is one-dimensional mode with the best temporal resolution.

Anatomical M mode is the newest version of M mode, in which the M mode cursor can be

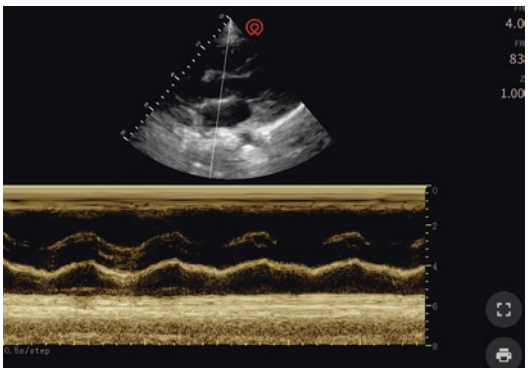

Fig. 2.1 Figure shows the M mode

N. Bouarroudj (✉)
Department of Anesthesiology and Critical Care, Clinique Maissalyne, Constantine, Algeria

C. Bouzid
Department of Anaesthesia and Critical Care, El Afia Hospital, Mila, Algeria

© The Author(s), under exclusive license to Springer Nature Switzerland AG 2024

N. Bouarroudj et al. (eds.), *POCUS in Critical Care, Anesthesia and Emergency Medicine*,
https://doi.org/10.1007/978-3-031-43721-2_2

placed separately from the probe. The result is more accurate assessment, mainly left ventricular regional wall motion.

2.2 The 2D Mode or B Mode or Brightness Mode

The 2D mode is a live display and representation in two-dimensional plan of echoes received by the ultrasound transducer, the latter is counted as the most used mode of imaging in CPOCUS; each echo is represented by gray-scale point in the screen corresponding to one pixel.

A sequential line scan (phased array probe) creates every image or frame. The number of images per second determines the frame rate.

The 2D mode serves as basis for all modalities of echocardiography that allows the practitioner to choose the exact location for the modality to be applied.

Echogenicity is the ability for the structure to generate brightness (reflect echo). It is pinpointing the liver as a landmark; the structure is hypoechoic, or hyperechoic, if it is darker or brighter, respectively, than the liver and anechoic if there is no brightness.

2.3 The Doppler Effect

The Doppler Effect is generated when the ultrasounds emitted from a source (transducer) with a frequency of f_0 is reflected by a target in motion, most often a blood cell or tissue. The ultrasound reflected is received with a new frequency f_1. This variation or shift in frequency is called the Doppler Effect ($f_1 - f_0$). From the Doppler signal collected, the velocity and the direction relative to the probe of the target are determined by using the following equation:

$$\text{Doppler shift}\left(f_1 - f_0\right) = 2 \times f_0 \times V \times \cos\theta / C$$

f_0: ultrasound beam frequency
C: propagation speed of ultrasound in tissues
Cosθ: cosine of angle of insonation
V: blood flow velocity

Based on this equation, the alignment of Doppler beam relative to the flow is crucial; the more is the angle narrowed to a zero degree, the more accurate is the assessment.

2.3.1 Flow Doppler

2.3.1.1 Spectral Doppler

Spectral Doppler is a graphical representation of the Doppler Effect in which velocity is plotted relatively to the time. Every point of the plot is represented by nuance of gray (brightness) proportionally to the intensity of the Doppler signal; Furthermore, from the spectrum plot, the flow type can be identified as laminar or turbulent.

By convention the velocity which moves toward the probe appears above the baseline; otherwise, it appears below the baseline.

The two subtypes of spectral flow Doppler that can be applied in echocardiography are: pulsed and continuous wave Doppler.

Pulsed Wave Doppler (PWD)

The ultrasound waves are emitted by a pulse; between two pulses is silence, during which the transducer waits for the echo's return before sending a new pulse. The number of cycles achieved per second is called period repetition frequency (PRF).

The maximum PRF possible is determined by the depth of the structure (time spent by ultrasound goes forth and back from the transducer to the structure). Once this value of PRF is reached, the aliasing phenomenon occurs. This maximum frequency before aliasing occurs, it is the Nyquist limit; it equals one half of the maximum PRF. The Nyquist limit means that every ultrasound wave has to be sampled at least two times by one wavelength; otherwise, the velocity and the direction will be ambiguous.

In PWD, a unique crystal is used to send and receive ultrasounds. The advantage is to investigate the velocity in a specific area. However, this advantage is limited by the occurrence of aliasing.

High PRF is the newest technology invented to avoid the occurrence of aliasing.

Continuous Wave Doppler (CWD)
The CWD allows to assess the velocities across all lengths of the ultrasound beam; thus, a non-specific area at a specific depth can be investigated individually. CWD uses two piezoelectric crystals for the emission and reception instantly; therefore, aliasing cannot occur. CWD is used to assess high velocities, which the PWD fails to evaluate.

2.3.1.2 Color Flow Doppler (CFD)
The CFD was built using the same principles as the pulsed wave Doppler. The 2D image is divided into small areas, which are separately assessed by using PWD. Each area receives a color corresponding to the mean velocity and flow direction (mapping) and superimposed on the 2D image; by convention, the blue color is used for blood flow going far from the transducer and the red color for blood flowing toward the transducer; when aliasing occurs, a mosaic of color is seen.

2.3.2 Tissue Doppler Imaging (TDI)

This imaging modality uses the ultrasound Doppler to assess tissue velocities (myocardium) instead of blood flow. The Doppler signal with high amplitude and low frequency generated by myocardium in motion can be represented either with pulsed spectral or color Doppler. The tissue Doppler evaluates the systolic and diastolic function of the left and right ventricles; however, it has a limitation to answer the question: does a segment of the myocardium contract, or does the other segment's contraction just attract it? This question is often encountered in the evaluation of regional motion of the myocardium. The response to this question is a new technology known as deformity imaging or speckle tracking (strain and strain rate).

2.4 Three-Dimensional Imaging

The three-dimensional echocardiography (3DE) imaging can be considered as a multimodality three-dimensional acquisition and display of the heart beating structures; it is regarded as a big step forward in the history of cardiac imaging. In the early twentieth century, the technological advances in information technology and transducer miniaturization allowed the creation of a fully sampled matrix-array transducer; it is a matrix arrangement of almost 3000–5000 piezoelectric elements. The reception and treatment of information relays on a massive number of miniaturized electronic circuits and programs. The place of 3DE in CPOCUS is still to be identified because it can be challenging to perform in emergency, when the patient has polypnea or arrhythmia.

2.4.1 Data Acquisition

The two data acquisition methods are real-time or live 3DE imaging and electrocardiographically triggered multiple-beat 3D imaging.

2.4.1.1 Real-Time or Live 3DE Imaging
Real-time or live 3DE imaging is the acquisition and display of multiple pyramidal data sets in one heartbeat; it permits avoidance artifacts caused by patient motion, breath, or arrhythmia; however, it has the disadvantage of low spatial and temporal resolution.

2.4.1.2 Electrocardiographically Triggered Multiple-Beat 3D Imaging
The electrocardiographically triggered multiple-beat 3D imaging is the acquisition of several subvolumes of data over multiple heartbeats, which are joined together to create a full volumetric data set. This mode of acquisition has the advantage of best spatial and temporal resolution, but it is limited by the occurrence of the artifacts caused by patient motion, breath, or arrhythmia (stitch artifact).

2.4.2 Data Acquisition Modes

2.4.2.1 Simultaneous Multi-plane Mode

Simultaneous multi-plane mode is a dual-screen display of two concomitant live images; the first one serves as reference plan of a particular structure, and the second image is a plan rotated from the reference plan (Fig. 2.2).

2.4.2.2 Real-Time 3D Narrow Sector

Real-time 3D narrow sector is a real time display of part of a pyramidal volume which is relatively small to allow the study and display of the cardiac structure of interest; it enables a precise diagnostic due to its superior spatial and temporal resolution.

2.4.2.3 Focused Wide Sector–Zoom

Focused wide sector–zoom allows a wide sector view of the cardiac structures; however, the cost is low temporal and spatial resolution.

2.4.2.4 Full Volume-Gated Acquisition

(Review the electrocardiographically triggered multiple-beat 3D imaging)

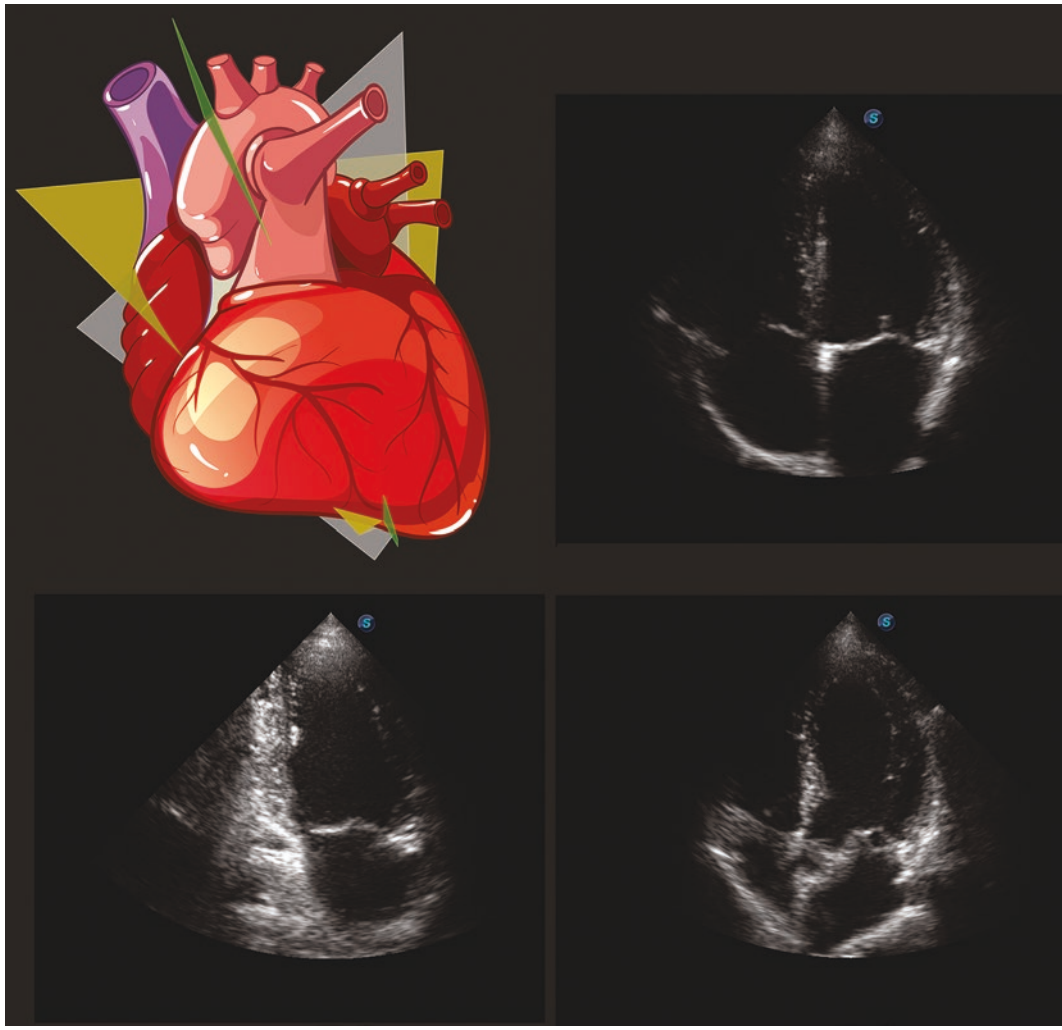

Fig. 2.2 This figure provides an overview of simultaneous multi-plane mode

2.4.2.5 Full Volume with Color Flow Doppler

2.4.3 3DE Display

2.4.3.1 Cropping

Cropping in 3DE is the removal of cardiac structures to gain access to the zone of interest, which is seen in perspective from an angle chosen by the operator; the aim is to get the maximum information about the complex anatomic defects. This process can be accomplished before, during, or after data acquisition.

2.4.3.2 Post-Acquisition Display

The display of 3DE images after acquisition can be performed using one or more of the following processes: volume rendering, surface rendering (Fig. 2.3), wire-frame (Fig. 2.4), or the tomographic slice.

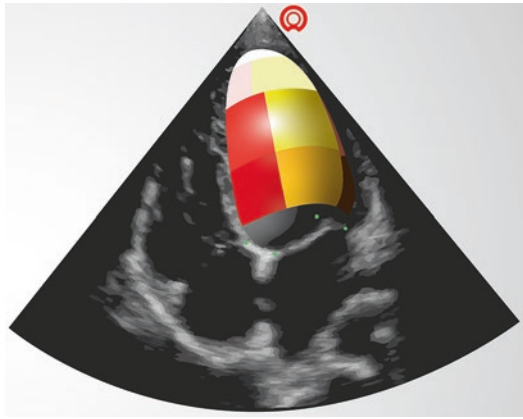

Fig. 2.3 Three-dimensional echocardiography display: surface rendering of the LV

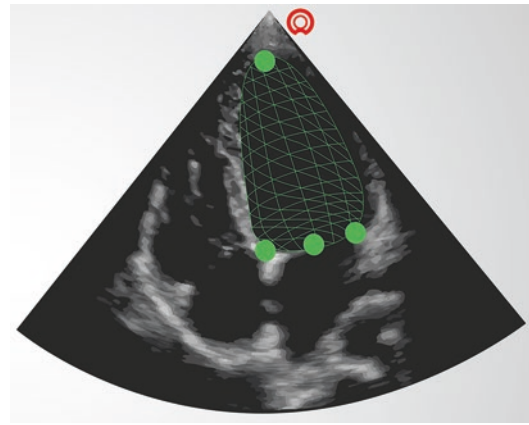

Fig. 2.4 Three-dimensional echocardiography display: wire frame rendering of the LV

3 Preparation, Equipment, and Techniques

Noreddine Bouarroudj and Cherif Bouzid

3.1 Preparation

- Check the battery autonomy.
- Clean the ultrasound machine using appropriate antiseptic and pay particular attention to the parts of the ultrasound machine that are exposed with the patient or care providers.
- In case of contact isolation, use appropriate sleeves and covers.
- Check the amount of gel available for the exam.
- Adjust environment lights. However, keep an eye on the patient and monitoring. Otherwise, a nurse is asked to monitor the patient.
- Ergonomic conditions and position are crucial for the success of the exam or the procedure in order to avoid any accidents or injuries to the patient and care provider.
- Turn on the ultrasound machine, choose the appropriate transducer, enter the data of the patient and select the type of exam.
- Most of the time the patient is laying on his back. However, this position may be inconvenient for images acquisition in apical and parasternal windows; nevertheless, sometimes changing the patient position is challenging or dangerous.

3.2 Equipment and Techniques

The phased-array transducer (Fig. 3.1) is mainly used for echocardiography applications in CPOCUS. Nevertheless, in some situations when the latter is not available, a curved transducer can be used, mainly in the sub-costal view.

For novices, the first use of ultrasound machine may cause discomfort. This chapter briefly exposes the basic settings and knobs of routine use (Fig. 3.2).

3.2.1 2D Mode

- Depth: Adjust the depth to get a whole heart echogram in the center of the screen. Moreover, the most compact portable ultrasound machine has the focal zone non-adjustable preset by constructor in the middle of the screen. Setting the depth is crucial for lateral resolution.
- Gain: The gain is used to compensate the attenuation of ultrasounds beam. The two

N. Bouarroudj (✉)
Department of Anesthesiology and Critical Care, Clinique Maissalyne, Constantine, Algeria
e-mail: bouarroudj@bouarroudj.net

C. Bouzid
Department of Anaesthesia and Critical Care, El Afia Hospital, Mila, Algeria

© The Author(s), under exclusive license to Springer Nature Switzerland AG 2024

N. Bouarroudj et al. (eds.), *POCUS in Critical Care, Anesthesia and Emergency Medicine*,
https://doi.org/10.1007/978-3-031-43721-2_3

Fig. 3.1 This figure represents the classical phased-array transducer used routinely in echocardiography

Fig. 3.2 This figure shows an example of the control panel of an ultrasound machine with the buttons 2D mode and doppler imaging CW Doppler PW Doppler Figure

types of gain control are: the time gain compensation that allows adjusting gain to the depth (Fig. 3.3) and the global gain which affects the whole image.

- Focus: Focus is the zone of screen with the best lateral resolution.
- Frame rate: Frame rate can be increased by reducing the depth and the sweeping angle.

Fig. 3.3 Figure illustrates the Time-Gain compensation control panel at the top right of the image

3.2.2 M-Mode

To achieve M-mode imaging of structures:

- Display the structure in 2D mode and optimize the image.
- Place the cursor line of the M-mode across the structure to assess and start imaging.
- Freeze the image and take measurements.

3.2.3 Doppler Imaging

3.2.3.1 Color Doppler (Fig. 3.4)

- Display the structure in 2D mode and optimize the image.
- Reduce the color Doppler box size to fit with the structure of interest in order to preserve the temporal resolution.
- Adjust color Doppler gain, the color image is over-gained; if there is over-painting and cluttering, under-gained flow will not be detectable.

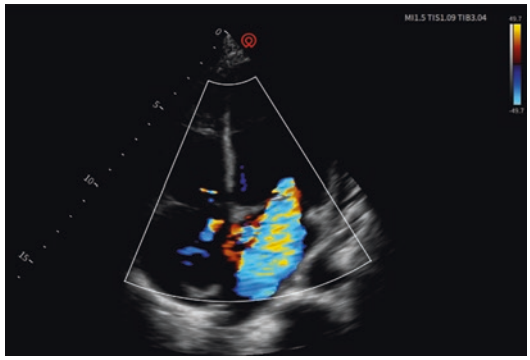

Fig. 3.4 The typical ultrasound image of color doppler is shown in this figure

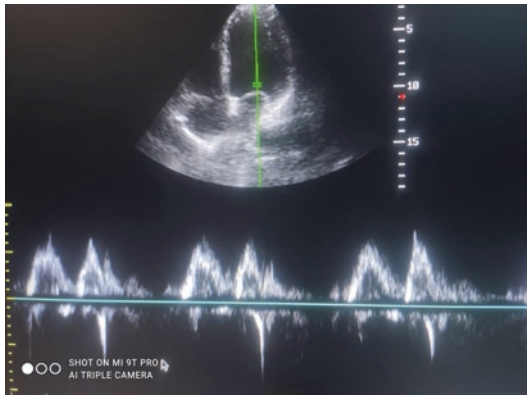

Fig. 3.5 A Pulsed Wave Doppler is illustrated in this figure

- Adjust velocity scale using PRF knob; if it is set too high low velocity will not be detectable, or too low aliasing may occur.

3.2.3.2 Spectral Doppler

PWD (Fig. 3.5)

- Display the structure in 2D mode and optimize the image.
- Select PWD and place the sample volume in the zone of interest.
- Activate PWD; if aliasing occurs increase PRF, shift the base line, use a lower frequency for Doppler, reduce the depth of sampling volume, or in the end switch to CWD.

CWD

- Display the structure in 2D mode and optimize the image.
- Select CWD and place the cursor over the zone of interest.
- Activate CWD; caution must be taken to alinate correctly the cursor relative to the flow direction.

Windows

4

Noreddine Bouarroudj and Cherif Bouzid

The heart is a structure deeply included in the thorax; it is entirely surrounded by other organs and tissues to increase its security, like the lungs and ribs, which may make an obstacle for the ultrasound propagation rendering the ultrasounds investigation complicated; because of those reasons and to establish a systematic approach for the heart ultrasonography exam, the echocardiographic windows are defined. The term echocardiographic windows refer to a chest wall landmark located in the intercostal spaces or thorax vicinity, where the heart may be explored by ultrasounds. The location of echocardiographic windows may vary according to the morphologic habits, location, and size of the heart, and some pathologic conditions like pneumonectomy. Sometimes no window is possible, which is a limit for transthoracic echocardiography (TTE) exam. In TTE exam, four windows are described: apical, subcostal, parasternal, and suprasternal.

For every window, the combination of basic movements of the transducer (Fig. 4.1) in one or more plans of reference (transverse, coronal, and sagittal plan) allows to display the standard echocardiographic views; furthermore, every ultrasound transducer has a landmark called pointer in the lateral side, which fits with the corresponding lateral landmark or pointer on the screen; thus, the ultrasounds transducer has an orientation which is standardized for each view. By convention, the screen pointer is placed on the right of the screen for TTE exam.

N. Bouarroudj (✉)
Department of Anesthesiology and Critical Care, Clinique Maissalyne, Constantine, Algeria

C. Bouzid
Department of Anaesthesia and Critical Care, El Afia Hospital, Mila, Algeria

© The Author(s), under exclusive license to Springer Nature Switzerland AG 2024

N. Bouarroudj et al. (eds.), *POCUS in Critical Care, Anesthesia and Emergency Medicine*,
https://doi.org/10.1007/978-3-031-43721-2_4

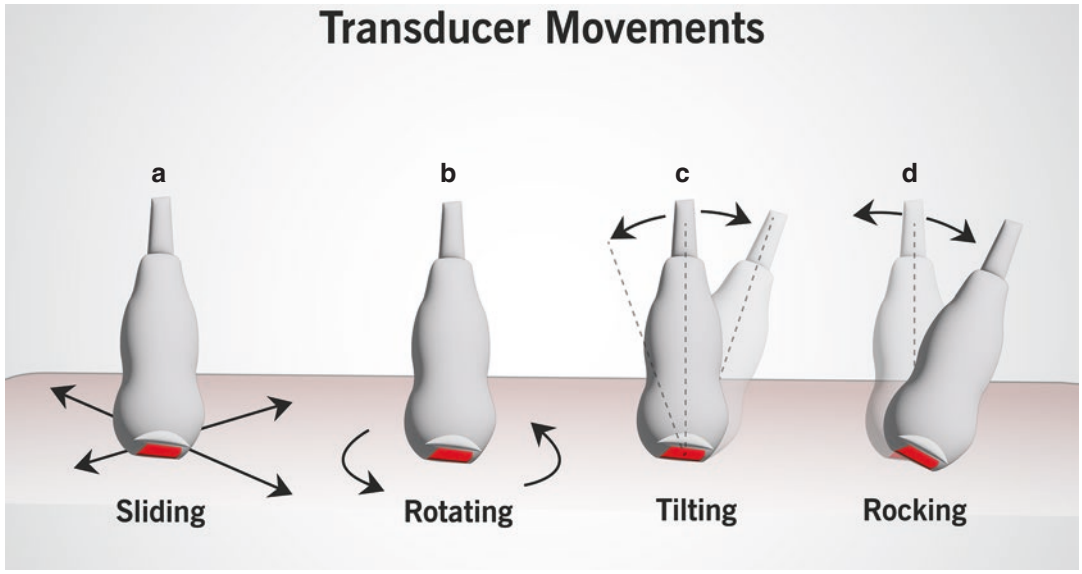

Fig. 4.1 Figure shows the different movements of the transducer used routinely Sliding Rocking Tilting and Rotating

Sonoanatomy of Standard Views

5

Noreddine Bouarroudj and Cherif Bouzid

5.1 Parasternal Long-Axis (PLAX) View

5.1.1 Introduction

Acquisition of PLAX view is a primary step in TTE exam; it serves as a basis to acquire the other parasternal standard views; it is a tomographic cross section of the heart in the axis joining the apex to a base called long axis.

5.1.2 Technique

Classically, the PLAX view is acquired by placing the transducer in the third or fourth left intercostal space just lateral to the sternum, with the pointer oriented to the right shoulder of the patient at 10 o'clock (Fig. 5.1); however, slight adjustments of the transducer or changes of the intercostal space are often required to achieve the ideal view. It is worth mentioning that patients with conditions that cause hyperinflation of the thorax like chronic obstructive pulmonary disease or those mechanically ventilated, the heart tends to be pushed down by the hyperinflated lungs, therefore, in these conditions, placing the transducer in the inter-costal spaces further down may be suitable. Figure 5.2 shows schematically the findings in the PLAX view: aorta, aortic valve, mitral valve, right ventricle, left atrium, and left ventricle. A variant of the classic PLAX view is the right PLAX view, which is acquired by placing the transducer symmetrically to its placement one acquiring the PLAX view, relatively to the sternum; it allows visualization of the aortic valve (AOV) and the proximal ascending aorta.

Fig. 5.1 Figure shows how to do a PLAX view: place the probe in the third–fourth at the left inter-costal space and sternum toward right shoulder precisely at 10 o'clock

N. Bouarroudj (✉)
Department of Anesthesiology and Critical Care, Clinique Maissalyne, Constantine, Algeria
e-mail: bouarroudj@bouarroudj.net

C. Bouzid
Department of Anaesthesia and Critical Care, El Afia Hospital, Mila, Algeria

© The Author(s), under exclusive license to Springer Nature Switzerland AG 2024

N. Bouarroudj et al. (eds.), *POCUS in Critical Care, Anesthesia and Emergency Medicine*,
https://doi.org/10.1007/978-3-031-43721-2_5

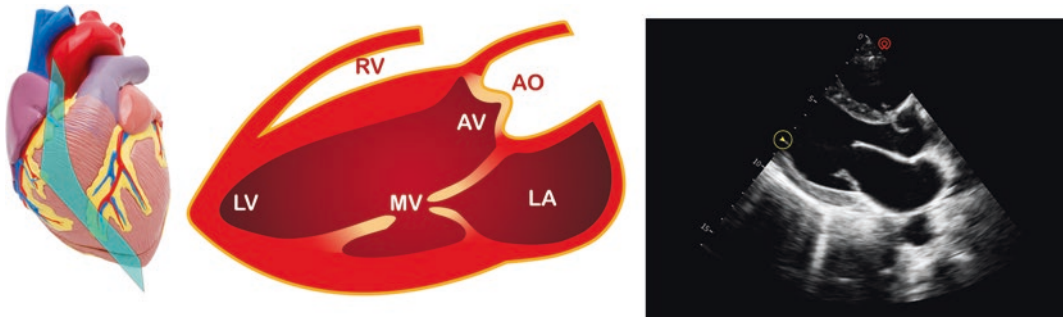

Fig. 5.2 Figure depicts ultrasound findings in this view: aorta, aortic valve, mitral valve, right ventricle, left atrium, and left ventricle

5.1.3 Assessments and Measurements

5.1.3.1 Left Ventricular (LV) Systolic Function

- Visual assessment of ejection fraction (EF).
- Measurement of EF: if the LV is not correctly imaged in its long axis, it appears more round shaped, the risk is the overestimation of EF and the underestimation of the LV cavity size.
- E-point septal separation (ESS).
  - Aortic valve (AOV): motion and morphology of the valve.
  - The aortic root and the initial ascending AO.
  - Left ventricular outflow tract (LVOT) diameter to calculate stroke volume and cardiac output.
  - Left atrial (LA) size notably the antero-posterior diameter.
  - Mitral valve (MV).
- Morphology and motion of anterior and posterior leaflets.
- Mitral stenosis and regurgitation mainly leaflet prolapse.
- Chordate and papillary muscle.
  - Right ventricular (RV) size and function; however, the RV is not imaged in its long axis for correct size evaluation.
  - Pericardium anterior and posterior to the heart, this view allows the differentiation between pericardial and pleural effusion (see chapter pericardial effusion).
  - Descending AO.
  - Coronary sinus in short axis.

5.2 Parasternal Short Axis (PSAX) View

5.2.1 Introduction

The PSAX view is the logical second step to achieve after assessing the heart in PLAX view; it is a serial tomographic cross section of the heart in a short axis, from the base to the apex.

5.2.2 Technique

From an optimized PLAX view, the transducer is rotated 90° clockwise, placing the pointer toward the left shoulder of the patient at 2 o'clock (Fig. 5.3), by tilting the transducer from the base to the apex four imaging plans are acquired, which are:

1. PSAX view at the level of AOV. Figure 5.4 depicts ultrasound findings in this view: right and left pulmonary arteries, aorta and aortic valve with three leaflets or cusps (a coronary cusp, left coronary cusp, and right coronary cusp), right atrium, right ventricle, and left atrium. Note the Mercedes-Benz sign given by the aortic leaflets.
2. PSAX view at the level of MV. From the PSAX view at the level of aortic valve perform an inferior-lateral angulation of the transducer.

   Figure 5.5 illustrates this view with the right ventricle and the mitral valve. Observe the mitral valve with a fish mouth appearance.

Fig. 5.3 Figure shows how to do a PLAX view: from the PLAX view rotate the probe 90° the probe is still in the third–fourth at the left inter-costal space and sternum toward left shoulder precisely at 2 o'clock

3. PSAX view at the level of papillary muscles. More inferiorly and lateral angulation allows the view of papillary muscles as shown in Fig. 5.6.
4. PSA view at the level of apex.

A technique using two hands may be suitable to avoid the accidental translation of the transducer on the thoracic wall when rotating from the PLAX view to acquire PSAX view.

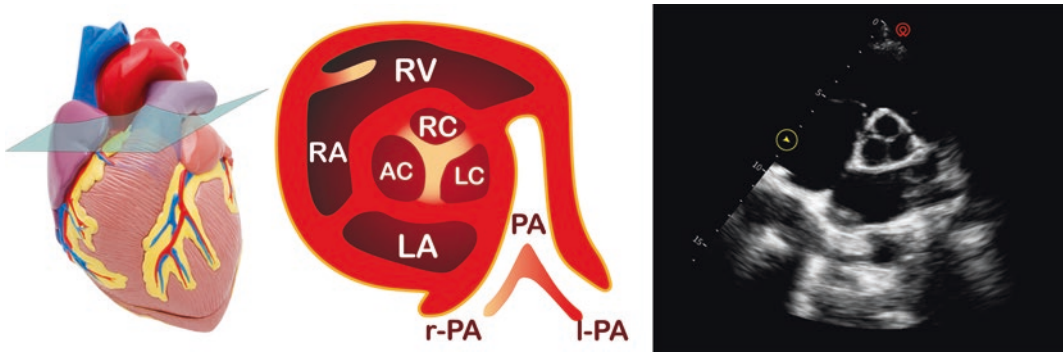

Fig. 5.4 This figure depicts ultrasound findings in this view: observe the level of the view in the left. Identify: Right and left pulmonary arteries, aorta and aortic valve with three leaflets or cusps (a coronary cusp, left coronary cusp, and right coronary cusp), right atrium, right ventricle, and left atrium. The Mercedes-Benz sign is obvious in ultrasound image corresponding

Fig. 5.5 PSAX view at the level of MV. From the PSAX view at the level of aortic valve obtained by an inferior-lateral angulation of the probe. Identify the right ventricle and the mitral valve. Observe the mitral valve with a fish mouth appearance

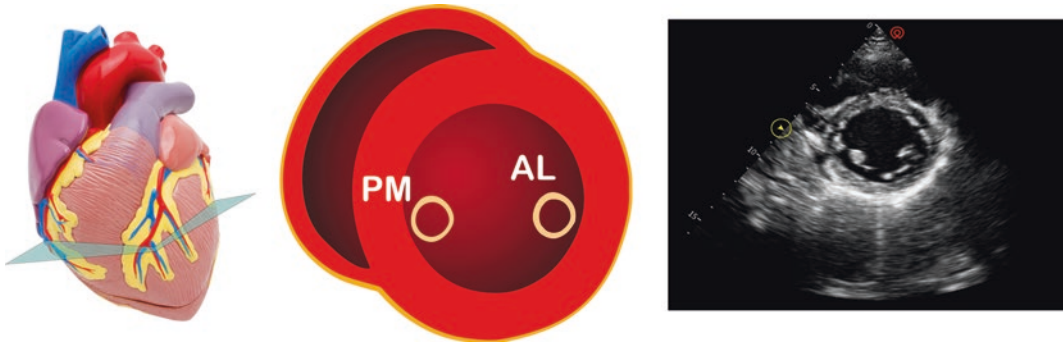

Fig. 5.6 PSAX view at the level of papillary muscles. An inferior and lateral angulation allows the view of the two papillary muscles: antero-lateral and posteromedial

5.2.3 Assessments and Measurements

5.2.3.1 PSAX View at the Level of AOV

- AOV: morphology, opening, and the number of cusps.
- Left and right atria with the inter-atrial septum (IAS).
- Tricuspid valve (TV) notably is the measurement of pulmonary artery systolic pressure (PSAP) using the velocity max of tricuspid regurgitation (TR).
- Right ventricle outflow tract (RVOT).
- Pulmonary valves (PV), mainly the assessment of pulmonary artery mean pressure (PAMP) and the pulmonary artery diastolic pressure (PADP) using the pulmonary regurgitation spectrum.
- Pulmonary trunk and mean bifurcation, patent dectus arteriosis (PDA).

5.2.3.2 PSAX View at the Level of MV

- MV with anterior and posterior leaflets; appreciate morphology and opening (fish mouth).
- If Mitral stenosis is suspected, planimetry of mitral orifice is performed.

5.2.3.3 PSAX View at the Level of Papillary Muscles

- LV and RV systolic function and size.
- Relative size of the RV to the LV.
- Inter-ventricular septum (IVS) motion and orientation, IVS is normally pushed toward the RV.

5.2.3.4 PSAX View at the Level of Apex

- Check for IVSD, thrombosis, and akinesis.

5.3 Apical Four Chamber (A4C) View

5.3.1 Introduction

The A4C view is the cornerstone for the heart assessment using ultrasounds at the apical window; it is an echotomographic cross section of the heart in the coronal plan and serves as a starting point to acquire the other apical views.

5.3.2 Technique

Classically, A4C view is acquired by placing the transducer at the fourth or fifth left inter-costal space just lateral to the mid-clavicular line, pointer toward 3 o'clock (Fig. 5.7); however, in practice, the exact location may vary considerably between patients; therefore, placing the transducer over the maximal apical beat may be more suitable. Care must be taken to avoid foreshortening the echotomographic cross section of the heart; in this condition, the heart tends to be more globular than oval shaped.

Fig. 5.7 The four-chamber view is performed by placing the probe at the fourth–fifth inter-costal space lateral to the mid-clavicular line exactly at 3 o'clock

5.3.3 Assessment and Measurements (Fig. 5.9)

- LV morphology, regional wall motion of the lateral wall, infero-septal wall, and apex.
- LV global systolic function and diastolic function.
- MV and TV morphology and function, notably stenosis or regurgitation.
- RV function and morphology relatively to the LV.
- Pulmonary veins may be displayed in the far field; however, alignment of PWD may be difficult.
- Right and Left atria with descending AO behind the latter.
- IVS and IAS shape and motion.

5.4 Apical Five-Chamber (A5C) View

5.4.1 Technique

From the A4C view, the transducer is tilted anteriorly until the fifth cavity, which is represented by the AOV, and LVOT is displayed on the screen.

5.4.2 Assessment and Measurements

All structures seen in the A4C view are displayed. Fig. 5.8 illustrates the findings of apical five

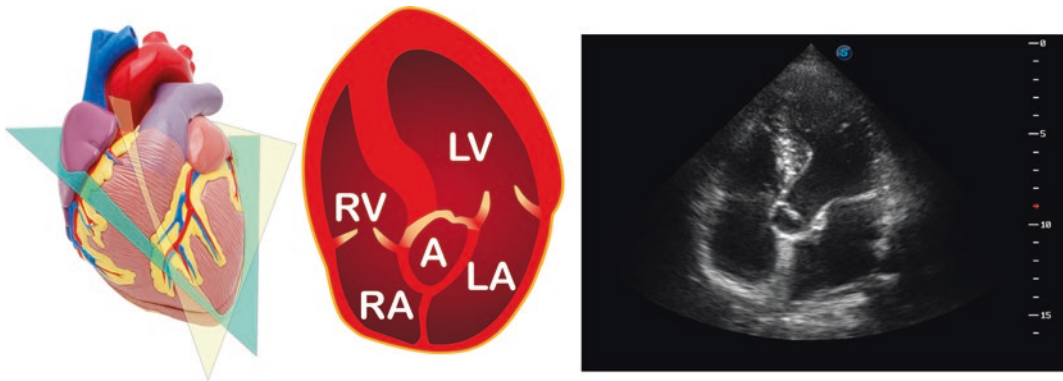

Fig. 5.8 shows the ultrasound findings of apical five chamber view: LV,RV,LA,RA and aorta. This view is obtained by an anterior tilt of ultrasound probe from the 4 chamber view

chamber view: LV, RV, LA, RA, and aorta. Furthermore, this view assesses:

- AOV morphology and function.
- LVOT, stroke volume, and cardiac output.

5.5 Apical Two-Chamber (A2C) View (Fig. 5.9)

5.5.1 Technique

From the A2C view the transducer is rotated 90° counterclockwise, pointer toward 9 o'clock, the ideal view displays only the LV, MV, and left atrium (LA).

5.5.2 Assessment and Measurements

- MV and LA.
- Global LV systolic function notably in Sampson's measurement of EF.
- Regional motion of anterior and inferior LV walls.

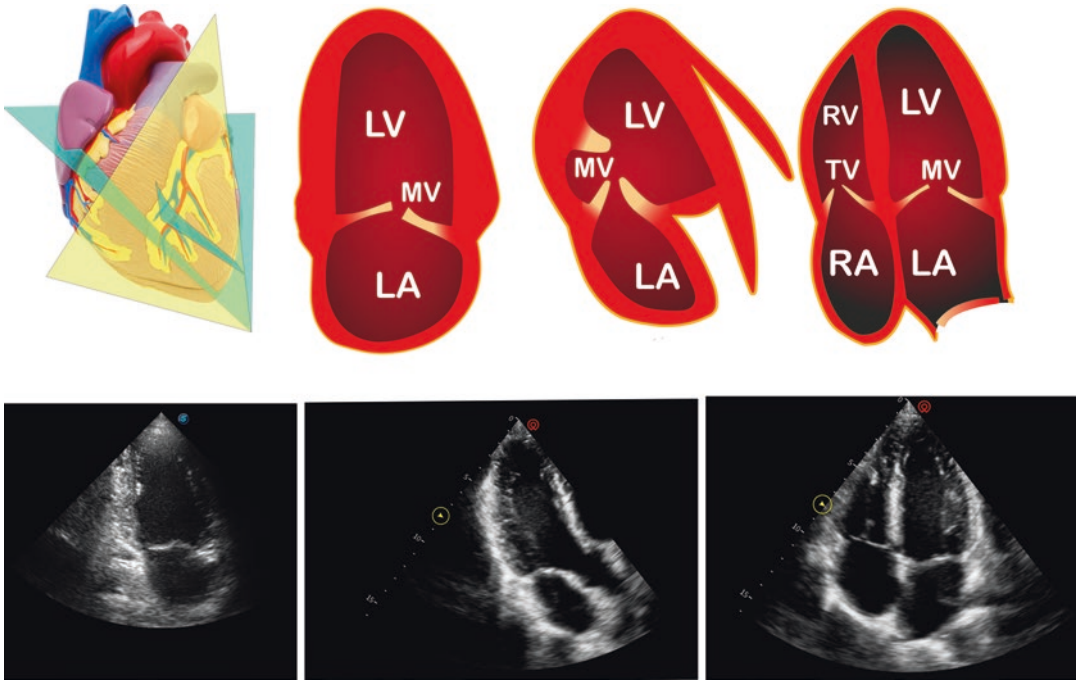

Fig. 5.9 Figure illustrates the two-, three-, and five-chamber views. The two-chamber view is obtained by rotating the probe 90° counterclockwise. The three-chamber view 120° counterclockwise at 11 o'clock. Identify LV, RV, LA, RA

5.6 Apical Three-Chamber (A3C) View (Fig. 5.9)

5.6.1 Technique

From the A4C view, the transducer is rotated 120° counterclockwise, pointer toward 11 o'clock, bringing the third chamber into view, represented by the AOV and the LVOT.

5.6.2 Assessment and Measurements

A particular interest is in regional wall motion assessment of the infero-lateral and the antero-septal LV walls.

5.7 Sub-costal Views

5.7.1 Sub-costal Four-Chamber View

5.7.1.1 Introduction

The sub-costal or sub-xiphoid four-chamber view is a horizontal echotomographic cross section of the heart, in which the liver is used as a window for ultrasound propagation. It has some advantages over the other echocardiographic views, mainly:

- Supine position provides good images.
- No necessity to interrupt resuscitation maneuvers when imaging the heart.
- In some conditions which cause lung hyperinflation, like in chronic obstructive pulmonary lung disease or in mechanically ventilated patient, it may be the only way to imaging the heart.
- Particular interest in assessing the RV and the IAS because the ultrasound beam is perpendicular to these structures, therefore, good quality of echographic images.

This view is integrated in the FAST and RUSH protocols, which used curved transducer with abdominal preset.

Fig. 5.10 illustrates how to perform sub-costal four-chamber view. The probe is oriented toward the left shoulder

5.7.1.2 Technique

To achieve sub-xiphoid four-chamber view, place the transducer just adjacent to the xiphoid process, with steep angle relatively to horizontal plan less than 20° (Fig. 5.10) and orient the transducer toward the left shoulder of the patient. Cooperating patients can be asked to bend their knees to relax the abdominal wall muscles.

5.7.1.3 Assessment and Measurements

The ultrasound findings of this view are the same as the four-chamber view except the liver which is found at the left of the heart (Fig. 5.11).

- RV function, RV-free wall.
- Pericardial effusion.
- LV function.
- Right atrium (RA), LA, and IAS.

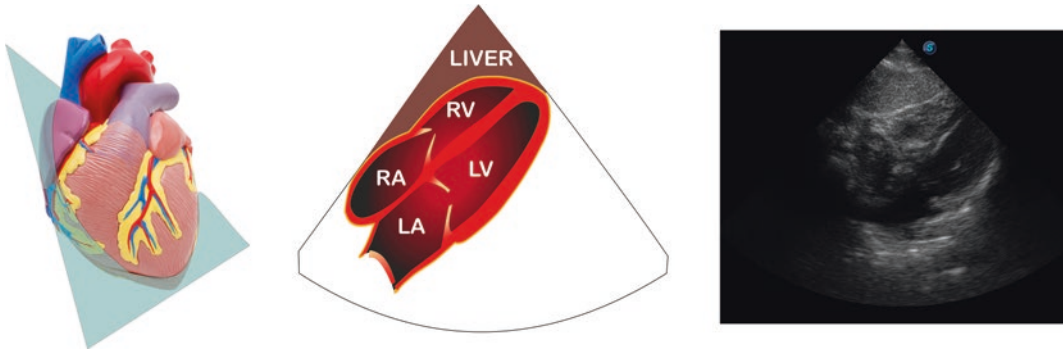

Fig. 5.11 illustrates the sub-costal four-chamber view. The ultrasound findings of this view are the same as the four-chamber view except the liver which is found at the left of the heart

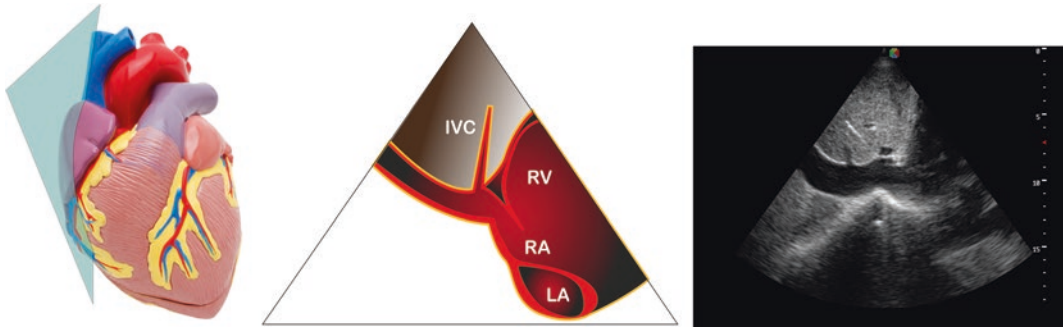

Fig. 5.12 The inferior vena cava view is obtained by rotating the probe 90° counterclockwise from sub-costal view

5.7.2 Inferior Vena Cava (IVC) View

From the sub-costal four-chamber view, the transducer is rotated 90° counterclockwise, pointer toward 12 o'clock, by rocking the transducer to the right of the patient until the inferior vena cava in its long axis comes into view (Fig. 5.12). The ideal image displays the inferior vena cave coursing under the liver, draining the hepatic veins and the inferior vena cava-RA junction. Measurements are performed 2 cm distal to the junction IVC-RA or just distal to the junction IVC-hepatic vein. Pay attention to differentiate the IVC from aorta; the last one is pulsatile structure with a thick wall that gives rise to the superior mesenteric artery when applying Doppler shows artery profile.

5.7.3 Sub-costal Short-Axis View

From the sub-costal four-chamber view rotate the transducer 90° counterclockwise pointer toward the head of the patient at 12 o'clock. By tilting laterally, the transducer from medial to lateral, four imaging plans are acquired, which have the same sonoanatomy as those acquired in the PSAX view (Fig. 5.13). Sub-costal short-axis view is equivalent to the PSAX view; it is a useful one; the latter cannot be acquired essentially with patients mechanically ventilated or with pulmonary conditions which causes lung hyperinflation.

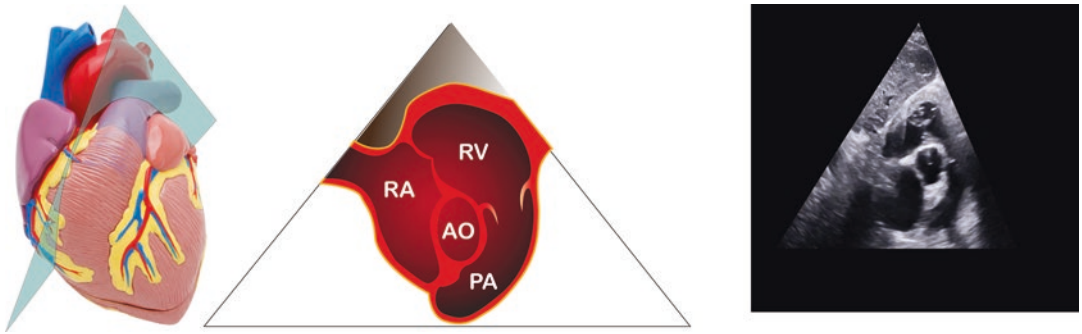

Fig. 5.13 illustrates sub-costal short-axis view which is obtained by rotating probe 90° counterclockwise. The sonoanatomy is the same as PSAX view

5.7.4 Supra-sternal Long Axis View

Patient laying in supine position with neck extended. Place the transducer in the supra-sternal notch (Fig. 5.14), the pointer toward the left shoulder of the patient, and tilt the transducer inferiorly toward the mediastinum; thus, the ideal view displays the aortic valve, the aortic arch, ascending aorta with a portion of the descending aorta, and the right pulmonary artery (PA) in cross section (Fig. 5.15).

5.7.5 Supra-sternal Short-Axis View

From the supra-sternal long-axis view the transducer is rotated 90° clockwise. The ideal view displays the AO in cross section, the PA, LA, and the four pulmonary veins.

This view is helpful to confirm the supra-sternal long-axis view finding, and to assess the pulmonary vein return.

Fig. 5.14 This figure shows how to place ultrasound probe in the supra-sternal probe pointed toward the left shoulder

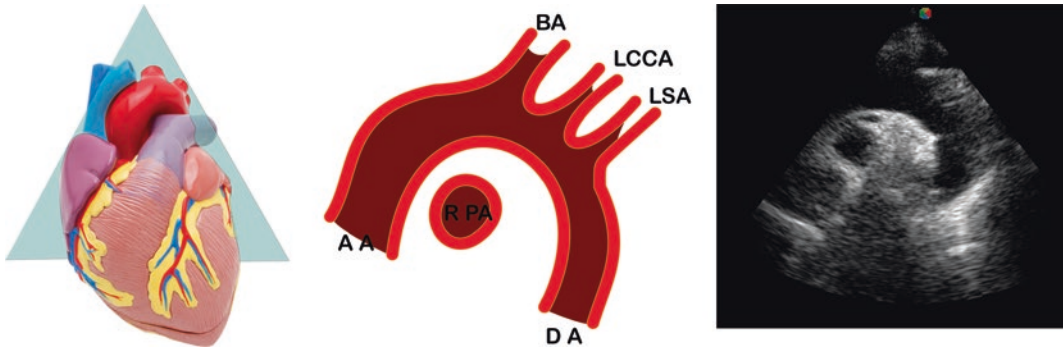

Fig. 5.15 The sonoanatomy of supra-sternal long-axis view is obvious. Structures can be readily identified: ascending aorta, descending aorta, brachiocephalic artery, left common carotid artery, left subclavian artery, and right pulmonary artery

6 Aorta, Vena Cava, and Heart Chambers

Noreddine Bouarroudj and Cherif Bouzid

6.1 LV Systolic Function

The state of LV systolic function is one of the vital questions that the physicians often have to answer.

6.1.1 Introduction

The state of LV systolic function is one of the vital questions that the physicians often have to answer, either in emergency setting or in perioperative medicine; the answer to this question has a direct impact on the care provided for the patients, often expressed by EF qualitatively estimated in CPOCUS setting. However, other parameters mainly derived from Doppler uses, which are relatively simple to acquire, may have a place in CPOCUS protocol in the setting of multi-parametric approach to assess LV systolic function.

In all cases, the parameters reflecting the LV function must be interpreted according to the clinical context because these parameters depend on load conditions.

N. Bouarroudj (✉)
Department of Anesthesiology and Critical Care, Clinique Maissalyne, Constantine, Algeria
e-mail: bouarroudj@bouarroudj.net

C. Bouzid
Department of Anaesthesia and Critical Care, El Afia Hospital, Mila, Algeria

6.1.2 Approaches to Estimate EF

The estimation of the EF can be divided into two groups which are quantitative and qualitative approaches.

6.1.2.1 Quantitative Approach

The use of quantitative approach to estimate EF is the rule in cardiologic practice [1]. Nevertheless, integration of this practice in CPOCUS protocols may face obstacles: they are time-consuming, need a careful acquisition of images in multiple plans and complex calculations, a sophisticated ultrasound machine, and need longer learning curve with no evidence of being superior to the qualitative approach in estimation of left ventricle ejection fraction (LVEF) [2]; however, this method may be useful to asses LV systolic function in patients more or less hemodynamically stable to flow trends, with the aim of reducing the variability intra- and inter-observer. This chapter will briefly review the principal quantitative methods to estimate the EF.

Fractional Shortening Method

Fractional shortening is calculated using the formula:

$$\text{Fractional shortening} = \text{EDD} - \text{ESD} / \text{EDD}$$

EDD: end diastolic diameter
ESD: end systolic diameter

© The Author(s), under exclusive license to Springer Nature Switzerland AG 2024

N. Bouarroudj et al. (eds.), *POCUS in Critical Care, Anesthesia and Emergency Medicine*,
https://doi.org/10.1007/978-3-031-43721-2_6

The normal range is between 28% and 42%, the measure of the diameters is performed using M-mode, which shows a good correlation with the angiographic fractional shortening [3]; in order to accurately estimate the fractional shortening, a symmetrical contraction of LV and good quality of 2D images are required.

Ventricular Volumes Method

Ventricular volumes are calculated using geometrical assumption, in which the LV is assimilating to an ellipsoid shape. Whereas the Teicholz approach (Fig. 6.1) is the most used, the diameter measures are performed using the M-mode and EF is calculated using the formula:

$$EF = EDV - ESV / EDV$$

EDV: end diastolic volume

ESV: end systolic volume

Conditions are required to validate the ventricular volumes method: a symmetrical contraction of the LV, perfect alienation of the M-mode cursor relative to the LV and good quality of 2D images.

Biplane Method of Discs (Modified Simpson's Rule) (Fig. 6.2)

Biplane method of discs is the referent method for EF estimation nowadays recommended by the American society of echocardiography and the European society of echocardiography [1]. The LV cavity is divided into serial sub-volumes discoid shaped and disposed along the axis joining the apex to the center of mitral valve; the LV volume is obtained by summation of all sub-volumes. To achieve the estimation of EF using this method, the operator has to trace the endocardial border in two orthogonal plans: A4C and A2C, in end-systole and end-diastole, the papillary muscles and trabeculations are considered part of the LV cavity, EF, and volumes are automatically displayed.

The limitations to this method are represented by the absolute necessity to acquire an actual 4 and 2 AC views without foreshortening, and a good definition of endocardial border; otherwise, intravenous contrast agents may be used to enhance the delineation of the endocardium.

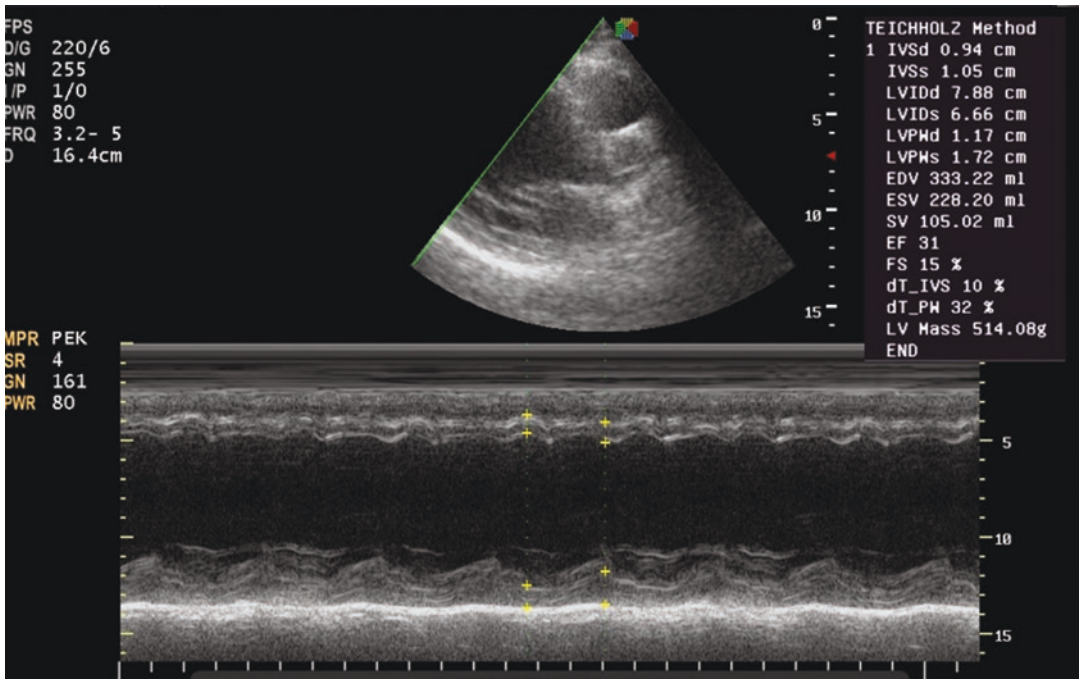

Fig. 6.1 Illustrates the Teicholz Approach: *Observe the EDV (end diastolic volume) and ESV (end systolic volume)*.In this case, the ejection fraction calculated is low =31%

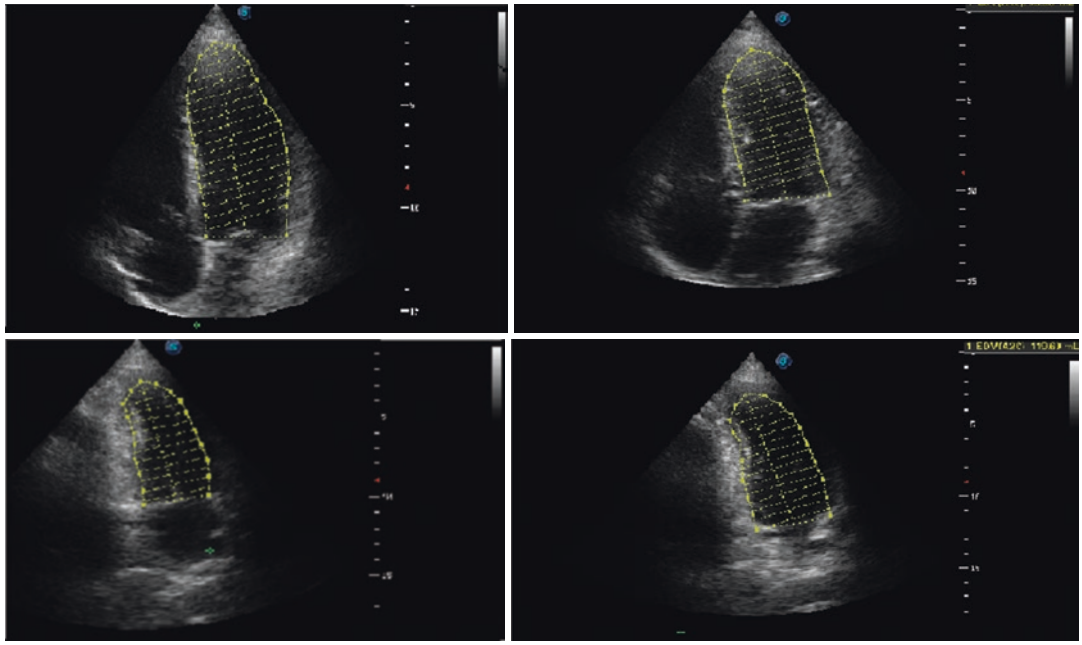

Fig. 6.2 As shown in this figure the *Biplane method of discs (modified Simpson's rule)*. Observe the endocardial border traced in two orthogonal plans: A4C and A2C

6.1.2.2 Qualitative Approach

The qualitative approach to estimate EF in CPOCUS is the standard practice. Studies attest the pertinence of CPOCUS protocol based on a qualitative approach managing the critically ill patients [2]. To avoid mis-estimation of LVEF using qualitative approach, a careful analysis of all segments of the LV wall is the rule; the goal of the qualitative approach is to grade the LV systolic function in one of four broad classes: normal, hyperdynamic, reduced, and severely reduced LV function, using three basic elements:

- Endocardial motion: describes the systolic shifting of the endocardium toward the center of the LV cavity.
- Myocardial thickening: describes the amount of thickness gained consecutively to the LV contraction.
- The septal motion of the tip of anterior mitral valve leaflet or E-point septal separation: describes the minimal distance separating the tip of the anterior leaflet from the septum in its maximum excursion corresponding to the first component of the LV filling. It reflects the gradient of pressure between the LA and the LV; the more the EF is good, the more the LV emptying is complete; consequently, the transmitral diastolic gradient is substantial; moreover, dilated LV by greater end-systolic volume tract the mitral chordae tendineae restricts the motion of the anterior mitral valve toward the septum in early diastole.

The ESS is ideally assessed using PLAX view, the existence of significant mitral regurgitation (MR) or aortic regurgitation (AOR) are limits to the use of the ESS.

Normal Left Ventricular Systolic Function

In a heart with normal systolic function, all segments of the myocardium wall gain in thickness by 40% at least, with a shifting of the underlying endocardium concentrically toward the center of the LV, and the minimal distance from the tip of the anterior mitral leaflet to the septum is less than 1 cm.

Hyperdynamic Left Ventricular Systolic Function

Under these circumstances, all aspects of the LV systolic function are exaggerated, the endocardial motion and myocardial thickening are maximal, giving the impression of total or subtotal erasing of the LV cavity in systole, whereas the maximal erasing realizes the "kissing heart" aspect. Often this hyperdynamic stat is encountered in the situations of true or relative hypovolemia; other possible etiology are: pulmonary embolism, severe valvular dysfunction, cardiac tamponade, and all etiology of high output cardiac failure.

Reduced Left Ventricular Systolic Function

The LV with reduced systolic function exhibits a profile of poor function, all three components are affected, the endocardium stays away from the center of the LV cavity giving the aspect of full end-systolic left ventricle, systolic changes in myocardium thickening are less noticeable, and the tip of the anterior mitral leaflet is far from the septum.

Severely Reduced Left Ventricular Systolic Function

At this stage of reduction in systolic left ventricular function, the LV exhibits little changes in the cardiac cycle, giving the impression of non-moving LV, the endocardium stays almost in its diastolic position, the myocardium wall barely gains thickening at systole, the tip of the anterior mitral leaflet is very far from the septum.

6.1.2.3 Other Approaches

Other approaches, mainly Doppler derived, may be integrated in the estimation of LV systolic function (multi-parametric evaluation):

1. dp/dt Index

   The dp/dt index represents an indirect measure of LV contractility; it describes the raising of the pressure in LV relative to the time. After acquiring a spectral Doppler of mitral regurgitation, the time spent to arise from 1 to 4 m/s corresponding by the application of simplified Bernoulli equation to arising from 4 to 36 mmHg is measured, dp/dt is calculated using the formula:

$$dp / dt = 4 - 36 / dt = 32 / dt$$

2. Stroke Volume and Cardiac Output

   Stroke volume represents the amount of blood ejected by the ventricle per one cardiac cycle; when multiplied by heart rate, it represents the cardiac output. Stroke volume in practice can be estimated by measuring the integral time velocity (ITV) at the LVOT by applying PWD in 3 or 5 AC views; LVOT surface is estimated by measuring the diameter of the LVOT in PLAX, approximately at the same location used to estimate the ITV of the LVOT; the stroke volume is measured by multiplying the ITV LVOT by the surface of the LVOT; normal values of stroke volume range between 50 and 80 mmHg.

   Careful interpretation of stroke volume value is the rule because this method of measure assumes that the LVOT has a circular and constant section which is not often the case [1], the mis-estimation of the LVOT surface elevated to the square causes more mis-estimation of the stroke volume.

3. Mitral Annular Plan Systolic Excursion (MAPSE)

   MAPSE measures the systolic motion of the MV annulus toward the apex, which reflects the LV global systolic function and especially the longitudinal component of the latter [1]; it is evaluated by applying the TM cursor through the lateral aspect of the MV annulus, and measurement of the systolic displacement.

6.2 LV Diastolic Function

6.2.1 Introduction

Well filled left venticle is a required element for efficient pump function during systole although this part of LV function cycle was underestimated in the past decades; actually, it is the subject of increasing interest either in the cardiologic prac-

tice or in the acute and perioperative medicine; however, correctly assessing the LV diastolic function is complicated; such complexity is reflected by the numerous parameters used for this purpose, making the approach to the LV diastolic assessment beyond the scope of CPOCUS; it relates from the advanced critical care echocardiography [4], and requires competences similar to those of our cardiology colleague, it is time-consuming and needs high quality images, making the adoption of this standard protocol difficult in daily practice for acute and perioperative medicine; therefore, in order to get access to the assessment of LV diastolic function in these conditions, more simplified approaches are under evaluation but need more validation to be integrated in practice.

6.2.2 Pertinence of LV Diastolic Function Evaluation

The evaluation and grading of the LV diastolic function is the indirect reflection of the LV end-diastolic pressure, and LA mean pressure; it may be crucial to assess in some clinical scenarios like:

- Patients in acute respiratory failure with diffuse pulmonary opacity in thorax radiography, the estimation of LA pressure may help in etiology differentiation between acute respiratory distress syndrome (ARDS) and acute heart failure.
- The occurrence of diastolic failure in septic patient is found to be a poor prognostic factor [4].
- Predict the issue of weaning in mechanically ventilated patient.
- Screening and management of patients with diastolic dysfunction perioperatively with a higher risk of adverse hemodynamic outcomes. Notably the use of more aggressive monitoring and fluid management policy.

6.2.3 Standard Cardiology Assessment of LV Diastolic Function

1. Flow Doppler measurements
   (a) MV inflow (Fig. 3.5)

   Diastole is defined as the part of cardiac cycle spent between the closing of AOV and the opening of MV; the PWD envelope is acquired by placing the sample volume between the tips of MV in A4C view; it represents the pressure gradient between the LA and LV [1].

   The E wave or early wave is the first to be recorded, it corresponds to the rapid filling of the LV; the second wave is the atrial wave, or A wave corresponding to the LA contraction. Its contribution to the LV filling is lesser than the E wave in normal diastolic functioning. Between the two waves is a period of low filling corresponding to the diastasis, in some pathologic conditions, a wave named L appears when the LV active relaxation is slow.

   It is worth mentioning that only the E wave is present in patients with atrial fibrillation. The values of E wave max velocity lowers with aging. In some conditions like tachycardia or atrial-ventricular first-degree block, the E and A wave merges, complicating the measures. It is important to note that through the different steps of diastolic function aggravation, the values of E wave decrease then increase, rendering the unique use of E max velocity to asses LV diastolic function not recommended, a significant MS or MR renders these parameters obsolete.

   (b) Tricuspid jet regurgitation maximum velocity (*see PHT chapter)*
2. TDI measurements (mitral annulus velocity) (Fig. 6.3)

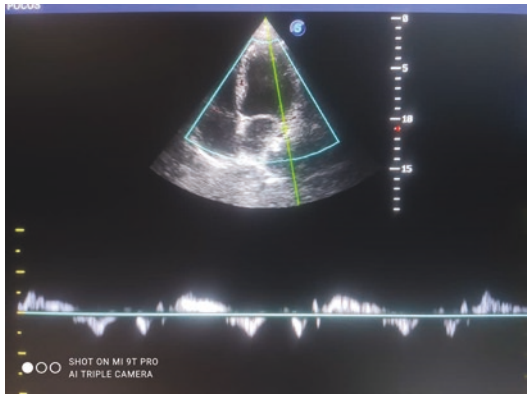

Fig. 6.3 TDI measurements (mitral annulus velocity)

Pulsed wave TDI allows the assessment of myocardial velocity throughout the cardiac cycle; it is the assessment of mitral annulus diastolic velocity which is used in LV diastolic function evaluation, to acquire the tracing of mitral annulus velocity, place the TDI PW sampling volume over the mitral annulus in the strict A4C view and record the tracing, the first negative deflection is the e' wave and the second one is a' wave.

The e' wave is relatively independent of pre-load conditions [1], the value of e' decreases progressively with the progression of LV diastolic dysfunction—these two aspects make it an excellent choice to assess the LV diastolic function. However, the absence of consensus over using the septal or lateral values, the wide range of normality of this parameter, making persons in the low range not certainly exempt from LV diastolic dysfunction, and the presence of regional abnormality motion of the base of the heart are limitations for the use of this parameter.

3. Measurement using 2D imaging

   Chronic pressure elevation in LV and LA causes enlargement of the latter to asses LA size (see LA chapter).

4. American Society of Echocardiography/ European Association of Cardiovascular Recommendation for the Evaluation of LV Diastolic Function 2016

   In patients with normal LVEF, assessment of the diastolic function follows the steps of the A algorithm, if diastolic dysfunction is present, grading of the latter follows the steps of the B algorithm (Fig. 6.4).

In a patient with reduced LVEV, assessment of the LV diastolic function follows the steps of the B algorithm.

6.2.3.1 Simplified Approach to Assess LV Diastolic Function

To make the evaluation of the LV diastolic function possible in routine practice and for more integration in CPOCUS protocol, abundant studies, and trials are performed; however, it needs more validation and consensus to be applied in practice. One of the simplified approaches is using a binary method [4], in which the response generated will be presence or absence of LV diastolic dysfunction without grading, this approach uses the two parameters e' and E/e', with a cut-off value of e' less than 8 cm/S and E/e' more than 14 to attest the presence of LV diastolic dysfunction. The adjunction of the finding derived from application of the POCUS protocol to the lungs, mainly the B lines may be useful.

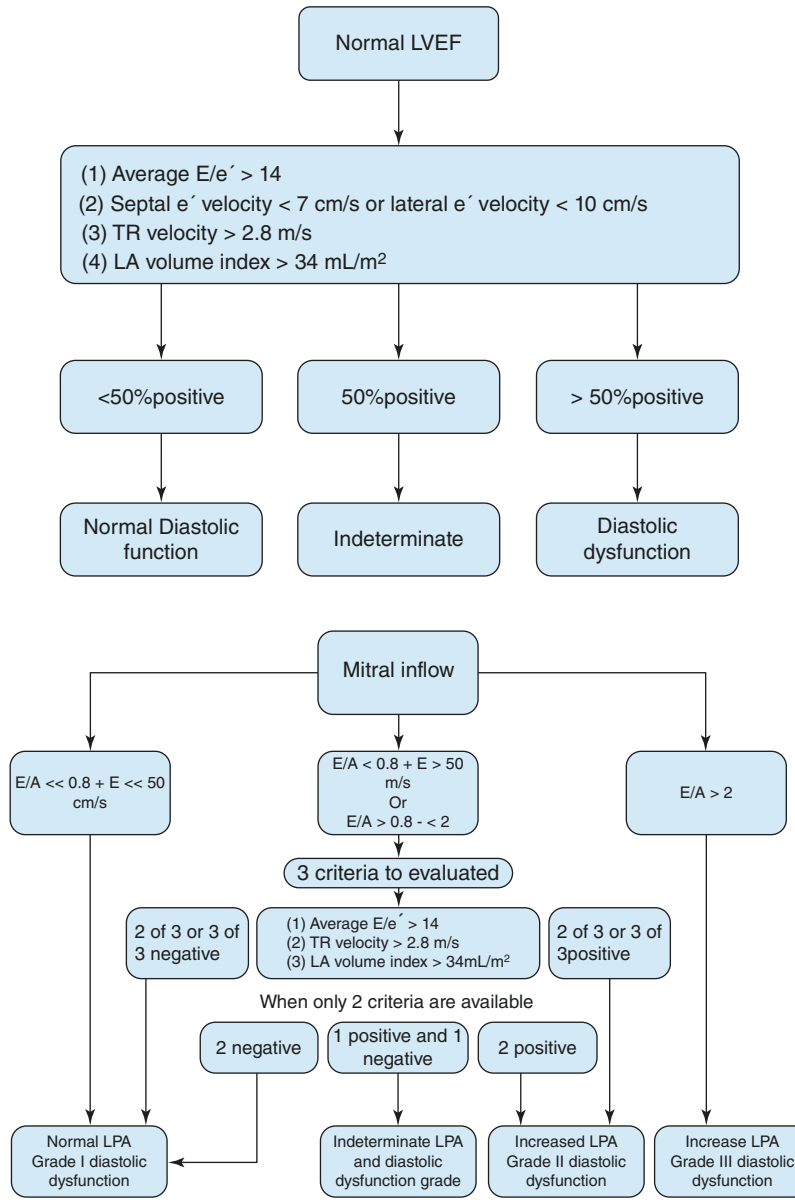
Normal LVEF
(1) Average E/e´ > 14
(2) Septal e´ velocity < 7 cm/s or lateral e´ velocity < 10 cm/s
(3) TR velocity > 2.8 m/s
(4) LA volume index > 34 mL/m2
<50%positive
50%positive
> 50%positive
Normal Diastolic function
Indeterminate
Diastolic dysfunction
Mitral inflow
E/A << 0.8 + E << 50 cm/s
E/A < 0.8 + E > 50 m/s Or E/A > 0.8 - < 2
E/A > 2
3 criteria to evaluated
2 of 3 or 3 of 3 negative
(1) Average E/e´ > 14
(2) TR velocity > 2.8 m/s
(3) LA volume index > 34mL/m2
2 of 3 or 3 of 3positive
When only 2 criteria are available
2 negative
1 positive and 1 negative
2 positive
Normal LPA Grade I diastolic dysfunction
Indeterminate LPA and diastolic dysfunction grade
Increased LPA Grade II diastolic dysfunction
Increase LPA Grade III diastolic dysfunction

Fig. 6.4 American Society of Echocardiography/ European Association of Cardiovascular Recommendation for the Evaluation of LV Diastolic Function 2016. WOLTERS KLUWER HEALTH, INC. LICENSE number 5538341104745

6.3 Left and Right Atria

6.3.1 Left Atrium

6.3.1.1 Introduction

The LA is the cardiac cavity interposed between the pulmonary circulation and the LV; LA accomplishes the function of reservoir, conduit, and pump for the blood originating from the pulmonary circulation toward the LV; furthermore, the LA has a neuroendocrine function by the mean of secretion of atrial natriuretic peptide involved in phenomenon of heart remodeling.

CPOCUS assessment of LA aims: ensuring its vacuity from mass and thrombosis, and to assess its size, which is increased in chronic atrial arrhythmia, MV pathology, and increased LV diastolic pressure.

6.3.1.2 Assessing the LA Vacuity

LA vacuity is checked by performing multiple scans of LA in different views; mass and thrombosis appears usually as hyperechoic structures which can be free in the LA cavity or adherent to the walls of the latter.

6.3.1.3 Assessment of LA Size

LA size may increase in some pathological processes; therefore, this parameter is used to assess the effect of atrial fibrillation, mitral valve pathology, and elevated LV end diastolic pressure; mainly in the setting of LV diastolic function estimation, two approaches may be used: the simplified approach and the LA volume measure. In all cases, the maximum or the end-systolic size is used.

Simplified Approach

In this approach (Fig. 6.5), the antero-posterior diameter of the LA is measured by acquiring PLAX view, then placing the cursor of TM-mode across the aorta and LA. It is generally accepted that once this diameter is superior to the diameter of aorta, the LA is enlarged [4]. However, despite the facility to integrate this parameter in the CPOCUS protocol, it neglects the other dimensions of the LA.

LA Volume Measure (Simpson's Approach)

The LA cavity is divided into serial discoid shaped sub-volumes and disposed along the axis joining the mid-mitral valve plan to the posterior wall of LA; the LA volume is obtained by summation of all sub volumes. To estimate LA volume using this method, the operator traces the endocardial border in two orthogonal plans, which are A4C and A2C, at end-systole (Fig. 6.6). The quality of the image required and the time consumed are the two obstacles for routine use of LA volume measure in the CPOCUS protocol.

6.3.2 Right Atrium

The RA is the heart cavity between the systemic venous system and the RV. In CPOCUS protocol, one parameter derived from this cavity is of particular interest: it is the RA pressure, mainly used

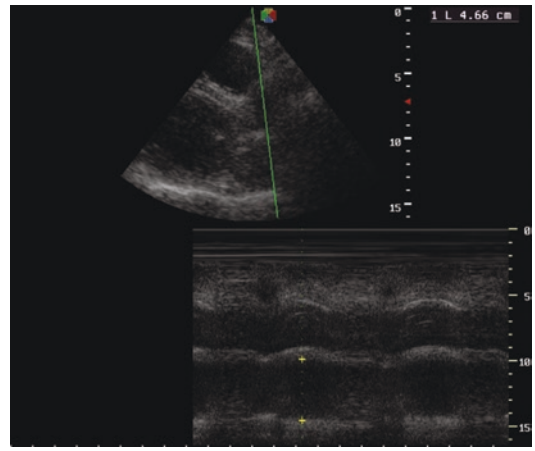

Fig. 6.5 PLAX view with TM mode across the aorta and LA allows the calculation of the antero-posterior diameter of the LA

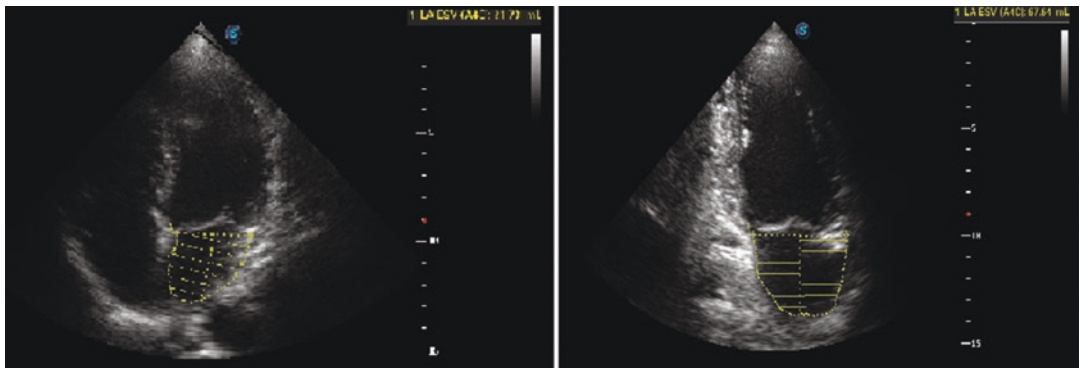

Fig. 6.6 A volume measure (Simpson's approach)

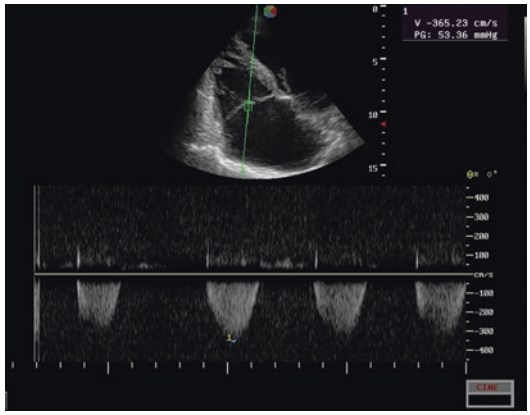

Fig. 6.7 RA pressure routinely used to estimate PASP

to estimate PASP; however, this parameter is best approached by studying a vein connected with the RA directly, it is the IVC (Fig. 6.7).

6.4 Thoracic Aorta

6.4.1 Introduction

Acute chest pain is a frequent motif for emergency consultation and hospitalization; aorta pathology, although rarely involved compared to the other causes of acute chest pain, is still a cause of high mortality and morbidity, which is increased by the delay in diagnosis and therapeutic start. The aortic dissection mortality rate is raised by more than 1% every hour passed after the onset, with overall mortality of 36–72% within the first 48 h from the establishment of the diagnosis [5].

In an emergency setting, the contribution of the clinic and the standard exams in thoracic aorta dissection diagnosis is deficient, the TTE, although less reliable as the transesophageal echocardiography (TOE), can solely establish or yield orientation elements for the diagnosis; TTE is enabled to eliminate the diagnosis owing to its low negative predictive value.

6.4.2 Thoracic Aorta Anatomy

The thoracic aorta is classically divided into three segments:

1. The first one is the ascending thoracic aorta, which extends from the AOV to the arising of the innominate artery; the first segment of the ascending aorta is the aortic root, which starts from the annulus to the sino-tubular junction which includes the Valsalva sinus.
2. The second segment is the aortic arch extending from the innominate artery to the left subclavian artery, which gives a rise to the three major arteries.
3. The third segment is the descending aorta from the subclavian artery to the iliac bifurcation.

Measurements are performed from the leading edge to the leading edge, in plan perpendicular to the aortic walls; in the ascending aorta, three diameters are of particular interest, which are the diameter at the annulus, sinus of Valsalva, and sino-tubular junction.

Diameters and measurement of the thoracic aorta are a function of age, gender, and the body surface area [6], the upper limits of normal range are 4 cm for ascending aorta and arch, 3 cm for descending aorta [5].

6.4.3 Technique

- Aortic root: PLAX view, PLAX right view (Fig. 6.8).
- Ascending AO: PLAX view, PLAX right view, suprasternal view.

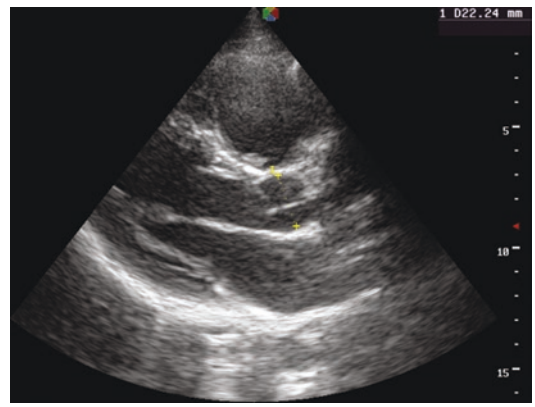

Fig. 6.8 Calculation of the antero-posterior diameter of the aorta

- Descending AO: PLAX view, PSAX view, A2C view, A4C view, A5C view, subcostal long and short axis, abdominal view.
- In all views that allow the visualization of descending AO in a short axis; when rotating the probe 90° in a clockwise direction displays a segment of the latter in the long axis; visualization of the AO in both long and short axis allows for ruling out some artifacts.
- In the presence of lung consolidation or pleural effusion, these pathologic conditions can be exploited in order to yield non-standard views of the AO.

6.4.4 Pathologic Finding

6.4.4.1 Dilatation and Aneurysm

Dilatations exceeding 4.5 cm are considered aneurismal dilatation [5]; it is rarely an isolated lesion that has the same distribution as atherosclerosis; however, in some congenital and genetic conditions like bicuspid aortic valve, Marfan's, and Ehlers-Danlos diseases, the proximal localization is the rule, which is fortunately very accessible to the TTE exam as shown in Fig. 6.9 an aneurysmal dilated aorta can be readily identified in the suprasternal long axis view. Atherosclerosis is one of the risk factors of aortic complication, it is simultaneously a risk factor of coronary artery disease, and it affects population at high risk of thromboembolic incidents. Therefore, the critical question in CPOCUS protocol is whether the aneurismal dilatation is a random discovery or relates to the current symptoms? The raising of any suspicion must promote the realization of available referent exams to rule out acute aortic syndrome.

Fig. 6.9 Example of an aneurysmal dilated aorta seen in a suprasternal long axis view

6.4.4.2 Aortic Dissection

Acute aortic syndrome is represented by aortic dissection, intramural hematoma, and aortic ulcer; however, the intramural hematoma and aortic ulcer are out of the scope of the CPOCUS protocol.

The diagnosis of aortic dissection in the CPOCUS protocol relays on two findings which are the aortic dilatation and the intimal flap.

The ability of TTE to diagnose aortic dissection is less than the other exams considered as a gold standard, the sensitivity in diagnosing aortic dissection of ascending aorta is 78–90%, but decreasing only to 31–51% for the descending aorta [6], this is owing to its incapability to explore the latter in all its length.

The differentiation between intimal flaps and artifacts may be difficult. Here are some tips to make the difference:

- The flaps motion is random; however, artifacts tend to reproduce the motion of adjacent structures (reverberation artifact), and the best modality to assess motion in this setting is the M-mode.
- Side lobe artifacts tend to be progressively attenuated, which is not the case for the flaps.
- A careful real-time scan to identify the adjacent structures. Do not confuse the innominate vein with a false channel!

6.4.5 Complications Diagnosis

- Assess pericardial effusion that can indicate the rupture of the false channel in pericardium.
- Assess the presence of pleural effusion that can indicate the aortic rupture in the mediastinum.

- Assess the regional motion of myocardium that can indicate the progression of dissection to the coronary arteries.
- Assess the presence of acute severe AOR.
- Assess the extension of the dissection to the abdominal aorta that can cause visceral ischemia.

6.5 Inferior Vena Cava

6.5.1 Introduction

The echographic study of IVC is often used to assess the RA pressure, and get estimation of the CVP, to get access to a more advanced parameter like the calculation of PASP, using the echographic assessment of the IVC to estimate the volume status and volume responsiveness of patients, it may seem attractive. However, it needs a thorough knowledge of hemodynamic and respiratory physiology and integration in multi-parametric strategy.

6.5.2 Physiology

Multiple factors may influence the diameter of the IVC and its respiratory variation:

- Volumic status of the patient.
- Intrathoracic pressure: in spontaneous ventilation, the IVC collapses, the opposite is true in controlled ventilation.
- RV failure and TR cause dilatation and reduced respiratory variation of IVC.
- Intra-abdominal pressure.

6.5.3 Technique

The most often used view to assess the IVC is the subcostal IVC view (see the IVC view chapter Figs. 5.12 and 6.10); however, in some circumstances, IVC can be imaged using the transhepatic longitudinal view; this view uses the liver as an optimal window, the transducer is placed over the last intercostals space at the right mid-axillary line, the pointer is toward the head and the transducer oriented posteriorly, the latter view allows the acquisition of both the IVC and AO in long axis.

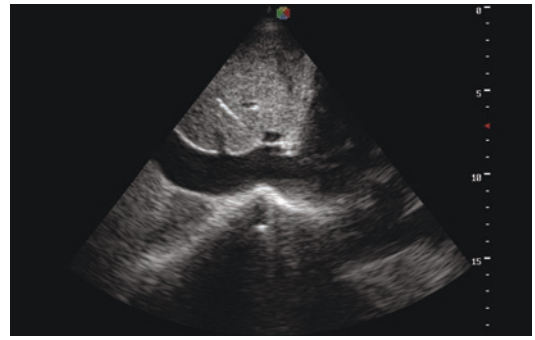

Fig. 6.10 The figure illustrates a dilated vena cava

After image acquisition, the M-mode cursor is placed perpendicularly to the IVC wall, and measures are performed, the off-axis view is a source of underestimation of the IVC diameter and must be avoided.

Analysis of the IVC relies on static parameters (minimal and maximum diameters), and dynamic index which are the IVC distensibility index (in mechanically ventilated patients) and collapsibility index (in spontaneously breathing patients).

6.5.4 Clinical Applications

6.5.4.1 Volume Responsiveness

Spontaneous Ventilation

Two parameters are used to assess the volume responsiveness of patients that totally and spontaneously ventilate: the IVC minimum diameter and the IVC collapsibility index (IVC max diameter on expiration—[IVC min diameter on inspiration/IVC max diameter on expiration]); the studies evaluating all these parameters used to predict the volume responsiveness show conflict; the current trend is the use of the extreme values to predict the responsiveness [2]; in all cases, these parameters must be integrated in multiparametric strategy.

Controlled Ventilation

With patients under total controlled ventilation, the pre-load conditions are relatively constant, making them better candidates to be assessed for volume responsiveness by means of IVC changes, despite the conflicting studies, a patient with IVC distensibility index (IVC max diameter on inspiration—IVC min diameter on expiration/IVC min diameter on expiration) of more than 12–18% is considered as potential volume responder [2]. In all cases, the presence of small collapsed IVC, with mechanically ventilated patients is a reliable argument in favor of volume responsiveness.

6.5.4.2 Tamponade Physiology

Pericardial effusion is common in critically ill patients; the IVC may be a useful tool to assess the compressive character of the effusion. An IVC that collapses more than 50% in deep inspiration attests to the non-compressive character of pericardial effusion [2].

6.5.4.3 RA Pressure and CVP Assessment

With spontaneously breathing patients, the ASE guidelines 2005 and 2010 are the references in the assessment of the RA mean pressure, 2005 ASE guidelines use a quantitative approach in the estimation of the RA pressure, which allows the calculation of the PASP:

- 0–5 mmHg: IVC maximum ≤ 7 mm, collapsibility index ≥ 50%
- 6–10 mmHg: IVC maximum > 7 mm, collapsibility index ≥ 50%
- 11–15 mmHg: IVC maximum > 7 mm, collapsibility index < 50%
- >15 mmHg: IVC maximum > 7 mm, collapsibility index < 25%

References

1. Lancellotti P, Zamorano JL, Habib G, Badano LP. European Association of Cardiovascular Imaging, editors. The EACVI Textbook of Echocardiography. 2nd ed. Oxford: Oxford University Press; 2017. 651 p.
2. Soni NJ, Arntfield R, Kory P. Point-of-care ultrasound. 2nd ed. Philadelphia, PA: Elsevier; 2020. p. 525.
3. Klimczak C, Fumat C. Échocardiographie clinique. 7th ed. Issy-les-Moulineaux: Elsevier Masson; 2016. (Collection de cardiologie pratique)
4. Greenstein YY, Mayo PH. Evaluation of left ventricular diastolic function by the intensivist. Chest. 2018;153(3):723–32.
5. Connolly J, Dean AJ, Hoffmann B, Jarman RD, editors. Emergency point-of-care ultrasound. 2nd ed. Wiley-Blackwell: Chichester, West Sussex, UK; 2017.
6. Evangelista A, Flachskampf FA, Erbel R, Antonini-Canterin F, Vlachopoulos C, Rocchi G, et al. Echocardiography in aortic diseases: EAE recommendations for clinical practice. Eur J Echocardiogr. 2010;11(8):645–58.

Part II

Adults and Pediatrics Diseases

Adult Heart Diseases

7

Noreddine Bouarroudj and Cherif Bouzid

7.1 Coronary Artery Disease

7.1.1 Introduction

Acute coronary syndrome currently represents a heavy burden for the healthcare system; the primary clinical manifestation of the acute coronary syndrome is represented by a chest pain. The role of CPOCUS in this context is well established; it allows the diagnosis of heterogeneous contractility pattern mainly after a successful resuscitation of circulatory arrest [1], despite the fact that the assessment of abnormality in LV regional wall motion is in the scoop of the advanced critical care echocardiography, the CPOCUS allows to rule out the other diagnosis of acute chest pain, which may contraindicate the thrombolysis and permit diagnosis of acute complication of myocardial infarction.

7.1.2 Regional Wall Motion Abnormality

Currently, TTE usage in the context of myocardial infarction is considered as appropriate; it has good sensitivity (approximately 93%) but low specificity (approximately 31%) [2]. LV wall is divided into 17 segments, the motion of every segment is assessed in all views possible, and it permits to judge the segmental motion as a normokinetic, hypokinetic, akinetic, or dyskinetic; the identification of all segments with abnormality motion allows the recognition of the occluded coronary artery; furthermore, TTE gives clues to distinguish current from former LV wall infraction, segments with a relative hyperechogenicity, and thinner than other segments are an argument in favor of a sequela from former infraction [2].

7.1.3 Mechanical Complications of Acute Myocardial Infarction

1. Acute MR:

   Ischemic acute MR may result from two mechanisms:

   (a) MV restriction: It is caused either by failed dilated LV or papillary muscle dysfunction, most often the posterior papillary muscle, in this case 2D mode objective non-coaptation of the two mitral leaflets. One restriction is caused by dilatation of the LV, the two leaflets are restricted by tethered chordae tendineae, and jet flow of MR is central, whereas in the restriction caused by papillary muscle dysfunction the jet flow is lateralized;

N. Bouarroudj (✉)
Department of Anesthesiology and Critical Care, Clinique Maissalyne, Constantine, Algeria
e-mail: bouarroudj@bouarroudj.net

C. Bouzid
Department of Anaesthesia and Critical Care, El Afia Hospital, Mila, Algeria

© The Author(s), under exclusive license to Springer Nature Switzerland AG 2024

N. Bouarroudj et al. (eds.), *POCUS in Critical Care, Anesthesia and Emergency Medicine*,
https://doi.org/10.1007/978-3-031-43721-2_7

Concerning this cases, the symptoms are alleviated by medical treatment optimization and revascularization.

(b) Rupture of the papillary muscle (mitral leaflet flail): Rupture of papillary muscle is attested by random motion of the hyperechoic structure, which is the tip of papillary muscle in the LA. The logical treatment in these cases is the mitral valve replacement.

2. Free Wall LV Rupture

Free wall LV rupture in the setting of myocardial infarction is often a postmortem diagnosis. The presence of pericardial effusion is often a constantly associated sign, which is unfortunately a non-specific finding in this setting.

3. IVS Rupture

IVS rupture is a rare complication in the myocardial infarction setting; the diagnosis is often suspected in presence of an acute RV dilatation and PHT; the septal defect is localized by color flow Doppler as a turbulent high-speed jet from the LV toward the RV.

4. Aneurysm and Pseudoaneurysm

LV wall true aneurysm refers to bulging or expansion of the LV free wall; this neo cavity is limited internally by a weakened, fibrotic, and well-delineated wall, a sequela of transmural myocardial infarction, and it can be either akinetic or dyskinetic.

LV wall pseudoaneurysm occurs once a myocardial rupture is sealed by pericardium; therefore, this neo cavity has non-proper wall at high risk of rupture and needs a prompt diagnosis to avoid this fatal complication.

Echocardiographic differentiation between true and pseudoaneurysm is problematical; the presence of a tight neck which connects the neo cavity and the LV is in favor of pseudoaneurysm.

5. LV Thrombi

LV thrombi typical presentation is a hyperechoic materiel adherent to an akinetic or dyskinetic myocardial zone. However, the diagnosis is sometimes more difficult to establish.

6. Pericardial Effusion: (*7.4. Pericardial Effusion and Tamponade*).

7.2 Right Heart Diseases

7.2.1 Introduction

RV is currently the center of interest in hemodynamic resuscitation in critically ill patients; functionally, it is the cavity responsible for the filling of the LV, anatomically placed with the LV within the same non-extensible space which is the pericardium; owing to the anatomic and functional relationship, separating these two cavities of the heart is inconceivable.

7.2.2 Assessment of the RV in the Different Standard Views

Owing to its complex three-dimensional shape, similar to a crescent, the latter must be evaluated from all possible views.

1. PLAX view

The PLAX view allows the assessment of the RV free wall, the RVOT, and the septum; this is an off-axis view of the RV; therefore, only significant RV dysfunction and dilatation can be objectified.

2. PSAX view (mid ventricular level)

This view allows comparison of the size of ventricles, and the analysis of the septum kinetic.

3. A4C view

This view allows assessment of the RV size relatively to the LV, analysis of the septum kinetic, qualitative assessment of RV systolic function, measurement of tricuspid annular plan systolic excursion (TAPSE), PSAP, and Doppler tissue S-wave.

4. Sub-costal long axis view

The sub-costal long axis view allows the same assessment as in the A4C view; furthermore, the ultrasound beam is perpendicular to the free wall of the RV, which permits good accuracy in measuring the thickness of the RV free wall.

7.2.3 The Interpretation of Pathological Finding

7.2.3.1 RV Size

In the normal heart, the RV size is less than 2/3 of the LV size [3], in acute RV failure, the RV is dilated; this situation results either from reduced contractility of the RV or an acute increase in RV after load.

The increase in RV size is measured relatively to the LV size, the RV/LV ratio is calculated by measuring the maximum diameter of the two ventricles in end-diastole, or most often qualitatively using the following nomenclature [3]:

- Normal RV size: less 2/3 of LV size.
- Moderately dilated RV: more than 2/3 LV size.
- Severely dilated RV: more than the LV size.

Once the RV is dilated, the apex belongs more to the latter, and the RV becomes more ovoid than crescent.

7.2.3.2 Wall Thickness of the RV

The normal RV free wall thickness is less than 0.5 cm, once greater to 1 cm, favoring the chronic process [3].

7.2.3.3 IVS

The kinetic of the IVS reflects the equilibrium of pressure between the two cavities; in normal physiology, the IVS has bow-shaped convex toward the RV, and the rise in the RV pressure pushes the IVS toward the LV cavity; firstly, the IVS is flattened in diastole realizing in PSAX view the D sign, with the increase of the RV pressure, the IVS becomes paradoxical, and bounce motion can be seen between systole and diastole.

7.2.3.4 Systolic Function of RV

Qualitative Method

The qualitative method uses the same principles as the qualitative evaluation of the LV systolic function, permitting the description of the RV function as normal, mildly, moderately, or severely reduced based on the subjective visual estimation.

Quantitative Method

1. Tricuspid Annular Plan Systolic Motion (TAPSE)

   TAPSE describes the anterior longitudinal motion of the lateral tricuspid annulus in systole; it is measured in 4 AC view by Applying the TM cursor across the lateral annulus, which provides a plot overtime of the systolic motion of the latter, the range between systole motion and diastole is measured when less than 17 mm, it attests a decrease in the RV systolic function.
2. Measurement of Peak Systolic Velocity at the TV (S'tv)

   S'tv measures the velocity of the annulus in systole through TDI, it's pertinence is attested in large cohort [4], the S'tv is measured in A4C view, by applying the cursor of TDI PW across the lateral tricuspid annulus, the peak of the systolic motion of the latter is recorded; once less than 10 cm/s it attests severely to the reduced RV systolic function [4].

7.2.3.5 Measurement of Pulmonary Artery Pressure

(See the PHT chapter).

7.3 Pulmonary Hypertension(PHT)

7.3.1 Introduction

PHT is presented when the mean pulmonary artery pressure (MPAP) is more than 25 mmHg at the resting state; the leading causes of PHT are the LV pathology, chronic lung diseases, and the primary causes affecting small pulmonary arteries; however, acute PHT results often from acute elevation in RV after load, in the setting of massive pulmonary embolism or ARDS. In all cases, elevation in pulmonary pressure correlates with a poor prognosis in terms of mortality [5].

The gold standard for measuring pulmonary artery is the right heart catheterization; nevertheless, non-invasive measurements using echocardiography are pertinent and secured [5].

7.3.2 Pertinence of Measurement of Pulmonary Pressure

- Identify patients with PHT, considered at higher risk in acute medicine and in perioperative setting.
- For patients with ARDS combined with RV dilatation, estimating pulmonary pressure allows the evaluation of RV after load; therefore, considering the use of pulmonary vasodilators and adjustment of ventilator setting to maximize the oxygen transport.
- Giving more arguments to consider the diagnosis of pulmonary embolism, in the presence of 60/60 sign and McConnell's sign.

7.3.3 Technique of Measurement

7.3.3.1 Quantitative Estimation

PHT is suspected in the presence of one or more of the following:

- RV size/LV size >1.
- Flattening of the IVS, realizing D-shaped LV.
- Enlarged RA and IVC with a loss of IVC diameter variations.

7.3.3.2 Estimation Using the Tricuspid Valve Regurgitation Maximum Jet

This technique allows the measurement of pulmonary systolic pressure using the modified Bernoulli equation:

$$\text{PASP} = \left(\text{TR Vmax}\right)^2 + \text{RA pressure}$$

All standard views can be exploited to identify a regurgitant jet of the TV using the CFD, CWD is placed through the regurgitant jet, and the envelope of the tricuspid regurgitation is acquired, allowing the measurement of the maximum velocity tricuspid regurgitation. After estimating the RA pressure (*see chapter IVC)*, the PASP is calculated using the Bernoulli modified equation. The American Society of Cardiology proposes the direct use of TR Vmax instead of calculate the PSAP in order to avoid mistakes caused by the approximation of the RA pressure, TR Vmax ≤2.8 m/s indicates a low probability, a value of 2.9–3.4 m/s indicates the intermediate probability, and a value of >3.4 m/s indicates the high probability of PHT.

The presence of pulmonic valve or RVOT stenosis are considered as limitations for the use of this technique of measurement.

7.3.3.3 Assessment of Flow Through the RVOT

1. Pulmonary Time Acceleration

   From PSAX view at the level of AOV, the sample volume of PWD is placed just underneath the pulmonic valves, acquire the tracing at that level, then measure time spent from the opening of pulmonic valve to the peak flow of the tracing; normal value is superior to 130 ms, less than 80 ms, it indicates a severe PHT.
2. Pulmonary Artery Systolic Flow Pattern

   The normal pulmonary artery systolic flow has a parabolic shape; the appearance of mid-systolic notch indicates an elevation of pulmonary vascular resistance.

7.3.3.4 Estimation Using the Pulmonic Regurgitant Diastolic Flow

In some conditions, applying the Bernoulli equation for the tricuspid regurgitant jet is not feasible; alternatively, in these cases, the tracing of pulmonic diastolic regurgitation is exploited in order to assess the pulmonary pressure. In PSAX view, at the level of the AOV, the pulmonic regurgitant jet is recognized using the color Doppler, placing the CWD cursor through the jet, tracing is acquired by measuring the peak pulmonary regurgitant jet; the MPAP may be calculated by applying the Bernoulli equation:

$$\text{MPAP} = 4\left(\text{peak velocity pulmonary jet regurgitation}\right)^2 + \text{RAP}$$

Measuring the end pulmonary regurgitant jet, the diastolic pulmonary artery pressure (DPAP) may be calculated by applying the Bernoulli equation:

$$\mathrm{DPAP} = 4\left(\mathrm{end\,pulmonary\,regurgitant\,jet\,velocity}\right)^2 + \mathrm{RAP}$$

7.4 Pericardial Effusion and Tamponade

7.4.1 Introduction

Pericardial effusion is the presence of fluid between the two layers of the pericardium; the etiology may vary from malignancy, uremia, trauma, infection, autoimmune diseases. When a non-cause is identified, the effusion is said to be idiopathic. It is estimated that more than 13.6% of patients consulting urgently for dyspnea with non-identified causes [3] also have pericardial effusion with varying clinical impact.

Clinical presentation in the setting of a significant pericardial effusion may be not specific; CPOCUS allows fast and reliable diagnosis of the pericardial effusions, and it has been shown that non-cardiologist physicians with appropriate training, can accurately diagnose pericardial effusion in more than 95% [3] compared to the comprehensive echocardiography as a gold standard. Furthermore, CPOCUS allows the following of trends and evaluation of the clinical impact of the pericardial effusion.

7.4.2 Positive Diagnosis of Pericardial Effusion

Classically, pericardial effusion is seen as an anechoic band between the two layers of pericardium (Fig. 7.1); the visceral pericardium is too thin; therefore, not outlined from the adjacent myocardium, at the beginning the free flowing pericardial effusion accumulates in the declivitous zones; thus, it is best identified anterior to the RV free wall in sub-costal 4C view, or posterior to the LV lateral wall in PLAX view, localated or clotting pericardial effusion is a particular entity in which fluid accumulates or clots in a localized area of the pericardium, with the potential compression of the adjacent heart chamber.

7.4.3 Differential Diagnosis

1. Epicardial fat deposits: Located between myocardium and visceral pericardium, some elements permit to distinguish the latter from pericardial effusion; the epicardial fat is often hypoechoic rather than anechoic, holds the same localization while the patient changes his position, and is most abundant in right atrio-ventricular sulcus and the RV free wall [6].
2. Pleural effusion: In PLAX view, the pericardial effusion passes anterior to the descending aorta, it is not the case for pleural effusion.
3. Ascites.

Fig. 7.1 Pericardial effusion appears as an *echo*-free into pericardium layers

7.4.4 Pathological Finding

The hemodynamic tolerance of pericardial effusion depends on four factors which are as follows:

1. Fluid volume and accumulation rate, a large volume of fluids slowly accumulating, can be accommodated with a little elevation in pericardial pressure; in contrast, the fast accumulation of a small volume may be life-threatening.
2. Pericardial compliance.
3. Hemodynamic and volume status of the patient.
4. Thickness and function of underneath heart chambers.

7.4.4.1 Pericardial Effusion Size

The hemodynamic tolerance of pericardial effusion depends on the volume and the rate of accumulation; however, to follow trends and therapeutic efficacy, the classification using the thickness of the pericardial effusion is widely accepted [3], it is based on the highest pericardial separation measured in end-diastole, the pericardial effusion is judged as small, moderate, or large if the maximum separation between the two layers of pericardium is less than 1 cm, 1–2 cm, and more than 2 cm, respectively.

7.4.4.2 Cardiac Tamponade

Cardiac tamponade is a clinical diagnosis that must be suspected in every patient with a large pericardial effusion associated with a hemodynamic collapse; it is the stat when the raising in pericardial pressure is sufficient to impede the diastolic filling of one or more heart chambers, resulting in fall of cardiac output.

The echocardiographic signs of tamponade are as follows:

1. RA systolic collapse.
2. RV diastolic collapse.
3. Dilatation and a loss of the IVC respiratory variations; mostly, this sign has a negative predictive value.
4. Paradoxical septum motion: in inspiration with the increase of diastolic filling of the RV, the IVS is pushed toward the LV cavity through the ventricular interdependence phenomenon, which reduces the LV stroke volume; it is the classical paradoxical pulse which is best appreciated in A4C view.
5. Mitral valve inspiratory reducing inflow more than 30%.

Due to tachycardia, all these finding are best interpreted using the M-mode. In order to avoid over diagnosis of tamponade, it is worth mentioning that:

1. IVC dilatation is not specific for cardiac tamponade.
2. RA collapse may be seen in hypovolemic patient—it is the continuum of the IVC collapse.
3. Small RV collapse, mainly the RVOT collapse, may be seen in the non-compressive pericardial effusion.

7.5 Heart Valve Disease

7.5.1 Introduction

Comprehensive assessment of the heart valves is clearly beyond the scope of CPOCUS; however, patients with a respiratory and circulatory failure or both; with no complete understanding of the underlying causal pathological process, a basic valves evaluation may be the answer; it includes a careful inspection of valves in multiple plans, combined with investigation by color Doppler, atrial, aortic root, and ventricular size and function estimation [3]. Conditions in which basic assessment of heart valves may be helpful include acute pulmonary edema, heart failure, septic shock, heart murmur finding, and a difficulty in weaning mechanical ventilation.

Mitral and aortic valves regurgitation represents the cornerstone in CPOCUS valves evaluation; a quantitative approach using 2D and color Doppler is the rule [1]; therefore, regurgitate

valve lesion is classified as severe or not severe; when in doubt, a request to perform comprehensive echocardiography is mandatory.

7.5.2 The Technique of the Echocardiographic Exam

1. Two-Dimensional Exam

   All components of the valve in question and adjacent structures must be inspected in all possible views; abnormality must be described in terms of:
   (a) Localization: leaflet, annulus, chordate…
   (b) Mechanism: perforation, restriction, flail, prolapse
   (c) Etiology: endocarditis, dystrophy, ischemia, ventricular dilatation…

   The evaluation of the cardiac chamber's adaptation, non-dilated cavity with hyperdynamic heart attests to the acute character of the valve lesion, dilatation of the cardiac chamber attests to the chronic character, often this dichotomy is not obvious, and the only review of the old echography reports allows to make the difference.
2. CFD

   CFD allows the diagnosis and grading of valvular regurgitation, regurgitant flow area and vena contracta are two parameters which can easily be integrated into CPOCUS protocol
   (a) The regurgitant flow area represents the rate of the LA surface occupied by the regurgitant jet; it is widely used despite numerous limitations represented by the dilatation of the LA, variable load conditions, and the LV systolic function.
   (b) Vena contracta diameter: It represents diameter of the tightest zone of the regurgitant jet, between the proximal flow convergence and the distal jet expansion.
3. Spectral Doppler

   The use of the spectral Doppler is not integrated into the routine CPOCUS protocol; however, some aspects of this modality can be used reliably in assessing stenotic valvular lesion after a short training.

7.5.3 Pathologic Findings

7.5.3.1 MR

MR represents the systolic reflux of blood from the LV; it is caused by the non-hermetic closure of the MV, the amount of blood regurgitated in the LA depends on the size of the regurgitant orifice, pressure gradient between the LV and LA and, to a lesser extent, the systole duration. The causes of MR may be divided into primary MR caused by lesion of the mitral apparatus, and secondary mitral regurgitation caused by LV dilatation.

1. Two Dimensional Finding

   The pathologic modifications of the MV are represented by thickening, calcifications and the presence of perforations and vegetations, the coaptation leaflets' abnormality may be caused by prolapsed or flail leaflets and the restriction that may be the result of LV dilatation, ischemia, and rheumatic disease (Carpentier classification). The systolic anterior motion (SAM) of the MV represents a particular entity mainly seen in the hypertrophic myocardiopathy; however, it may be encountered in all hyperdynamic status with a small LV cavity and increased contractility. SAM refers to the systolic aspiration of the anterior mitral valve leaflet toward the septum that might cause LVOT dynamic obstruction.

   The association of normal-size left heart cavity with a hyperdynamic stat favors acute mitral valve regurgitation.
2. CFD Finding

   Mitral regurgitation is considered as severe when the jet area occupies more than 50% of the LA surface, a vena contracta width of more than 0.7 cm.

   The direction of the regurgitant jet can suggest the mechanism of the mitral regurgita-

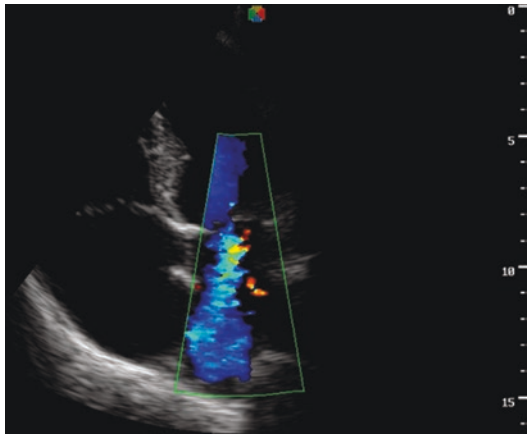

Fig. 7.2 Mitral regurgitation

tion; the central regurgitant jet often orients toward the primary mitral regurgitation causes (Fig. 7.2); while the lateralized regurgitant jet orients toward a secondary mitral regurgitation.

7.5.3.2 Aortic Regurgitation

Aortic regurgitation represents the diastolic blood reflux from the AO to the LV; it is caused by non-hermetic closure of the aortic valve; the amount of blood regurgitated in the LV depends on the size of the regurgitant defect, the gradient of pressure between AO and LV, and the diastole duration; the aortic regurgitation causes are represented by a degenerative and inflammatory diseases, infective endocarditis, aortic dissection, thoracic traumatism, and bicuspid aortic valve.

1. Two-Dimensional Finding

   The pathologic modifications of the aortic valve and the ascending aorta are represented by thickening and calcification of cusps, vegetations and cusp perforation, bicuspid aortic valve, aortic dilatation, aortic flap, and cusp prolapsed in the LV cavity (Carpentier classification).

   The size and function of the LV attest to the chronicity of the aortic regurgitations; non-dilated hyperdynamic LV favors acute aortic regurgitation.
2. Color Flow Doppler Finding

   Aortic regurgitation is generally considered as severe in presence when the ratio jet width to the LVOT diameter is more of 65%, or vena contracta width of more than 0.6 cm.
3. Tricuspid Regurgitations

   Tricuspid regurgitations are often secondary to RV dilation; the primary causes of tricuspid valve regurgitation are represented by endocarditis, rheumatic and degenerative diseases, Ebstein anomaly, carcinoid syndrome.
4. Two-dimensional finding: Are similar to MV regurgitation finding.
5. Color Doppler Flow

   Tricuspid regurgitation is considered as severe when the regurgitant jet occupies more than 50% of the RA surface or vena contracta width of more than 0.7 cm.

7.5.3.3 Stenotic Valvular Lesions

The normal anatomy with normal leaflets and cusp motion in 2D ultrasound exam excludes often severe stenotic valvular lesions; in the opposite presence of valvular thickening, calcifications are in favor of the latter. The surface opening of the mitral valve and aortic valve could be measured in PSAX view in the absence of significant calcifications. Otherwise, assessing the cavity in upstream relative to the stenosis can reflect the importance of the stenosis, the usage of the spectral Doppler to assess the stenotic valvular lesions belongs more to the advanced critical care echocardiography; however, using CWD through the aortic and mitral valve with measurement of the corresponding ITV can accurately assess the stenotic lesions, the mean gradient of a more than 15 mmHg for mitral valve and 40 mmHg for the aortic valve attests to the severity of the stenotic lesions.

7.6 Cardiomyopathies

7.6.1 Hypertrophic Cardiomyopathy

Hypertrophic cardiomyopathy (HCM) is a primary myocardial disease, it is a myocardial

hypertrophy not justified by the loading conditions; therefore, excluding the other causes of secondary myocardial hypertrophy is crucial before retaining the diagnosis of HCM. The HCM phenotype is estimated to be present in at least 0.2% of the general adult population [2]. HCM clinically and anatomically is a heterogeneous entity; it can be divided into obstructive and non-obstructive forms, and the LV wall hypertrophy may be localized or diffused.

7.6.1.1 Echographic Diagnosis of HCM

Asymmetrical isolated septal hypertrophy is the most encountered form of HCM, the obstruction at the level of LVOT is an inconstant finding.

7.6.1.2 Echographic Finding

1. Asymmetrical Septal Hypertrophy

   Asymmetrical septal hypertrophy is a common finding in HCM; however, it can be encountered in other pathologic circumstances, septal thickening of more than 15 mm, or septal to posterior wall thickening ratio of more than 1.3 attests to the presence of this condition [2], the hypertrophied segment of the IVS exhibits a hypokinetic pattern compared to the other heart segments appears hyperechoic. The 2D mode allows the diagnosis of the septal localization and possible extension to the other segments of the wall heart and apex.
2. Systolic Anterior Motion (SAM)

   SAM refers to the anterior systolic displacement of the mitral valve toward the IVS; the pathophysiology of this phenomenon is complex and it includes functional and anatomic modifications responsible for the aspiration of the MV in the LVOT by means of the Venturi phenomenon, which causes LVOT dynamic obstruction. The SAM is not specific to HCM; it is described only with 69% of HCM cases [7]; it may be encountered in all pathologic circumstances with hyperdynamic stats and small LV cavity.

   SAM is best seen in A4C view, and more delineated in PLAX view using the M-mode.
3. Mesosystolic Closure of the Aortic Cusps

   Mesosystolic closure of the aortic cusps reflects the dynamic obstruction of the LVOT; it can be identified in PLAX view by using the M-mode, placing the TM cursor through AOV shows a mid-systolic notch of the aortic box.
4. Intraventricular Obstruction

   The left ventricular outflow obstruction (LVOTO) is first located by the CFD, which shows the flow acceleration as aliasing zone, the confirmatory diagnosis is established by the CWD in A5C by applying CWD cursor through the LVOT aliasing zone, peak gradient is derived from the dagger-shaped envelope of the CWD by applying the Bernoulli modified equation, a peak gradient greater than 32 mmHg attests to a significant intraventricular obstruction.
5. MR

   MR is quasi-constant in the presence of LVOT dynamic obstruction; a careful observation must be paid in order to not confuse between the systolic mitral regurgitation jet and the flow acceleration of the dynamic obstruction.
6. Diastolic Dysfunction

   Diastolic dysfunction's severity is variable, most often impaired relaxation is mainly encountered, and a restrictive profile is seen more tardily.
7. Systolic Dysfunction

   Systolic dysfunction is seen later in the evolution of the disease.

7.6.2 Dilated Cardiomyopathy

Dilated cardiomyopathy (DCM) is an entity of heart disease in which the LV undergoes progressive dilatation concomitant with homogeneous fall in its systolic function; nevertheless, the LV wall thickness stays in the normal range. The whole morphologic and functional modifications are not in response to pathologic load conditions or coronary artery disease [2]. The main cause of the DCM is sporadic.

7.6.2.1 Echographic Finding

1. *Systolic function impairment (see the corresponding chapter).*
2. *Diastolic function impairment (see the corresponding chapter).*
3. *Other anomalies.*
   (a) *Valvular regurgitations:* caused by annulus dilatation and valvular restriction.
   (b) *PHT (see the PHT chapter).*

7.6.3 Restrictive Cardiomyopathy

Restrictive cardiomyopathy refers to an entity of myocardial disease characterized by a reduced ventricular compliance, causing very steep elevation of ventricular pressure in response to low volume modifications; the LV diastolic volume is normal or reduced; however, ventricular wall thickness is in the normal range [2], the echographic features may vary with the supposed etiology, and in most cases associate:

1. A modified echocardiographic aspect of the myocardium, which is heterogeneous and more hyperechogenic than usual, giving the myocardium the aspect of (granular sparkling).
2. Systolic dysfunction: Systolic dysfunction is seen in an advanced stage of the disease.
3. Diastolic dysfunction: It represents the cornerstone of echographic features and may vary from impaired relaxation to restrictive profile.
4. Other finding: Their presence can yield etiologic clues; the main anomaly can be associated variably with: pericardial effusion, IAS and atrio-ventricular (AV) valves thickening, atrial dilatation, and LV clot.

7.7 Acute Fibrillation and Other Arrhythmias

7.7.1 Atrial Fibrillation

Atrial fibrillation is the form of arrhythmia most commonly encountered in the general population; atrial fibrillation's prevalence seems to increase with age [8]; in acute atrial fibrillation, TTE can help to establish the diagnosis by applying TM cursor or PWD sampling volume through the MV when the electrocardiogram interpretation is doubtful or in the presence of artifact making its interpretation difficult; however, in the presence of tachycardia, the E and A waves merge making the rhythm distinction impossible; TTE allows the diagnosis of underlying cardiopathy like severe valvulopathy, which may require an emergency treatment to improve the clinical status of the patient; TTE can provide clues to estimate the systemic embolic risk, mainly by measuring the antero-posterior diameter or the volume of the LA *(see the biatrial enlargement in Fig. 7.3.)*, or establishing emergency anticoagulation when clot inside the LV is seen; however, performing an electro-version of an acute fibrillation on the basis of data yielded from TTE is not a wise decision due to its low sensitivity in clot detection, mainly the non-adequate visualization of the auricle.

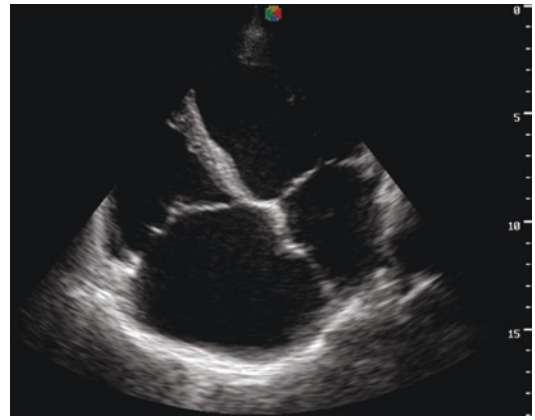

Fig. 7.3. *Biatrial enlargement* seen in patient with atrial fibrillation

7.7.2 Other Arrhythmia

(See Chapter Advanced Life Support)

7.8 Prosthetic Valves

7.8.1 Introduction

Prosthetic valves are the invention supposed to cure definitively the valvular pathology; owing to the technological advances, prosthetic valves are safer and can reliably be assessed in order to detect precociously any dysfunction. In acute medicine, encountering patients with prosthetic replacement is not uncommon; therefore, knowing the basic assessment of the prosthetic valves is useful. This chapter aims to introduce the basic assessment of prosthetic valve and gives clues to the confirmed practitioner in CPOCUS protocol to judge grossly the prosthetic valve function; if any doubt arises, asking for a comprehensive TTE or more TOE is mandatory. Whenever possible, consider asking for the reference values of the prosthetic valve initial exam to compare the current with the ex-values; the results of the echocardiographic exam must be interpreted according to the clinical context.

7.8.2 2D and TM Features of Replacement Valves

7.8.2.1 Mechanical Replacement Valves

1. Ball-Cage Type

   An echographic study is performed in A4C view for the mitral insertion and A3C view for the aortic insertion, allowing the ultrasounds beam to be aligned relatively to the ball motion, in TM-mode ball motion draws a niche aspect, a slight bounce at the beginning of the diastole and systole for the mitral and aortic insertion of the valve, respectively, may attest to the normal functioning of the valve. The 2D mode allows visualization of all components of the valve.
2. Single Tilting Disc

   Ultrasound scanning of these types of mechanical replacement valves must consider a view in which the ultrasound beam meets the tilting disc vertically at its maximum excursion for optimal visualization of the latter.

   In both mitral and aortic localization of the replacement valve, TM mode visualizes the motion of the sewing ring and the disc which shows a niche motion, the latter open in systole or diastole for the aortic and mitral localization, respectively; in 2D mode, the disc is perfectly seen in its maximum tilting.
3. Bi-Leaflet

   This type of valve replacement is best explored in PLAX or PSAX views, the sewing ring is showed as two parallel lines with the same pattern motion as the aortic wall; between the two lines, the opening leaflets draw a double opposite niche aspect, 2D mode shows the circular sewing ring, with two line corresponding to the opening of the two leaflets, disappears when the valve is closed.
4. Biological Valves

   Biological valves are best explored in PLAX or PSAX views; in TM-mode, the sewing ring is shown as two parallel lines with the same pattern motion as the aortic wall, the leaflets describe the same box pattern as native valves; PSAX view permits the visualization of the sewing ring and the three leaflets, when all leaflets are closed, they describe the Y character. The stentless biological valves give the same echographic pattern as native valves, with thickening zone corresponding to the surgical stitches.

7.8.3 Doppler Features of Replacement Valves

In all cases, when performing Doppler study of replacement valves, preferably the view that allows the best alignment with the flow through the replacement valve; therefore, the Doppler study is best performed in A4C view for mitral location and the PLAX right, A5C, A3C, and suprasternal views for the aortic location, in CPOCUS protocol setting CWD with measurement of mean gradient seem to be the most adapted; in all cases, a careful interpretation of the mean gradient is essential because it is influenced by the flow through the replacement valve and the heart rate. Color Doppler allows assess-

ment of the trans-prosthetic flow, trans- and para-prosthetic regurgitations, trans-prosthetic physiologic jets are a normal finding which is called washing jets, it is a small leakage intentionally created by the producer to reduce the valve thrombosis incidence, its flow profile is predictable according to the type of the replacement valve.

7.8.4 Pathologic Findings

Valve replacement dysfunction may result from valve replacement disinsertion, thrombosis, and biologic valve degeneration.

1. Valve Replacement Disinsertion
   Valve replacement disinsertion is the result of one or more stitch failures; it may happen spontaneously or in the setting of endocarditis; in TM- and 2D-mode when disinsertion is significant, the prosthetic valve may present a tilting motion, TM-mode may show signs of volume overload as a consequence of the regurgitations, while color Doppler can confirm the presence of prosthetic disinsertion when visualizing and quantifying the para-prosthetic regurgitation flow; any presence of paraprosthetic regurgitation causes an elevation in trans-prosthetic gradient; the estimation of paraprosthetic regurgitation uses the same modality as in native valve; however, it is more difficult to apply.
2. Prosthetic Thrombosis
   Prosthetic thrombosis can cause a prosthetic obstruction and less frequently trans-prosthetic regurgitation. TM-mode shows motion abnormality of the mobile part of the prosthetic valve. 2D-mode may visualize directly the thrombosis; however, differential diagnosis between thrombosis, vegetation, stitch, or fibrin strands is complicated, the measurement of mean gradient trans-prosthetic flow allows the estimation of the prosthetic valve obstruction; the value calculated is compared to the reference value, mean gradient of more than 5 mmHg raises suspicion about the mitral prosthetic valve obstruction; when it is more than 10 mmHg, the obstruction is considered as severe [2]; for the aortic emplacement, mean gradient greater than 35 mmHg favors aortic prosthetic valve obstruction [2], color Doppler in these circumstances may show an abnormal eccentric flow with abnormal aliasing, or the disappearance of the normal physiologic trans-prosthetic valve regurgitation.
3. Biologic Valve Replacement Degeneration
   2D- or TM-mode may show thickening or calcification of the cusps of the prosthetic valve, and replacement valve may show signs of obstruction or the appearance of neo-regurgitations; moreover, cusps may be prolapsed.

7.9 Endocarditis

Any suspicion of endocarditis imposes prompt realization of TOE.

7.9.1 Introduction

Endocarditis is the infective inoculation of the endocardium, TTE is the cornerstone in the initial evaluation and diagnosis of patients with endocarditis suspicion; furthermore, it allows diagnosis of complications, hemodynamic evaluation, therapeutic adaptation, and close follow-up. The main echocardiographic lesions in endocarditis are vegetations and destructive lesions.

7.9.2 Vegetations

Vegetations may not be visualized in the early stages of endocarditis; therefore, repeating echographic exam is crucial. Valvular vegetations are the common form, frequently located in the valvular surface facing up the heart cavity with lower pressure; however, vegetations may be located everywhere in the endocardium and implanted material, moreover in the proximal aorta or the pulmonary artery. Vegetations appear

in TM- or 2D-mode as hyperechogenic pedunculated, or sessile structures with different sizes; when vegetations are pedunculated, they are animated with a random motion. Pedunculate feature, mobility, size, and the mitral location of the vegetation determined the embolic potential; sometimes vegetation diagnosis may be complex, mainly in the presence of old scars of endocarditis, or non-infective vegetations, and in valve replacement.

7.9.3 Destructive Lesions

Destructive lesions represented mainly by:

- Valvular lesion: perforation, rupture, and prolapsed leaflets valve, chordae tendineae rupture.
- Annular and peri-annular abscess mainly in the aortic valve, IVS abscess can be complicated with atrio-ventricular block.

7.9.4 Hemodynamic Consequences

Hemodynamic consequences are mainly represented by the acute valvular regurgitation, pulmonary embolism of the right heart vegetations mainly in intravenous drug abuse, and pericardial effusion.

7.10 Advanced Cardiac Life Support (Cardiac Arrest)

7.10.1 Introduction

Cardiac arrest is considered as the absolute emergency in acute medicine; therefore, any delay or improvisation is accepted when providing adapted advanced cardiac life support. The American Heart Association states that integration of ultrasounds in the setting of cardiac arrest is feasible in the presence of a qualified sonographer [9]; CPOCUS protocol allows the understanding of the causal mechanism; therefore, it allows to act etiologically when the mechanism in cause is potentially reversible, it distinguishes the underlying electrical activity pattern and screening for the return to an efficient, mechanical, spontaneous activity; finally, it gives clues to stop resuscitation effort in standstill cardiac arrest.

7.10.2 Diagnostic Approach

The underlying electrical activity guides the advanced cardiac life support efforts, correcting reversible causes of cardiac arrest is crucial and life-saving.

7.10.2.1 Ventricular Fibrillation

In presence of ventricular fibrillation or any other pulseless arrhythmia, defibrillation must be performed without any delay, ventricular fibrillation with small tremulations sometimes can be mistakenly considered as asystole; therefore, echocardiography can redress the diagnosis; it is worth mentioning that after restituting mechanically effective activity, the presence of non-homogenous LV contraction may orient the diagnosis toward an ongoing myocardial infarction [1].

7.10.2.2 Pulseless Electrical Activity and Asystole

These rhythm patterns may result from potentially reversible causes of cardiac arrest.

1. Hypovolemia

   The occurrence of a cardiac arrest in the setting of deep hypovolemia is suspected in the presence of a low preload statue; the analysis of the diameter of the IVC and the respiratory variability is inaccurate in the presence of chest compression and mechanical ventilation; however, the presence of underfilled heart chambers may be evocative; otherwise, the extra cardiac application of POCUS protocol can detect blood collection in the chest, abdomen, pelvis; in order to reverse the cause of the cardiac arrest, emergent perfusion of fluids after a blood transfusion is started and urgent surgical consultation is mandatory.

2. Pneumothorax

   Ultrasound scanning of the wall chest may visualize the presence of physiological pleura sliding; therefore, it excludes the presence of pneumothorax in the scanning zone; absence of pleura sliding is not, however, pathognomonic of pneumothorax presence, in all cases in the presence of clinical or echographic suspicion of pneumothorax, a needle decompression must be considered.
3. Cardiac Tamponade

   The presence of a large pericardial effusion must be considered as a potential cause of cardiac arrest; therefore, an immediate thoracocentesis must be considered.
4. Pulmonary Embolism

   In a cardiac arrest setting, after restituting mechanically effective activity, the presence of RV dilatation may orient the etiological diagnosis toward the pulmonary embolism mechanism; nevertheless, in this context, the RV dilatation may be the consequence of high-volume fluid perfusion combined with the fact that can be a usual finding after reversal of a prolonged ventricular fibrillation [10], without ignoring the ongoing mechanical ventilation effect, the fast scan of low limb veins may visualize the thrombosis and orient toward the embolic mechanism; in all cases, thrombolysis must be considered in presence of high clinical probability of embolism.

7.10.3 Prognostic

Standstill cardiac arrest has a poor prognosis; it must be differentiated from the valve flutter, which may be caused by breast compression, mechanical ventilation, and fluid shift, patient diagnosed with pseudo pulseless electrical activity that is defined as the absence of palpable pulse; however, electrical activity in the monitor and mechanical heart activity ultrasound are detectable, is considered as sub-group of pulseless electrical activity with better prognosis [11].

7.10.4 Technique

1. Ultrasound Transducer

   Phased-array transducer is the most adapted transducer for the heart imaging; however, the linear ultrasound transducer may be preferable for thoracic or vein exams.
2. Ergonomy

   Echographer placing himself at the patient's right hip is the best ergonomic place because it allows free access to the thorax abdomen and inferior limbs.
3. Image Acquisition

   To avoid interference with the resuscitation maneuvers, the sub-costal is the only window accessible for the heart imaging when heart compressions are performed; during this phase, imaging of the abdomen, IVC, and veins of the inferior limbs is feasible, when pulse check is performed, the sonographer may use the other windows to best imaging the heart and assessing the potential presence of pneumothorax.
4. Protocols

   The local protocol may be developed in every institution, considering the availability of personnel and equipment.

7.11 Pericardiocentesis

7.11.1 Introduction

The only logical treatment for patients with tamponade condition is pericardial removal of fluid or pericardiocentesis. Surgical drainage is more used for traumatic and bacterial pericarditis; also, pericardiocentesis may be performed for etiological diagnosis.

7.11.2 Contraindications

Except for emergency setting, before performing pericardiocentesis, hemostasis disturbance must be corrected.

7.11.3 Ultrasound Technique

Except an extreme emergency, a blind technique for pericardiocentesis must be avoided; ultrasound-guided pericardiocentesis has a success ratio of 97% and complication rate of 4.7% [3]. Apical, sub-costal, and parasternal windows can be used for the procedure, while sub-costal window is the most used. An initial ultrasound scan allows to identify the largest zone of the pericardial effusion and the thoracic wall entry point with the shallowest trajectory; for more safety, the max needle penetration distance may be measured, in plan technique is may be the safest method to enter the pericardial sac; however, out of plan technique is feasible, placing the patient in semi-supine position at 30–45° may be helpful; using the sub-costal approach, angiocath 18 gauge or long spinal needle G20 is inserted in plan, aiming for the pericardial sac, the aspiration of fluid attests to the optimal needle tip position; for more confirmation, agitated saline can be injected through three-way stopcock; the observation of bubbles in the pericardial sac is a confirmatory finding, indwelling catheter may be placed using the Seldinger technique.

7.11.4 Complications

- Cardiac dysrhythmias.
- Cardiac puncture.
- Pneumothorax.
- Coronary artery and internal thoracic artery injury.
- Peritoneal, stomach puncture, and liver injury.

References

1. Mayo PH, Beaulieu Y, Doelken P, Feller-Kopman D, Harrod C, Kaplan A, et al. American College of Chest Physicians/La Société de Réanimation de Langue Française statement on competence in critical care ultrasonography. Chest. 2009;135(4):1050–60.
2. Lancellotti P, Zamorano JL, Habib G, Badano LP. European Association of Cardiovascular Imaging, editors. The EACVI Textbook of Echocardiography. 2nd ed. Oxford: Oxford University Press; 2017. p. 651.
3. Soni NJ, Arntfield R, Kory P. Point-of-care ultrasound. 2nd ed. Philadelphia, PA: Elsevier; 2020. p. 525.
4. Salerno A, Haase DJ, Murthi SB, editors. Atlas of critical care echocardiography. Switzerland: Cham, Springer; 2022.
5. Parasuraman S, Walker S, Loudon BL, Gollop ND, Wilson AM, Lowery C, et al. Assessment of pulmonary artery pressure by echocardiography—A comprehensive review. IJC Heart Vasc. 2016;12:45–51.
6. Bertaso AG, Bertol D, Duncan BB, Foppa M. Epicardial fat: definition, measurements and systematic review of main outcomes. Arq Bras Cardiol. 2013;101(1):e18–28. https://doi.org/10.5935/abc.20130138.
7. Klimczak C, Fumat C. Échocardiographie clinique. 7th ed. Issy-les-Moulineaux: Elsevier Masson; 2016. (Collection de cardiologie pratique)
8. Kim TS, Youn HJ. Role of echocardiography in atrial fibrillation. J Cardiovasc Ultrasound. 2011;19(2):51.
9. Link MS, Berkow LC, Kudenchuk PJ, Halperin HR, Hess EP, Moitra VK, et al. Part 7: Adult advanced cardiovascular life support: 2015 American Heart Association guidelines update for cardiopulmonary resuscitation and emergency cardiovascular care. Circulation. 2015;132(18_suppl_2):S444–64. https://doi.org/10.1161/CIR.0000000000000261.
10. Berg RA, Sorrell VL, Kern KB, Hilwig RW, Altbach MI, Hayes MM, et al. Magnetic Resonance Imaging During Untreated Ventricular Fibrillation Reveals Prompt Right Ventricular Overdistention Without Left Ventricular Volume Loss. Circulation. 2005;111(9):1136–40.
11. Prosen G, Križmarić M, Završnik J, Grmec Š. Impact of modified treatment in echocardiographically confirmed pseudo-pulseless electrical activity in out-of-hospital cardiac arrest patients with constant end-tidal carbon dioxide pressure during compression pauses. J Int Med Res. 2010;38(4):1458–67.

Pediatric and Congenital Heart Disease

8

Noreddine Bouarroudj and Cherif Bouzid

8.1 Patent Foramen Ovale

8.1.1 Introduction

Patent foramen ovale (PFO) is a remnant of the fetal circulation which is supposed to be shut with the first breaths of the newborn; however, it is not the case with 15–35% of the normal population [1], this sub-group of subjects is more exposed to ischemic stroke, mainly cryptogenic. The atrial septal aneurysm is another abnormality of IAS, defined as protrusion of more than 1 cm of the IAS in either atria; this abnormality is associated to PFO with more than 60% of cases [1].

8.1.2 Diagnosis of PFO

The opening of the foramen ovale depends on the pressure gradient between two sides of the IAS; therefore, maneuvers allowing the increase of the RA pressure and the reduction of the LA pressure are employed. The spontaneous visualization of PFO in 2D-mode is rare. The use of color Doppler and contrast test, combined with dynamic tests, is the standard practice; by all means, the sensitivity of TTE is estimated approximately to be 90%, inferior to the sensitivity of TOE estimated approximately to be 100% [1], a contrast test is performed by using two syringes containing air and saline, which is passed from syringe to another through a three-way stopcock, the agitated saline is then injected intravenously to the patient, which is asked to perform concomitantly Valsalva maneuver, the presence of the bubbles in the LA in two or three heartbeats attests to the presence of PFO.

8.2 Atrial Septal Defects

8.2.1 Introduction

Atrial septal defect (ASD) is a group of pathology, a consequence of a defect in the IAS, the sinus venosus, or in the roof of the coronary sinus; it represents 7–10% of the overall congenital cardiac defect [2].

8.2.2 Anatomic Classification

8.2.2.1 ASD Ostium Secundum

ASD ostium secundum is the most common form, usually located in the center of the fossa ovale, in the septum premium. As shown in Fig. 8.1, a large ASD ostium secundum.

N. Bouarroudj (✉)
Department of Anesthesiology and Critical Care, Clinique Maissalyne, Constantine, Algeria
e-mail: bouarroudj@bouarroudj.net

C. Bouzid
Department of Anaesthesia and Critical Care, El Afia Hospital, Mila, Algeria

© The Author(s), under exclusive license to Springer Nature Switzerland AG 2024

N. Bouarroudj et al. (eds.), *POCUS in Critical Care, Anesthesia and Emergency Medicine*,
https://doi.org/10.1007/978-3-031-43721-2_8

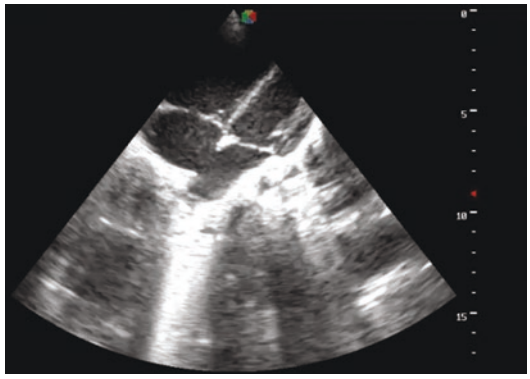

Fig. 8.1 ASD ostium secundum

8.2.2.2 ASD Sinus Venosus

ASD sinus venosus results from the left shifting of the superior vena cava (SVC), and rarely IVC. SVC overrides the IAS; this entity is frequently associated with a partial anomalous pulmonary venous connection, mostly abnormal connection of the superior right pulmonary vein directly in the SVC.

8.2.2.3 ASD Ostium Premium

ASD ostium premium is a manifestation of abnormal heart cushioning development, primarily associated with variable grade of atrioventricular canal abnormality. It is located in the most anterior and inferior part of the IAS.

8.2.2.4 ASD Coronary Sinus

ASD coronary sinus is a rare entity that results from a defect or the total absence of the roof of the coronary sinus; the left superior vena cava is the abnormality which is frequently associated with this defect.

8.2.3 Technique

The sub-costal window is the most appropriate for the diagnosis of ASD, owing to the perpendicular orientation of the ultrasound beam relatively to the IAS; sometimes by rotating the ultrasound probe 90° counterclockwise from sub-costal view 4C, a view similar to the trans-esophageal bi-caval view may be acquired, and it is useful for the diagnosis of ASD sinus venosus essentially; in 2D echocardiography, ASD appears as solution of continuity of IAS; using color Doppler is mandatory for screening, confirmation, and assessment of the ASD.

8.2.4 Echographic Finding

8.2.4.1 Type of the ASD

- ASD ostium secondum is best visualized in the sub-costal view.
- ASD ostium premium is best visualized in sub-costal view and A4C view.
- ASD sinus venosus is best visualized in sub-costal view; however, in adults, it may require TOE.
- ASD coronary sinus is best suspected in the presence of enlarged coronary sinus in PLAX view, while a direct visualization of the defect is difficult to obtain.

8.2.4.2 Size of the Defect

The size of the defect is measured at the end of the diastole in multiple views because the defect may have shapes other than circular; the maximal measured diameter when it is between 3 to 5 mm and 5 to 8 mm and greater than 8 mm is respectively considered as small, moderate, and large ASD.

8.2.4.3 Evaluation of the Effect of the Shunt

The left to right shunt is considered as important in the presence of one or more of the following elements:

- Right heart cavity enlargement: RA, RV, pulmonary artery.
- LA enlargement.
- Diastolic flattening of the IVS, sometimes IVS may be paradoxical.
- PHT.

8.3 Ventricular Septal Defect

8.3.1 Introduction

Ventricular septal defect (VSD) is the presence of abnormal communication between the two ventricles or between the LV and the RA (Gerboud defect); they may be isolated or associated with other congenital abnormalities, and it is considered as one of the most frequent congenital defects, it represents at least 20–30% of the overall congenital defects [3].

8.3.2 Pathophysiology

VSDs are responsible for left to right heart shunting, the volume of the shunted blood on the defect size and the pressure difference between the two ventricles; therefore, VSDs are responsible for RV, LA, and LV volume-overload and dilatation, combined with high pulmonary blood flow; the latter causes initially a reversible PHT, then with the development of media hypertrophy and the intimal hyperplasia, PHT becomes irreversible; in long-standing VSDs, the PHT is or more higher than the systemic arterial pressure, causing a shunt direction inversion (this phenomenon is named Eisenmenger syndrome).

Regional effect and complications on the location of the defect, the high jet velocity in the mid-RV may cause a muscular bundle hypertrophy, which tends to divide the RV cavity into two subcavities, giving the aspect of a double-chambered RV. In supracristal and perimembranous VSDs, the poor support to the aortic valve caused by the VSD defect, and the close relation to the aortic valve relatively to the shunting jet may cause aortic valve regurgitation; in all VSD locations, the endocarditis occurrence is a potential and redoubtable complication.

8.3.3 Anatomy and Imaging

8.3.3.1 Membranous VSD (Gerboud Defect)

- The membranous septum is divided by the septal insertion of the tricuspid valve into two portions called atrioventricular (AV) and interventricular components; owing to the anterior shifting of the tricuspid valve, the atrioventricualr portion is located between the LV and the RA and extends from the tricuspid to the mitral insertion of the two valves.
- A defect at the posterior level of the membranous septum causes a direct shunt from the LV to the RA.
- This defect is best visualized in A4C view.

8.3.3.2 Perimembranous VSD (Infracristal)

- The interventricular portion of the membranous septum is superiorly limited by the atrioventricular portion of the membranous septum, anteriorly by the outlet septum, inferiorly by the trabecular septum, and posteriorly by the inlet septum.
- Perimembranous VSD involves the membranous septum and the adjacent area, the fundamental adjacent landmark is represented by the septal leaflet of the tricuspid valve.
- Atrioventricular conduction system lies in close relationship to the posterior and inferior border of the perimembranous VSD.
- Pay close attention to the septal leaflet of the tricuspid valve which can obstruct totally or partially the VSD or allows flow shunting in the RA.
- It is the most prevalent VSD type—80%.
- The defect is best visualized in PLAX, PSAX, and A4C views.

8.3.3.3 Muscular VSD

- The most common VSD is in newborns.
- Relatively to the location in the muscular septum, VSDs are divided into: anterior, posterior, mid, and apical.
- Multiple small VSD gives the aspect of a Swiss cheese. Sometimes too small to be seen in 2D; however, applying color Doppler allows the overcoming of this limitation.
- The defects are best visualized in PLAX, PSAX, sub-costal 4C views.

8.3.3.4 Inlet VSD

- The inlet septum is located posteriorly and inferiorly to the membranous septum, the

basal and apical borders are represented by the atrioventricular valve and the septal insertion of the latter, respectively.
- Inlet VSDs are almost exclusively integrated in the setting of endocardial cushion defect spectrum.
- The defect is best visualized in the PSAX, A4C, and sub-costal views.

8.3.3.5 Supracristal VSD (Sub-pulmonic, doubly-committed, Sub- and Juxta-Arterial, Outlet VSD)

- Supracristal VSD involves the infundibular septum, which separates the outflow tract of both ventricles, inferiorly limited by the membranous septum, conus papillary muscle, and superiorly by the pulmonary valve.
- More prevalent in oriental population.
- The defect is best imaged in the short and long axis of parasternal and sub-costal windows.

8.3.4 Steps of Echocardiography Exam

8.3.4.1 Location of the VSD

IVS must be inspected in all views, 2D is combined with color Doppler sweep to avoid missing of the small VSD; the more the pressure gradient between the two ventricles is low, the visualization of the defect becomes harder to spot.

8.3.4.2 Size of the Defect

The size of the VSD is estimated relative to the size of the aortic annulus in 2D mode; VSD is small, moderate, or large if the VSD diameter is less than one third, between one and two third, and more than two third of aortic annulus diameter, respectively.

8.3.4.3 Flow Direction

The flow direction is determined by the pressure gradient between the two ventricles; in small restrictive VSD it is left to right shunt; in the presence of PHT, the shunt may be bidirectional, further inversed in the presence of Eisenmenger syndrome.

8.3.4.4 Estimation of the Size of Shunt

The volume of blood shunting across the VSD is function of the size of the defect and the pressure gradient between the two ventricles; the latter is estimated by perfect alignment of the CWD cursor through the defect and the measurement of the max velocity, applying the modified Bernoulli equation allows the measurement of the pressure gradient between the two ventricles. The pulmonary artery pressure may be calculated by assuming the LV max pressure equals the systemic blood pressure:

$$LV\max P - RV\max P = 4V\max^{2}$$

$$\mathrm{RV}\max \mathrm{P}^{2} = 4V\max \mathrm{P}^{2} - LV\max \mathrm{P}^{2}$$

$$PASP = RV\max P^{2} + RAP$$

8.3.4.5 Estimation of the Effect of the VSD

- The volume is reflected by the dilatation of the RV, LA, and the LV.
- Estimation of the pulmonary artery resistance is reflected by PASP measured by applying the Bernoulli equation in the absence of RVOT or pulmonary stenosis through the tricuspid regurgitant jet, or at the level of the VSD.
- Look for hypertrophied RV muscle bundle in 2D, particularly PSAX view at the level of AOV.
- Look for aortic regurgitation in paramembranous and supracristal VSDs.
- Assessing alignment of the conal septum, anterior malalignment is responsible for RVOT obstruction (RVOT); however, the posterior malalignment is responsible for LVOT obstruction.
- Endocarditis is a redoubtable complication.

8.4 Patent Ductus Arteriosus

8.4.1 Introduction

Patent ductus arteriosus (PDA) refers to the persistence of fetal circulatory relic, which usually connects the descending aorta at the level just below the sub-clavian artery to the pulmonary

artery; normally ductus arteriosus is spontaneously closed within the first week after birth, PDA incidence is estimated to be 56.7 cases per 100,000 live births [1].

8.4.2 Steps of Echocardiography Exam

8.4.2.1 Positive Diagnosis of PDA

PDA is suspected in PSAX view at the level of the AOV when CFD applied through the pulmonary artery shows retrograde flow mainly along the left border of the pulmonary artery (Fig. 8.2); more cranial tilting or placing the transducer few inter-costal spaces up allows a direct visualization of the PDA, the main pulmonary artery trifurcate (prong view), by rotating the probe in clockwise manner may allow a visualization of the PDA in all its length—another alternative is the visualization of the PDA in a suprasternal view.

When PDA shunts from right to left, the retrograde jet in the pulmonary artery is absent, where only the direct visualization of PDA allows the diagnosis.

8.4.2.2 Evaluation of the Size of PDA

- Indirect evaluation by assessing the effect of shunt in the left heart and pulmonary pressure.

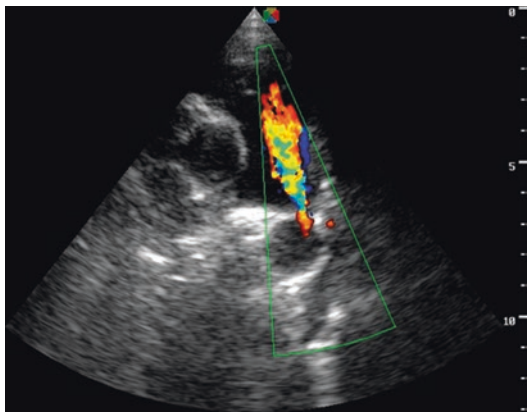

Fig. 8.2 PDA is suspected in PSAX view at the level of the AOV. Observe the retrograde jet in the pulmonary artery

- Direct evaluation by calculating the ratio of the minor diameter of the PDA relatively to the diameter of the left pulmonary artery at its origins, a ratio less than 0.5, between 0.5 and 1, and greater than 1 reflects the presence of small, moderate, and large PDA, respectively.

8.4.2.3 Evaluation of the Direction of the Shunt

The direction of the shunt is attested by applying color Doppler through the PDA, or aligning CWD relatively to the shunt.

8.4.2.4 Evaluation of the Effect of PDA

- Evaluate the LV cavity size.
- Assess the PA pressure.
- Endarteritis is a possible complication.

8.5 Tetralogy of Fallot

8.5.1 Introduction

Tetralogy of Fallot (ToF) is the cyanotic heart defect that is the most prevalent, encountered in 0.33 per 1000 live births, and represents 6.7% of the overall congenital heart defects [1]; the four main components of the defect are the VSD, overriding aorta, pulmonary stenosis, and RV hypertrophy; however, the anatomic point of view considers the main lesion as the anterior displacement of the conal septum which causes: malalignment of large VSD, the overriding of the aorta, the pulmonary stenosis, and the RV hypertrophy which is the consequence of the pulmonary stenosis. There is a spectrum of the disease with different degrees of the four lesions:

- Form with moderate pulmonary stenosis, with predominant left-to-right shunting, closer to a large VSD presentation.
- In the severe form, the pulmonary stenosis is too critical, the pathology becomes ductal dependent.
- In the extreme forms of pulmonary atresia with an absence of main pulmonary artery, the pulmonary vasculature is insured by aortic collaterals.

- A particular form of ToF is the absence of a pulmonary valve and the ductus arteriosus, associated with aneurismal dilatation of the main pulmonary artery branches, which may compress the airway causing respiratory distress in the newborn.

8.5.2 Objective of the Echographic Exam: Fig. 8.3

- Identify underlying anatomy, mainly the conal septum deviation and the resulting RVOT obstruction.
- Demonstrate the presence of the pulmonary artery main trunk and branches.
- Assess the presence of PDA.
- Assess the presence of associate lesions.

8.5.3 Echography Imaging of the Main Lesions

8.5.3.1 VSD

The large VSD consequent to the malalignment is best seen in PLAX and A5C views; the degree of the aortic overriding gives a clue to estimate the conal deviation, the PSAX view differentiates ToF from the other truncal abnormalities, the pulmonary atresia with open septum is excluded by the presence of anterograde flow in the RVOT and main pulmonary artery, the common truncus arteriosus by the presence of the two great arteries, mitral–aortic fibrous continuity excludes the diagnosis of the double right ventricle outflow tract, it is difficult to assess the presence of additional VSDs despite the use of color Doppler, owing to the presence of the large VSD, which reduces the gradient between the two ventricles.

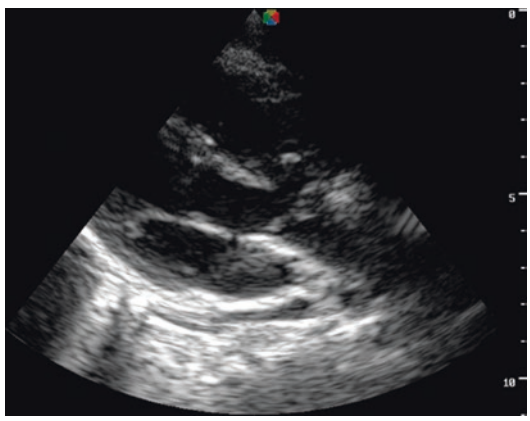

Fig. 8.3 Tetralogy of Fallot with VSD with Aortic override

8.5.3.2 Assessment of Pulmonary Tract

The 2D imaging coupled with CFD in the PSAX view allows the assessment of obstacles and stenosis of the RVOT, the pulmonary valve, pulmonary artery main trunk and main branches; the main right pulmonary artery is visualized in suprasternal long axis view; nevertheless, the left main pulmonary artery is difficult to image, CWD applied along the pulmonary tract shows high velocity in the obstructed zone, dynamic obstruction is suspected in the presence of late peak with dagger aspect of the spectral Doppler envelope.

8.5.3.3 Associated Lesions

- Right aortic arch visualized in suprasternal long and short axis.
- Atrioventricular septal defect (AVSD).
- Coronary artery abnormality.
- PDA and ASD.

8.6 Transposition of the Great Arteries (Complete TGA or D-TGA)

8.6.1 Introduction

Transposition of the great arteries occurs when the aorta arises from the RV and pulmonary artery arises from the LV; therefore, it is a discordant ventriculo-arterial connection; in D-TGA, the other segments of the heart are normally connected; however, the great artery is transposed, often the aorta arises anteriorly and to the right of the pulmonary artery, the D-TGA represents the second cause of cyanotic heart disease after ToF with an incidence approximately 31.5 per 100,000 live births [4].

ALGrawany

8.6.2 Pathophysiology

In D-TGA condition, the systemic and pulmonary artery circulations are placed in parallel each relatively to the other:

- The deoxygenate blood arrives to the RA, the RV, then the aorta toward the organs.
- The oxygenate blood arrives to the LA, the LV, then to the pulmonary artery toward the lungs.

The only possible mixing sites of the oxygenate and deoxygenate blood are represented by the presence of ASD, PDA, and VSD as associated lesions.

8.6.3 Objective of the Echographic Assessment

- Identify the segmental anatomy: {S,D,D}.
- Evaluation of shunts.
- Relative size and function of the aortic and pulmonary valve.
- Associated lesions: mainly VSD and pulmonary stenosis.

8.6.4 2D-Imaging Mode

8.6.4.1 Acquisition

1. Sub-costal Window
   (a) Sub-costal long axis view with sweep from posterior to anterior:
      - Situs solitus.
      - D-loop.
      - Transposed ventriculo-arterial connection, the bifurcate vessel representing the PA arises posteriorly from the LV; the anterior vessel represents the aorta.
      - Assess the presence of ASD and PFO.

   (b) Sub-costal short axis view with sweep from the base to the apex, confirms the situs, looping, and transposition of the great vessels.
2. Apical Window
   Apical views with sweeping from posterior to anterior confirm the transposition of the great vessels, allow screening for VSD, and the anatomic evaluation of the outflow tracts.
3. Parasternal Window
   (a) PLAX View
      - Great vessels posed in parallel manner (shotgun barrel image).
      - Fibrous mitral-pulmonary continuity excludes the diagnosis of the double outlet RV.
      - Assess the presence of VSD and outflow tract obstruction.

   (b) PSAX View
      - The AOV is anterior and often placed on the right side of the pulmonary valve.
      - Assess the presence of VSD.

   (c) Suprasternal View
      - Assess the presence of PDA and its size.

8.6.4.2 Analysis

- Assess the size of the shunts: ASD, PDA, and possibly VSD.
- Assess the presence of pulmonary stenosis.

8.6.5 Doppler Imaging

8.6.5.1 Acquisition

1. Sub-costal View
   (a) Assess the presence of ASD by applying color Doppler over the IAS.
   (b) Assess the presence of VSD by applying color Doppler over the IVS, in the presence of a large VSD or PDA, the gradient between the two ventricles decreases, making the diagnosis of associated VSD hard; acquire the max velocity of the flow by means of CWD.
   (c) Assess the presence of obstruction in the RVOT, LVOT, and corresponding valves.
2. Apical View
   (a) Assess the presence of VSD.
   (b) Assess the presence of obstruction in the RVOT, LVOT, and corresponding valves.
3. Parasternal View
   (a) Assess the presence of VSD.
   (b) Assess the presence of obstruction in the RVOT, LVOT, and corresponding valves.

4. Suprasternal view
   (a) Use color Doppler and PWD to determine the direction of the shunt.
   (b) Assess the presence of hypoplasia of the arch using color and spectral Doppler, mainly in the presence of RVOT obstruction.

8.7 Atrioventricular Septal Defects

8.7.1 Introduction

The term *atrioventricular septal defect* (AVSD) refers to an entity of congenital defects, characterized by the presence of a common atrioventricular (AV) junction associated with AV septation defects, resulting from primary abnormality of endocardial cushion development. AVSD is present in more than 40% of patients with Down syndrome [4].

The group of AVSD is divided into three sub-groups:

- Complete AVSD associates Inlet VSD (IVSD), premium ASD, and single AV junction.
- Transitional AVSD associates IVSD which may be variably occluded by AVV chordal tissue, two AVV orifices, cleft of the left AVV.
- Partial AVSD associates two AVV orifices, cleft of the anterior leaflet of the left-sided AVV.

Rastelli classification of AVSD is based upon the anterior bridging leaflet insertion:

- Rastelli A: anterior bridging leaflet attached to the crest of the IVS.
- Rastelli B: anterior bridging leaflet attached to the right side of the IVS.
- Rastelli C: anterior bridging leaflet has non-attachment to the crest of the IVS.

8.7.2 2D-Imaging Mode

8.7.2.1 Anatomic Finding

- A4C view allows assessment of the premium ASD, IVSD, and the AVV(s), the AVV(s) is situated in the same plan with no advancement of the right-sided AVV relatively to the left one, the premium ASD and the IVSD are just above and below the plan of the AVV(s), respectively; furthermore, the balance of the AVV(s) relatively to the ventricles and AVV regurgitation are assessed in the A4C view.
- The premium ASD is best evaluated in sub-costal view, the PSAX and sub-costal short axis views allow the best visualization of the AVV(s), the balance of the AVV(s) relatively to the ventricles; furthermore, establishment of Rastelli classification.
- Classically, in a normal heart, the aortic valve is wedged between the mitral and tricuspid valves; in all AVSD and notably partial AVSD, the aortic valve is high placed (unwedged) causing elongation of the LVOT; LVOT obstruction is evaluated in the A5C.
- The two AVV(s) of the partial AVSD with the cleft of the left-sided AVV are best seen in PSAX, the premium ASD is visualized in sub-costal and A4C views, in partial AVSD exceptionally the premium ASD is absent with the presence of IVSD.

8.7.2.2 Acquisition

1. Complete and Transitional AVSD.
   (a) Assessment of the AVV
      - In PSAX or sub-costal short axis views establish the Rastelli classification.
      - In A4C view, assess the AVV regurgitation.
      - Balancing of the valve relatively to the corresponding ventricles is best determined in A4C and PSAX; color Doppler may be a good adjunction,

showing the flow distribution relatively to the two ventricles.

(b) Assessment of IVSD
- IVSD is best visualized in A4C, PLAX, and PSAX views.
- Determine size, direction, and the peak gradient through the IVSD, mainly in PSAX.
- Verify the presence of other VSD.

(c) Assess the premium ASD:
- Best seen in sub-costal and A4C views.
- Using the CFD and PWD to determine the direction of flow.

(d) Screening and assessment of associated lesions:
- LVOT obstructions in A5C view using color and CWD, consequence of the unwedged AOV or oriented toward aortic coarctation.
- RVOT obstruction may reflect association of the AVSD with ToF.
- Unbalanced AVSD with RV dominance imposed to assess the aortic arch for possible coarctation; in case of LV dominance, RVOT obstruction is possible.

(e) Assess the effect of shunts:
- Premium ASD may cause RA, RV, and pulmonary artery dilatation.
- IVSD may cause LV dilatation.
- PHT.

2. Partial AVSD:

(a) Assessment of the AVV:
- In A4C view coupled with CFD allows the assessment of AVVs regurgitation.

(b) Assess the premium ASD:
- Premium ASD is best seen in sub-costal and A4C views; determine the flow direction using color and PWD.
  - Screening and assessment of associated lesions:
- Mainly the presence of LVOT obstruction.
  - Assess the effect of shunts:
- Right cavity dilatation may be caused by the premium ASD.
- LA enlargement may be caused by the AVVs regurgitant jet.
- PHT.

8.7.3 Doppler Finding

8.7.3.1 AVV Assessment

1. Assess the AVV regurgitation using the CFD.
2. Pulmonary regurgitation may be used to assess the PA pressure.

(a) Premium ASD Assessment
- Assess the direction using the CFD.

(b) IVSD Assessment
- Use the CFD to assess the direction and CWD to record the peak velocity jet.

(c) Outflow Obstruction
- Apply color and spectral Doppler to assess the right and left ventricular outflow obstruction.

8.8 Other Anomalies

8.8.1 Pulmonary Stenosis

The obstruction may occur at the sub-valvular, valvular, or supra-valvular levels; severe forms cause cyanosis in neonates due to the right-to-left shunt through ASD or PFO, and reduced pulmonary blood flow, the latter may be dependent on blood supply from PDA. 2D-imaging visualizes a dome-shaped, or dystrophic with reduced leaflets pulmonary valve. CFD visualizes aliasing in the stenotic zone. CWD applied across the stenotic pulmonary valve shows a systolic peak velocity and a peak pressure gradient greater than 4 m/s and 60 mmHg, respectively, in severe pulmonary stenosis according to the American Heart Association and American College of Cardiology recommendations Fig. 8.4.

8.8.2 Coarctation of the Aorta: Fig. 8.5

Coarctation of the aorta is a congenital narrowing or stenosis of a segment of the AO; frequently, this condition affects the isthmus just distal to the origin of the left subclavian artery; when coarctation of the aorta is critical, aorta blood supply may depend on the patency of the ductus arteriosus, the physiologic closer of the latter may cause LV failure in infants, the diagnosis is suspected in

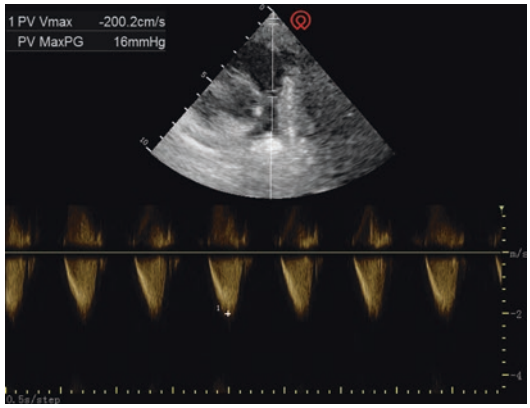

Fig. 8.4 CWD applied across the stenotic pulmonary valve

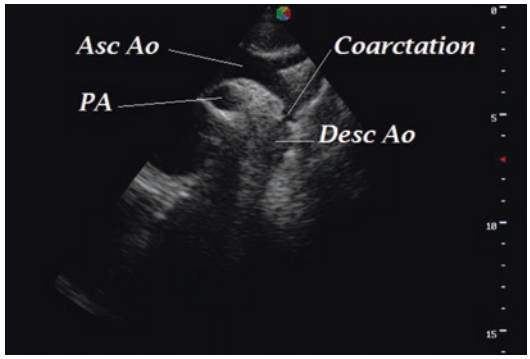

Fig. 8.5 Coarctation of the aorta

2D-imaging at the long axis suprasternal view which visualizes a narrowing of the aorta at the isthmus, CFD shows aliasing at the same zone and allows the assessment of the contribution of the PDA in aortic blood supply.

8.8.3 Aortic Aneurysm Can Lead to Dissection or Rupture

As shown in Fig. 8.6, an aneurysmal dilated ascending aorta in pediatric in suprasternal view. Figure 8.7 depicts aneurysm in parasternal long axis view.

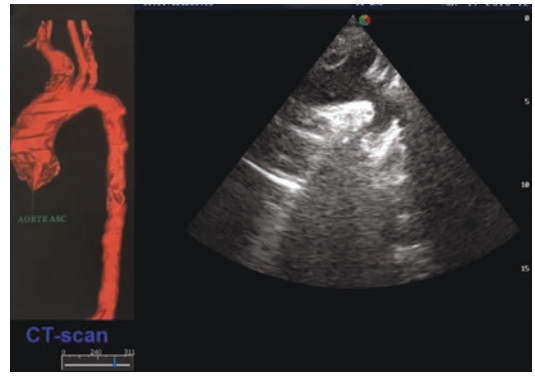

Fig. 8.6 Aneurysmal dilated ascending aorta in pediatric in suprasternal view

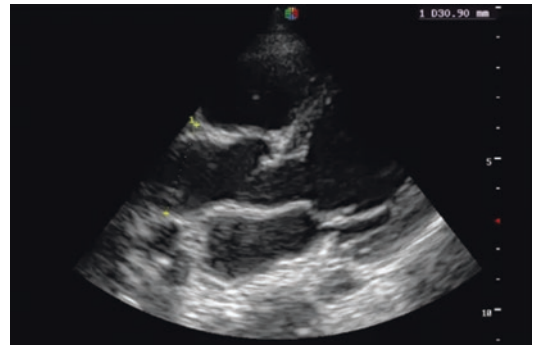

Fig. 8.7 Aneurysmal dilated ascending aorta in pediatric in parasternal long axis view

References

1. Otto CM, editor. The practice of clinical echocardiography. 5th ed. Philadelphia, Pennsylvania: Elsevier; 2017. p. 1002.
2. Eidem BW, O'Leary PW, Cetta F, editors. Echocardiography in pediatric and adult congenital heart disease. 2nd ed. Philadelphia, PA: Wolters Kluwer; 2015. p. 720.
3. Hyun WG, Soo-Jin K, Hye-Sung W. An illustrated guide to congenital heart disease. Disponible sur:704. https://doi.org/10.1007/978-981-13-6978-0.
4. Lai WW, Mertens L, Cohen M, Geva T, editors. Echocardiography in pediatric and congenital heart disease: from fetus to adult. 2nd ed. Chichester, West Sussex ; Hoboken, NJ: John Wiley & Sons Ltd; 2015. p. 1.

Tips and Tricks

9

Noreddine Bouarroudj and Cherif Bouzid

- Echographic windows vary according to the body habits and underlying pathologic conditions; therefore, instead of using fixed landmarks, sweep the zone of interest.
- Parameters reflecting the LV systolic function must be interpreted according to the clinical setting.
- Assessment of the LV diastolic function relies on multi-parametric approach; however, E/e' and e' are the two parameters potentially integrable in the CPOCUS protocol.
- When assessing thoracic aorta for dissection, care must be paid to not mistake artifacts as intimal flaps.
- Tamponade is a clinical diagnosis, it must be suspected in every patient with large pericardial effusion.
- When assessing patient with prosthetic valve replacement, the results of the current exam must be compared to the results of the reference values and interpreted according to the clinical context.
- Identifying reversible cause of cardiac arrest and assessment of underlying cardiac rhythm are the primary focus of the POCUS protocol.
- PFO diagnosis procedure must include dynamic maneuvers combined with contrast test.
- ASD may be silent for a long time; however, shunt increases with reduction in the LV compliance caused by aging, systemic arterial hypertension, and LV pathology, causing worsening of the symptoms.
- VSDs are responsible of systemic complication, mainly PHT, endocarditis, and Eisenmenger syndrome. Local complications are in close relationship with VSDs' locations.
- ToF is represented by a spectrum, the clinical presentation varies with the severity of the four underlying abnormalities.
- In D-TGA condition, survival relies on the patency of the zones of blood mixing; therefore, estimation of the blood flow through the shunts is crucial.

N. Bouarroudj (✉)
Department of Anesthesiology and Critical Care, Clinique Maissalyne, Constantine, Algeria
e-mail: bouarroudj@bouarroudj.net

C. Bouzid
Department of Anaesthesia and Critical Care, El Afia Hospital, Mila, Algeria

© The Author(s), under exclusive license to Springer Nature Switzerland AG 2024

N. Bouarroudj et al. (eds.), *POCUS in Critical Care, Anesthesia and Emergency Medicine*,
https://doi.org/10.1007/978-3-031-43721-2_9

Part III

US in Different Settings

Lung Ultrasound in Acute Care

10

Lim Teng Cheow, Nur Hafiza Yezid, and Shahridan bin Mohd Fathil

10.1 Introduction

Lung ultrasound has been proven to be superior compared with chest radiography in the diagnosis of various lung conditions, such as pulmonary oedema, pleural effusion, pneumothorax and consolidation. [1, 2]

10.2 Principles

Normal lung which is filled with air cannot be visualized as a discrete organ under ultrasound examination. However, when relative composition of air and fluid changes in a diseased lung, predictable patterns can be recognized with ultrasound.

Lung ultrasound findings are broadly classified into artefacts and real images. Artefacts can be formed by normal and abnormal lung, while real images are always pathological when relative proportion of air and fluid varies abnormally [3].

10.3 Technical Considerations

Pre-examination technical considerations focus on type of probe to be used, as well as examination mode.

(a) Probe: either linear probe which is the best in examining the lung, or curvilinear probe (Fig. 10.1). Linear probe offers us superior resolution while curvilinear probe has the advantage of providing better wave penetration.
(b) Modes: B- and M-mode are the commonly used modes in lung sonography. B in B-mode originates from the word brightness, and in this mode structural information of the lung will be obtained. It is shown as an image that consists of dots of different brightness. M in M-mode represents motion, which enables us to observe the motion of the structure being examined (Fig. 10.2).

L. T. Cheow
Department of Anaesthesia and Intensive Care, Malacca General Hospital, Melaka, Malaysia

N. H. Yezid
Department of Emergency Medicine, Hospital Sultanah Bahiyah, Alor Setar, Malaysia

S. M. Fathil (✉)
Department of Anaesthesia, Gleneagles Medini Hospital Johor, Iskandar Puteri, Johor, Malaysia

© The Author(s), under exclusive license to Springer Nature Switzerland AG 2024
N. Bouarroudj et al. (eds.), *POCUS in Critical Care, Anesthesia and Emergency Medicine*,
https://doi.org/10.1007/978-3-031-43721-2_10

Fig. 10.1 Ultrasound probes commonly used for lung ultrasound: linear probe (left) and curvilinear probe (right)

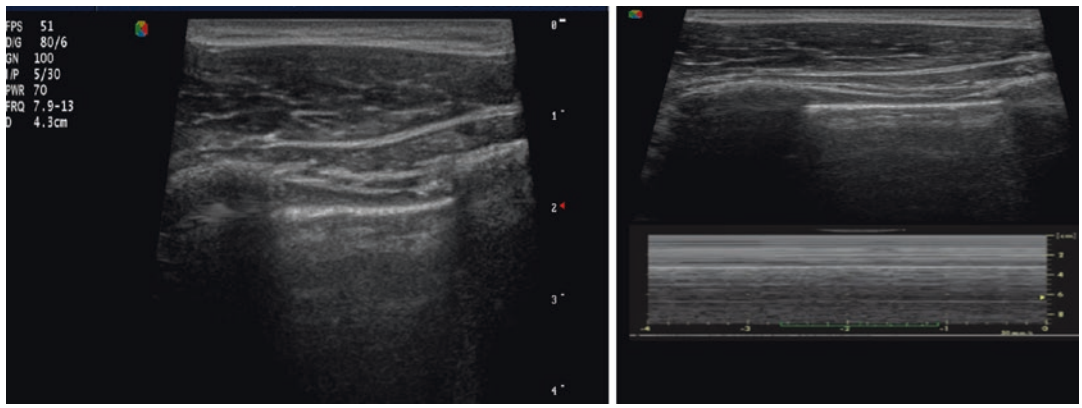

Fig. 10.2 B-mode (left) and M-mode (right). In B-mode dots of different brightness are the elements to construct the image, while in M-mode, motion of the underlying structure can be visualized

10.4 Technique of Examination

The patient can be placed in supine, prone or semi-recumbent position for lung examination. Typically, patient is examined in supine position. The lung is scanned over several standardized zones to detect abnormalities. Conventionally, each lung is divided into four areas (Fig. 10.3) [4]. The anterior and lateral aspects of each lung are examined systematically. Anteriorly, area 1 represents upper anterior chest and area 2 looks into the lower anterior chest. Laterally, areas 3 and 4 examine the upper lateral and basal lateral chest areas, respectively.

For each of these areas, examination can be done through two views, namely the longitudinal and transverse views (Fig. 10.4).

In order to optimize the ultrasound examination, the depth of ultrasound should be adjusted until the structures of interest, for instance the pleura appear in the middle of the screen (Fig. 10.5).

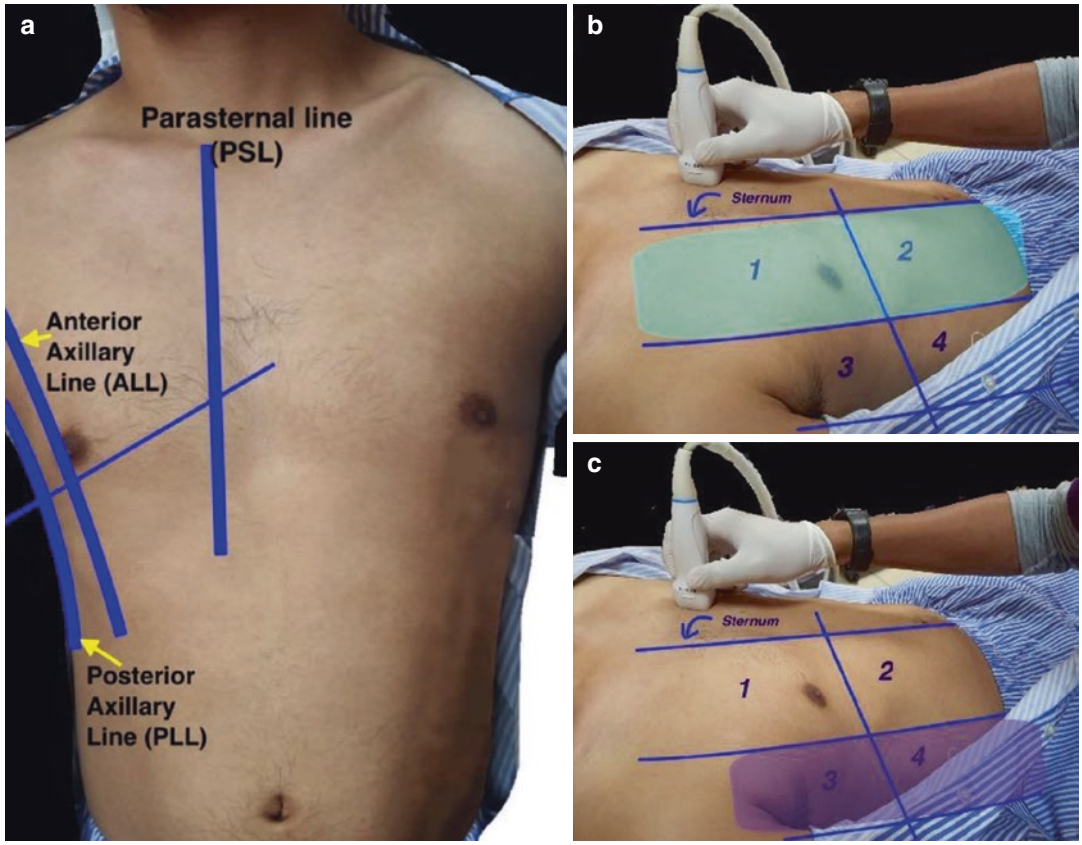

Fig. 10.3 (**a**) The related anatomical landmarks to delineate the areas of each lung. (**b**) The anterior chest is divided into upper and lower areas (area 1 and area 2). (**c**) The lateral chest is divided into upper and basal areas as well (area 3 and area 4)

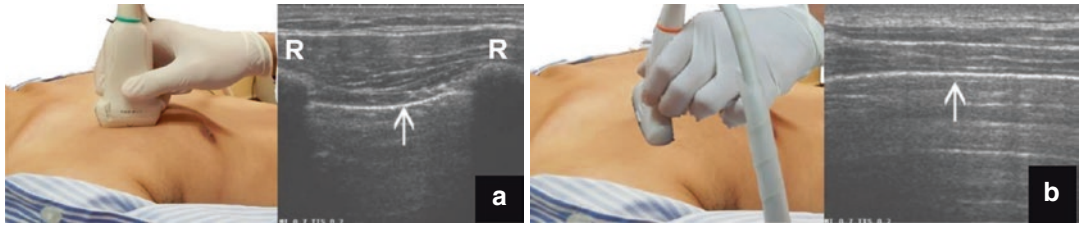

Fig. 10.4 (**a**) Lung ultrasound in longitudinal view. The pleura is represented by a hyperechoic line indicated by the arrowhead, and it is seen to be oscillating between two consecutive ribs (R). (**b**) Lung ultrasound in transverse view. The lung is examined from a window located between two consecutive ribs (intercostal space). The pleura is again represented by an oscillating hyperechoic line, as indicated by the arrowhead

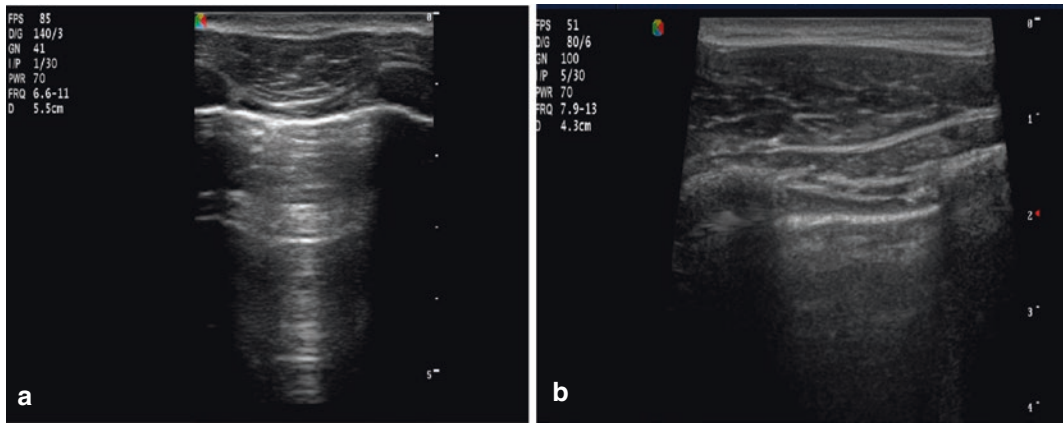

Fig. 10.5 (**a**) With the pleura as the structure of interest, it is not shown in the middle of the screen. With the appropriate adjustment, the pleura is now placed optimally in the middle of the screen (**b**)

10.5 Sonography of Normal Lung

Lung ultrasound findings are based on patterns, and normal lung patterns will be briefly described here. Any pattern that deviates from these descriptions is deemed to be abnormal [5–8].

(a) Pleural line: Due to difference in composition between chest wall soft tissues and lung, they have very different acoustic impedance. Chest soft tissues are generally rich in water while normal lung is relatively richer in air. When ultrasound beams encounter an interface formed by chest wall and lung, they are reflected as both chest wall and lung have large difference in acoustic impedance. This is the basis of pleural line. One may not be able to always identify both layers of pleura due to restriction caused by resolution of ultrasound machines.

(b) A lines: Reflected ultrasound beams encountering ultrasound probe will be detected and shown as a hyperechoic line. Subsequently, these beams will also be directed back into the chest wall and pleurae and get reflected. This causes the ultrasound beams to travel repetitively between the ultrasound probe and chest wall-pleura interface. A hyperechoic line will be formed whenever ultrasound beam is detected by ultrasound probe. Due to these repetitive movements of ultrasound beam, multiple such hyperechoic lines are formed, and they are collectively named as A lines. The distance between two consecutive lines is generally similar for the same reason (Figs. 10.6 and 10.7).

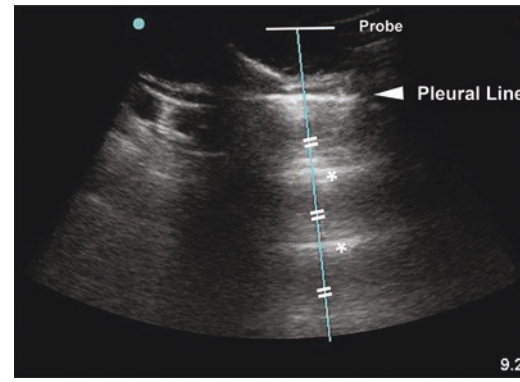

Fig 10.6 A lines in B-mode. These lines (marked with asterisks) are parallel to each other, and the distance between two consecutive lines is constant

(c) Lung sliding: It is a sign arising from pleural line, representing inspiratory descent and expiratory ascent of visceral pleura against parietal pleura. On B-mode ultrasound, this appears as a shimmering mobile pleural line, which moves synchronously with respiratory cycle. The presence of lung sliding can also be demonstrated on M-mode, as what is typically named as sea-shore sign (Fig. 10.8).

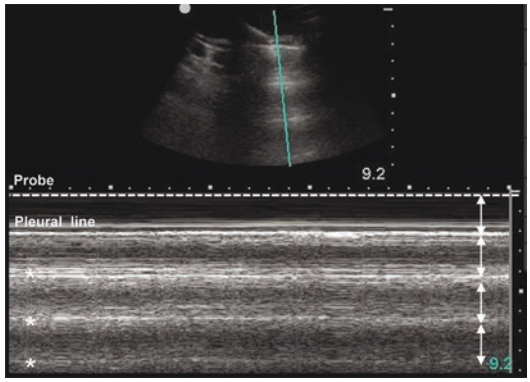

Fig 10.7 A lines in M-mode. The similar artefacts are demonstrated in M mode. A lines are evenly spaced at multiples of the distance between ultrasound probe and pleural line

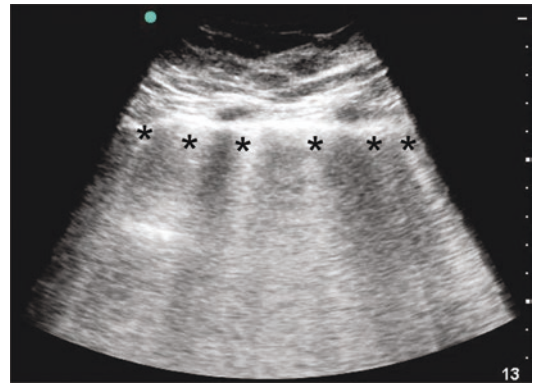

Fig. 10.9 B-lines. They are hyperechoic white lines that extend from the pleural line to the edge of the screen, which move with respiration. B-lines are marked with asterisks in the diagram

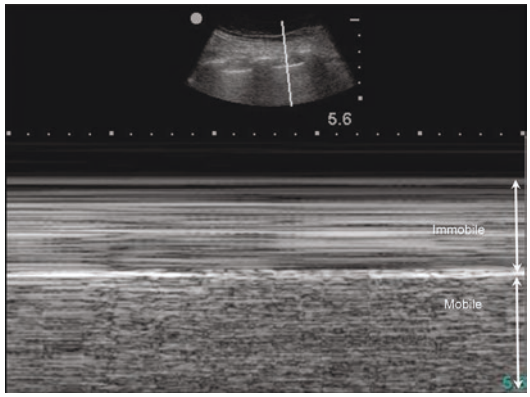

Fig. 10.8 Sea-shore sign. Two components form this sign, namely the sea and the shore. Sea is caused by immobile chest wall structures like skin and subcutaneous tissue, while the beach is caused by the moving pleura. The sea is named as such as the artefact produced mimics the wave lines in the sea. The artefact caused by moving pleura mimics the sandy appearance of a beach

10.6 Sonography of Lung Pathologies

10.6.1 Interstitial Syndrome

This syndrome comprises various conditions that give rise to an abnormal lung interstitium. The alveoli are relatively normal and aerated. It is diagnosed with presence of ≥3 B-lines between two successive ribs. B-line is formed whenever there is an increase in relative ratio of water-to-air content in the lung, and this happens in fluid accumulation of deposition of collagen tissues [9–11]. The aetiology of this syndrome can be divided into cardiogenic and non-cardiogenic causes, which typically include fluid overload, cardiac failure, interstitial pneumonitis, and pulmonary fibrosis [12]. B-line is a hyperechoic vertical line that extends from the pleural line to the bottom of the ultrasound screen (Fig. 10.9). It erases the normal A lines and moves in synchrony with lung sliding [4]. Lung ultrasound is very sensitive in the diagnosis of interstitial syndrome with a sensitivity of >90% [2].

10.6.1.1 Number of B-Lines

As the number of B-lines increases with decreasing air content and increasing lung density, it can be used to estimate the severity of lung disease [13]. Three or four B-lines between two ribs indicates thickened subpleural interlobular septa. With appearance of five or more B-lines, this signifies ground-glass opacities on computerized tomography, indicating a severe interstitial syndrome [14]. The number of B-lines is found to correlate closely with extravascular lung water content as well as NT-proBNP levels [15, 16]. Based on this finding, the number of B-lines can be used as a tool to assess the response to therapy in acute pulmonary oedema [17].

All the relevant considerations are summarized in the table below [18, 19].

Conditions	Characteristics
Pulmonary oedema	B-lines + bilateral, diffuse distribution
Acute respiratory distress syndrome	B-lines + non-homogeneous and irregular pattern with areas of patchy B-lines alternating with regular A-lines zones (spared areas or skip lesions)

10.6.2 Pleural Effusion

Quad sign and sinusoidal sign are two useful signs to diagnose pleural effusion. Both signs are demonstrable only in M-mode. As indicated by the name, Quad sign illustrates the four borders seen on ultrasound screen surrounding a collection of fluid (Fig. 10.10). It is made up of an anechoic area signifying presence of fluid, bordered by pleural line, lung line and shadows produced by successive ribs. Pleural effusion can be demonstrated in both longitudinal and transverse views (Fig. 10.11). With fluid in pleural cavity, this apparently has amplified the visceral pleura movement towards and away from chest wall throughout the respiratory cycle, and this forms the basis of sinusoidal sign [20] (Fig. 10.12) which is well seen with examination performed in M-mode. Identification of pleural effusion, in fact, is reported to be the most established application of lung ultrasound [10, 21].

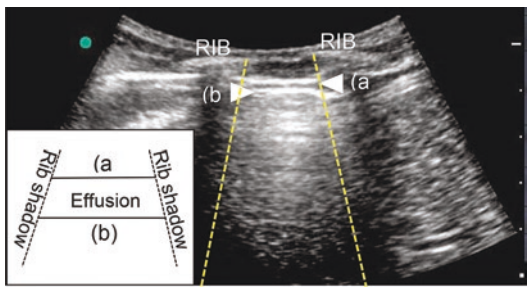

Fig. 10.10 Quad sign. Anechoic area surrounded by four borders, namely the pleural line (**a**), lung line (**b**) and shadows contributed by the two successive ribs (yellow broken lines). Lung line is an ultrasound indicator of visceral pleura in pleural effusion

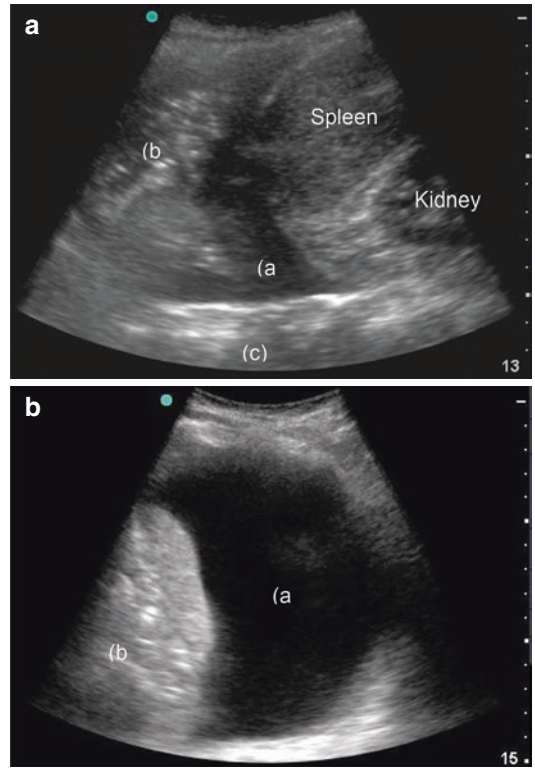

Fig. 10.11 (**a**) Sonographic image of pleural effusion in longitudinal view. The sonographic features of pleural effusion are demonstrated here. The anechoic region (a) represents pleural effusion. Due to change in relative ratio of water-to-air content, texture of lung has now changed to tissue-like pattern (b), which suggests consolidation. As fluid allows ultrasound beam penetration, the underlying vertebral column deep to the lung is now visible and is marked with (c). (**b**) Sonographic image of pleural effusion in transverse view. Pleural effusion is seen as an anechoic area marked with (a), with the underlying lung showing consolidation and air bronchogram (b)

10.6.3 Pneumothorax

Diagnosis of pneumothorax is made based on the findings of presence of lung point, with absence of lung sliding, B-lines and lung pulse [10] (Fig. 10.13). Except for the presence of B-lines, the rest of the findings are more readily demonstrated in M-mode. Absence of lung sliding is conveniently portrayed as stratosphere or barcode sign (Fig. 10.14). As there are other conditions which may give rise to absent lung sliding,

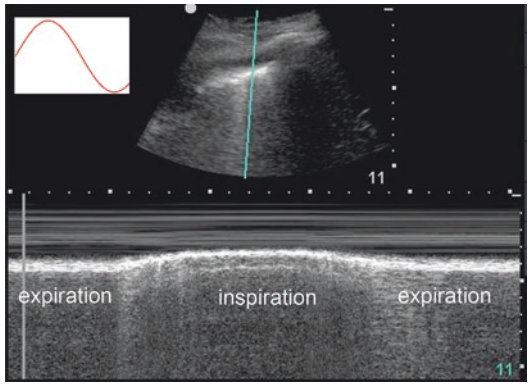

Fig. 10.12 Pleural effusion in M-mode. As the visceral pleura moves throughout the respiratory cycle, a sinusoidal pattern is seen, similar to a graph of a sinusoidal function (inlet)

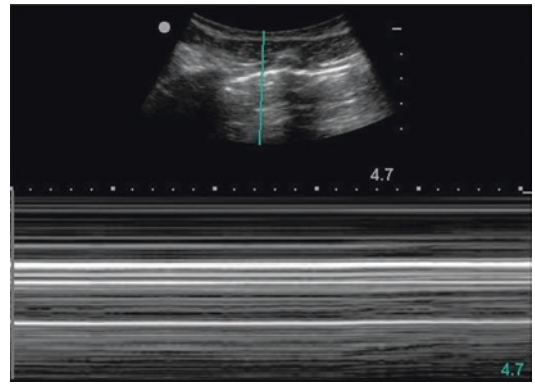

Fig. 10.14 Barcode (stratosphere) sign. This sign is caused by the absence of lung sliding with the chest wall and lung remaining static and immobile. Although this sign by itself suggests pneumothorax, but it is not an absolute distinctive feature of pneumothorax

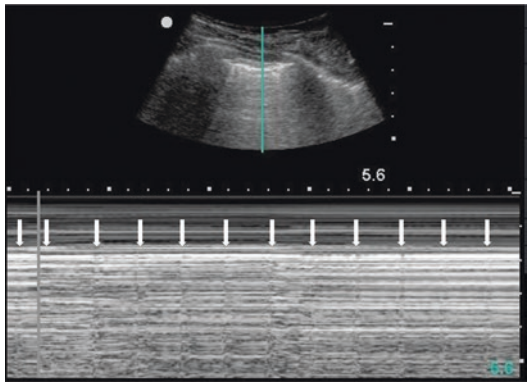

Fig. 10.13 Lung pulse. Transmission of cardiac beating to ultrasound probe through a poorly aerated lung is observed as lung pulse on M-mode. Its presence rules out pneumothorax. Cardiac contraction pulse is indicated by arrows in the diagram

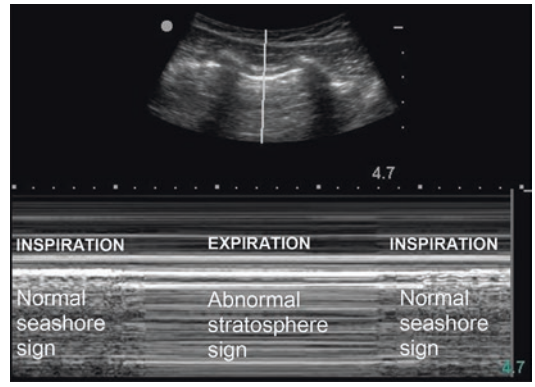

Fig. 10.15 Lung point. Alternating normal sea-shore sign during inspiration and abnormal stratosphere sign during expiration is seen at the border of the pneumothorax. It marks the border of pneumothorax and hence the approximate size of pneumothorax

this feature alone is not reliable in diagnosis of pneumothorax. The other conditions which are associated with the absence of lung sliding include adult respiratory distress syndrome (ARDS), massive atelectasis, pleural adhesions, endobronchial intubations, cardiopulmonary resuscitations and phrenic nerve palsy [22–24]. In a living human, activity of a beating heart can be transmitted to ultrasound probe through a non-expanding lung as the pleura is now moving synchronously with cardiac rhythm [25]. As intact and adherent pleura is required to generate B-lines, its presence can rule out pneumothorax safely [26]. Lastly, lung point actually represents the border of pneumothorax, and it is visualized as alternating sea-shore and stratosphere patterns on ultrasound [27] (Fig. 10.15).

10.6.4 Alveolar Syndrome

In alveolar syndrome, the alveolus is abnormally filled with fluid, leading to massive loss of air [28]. It is diagnosed with the presence of poorly echogenic or tissue-like image arising from pleural line, which is sometimes being referred to as hepatization [10] (Fig. 10.16). The irregular deep margin of this pattern serves to separate consolidated lung from the part which is aerated. This is known as shred sign [29] (Fig. 10.17). The common aetiologies of alveolar syndrome are consolidation and atelectasis [11]. Further clinical history

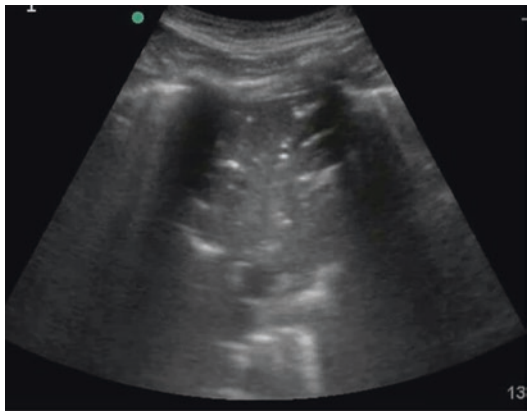

Fig. 10.16 Consolidation. Relative hypoechoic heterogenous echotexture on ultrasound

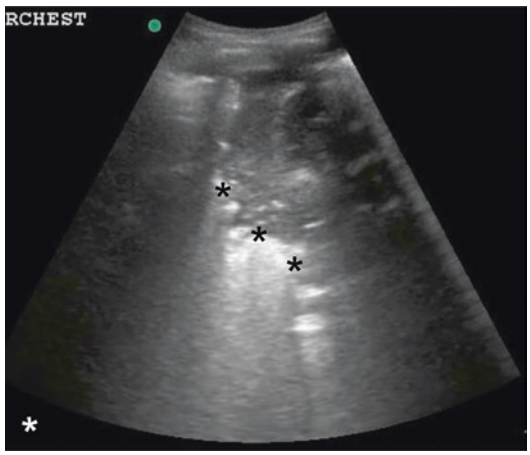

Fig. 10.17 Shred Sign. Consolidated lung tissue appears as a subpleural hypoechoic region which has an irregular (shredded) deep border adjacent to normal lung. Border is marked with asterisks in diagram

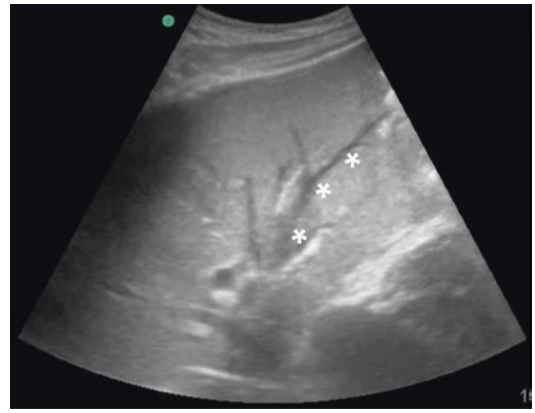

Fig. 10.18 Hepatized lung with air bronchograms. A bronchogram is marked with asterisks

and additional relevant lung sonographic findings are essential to formulate the differential diagnosis of this syndrome. Among the sonographic features which are useful in determining the aetiology include shape, margin, distribution, vascularization pattern and the presence of air bronchograms [28, 30–33]. Punctiform or linear hyperechoic artefacts seen within a consolidated lung forms air bronchograms, which is useful to rule out the possibility of atelectasis [32] (Fig. 10.18).

10.7 Conclusion

Lung ultrasound can be used to diagnose and manage acute and chronic pulmonary conditions. Lung ultrasound can provide practical, real time, and reliable tool for acute care. Each condition is characterized by its own unique sonographic features.

References

1. Ross AM, Genton E, Holmes JH. Ultrasound examination of the lung. J Lab Clin Med. 1968;72:556–64.
2. Díaz-Gómez JL, Renew JR, Ratzlaff RA, et al. Can lung ultrasound be the first-line tool for evaluation of intraoperative hypoxemia? Anesth Analg. 2018;126:1769–73.
3. Mojoli F, Bouhemad B, Mongodi S, et al. Lung ultrasound for critically ill patients. Am J Respir Crit Care Med. 2019;199:701–14.

4. Volpicelli G, Elbarbary M, Blaivas M, et al. International liaison committee on lung ultrasound (ILC-LUS) for the international consensus conference on lung ultrasound (ICC-LUS). International evidence-based recommendations for point-of-care lung ultrasound. Intensive Care Med. 2012;38:577–9.
5. Lichtenstein DA. Introduction to lung ultrasound. In: Whole body ultrasonography in the critically ill. Berlin Heidelberg: Springer-Verlag; 2010. p. p117–28.
6. Goffi A, Kruisselbrink R, Volpicelli G. The sound of air: point-of-care lung ultrasound in perioperative medicine. Can J Anaesth. 2018;65:399–416.
7. Williams D. The physics of ultrasound. Anaesth Intens Care Med. 2012;13:264–8.
8. Dietrich CF, Mathis G, Cui XW, et al. Ultrasound of the pleurae and lungs. Ultrasound Med Biol. 2015;41:351–65.
9. Lichtenstein D, Mézière G, Biderman P, et al. The comet-tail artifact. An ultrasound sign of alveolar-interstitial syndrome. Am J Respir Crit Care Med. 1997;156:1640–6.
10. Gargani L, Volpicelli G. How I do it: lung ultrasound. Cardiovasc Ultrasound. 2014;12:25.
11. Leidi F, Casella F, Cogliati C. Bedside lung ultrasound in the evaluation of acute decompensated heart failure. Intern Emerg Med. 2016;11:597–601.
12. Miller A. Practical approach to lung ultrasound. Br J Anaesth Educ. 2016;16:39–45.
13. Dietrich CF, Mathis G, Blaivas M, et al. Lung B-line artefacts and their use. J Thorac Dis. 2016;8:1356–65.
14. Lichtenstein DA. Current misconceptions in lung ultrasound: a short guide for experts. Chest. 2019;156:21–5.
15. Agricola E, Bove T, Oppizzi M, et al. Ultrasound comet-tail images: a marker of pulmonary edema: a comparative study with wedge pressure and extravascular lung water. Chest. 2005;127:1690–5.
16. Gargani L, Frassi F, Soldati G, et al. Ultrasound lung comets for the differential diagnosis of acute cardiogenic dyspnoea: a comparison with natriuretic peptides. Eur J Heart Fail. 2008;10:70–7.
17. Volpicelli G, Caramello V, Cardinale L, et al. Bedside ultrasound of the lung for the monitoring of acute decompensated heart failure. Am J Emerg Med. 2008;26:585–91.
18. Falcetta A, Leccardi S, Testa E, et al. The role of lung ultrasound in the diagnosis of interstitial lung disease. Shanghai Chest. 2018;2:41.
19. Copetti R, Soldati G, Copetti P. Chest sonography: a useful tool to differentiate acute cardiogenic pulmonary edema from acute respiratory distress syndrome. Cardiovasc Ultrasound. 2008;6:16.
20. Lichtenstein DA. Lung ultrasound in the critically ill. Ann Intensive Care. 2014;4:1.
21. Maskell N, Butland R. BTS guidelines for the investigation of a unilateral pleural effusion in adults. Thorax. 2003;59(4):8–17.
22. De Luca C, Valentino M, Rimondi M, et al. Use of chest sonography in acute-care radiology. J Ultrasound. 2008;11:125–34.
23. Murphy M, Nagdev A, Sisson C. Lack of lung sliding on ultrasound does not always indicate a pneumothorax. Resuscitation. 2008;77:270.
24. Ball CG, Kirkpatrick AW, Feliciano DV. The occult pneumothorax: what have we learned? Can J Surg. 2009;52:E173–9.
25. Lichtenstein DA, Lascols N, Prin S, et al. The "lung pulse": an early ultrasound sign of complete atelectasis. Intensive Care Med. 2003;29:2187–92.
26. Mittal AK, Gupta N. Intraoperative lung ultrasound: a clinicodynamic perspective. J Anaesthesiol Clin Pharmacol. 2016;32:288–97.
27. Lichtenstein D, Mezierre G, Biderman P, et al. The 'lung point': an ultrasound sign specific to pneumothorax. Intensive Care Med. 2000;26:1434–40.
28. Volpicelli G. Lung sonography. J Ultrasound Med. 2013;32:165–71.
29. Lichtenstein DA, Lascols N, Mezierre G, et al. Ultrasound diagnosis of alveolar consolidation in the critically ill. Intensive Care Med. 2004;30:276–81.
30. Volpicelli G, Caramello V, Cardinale L, et al. Diagnosis of radio-occult pulmonary conditions by real-time chest ultrasonography in patients with pleuritic pain. Ultrasound Med Biol. 2008;34:1717–23.
31. Mathis G, Blank W, Reissig A, et al. Thoracic ultrasound for diagnosing pulmonary embolism: a prospective multicenter study of 352 patients. Chest. 2005;128:1531–8.
32. Lichtenstein D, Mezierre G, Seitz J. The dynamic air bronchogram. A lung ultrasound sign of alveolar consolidation ruling out atelectasis. Chest. 2009;135:1421–5.
33. Nazerian P, Volpicelli G, Vanni S, et al. Accuracy of lung ultrasound for the diagnosis of consolidations when compared to chest computed tomography. Am J Emerg Med. 2015;33:620–5.

11 Ultrasound-Guided Vascular Access

Noreddine Bouarroudj and Cherif Bouzid

11.1 Introduction

The central venous cannulation (CVC) is a typical example of the invasive procedure which is widely modified by the POCUS (point-of-care ultrasound) protocol adoption in daily practice; despite the initial interest in the internal jugular vein (IJV) emplacement, the application of the POCUS protocol over the other possible sites of CVC gains an increasing interest; moreover, the safety profile of the latter permits the renaissance of older non-conventional approaches for CVC, such as the supraclavicular approach to the subclavian vein that was judged before as a high-risk procedure.

The integration of the ultrasound in the CVC procedure is currently regarded as the key to reducing mechanical complications, the number of cannulation attempts, and the overall time dedicated in performing the procedure; these presumptions are particularly verified for the IJV cannulation; meta-analyses of randomized controlled trials with two groups (conventional group procedure versus echo-guided group procedure) are all in favor of the adoption of the echo-guided procedure, with increased success rates in the first insertion attempt [1], increased overall success rates [1, 2], decreasing rates of arterial accidental puncture [2, 3], and a decrease in the number of tentative insertions [1].

The echography is currently integrated into different steps of a CVC setup, from the initial scan before sterile preparation to the verification of the guide wire and catheter tip location, and the verification of any mechanical complication occurrence rather than being limited to the sole guidance of venous puncture.

11.2 General Considerations

11.2.1 Blood Vessel Identification

Blood vessel echographic aspect is typical; depending on the echographic long or short axis view; the vessel appears respectively as rectangular or circular anechoic structure (Figs. 11.1 and 11.2) well delineated from the surrounding tissue with a posterior enhancement, when thrombosed a hyper or hypoechoic material, moreover, anechoic material could occupy the lumen (Fig. 11.3).

Several echographic aspects oppose veins and arteries; arteries are more round shaped, with thick walls (Fig. 11.1), and show more resistance to being collapsed under the transducer pressure; depending on the underlying local and systemic conditions(Fig. 11.4), they show a pulsate pat-

N. Bouarroudj
Department of Anaesthesia and Critical Care, Maissalyne Hospital, Constantine, Algeria

C. Bouzid (✉)
Department of Anaesthesia and Critical Care, El Afia Hospital, Mila, Algeria

© The Author(s), under exclusive license to Springer Nature Switzerland AG 2024

N. Bouarroudj et al. (eds.), *POCUS in Critical Care, Anesthesia and Emergency Medicine*,
https://doi.org/10.1007/978-3-031-43721-2_11

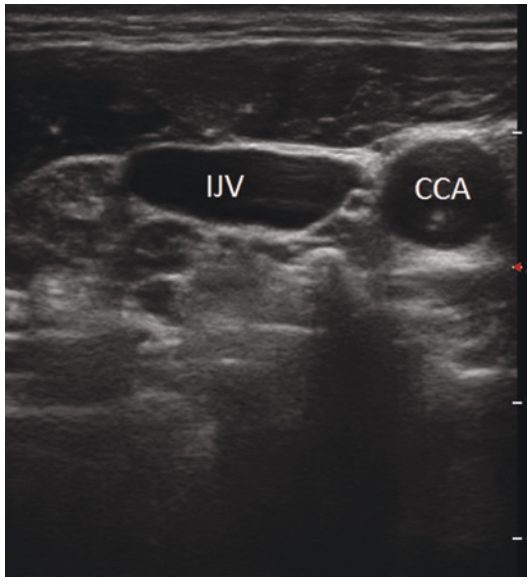

Fig. 11.1 Short axis view of the internal jugular vein (IJV) and the common carotid artery (CCA)

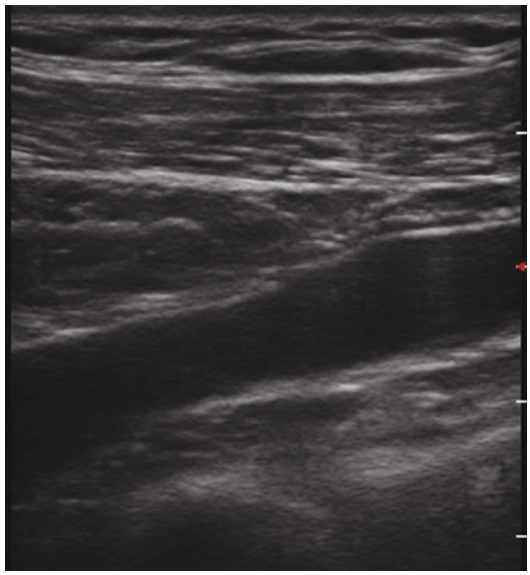

Fig. 11.2 Long axis view of the axillary vein

tern; however, veins show continuous flow with respiro-phasic variations; sometimes pulsations from the arteries are transmitted to the adjacent veins, and more information derived from the application of the color Doppler flow and the pulsed wave Doppler confirms the two-dimensional finding (Figs. 11.5 and 11.6).

Fig. 11.3 Thrombosis of the femoral vein, appearing as a hypoechoic material occupying partially the lumen of the vein

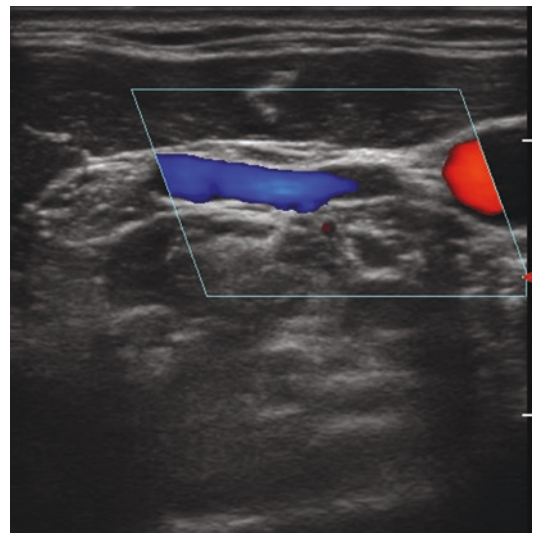

Fig. 11.4 Gentle pressure over the neck vessel applied using the transducer in short axis view, causing partial internal jugular vein collapse

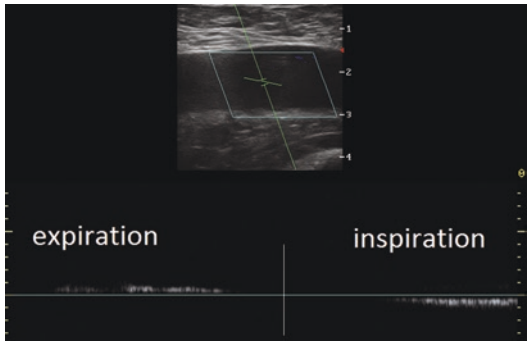

Fig. 11.5 Pulsed wave Doppler with the sample volume applied over the femoral vein, showing a pulseless, low velocity with respiratory variation pattern

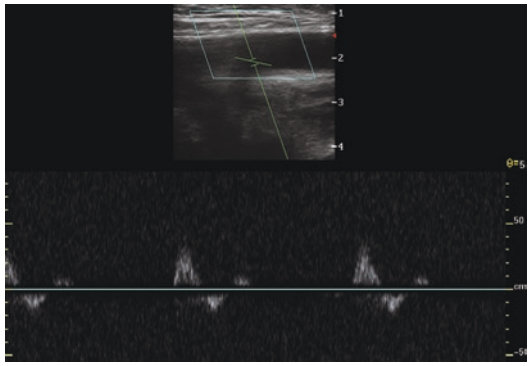

Fig. 11.6 Pulsed wave Doppler with the sample volume applied over the common femora artery, showing pulsed with high velocity pattern

11.2.2 Approaches for Vascular Cannulation

11.2.2.1 Out-of-Plane Approach

In the out-of-plane approach, the targeted vessel is displayed on its short axis (Fig. 11.1), ideally placed in the center of the screen; the needle is inserted at a variable distance from the midpoint of the transducer's long axis, and it advances perpendicularly to the ultrasound beam toward the targeted vessel (Fig. 11.7); once the needle crosses the ultrasound beam, it appears as a hyperechoic dot with posterior reverberation artifacts.

By combining the movements of tilting and translation of the transducer, the operator follows the needle's shaft in short axis right until it disappears—this point is judged as the location of the needle's tip; the process of progression of the needle of 1–2 mm at the time and relocation of the needle tip is repeated till the latter causes a tenting in the anterior wall vessel, and it penetrates the vessel, giving the "target sign"; more tilting of the transducer is required to rule out puncture of the posterior wall of the vessel.

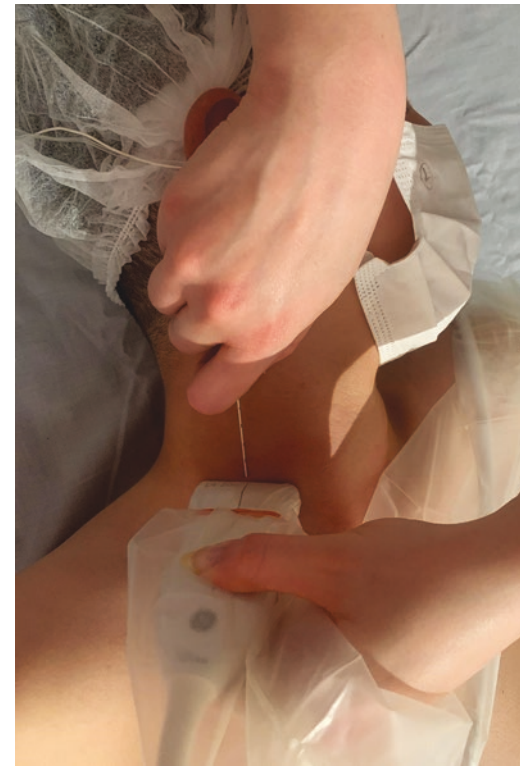

Fig. 11.7 Shows the relative position of the needle and the transducer over the lateral aspect of the neck for out-of-plane internal jugular vein cannulation

The out-of-plane approach allows both visualization of the vessel and the surrounding structures, which may reduce the complications incidence, permits orientation of the tip of the needle toward the center of the vessel which reduces the "cylinder tangential effect": the tendency of the needle tip, however, is to push and roll the vessel rather than puncture its wall; the failure to locate the needle's tip which may lead to a puncture of the surrounding structures counts as a concern for this approach.

Fig. 11.8 Shows the relative position of the needle and the transducer over the lateral aspect of the neck for in-plane internal jugular vein cannulation

11.2.2.2 In-Plane Approach

In an in-plane approach (Fig. 11.8), the targeted vessel is displayed in its long axis (Fig. 11.2), and the needle is visualized in all its length in the same plan; no further mobilization is needed to continually visualize the needle tip. However, keeping the alignment of the ultrasound beam, the needle, and the vessel may be difficult, especially when the targeted vessel has a small diameter. A slight translation of the probe from the true axis of the vessel may cause the cylinder tangential effect. It is worth mentioning that only structures situated in the same plane are displayed, even a slight translation of needle's tip out of the ultrasound plan may cause inadvertent punctures.

11.2.2.3 Oblique Approach

The oblique approach is the result of a combination of the in-plane and out-of-plane approaches; the vessel is insonated in the plan corresponding to the bisectrix of the angle formed by its long and short axes. The needle is advanced in plan along this axis. This approach allows the combination of the advantages of simultaneous visualization of the needle in all its length and the surrounding structures.

11.2.3 Transducer and Imaging Mode

11.2.3.1 Transducer

The standard practice is the use of a linear high frequency transducer; however, in obese patients, curvilinear transducer may be required. In the pediatric population and for some vascular locations like the supraclavicular region, a transducer with a small footprint may be useful, mainly the hockey stick transducer; an alternative to the latter is the use of endocavitary transducer with the inconvenience of difficult stabilization during the procedure.

A new transducer known as the T-shaped transducer is specially designed to accomplish vascular cannulation procedure by combining real-time in- and out-of-plane approaches simultaneously; however, it needs more evaluation for clinical routine usage.

11.2.3.2 Imaging Mode

The use of the two-dimension mode is the standard practice; however, the Doppler mode is used for vascular identification (pulsed, color, and power Doppler).

11.2.4 Preparation

11.2.4.1 Pre-procedural Checklist

- Review the medical history of the patient and hemostasis tests.
- Choose the bore of cannula or catheter, the current trend for venous access is to choose the minimal bore adapted for clinical request in venous cannulation.
- Choose the length of the central venous catheter according to the presumed emplacement.
- Review the indication for vascular access and choose the adapted emplacement.

11.2.4.2 Equipment

- An ultrasound machine with at least linear and curvilinear transducers.

- Sleeves for transducer with sterile gel.
- Tourniquet for peripheral venous cannulation.
- Sterile gloves.
- Syringes 3–5 mL.
- Antiseptic solution (chlorhexidine gluconate, povidone-iodine).
- Needles for anesthetic infiltration, sometimes needle block for cervical intermediate block in IJV emplacement.
- Sterile gauzes.
- Local anesthetic (lidocaine 2%).
- Sterile transparent dressing.
- Sterile drapes, gown, mask, and hat.
- Adapted cannula or catheter.

11.2.4.3 Positioning and Ergonomy

1. Patient
   (a) Lying supine or in a sitting position.
   (b) Trendelenburg if presumed CVC emplacement in the upper extremity.
   (c) Keep a visual and verbal contact with the patient and monitor (EKG, Spo2) in the event of acute complication.
2. Operator
   (a) Comfortable and ergonomically positioned, depending on the vascular access emplacement.
   (b) Respect the line: operator, sight-access point, ultrasound screen.

11.3 Ultrasound-Guided Internal Jugular Vein Cannulation

IJV ultrasound canulation represents the preferable CVC site emplacement for most practitioners; this choice is justified by the relative facility of the emplacement technique, being an accessible site for a manual compression in the advent of arterial puncture or hematoma formation, and the lower rate of catheter-related infection relative to the femoral emplacement [4].

11.3.1 Anatomic and Sonoanatomic Considerations

11.3.1.1 Anatomic Considerations

- The IJV vein drains the cerebral venous blood; it coursed in the anterolateral aspect of the neck from the jugular foramen to the thorax.
- The IJV joins the subclavian vein to form the brachiocephalic trunk; the latter drains in the superior vena cava.
- The IJV has close relation with the common carotid artery (CCA), the pleural dome, the thoracic duct on the left side.
- The Right IJV is in direct continuity of the superior vena cava.

11.3.1.2 Sonoanatomic Considerations

- A slight turn of the patient's head with the aim of reducing the IJV and the CCA overlapping (Fig. 11.9).
- Trendelenburg position causes IJV engorgement; facilitates venous puncture and reduces the probability of air embolism.
- Choose the segment of the IJV with the maximum diameter and the minimal overlapping between the IJV and the CCA.
- IJV thrombosis is a common finding; compressibility test and Doppler permit ruling out of this condition.

11.3.2 Cannulation Technique

Patient is lying supine in the Trendelenburg position, with the head rotated to the opposite side of the IJV to be cannulated, practitioner stands at the patient's head.

An initial scan is performed before proceeding to the IJV cannulation; it allows the evaluation of the IJV anatomy, verifies its patency, and allows the selection of a more superficial segment of the vein with the maximum diameter.

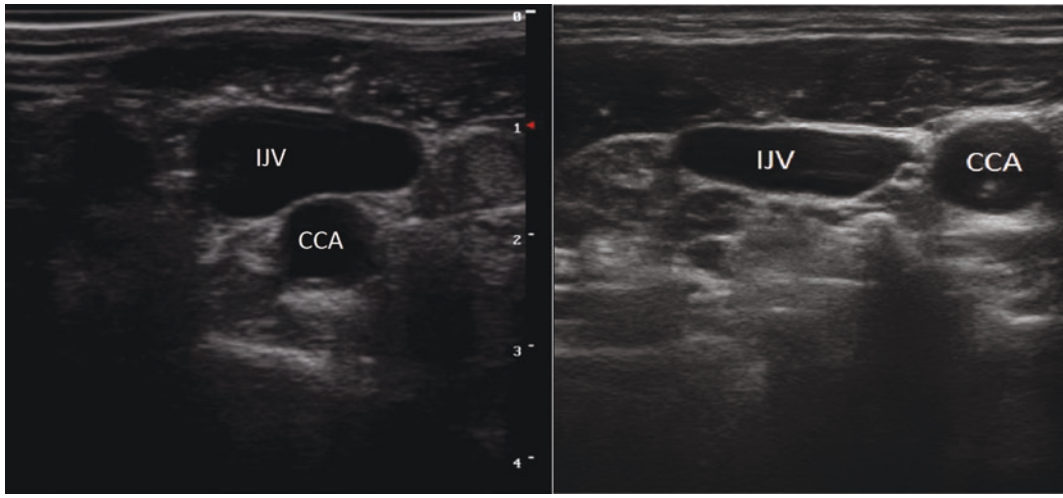

Fig. 11.9 Shows the effect of slight head rotation in reduction of the internal jugular vein (IJV) and the common carotid artery (CCA) to avoid inadvertent puncture of the latter

The IJV is cannulated using in-plane, out-of-plane, or oblique approaches; moreover, a new in-plane approach with IJV visualization in short axis has recently been described, it is performed by placing the transducer oriented in an antero-posterior manner, in the lateral aspect of the neck [5]. After threading the guide wire in the IJV, the correct position of the latter is confirmed by scanning the IJV more distally. The exact location of the catheter tip in the cavo-atrial junction may be verified directly when performing a suprasternal short axis view (Fig. 11.10) or more often indirectly by injection of the agitated saline through the catheter with echocardiographic visualization of the right atrium.

Scanning the anterior chest wall at the end of the procedure allows for ruling out inadvertent pleural puncture with pneumothorax occurrence.

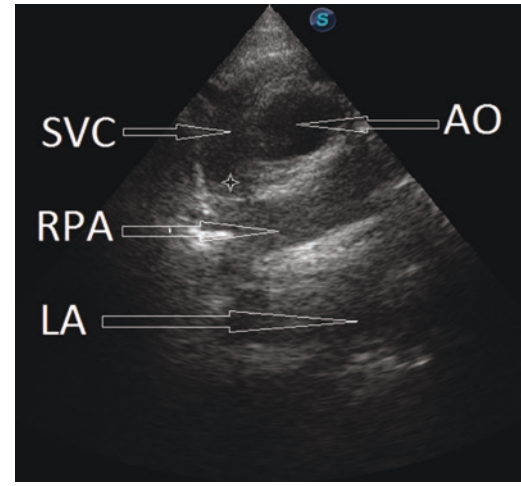

Fig. 11.10 Parasternal short axis view allowing verification of the correct catheter trajectory and tip location. *SVC* superior vena cava, *Ao* aorta, *RPA* right pulmonary artery, *LA* left atrium. The star within the SVC represents the expected correct location of the catheter tip

11.3.3 Complications

- Pneumothorax, hemothorax.
- Pericardial effusion.
- CCA puncture, hematoma, pseudo aneurysm, arterio-venous fistula.
- Arrhythmia.
- Thoracic duct lesion.

11.4 Ultrasound-Guided Subclavian Vein Cannulation

The subclavian vein cannulation is repeated as the CVC emplacement with the lowest rate of infectious complications, in this regard, centers

for disease control and prevention recommend the subclavian CVC emplacement over the femoral and IJV sites [6]; moreover, the subclavian vein is still patent even in the situation of deep hypovolemia; however, the subclavian vein courses in a non-accessible zone for external compression, in close relation to the pleura, subclavian artery, brachial plexus, and thoracic duct; all these factors make the subclavian vein cannulation a high risk procedure; ultrasound guidance is regarded as the adapted tool to reduce the incidence of these complications.

The two approaches for subclavian vein cannulation are described as:

- The infraclavicular approach: often, allows cannulation of the distal part of the axillary vein; nevertheless, it is commonly accepted as subclavian vein cannulation.
- The supraclavicular approach: is uncommonly performed; nevertheless, it allows a true subclavian vein cannulation.

11.4.1 Anatomic and Sonoanatomic Considerations

11.4.1.1 Anatomic Considerations

The union of the brachial and the basilic vein give a rise to the axillary vein; the latter courses in the lateral chest wall in the deltopectoral groove, at the lateral border of the first rib; the axillary vein receives the cephalic vein and becomes the subclavian vein (Fig. 11.11). The subclavian vein courses initially in cranial direction, from the clavicle until its union with the ipsilateral IJV to give a rise to the brachiocephalic trunk, the subclavian vein courses medially; the subclavian artery runs posterior and superior to the subclavian vein, the pleura and the lung are underneath the subclavian vein.

11.4.1.2 Sonoanatomic Considerations

- The subclavian vein is a deep structure comparatively to the IJV.

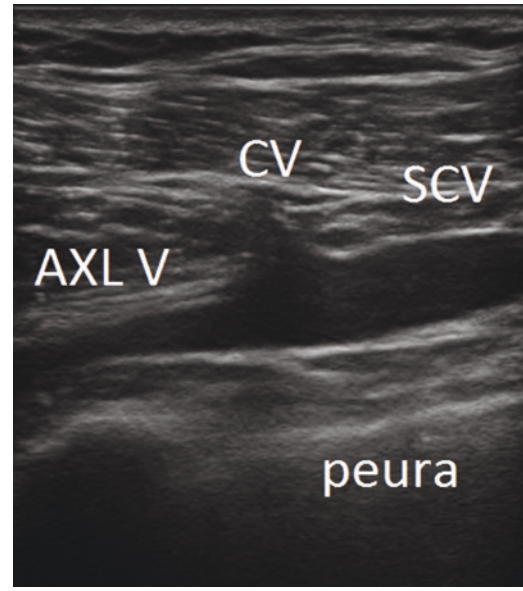

Fig. 11.11 Long axis view of the proximal segment of the axillary vein (AXL V), the distal segment of the subclavian vein (SCV), and the cephalic vein connection to the AXL V

- The subclavian vein runs underneath the clavicle, which greatly interferes with its echographic imaging.
- The subclavian vein is closely related to vital structures: pleura and lung, the subclavian artery, and the brachial plexus; therefore, imaging of these structures before proceeding is mandatory.
- Cannulation of the subclavian vein more distal to the clavicle reduces the risk of pneumothorax but exposes the patient to the risk of brachial plexus and long thoracic nerve injury.
- The trajectory of the right subclavian vein is more horizontal and shorter; it is preferred for venous cannulation over the left one.

11.4.2 Cannulation Technique

Patient is lying supine in the Trendelenburg position, the practitioner comfortably positioned at either the head or the arm on the same side as the subclavian vein to be cannulated, abduction and

external rotation of the arm helps to visualize the subclavian vein.

11.4.2.1 The Infraclavicular Approach

Scan the anterior chest wall to identify the axillary vein and assess its anatomy and patency, place the transducer in horizontal position with the medial side over the clavicle seen in the screen as a hyperechoic structure, identify the proximal axillary vein, the union between the cephalic vein and the axillary vein represents the border between the proximal axillary vein and the subclavian vein (Fig. 11.11), more cephalic tilting of the transducer brings the subclavian artery into view, subclavian vein can be cannulated using an in-plane (Fig. 11.11) or out-of-plane approach (Fig. 11.12); the optimal subclavian vein cannulation site is the more proximal and superficial segment of the latter, with the best delineation of the surrounding structures; after success in the cannulation of the subclavian vein and threading of the guide wire, the correct location of the latter is verified, in case of ectopic trajectory in the ipsilateral IJV, the guide wire is withdrawn, a firm compression at the base of the neck with caudal orientation of the j end of the guide wire may help to advance the guide wire to the superior vena cava.

The exact location of the catheter tip in the cavo-atrial junction may be verified directly when performing a suprasternal short axis view (Fig. 11.10) or more often indirectly by injection of the agitated saline through the catheter with an echocardiographic visualization of the right atrium.

Scanning the anterior chest wall at the end of the procedure allows ruling out an inadvertent pleural puncture with a pneumothorax occurrence.

11.4.2.2 The Supraclavicular Approach

In the supraclavicular approach, the subclavian vein is cannulated between the medial border of the clavicle and the clavicular insertion of the sternocleido-mastoid muscle, the ipsilateral IJV is swiped in all its length caudally till the clavicle; at this point, the transducer is tilted anteriorly which brings to the view the union of the IJV and the subclavian vein, a slight adjustment of the transducer allows visualization of the subclavian vein in its long axis (Figs. 11.13 and 11.14), the subclavian vein is cannulated using an in-plane

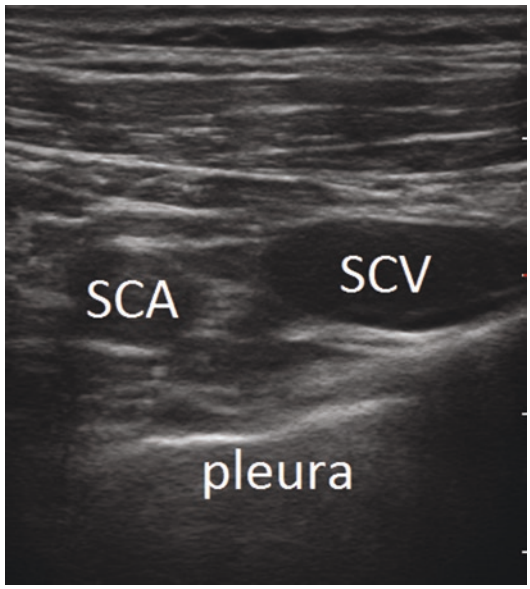

Fig. 11.12 Short axis view of the subclavian vessel showing the close relation with the pleura. *SCA* subclavian artery, SCV subclavian vein

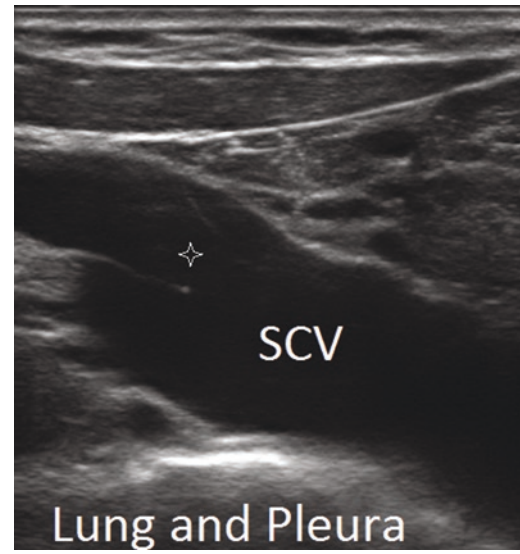

Fig. 11.13 Long axis view of the subclavian vein (SCV) for supraclavicular approach. The star represent venous valve

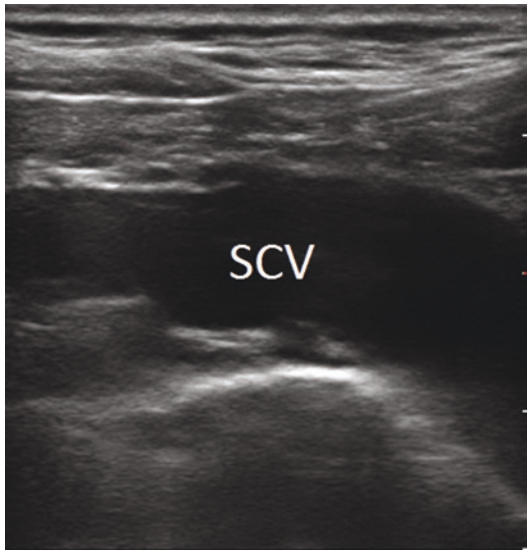

Fig. 11.14 long axis view of the subclavian vein (SCV) for supraclavicular approach

approach with the aim to avoid pleural puncture, after a successful cannulation of the subclavian vein, the remainder of the procedure is performed as the infraclavicular approach.

11.4.3 Complications

- Pneumothorax, hemothorax.
- Pericardial effusion.
- Subclavian artery puncture, hematoma, pseudo aneurysm, arterio-venous fistula.
- Arrhythmia.
- Thoracic duct lesion.

11.5 Femoral Vein Cannulation

Common femoral vein cannulation represents an alternative for CVC insertion when access to the upper extremity is restricted; when the current indication represents the extracorporeal membrane oxygenation (ECMO) cannulation emplacement, temporary intravenous pacing, and urgent CVC emplacement in non-ideal aseptic conditions which demand to be replaced in the upper body when aseptic conditions are right.

11.5.1 Anatomic and Sonoanatomic Considerations

11.5.1.1 Anatomic Considerations

The common femoral vein drains blood from the lower limb.

In the inguinal crest, it is located medially to the common femoral artery.

11.5.1.2 Sonoanatomic Consideration

- The common femoral vein is a relatively deep structure that may require a curvilinear transducer for an optimal visualization.
- The common femoral vessels overlapping can cause an accidental femoral artery puncture when attempting CVC emplacement at this level.

11.5.2 Cannulation Technique

The patient is lying supine with the inferior leg abducted and externally rotated. The operator is placed on the ipsilateral side to be cannulated, common femoral vein cannulation may be performed using in-plane approach (Fig. 11.15);

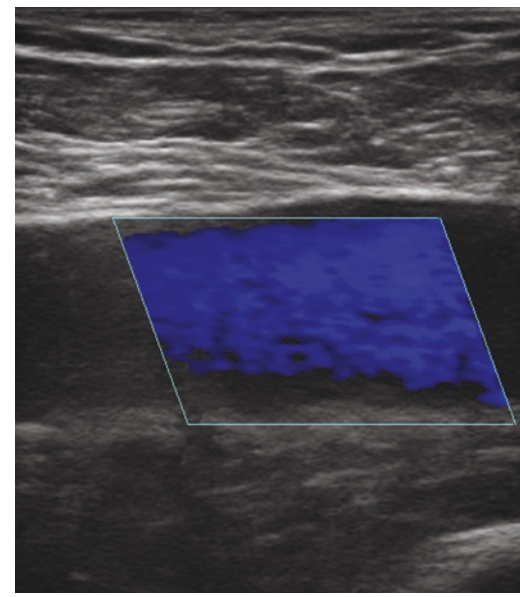

Fig. 11.15 Long axis view of the femoral vein with color Doppler aspect

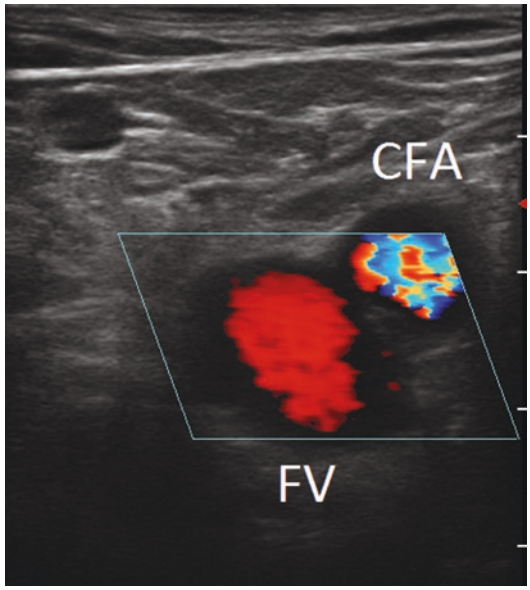

Fig. 11.16 Short axis view of the femoral vessels with color Doppler aspect

however, out-of-plane is the standard practice (Fig. 11.16); ultrasound transducer is placed transversally just below the inguinal crest, the common femoral vein appears as an oval-shaped, anechoic structure located medially and often posteriorly to the common femoral artery.

11.6 Peripherally Inserted Central Catheter Lines

11.6.1 Definition

Peripherally inserted central catheter lines (PICCs lines) are a subgroup of the central venous catheters, with length ranging from 50 to 60 cm, inserted in the upper limb peripheral vein and advanced till the catheter tip is in central position (superior vena cava–right atrium junction), it is a medium-term venous access, the predictable usage period ranges from a few weeks to 6 months.

11.6.2 Indications

PICCs lines are indicated for all patients, requiring midterm reliable venous access, for perfusion or repeated blood sampling, either with inpatients or with outpatients, the principal indications are:

- Difficult venous access.
- Medium term intravenous medication administration.
- Continuous or repeated administration of medications or solutions which potentially irritate peripheral veins.
- Repeated blood or blood-derived products administration.
- Repeated blood sampling.
- Anatomic conditions complicating CVC insertion.
- Coagulation disorders.
- High flow infusions.

11.6.3 Contraindications

The relative contraindications for PICCs lines insertion are:

- Burns, local skin infection, trauma, and venous thrombosis in the insertion site.
- Bacteremia.
- Prevision dialysis access insertion or arteriovenous fistula creation.
- Small peripheral venous diameter.
- Conditions cause a repeated cough and vomiting.

11.6.4 Technique

11.6.4.1 Initial Scan

The aim of the initial scan is the identification of a patent's upper limb peripheral vein which can accommodate PICC line catheter.

The choice of insertion site is made among the following peripheral veins:

- Right basilic vein (Fig. 11.17): is the best choice, given its caliber and its direct continuity with the right subclavian vein, which has a short course and in direct continuity with the superior vena cava.

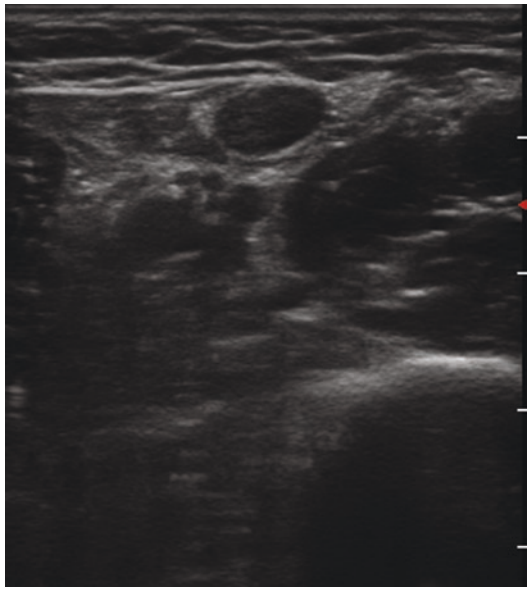

Fig. 11.17 Basilic vein short axis view

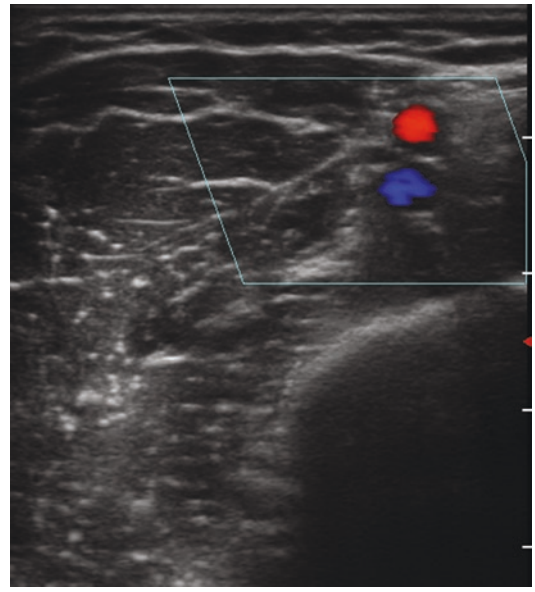

Fig. 11.18 Cephalic vein short axis view

- Median cubital vein: elbow bending may cause patient discomfort, phlebitis, and PICC line displacement.
- Cephalic vein (Fig. 11.18): it has a tortuous course and a relatively sharp angle connection to the subclavian vein making PICC line catheter advancement difficult.
- Brachial vein (Fig. 11.19): is a deep vein with risks of brachial artery puncture and median nerve injury.

11.6.4.2 Material and Preparation

- The modified Seldinger technique is the most used for PICC lines insertion.
- The PICC line catheter differs in length, lumen number, valves may be present or absent.
- To the classical set used for ultrasound-guided CVC, add PICC insertion kit which includes:
  - PICC catheter.
  - Guide wire.
  - Dilatators.

11.6.4.3 Procedure (Modified Seldinger Method)

- Measure the length of the PICC line catheter to be inserted, by measuring the distance from the insertion site to the mid-clavicular line then to the third intercostal space.

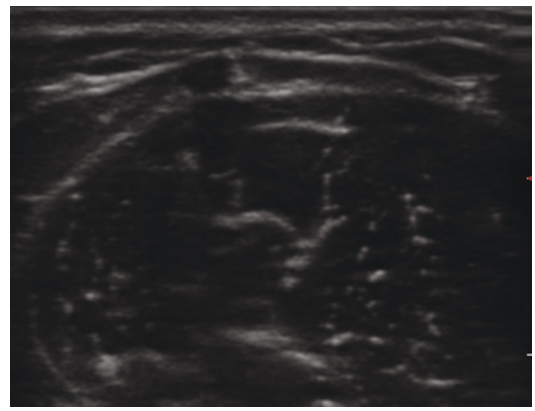

Fig. 11.19 Brachia artery and vein short axis view, with color Doppler aspect

- Absolute aseptic conditions must be observed throughout the procedure, the same as for CVC insertion.
- Skin disinfection according to the local protocol.
- Anesthetize skin.
- Ultrasounds scan.
- Needle insertion using transverse or longitudinal approach till successful vein puncture.
- Thread guide wire and verify its venous location using ultrasound.
- Create a small nick at the insertion site using a scalpel.

- Insert dilator and introducer through the guide wire.
- Remove the guide wire and dilator.
- Insert catheter through the introducer till the measured length.
- Remove the introducer.
- Confirm the correct placement of the catheter by scanning all the length of the peripheral vein used for PICC insertion and the axillary vein.
- The catheter tip location may be verified directly using phased array transducer in suprasternal notch (Fig. 11.10), or indirectly by injection of agitated saline through the catheter with right atrium visualization.
- Secure the catheter and cover using sterile dressing.

11.6.5 Complications

- Infection.
- Catheter malposition or secondary migration.
- Catheter malfunction.
- Phlebitis.
- Air embolism.
- Arrhythmia.
- Pericardial effusion.

11.7 Ultrasound-Guided Arterial Cannulation

The adjunction of ultrasound to guide arteries cannulation improves the success rate of the procedure, decreases the numbers of attempts, time spent till cannulation, and complications rate [7]; moreover, ultrasound allows cannulation of non-conventional insertion sites, for example, the temporal, axillary arteries [8].

11.7.1 Technique

11.7.1.1 Preparation

- Patient lying comfortably supine.
- Ultrasound machine with a high-frequency ultrasound transducer.
- Ergonomy is crucial, respect axis: operator, insertion site, and screen.
- Cannulation site preparation and sterilization according to the local protocol.
- The overall procedure must be performed using sterile technique.
- To the classic set used for blind arterial cannulations, adding a sterile sleeve for ultrasound transducer and sterile gel.

11.7.1.2 Transverse Versus Longitudinal Approach

Transverse Approach

In transverse approach, the artery is visualized in its short axis; this approach permits to puncture the artery in its midline; however, it requires a dynamic tracking of the needle tip.

Longitudinal Approach

In the longitudinal approach, the artery is visualized in its long axis; this approach permits the needle to be visualized in all its length; however, artery puncture may occur laterally to the midline, which complicates the guide wire progression; it is worth mentioning that keeping the alignment of the ultrasound beam with the needle and the artery may be challenging.

11.7.2 Arteries Cannulation Sites Particularities

11.7.2.1 Radial Artery

For radial artery cannulation (Figs. 11.20 and 11.21), the use of an arm board to support the upper limb may be a useful adjunct. Mild dorsiflexion of the hand helps to introduce the needle with a flat angle; the transducer is placed transversally in the lateral aspect to identifier, then advance the needle toward the radial artery in the transverse approach.

11.7.2.2 Femoral Artery

For femoral artery cannulation (Fig. 11.16), the lower limb is abducted and externally rotated, it is the same procedure as for common femoral vein cannulation.

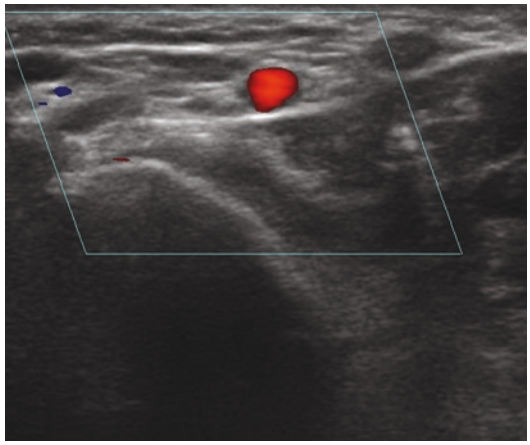

Fig. 11.20 Short axis view of the radial artery, with color Doppler aspect

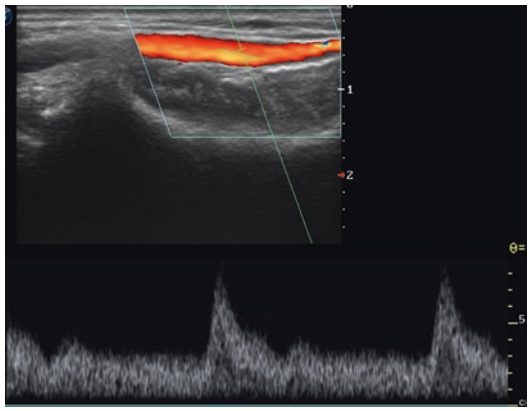

Fig. 11.21 Radial artery long axis view with color and pulsed wave Doppler aspect

11.7.2.3 Dorsalis Pedis Artery

Dorsalis pedis artery is a small artery that is easily compressed by the transducer; mild foot planter flexion helps to introduce the needle with flat angle.

11.7.2.4 Posterior Tibial Artery Cannulation (Figs. 11.22 and 11.23)

The posterior tibial artery cannulation may be an alternative for radial cannulation with children, the ankle is maintained in dorsiflexion and eversion position, the transducer is placed transversally between the lateral malleolus and Achilles

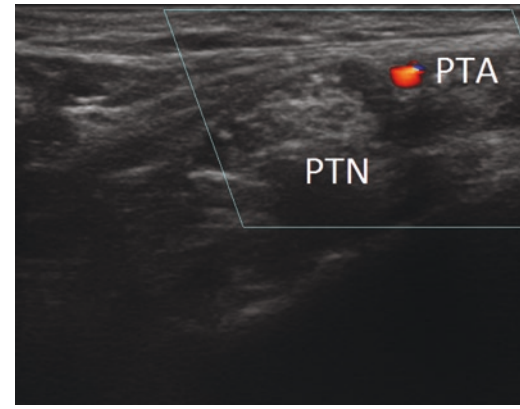

Fig. 11.22 Posterior tibial artery (PTA) short axis view with color Doppler aspect; *PTN* posterior tibial nerve

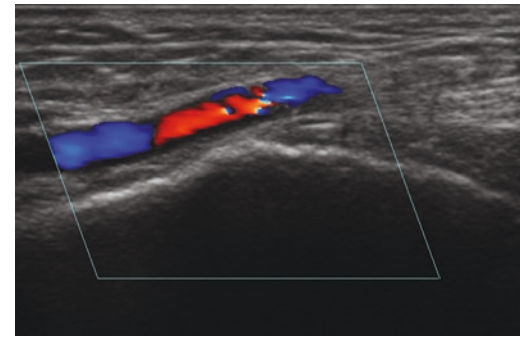

Fig. 11.23 Long axis view of the posterior tibial artery with color Doppler aspect

tendon; at this level, the posterior tibial vessels are beside the posterior tibial nerve.

11.8 Ultrasound-Guided Peripheral Venous Cannulation

Despite the fact that peripheral venous cannulation is usually a simple procedure; the presence of some pathologic or physiologic conditions renders the blind procedure difficult or even more impossible; delay or failure in peripheral venous cannulation insertion may lead to medications administration delay and may require CVC emplacement, with all inherent complications.

Ultrasound-guided peripheral venous cannulation is seen as the adapted technique to over-

come peripheral venous cannulation difficulties. Despite the conflicting literature, there is wide agreement that ultrasound-guided peripheral venous cannulation at least increases the overall success rate compared to the blind technique [9, 10].

11.8.1 Indications

There is no data or consensus which shows the precise indication for ultrasound peripheral venous cannulation; nevertheless, these indications may be divided into two groups:

11.8.1.1 Primary Indications

Primary indications are represented by clinical situations with predicted difficulty for peripheral venous insertion, the common factors associated with difficult peripheral venous access are: body habitus, anatomical variations, soft-tissue edema, intravenous drugs abuse, dehydration, medical conditions (diabetes, sickle cell disease) [11, 12].

11.8.1.2 Secondary Indications

Secondary indications are represented by all situations when the blind approach fails.

11.8.2 Technique

11.8.2.1 Initial Scan

The three potential veins to be cannulated in the upper arm are basilica (Fig. 11.17), cephalic (Fig. 11.18), and brachial veins (Fig. 11.19); therefore, the scan is performed with the transducer in transverse position after tourniquet application, starting from the antecubital fossa to the medial and lateral aspects of the arm. The basilic vein is a superficial vein; however, in close relation with the medial cutaneous nerve of the forearm; the brachial vein is relatively a deep target in close relation with the humeral and median nerve; cephalic vein may be a reasonable choice.

11.8.2.2 Distinguish Vein from Artery

Classically, veins are oval-shaped with a thin wall, easily collapsed with gentle pressure from the transducer, does not express pulsations, distal limb pressure increase blood flow in the vein, and valves may be present within the vein lumen.

11.8.2.3 Choice of the Vein to be Cannulated

The ideal vein to be cannulated has four criteria:

1. Shallow Vein

   Overall success increases when the vein is located within depth ranging between 0.3 and 1.5 cm and decreases for depth greater than 1.6 cm [13]; for shallowest vein to overcome artifacts situated in the near echographic sector, a small saline bag may be placed between the transducer and the skin.
2. Large Vein

   The selection of vein with the internal diameter of more than 0.4 cm is shown to increase the success rate [13].
3. Straight Vein

   As in the blind technique, selections of vein with straight course facilitate the venous cannulation process.
4. Patent Vein

   Vein easily compressible by applying gentle pressure; totally colored when using color Doppler, and the absence of material occupying the lumen.

11.8.2.4 Material and Preparation

- High-frequency transducer, with superficial depth and focal setting.
- Patient in sitting or supine position.
- Upper limb fully extended and externally rotated; the use of arm board support is a useful adjunction.
- Choose a long intravenous catheter to reduce the risk of dislodgement from the vein.
- Higher application of the tourniquet relatively to the insertion site.
- Skin sterilization according to the local protocol.

- To the classical material used for peripheric venous cannulation, add sterile gel and sleeve for transducer.
- It is recommended to execute the procedure under aseptic conditions.

11.8.2.5 Transverse Versus Longitudinal Approach

Transverse Approach

In transverse approach, the transducer is placed perpendicular to the upper limb axis, the selected vein for cannulation therefore is visualized in its short axis, the needle is inserted at the center of the transducer long axis, and steep angle of insertion relative to the skin is recommended to increase the intravenous catheter length, which reduces the risk of dislodgement of the catheter. After initial catheter insertion, the operator will focus on needle tip location using a combination of tilt and translation movement of the transducer; the needle shaft is visualized as a hyperechoic dot; its disappearance when the transducer is sequentially translated and tilted indicates the needle tip location; once the needle tip is located, the needle is advanced a few millimeters toward the targeted vein; this process is repeated till the needle tip induces tenting of the anterior vein wall. At this level, a firm needle advancement allows vein puncture, more anterior transducer tilting allows verification with respect to the posterior wall, venous blood reflux in the hub catheter and catheter flush using agitated saline confirm the intravenous needle location. At this stage, lowering of the needle hub allows more alignment of the catheter relatively to the vein which makes the catheter advancement easier.

Longitudinal Approach

Start by visualizing the targeted vein in the center of the screen, a 90° rotation of the transducer allows vein display in its long axis; the needle is inserted in the center of the transducer's short axis and advanced toward the targeted vein under real-time visualization of the needle in all its length; once the needle tip punctures the anterior vein wall, lowering of the needle hub allows easy intravenous catheter advancement.

11.8.3 Complication

- Arterial puncture.
- Nerve injury: median nerve, medial cutaneous nerve of the forearm.
- Thrombophlebitis.

11.9 Pediatric Considerations

11.9.1 Central Venous Access

- The use of ultrasound guidance for CVC insertion is consensually recommended by multiple organizations [14, 15].
- The anatomic particularity is mainly represented by a shorter vessel with reduced diameter, close relation with the surrounding structure which increases the likelihood of inadvertent puncture, and higher incidence of anatomic variability and infection relatively to the adult population [16–18].
- Advantage of ultrasound guidance for IJV insertion in pediatric population is clearly demonstrated [19].
- Ultrasound-guided insertion of PICC in pediatric population shows advantages relatively to the blind technique [20].
- The supraclavicular approach for CVC of the brachiocephalic vein is well described for the pediatric population; however, more validation is needed to be adapted into clinical routine practice.

11.9.2 Peripheral Venous Cannulation

In the emergency setting, ultrasound peripheral intravenous cannulation is superior to the blind technique, with increase in the overall success rate (80% vs. 64%), decreasing in the number of puncture (1 vs. 3) [21].

11.9.3 Arterial Cannulation

The adoption of ultrasound technique compared to the blind technique allows increasing of the ratio of first attempt success and decreasing of the complication ratio [22].

References

1. Practice guidelines for central venous access 2020. Anesthesiology. 2020;132(1):8–43.
2. Verghese ST, McGill WA, Patel RI, Sell JE, Midgley FM, Ruttimann UE. Ultrasound-guided internal jugular venous cannulation in infants. Anesthesiology. 1999;91(1):71–7.
3. Denys BG, Uretsky BF, Reddy PS. Ultrasound-assisted cannulation of the internal jugular vein. A prospective comparison to the external landmark-guided technique. Circulation. 1993;87(5):1557–62.
4. McGee DC, Gould MK. Preventing complications of central venous catheterization. N Engl J Med. 2003;348(12):1123–33.
5. Aithal G, Muthuswamy G, Latif Z, Bhaskaran V, Haji Sani HS, Shindhe S, et al. An alternate in-plane technique of ultrasound-guided internal jugular vein cannulation. J Emerg Med. 2019;57(6):852–8.
6. O'Grady NP, Alexander M, Burns LA, Dellinger EP, Garland J, Heard SO, et al. Summary of recommendations: guidelines for the prevention of intravascular catheter-related infections. Clin Infect Dis. 2011;52(9):1087–99.
7. Shiver S, Blaivas M, Lyon M. A prospective comparison of ultrasound-guided and blindly placed radial arterial catheters. Acad Emerg Med. 2006;13(12):1275–9.
8. Troianos CA, Hartman GS, Glas KE, Skubas NJ, Eberhardt RT, Walker JD, et al. Guidelines for performing ultrasound guided vascular cannulation: recommendations of the American Society of Echocardiography and the Society of Cardiovascular Anesthesiologists. J Am Soc Echocardiogr. 2011;24(12):1291–318.
9. Egan G, Healy D, O'Neill H, Clarke-Moloney M, Grace PA, Walsh SR. Ultrasound guidance for difficult peripheral venous access: systematic review and meta-analysis. Emerg Med J. 2013;30(7):521–6.
10. Stolz LA, Stolz U, Howe C, Farrell IJ, Adhikari S. Ultrasound-guided peripheral venous access: a meta-analysis and systematic review. J Vasc Access. 2015;16(4):321–6.
11. Fields JM, Piela NE, Au AK, Ku BS. Risk factors associated with difficult venous access in adult ED patients. Am J Emerg Med. 2014;32(10):1179–82.
12. Loon FHJV, Puijn LAPM, Houterman S, Bouwman ARA. Development of the A-DIVA scale: a clinical predictive scale to identify difficult intravenous access in adult patients based on clinical observations. Medicine (Baltimore). 2016;95(16):e3428.
13. Witting MD, Schenkel SM, Lawner BJ, Euerle BD. Effects of vein width and depth on ultrasound-guided peripheral intravenous success rates. J Emerg Med. 2010;39(1):70–5.
14. Brass P, Hellmich M, Kolodziej L, Schick G, Smith AF. Ultrasound guidance versus anatomical landmarks for internal jugular vein catheterization. Cochrane Emergency and Critical Care Group, éditeur. Cochrane Database Syst Rev. 2015;1(1):CD006962. https://doi.org/10.1002/14651858.CD006962.pub2.
15. Brass P, Hellmich M, Kolodziej L, Schick G, Smith AF. Ultrasound guidance versus anatomical landmarks for subclavian or femoral vein catheterization. Cochrane Emergency and Critical Care Group, éditeur. Cochrane Database Syst Rev. 2015;1(1):CD011447. https://doi.org/10.1002/14651858.CD011447.
16. Mallinson C, Bennett J, Hodgson P, Petros AJ. Position of the internal jugular vein in children. A study of the anatomy using ultrasonography. Pediatr Anesth. 1999;9(2):111–4.
17. Bhatia N, Sivaprakasam J, Allford M, Guruswamy V. The relative position of femoral artery and vein in children under general anesthesia - an ultrasound-guided observational study. Pediatr Anesth. 2014;24(11):1164–8.
18. Ullman AJ, Marsh N, Mihala G, Cooke M, Rickard CM. Complications of central venous access devices: a systematic review. Pediatrics. 2015;136(5):e1331–44.
19. Bruzoni M, Slater BJ, Wall J, St Peter SD, Dutta S. A prospective randomized trial of ultrasound- vs landmark-guided central venous access in the pediatric population. J Am Coll Surg. 2013;216(5):939–43.
20. Katheria AC, Fleming SE, Kim JH. A randomized controlled trial of ultrasound-guided peripherally inserted central catheters compared with standard radiograph in neonates. J Perinatol. 2013;33(10):791–4.
21. Doniger SJ, Ishimine P, Fox JC, Kanegaye JT. Randomized controlled trial of ultrasound-guided peripheral intravenous catheter placement versus traditional techniques in difficult-access pediatric patients. Pediatr Emerg care. 2009;25(3):154–9.
22. Aouad-Maroun M, Raphael CK, Sayyid SK, Farah F, Akl EA. Ultrasound-guided arterial cannulation for paediatrics. Cochrane Emergency and Critical Care Group, éditeur. Cochrane Database Syst Rev. 2016;9(9):CD011364. https://doi.org/10.1002/14651858.CD011364.pub2.

E-FAST and Abdominal Ultrasound

12

Divesh Arora, Hetal Vadera, and Amrita Rath

12.1 Introduction

Extended Focused Assessment with Sonography in Trauma (E-FAST) is defined as a point-of-care ultrasound examination (POCUS) for the detection of free fluid and pathological condition in the abdominal, pelvic, pericardial, and thoracic cavity with an additional ability to detect pneumothorax.

Before the introduction of Focused Assessment with Sonography in Trauma (FAST), Diagnostic Peritoneal Lavage (DPL) was used to diagnose haemoperitoneum in trauma patients. DPL is an invasive procedure with excellent sensitivity but poor specificity [1]. Computed tomography (CT) scan is considered the gold standard for blunt abdominal trauma patients, but it is not suitable for unstable patients for whom it is difficult to transfer patients to the CT room [2] and also carries the risk of radiation exposure. At the same time, E-FAST is a bedside, quick, and repeatable procedure with excellent specificity and moderate sensitivity.

D. Arora (✉)
Department of Anaesthesia and OT Services, Asian Hospital, Faridabad, Haryana, India

H. Vadera
Department of Anaesthesia, Sterling Hospital, Rajkot, Gujarat, India

A. Rath
Department of Anaesthesia, IMS, BHU, Varanasi, UP, India

FAST has become quite popular amongst emergency physicians, intensivists, and anaesthesiologists in the last few decades. It has been used in Europe since the 1980s but became popular in the USA after the 1990s. Grace Rozycki, a trauma surgeon, coined the word FAST and introduced the protocol of imaging at four potential spaces where fluids get collected [3].

Over the years, FAST has become a standard of care for the management of patients with a history of trauma at the emergency department. The FAST examination was initially designed for the detection of blood in peritoneal and pericardial cavity in trauma patients. In the era prior to FAST examination, trauma survey involved the use of physical signs, auscultation, and chest X-ray evaluation to detect pneumothorax and haemothorax. However, ultrasound has better sensitivity and specificity for diagnosis of pneumothorax in comparison to a chest X-ray [4]. The concept of E-FAST was propounded by Kirkpatrick and colleagues in 2004 [5]. E-FAST examination allows for concomitant evaluation of pneumothorax and fluid in pleural cavities using bilateral anterior thoracic views and bilateral costophrenic views, respectively, in addition to the detection of haemopericardium and haemoperitoneum as is being done using FAST examination. In the last two decades, the applicability of POCUS has increased because of the availability of portable ultrasound machines with better resolution and advanced software technology. E-FAST is a reli-

© The Author(s), under exclusive license to Springer Nature Switzerland AG 2024

N. Bouarroudj et al. (eds.), *POCUS in Critical Care, Anesthesia and Emergency Medicine*,
https://doi.org/10.1007/978-3-031-43721-2_12

able decision-making tool for trauma patients. Though originally designed for decision-making in abdominal and thoracic injury patients for immediate surgery, it is now being extensively used in the perioperative period for non-trauma settings.

David Bahner et al. in 2012 described the novel Indication, Acquisition, Interpretation, and Medical Decision-Making (I-AIM) framework as a novel teaching model to learn the FAST exam. Since its original description, the I-AIM framework remains a standardised mnemonic and checklist tool for POCUS [6].

12.2 Preparation Equipment and Technique

E-FAST examination is possible with most modern-day ultrasound machines.

12.2.1 Transducer Selection

Curvilinear transducer (2–5 MHz frequency) or phased array transducer (1–5 MHz transducer) used for echocardiography are preferred transducers for E-FAST examination as it involves visualisation of deeper structures in thoracic and abdominal cavity (Fig. 12.1). A linear transducer having high frequency (6–14 MHz) is sometimes used for scanning pleura as it is a superficial structure, and linear transducer provides higher resolution images.

An advantage of using phased array transducer is that it has a smaller footprint which helps to place it in between ribs and the transducer change is not needed for obtaining a cardiac subcostal view. However, it has a poor resolution as compared to a curvilinear transducer while scanning abdominal cavity.

12.2.2 Orientation Marker

The orientation marker is the notch on the transducer which corresponds to an orientation indicator which is a dot on the screen. By convention, it is kept cranially in sagittal scanning and towards the right side of the patient in transverse scan.

The orientation indicator appears on the left side of the ultrasound machine for abdominal scanning using a curvilinear transducer or doing an anterior thoracic cavity scan using a linear transducer (Fig. 12.2). If a phased array transducer is used for performing subcostal examination, the orientation indicator is located on the right side of the ultrasound machine. This fact

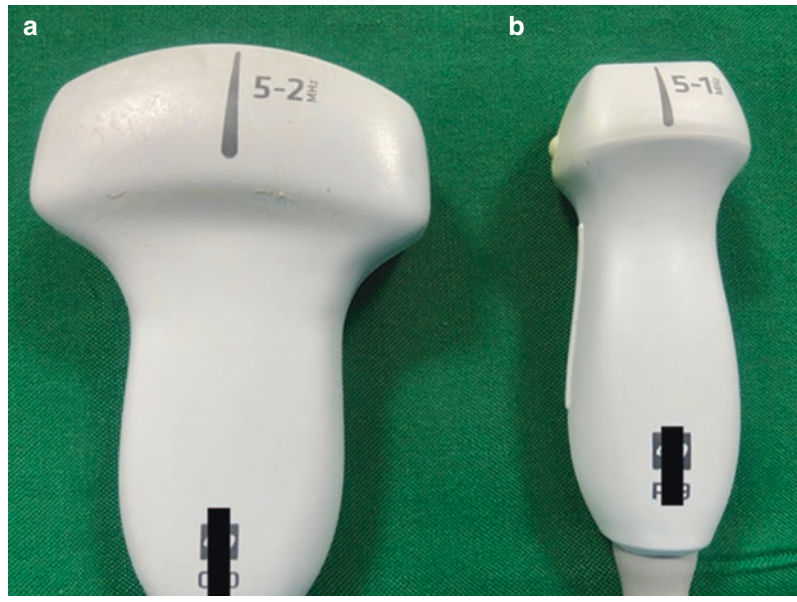

Fig. 12.1 (**a**) Curvilinear transducer. (**b**) Phased array transducer

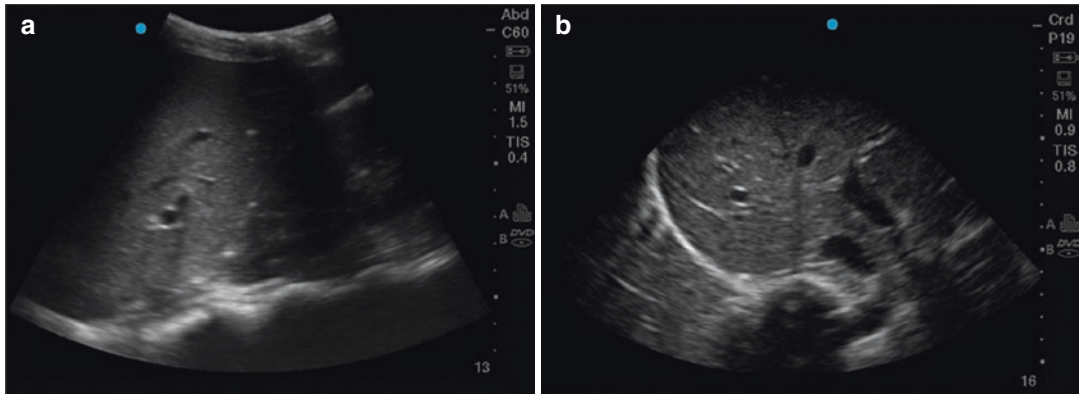

Fig. 12.2 (**a**) Orientation indicator curvilinear transducer. (**b**) Orientation indicator phased array transducer

must be kept in mind when using a phased array for obtaining subcostal window for E-FAST examination.

12.2.3 Patient Position

The patient is positioned in a supine position with arms abducted if possible. Trendelenburg position improves sensitivity of the right upper quadrant (RUQ) view, and the reverse Trendelenburg position improves sensitivity of the left upper quadrant (LUQ) view. It helps to detect the smaller quantity of blood inside the peritoneum.

12.2.4 E-FAST Sequence

E-FAST examination is performed during the circulatory phase of the primary survey following trauma. E-FAST examination involves eight views. The E-FAST examination can be performed in any sequence but is started in RUQ as this area has the maximum sensitivity for fluid accumulation. The typical sequence to be followed for the E-FAST examination as per author's experience is shown in Fig. 12.3.

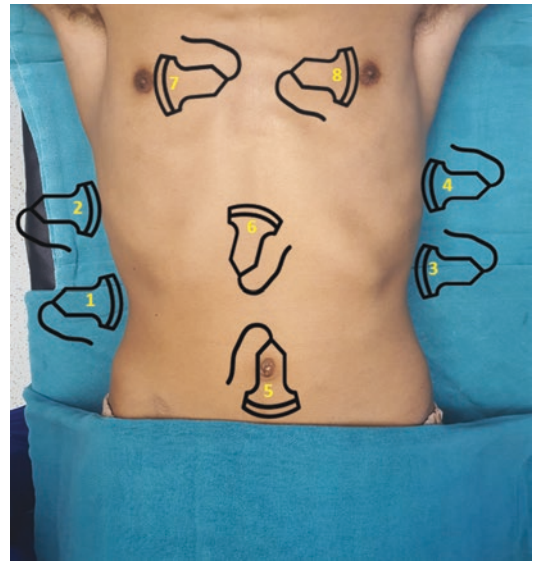

Fig. 12.3 Patient position and scanning sequence for E-FAST examination. **1** RUQ view **2** Right costophrenic space view **3** LUQ view **4** Left costophrenic space view **5** Pelvic (longitudinal and transverse view) **6** Subcostal view **7** Right anterior thoracic cavity view **8** Left anterior thoracic cavity view

12.3 Anatomy

E-FAST examination relies on finding free fluid in either of the four cavities:

- Abdominal cavity
- Pelvic cavity
- Pericardial sac
- Pleural cavity

E-FAST examination assumes that fluid which accumulates in any of the cavities in a trauma patient reflects blood collection in these cavities. With patient in supine position, hepatorenal space, splenorenal recess, and pelvic cavity are the most dependent regions of the peritoneal cavity where fluid accumulates [7]. With abdominal injury secondary to trauma, free fluid or blood will first collect in the dependent part of the abdominal cavity (pelvis) in a supine patient. As the blood keeps accumulating, it spills over to the Morrison's pouch through the right paracolic gutter. In case of abdominal organ injury arising in the left hypochondrium, free fluid or blood will accumulate first in subphrenic space and subsequently will spill over into the splenorenal recess and finally find its way to the Morrison's pouch. Air collects anteriorly in a patient in the supine position secondary to blunt or penetrating thoracic trauma.

12.4 Sonoanatomy E-FAST Views

12.4.1 Right Upper Quadrant View

RUQ view of E-FAST examination involves visualisation of liver, kidney, diaphragm, and lung. RUQ view, the most important view, is done first in the E-FAST sequence. It is considered the most sensitive view for detecting free fluid in the upper peritoneal cavity as it is the most dependent point of the upper peritoneum when supine. In this view, the areas assessed are Morrison's pouch (between liver and kidney), right subdiaphragmatic area, and right paracolic gutter. A curvilinear transducer with the orientation marker directed cephalad is placed in the coronal plane at the mid-axillary line in the eighth to eleventh right intercostal space (Fig. 12.4). Clinician should aim for the identification of the liver, kidney, diaphragm, and spine. Slight counterclockwise rotation of transducer is helpful if rib shadow obscures the view. Tilting of the transducer in anteroposterior direction will help to find Morrison's pouch. The transducer is moved caudally to evaluate the inferior edge of the liver and to identify right paracolic gutter, which represents a space between the lateral abdominal wall and ascending colon and is a potential space for free fluid collection.

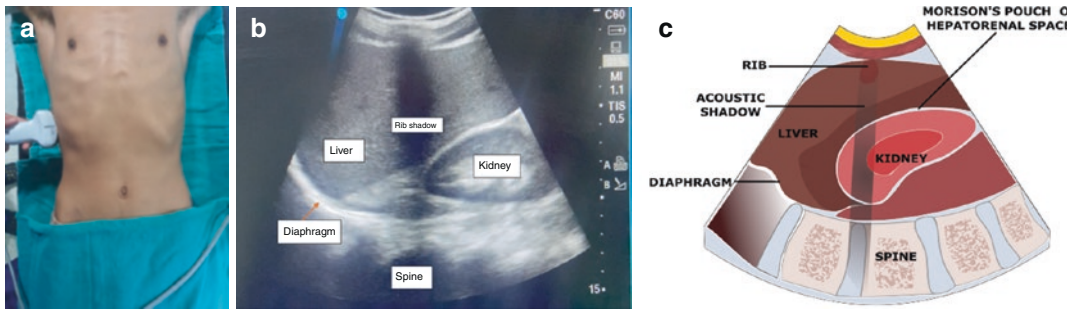

Fig. 12.4 (**a**) Transducer position for RUQ examination. (**b**) Sonoanatomy RUQ view. (**c**) RUQ view schematic

After the E-FAST examination of the right upper quadrant is complete, the ultrasound probe is moved cranially in the midaxillary line at the sixth to eighth intercostal space to visualise the lungs and the right costophrenic space for fluid accumulation. Diaphragm appears as a bright hyperechoic line on ultrasound. Fluid, if present, will be seen as a black anechoic or at times hypoechoic collection between the lungs, pleural cavity, and diaphragm. In normal individuals, liver may be seen as artefact superior to diaphragm because of ultrasound waves getting reflected from the diaphragmatic surface.

12.4.2 Subcostal View

Subcostal or subxiphoid view of the E-FAST examination involves visualisation of liver, heart, pericardium, and evaluation of the pericardial sac. The subcostal view helps in the optimal evaluation of dependent regions of the pericardial sac. The examination is performed in abdominal preset with a starting depth of 20–25 cm which can be modified according to patient habitus. The curvilinear transducer is placed caudal to the xiphoid process with the orientation marker pointing to the patient's right shoulder. The operator holds the transducer with an overhand grip to depress the transducer into the abdomen. An overhand grip is used to keep the plane of the transducer as parallel as possible to the abdominal wall without the operator's hand interfering with the flattening of the transducer. Once this is achieved, transducer is turned 10°–15° counterclockwise to get the optimal image on the screen (Fig. 12.5). Clinician should aim for the identification of the four chambers of the heart, liver, and pericardial sac. Heart chambers are visualised through the acoustic window of liver. The chamber closest to liver is right ventricle. Pericardium appears as a white hyperechoic line between the liver and heart. At times, it is difficult to obtain the subcostal view in patients with higher body mass index and non-cooperation from the patient. Deep inspiration manoeuvre, which results in

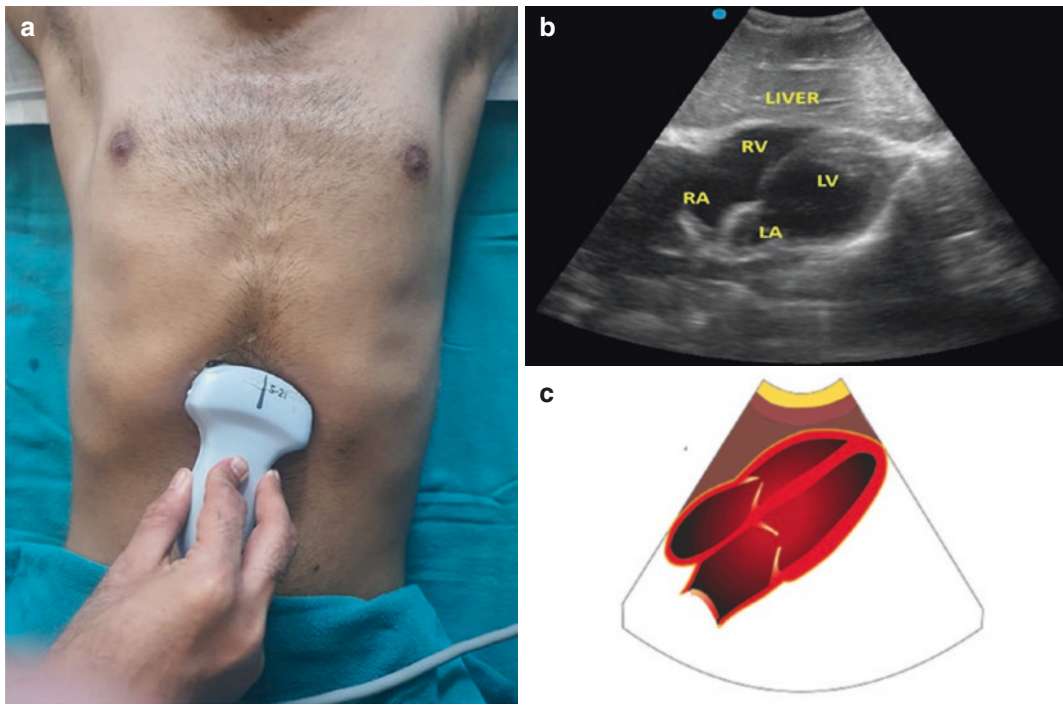

Fig. 12.5 (**a**) Transducer position for subcostal cardiac examination. (**b**) Sonoanatomy subcostal view. (**c**) Subcostal view schematic

negative intrathoracic pressure and improves cardiac filling, helps in the caudal movement of the diaphragm, thereby improving the subcostal view. If possible, patient can be asked to flex their limbs to relax abdominal muscles and improve subcostal view. Alternatively, a long-axis parasternal view can be used to identify the pericardial sac. A phased array cardiac transducer can also be used with cardiac preset and orientation marker towards the patient's left shoulder for subcostal view and towards the patient's right shoulder for long axis parasternal view.

12.4.3 Left Upper Quadrant View

LUQ view of E-FAST examination involves visualisation of spleen, kidney, diaphragm, and lungs. LUQ E-FAST examination is more challenging than RUQ examination because of cephalad position of left kidney and posterior position of spleen. In this view, areas assessed are perisplenic space, left paracolic gutter, and left subdiaphragmatic space. Free fluid is less likely to collect in splenorenal space as the phrenicocolic ligament prevents fluid from migrating into this space. A Curvilinear transducer with orientation marker directed cephalad is placed longitudinally in the posterior axillary line in the sixth to eighth left intercostal space (Fig. 12.6). The clinician needs to knuckle his hand to place the transducer in the posterior axillary line while performing LUQ examination. Slight clockwise rotation of transducer is helpful if rib shadow obscures the view. Tilting the transducer in anterior posterior direction is helpful to assess spleen and perisplenic space. Transducer is moved caudally to visualise the left paracolic gutter, a potential space for free fluid collection located between the lateral abdominal wall on the left side and the descending colon. The transducer is moved cranially to visualise the diaphragm and subdiaphragmatic space, which is a space between the diaphragm and spleen.

After the examination of the left upper quadrant is complete, the transducer is moved cranially to visualise the lungs and the left costo-phrenic space for fluid accumulation. Fluid if present will be seen as a black anechoic or at times hypoechoic collection between the lungs, pleural cavity, and diaphragm. In normal individuals, spleen may be seen as an artifact superior to left side of diaphragm because of ultrasound waves getting reflected from the diaphragmatic surface.

12.4.4 Pelvic View (Long and Short Axis)

Pelvic view of E-FAST examination involves visualisation of bladder, prostate, and rectum in males and visualisation of bladder, uterus, and rectum in females. As pelvis is the dependent part of the peritoneum, pelvic views are of immense importance. In females, the most dependent location is the pouch of Douglas, which is the space between the uterus and the rectum. In males, the rectovesical pouch, which is a space between the bladder and the rectum, is the most dependent location. Pelvic views are obtained in longitudinal as well as transverse orientation.

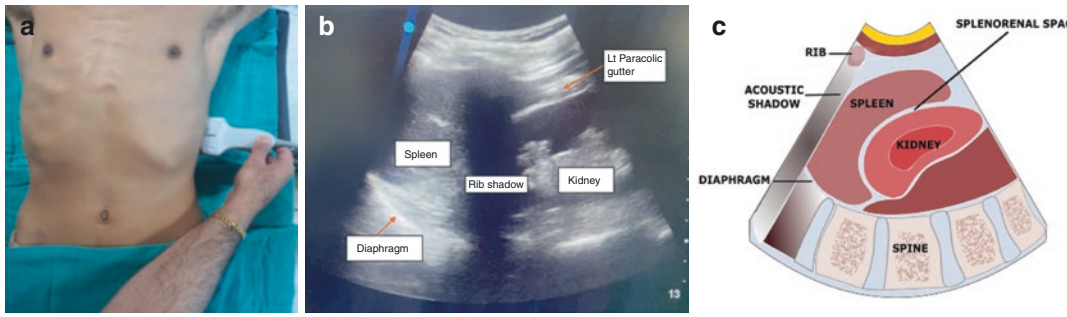

Fig. 12.6 (**a**) Transducer position for LUQ examination. (**b**) Sonoanatomy LUQ view. (**c**) LUQ view schematic

12.4.5 Rectovesical Pouch in Males

In the pelvic view, the bladder is used as the acoustic window for locating free fluid. The detection of fluid becomes easy in head low position and in the presence of bladder which is fluid filled [8]. A full bladder is essential for getting a good sonographic window. However, emptied bladder consequent to catheterisation compromises the detection. The curvilinear transducer is placed cranial to the pubic symphysis with the orientation marker directed towards patient head end to obtain a long axis view. The transducer is gently rocked towards the pelvis (Fig. 12.7). The urinary bladder is seen superior to the pubic bone. The bladder must be kept at the centre of the screen and the structures situated around the bladder are identified. The assessment is done systematically to differentiate each structure. Clinician should aim for the identification of the bladder, the rectum, and the prostate. The transducer is tilted left and right to find the rectovesical pouch. Transverse view of the urinary bladder is obtained by turning the transducer 90° anticlockwise with orientation marker towards the right side. Identification of the bladder, seminal vesicles, and rectum is done in the transverse view (Fig. 12.8).

12.4.6 Rectouterine Pouch in Females

Similarly, as in males, the transducer is placed superior to pubic symphysis and scanned in both long axis (Fig. 12.9) and transverse axis in females (Fig. 12.10). Clinician should aim for the identification of the bladder, uterus, and rectum. In females, the free fluid is visualised as hypoechoic or anechoic collection posterior to the uterus between the rectum and the uterus. The transducer is moved from side to side and in cranial caudal direction to look for the collection between the uterus and bladder. Fifty mL of free

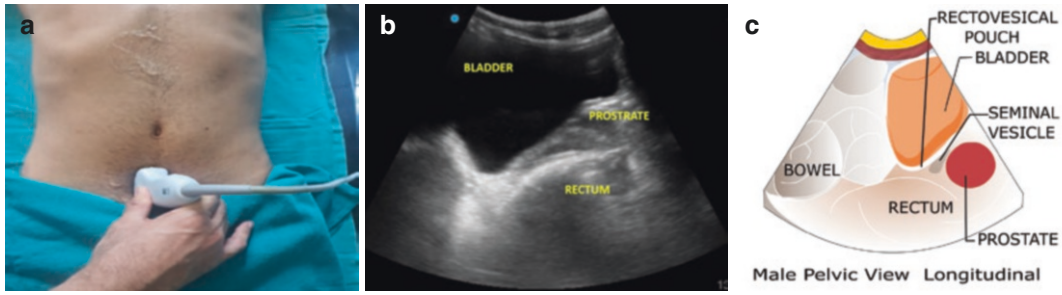

Fig. 12.7 (**a**) Transducer position for pelvic examination longitudinal axis. (**b**) Sonoanatomy male pelvic view longitudinal axis. (**c**) Male pelvic view longitudinal axis schematic

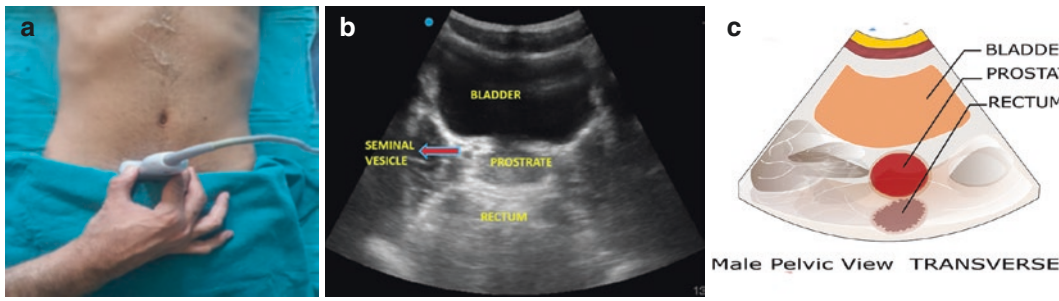

Fig. 12.8 (**a**) Transducer position for pelvic examination transverse axis. (**b**) Sonoanatomy male pelvic view transverse axis. (**c**) Male pelvic view transverse axis schematic

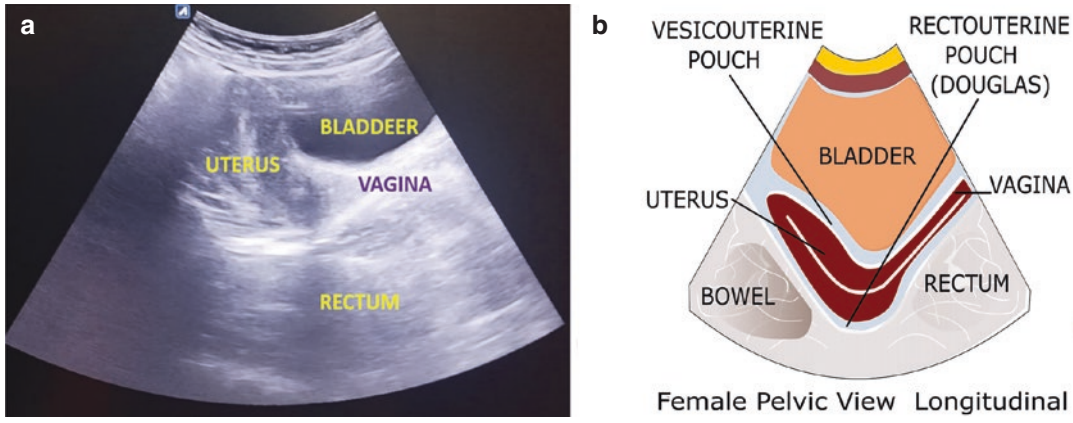

Fig. 12.9 (**a**) Sonoanatomy female pelvic view longitudinal axis. (**b**) Female pelvic view longitudinal axis schematic

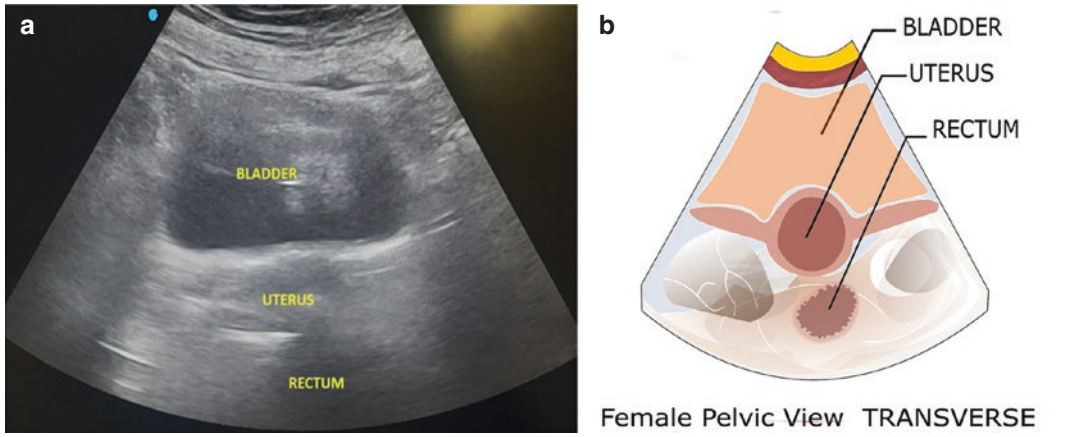

Fig. 12.10 (**a**) Sonoanatomy female pelvic view transverse axis. (**b**) Female pelvic view transverse axis schematic

fluid in the pouch of Douglas in women of child-bearing age group is considered physiological. However, fluid around the anterior or lateral aspects of the bladder is always pathological [9].

12.4.7 E-FAST Thoracic View

Thoracic view of E-FAST examination allows for the evaluation of bilateral thoracic cavities for pneumothorax and haemothorax. Pneumothorax evaluation is carried out in supine position as air rises anteriorly towards the chest surface. For evaluation of the anterior chest cavity, with the patient in supine position, a curvilinear transducer is placed in the second to fourth intercostal space with an aspect marker directed towards the patient's head in the mid-clavicular line. Lung sliding is observed because of the movement of visceral and parietal pleura against each other (Fig. 12.11). When pleura is visualised on M-mode, a characteristic sea-shore sign is seen. Chest wall with minimal movement appears as straight lines on M-mode, pleura appears as shoreline and lung parenchyma appears as the sandy granular beach. Normal lung also shows B-lines which are vertical laser-like hyperechoic lines originating from the parietal pleura and travelling towards the far field of ultrasound screen. B-lines occur because of interaction between the fluid-filled interlobular septa and ultrasound waves. Up till three, B-lines are considered normal. Lung pulse, which is a passive pleural movement corresponding with cardiac

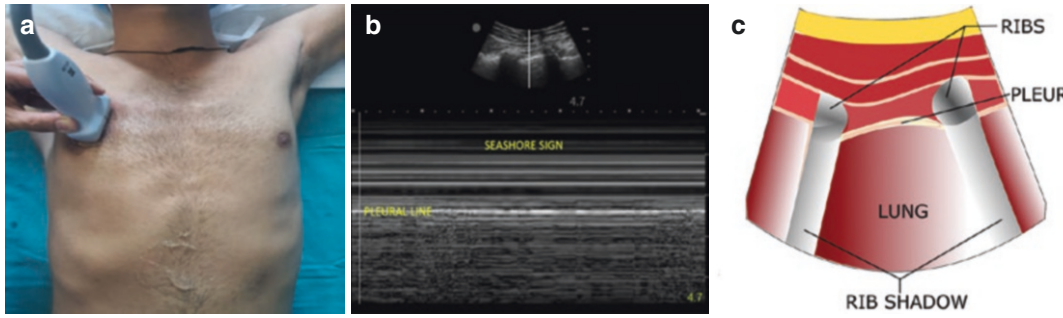

Fig. 12.11 (**a**) Transducer position for E-FAST thoracic cavity view. (**b**) Sea-shore sign seen in normal lung on M-mode. (**c**) E-FAST thoracic cavity view schematic

cycle, can be observed in a normal patient particularly on the left side. The presence of lung sliding, B-lines and, lung pulse helps to rule out pneumothorax.

12.5 Other Abdominal Views

12.5.1 Liver Ultrasound

The liver ultrasound helps in the identification of various disease pathologies like acute hepatitis, chronic hepatitis, cirrhosis, and steatohepatitis. The size, parenchymal texture, echogenicity, and capsular contour is assessed using ultrasound to determine the liver pathology. Also, important vascular structures like aorta, hepatic veins, portal vein, and Inferior Vena Cava can be visualised in this window. Liver ultrasound is performed using curvilinear transducer placed in the mid-axillary line in the coronal plane between ninth to eleventh right intercostal space with the orientation marker directed towards head end of patient. A deep breathing manoeuvre and right arm above the head helps in widening the intercostal space and leads to optimal view. The right kidney, liver, and diaphragm are visualised in the longitudinal axis [10]. Span of the liver is assessed in craniocaudal direction in the mid-clavicular line. When the span is more than 16.0 cm, it is termed as hepatomegaly. Liver parenchyma in normal individuals has a homogenous texture and echogenicity with a smooth contour.

12.5.2 Liver Pathology

1. In patients with acute hepatitis, the span of the liver is enlarged. Along with this, the echogenicity of the liver is decreased along with increased brightness of portal vein walls. A starry sky appearance is seen in the inflammation of liver with walls of portal vein appearing as stars on the background of oedematous hepatocytes.
2. In patients with chronic hepatitis or cirrhosis, the span of the liver is decreased. The echogenicity is increased along with decreased brightness of the portal vein walls. The findings are just the opposite to that of an acute condition.

12.5.3 Gall Bladder and Common Bile Duct Ultrasound

Ultrasound is used for diagnosing the majority of biliary tree pathologies like cholelithiasis, cholecystitis, and choledocholithiasis. As the gallbladder is not attached to the body wall like other intestinal organs, it is challenging to obtain an adequate window. In the full stomach condition, the gall bladder is contracted, which compromises the visibility whereas, on an empty stomach, it is dilated with anechoic bile. However, in emergency presentation with acute abdomen, it is difficult to expect a fasting state. Turning the patient towards their left side helps to bring the gallbladder more anteriorly which

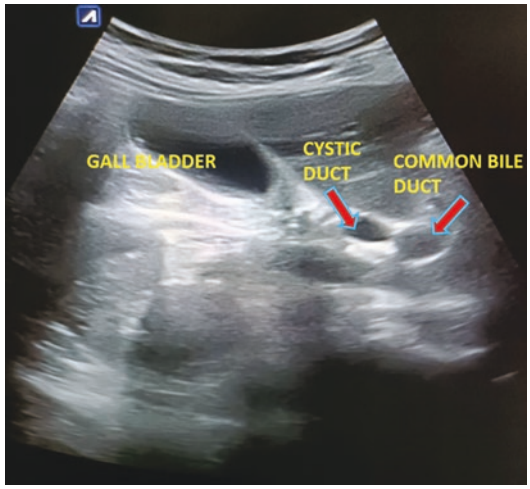

Fig. 12.12 Gall bladder ultrasound

helps in better scanning. A curvilinear probe is placed in the sagittal plane in the epigastrium in the longitudinal orientation with the orientation marker directed cephalad with an aim to find the portal vein curving into the liver. The transducer is turned 90° counterclockwise to obtain the short axis view of portal triad which comprises the hepatic artery, the portal vein, and the common bile duct. The characteristic appearance of the portal triad is called as "mickey mouse sign" where the common bile duct and the hepatic artery are the ears and portal vein represents the head of mickey mouse (Fig. 12.12). Colour Doppler can be used to differentiate between hepatic artery and the common bile duct. Pulsatile flow is seen in the hepatic artery, whereas there will be no flow in the common bile duct, and it will appear anechoic. The transducer is moved towards the right costal margin to localise the main lobar fissure to which the gall bladder neck is attached. The characteristic view that is obtained is called as "Exclamation point sign" where portal triad represents the point of exclamation mark and the gall bladder is the line of exclamation. The diameter of the common bile duct is measured in longitudinal axis. A normal CBD measures <5 mm in the majority of the adult population. The anterior wall thickness of gallbladder is measured in short axis. The normal anterior wall thickness of gallbladder is usually <3 mm.

12.6 Gall Bladder and CBD Pathology

12.6.1 Cholelithiasis

Cholelithiasis is defined as gallstone formation occurring in the biliary tree. Ultrasound is considered the diagnostic modality of choice for the detection of gallstones. Within the lumen of gallbladder stones larger than 5 mm appear as hyperechoic collections with posterior shadowing. When the patient changes position, the stones may be seen rolling within the gall bladder. Tiny stones are difficult to appreciate and may be confused as artefacts. The sensitivity (89.8%) and specificity (88%) of gall bladder POCUS for the detection of cholelithiasis is quite high [11].

12.6.2 Cholecystitis

Cholecystitis is defined as inflammation of the gall bladder. Pathophysiology involves obstruction of the lumen of cystic duct by a gallstone, thereby resulting in an inflamed gall bladder (Fig. 12.13). Acute cholecystitis results in sudden onset of pain in the right hypochondrium or epigastric region of the stomach. When the ultrasound transducer is pressed against the visualised gall bladder, the patient complains of pain. This is called as sonographic murphy sign and has high sensitivity. Because of the inflammation, the anterior gallbladder wall thickening measured in short axis view is increased to >3 mm. Visualisation of gall stones, increased thickness of anterior wall of gall bladder, presence of pericholecystic fluid are diagnostic features of acute inflammation in gall bladder. Presence of gallstones and positive sonographic Murphy's sign has a positive predictive value of 92% for acute cholecystitis [12].

Fig. 12.13 (**a**) Cholelithiasis. (**b**) Cholecystitis with pericolic collection. (**c**) Choledocholithiasis

12.6.3 Choledocholithiasis

Choledocholithiasis refers to the presence of stones within the common bile duct. Presence of stones in common bile duct predisposes to acute bacterial infection referred to as ascending cholangitis associated with high morbidity and mortality, thereby necessitating removal of stones from the common bile duct. Stones are visualised in gall bladder and common bile duct during ultrasound examination. The diameter of common bile duct is increased >5 mm.

12.6.4 Appendicitis

Fig. 12.14 Appendicitis ultrasound

Appendicitis is defined as an inflammatory process which is caused by obstruction of the lumen of appendix, thereby leading to compromise in blood supply and ultimately leading to necrosis and perforation of the appendix. CT scan is usually the diagnostic modality in the detection of appendicitis, but owing to the reduced radiation exposure, ultrasound remains the primary modality of choice. The ultrasound imaging of appendix is highly challenging as the gaseous and faecal loading of the caecum and patient habitus are the biggest limiting factors which obscure the window to visualise the appendix. Hence, the learning curve is quite high. POCUS examination has a sensitivity of 91% for detection of acute changes in appendix [13] (Fig. 12.14).

Curvilinear transducer placed in the right flank, with abdominal preset and orientation marker directed cranially, is used for the scanning of appendix. The ultrasound probe is placed over the location of maximal tenderness and an attempt is made by applying pressure onto the probe for displacing bowel gas. The probe is moved caudally till ascending colon is visualised. The colonic shadowing/hepatic flexure is visibly distinguished from the small bowel by the presence of undulations called haustra. The probe is moved further caudally to visualise the insertion of the terminal ileum into the caecum. With graded compression technique, the caput of the caecum and the origin of appendix is visualised. Clinician should also try to visualise the right psoas muscle and external iliac artery which is another landmark for appendix localisation as the appendix is often seen overlying it.

In children, appendix appears on ultrasound as having an inner hypoechoic band without folds, which is not present in other bowel structures. The outer diameter of the appendix ranges from 2–13 mm in the adult population, and for paediat-

ric population, it ranges between 3–9 mm. The appendix might be filled with gases, a more sensitive indicator called maximal mural thickness must be measured which is less than 3 cm in a normal appendix.

In acute appendicitis, appendix appears as a non-compressible, concentric structure with hypoechogenic inner lumen surrounded by hyperechogenic oedema. Although maximum outer diameter of more than 6 mm raises the suspicion for diagnosis of appendicitis, it is, however, not a very sensitive marker. The maximum mural thickness of more than 3 cm is strongly suggestive of acute appendicitis. Other findings suggestive of acute appendicitis are distorted irregular mucosa, thickened omentum, enlarged lymph nodes, free fluid in the periappendiceal region, and presence of a fecalith. Inflammation of appendix is indicated by its non-compressibility. Asymmetrical wall thickening may indicate perforation.

12.7 Pathology

12.7.1 Hemoperitoneum in the Hepatorenal Space

RUQ view of E-FAST examination involves visualisation of the diaphragm, liver, and kidney. In normal individuals, liver and kidney are juxtaposed. Fluid accumulation is seen as a hypoechoic or anechoic collection either in right subdiaphragmatic space or in the Morrison's pouch or just at the caudal tip of the liver (Fig. 12.15). Clinician should remember that the Morrison's pouch is a three-dimensional space, and an attempt should be made to scan the space in all directions before commenting as indeterminate or negative examination [14].

12.7.2 Haemothorax in the Right and Left Pleural Space

Pleural space view of E-FAST examination involves visualisation of the lung parenchyma, diaphragm, and pleura. Haemothorax evaluation

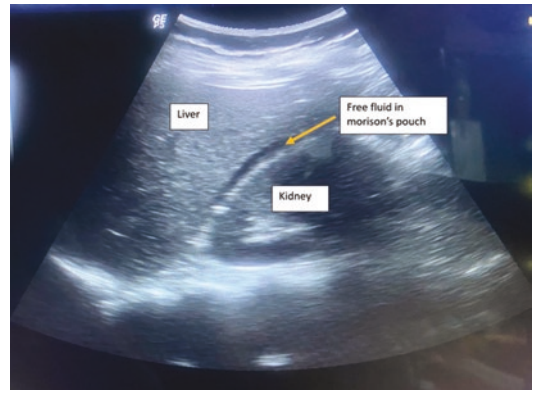

Fig. 12.15 Hemoperitoneum in hepatorenal space

is best carried out in a sitting position as fluid accumulates in dependent zones because of the gravitational effect. However, in the trauma patient, this may not be feasible at all times. Turning the patient towards the side of the examination helps in detecting fluid in the pleural cavity. The presence of fluid in the costo-phrenic space is seen as a black anechoic or at times hypoechoic collection between the chest wall and the diaphragm (Fig. 12.16). The presence of effusion in a patient with history of trauma is presumed to be haemothorax unless proved otherwise. Vertebral bodies are seen up to the level of the diaphragm, but it is not visible cranial to the diaphragm because the air in the diaphragm attenuates echoes returning from the spine. Vertebral bodies are visible above the diaphragm if there is free fluid inside the pleural cavity. This is called a spine sign.

12.7.3 Haemoperitoneum in the Splenorenal Space

LUQ view of E-FAST examination involves visualisation of the diaphragm, spleen, and kidney. Fluid accumulation is seen as a hypoechoic or anechoic collection either in left subdiaphragmatic space or in the splenorenal space (Fig. 12.17). Similar to RUQ examination, clinician should remember that perisplenic space is a three-dimensional space, and an attempt should be made to scan the space in all directions before

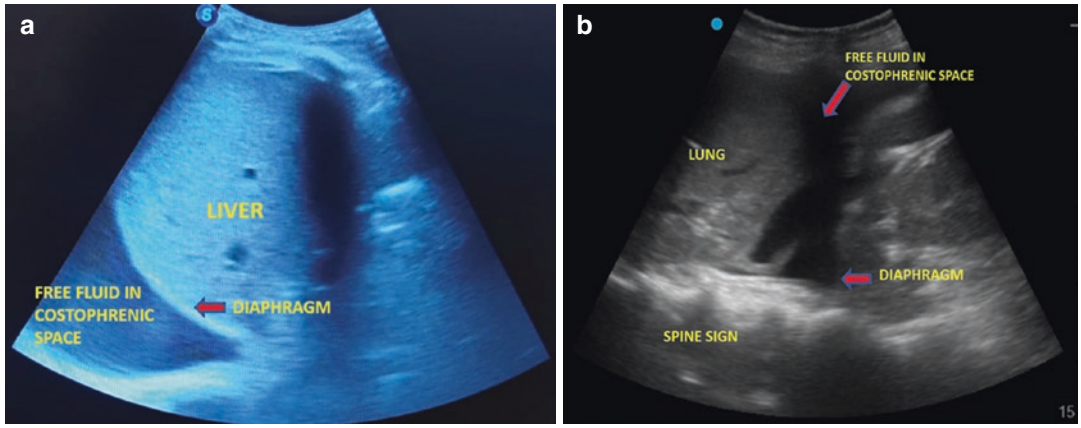

Fig. 12.16 (**a**) Hemothorax in right costophrenic space. (**b**) Hemothorax in left costophrenic space

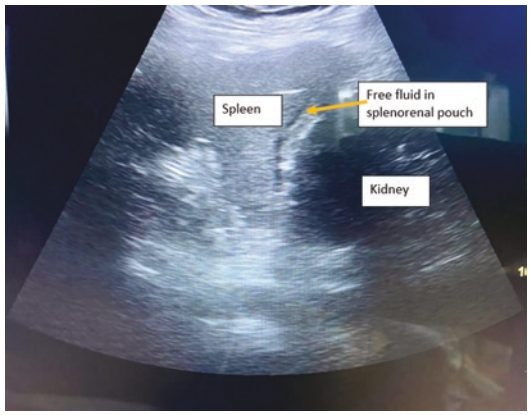

Fig. 12.17 Hemoperitoneum in splenorenal space

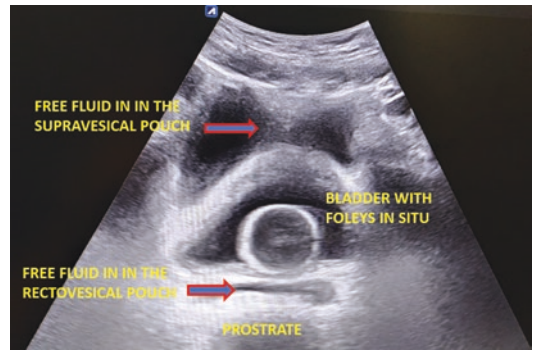

Fig. 12.18 Hemoperitoneum in the rectovesical pouch

commenting as indeterminate or negative examination [14].

12.7.4 Haemoperitoneum in the Rectovesical and Rectouterine Excavation

Pelvic view of E-FAST examination involves visualisation of free fluid in the pelvis. The collection of fluid in the pelvis is possible either lateral, posterior, or anterior to bladder and along the walls of the uterus in female patients. Position of patient, prostate size, flexion state of uterus are some of the factors which will determine ease of visibility on ultrasound [15]. The localisation of the free fluid should be done in a serial order. The transducer should be focused to visualise the free fluid anterior to the bladder. It is always pathological if not proven otherwise. In an empty bladder, free fluid collection either anterior or cephalad to the bladder can be mistaken for the urinary bladder. The transducer is tilted in all planes to look for the 'wedge-shaped' free fluid collection in cavities lateral to the bladder and in between the bowel folds. The pelvis is scanned in all planes to detect the presence of fluid posterior to the urinary bladder, i.e. in the rectovesical pouch (Fig. 12.18) and Pouch of Douglas (Fig. 12.19).

12.7.5 Haemopericardium

The subcostal view of E-FAST examination involves visualisation of liver, heart, pericardium,

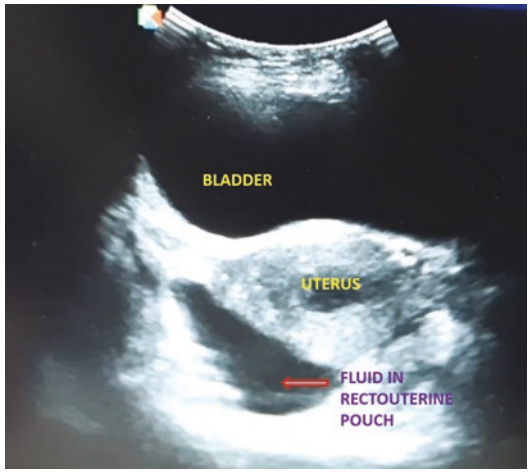

Fig. 12.19 Hemoperitoneum in the rectouterine pouch

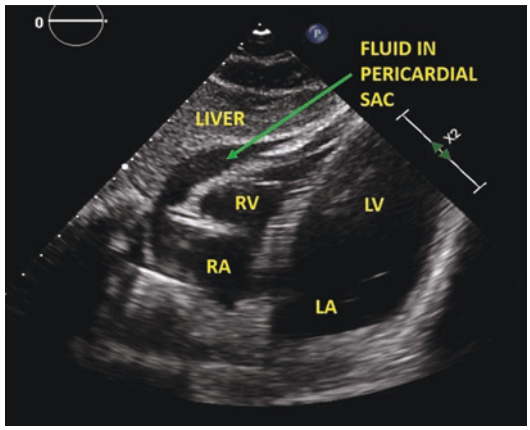

Fig. 12.20 Hemopericardium in the subcostal view

and evaluation of the pericardial sac. In patients with thoracoabdominal trauma, presence of fluid in pericardial cavity is seen as a black anechoic or at times hypoechoic collection separating the hyperechoic pericardium from the grey myocardium and is a highly specific marker for pericardial effusion (Fig. 12.20). Pericardial effusion can be acute or chronic; however, in the context of a history of trauma, it should be assumed to be acute. The amount of fluid and rate of accumulation of fluid will determine if tamponade physiology results or not. Because of rapid accumulation of fluid in the pericardial cavity, pressures in the pericardial cavity exceed the right-side filling pressures, thereby leading to compromised heart filling and ultimately leading to a fall in cardiac output and hypotension.

12.7.6 Detecting Pneumothorax

Anterior thoracic cavity view of E-FAST examination involves visualisation of lung parenchyma and pleural movement. Chest X-ray in supine position in comparison with ultrasound is time-consuming and less sensitive for detection of pneumothorax [16]. Visualisation of lung sliding on ultrasonography excludes the diagnosis of pneumothorax. However, non-visualisation of lung sliding on ultrasound should increase the suspicion of pneumothorax in a patient with history of trauma. Absence of lung sliding on M-mode is seen as a barcode or stratosphere sign with straight lines arising from the chest wall reaching until the far field of the ultrasound screen. The lung point, diagnostic feature of pneumothorax is seen on M-mode as an alternating zone of the sea-shore sign and barcode sign (Fig. 12.21). The algorithm listed in Table 12.1 guides the clinician for decision-making in a patient with pneumothorax.

12.7.7 Abdominocentesis

Abdominal paracentesis is defined as the removal of the ascitic fluid either for diagnostic or thera-

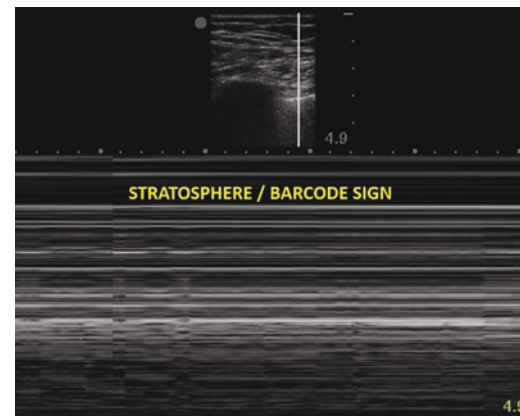

Fig. 12.21 Barcode or stratosphere sign seen on M-mode in a patient with pneumothorax

Table 12.1 Algorithm for pneumothorax detection

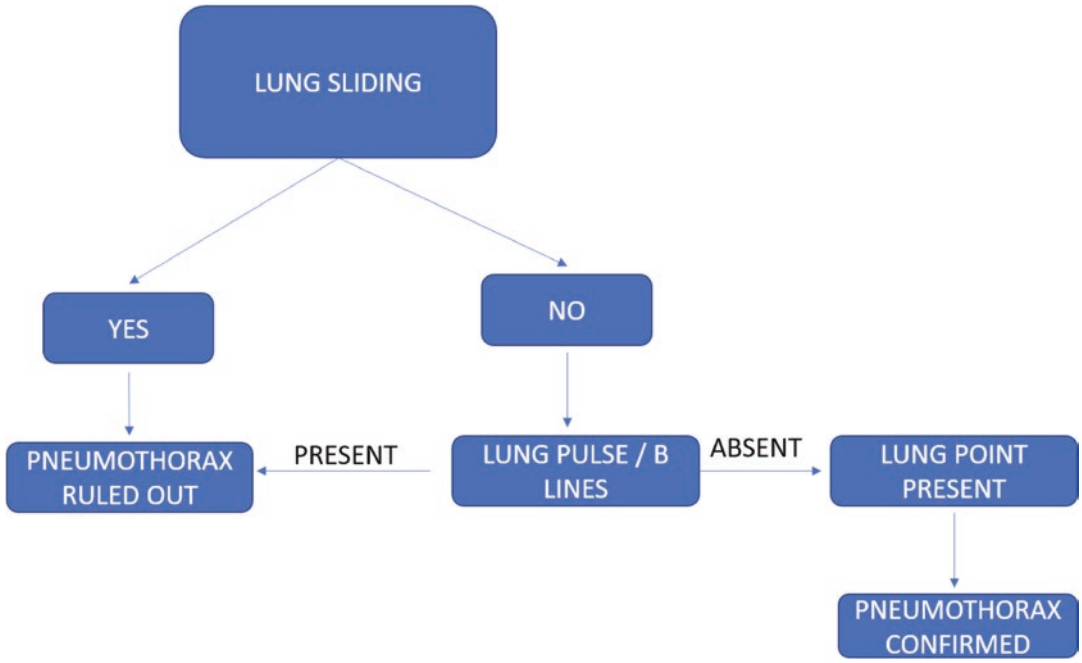

peutic purpose. This procedure can be done as a landmark-based technique; however, this is associated with increased chances of bleeding, hematoma formation, visceral injury, and procedure failure ultrasound-guided or ultrasound-assisted abdominal paracentesis has become the standard of care as per the Society of Hospital Medicine [17]. Ultrasound can be used to assess the location and volume of intraperitoneal free fluid along with position of abdominal organs and helps the clinician to ascertain the site where a puncture can be made for performing paracentesis.

Ultrasound is used to select the avascular plane where cannula or needle can be placed to avoid vascular injury. Lateral avascular plane can be identified on ultrasound as an echogenic plane which is situated lateral to the rectus abdominis. Using colour Doppler, inferior epigastric artery, deep circumflex iliac artery along with veins can be seen in this region during ultrasound scan. Under aseptic precautions and following local site infiltration, the paracentesis needle is inserted using a Z-track technique. In therapeutic paracentesis, a 16-gauge needle is used for a therapeutic paracentesis and an 18 G for diagnostic purpose. Post procedure, ultrasound is used to perform a scan to identify any complications like vascular bleeding.

12.8 Advantages of E-FAST

1. Bedside examination.
2. Simple and effective.
3. Non-invasive.
4. Can be done rapidly.
5. Can be repeated.
6. Real time.
7. Relatively inexpensive.
8. Avoids complication associated with DPL.
9. Avoids radiation exposure and shifting of the patient to the radiology suite.
10. Time and resource saving.

12.9 Tips and Tricks

E-FAST examination is a diagnostic modality which is patient habitus-, operator-, and ultrasound machine-dependent. The following tips and tricks can help clinicians to improve E-FAST examination views.

1. The depth and gain need to be adjusted when transitioning between views. Depth needs to be increased to 20–25 cm for the subcostal view and needs to be decreased for the pelvic view. Examiner-dependent errors, like not adjusting proper depth in obese patients or too much gain, will lead to false negative examinations.
2. Deep breathing and holding help to get a better ultrasound image in LUQ and subxiphoid view.
3. Trendelenburg position improves the RUQ and LUQ examination views and head low position improves the pelvic cavity view.
4. In RUQ view, hepatic veins, bile ducts, and even sometimes the gall bladder can be confused with free fluid. In the LUQ view, splenic hilum and gastric contents can be confused as free fluid. Scanning from different angles helps to differentiate free fluid from other organs.
5. The E-FAST examination has poor sensitivity and specificity for diagnosing organ injury and retroperitoneal haematoma. It is advisable to go for a CT scan in case of serial negative E-FAST in unstable patients.
6. Fluid accumulation is a dynamic process. Early examinations in case of small fluid collections can be missed. Serial E-FAST examinations help improve sensitivity and are indicated in patients with negative examination who are unstable.
7. Clinician should be mindful of false positive results associated with E-FAST examination. Pre-existing free fluids like ascitic fluid, peritoneal fluid in a patient on peritoneal dialysis, fluids from bladder or bowel rupture, intrapleural transduction because of aggressive fluid resuscitation or overflow from VP shunt can lead to false positive E-FAST. A ruptured ovarian cyst or fluid from the ruptured ovarian follicle in a polycystic ovary can mimic free fluid collection in the pelvic view.
8. As blood clots, it becomes isoechoic or hyperechoic. Clotted blood is difficult to differentiate from surrounding organs. Scanning from different angles helps to differentiate clotted blood from other organs.
9. Fat can appear hypoechoic with hyperechoic striae and at times mimic free fluid or organising haematoma. Perinephric fat mimics a free fluid at the splenorenal or hepatorenal interphase. It is known as a Double Line sign. Examination of a patient with the change of position will not alter the appearance of perinephric fat whereas an organising haematoma would give an altered appearance due to the movement of fluid and clot. Pericardial fat may mimic effusion in the subcostal view.
10. Mirror artefacts which occur because of ultrasound waves striking a refractile surface like a diaphragm can give the appearance of the liver or spleen in the thoracic cavity above the diaphragm and can mimic consolidation. Scanning in an anterior-posterior direction along with cranial-caudal movement will help eliminate this artefact.
11. In case of poor visualisation of heart chambers and pericardium in subcostal view with a curvilinear transducer, a phased array transducer can be used, and a long parasternal axis view can be obtained in addition.
12. In the pelvic view, seminal vesicles which are located posteriorly and appear as hypoechoic can mimic free fluid. Seminal vesicles have a symmetrical smooth contour which helps to distinguish them from the free fluid.
13. The sensitivity and specificity of the pelvic view in an empty bladder state is less. It is always better to catheterise the patient only after doing an E-FAST examination. IV fluid therapy helps if the bladder is empty. Posterior acoustic enhancement as an artefact is often observed posterior to the urinary bladder and can affect the visualisation of fluid in pelvic cavity. Decreasing far field gain can help overcome this artefact.
14. CT scan should be considered when E-FAST examination findings are not matching with the clinical situation.

12.10 E-FAST Examination in Medical Decision-Making

E-FAST examination in a patient with history of thoracoabdominal trauma helps the clinician to plan an urgent laparotomy, thoracostomy tube insertion depending on the clinical findings and point of care ultrasound findings. Small pneumothorax can go undetected at the time of initial assessment during primary survey and may deteriorate as the patient is placed on ventilator during general anaesthesia for trauma laparotomy. Serial E-FAST examination by anaesthesiologists can help detecting pneumothorax in such situations. The algorithm listed in Table 12.2 guides the clinician for decision-making in patients with trauma. However, the clinician must understand that E-FAST examination has a high specificity close to 99% and moderate sensitivity of 60–80% [18]. As a result, E-FAST examination cannot be used to rule out presence of free fluid. E-FAST examination therefore is an initial diagnostic modality in trauma setting; however, in case of E-FAST negative patient who is unstable, CT scan should be considered. Although described in context of trauma, E-FAST examination can be performed by the anaesthesiologist following abdominal surgery in a patient who becomes unstable in recovery room and surgical intensive care unit (SICU). E-FAST examination has been used to diagnose peritoneal fluid in individuals who have undergone hip arthroscopy [19] and thereby preventing the occurrence of life-threatening complications. E-FAST has been used in perioperative period for diagnosing peritoneal fluid accumulation, pneumothorax, and haemothorax following percutaneous nephrolithotomy (PCNL) [20]. E-FAST examination is an easy-to-learn POCUS technique and requires 30 Level 1 examinations (performed and interpreted) and 20 Level 2 examinations (interpreted) as per American Society of Regional Anesthesia (ASRA) recommendations [21].

Table 12.2 Algorithm for E-FAST examination

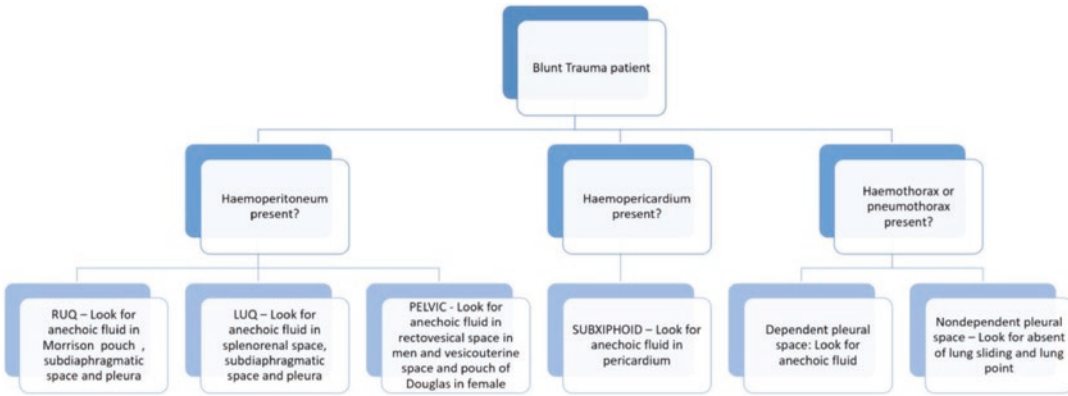
Blunt Trauma patient
Haemoperitoneum present?
Haemopericardium present?
Haemothorax or pneumothorax present?
RUQ – Look for anechoic fluid in Morrison pouch , subdiaphragmatic space and pleura
LUQ – Look for anechoic fluid in splenorenal space, subdiaphragmatic space and pleura
PELVIC - Look for anechoic fluid in rectovesical space in men and vesicouterine space and pouch of Douglas in female
SUBXIPHOID – Look for anechoic fluid in pericardium
Dependent pleural space: Look for anechoic fluid
Nondependent pleural space – Look for absent of lung sliding and lung point

12.11 Conclusion

POCUS is the modern-day stethoscope available to clinicians in their armamentarium. Ultrasound machines over the years have become portable, small, with innovations in software technology for better visualisation of target structures. E-FAST examination, a point-of-care ultrasound examination can be lifesaving in patients with history of trauma and has a wide array of applications in non-trauma setting. As the progress in medical field continues, artificial intelligence-based algorithms will be helpful in guiding the clinicians for management of trauma patients.

References

1. Liu M, Lee CH, P'eng FK. Prospective comparison of diagnostic peritoneal lavage, computed tomographic scanning, and ultrasonography for the diagnosis of blunt abdominal trauma. J Trauma Acute Care Surg. 1993;35(2):267–70.
2. Cinquantini F, Tugnoli G, Piccinini A, Coniglio C, Mannone S, Biscardi A, Gordini G, Di Saverio S. Educational review of predictive value and findings of computed tomography scan in diagnosing bowel and mesenteric injuries after blunt trauma: correlation with trauma surgery findings in 163 patients. Can Assoc Radiol J. 2017;68(3):276–85.
3. Rozycki GS, Ochsner MG, Jaffin JH, Champion HR. Prospective evaluation of surgeons' use of ultrasound in the evaluation of trauma patients. In: 50 Landmark papers every trauma surgeon should know. CRC Press; 2019. p. 89–92.
4. Ding W, Shen Y, Yang J, He X, Zhang M. Diagnosis of pneumothorax by radiography and ultrasonography: a meta-analysis. Chest. 2011;140(4):859–66.
5. Kirkpatrick AW, Sirois M, Laupland KB, Liu D, Rowan K, Ball CG, Hameed SM, Brown R, Simons R, Dulchavsky SA, Hamiilton DR. Hand-held thoracic sonography for detecting post-traumatic pneumothoraces: the extended focused assessment with sonography for trauma (E-FAST). J Trauma Acute Care Surg. 2004;57(2):288–95.
6. Bahner DP, Hughes D, Royall NA. I-AIM: a novel model for teaching and performing focused sonography. J Ultrasound Med. 2012;31(2):295–300.
7. Meyers MA. The spread and localization of acute intraperitoneal effusions. Radiology. 1970;95(3):547–54.
8. Abrams BJ, Sukumvanich P, Seibel R, Moscati R, Jehle D. Ultrasound for the detection of intraperitoneal fluid: the role of Trendelenburg positioning. Am J Emerg Med. 1999;17(2):117–20.
9. Ingelfinger JR. Use of eFAST in patients with injury to the thorax or abdomen. N Engl J Med. 2022;386(10):e23.
10. Macnaught F, Campbell-Rogers N. The liver: how we do it. Australas J Ultrasound Med. 2009;12(3):44.
11. Ross M, Brown M, McLaughlin K, Atkinson P, Thompson J, Powelson S, Clark S, Lang E. Emergency physician-performed ultrasound to diagnose cholelithiasis: a systematic review. Acad Emerg Med. 2011;18(3):227–35.
12. Zenobii MF, Accogli E, Domanico A, Arienti V. Update on bedside ultrasound (US) diagnosis of acute cholecystitis (AC). Intern Emerg Med. 2016;11:261–4.
13. Matthew Fields J, Davis J, Alsup C, Bates A, Au A, Adhikari S, Farrell I. Accuracy of point-of-care ultrasonography for diagnosing acute appendicitis: a systematic review and meta-analysis. Acad Emerg Med. 2017;24(9):1124–36.
14. Pace J, Arntfield R. Focused assessment with sonography in trauma: a review of concepts and considerations for anesthesiology. Can J Anesth. 2018;65(4):360–70.
15. Manson WC, Kirksey M, Boublik J, Wu CL, Haskins SC. Focused assessment with sonography in trauma (fast) for the regional anesthesiologist and pain specialist. Reg Anesth Pain Med. 2019;44(5):540–8.
16. Zhang M, Liu ZH, Yang JX, Gan JX, Xu SW, You XD, Jiang GY. Rapid detection of pneumothorax by ultrasonography in patients with multiple trauma. Crit Care. 2006;10(4):1–7.
17. Cho J, Jensen TP, Reierson K, Mathews BK, Bhagra A, Franco-Sadud R, Grikis L, Mader M, Dancel R, Lucas BP, Soni NJ. Recommendations on the use of ultrasound guidance for adult abdominal paracentesis: a position statement of the Society of Hospital Medicine. J Hosp Med. 2019;14:E7.
18. Boulanger BR, McLellan BA, Brenneman FD, Ochoa J, Kirkpatrick AW. Prospective evidence of the superiority of a sonography-based algorithm in the assessment of blunt abdominal injury. J Trauma Acute Care Surg. 1999;47(4):632.
19. Haskins SC, Desai NA, Fields KG, Nejim JA, Cheng S, Coleman SH, Nawabi DH, Kelly BT. Diagnosis of intraabdominal fluid extravasation after hip arthroscopy with point-of-care ultrasonography can identify patients at an increased risk for postoperative pain. Anesth Analg. 2017;124(3):791–9.
20. Sharma A, Bhattarai P, Sharma A. eFAST for the diagnosis of a perioperative complication during percutaneous nephrolithotomy. Crit Ultrasound J. 2018;10(1):7.
21. Haskins SC, Bronshteyn Y, Perlas A, El-Boghdadly K, Zimmerman J, Silva M, Boretsky K, Chan V, Kruisselbrink R, Byrne M, Hernandez N. American Society of Regional Anesthesia and Pain Medicine expert panel recommendations on point-of-care ultrasound education and training for regional anesthesiologists and pain physicians—part I: clinical indications. Reg Anesth Pain Med. 2021;46(12):1031–47.

Point-of-Care Gastric Ultrasound

13

Noreddine Bouarroudj

13.1 Introduction

13.1.1 Gastric Ultrasound: An Emerging Technique

Original description of Gastric Ultrasound was first made more than 40 years ago to assess gastric em*ptying* by a team of radiologists, Whittingham and colleagues [1]. The first team of anesthesiologists to describe the technique was from Nagasaki department of Anesthesiology in 1993 [2]. They were the first to develop a method to estimate and assess gastric contents by measuring cross-sectional area of the stomach. Recently, Gastric Ultrasound has caused considerable interest within the community due to the fact that the POCUS has revolutionized the practice of anesthesia emergency and critical care. In addition, the rise of technology has allowed easy access to ultrasound machines for practitioners. There exists a very extensive literature on the topic as shown in the Fig. 13.1 which illustrates the number of publications for the request: "Gastric Ultrasound on PubMed." Ultrasonography is known to have indisputable advantages: mobility and lower cost, non-invasive and does not expose to radiation, and finally the time of examination has decreased. The disadvantage which may be summarized is the fact that it requires extensive knowledge of sonoanatomy and anatomy, knowledge of anatomical variations, and knowledge of its limitations.

13.1.2 Gastric Ultrasound to Prevent Perioperative Pulmonary Aspiration

Gastric ultrasound allows anesthesiologists to assess the contents and the volume of the stomach. Preoperative gastric ultrasound has a clear impact on the conduct and management of general anesthesia. Knowing that preventing aspiration is the sine qua non condition of safety in anesthesia, this technique has an inevitable place in current practice.

Perioperative pulmonary aspiration can be defined as aspiration of gastric contents occurring after induction of general anesthesia either immediately at induction or it may even occur postoperatively. It is well-known that pulmonary aspiration comes with it a risk of mortality. Pulmonary aspiration is a rare but dramatic event both for the anesthesiologist and for the patient. Reminiscences and memories of general anesthesia take us a little far back in history. James Simpson, in 1848, 1 year after the description of the first general anesthesia, described the clinical case concerning a 15-year-old young child after surgical removal of an ingrown toenail [3]. The

N. Bouarroudj (✉)
Department of Anaesthesia and Critical Care, Maissalyne Hospital, Constantine, Algeria

© The Author(s), under exclusive license to Springer Nature Switzerland AG 2024

N. Bouarroudj et al. (eds.), *POCUS in Critical Care, Anesthesia and Emergency Medicine*,
https://doi.org/10.1007/978-3-031-43721-2_13

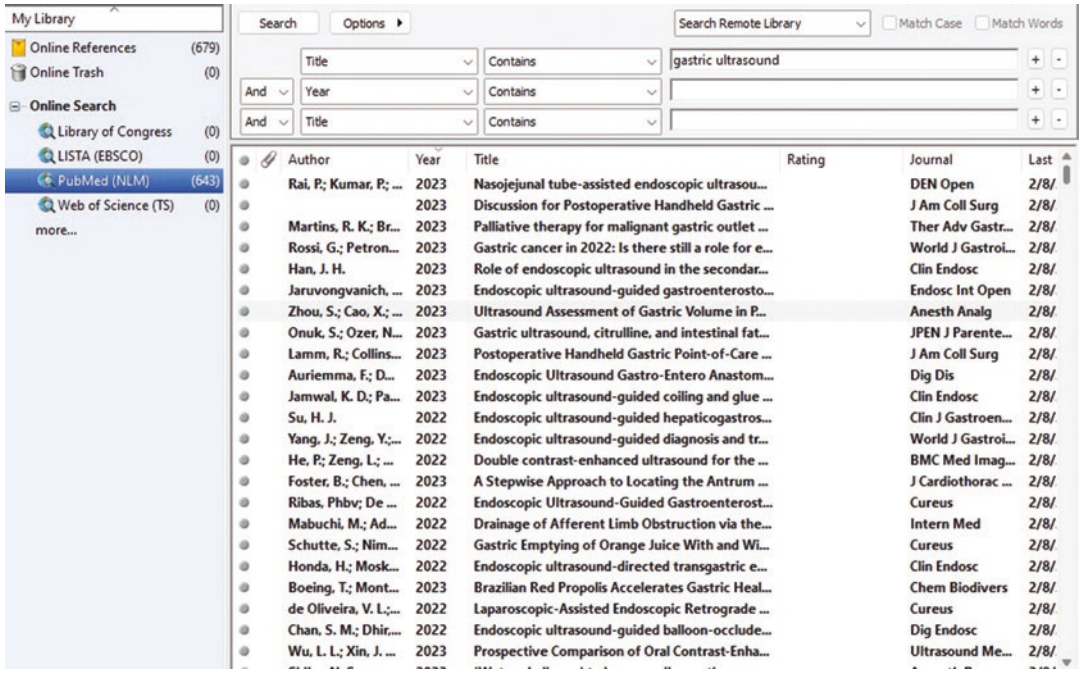
My Library
Online References (679)
Online Trash (0)
Online Search
Library of Congress (0)
LISTA (EBSCO) (0)
PubMed (NLM) (643)
Web of Science (TS) (0)
more...
Search
Options
Search Remote Library
Match Case
Match Words
Title
Contains
gastric ultrasound
And
Year
Contains
And
Title
Contains
Author
Year
Title
Rating
Journal
Last
Rai, P.; Kumar, P.; ... 2023 Nasojejunal tube-assisted endoscopic ultrasou... DEN Open 2/8/
2023 Discussion for Postoperative Handheld Gastric ... J Am Coll Surg 2/8/
Martins, R. K.; Br... 2023 Palliative therapy for malignant gastric outlet ... Ther Adv Gastr... 2/8/
Rossi, G.; Petron... 2023 Gastric cancer in 2022: Is there still a role for e... World J Gastroi... 2/8/
Han, J. H. 2023 Role of endoscopic ultrasound in the secondar... Clin Endosc 2/8/
Jaruvongvanich, ... 2023 Endoscopic ultrasound-guided gastroenterosto... Endosc Int Open 2/8/
Zhou, S.; Cao, X.; ... 2023 Ultrasound Assessment of Gastric Volume in P... Anesth Analg 2/8/
Onuk, S.; Ozer, N... 2023 Gastric ultrasound, citrulline, and intestinal fat... JPEN J Parente... 2/8/
Lamm, R.; Collins... 2023 Postoperative Handheld Gastric Point-of-Care ... J Am Coll Surg 2/8/
Auriemma, F.; D... 2023 Endoscopic Ultrasound Gastro-Entero Anastom... Dig Dis 2/8/
Jamwal, K. D.; Pa... 2023 Endoscopic ultrasound-guided coiling and glue ... Clin Endosc 2/8/
Su, H. J. 2022 Endoscopic ultrasound-guided hepaticogastros... Clin J Gastroen... 2/8/
Yang, J.; Zeng, Y.;... 2022 Endoscopic ultrasound-guided diagnosis and tr... World J Gastroi... 2/8/
He, P.; Zeng, L.; ... 2022 Double contrast-enhanced ultrasound for the ... BMC Med Imag... 2/8/
Foster, B.; Chen, ... 2023 A Stepwise Approach to Locating the Antrum ... J Cardiothorac ... 2/8/
Ribas, Phbv; De ... 2022 Endoscopic Ultrasound-Guided Gastroenterost... Cureus 2/8/
Mabuchi, M.; Ad... 2022 Drainage of Afferent Limb Obstruction via the... Intern Med 2/8/
Schutte, S.; Nim... 2022 Gastric Emptying of Orange Juice With and Wi... Cureus 2/8/
Honda, H.; Mosk... 2022 Endoscopic ultrasound-directed transgastric e... Clin Endosc 2/8/
Boeing, T.; Mont... 2023 Brazilian Red Propolis Accelerates Gastric Heal... Chem Biodivers 2/8/
de Oliveira, V. L.;... 2022 Laparoscopic-Assisted Endoscopic Retrograde ... Cureus 2/8/
Chan, S. M.; Dhir,... 2022 Endoscopic ultrasound-guided balloon-occlude... Dig Endosc 2/8/
Wu, L. L.; Xin, J. ... 2023 Prospective Comparison of Oral Contrast-Enha... Ultrasound Me... 2/8/

Fig. 13.1 Publications for the request: "Gastric Ultrasound on PubMed"

death was attributed to general anesthesia and the autopsy concluded that it was a pulmonary congestion due to the chloroform. A direct causal link was not established between general anesthesia and pulmonary aspiration. Historically, the original description of pulmonary aspiration was made by Mendelssohn in 1946. The description was made during anesthesia in obstetrics. The study involved 66 cases observed between the years 1932 and 1945 that resulted in the death of two women [4]. Such findings are also seen in a more recent report in the literature. Large and several studies reported incidence of pulmonary aspiration in the general surgical population. Incidence related to perioperative pulmonary aspiration is as follows: A Swedish study reported an incidence of 1/2131, USA 1/3216, and UK 1/14,139. The respective mortality [5] of his studies is 1/45,454, 1/71,829, and 1/84,839.

13.2 Principles

The principle of point-of-care gastric ultrasound consists in allowing assessment of its content in either qualitative or quantitative terms prior to surgery and anesthesia. In any case, point-of-care gastric ultrasound is:

- A safe, non-invasive, and rapid technique that allows anesthesiologists to assess the gastric contents and volume at the bedside in real time.
- A valuable, simple, and repeatable tool that informs a possible risk of aspiration in anesthesia critical care and emergency medicine.
- Useful to manage anesthesia and airway before general anesthesia in unclear situations with difficulty to predict gastric emptying.
- It allows not only quantitative but also qualitative evaluation.

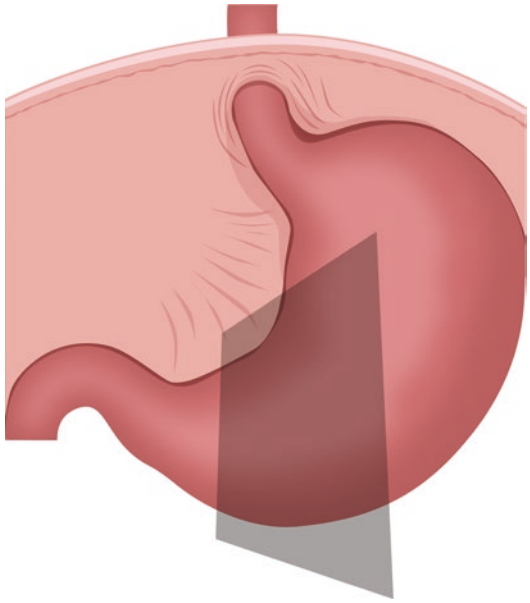

Fig. 13.2 Sagittal cross section beam

This assessment is done by using sonography. The quantitative evaluation consists of the measurement of the cross-sectional diameter while the qualitative evaluation allows to see most of the time the existence of liquid or solid contents. In total, the principle is based on an ultrasound examination which is based on a sagittal cross section depicted in Fig. 13.2.

13.3 Assessment of Gastric Content vs. Schrödinger's Cat Thought Experiment

A thought experiment is a method of reasoning, often used in science, that involves imagining a hypothetical scenario to explore the implications and consequences of a particular idea or theory. These imaginary scenarios are used when real-world experiments are impractical or impossible to perform.

13.3.1 Teaching Schrödinger's Cat to Evaluate the Clinical State of Superposition?

The idea originated in the literature under the name of "Schrödinger's gut" and introduced by raising the question: "Should we look inside Schrödinger's gut?" [6]. Indeed, the Schrödinger's cat is a powerful springboard to understand complex ideas as the concept of superposition of clinical states for example.

Let's remember the Schrödinger's cat paradox, this well-known thought experiment in quantum mechanics that illustrates the concept of superposition. Schrödinger's original description stipulates that a cat is placed in a closed box with a vial of poison and a radioactive material (Fig. 13.3). If the Geiger counter detects radioactivity, the vial breaks that kills the cat. According to "Copenhagen Interpretation," the cat is alive and dead at the same time [7]. So, until the box is opened and observed, the cat exists in a state of superposition where it is both alive and dead at the same time. One possible solution is to open

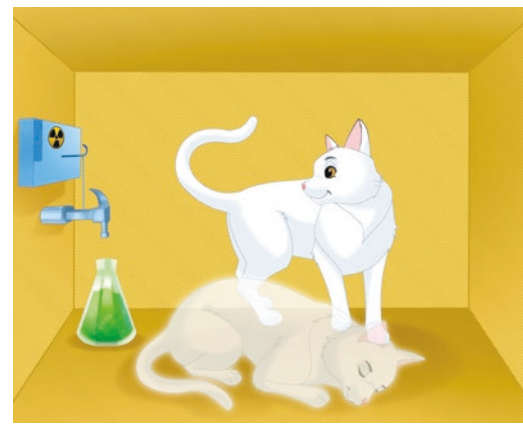

Fig. 13.3 Schrödinger's cat thought experiment. The cat is placed in a closed box with a vial of poison, radioactive material and the Geiger counter

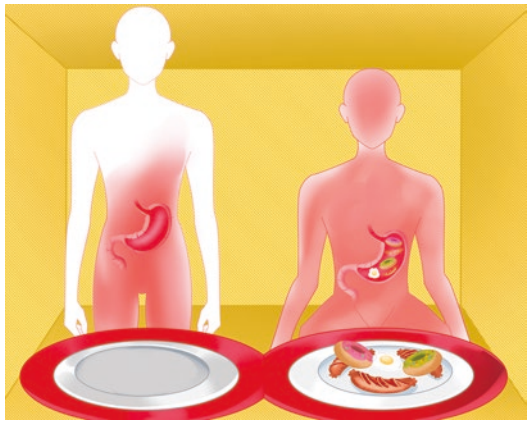

Fig. 13.4 Concerning the gastric content assessment, the stomach is neither full nor empty before anesthesia. This situation illustrates the clinical state of superposition

the box. By analogy, in the case of gastric content assessment, looking at stomach contents, the stomach is neither full nor empty before anesthesia, and the only way to resolve this conundrum is to take a look inside the stomach by performing an ultrasound scan. In fact, "quantum mechanics" can aid to understand the dilemma "full or empty" and can also examine the limits of our understanding. Several studies have shown a possibility of pulmonary aspiration during general anesthesia despite the patient's compliance with the fasting rules. This supports the idea and concept.

Schrödinger's cat thought experiment may be directly applicable to gastric ultrasound and may illustrate the concept of superposition (Fig. 13.4). Until further testing is conducted, the patient's diagnosis is in a state of superposition, where the stomach is both full and empty at the same time. When it comes to applying this concept to gastric ultrasound, it's important to note that the Schrödinger's cat paradox is typically used in discussions about the uncertainties and unknowns that may exist in unclear situations of gastric emptying [6]. In terms of Schrödinger's gut or Schrödinger's stomach, it is about patients who are in what could be called a Superposition of clinical states. This is one way in which Schrödinger's cat paradox could be applied to gastric ultrasound and this by considering the uncertainties and unknowns. For example, a gastric ultrasound might reveal a full stomach in a fasting patient. Similarly, when performing a gastric ultrasound, the sonographer may obtain additional information and get an opinion of gastric ultrasound images that exists in a state of certainty, of an empty stomach.

In summary, Schrodinger's cat is simply a teaching tool that we can use to understand and illustrate the superposition of clinical states. This concept is both easy to understand and straightforward to implement.

13.4 Anatomy and Physiology

Understanding anatomy and physiology is fundamental to the rational practice and the success of the point-of-care gastric ultrasound. The stomach is an important organ in the upper abdomen; it's an important part of the gastrointestinal tract. The stomach is a "j"-shaped organ, with two openings: the end esophagus and the duodenum. Topographically, the stomach consists of several parts: cardia, fundus, corpus, and the antropyloric region. Each topographic region has a distinct function. The fundus stores gases. The Corpus provides the secretion of hydrochloride acid and pepsinogen. Pylorus provides gastrin pepsinogen and the mucus. The major functions of the stomach are temporary food storage, preliminary digestion, mixing boluses of food with gastric secretions, and emptying of the stomach.

13.4.1 Applied Anatomy

Applied anatomy greatly simplifies the understanding of the sonoanatomy of the preoperative gastric ultrasound. In this chapter, we will discuss the anatomy of the stomach applied to gastric ultrasound. The stomach is the outermost abdominal viscera. It has several anatomical relations with the liver, pancreas, aorta, and superior mesenteric artery (SMA). As the gastric ultrasound consists of a sagittal view, it is relevant to describe anatomical structures according to cross sections of the abdominal cavity. When performing gastric ultrasound, these anatomical struc-

tures mentioned above are important to consider: the superior mesenteric artery, left lobe of the liver abdominal, aorta, and vertebral bodies. Figure 13.5 shows the cross-sectional anatomy of the abdominal cavity and all landmarks.

The most important landmarks are highlighted in Fig. 13.6. Abdominal aorta gives rise to the superior mesenteric artery, about 1 cm below the celiac trunk. Its trunk descends vertically behind the pancreas more exactly the uncinate process of pancreas. The anatomical relationships of the superior mesenteric artery are represented by the head of the pancreas anteriorly with the antrum of the stomach and the splenic vein. The posterior anatomical relationships are represented by the left renal vein, the lower portion of the duodenum, and the uncinate process of the pancreas.

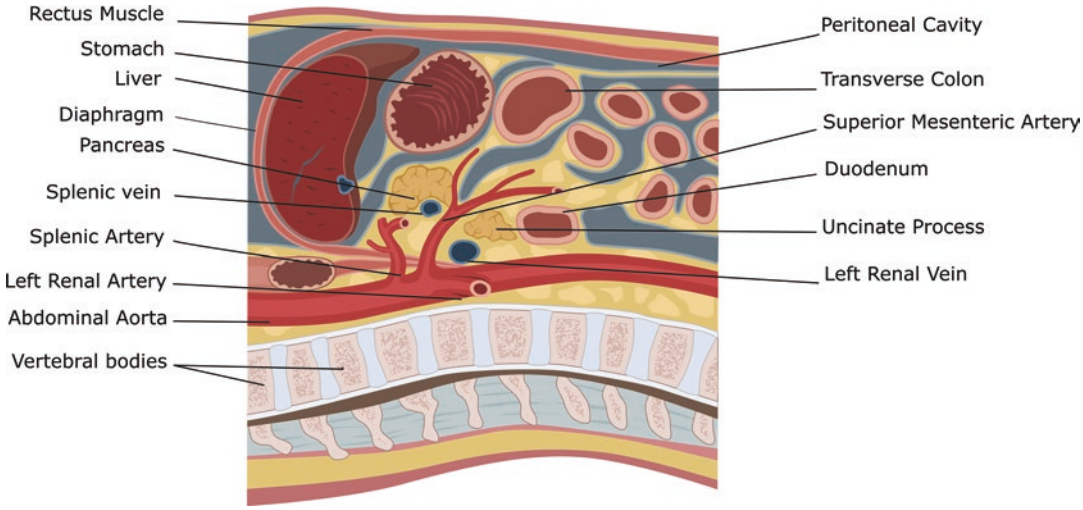

Fig. 13.5 Sagittal cross section of peritoneal cavity. The anatomy applied to gastric ultrasound is based on the identification of landmarks: superior mesenteric artery, left lobe of liver abdominal, aorta, and vertebral bodies

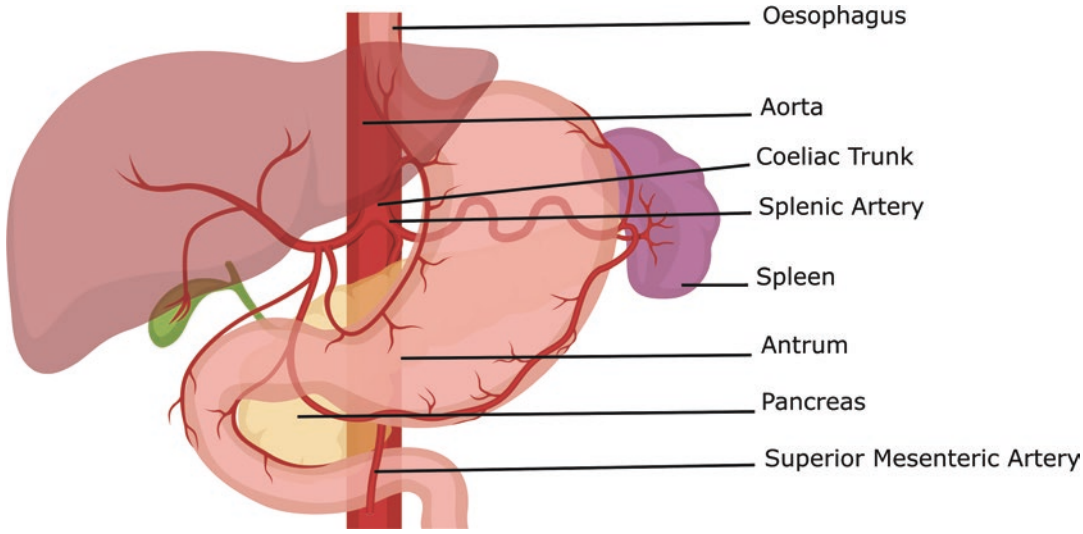

Fig. 13.6 Clearly shows the different anatomical relationships of superior mesenteric artery

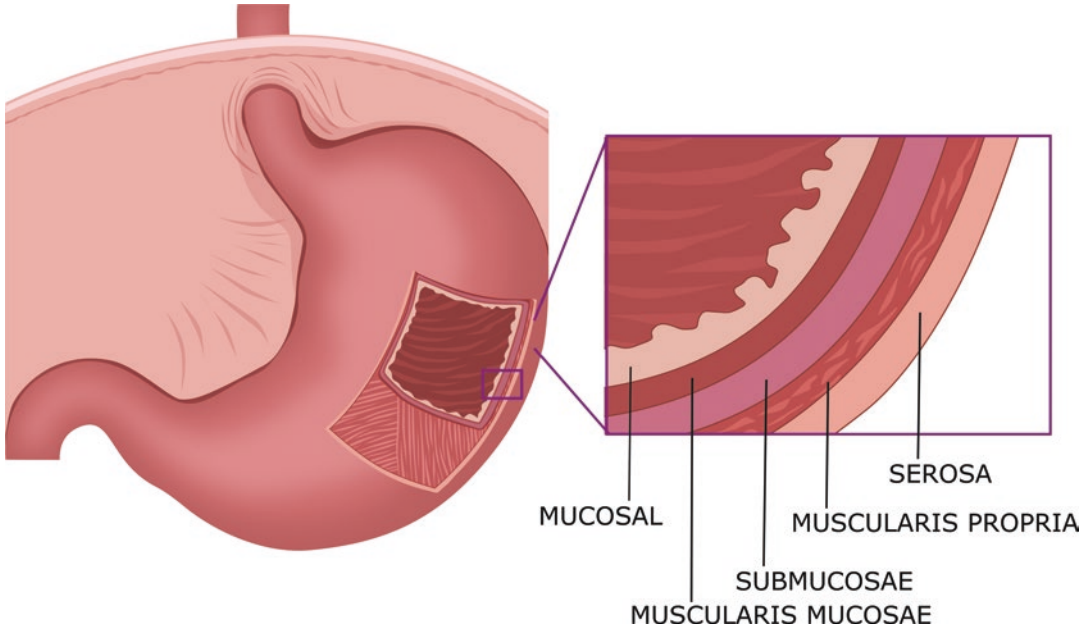

Fig. 13.7 Illustrating the different layers of gastric wall: serosa, muscularis propria, submucosae, muscularis mucosae, and mucosal/lumen

13.4.2 Gastric Wall Histology

As shown in Fig. 13.7, the different layers that constitute the gastric wall. From outside the different layers of the gastric wall are:

1. Serosa is the outermost layer of connective tissue.
2. Muscularis propria is a muscular layer.
3. Submucosa A is a fibrous structure of connective tissue.
4. Muscularis mucosae is a muscular layer.
5. Mucosal the lumen interface the innermost layer of epithelium which has a close relationship with the peritoneum.

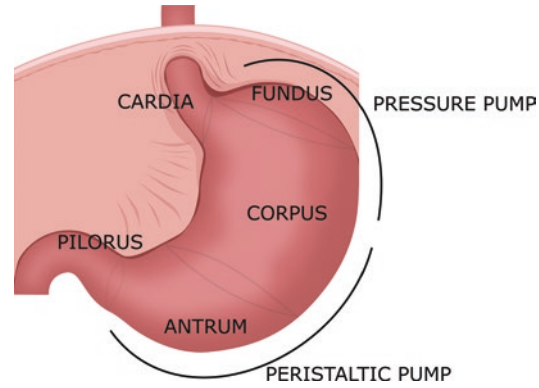

Fig. 13.8 Shows the different parts of stomach with the two pumps: pressure pump and peristaltic pump

13.4.3 Gastric Motor Function Physiology and Pathophysiology

It is important to understand the theoretical basis of gastric motility and emptying. The major functions of the stomach are: temporary food storage, chemical and mechanical digestion of food, mixing boluses of food with gastric secretions, and emptying of the stomach.

Anatomically, the stomach is considered a single chamber, but in reality, it is a multifunctional organ as shown in Figs. 13.8 and 13.9. The interaction of two important regions of the stomach is involved in the motor function of the stomach: the proximal and the distal stomach. The separation between the two gastric regions was determined and clearly highlighted by myoelec-

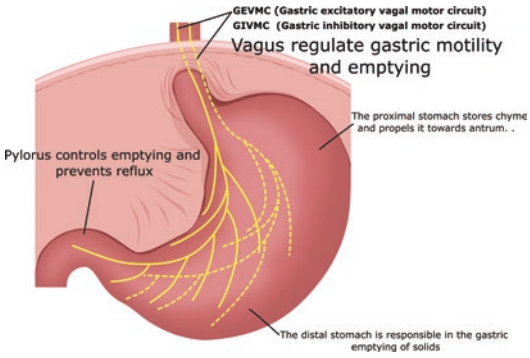
GEVMC (Gastric excitatory vagal motor circuit)
GIVMC (Gastric inhibitory vagal motor circuit)
Vagus regulate gastric motility and emptying
The proximal stomach stores chyme and propels it towards antrum. .
Pylorus controls emptying and prevents reflux
The distal stomach is responsible in the gastric emptying of solids

Fig. 13.9 Shows the two gastric regions, proximal and distal stomach. In addition, this figure illustrates two parallel circuits: GEVMC (the gastric excitatory vagal motor circuit) and GIVMC (the gastric inhibitory vagal motor circuit)

tric and motor criteria ref. The proximal stomach stores chyme and propels it towards antrum. This part is responsible in gastric emptying of liquids due to its slow and sustained contractions. On the other hand, the peristaltic and terminal antral contractions of the distal stomach are responsible for the gastric emptying of solids. The biomechanics of gastric emptying is summarized by the intervention of two pumps within the same crushing organ: a "pressure" pump and a "peristaltic" pump (Fig. 13.8).

Activation of the proximal stomach contractions involves hormonal as well as external neural controls. The vagus nerve plays an important role in both excitation and inhibition messages. The two parallel mechanisms responsible are the GEVMC (the gastric excitatory vagal motor circuit) and GIVMC (the gastric inhibitory vagal motor circuit). These two vagal circuits regulate gastric motility and emptying. Otherwise, in digestion time the hormonal secretion of cholecystokinin and GLP-1 leads to inhibition of gastric emptying involving the GIVMC. On the other hand, between the digestion periods the hormonal secretion of ghrelin and motilin leads to excitation of gastric emptying involving GEVMC [8].

A lot of clinical situations can lead to disrupt the motility of the proximal and distal stomach with altered gastric emptying of liquids and solids: Severe obesity, diabetes, critical illness, pregnancy and labor, severe liver or kidney dysfunction, neuromuscular disorders. Understanding the physiology and pathophysiology of the motor function of the stomach is important not only for performing gastric ultrasound but also for preventing pulmonary aspiration of disorders of the gastric motility, anticipate the risk of inhalation and medical decision-making.

13.5 Indications

One of the main reasons for performing gastric ultrasound is that it helps the anesthesiologist to know the status of the gastric contents, so that he can easily evaluate the risk and influence the management of the anesthesia [9].

More recent work by Johnson and colleagues [10] suggested that ultrasound assessment of gastric content is sensitive and specific to inform anesthesiologists if the stomach is full in unclear and uncertain situations. In terms of Schrödinger's cat paradox, it is about patients who are in what could be called a superposition of clinical states. Many clinical situations are encountered with a degree of uncertainty and unknown. Uncertainty refers to the lack of information about the gastric emptying. Uncertainty can arise from many sources and situations that should be called superposition of clinical states.

13.5.1 Confirm Gastric Emptiness in Superposition of Clinical States

Schematically, two main scenarios can occur in the current practice concerning the evaluation of gastric contents. One may be confronted with communication problems with the patient or have clinical situations with potential delay in gastric emptying.

– **Miscommunication** in pediatric patients, altered state of consciousness, cognitive dysfunction, language barrier, and unclear history. In all these situations, there can exist a

lack of adherence to fasting instructions in non-fasted emergency patients and for patients scheduled for surgery.

– **Potential Delay in Gastric Emptying.**
– Several factors may also be associated with an increase in the risk of potential delay in gastric emptying such as:
  - Diabetes and scleroderma can cause chronic gastric atony.
  - Active labor and pregnancy.
  - Severe liver or kidney dysfunction.
  - Neuromuscular disorders.
  - Obesity.
  - Critical illness.
  - Patients with history of vagotomy and gastric resection, alkaline reflux gastritis, and Roux stasis syndrome (after Roux-en-Y Gastrojejunostomy) can present chronic gastric atony.

  - All these states deserve to be labelled superposition of clinical states so that stomach is neither full nor empty. Ideal solution in this case is to assess the gastric content with ultrasound.

13.5.2 Other Clinical Applications

Other rare indications can be highlighted: suspicion of a gastric foreign body, confirmation of the placement of a nasogastric tube, hypertrophic pyloric stenosis.

13.6 Preparation, Equipment, and Techniques

13.6.1 Preparation

First it is important to explain to the patients how the examination is carried out to obtain their consent. Always remember to cover the patient's private parts, in this case the upper abdomen (more precisely the epigastrium) and lower part of the thorax are exposed. The wearing of gloves by the examiner is necessary to preserve the privacy of the patient and to avoid skin-to-skin contact. Patients always remember their first ultrasound exam, which is still mythical in their mentality, so we must always be careful with our behavior, attitude, gestures, and always give a good impression. In addition, the use of the gel soils the patients a little bit, it is necessary to think to give to the patients towels to wipe themselves.

– Use aseptic technique.
– It should be noted that proper ergonomics are crucial. Ergonomic workstations improve comfort and efficiency. The visual alignment must respect the axis between the patient, physician, and the ultrasound machine. This assumes that the sonographer is on the right side and that the machine is on the left side of the patient. For a right-handed person, this is the ideal configuration and ergonomics for a successful sonographic examination. This is not always the case, and the examiner must face technical constraints, especially in emergency situations.

13.6.2 Position

13.6.2.1 Supine Position

Firstly, scan in the dorsal decubitus position and thereafter continuing the gastric exam in the right lateral position. Classic descriptions of gastric ultrasound technique call for an examination in the supine position; however, the main difficulty with this approach is that the content can be underappreciated. Additionally, a negative ultrasound evaluation in dorsal decubitus position should not imply that the antrum is devoid of any content (Fig. 13.10).

13.6.2.2 Right Lateral Position

It goes without saying that in this position, the gastric contents tip downwards due to gravity. A precise and complete evaluation of the gastric contents imposes to change the patient's decubitus to the right lateral position.

In all cases, to allow an accurate assessment, it is necessary that the gastric exam is always performed in dorsal decubitus position first, then the

Fig. 13.10 Supine position

Fig. 13.11 Right lateral position

patient is returned to the right lateral decubitus position (Fig. 13.11).

13.6.2.3 Half Sitting Position

If for any reason the patient cannot turn over in the lateral decubitus position, we will have to adopt a half-sitting position, slightly head up at 45° (Fig. 13.12). More recently, it has been demonstrated that an angle of the bed at 45° has more impact on qualitative assessment than the supine position [11].

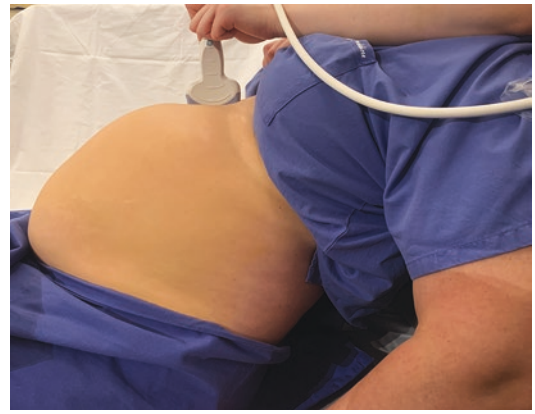

Fig. 13.12 Half-sitting position

13.6.2.4 Equipment

In practice, any ultrasound machine with abdominal settings can be used. The condition is that the CSA can be measured. The gel will serve as an interface between the patient and the probe.

Probes

The higher the frequency of ultrasound emitted by the transducer, the higher the resolution of the image. There are several types of transducers emitting different frequencies of ultrasound: low-frequency transducer, high-frequency transducer. Use a low-frequency 2–5 MHz curvilinear probe for adults (2–5 MHz).

For children whose weight is less than 35 kg, a high frequency probe 7–17 MHz is the most appropriate one.

13.6.2.5 Techniques

To perform POCGUS, the probe should be placed in the upper abdomen exactly in the midline between the xyphoid process and the umbilicus over the epigastric region. Scanning is done in the parasagittal plan; the marker should be oriented cephalad. Starting with the depth of 10 cm is usually adequate, except in very obese patients.

13.7 Sonoanatomy

It is relevant to correlate anatomic structures identified in the anatomy chapter with findings on ultrasound. Applied anatomy with ultrasound correlation can help to understand gastric sonoanatomy. The sagittal view offers a typical sonoanatomy (Fig. 13.13).

One approach to aid in identifying the stomach and more precisely the antrum is to start at the midline with a parasagittal orientation of ultrasound transducer.

- Scan abdomen from the midline. In most individuals, the antrum and other structures can be readily identified with ultrasound.
- Observe the abdominal contents deep to the skin, subcutaneous tissue, and rectus muscle.
- Observe peristaltic contractions of the stomach. If present, suggests recent ingestion of food.
- Identify the liver, pancreas, superior mesenteric artery, long axis view of aorta, and inferior vena cava vertebral bodies. The first cephalad structure to identify is the liver.
- Identify the stomach, the short axis of antrum.
- Begin again with the ultrasound transducer over the midline.
- Slowly move the transducer laterally maintaining a parasagittal view.
- Slightly angle to be parallel with the aorta or vena cava.
- Use color Doppler. It is important to mention that, when performing gastric ultrasound, color flow Doppler should be used to identify aorta and inferior vena cava (Fig. 13.14).
- Observe a pulsatile structure anterior to vertebral bodies corresponding to the aorta.
- Identify the celiac trunk and the SMA arising from the aorta then becomes parallel to it.
- Differentiate between the aorta and IVC. Aorta is pulsatile and slightly left of the midline. IVC is seen to the right of the midline. In addition, the diameter of IVC varies according to the inspiration increasing with expiration.
- Identify vena cava laterally until you are over the midline.
- Slowly move the transducer laterally maintaining a parasagittal view.
- Tilt may be applied to the transducer to better visualize anatomic structures. This allows identification of the antrum sandwiched between the pancreas posteriorly and the liver anteriorly.

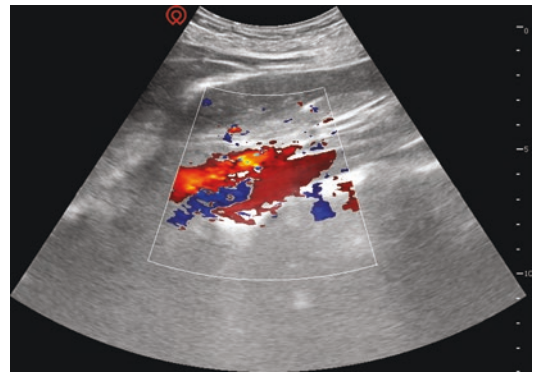

Fig. 13.14 Color Doppler allows visualization of vascular structures inferior vena cava aorta and superior mesenteric artery

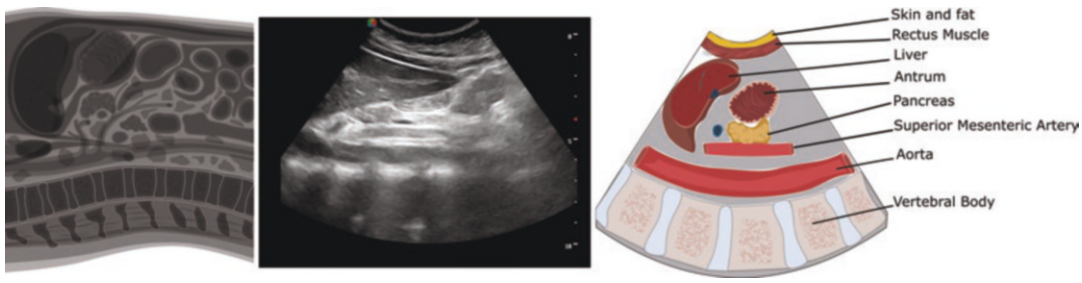

Fig. 13.13 Illustrates schematically the correlation by identifying relevant landmarks as liver, pancreas, superior mesenteric artery, aorta, and inferior vena cava antrum and vertebral bodies

Qualify the gastric contents and note the sonographic findings: solids thick or clear liquids (see the sub-chapter "Qualitative Assessment of Gastric Volume").

Quantify the gastric contents: Measure the cross-sectional area of the antrum (CSA) from the serosa to the serosa. Use the free tracing tool of the ultrasound machine as shown in Fig. 13.14 to measure diameters. The serosa is usually the most hyperechoic of the gastric wall layers with muscularis being the most hypoechoic (see the sub-chapter "Quantitative Assessment of Gastric Volume").

13.7.1 Sonographic Appearance of Gastric Wall Layers

Sonographic identification of gastric layers is characterized by an alternating echogenicity.

Figure 13.15 illustrates the correlation between gastric wall histology and ultrasound findings of the different layers.

- The serosa appears as a hyperechoic and thin layer.
- The muscularis is the thickest gastric wall layer that is hypoechoic. This sonographic feature is most obvious when the stomach is empty.
- The submucosa appears hyperechoic.
- The muscularis mucosae appears hypoechoic.
- The mucosal appears hyperechoic.

13.7.2 Sonographic Appearance of Gastric Content

Ultrasonography is a useful tool for imaging gastric content. It is first important to define what looks like sonographic features of gastric content. It is important to stress that:

- *Sonographic Appearance of solids*: The sonographic visualization of solids appears heterogeneous on ultrasound (Fig. 13.16).

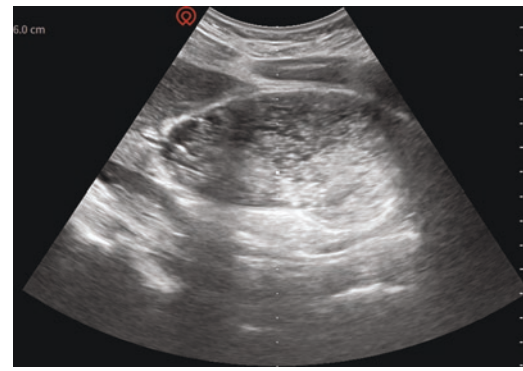

Fig. 13.16 Represents the sonographic visualization of solids that appear heterogeneous

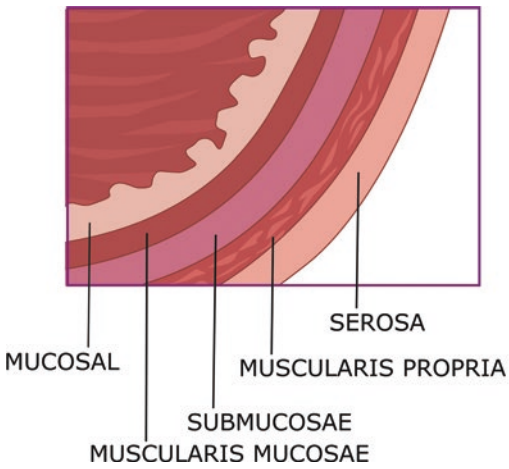

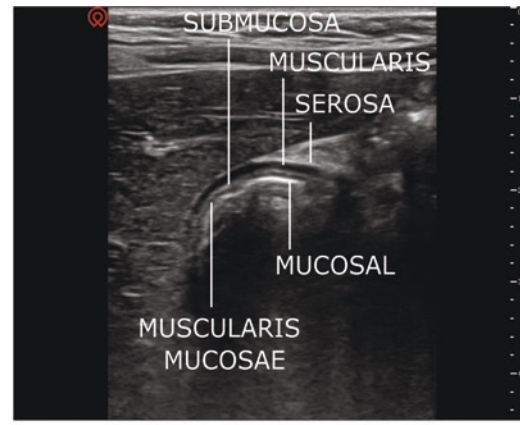

Fig. 13.15 Provides an overview of the sonographic appearance of gastric wall layers. Observe the correlation between ultrasound and gastric wall histology. Differentiate different layers with alternating echogenicity

– *Sonographic Appearance of thick fluids*: Milk and thick liquid contents have a hyperechoic and homogeneous appearance (Fig. 13.17).
– *Sonographic Appearance of clear liquids*: The baseline gastric secretions, water and clear liquids are anechoic or hypoechoic and homogeneous (Fig. 13.18).

13.7.3 Sonographic Appearance of Antrum

Various sonographic findings of antrum can be described.

Empty Antrum In fasted patients, empty antrum appears on ultrasound as a "Target" [12] or a "Bull's eye" (Fig. 13.19). Other authors describe the gastric antrum as a small flattened or round structure (Fig. 13.20).

Full Antrum A full antrum is rather distended and round shaped in non-fasted patients (Fig. 13.21). After a solid meal, the antrum is hyperechoic as shown in Fig. 13.22. Solid food with air bubbles gives a "starry night" appearance as depicted in Fig. 13.23, "frosted-glass" or air-mixed appearance. Crystalloid mixture creates ring-down artifacts with typical "blur." Recently ingested clear liquids contain air bubbles that appear hyperechoic with mobile punctuate echoes. Gastric peristaltic contractions suggest a recent food intake.

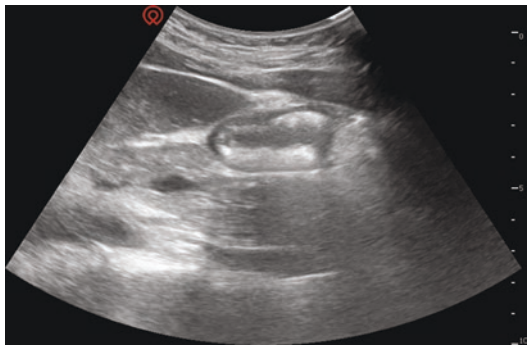

Fig. 13.17 Represents the sonographic visualization of milk and thick contents have a hyperechoic and homogeneous appearance

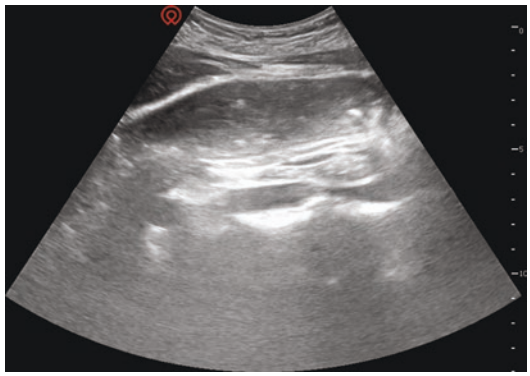

Fig. 13.18 Represents the sonographic visualization of baseline gastric secretions, water and clear liquids are anechoic or hypoechoic and homogeneous

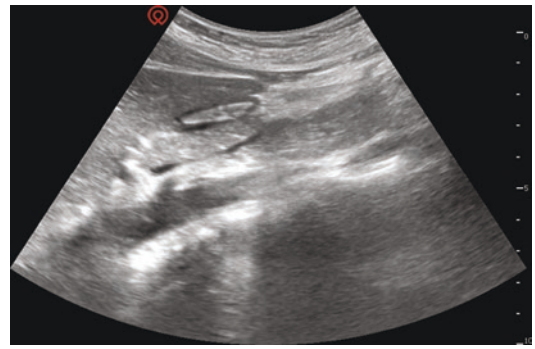

Fig. 13.19 Targetoid structure

Fig. 13.20 Empty antrum appearance shows a flattened structure

Fig. 13.21 Full antrum sonoanatomy

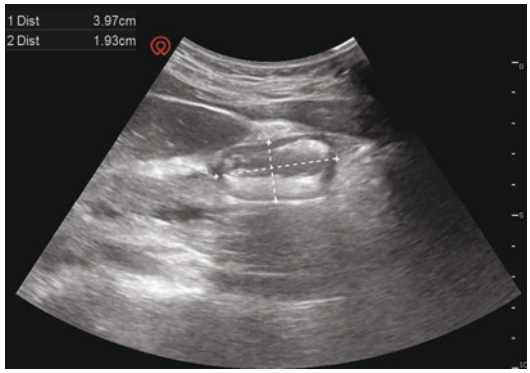

Fig. 13.22 Hyperechoic aspect of antrum after a solid meal

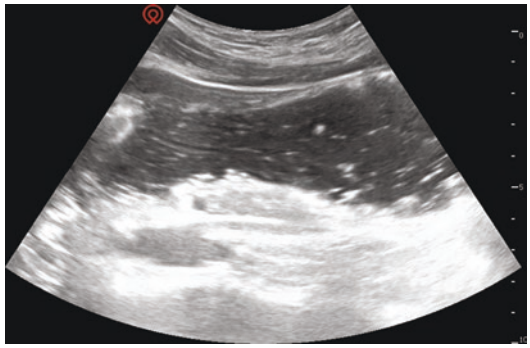

Fig. 13.23 "Starry night" appearance of solid food with air bubbles

13.8 Ultrasonographic Measurement of Antral Area

Different methods of volume assessment and measurement have been previously used and described by Perlas and colleagues [13].

13.8.1 Qualitative Assessment of Gastric Volume

- Antral Grading System (Grades 0, 1, 2)
- This grading system suggested by Perlas and colleagues is strictly assessed on the qualitative aspect of the gastric content. This grading system provides correlation with gastric volume predicted by previous mathematical models [13]. It consists of a three-point grading system:

Grade 0: Empty antrum in both supine and right lateral decubitus (RLD position) Negligible or minimal clear fluid visible in the antrum. Figure 13.24 shows an example of Grade 0.

Grade 1: Clear fluid visible in the antrum (distended antrum with hypoechoic content) only in the RLD position. This grade illustrated in Fig. 13.25 corresponds to low predicted gastric volume and low aspiration risk <1.5 mL/kg of clear fluid.

Grade 2: Clear fluid visible in the antrum (distended antrum with hypoechoic content) both

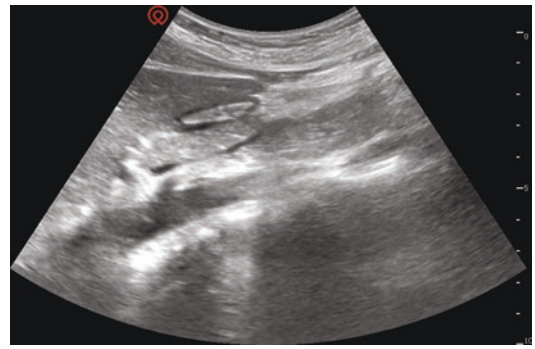

Fig. 13.24 Grade 0 empty antrum or minimal clear fluid visible

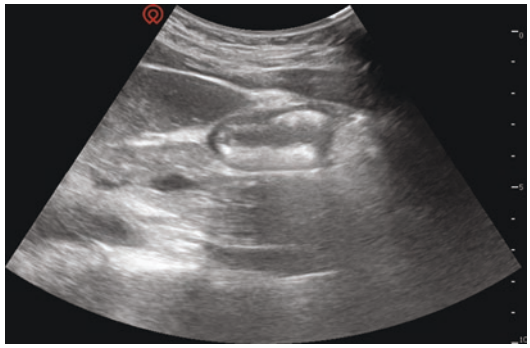

Fig. 13.25 Illustrates Grade 1: distended antrum with hypoechoic content only in the RLD position

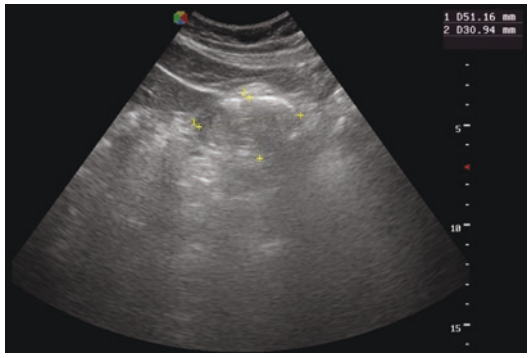

Fig. 13.26 Illustrates Grade 2: clear fluid visible in the antrum both in the supine and RLD positions

in the supine and RLD positions. This grade illustrated in Fig. 13.26 corresponds to high predicted gastric volume and high aspiration risk >1.5 mL/kg of clear fluid.

This antral grading system has been validated in children, obese and non-obese adults, and obstetric patients.

13.8.2 Quantitative Assessment of Gastric Volume

The purpose of the measure is to estimate the antral area of the antrum. This measure was

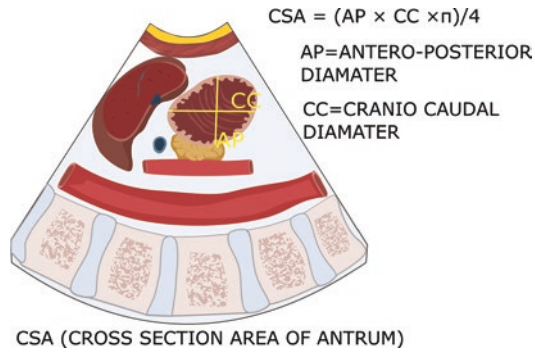

Fig. 13.27 Clearly shows how to measure the craniocaudal diameter (CC) and the antero-posterior diameter (AP) both are measured from serosa to serosa

found to be strongly correlated with gastric volume. In fact, the cross-sectional area of the antrum (CSA) has a linear correlation with the gastric volume. The details of the procedure have been reported previously by Bolondi and colleagues [14]. Measurements were performed according to a standardized protocol defined concerning the cross-sectional area of the antrum (CSA). It can be described through an equation such as the following:

$$\mathrm{CSA} = \left(\mathrm{AP} \times \mathrm{CC} \times \pi\right) / 4.$$

Measure the antero-posterior diameter of the antrum then the cranio-caudal diameter. A visual representation of the CSA can be seen here in Fig. 13.27.

The equation is based on two diameters corresponding to the cranio-caudal and the antero-posterior diameter. It is of high importance to obtain accurate measurements from serosa to serosa (Fig. 13.22). In addition, it is important to remember that the CSA of the antrum is an area and not a volume. The idea behind this measurement is that the antrum area correlates with the volume. This can be estimated as described in the following equation [13]:

$$\mathrm{Volume}\left(\mathrm{mL}\right) = 27.0 + 14.6 \times \mathrm{right\ lateral CSA}\left(\mathrm{cm}^2\right) - 1.28 \times \mathrm{Age}\left(\mathrm{years}\right).$$

Table 13.1 Predictive model to assess the gastric volume and relationship between age and the CSA in the right lateral decubitus position according to the mathematical model validated by Perlas [13]

Variable	Parameter estimate	Standard error	*P* value
Intercept	27.0	26.7	<0.3131
Right lat CSA	14.6	0.9	<0.0001
Age	−1.28	0.46	0.006
Rsq = 0.731			

CSA cross-sectional area
Table used with permission from gastricultrasound.org

The validation of this mathematical model has been approved for non-obese and non-pregnant adults and allow prediction of volumes in a range of zero to 500 mL [13]. *Use* Table 13.1 lists the predicted volumes according to the two parameters, age and CSA, in the right lateral decubitus position.

13.9 Interpretation and Scores

Perlas et al. describe a generalized framework [15] for interpreting and scoring of patients. The framework based on I-AIM mode (Indication Acquisition Interpretation Medical Management) brings together all elements of the clinical reasoning in a coherent and practical way. Figure 13.28 provides an overview of the framework.

13.9.1 Medical Decision-Making

Figure 13.29 shows the scenarios explained and decision-making algorithms according to the mathematical model validated by Perlas [13].

After evaluating the gastric contents and interpreting the results, we have to decide what to do:

- Canceling proceeding or delaying surgery and anesthesia.
  - Surgery and anesthesia should be cancelled or postponed when the stomach is full (grade 1 or 2 with high volume on gastric ultrasound) and surgery is scheduled and not urgent. This is common sense and the strict application of the rules of fasting to the letter. The fasting guidelines of the ASA are very explicit.
  - The second scenario represents the case where the stomach is frankly without content with obvious ultrasound criteria. In ultrasound terms, it corresponds to grade 0 with an evaluation of negligible volumes or <1.5 mL/kg.
- Decide a possible gastric tube placement and aspiration before induction and to maintain it preoperatively and postoperatively.
- Decide on the technique to be used: general anesthesia/regional anesthesia.
- Decide to use or not a rapid sequence induction.
- Decide to intubate the patient rather than use supraglottic device in patients with potential delay in gastric emptying such as diabetic.
- Decide to use a laryngeal mask with sedation rather than endotracheal tube.
- Decide to prescribe premedication with prokinetic such as Metoclopramide to accelerate gastric emptying.
- Decide to prescribe antacids.

I-AIM FRAMEWORK FOR GASTRIC SONOGRAPHY

(I) INDICATION

Pre-anesthetic aspiration risk assessment in the setting of questionable per os intake:
- elective procedures but NPO guidelines not followed
- urgent/emergency procedures
- NPO status unknown

(A) ACQUISITION

Patient	▪ Position: supine and RLD ▪ Adjust ambient light ▪ Expose the upper abdomen		**Probe**	▪ Adults: low frequency curved probe ▪ Pediatrics: consider high frequency linear probe ▪ Acoustic medium: gel ▪ Sagittal scanning plane in the epigastrium
Picture	Scan	▪ sweep widely from left to right subcostal margin to systematically identify the stomach as a hollow viscus located superficially between the left lobe of the liver and the pancreas with a prominent muscularis layer within its wall ▪ rock and slide to positively identify the antrum at the level of the aorta ▪ rotate to obtain a true cross section of the antrum avoiding oblique views ▪ heel to toe movement to optimize acoustic reflections		
	Knobology	▪ primary: adjust depth and gain ▪ secondary: adjust tissue harmonics and focal zone ▪ tertiary: color or power Doppler to confirm vessel identity if required		
	Capture	▪ still frame or video as required ▪ if clear fluid content, measure antral CSA in RLD as a mean of 3 readings, between peristaltic contractions and estimate gastric volume using a predictive model such as: (Volume(mL)=27.0 + 14.6 x Right-lat CSA – 1.28 x age)		
Protocol	Complete written report (fig.x)			

(I) INTERPRETATION

Pattern recognition: gastric content nature
- Empty stomach, grade 0 antrum: minimal clear fluid/air content, flat antrum or "bull's eye" pattern in both supine and RLD
- Clear fluid (distended antrum with hypoechoic content)
  - -Grade 1 antrum (fluid visible in RLD only, suggesting low gastric volume)
  - -Grade 2 antrum (fluid visible in both supine and RLD, suggesting high gastric volume)
- Thick fluid or solid (distended antrum with hyperechoic/heterogeneous content)

Volume estimation

Helps differentiate clinically insignificant volume or baseline gastric secretions (<1,5 mL/kg of clear fluid) from greater than baseline volumes (>1,5mL/kg)

(M) MEDICAL DECISION MAKING

Clinical context	▪ History and physical exam ▪ Elective versus urgent versus emergency procedure ▪ Time interval since last meal ▪ Type and amount of meal ▪ Other aspiration risk factors (diabetes, GERD, stroke, active labor, Neuromuscular disease)
Image analysis	▪ Adequate ▪ Technically difficult ▪ Inadequate

Physician interpretation and decision making

Classify findings into one of 3 categories:
- Empty stomach or baseline gastric secretions suggesting LOW aspiration risk
- Clear fluid content (>1,5mL/kg) suggesting higher than baseline gastric volume and HIGH aspiration risk
- Thick fluid or solid content suggesting HIGH aspiration risk

Medical decision making
- Decide on anesthetic/surgical timing: proceed, delay, cancel
- Decide on anesthetic technique: general versus regional
- Decide on the need for aspiration precautions (e,g, need for intubation, rapid sequence induction)

Fig. 13.28 Illustrates the basic model of the framework [15]. (The figure is used with permission from gastricultrasound.org)

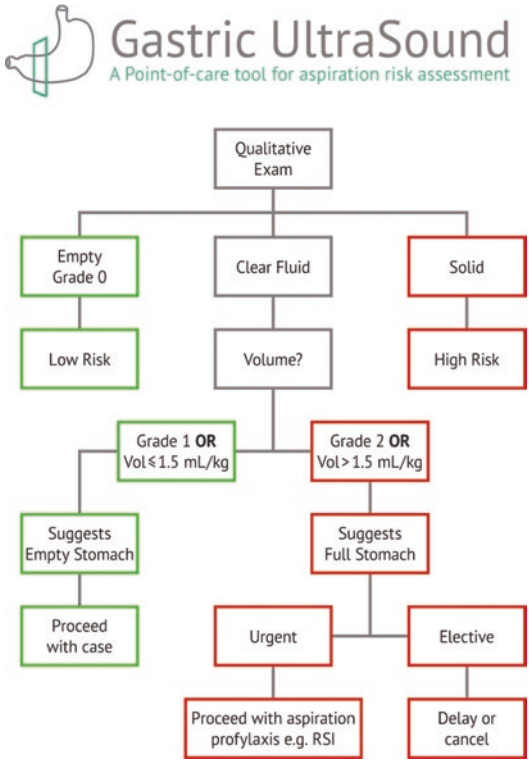

Fig. 13.29 Decision-making algorithms of gastric ultrasound findings. (Table used with permission from gastricultrasound.org)

13.10 Specific Patients

In some individuals (pregnant women, obese patients, non-fasting patients, existence of physiologic air…), it can be more challenging to identify which structure is which. These difficulties stem from the fact that the technique has its limitation and disadvantages that have already been mentioned at the beginning of this chapter. *However*, literature offers no clear methodology for the problem.

13.10.1 Point-of-Care Gastric Ultrasound in Adults

The adult has been included in this chapter as a specific patient in the sense that it serves as a reference examination for the rest of the patients (Fig. 13.30).

Fig. 13.30 Shows the reference sonoanatomy of gastric ultrasound

The details of the procedure are described as follows:

- Measure the antero-posterior diameter of the antrum then the cranio-caudal diameter as shown in Figs. 13.31 and 13.32.
- Measure the CSA = (AP × CC × π)/4. The CSA is an area and not a volume.
- Use the predictive model validated by Perlas to assess gastric volume Table 13.1.
- Use decision-making algorithms.

13.10.2 Point-of-Care Gastric Ultrasound in Pregnancy

Principle indications of gastric ultrasound are generally the same as for the adult non-pregnant except for some specificities. The first evidence was provided by O'Sullivan [16] whose study concludes that there is no significant difference of gastric emptying between a non-pregnant woman and the non-laboring pregnant women. However, the time of gastric emptying is delayed during labor. More recently, Howle [17] reported that the gastric emptying of fluid is unchanged during pregnancy and the postpartum period while the gastric emptying of solids is prolonged. The implication of this is that it is relevant to leave the parturients fasting during labor.

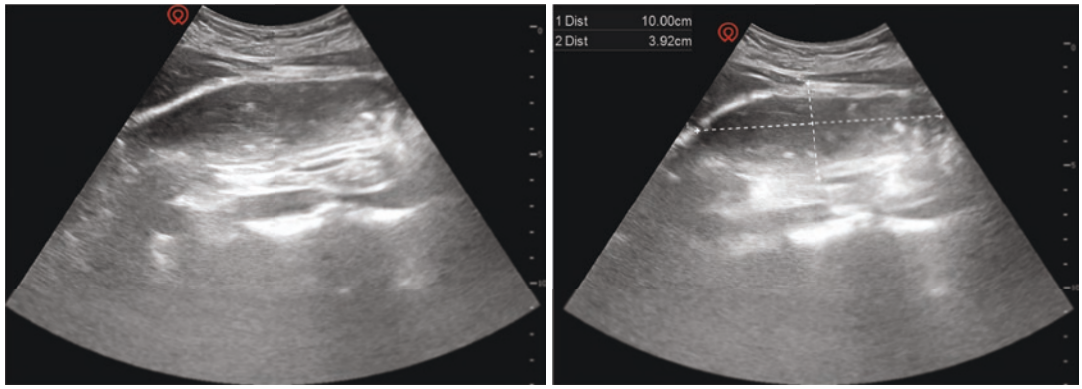

Figs. 13.31 and 13.32 Illustrates the ultrasound findings of a full stomach. The two diameters are measured, then the CSA is calculated

Characteristics of pregnancy that can make gastric ultrasound technically difficult:

- Enlarged uterus.
- Tachypnea with hyperdynamic circulatory.
- The uterine height also hinders the placement of the probe in the upper abdomen. The midline between xyphoid process and the umbilicus over the epigastric region present a steeper angle during the last trimester of pregnancy.
- Fetal movements sometimes interfere with the examination.
- The stomach is moved cephalad and right due to anatomical changes.
- The problem calls for a different optimization technique for pregnant women and this is an optimal solution to solve this problem:
- Semirecumbent position figure and right lateral decubitus (Fig. 13.33).
- Moving the uterus delicately.
- Asking the woman to control and slow breathing for a moment.

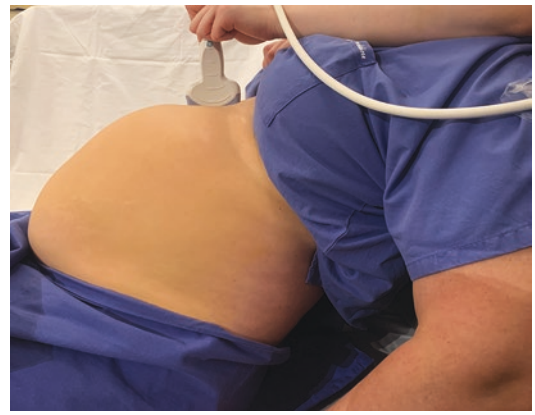

Fig. 13.33 Semirecumbent position

13.10.2.1 Ultrasound Findings During Pregnancy

The reference sonoanatomy is represented in Figs. 13.34 and 13.35 and is the same as in the adult with some exceptions.

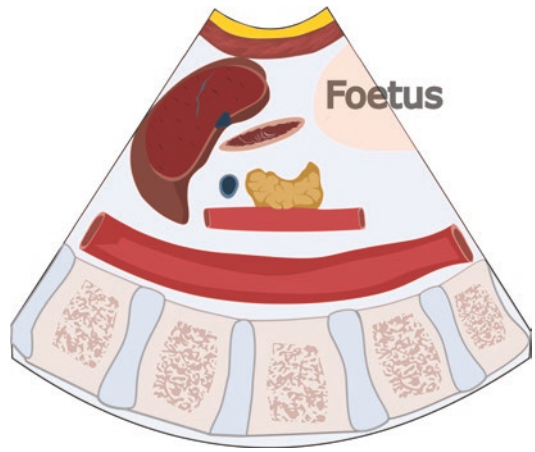

Fig. 13.34 Illustrates the ultrasound findings during pregnancy. Identify uterus the most caudad structure

– Identify antrum wedged between the liver (the first cephalad structure) and uterus (the most

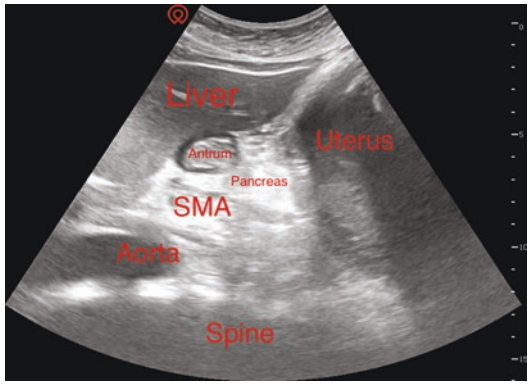

Fig. 13.35 Shows the details of the gastric ultrasound findings during pregnancy. Identify uterus the most caudad structure, liver, SMA, antrum, and pancreas

caudad structure). In cephalad to caudal direction, observe liver antrum then uterus wall.
- Identify antrum. As highlighted above, it's difficult to identify the antrum easily.
- Tilt the transducer to better visualize the antrum anatomically.
- Identify the pancreas, superior mesenteric artery, long axis view of aorta, and posteriorly vertebral bodies.
- Measure the cross-sectional area of the antrum (CSA) CSA = (AP × CC × π)/4 AP corresponding to the antero-posterior diameter of the antrum. AP the cranio-caudal diameter. It is important to note that this formula calculates an area and not a volume.
- Appreciate and quantify the gastric content. It is important to note that the model mentioned above (Volume = 27.0 + 14.6 × RL CSA − 1.28 × Age) is not applicable to pregnant women. Studies have proposed mathematical models to evaluate gastric content such as Roukhomovsky et al. [17]. Due to a lack of clarity, more studies are needed to validate the suggested models to estimate the gastric volume. In the meantime, it seems logical to continue using Perla's method and to combine qualitative assessment of gastric volume (Antral Grading System [0, 1, 2]) and measure the cross-sectional area.

13.10.3 Point-of-Care Gastric Ultrasound in Pediatrics

Gastric ultrasound is used in children in many circumstances to assess gastric:

- Miscommunication in pediatric patients.
- Unclear and uncertain situations before surgery and anesthesia.
- Potential delay in gastric emptying: pediatric intensive care unit and neonatal intensive care unit diabetes neuromuscular disorders.

Other rare indications: suspicion of a gastric foreign body, confirmation of the placement of a nasogastric tube, hypertrophic pyloric stenosis.

- A linear high-frequency probe allows to better visualize superficial location of structures that are expected in pediatric patients.
- Place the transducer in the upper abdomen in the midline between xyphoid process and the umbilicus over the epigastric region (Fig. 13.36).
- Scan in supine position then in right lateral position (Fig. 13.37).
- Scan in the parasagittal plan, the marker should be oriented cephalad.
- Avoid the collapsibility of the stomach.

Fig. 13.36 Probe placement

The sonoanatomy is the same as in adults and more obvious as shown in Figs. 13.38 and 13.39.

As in adults, the CSA is highly correlated with gastric volume.

First measure the antero-posterior diameter of the antrum then the cranio-caudal diameter; then calculate the CSA with the following equation: CSA = (AP × CC × π)/4.

Another mathematical model is approved in pediatrics different than adults and allows assessment of gastric volume:

$$\text{Gastric volume}(\text{mL}) = -7.8 + (3.5 \times \text{RLD} - \text{CSA}) + (0.127) \times \text{age}(\text{months}).$$

Fig. 13.37 Right lateral position

After calculating the CSA (Fig. 13.40), use predictive model to assess the gastric volume in Table 13.2.

13.10.4 Point-of-Care Gastric Ultrasound in Obese Patients

As mentioned by Riveros-Perez and colleagues [18], the body mass index predicts independently the antral cross-sectional area and gastric volume in term women planned for cesarean section.

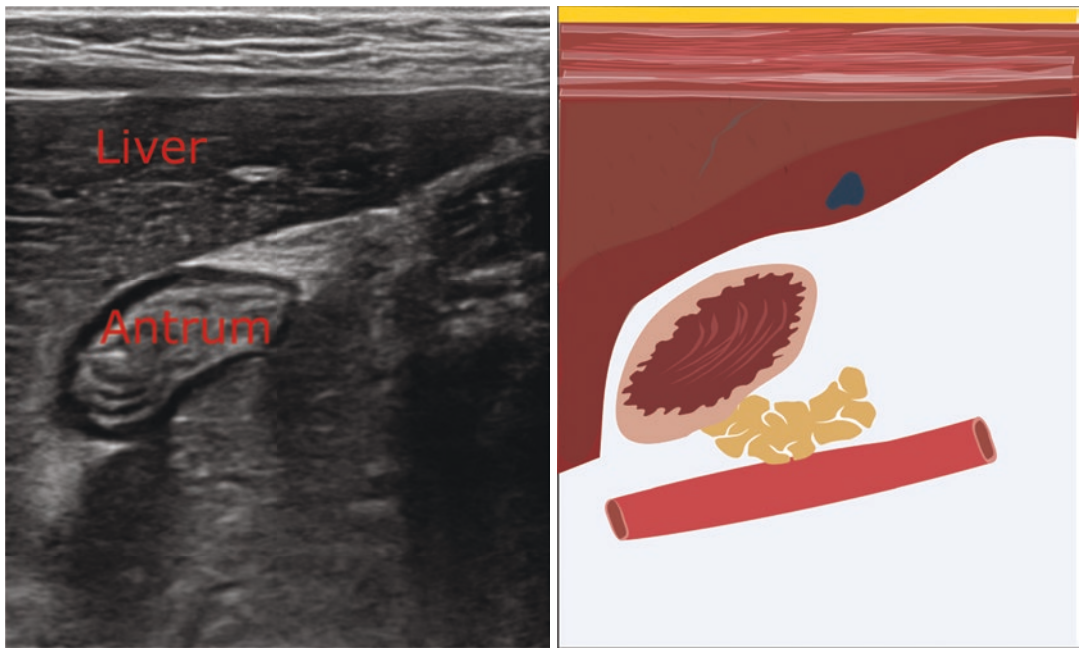

Figs. 13.38 and 13.39 The sonoanatomy is obvious. Antrum is easily identified. Observe the wall gastric layers well individualized

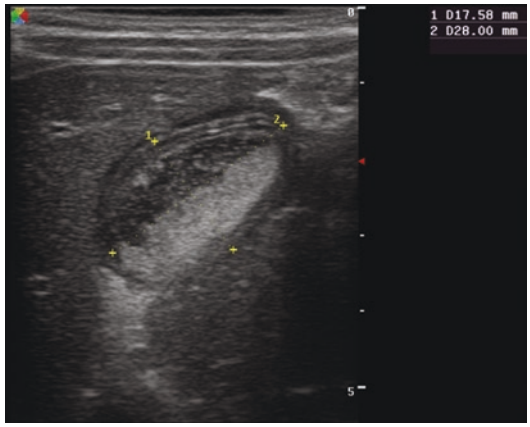

Fig. 13.40 Measure the two diameters of antrum to calculate antrum area

Perioperative fasting guidelines in pregnancy should be adjusted in obese and morbidly obese pregnant women. According to their validation study, Kruisselbrink and colleagues [19] suggest that the model mentioned above (Volume = 27.0 + 14.6 × RL CSA − 1.28 × Age) is applicable to obese patients. Clear, strong, and well-documented evidence suggests that the mathematical model to assess gastric volume is valid for severely obese individuals.

Table 13.2 Lists the predicted volumes according to the two parameters, age and CSA, in pediatrics

	Age (years)						
Right lat CSA (cm^2)	20	30	40	50	60	70	80
3	45	32	20	7	0	0	0
5	74	62	49	36	23	10	0
7	103	91	78	65	52	40	27
9	133	120	107	94	82	69	56
11	162	149	136	123	111	98	85
13	191	178	165	153	140	127	114
15	220	207	194	182	169	156	143
17	249	236	224	211	198	185	173
19	278	266	253	240	227	214	202
21	307	295	282	269	256	244	231
23	337	324	311	298	285	273	260
25	366	353	340	327	315	302	289
27	395	382	369	357	344	331	318
29	424	411	398	386	373	360	347

13.10.5 Point-of-Care Gastric Ultrasound for Critically Ill Patients

- Before induction or sedation in ICU, PICU, and NICU.
- Altered state of consciousness.
- Neuromuscular disorders.
- Ultrasound-guided enteral nutrition.
- Nasogastric tube placement.
- Detect foreign bodies in the stomach.

13.11 Tips and Tricks

- We need to tread very carefully and avoid any stomach compressibility which might lead to stomach compressibility, especially in children.
- The measurements are performed according to a standardized protocol. The view should be in the sagittal plan and oblique views lead to errors. Avoid being parallel to inferior vena cava. Probe should be parallel to aorta.
- Differentiate between colon and antrum: colon is more caudally situated than the stomach. The wall layers of the colon are not well individualized. In addition, the colon is identified as a hazy structure.
- Measure the CSA between peristaltic contractions.
- The existence of peristaltic contraction suggests a full stomach and a recent food intake.
- When assessing pregnant woman, move the uterus delicately and ask the woman to control and slow breathing for a moment.

References

1. Whittingham TA, Bateman. Volume measurements of the stomach. Br J Radiol. 1980;53:615–6.
2. Fujigaki T, et al. Quantitative evaluation of gastric contents using ultrasound. J Clin Anesth. 1993;5(6):451–5.
3. Simpson JY. The alleged case of death from the action of chloroform. Lancet. 1848;1:175.
4. Mendelson CL. The aspiration of stomach contents into the lungs during obstetric anesthesia. Am J Obstet Gynecol. 1946;52:191–205.
5. Engelhardt T, Webster NR. Pulmonary aspiration of gastric contents in anaesthesia. Br J Anaesth. 1999;83(3):453–60.
6. Charlesworth M, Wiles MD. Pre-operative gastric ultrasound—should we look inside Schrödinger's gut? Anaesthesia. 2019;74(1):109–12. https://doi.org/10.1111/anae.14516.
7. Schrödinger E. Die gegenwärtige Situation in der Quantenmechanik. Naturwissenschaften. 1935;23:807–12. https://doi.org/10.1007/BF01491891.
8. Goyal RK, Guo Y, Mashimo H. Advances in the physiology of gastric emptying. Neurogastroenterol Motil. 2019;31:e13546.
9. Alakkad H, et al. Point-of-care ultrasound defines gastric content and changes the anesthetic management of elective surgical patients who have not followed fasting instructions: a prospective case series. Can J Anaesth. 2015;62(11):1188–95.
10. Johnson EJ, Morbach J, Blake C, Pecka S. Sensitivity and specificity of gastric ultrasonography in determination of gastric contents. AANA J. 2021;89(1):9–16.
11. Bouvet L, et al. Effect of body position on qualitative and quantitative ultrasound assessment of gastric fluid contents. Anaesthesia. 2019;74(7):862–7.
12. Moake MM, Presley BC, Hill JG, Wolf BJ, Kane ID, Busch CE, Jackson BF. Point-of-care ultrasound to assess gastric content in pediatric emergency department procedural sedation patients. Pediatr Emerg Care. 2022;38:e178.
13. Perlas A, Davis L, Khan M, et al. Gastric sonography in the fasted surgical patient: a prospective descriptive study. Anesth Analg. 2011;113:93–7.
14. Bolondi L, Bortolotti M, Santi V, Calletti T, Gaiani S, Labo G. Measurement of gastric emptying by real time ultrasonography. Gastroenterology. 1985;89:752–9.
15. Perlas A, et al. I-AIM framework for point-of-care gastric ultrasound. Br J Anaesth. 2016;116(1):7–11.
16. O'Sullivan G. Gastric emptying during pregnancy and the puerperium. Int J Obstet Anesth. 1993;2:216–24.
17. Howle R, et al. Gastric point-of-care ultrasound (PoCUS) during pregnancy and the postpartum period: a systematic review. Int J Obstet Anesth. 2020;44:24–32.
18. Riveros-Perez E, Davoud S, Sanchez MG, Montesinos H, Rocuts A. Ultrasound your NPO: effect of body mass index on gastric volume in term pregnant women—retrospective case series. Ann Med Surg (Lond). 2019;48:95–8. https://doi.org/10.1016/j.amsu.2019.10.029.
19. Kruisselbrink R, et al. Ultrasound assessment of gastric volume in severely obese individuals: a validation study. Br J Anaesth. 2017;118(1):77–82.

Vascular Ultrasound

14

Fatima Zohra Ouichen and Lydia Nekmouche

14.1 Introduction

Blood circulation may be checked using a vascular ultrasound, a noninvasive ultrasound technique in which sound waves are delivered through the tissue to evaluate limbs, neck, and abdomen. Physicians are able to determine the rate of flowing blood cells inside blood arteries by using the reflected sound waves. The waves of sound are captured and shown graphically on a computer monitor.

14.2 Techniques

Vascular ultrasound includes several methods and approaches to study blood vessels and blood flow (Fig. 14.1). Continuous-wave Doppler is the simplest technique for evaluation. Ultrasound machines use pulsed-wave ultrasound in combination with B-mode and pulsed Doppler [1].

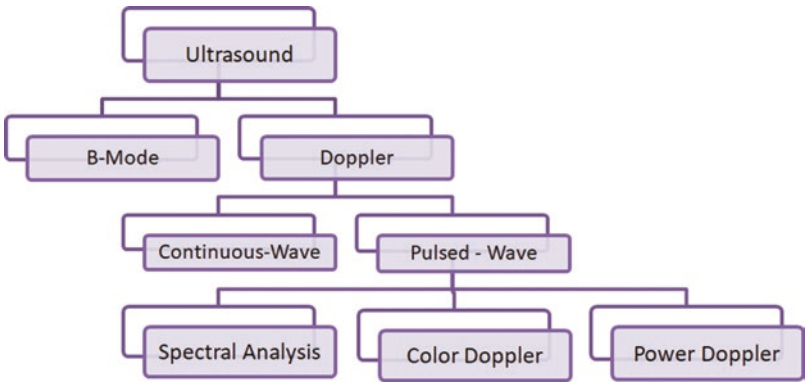

Fig. 14.1 This diagram illustrates different modes of Doppler

F. Z. Ouichen (✉)
Clinique Chifa, Algiers, Algeria

L. Nekmouche
EPH Laghouat, Laghouat, Algeria

© The Author(s), under exclusive license to Springer Nature Switzerland AG 2024
N. Bouarroudj et al. (eds.), *POCUS in Critical Care, Anesthesia and Emergency Medicine*,
https://doi.org/10.1007/978-3-031-43721-2_14

14.3 Assessment of Upper Limb Vessels

14.3.1 Anatomy

Knowledge of anatomy is important to know anatomical variations and vascular pathologies. It's the sine qua non condition for the success of the vascular ultrasound examinations.

14.3.1.1 Artery Anatomy of the Upper Extremity

There are five major arteries that deliver blood to the upper limb [2]. From proximal to distal, the different arteries are as follows:

1. Subclavian artery
2. Axillary artery
3. Brachial artery
4. Radial artery
5. Ulnar artery

Figure 14.2 clearly shows the different arteries of the upper limb.

Subclavian Artery: The subclavian artery is the starting point of the arterial blood flow to the upper regions. It branches out of the brachiocephalic trunk on the right of the organism and splits off the aortic arch straight to the left.

Axilla: Axillary Artery: Located inside the axillary sheath, it runs deep into the pectoralis minor muscle. Position in relation to the pectoralis minor allows for its separation into the following three distinct segments:

- **First part:** Found proximally to the pectoral muscles
- **Second part:** Located posteriorly to the pectoral minor muscle
- **Third part:** Distally to the pectoral minor muscle

The Brachial Artery:

It originates from the brachioradialis muscle and branches out to form the profunda brachii (also known as the Deep Artery) and an anastomotic network around the elbow.

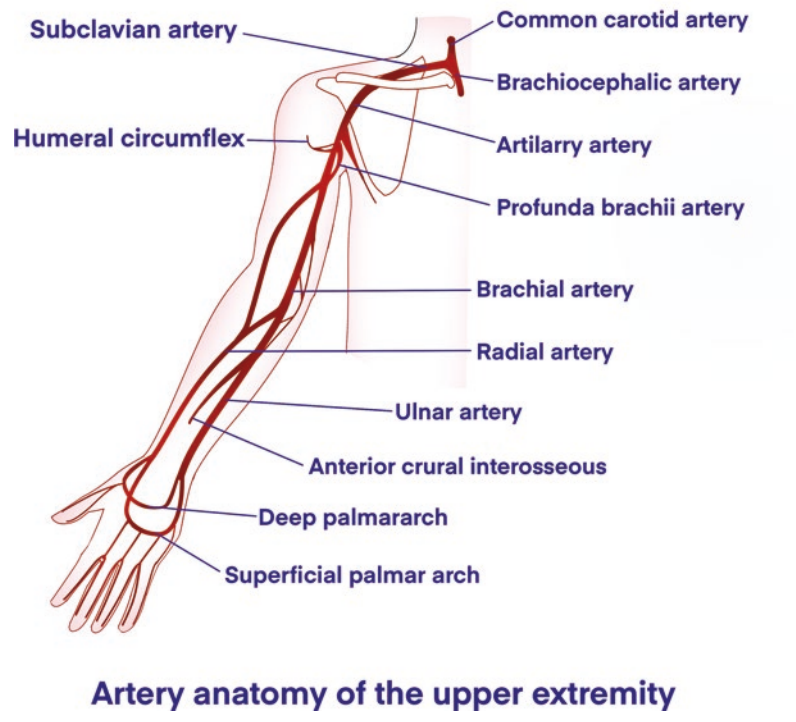

Fig. 14.2 Artery anatomy of the upper extremity

14.3.1.2 Venous Anatomy of the Upper Extremity

Main veins of the upper limb consist of a complex network of superficial and deep veins that are interconnected. In fact, upper extremity's veins drain blood both superficially and deeply; the cephalic vein and the basilic vein are two of the main superficial veins in the upper extremity, together with the dorsal-venous network.

As shown in Fig. 14.3, the main deep veins of the upper limb consist of the axillary vein, the anterior interosseous vein, the posterior interosseous vein, the radial vein, the ulnar vein, the anterior interosseous vein, and the posterior interosseous vein. The venous blood from the upper limbs travels up the axillary vein to the subclavian vein, from there to the brachiocephalic vein, and eventually back to the heart via the superior vena cava.

14.3.2 Sonoanatomy

The interest of the Doppler is to search for an occlusion with its location and extent, to search for an aneurysm or dissection.

Examination Protocol and Technique:

A 7.5 MHz transducer is used to evaluate the subclavian, axillary, and brachial veins. The examiner scans these veins while standing above the patient's head. In other terms, the physician will position himself so that he is looking down on the patient's head. Only the axillary and brachial veins are collapsible in the compression test; the subclavian vein is not collapsible.

The transducer is first used to determine the axillary vein's compressibility in a transverse configuration. Next, we get a Doppler waveform in the axial plane to rule out the possibility of a thrombosis or compression as causes of a blocked

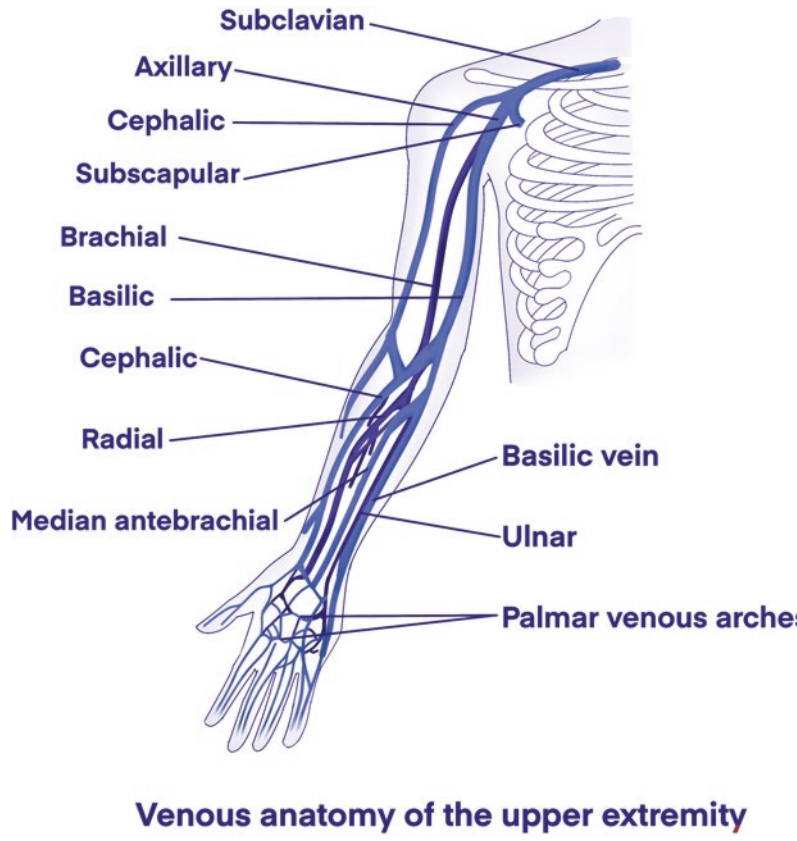

Fig. 14.3 Venous anatomy of the upper extremity

central outflow. The vein is followed as far as possible, and its compressibility is checked by pushing medially on the vein as it passes through the upper arm and into the humerus.

Materials

To carry out this exploration, we must have: Doppler ultrasound device fitted with a 6–8 MHz linear probe (Fig. 14.4), and if possible, a high-frequency probe (10–15 MHz) for the examination of the digital arteries.

Methods

Signal collection during the static study, in the supine position with an inclination of the torso of approximately 60° in relation to the plane of the bed. The arm is positioned along from the body. Dynamic maneuvers for exploring the thoracobrachial crossing are performed in a seated or standing position [3]. As during any Doppler ultrasound exploration, care must be taken to keep an angle of inclination of the probe relative to the axis of the vessel under study less than 60°.

The path of the vessels is examined in its entirety. Exploration is bilateral and comparative. It is completed by measuring the humeral pressure in both arms. In case of suspicion of digital arteriopathy (evocative clinical or positive Allen test), the examination is systematically completed by a digital pressure measurement.

Static Study

The subclavian artery (Figs. 14.5 and 14.6):

Fig. 14.4 An example of a 6–8 MHz linear probe

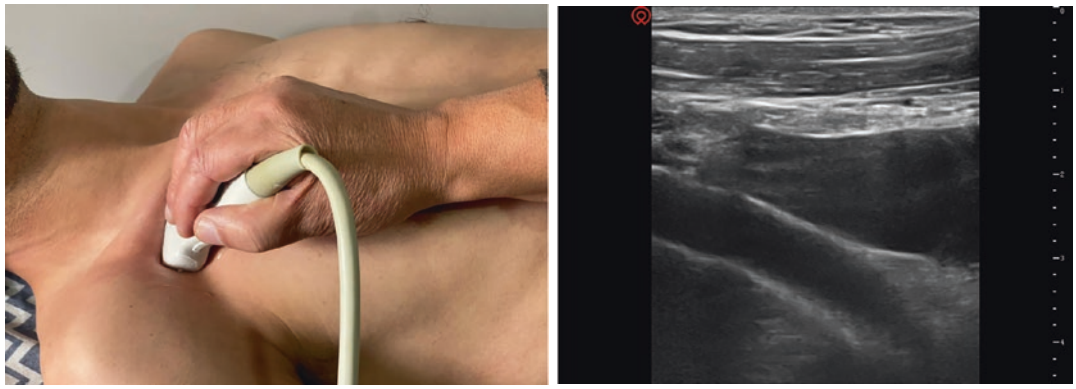

Fig. 14.5 Scan of the subclavian artery in supraclavicular fossa

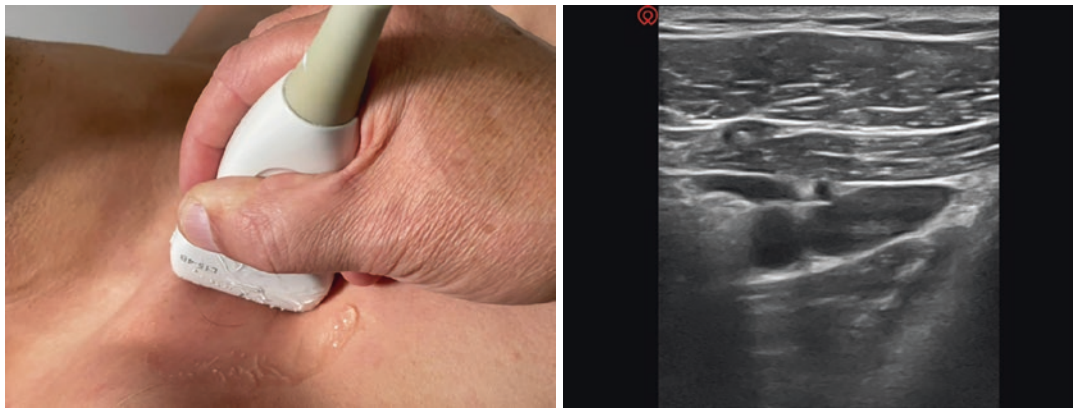

Fig. 14.6 Scan of the subclavian artery in infraclavicular region

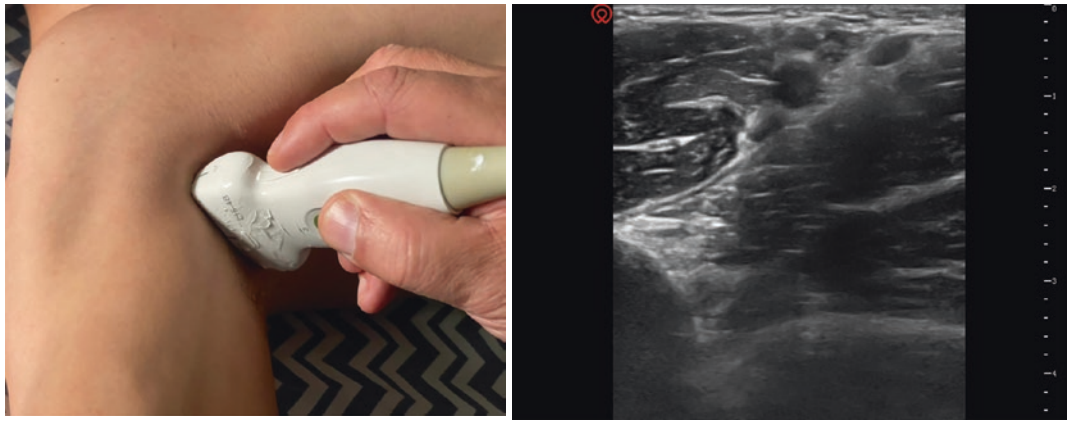

Fig. 14.7 Ultrasound exam of the axillary artery is sought in the axillary sulcus using transversal view

This artery is identified either in the supraclavicular fossa or in the subclavian in its distal segment.

The axillary artery: It is sought in the axillary sulcus or in the hollow axillary. Figure 14.7 shows the transversal position of the probe in scanning the axillary artery with corresponding sonoanatomy. On the other side, Fig. 14.8 illustrates longitudinal position of the probe and corresponding ultrasound image.

The brachial artery (Figs. 14.9 and 14.10): It can be recorded along its entire course in sections longitudinal and transverse in the event of anatomical variations (10–15% of normal population) to the antero-internal part of the arm.

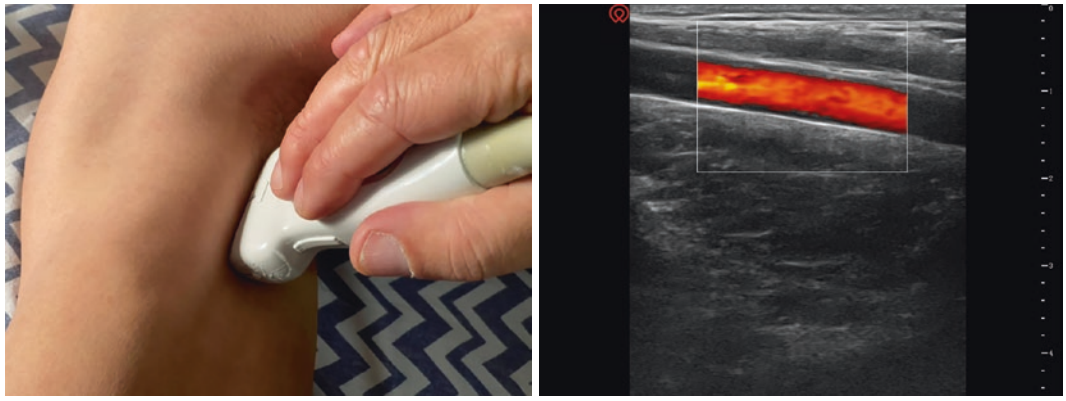

Fig. 14.8 Axillary artery is also sought in the hollow axillary using longitudinal position

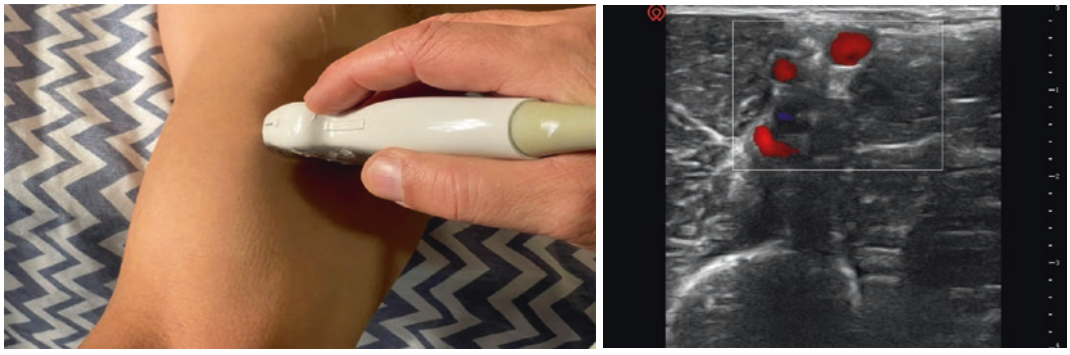

Fig. 14.9 Brachial artery using transversal view

The radial artery: It scans radial artery from the brachial bifurcation at the elbow until its end. Figure 14.11 shows how to place transducer and the ultrasound findings.

The ulnar artery: It is followed from the brachial bifurcation until its ends at the hypothenar eminence. Figure 14.12 illustrates the scanning and the sonoanatomy.

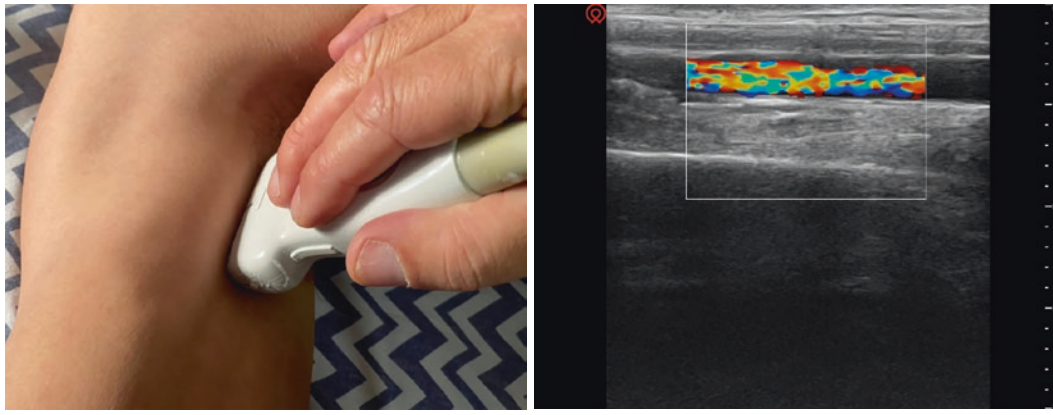

Fig. 14.10 Brachial artery using longitudinal view

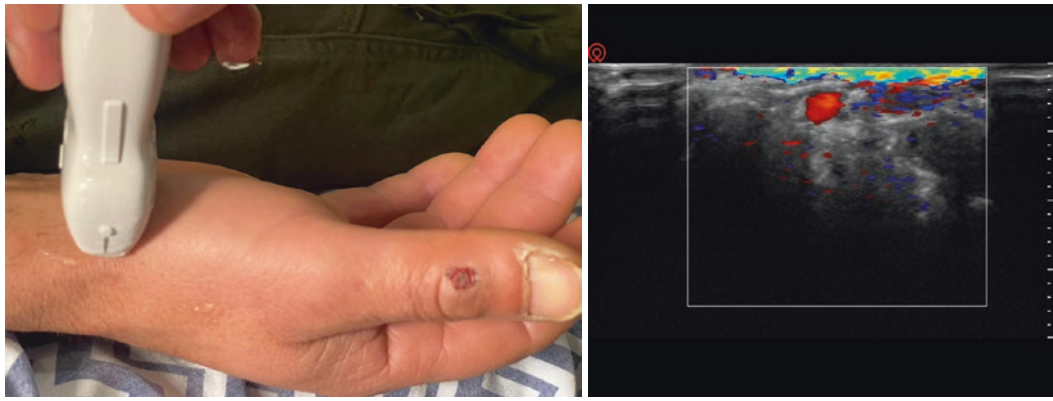

Fig. 14.11 Scanning the radial artery with linear probe and the corresponding ultrasound view

The deep interosseous artery: It is followed at the level of the anterior surface of the forearm along its midline more medially to the radial artery and lateral to the ulnar artery.

The carpal and metacarpal arteries: These are examined from the termination of the radial artery and the ulnar artery opposite the metacarpals, they are subject to many anatomical variations.

The digital network: The arteries are examined in the interdigital spaces then followed on the lateral faces of the fingers.

The pulp network: The probe is positioned at the level of the pulp.

Dynamic Study

Study of the Palmar Arches

The dynamic tests make it possible to specify the implication of the various pedicles in the pal-

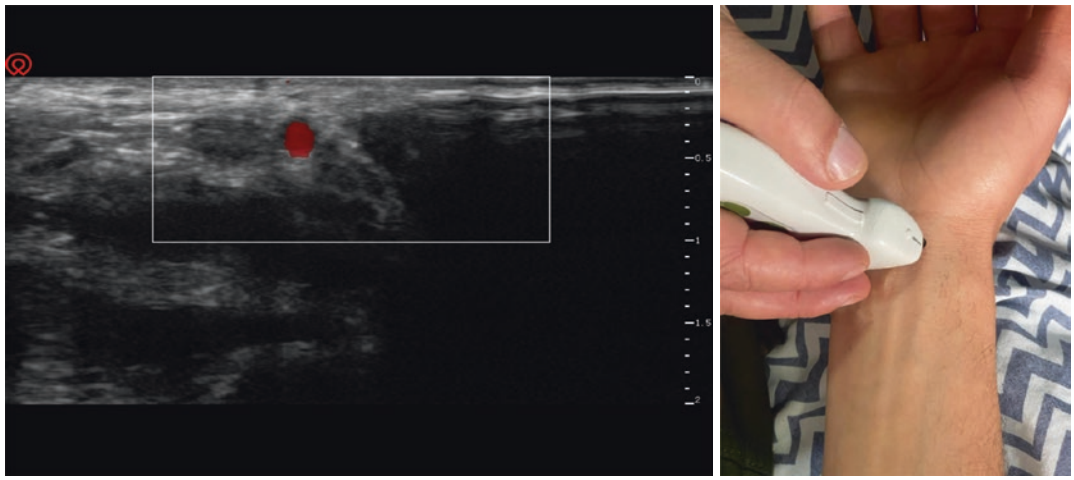

Fig. 14.12 Scan of the ulnar artery

mar and digital vasculature. First, the probe is positioned in view of the deep palmar arch region then the radial and the ulnar region.

The physician exerts a compression at the level of the ulnar artery.

Study of the thoracobrachial crossing syndrome is clinical and based on the chandelier sign.

The interest of the echo-Doppler is to look for a stenosis, a plaque ulcer, a thrombus, or an aneurysm, these lesions being perfectly detected by anatomical position.

14.3.3 Pathology

Upper Extremity Arterial Disease [4]

The Doppler is indicated if there is a suspicion of:

- Ischemia and diminished pulses in the arms and shoulders
- Systolic blood pressure measurements that differ between the two arms
- Possible arterial embolism in the upper limbs
- Assessment of arterial injury
- Subclavian "steal" syndrome or thoracic outlet syndrome

It is possible to highlight plaques of atheroma essentially at the subclavian level. The occlusion of the arteries of an upper limb is often of an embolic nature, we then visualize an intraluminal thrombus with an absence of flow in pulsed Doppler and color Doppler. Particular mention should be made of the possibility of concentric hypoechoic stenosis in the subclavian and axillary arteries in inflammatory arteriopathy, mainly Takayasu's disease and Horton's disease. In the case of Leo Burgers' disease, there may be a very distal involvement of the arches and digital arteries without initial involvement of the radial and ulnar arteries.

Upper Extremity Venous Disease

Signs of Deep Vein Thrombosis

The installation of a line or a pacemaker/implantable cardioverter defibrillator (ICD) might cause venous thrombosis due to the trauma that the patient experiences. Sometimes its thrombophilia. Figure 14.13 shows an example of subclavian thrombosis.

Non-compressibility

Normally, veins are readily collapsible with little force from the transducer because they are dilated when the pressure in the body is low. The vein is either not compressible at all or just somewhat compressible when venous thrombosis is present.

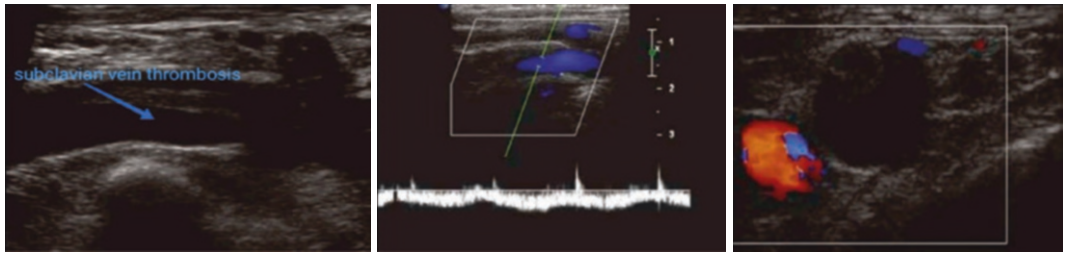

Fig. 14.13 Subclavian thrombosis

Flow Obstruction

The rate at which blood flows through the veins normally varies naturally with the breathing cycle. If you squeeze a muscle bed far enough away, blood will rush into the vein.

14.4 Neck Vessels

Introduction

The carotid and vertebral arteries deliver the bulk of blood to the head and neck. The anatomical course, branching and distribution of the carotid arteries are points of interest in this chapter. Figure 14.14 illustrates the different neck arteries.

– Carotid artery

Anatomy: The carotid arteries are the main blood vessels that provide oxygen and nutrients to the brain; the right carotid artery (RCCA) begins at the level of the brachiocephalic artery in the neck, and the left carotid artery (LCCA) begins at the level of the aortic arch in the chest.

Sonoanatomy

– Scanning with linear probe from bottom to top allows visualization of the common carotid artery at the bottom and the bifurcation at the top as shown in Fig. 14.15.
– The normal color Doppler of the common carotid artery with longitudinal position of the probe and in transverse position of the probe (Fig. 14.16).
– An example of carotid PW is shown in Fig. 14.17.

Pathology

Problems that can affect the carotid arteries include:

- Carotid artery disease: the most occurrent is the atherosclerosis.
- Carotid artery aneurysm.
- Carotid artery dissection.
- Fibromuscular dysplasia.

Carotid Atherosclerotic Plaque

It is a buildup of plaque on the arterial walls, and it often occurs in the area where the carotid arteries branch out (Figs. 14.18 and 14.19).

The occurrence of a TIA or a stroke is increased by arterial plaque buildup. That is because clots may develop on the plaque and then break off, making their way to a brain artery where they can completely block the flow of blood.

Jugular vein [5]

Anatomy

The human has two of jugular veins, external and internal. The internal jugular veins join with the subclavian veins more medially to form the brachiocephalic veins (Fig. 14.20).

Sonoanatomy

– Scan the internal jugular vein and evaluate the compressibility of the vein (Fig. 14.21).

Pathology

Pathologies of the jugular veins are not frequent; thus, the risk of thrombosis is very infrequent and external compressions are also very exceptional but that exist, and trauma, line placement, pacemaker/implantable cardioverter

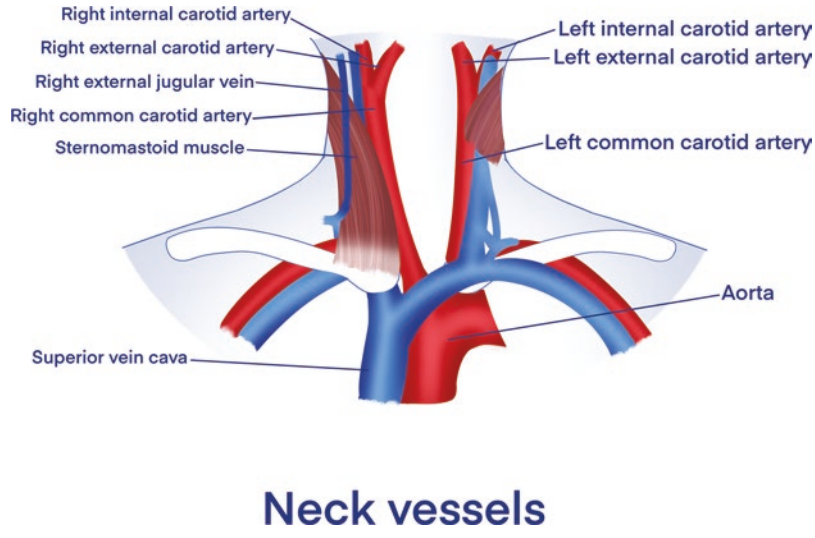

Fig. 14.14 Neck arteries

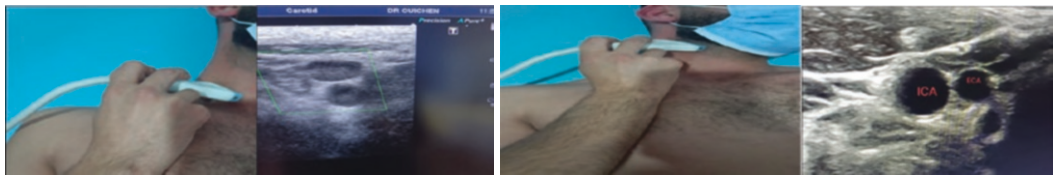

Fig. 14.15 Scanning from bottom to top allows visualization of the common carotid artery at the bottom (image on the left) and the bifurcation at the top (image on the right)

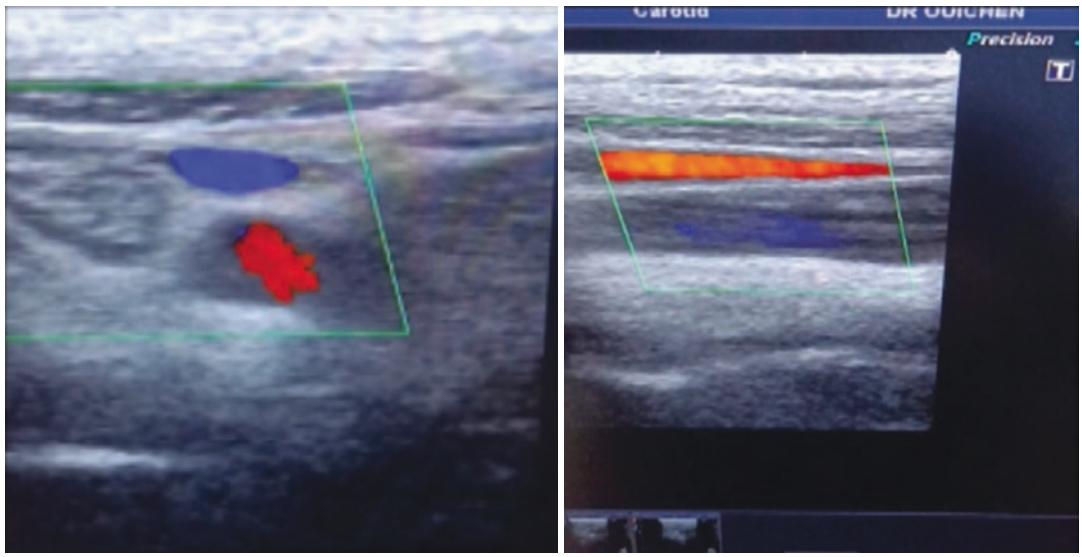

Fig. 14.16 Normal color Doppler of the common carotid artery. Longitudinal position of the probe (Image on the right). Transverse position of the probe (Image on the left)

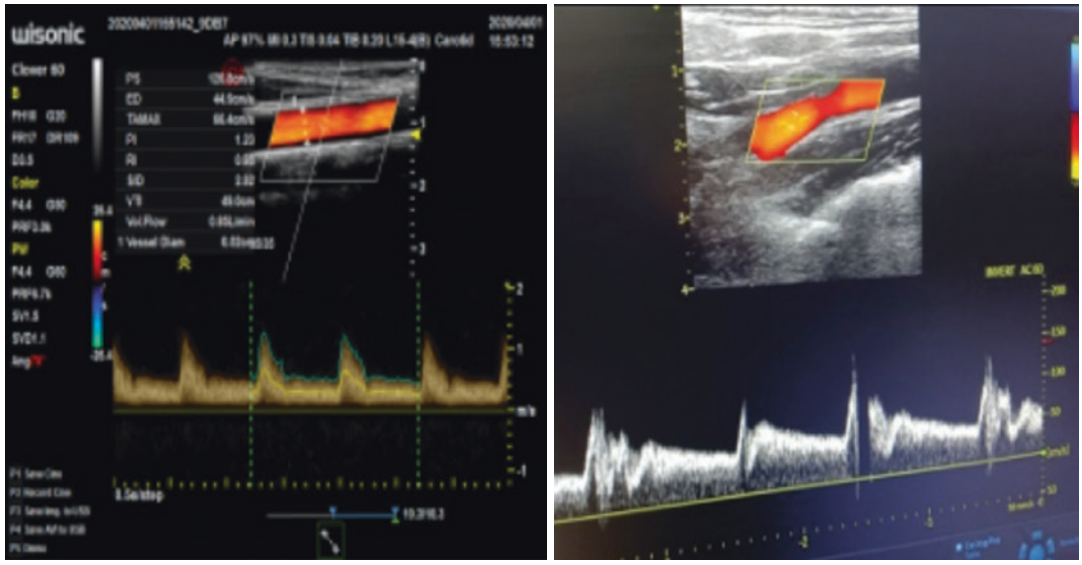

Fig. 14.17 Carotid PW

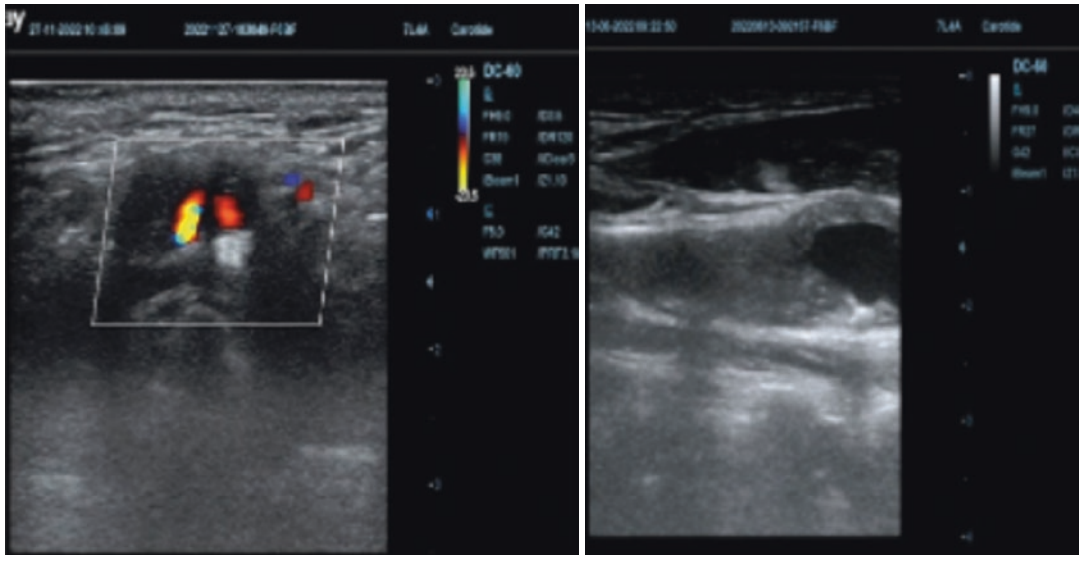

Fig. 14.18 Pre-occlusive stenosis of the internal carotid artery on the left. Total occlusion of the internal carotid artery with no flow on the right

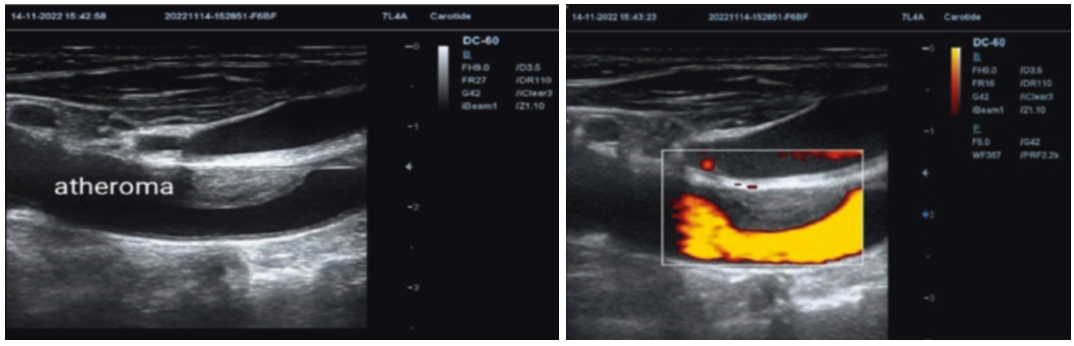

Fig. 14.19 Carotid atherosclerotic plaque. In the right carotid, atherosclerotic plaque view in Doppler color

Fig. 14.20 Neck veins

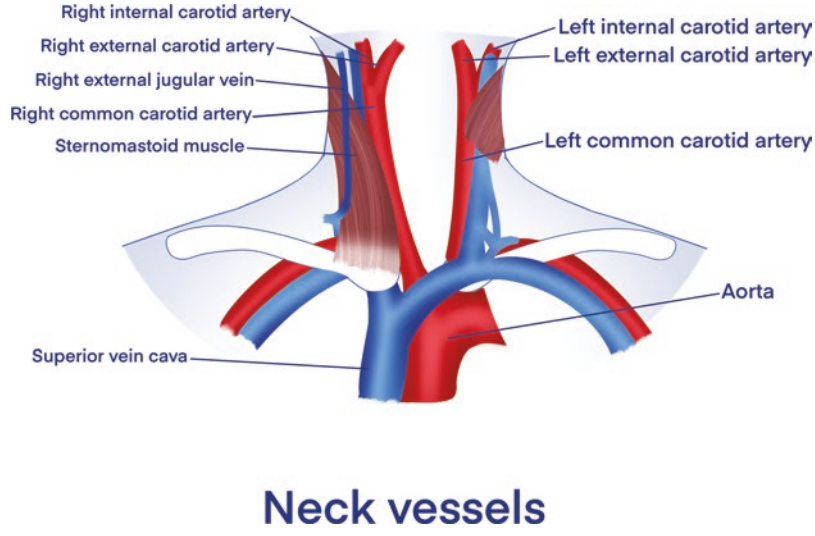

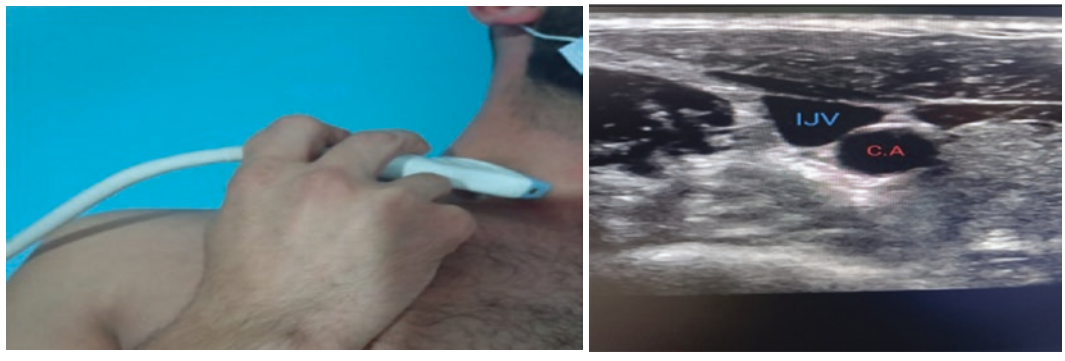

Fig. 14.21 Scanning the internal jugular vein and evaluation of the compressibility of the vein

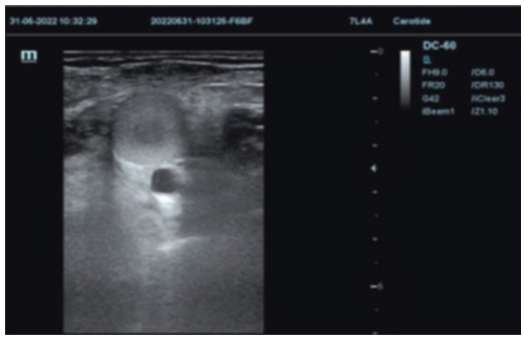

Fig. 14.22 Jugular thrombosis post cannulation with hemodialysis catheter

defibrillator (ICD) implantation, pericardial constriction, and thrombophilia are all potential causes. Figure 14.22 illustrates a jugular thrombosis post cannulation with hemodialysis catheter.

14.5 Assessment of Lower Limb Vessels

14.5.1 Assessment of Lower Limb Artery

Introduction

The study of the arteries of the lower limbs has benefited for several years from the use of ultrasound, because of their noninvasive, reliable, and moderate cost [6].

The pathologies that affect the arteries of the lower limbs are varied, largely dominated by obliterative arteriopathy of the lower limbs due to atheroma.

Anatomy

Figure 14.23 provides an overview of the anatomy of lower limb arteries.

Arteries Scanned for Reporting

CIA—Common iliac artery: Stretches from the sacrum to the SI joint. Length is around 4–5 cm. The two parts are the IIA and the EIA. Its corresponding common iliac vein (CIV) can be found to its left.

IIA—Internal iliac artery: Divides in half, front and back. Branches from the anterior division go to the bladder, rectum, and buttocks, as well as the reproductive organs. The pelvic muscles get their branches from the posterior division.

EIA—External iliac artery: Rests close to the skin's surface near the relevant vein. Creates a blood vessel in the lower epigastrium. The inguinal ligament is where the CFA officially begins.

CFA—Common femoral artery: It is just below the inguinal ligament, on the surface of the femoral triangle. It extends for 3–5 cm beyond the inguinal ligament and divides to form the SFA and PFA.

PFA—Profunda femoris artery: It provides perforating arteries to the thigh muscles.

SFA—Superficial femoral artery: It is located in the middle of the thigh and somewhat lengthy.

It penetrates the adductor magnus deep notch and follows the popliteal artery.

Popliteal artery: It starts when the adductor hiatus has healed. A vertical cut across the popliteal fossa. Separates into the TPT and ATA. The anterior tibial artery (ATA) and the tibioperoneal trunk (TPT).

ATA—Anterior tibial artery: It supplies the front compartment of the leg and continues down to the foot as the dorsalis pedis artery after passing anterior to the tibia.

TPT—Tibioperoneal trunk: PTA and peroneal artery are formed at this point.

PTA—Posterior tibial artery: It supplies the back of the calf and the foot as the plantar arteries, which run posterior to the tibia.

Peroneal artery: It supplies the deep compartment through a medial route to the fibula.

Material and Methods

- High-resolution B-mode imaging, color (and energy) Doppler, and pulsed Doppler spectrum analysis are all used in duplex or triplex systems.
- Probes operating at multiple frequencies and depths are required.
- Low-frequency probes (2–3 MHz) are used to study the aorta and iliac axes (Fig. 14.24).
- Higher frequency probes (5–8 MHz) are used to study the infra-inguinal axes (Fig. 14.24).
- A pneumatic cuff should be available to measure the systolic pressure index.

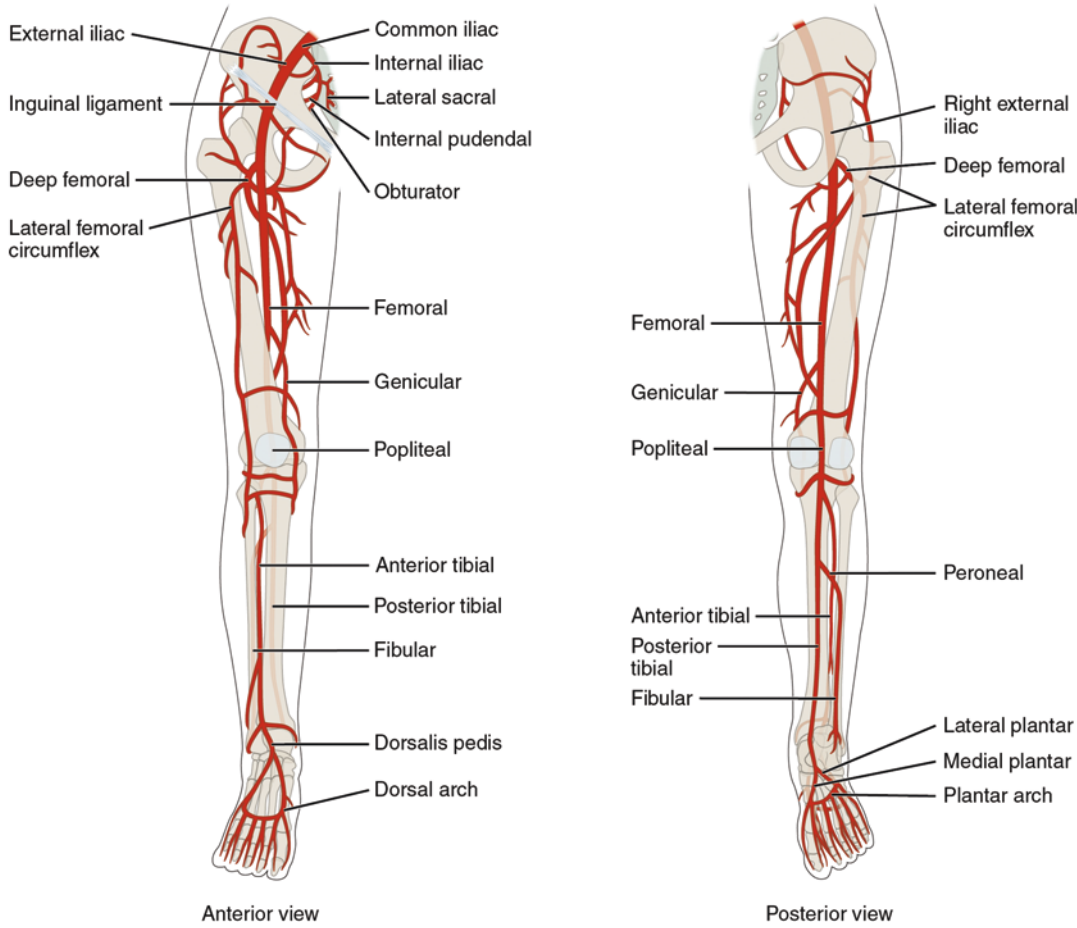

Fig. 14.23 Anatomy of lower limb artery (OpenStax College, Creative Commons Licenses CC BY 3.0)

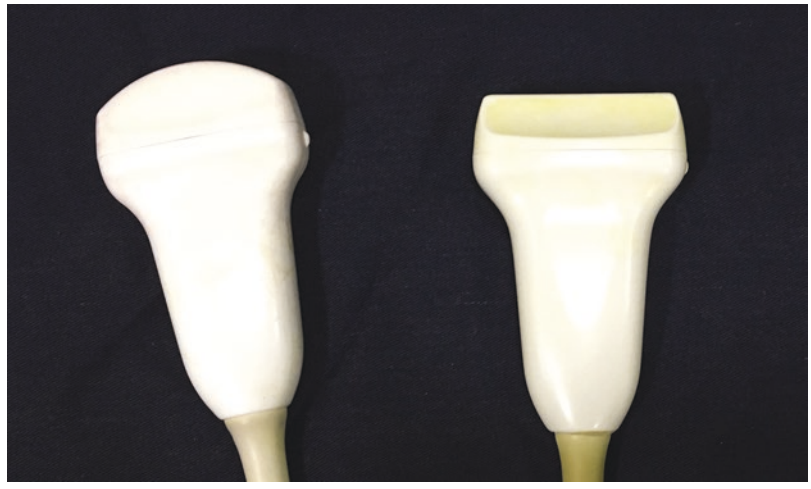

Fig. 14.24 Low-frequency probes (2–3 MHz) are used to study the aorta and iliac axes. Higher frequency probes (5–8 MHz) are used to study the infra-inguinal axes

The examination starts with the patient at rest, in dorsal recumbency, with legs extended. In the vast majority of cases, the examination is complete, from the origin of the abdominal aorta to the ankle or foot. The iliofemoral axes are studied in the supine position.

The distal part of the superficial femoral artery, the popliteal artery, and the leg axes are studied in semiflexed legs and in external rotation. The popliteal artery is usually approached posteriorly with the knee semiflexed. A prone or lateral decubitus study sometimes allows a more precise analysis of the popliteal artery and leg arteries.

Take pictures of the following structures in order: the aorta, the common iliac arteries, the external iliac arteries, the common femoral arteries, and the femoral bifurcation. Arteries of the upper portion of the profunda femoris. Proximal, intermediate, and distal superficial femoral arteries. Arteries in the thigh (popliteal) and the foot (dorsalis pedis). Ankle level posterior tibial arteries. The arterial axes are identified in axial sections and then studied in longitudinal sections. Ideally, the B-mode examination is performed with a probe perpendicular to the vessel. In Doppler, on the other hand, the examiner must angulate the probe to obtain the most tangential Doppler shot possible, in practice with an insonation angle of less than 60° or better than 45°.

Spectral Analysis at Rest

High resistance arteries are characterized by a triphasic appearance in the spectra observed in the arteries of the lower extremities as shown in Fig. 14.25.

- Rapid systolic rise with an ample and brief systolic peak.
- Rapid post-systolic deceleration.
- Clear spectral envelope allowing the identification of a sub-systolic dark window.
- Negative protodiastolic wave showing a transient reverse flow, reflecting peripheral resistance.
- Positive rebound wave, inconstant, reflecting a satisfactory arterial compliance.

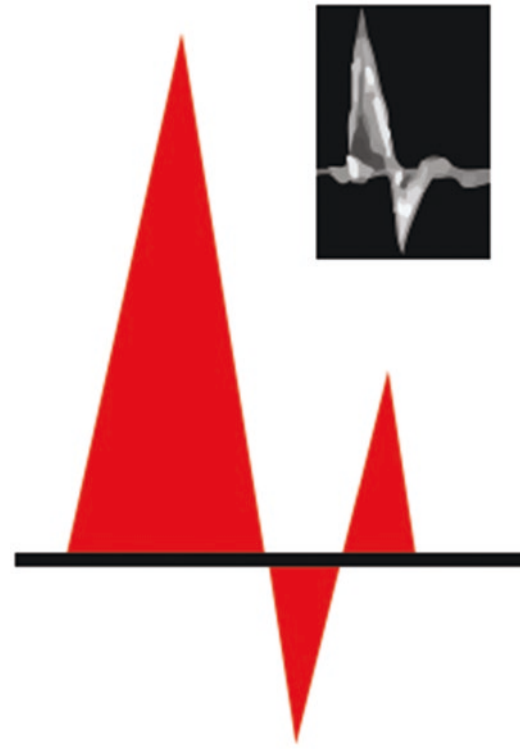

Fig. 14.25 The spectra recorded in the arteries of the lower limbs

- A meso- and telediastolic interruption of the flow.
- The flow is laminar, with most of the figured elements of the blood having similar velocities. This is reflected by a sharp spectrum envelope containing a narrow band of velocities and by the presence of a dark subsystolic window.

Sonoanatomy

Femoral artery (Fig. 14.26)
Popliteal artery (Fig. 14.27)
Anterior tibial artery (Fig. 14.28)
Posterior tibial artery (Fig. 14.29)

Pathology

Specific Study of Obliterating Lesions

The study of obliterating lesions is often long and complex because there is a relatively large potential for collateral circulation around stenoses or thromboses in the lower limbs.

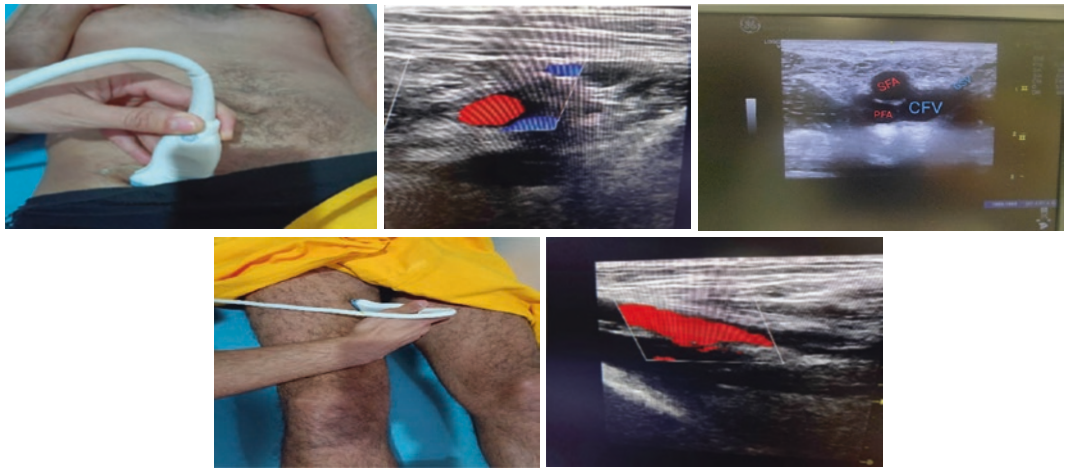

Fig. 14.26 Femoral artery

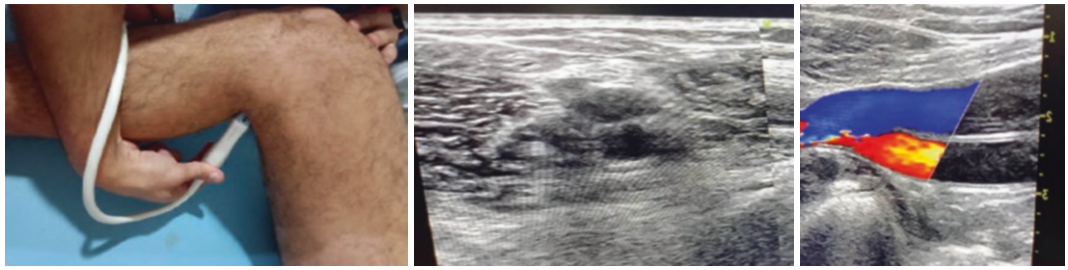

Fig. 14.27 Popliteal artery

The analysis should include:

1. Morphological Study of the Stenosis

- B-mode and color Doppler analysis.
- Specify the character of the lesions (single, multiple, length, severity, homogeneous or heterogeneous character, parietal thickening).
- Search for thrombosis.
- Spectral evaluation of the site of the stenosis as well as upstream and downstream because the existence and degree of upstream and downstream signs are important determinants in the assessment of the percentage of stenosis at the hemodynamic level. Figure 14.30 illustrates various clinical situations according to the percentage of stenosis: *No stenosis or stenosis <30%. *30–70% stenosis. *70–90% stenosis. *Stenosis >90%. *Total occlusion without collateral circulation effective. *Total occlusion with collateral circulation providing poor downstream reinjection.
- The spectral analysis must specify the maximum systolic velocity as well as the existence of turbulence and filling of the subsystolic dark window.

Fig. 14.28 Anterior tibial artery

Fig. 14.29 Posterior tibial artery

- In some ambiguous cases, it can be completed by dynamic maneuvers (stress test, compression test).
- Measurement of the systolic pressure index: the decrease of the systolic pressure index is correlated to the severity of the arterial ischemia.

*As shown in Fig. 14.31, an example of occlusion responsible for downstream repercussion.

*As illustrated in Fig. 14.32. 1/Very infiltrated popliteal artery; 2/Damped flow of an anterior tibial artery; 3/Flow or power flow to detect very weak flows; 4/Femoral stenosis.

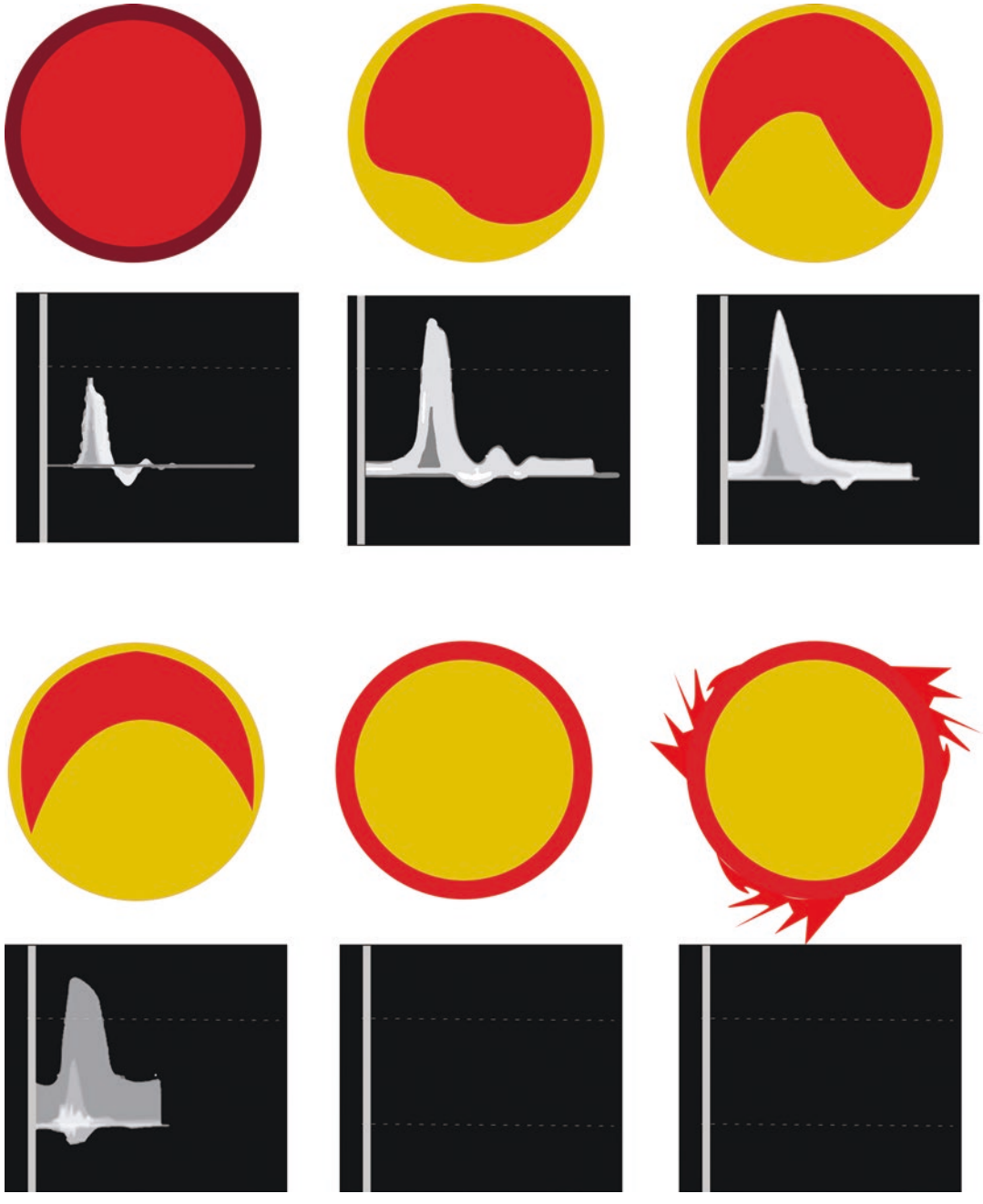

Fig. 14.30 Illustration of various clinical situations according to the percentage of stenosis: *No stenosis or stenosis <30%. *30–70% stenosis. *70–90% stenosis. *Stenosis >90%. *Total occlusion without collateral circulation effective. *Total occlusion with collateral circulation

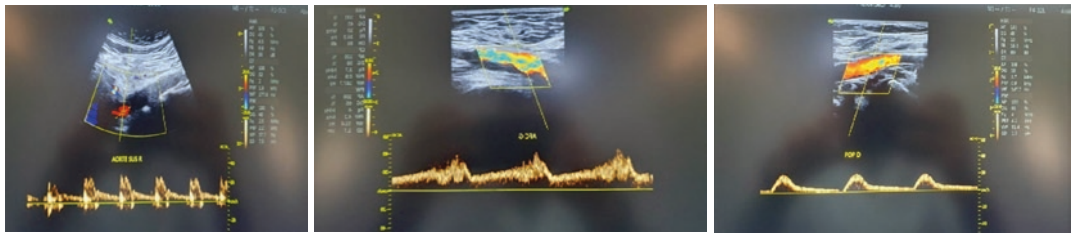

Fig. 14.31 Occlusion with downstream repercussion

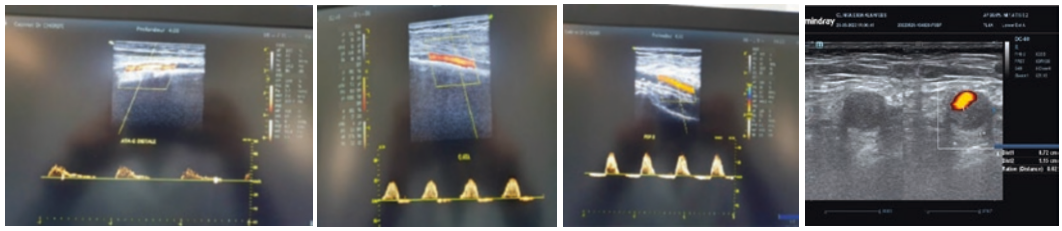

Fig. 14.32 1/Very infiltrated popliteal artery; 2/Damped flow of an anterior tibial artery; 3/Flow or power flow to detect very weak flows; 4/Femoral stenosis

14.5.2 Assessment of Lower Limb Venous

Introduction

It is crucial to understand the normal and abnormal architecture of the venous vasculature of the lower extremities.

Ultrasound is the most frequently used examination to search for deep or superficial venous thrombosis, to specify its location, and to evaluate its extent. The need of a complete and consistent duplex examination process.

Anatomy

There are three parts to the venous system in the lower limb:

1. Veins near the surface with a thick wall
2. Deep veins with thin walls
3. Veins that rupture

About 85% of venous return is handled by the deep venous system, while the superficial venous system handles the remaining 15%. Anatomy of lower extremity veins is illustrated in Fig. 14.33.

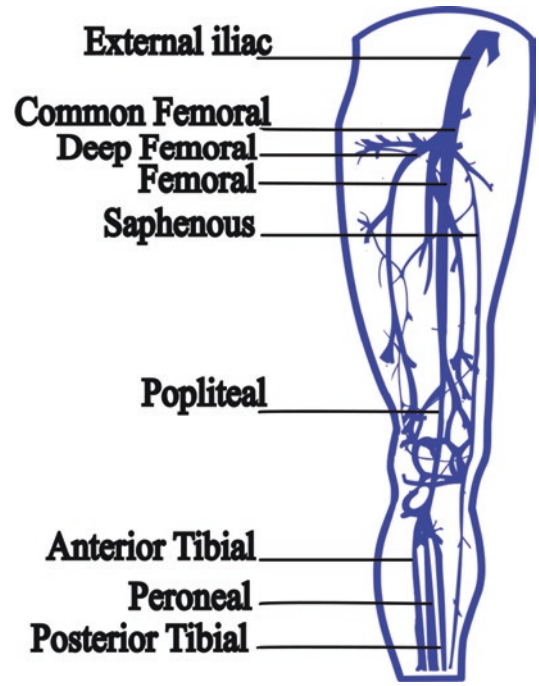

Fig. 14.33 Anatomy of lower extremity veins

- ***The Superficial Venous System***

Greater or Long Saphenous Vein

The saphenofemoral junction marks the point at which this vein merges into the common femoral vein in the groin.

Lesser or Short Saphenous Vein

As its name implies, the smaller saphenous vein is much shorter than the more common saphenous vein. Both the popliteal and the distal superficial femoral veins, as well as the gastrocnemius vein, are possible destinations for its drainage into the deep system.

- ***The Deep Venous System***

Veins on the outside of the body (you may need a different transducer if they're too high in frequency).

- Veina comn da fémura.
- The origin of the profunda femoris vein.
- The superficial femoral vein or femoral vein.
- Vena poplitea.
- Vein located behind the tibia.
- Veins in the peroneal and anterior tibia (only scanned when there is local discomfort; these veins are generally incompressible due to surrounding bones).

– **Characteristics of Normal Veins**

The ultrasonic characteristics of normal veins are as follows:

- Veins are compressible under probe pressure completely and easily.
- A venous wall is thinner than the artery.
- A venous diameter is greater than that of the homologous artery.
- A venous lumen with a clear contour.
- An anechoic venous lumen.
- Venous caliber increases with manual upstream compression that causes complete color filling of the venous lumen.
- Venous flow has respiratory pulsatility and is no longer recorded at the thigh veins during the Valsalva maneuver. As shown in Fig. 14.34, the anterograde flow decreases with inspiration. The reason for this is due to higher intra-abdominal pressure.
- The diameter of the VFC increases by approximately 15–20% during the Valsalva maneuver.

Materials and Methods

For the study of veins below the inguinal ring, use a medium to high frequency linear probe.

Use a Curved Probe with a Lower Frequency for the Examination of the Iliac Veins and the IVC Scanning

The patient is in a supine posture with his or her upper body elevated by about 45° (a reverse Trendelenburg position) to dilate the veins. The inspected leg is bent at the knee and externally rotated. From the inguinal ligament, a diagonal line is taken up the leg toward the umbilicus to scan the external iliac vein.

If thrombus is seen in the external iliac vein, grayscale imaging, color Doppler, and spectral Doppler are used to examine the common iliac vein and the IVC. Grayscale imaging is used to scan the common femoral vein in the groin all the way to where it splits off into two smaller veins.

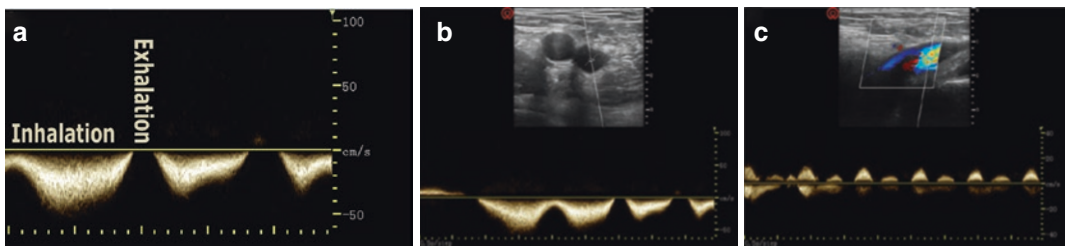

Fig. 14.34 A lower extremity–normal respirophasic: antegrade flow decreases with inspiration due to higher intra-abdominal pressure and increases with expiration due to decreased intra-abdominal pressure. (**b**) Normal respirophasic; (**c**) loss of respiratory modulation

Fig. 14.35 The Mickey Mouse sign representing schematically the normal sonoanatomy of the deep Venous System at the inguinal level. Common Femoral Artery, Great Saphenous Vein, and Common Femoral Vein drawing Mickey Mouse head on ultrasound

Every 1–2 cm, the transducer is used to provide pressure (enough to cause full vein collapse). The common femoral vein splits into the superficial femoral vein and the deep femoral vein. (When required, color Doppler flow-mapping may be utilized to pinpoint blood supply routes.)

It is common practice to scan the superficial femoral vein, also called the femoral vein, along the medial aspect of the thigh, usually located 1–2 cm distal to the femoral arterial bifurcation (it may be necessary and desirable to apply pressure with the free hand to the lateral thigh at the site of compression). From a posterior approach in the popliteal fossa, the popliteal vein is scanned all the way to the level of the tibioperoneal trunk.

Sonoanatomy

The following Fig. 14.35 describes the Mickey Mouse sign representing schematically the normal sonoanatomy of the deep Venous System at the inguinal level. Common Femoral Artery, Great Saphenous Vein, and Common Femoral Vein drawing Mickey Mouse head on ultrasound.

Pathology

– Diagnostic Criteria for Thrombosis

Direct Signs of Venous Thrombosis

Venous incompressibility: Thrombus prevents the venous walls from collapsing during compression. With incompletely occlusive thrombus, the vein may be partially compressed, whereas a completely occlusive thrombus results in incompressibility.

Endoluminal thrombus: A recent thrombus is hypoechoic, whereas an old thrombus appears increasingly echogenic over time. This appearance depends on image quality and device settings.

Absence of venous flow: No flow is demonstrated when the thrombosis is occlusive. When the thrombosis is only central and not occlusive, peripheral flow may be seen. This is an important sign for the diagnosis of iliac DVT, which is often inaccessible to the compressibility test.

Venous diameter: Venous diameter increases in the acute phase of thrombus and then gradually decreases to less than normal venous diameter in the chronic phase.

Venous wall thickening: The thickness of the venous wall gradually increases over time.

Indirect Signs of Thrombosis

- Loss of respiratory flow modulation, damping, or poor response to the Valsalva maneuver at the level of the VFC suggests venous obstruction proximal to the probe.
- Lack of change in venous caliber of the VFC during the Valsalva maneuver suggests an occlusive proximal thrombosis.
- A small increase in venous flow after muscle compression at the calf level suggests an occlusive thrombosis located between the area of examination and the area of increased flow.
- Presence of deep collaterals.

These two figures below illustrate examples of thrombosis. Figure 14.36 *clearly shows, respectively, thrombosis of femoral vein and thrombosis of popliteal vein.* Figure 14.37 *provides an overview of a GSV continent in the left and incontinent in the two other images.*

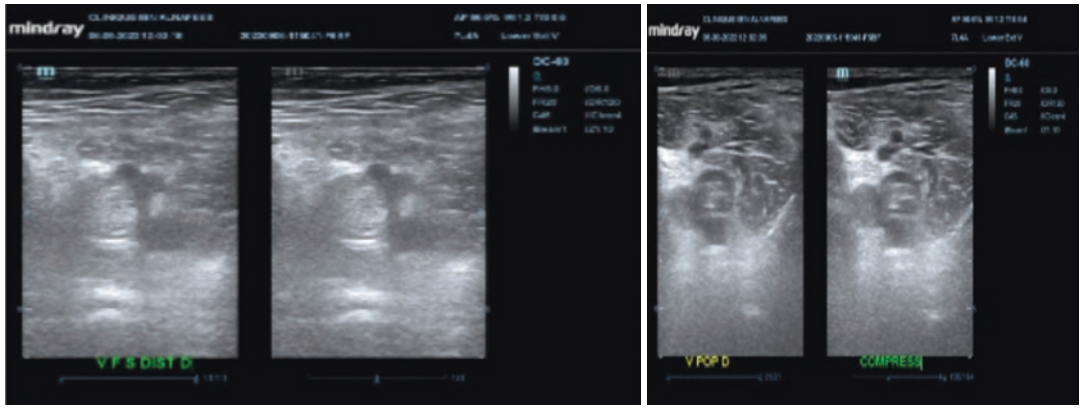

Fig. 14.36 Thrombosis of femoral vein and thrombosis of popliteal vein

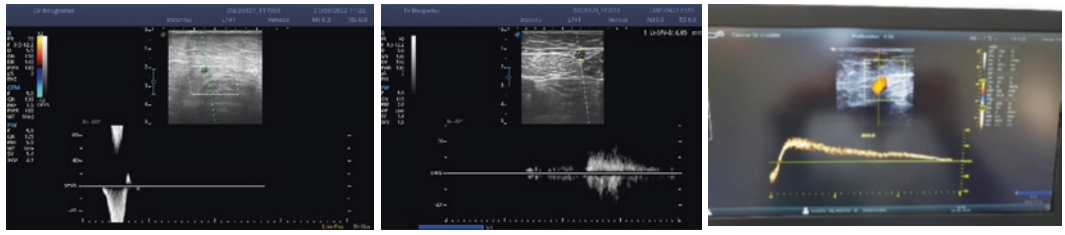

Fig. 14.37 Illustrates an overview of a GSV continent in the left and incontinent in the two other images

14.6 Abdominal Aorta

Introduction

The abdominal aorta is a major vessel that distributes blood to the abdominal organs and lower limbs. Aortic pathology is frequent and is dominated by aneurysms in the infrarenal portion and stenoses in its distal portion, vasculitis and aortic dissections especially in its thoracic portion. Ultrasound Doppler often detects asymptomatic pathologies and is used in the monitoring of many conditions. When performing an echo-Doppler examination of the arteries in the legs, kidneys, and stomach, the abdominal aorta is an essential part of the process [7]. As such, it serves as a common test of readiness.

Anatomy

The abdominal aorta (see Fig. 14.38) is an elastic artery. It follows the thoracic aorta at the level of the diaphragmatic orifice, at the level of T12. It runs in front of the spine, to the left of the midline, close to the inferior vena cava located to the right of the midline. It divides at L4 into two arteries: iliac commons which are its terminal branches.

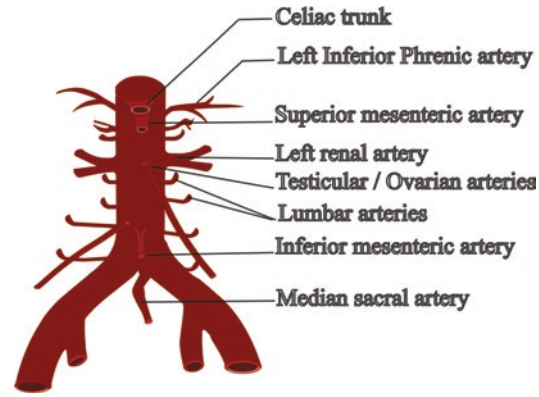

Fig. 14.38 Anatomy of the abdominal aorta

The height of the division is approximately at the level of the umbilicus. Its diameter gradually decreases from top to bottom, while it becomes more superficial as one approaches its termination. Its main collaterals visible in Doppler echo are the visceral arteries: Trunk celiac which arises from the anterior facing of T12, superior mesenteric artery opposite of L1, inferior mesenteric artery next to L3, renal arteries which arise laterally in gaze of L2. Branches with parietal destiny do not have sufficient caliber to be easily individualized in echo-Doppler.

Materials and Methods

Curvilinear probe 2–5 MHz (Fig. 14.39).

Scan the patient when they are resting supine. Patients who are bloated or experiencing gas problems should be positioned in the right lateral decubitus posture and seen via a coronal (flank) window.

Fig. 14.39 Curvilinear probe 2–5 MHz

B-mode: It determines the maximum anteroposterior diameter by first determining the maximum transverse diameter. It specifies the regularity of its walls, the state of its lumen, and the appearance of its main collateral branches and iliac arteries.

Color Doppler: It specifies the permeability of the aorta and looks for hemodynamic disturbances (acceleration, turbulence).

Pulsed Doppler for Spectral Analysis: The aorta has stronger walls, doesn't collapse, and beats with the heart. The aorta's triphasic appearance on pulse-wave Doppler during normal flow contrasts with the IVC's monophasic waveform, and its shape varies throughout different respiratory phases. It specifies the possible hemodynamic consequences and the velocimetric anomalies detected in color Doppler.

NB: The study of the aorta must be associated with that of the iliac axes. The study of the aortic, digestive, or renal collaterals is often associated with the study of the aorta without being systematic because it depends on the clinical indications. The diameter considered normal for the abdominal aorta is 20–25 mm with a commonly accepted tolerance of up to 30 mm.

Sonoanatomy

Normal sonoanatomy of abdominal aorta is shown in Fig. 14.40 **transverse view on the left and longitudinal view on the right.**

Pathology: Abdominal Aortic Aneurysm AAA

Figure 14.41 *illustrates types of Abdominal Aneurysm: Saccular, fusiform, dissection, and false aneurysm.*

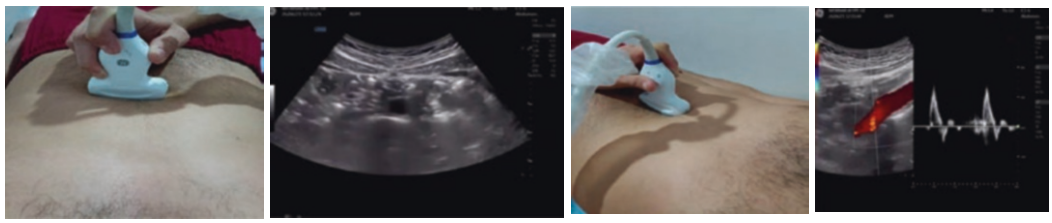

Fig. 14.40 Normal sonoanatomy of abdominal aorta transverse view on the left and longitudinal view on the right

Atherosclerosis is the common cause of abdominal aortic dilatation more than 30 mm. They can cause severe internal bleeding if they are larger than 5.5 cm in diameter.

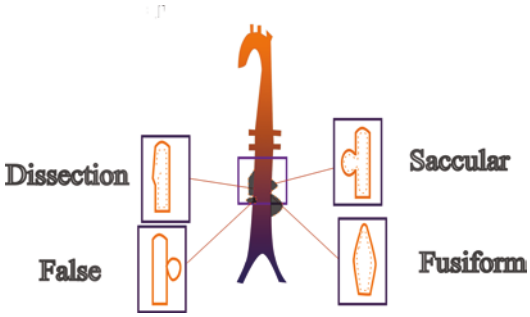

Fig. 14.41 Illustration of different types of abdominal aneurysm: saccular, fusiform, dissection, and false aneurysm

Diameter measurements should be made transverse to avoid underestimation. Because of the difference in size between systole and diastole, three measurements should be made and averaged. Compare the length of the most distal renal artery to the height of the collar to see where the AAA is located in respect to the renal arteries. Measurements taken on an aneurysm should include the total diameter including the thrombus and the lumen.

It is possible to use color Doppler in these circumstances, which will show the absence of flow at the level of thrombosis. The examination will be completed by a sagittal section in order to specify the extent of the aneurysm. Figure 14.42 illustrates a case of infrarenal abdominal aortic aneurysm.

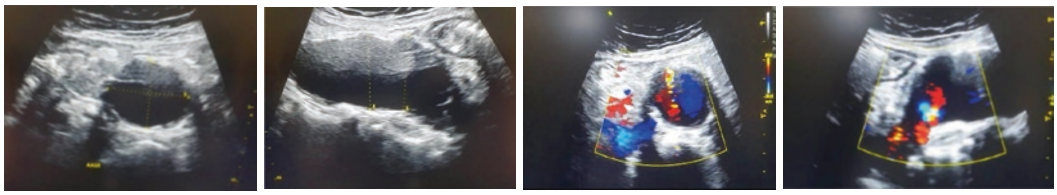

Fig. 14.42 Example of an infrarenal abdominal aortic aneurysm

14.7 Arteriovenous Fistula

Definition.

The arteriovenous fistula consists of connecting a superficial vein of the arm to an artery under the effect of arterial pressure, the vein expands and its wall thickens. After 4–6 weeks, the vein becomes strong enough to tolerate repeated punctures.

Different Types of AVF

Arteriovenous fistulas may take on a wide variety of shapes as illustrated in Fig. 14.43a–c. Most typically, radiocephalic, brachiocephalic, and brachiobasilic transpositions are performed on the upper limbs. Patients whose veins are too small to sustain the recommended radiocephalic or brachiocephalic fistulas have started turning more often to brachiobasilic transposition.

1. Radiocephalic fistula
2. Brachiocephalic fistula
3. Brachiocephalic transposition

Preoperative Arteriovenous Fistula Assessment

Duplex scanning is used to precisely assess the diameter of the cephalic and basilic veins in the forearm and upper arm prior to surgery (a vein diameter of more than 3 mm is ideal).

We have to scan the fistula in case any abnormal incident appears like:

High venous pressures during hemodialysis; having trouble cannulating; after receiving angioplasty or thrombolytic treatment; Symptoms to look out for include: pain, swelling, redness, and a palpable lump (from a hematoma, seroma, or lymphocele) around the access site.

Depending on the surgeon's desire, it is often done 4–6 weeks following surgery and subsequently at regular intervals to monitor the arteriovenous fistula.

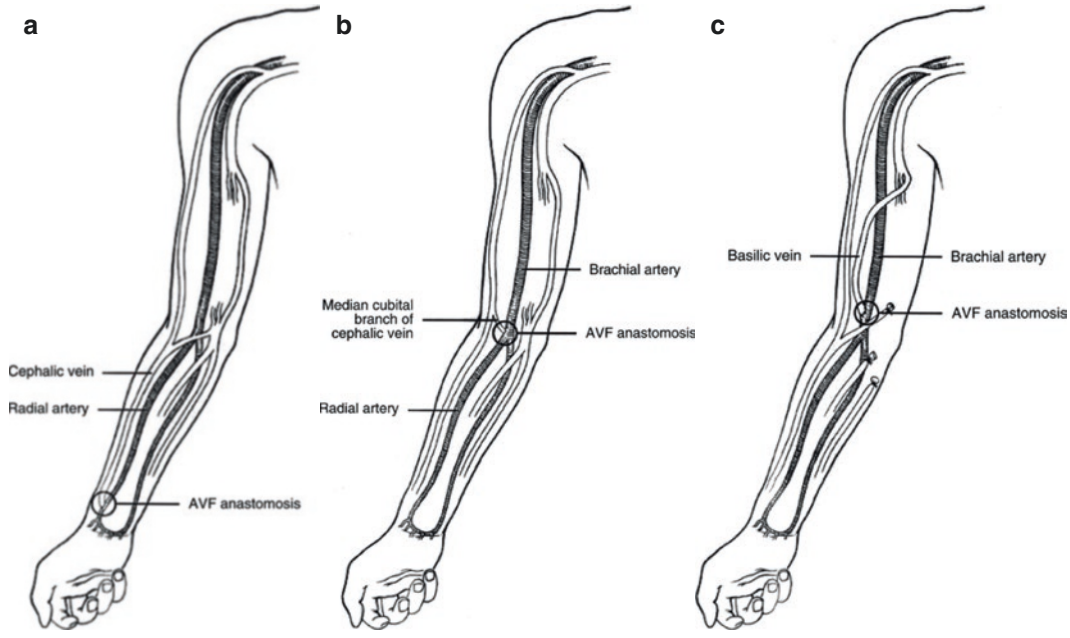

Fig. 14.43 Different types of arteriovenous fistulas. Increasing arteriovenous fistulas in hemodialysis patients: problems and solutions. (**a**) Radiocephalic fistula, (**b**) brachiocephalic fistula, (**c**) brachiocephalic transposition. (Michael Allon, Michelle L. Robbin 2002 License Elsevier)

14.8 Fistula Complication

True Aneurysm (Fig. 14.44)

An actual aneurysm is a localized ballooning out of the artery wall. Grayscale imaging reveals a pulsing mass..

False Aneurysm (Pseudoaneurysm) (Fig. 14.45)

Gray- and color-scale Doppler imaging may detect a pseudoaneurysm, which is characterized by a pulsing mass attached to an artery.

Thrombosis (Fig. 14.46)

It is the formation of the blood clot inside the arteriovenous graft.

Other Complications

Wall irregularities, infection, hematoma, and the most common complication associated with AVF was ischemic neuropathy.

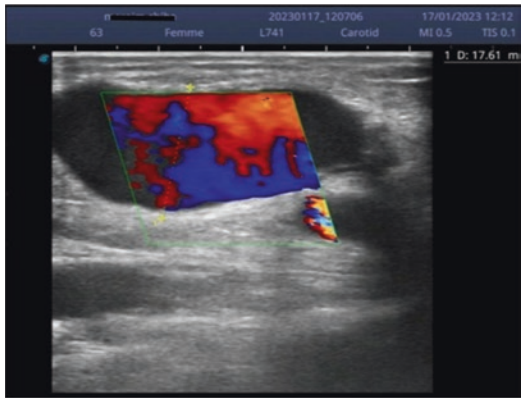

Fig. 14.44 Fistula true aneurysm

Fig. 14.45 Fistula false aneurysm

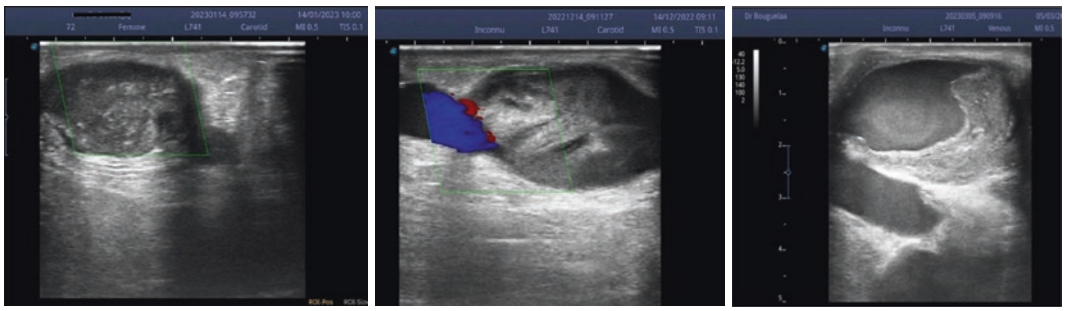

Fig. 14.46 Thrombosis

References

1. Stiegler H. Gefäßsonographie [Vascular ultrasonography]. Internist (Berl). 2012;53(3):298–308. https://doi.org/10.1007/s00108-011-2956-7.
2. Kong AC, Varacallo M. Anatomy, shoulder and upper limb, hand volar arch arteries. In: StatPearls. Treasure Island (FL): StatPearls Publishing; 2022.
3. Weber TM, Lockhart ME, Robbin ML. Upper extremity venous Doppler ultrasound. Radiol Clin N Am. 2007;45(3):513–24. https://doi.org/10.1016/j.rcl.2007.04.005.
4. Greenfield LJ, Rajagopalan S, Olin JW. Upper extremity arterial disease. Cardiol Clin. 2002;20(4):623–31. https://doi.org/10.1016/s0733-8651(02)00068-1.
5. Pucheu A, Evans J, Thomas D, Scheuble C, Pucheu M. Doppler ultrasonography of normal neck veins. J Clin Ultrasound. 1994;22(6):367–73. https://doi.org/10.1002/jcu.1870220603.
6. Finlay K, Friedman L. Ultrasonography of the lower extremity. Orthop Clin N Am. 2006;37(3):245–75. https://doi.org/10.1016/j.ocl.2006.03.002.
7. Clevert DA, Horng A, Reiser MF. Ultraschallbildgebung der Aorta abdominalis [Ultrasound imaging of the abdominal aorta]. Radiologe. 2009;49(11):1024–32. https://doi.org/10.1007/s00117-009-1875-2.

Role of Ultrasound in Airway Management

15

Peňafrancia C. Cano

15.1 Introduction

Two decades ago, ultrasound in the field of anesthesiology was initially used as a tool in the performance of peripheral nerve blocks. From then on, the use of the ultrasound has increased exponentially. From its use in Regional Anesthesia, it has been utilized as an adjunct in the insertion of catheters in the internal jugular vein, and at present, it is being used extensively for point-of-care ultrasound (POCUS). Its function for POCUS has gained a lot of popularity not only in anesthesiology but also among emergency room and critical care physicians, cardiologists, pediatricians, and other specialties as well. Since the machine is very compact without causing an emission of ionizing radiation, examination can be done repeatedly at any given time and can be used in different settings where diagnosis of clinical pathologies can be obtained instantaneously.

Since anesthesiologists routinely perform intubation as part of their practice, POCUS for evaluation of the airway has played an integral role. A good comprehension of the airway anatomy and its corresponding sonographic appearance will enable the recognition of an atypical or predict a difficult airway. Mastery of POCUS of the airway can simplify the performance of procedures such as percutaneous cricothyroidotomy, tracheostomy, and confirmation of endotracheal tube (ETT) placement. This chapter accentuates the role of ultrasound as an instrument in the evaluation of the airway and its management.

P. C. Cano (✉)
Division of Regional Anesthesia, Department of Anesthesiology, University of the Philippines-Philippine General Hospital, Manila, Philippines

15.2 Sonoanatomy of the Airway

Understanding the physics of ultrasound, together with adequate knowledge in transducer selection, probe orientation, and mastery in the anatomy of the upper airway will augment one's knowledge in the sonography of the airway.

With the use of a linear transducer, the tracheal cartilage in the transverse plane can be imaged as an inverted "U" shaped structure while underneath the cartilage is a strip line that is hyperechoic which is the air-mucosal (A-M) interface. Posterior to the left thyroid gland, the esophagus can be observed at the level of the first and second tracheal cartilage (Fig. 15.1). Peristaltic movement can be visualized and observed inside the esophageal lumen during swallowing. If the probe is moved cephalad, the cricoid cartilage will be seen. Same as the tracheal cartilage, it can be visualized as an inverted U shaped structure that is mixed-echoic in appearance, thicker and with a similar hyperechoic strip line of A-M interface directly beneath it (Fig. 15.2).

© The Author(s), under exclusive license to Springer Nature Switzerland AG 2024

N. Bouarroudj et al. (eds.), *POCUS in Critical Care, Anesthesia and Emergency Medicine*,
https://doi.org/10.1007/978-3-031-43721-2_15

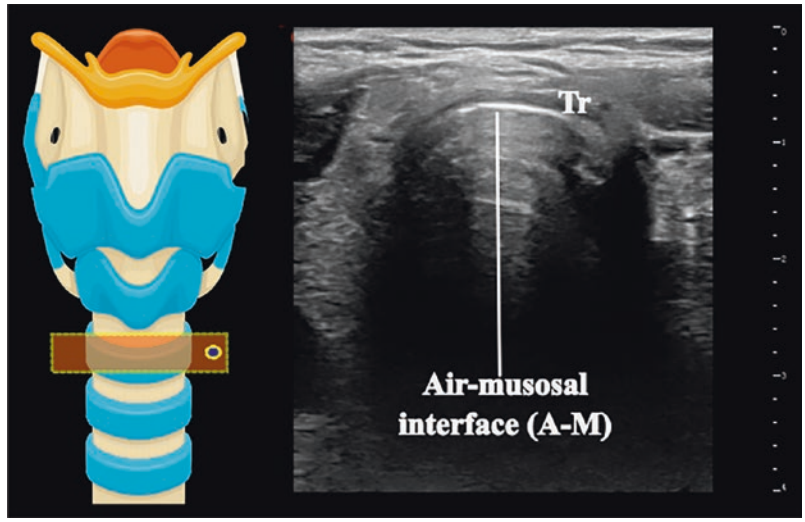

Fig. 15.1 The tracheal cartilage is seen as an inverted "U" shape hypoechoic structure. The air-mucosal interface (A-M interface) which is formed by reverberation artifacts is seen as a hyperechoic strip line beneath the trachea. *Tr* tracheal cartilage. (Image adapted from Osman A [1])

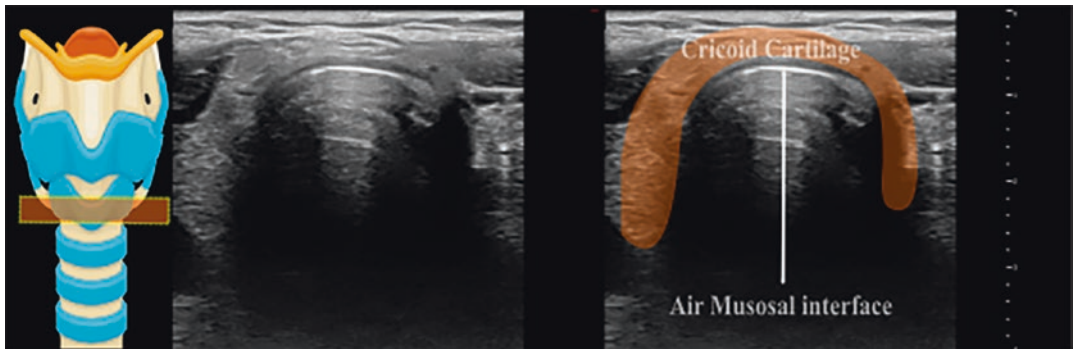

Fig. 15.2 Cricoid cartilage in transverse view. (Adapted from Osman A [2])

If the probe is moved further cephalad, the thyroid cartilage will be seen as a hyperechoic triangle-shaped structure. The transverse view at this level provides the best window to visualize the vocal cords. The hyperechoic appearance of the vocal ligaments delineates the vocal cord (Fig. 15.3).

In a longitudinal view, the tracheal cartilages have a hypoechoic appearance with the hyperechoic line, the A-M interface beneath. The series of tracheal cartilages is also called as the "string of beads" (Fig. 15.4). Cephalad to the tracheal cartilage is the bigger cricoid cartilage and further cephalad is also the bulky thyroid cartilage (Fig. 15.5). In between the two structures is the cricothyroid membrane.

A L G r a w a n y

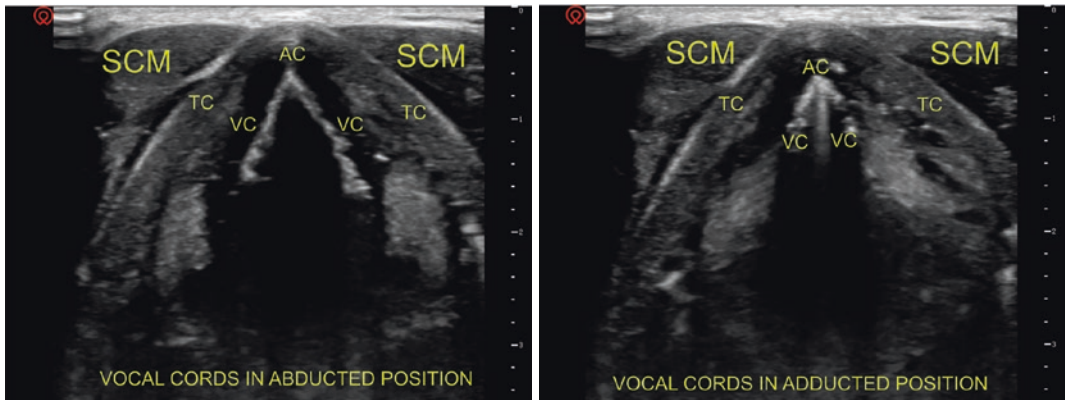

Fig. 15.3 Transverse view at the level of thyroid cartilage to observe the movements of vocal cord during abduction and adduction. *SCM* sternocleidomastoid muscle, *TC* thyroid cartilage, *AC* anterior commissure, *Vc* vocal cords, *A* arytenoids. (Adapted from Anusha C [3])

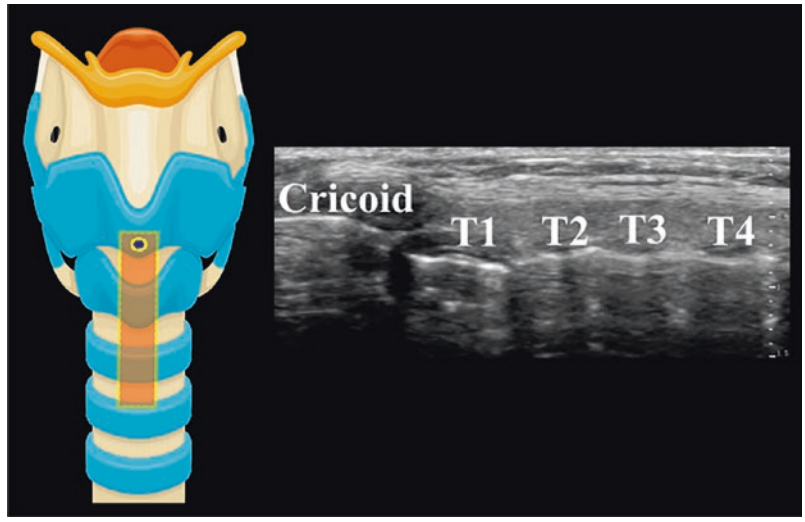

Fig. 15.4 Longitudinal view of the tracheal cartilages "string of beads" and the cricoid cartilage. (Adapted from Osman A [1])

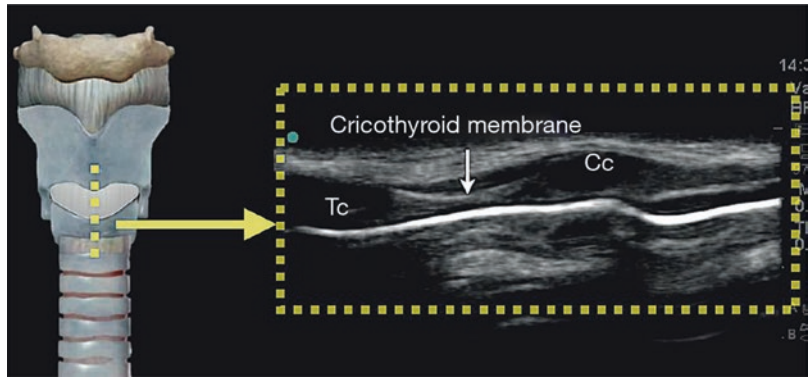

Fig. 15.5 Longitudinal view of the thyroid and cricoid cartilages. (Adapted from Osman A [1])

15.3 Functions of Ultrasound in the Airway

15.3.1 Cricothyroidotomy

Cricothyroidotomy can be a life-saving procedure, especially in "cannot intubate, cannot ventilate" circumstances. The most frequent problem of cricothyroidotomy, however, is the possibility of incorrect placement of the tube due to the mistake of correctly identifying the cricothyroid membrane, which can result in a catastrophic outcome.

Classically, cricothyroidotomy can be performed using surface landmarks to identify the cricothyroid membrane. However, the success rate with the landmark approach is achieved poorly which has been noted at 36% among anesthesiologists. Landmark guidance alone is insubstantial as a tool to mark the cricothyroid membrane and its identification is more difficult in obese patients. Evidence has shown that the use of ultrasound can perform better in recognizing the cricothyroid membrane as compared to the landmark approach. Based from the randomized controlled trial by Siddiqui et al. where a comparison was performed regarding the incidence of injury to the larynx and trachea in cadavers by non-experienced ultrasound trainees who performed digital palpation versus ultrasonography, results showed that there was a significant decrease in injury to the airway with the use of the ultrasound. Furthermore, among those cadavers with distorted anatomy, injuries of only 33% were recorded with the use of ultrasound as compared to the incidence of 100% with digital palpation.

15.3.2 Confirmation of Endotracheal Tube (ETT) Placement

It is of paramount importance to ascertain that the ETT is in the correct location upon intubation. Esophageal intubation when not immediately detected can result in catastrophic complications. Confirmation of correct ETT insertion is ordinarily performed by direct visualization of ETT placement through the vocal cords which can be validated by listening for bilateral breath sounds and direct observation of misting of ETT which are not definitive enough to precisely confirm the location of the ETT.

Capnography has been regarded as the gold standard for ETT placement verification, but it has several limitations. Cardiorespiratory arrest, pulmonary embolism, bronchoconstriction, and technical malfunction may disregard its use. In fact, based from the study that was performed by Li, for emergency capnography use, the false-negative failure rate (tube in trachea but capnography reports esophagus) was 7% and the false-positive rate (tube in esophagus but capnography reports trachea) was 3%. These findings render possible harm to one patient in every ten treated with capnographic confirmation alone.

In emergency cases, ultrasonography is a more reliable tool for ETT confirmation with several systematic reviews demonstrating its credibility. During the performance of transtracheal ultrasound, it is suggested to place the transducer in a transverse plane at the level of the suprasternal notch. Endotracheal intubation can be diagnosed through a longitudinal view with visualization of a hyperechoic linear image in the trachea (Fig. 15.6). On the other hand, esophageal intubation can be diagnosed when the "double tract sign" is observed which can be manifested as two air-mucosa interfaces, one in the trachea and the other in the esophagus (Fig. 15.7).

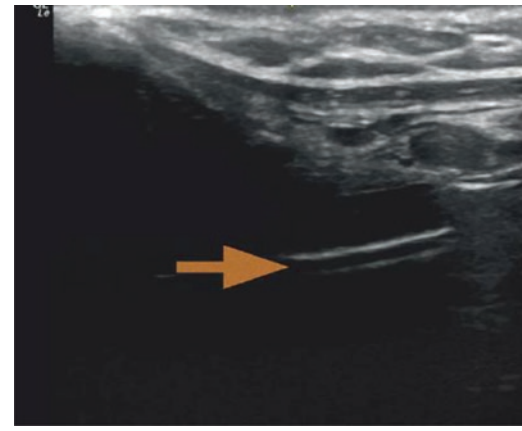

Fig. 15.6 Sonographic appearance of a saline-filled ETT cuff (arrow)

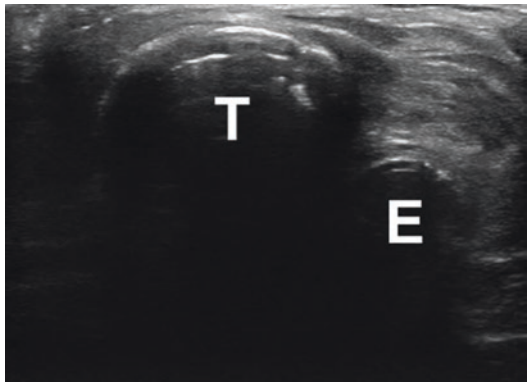

Fig. 15.7 Sonographic appearance of an esophageal intubation. *T* trachea, *E* esophagus. (Adapted from Gottlieb M [4])

15.3.3 Prediction of Difficult Laryngoscopy

By convention, airway assessment is initially performed by using the Mallampati score and thyromental distance, the results of which can anticipate difficult airway. Studies however have exhibited that the Mallampati score is only 51–53% sensitive and effective in foretelling difficult laryngoscopy. Relative to this, several pilot studies have been conducted to determine the significance of POCUS as a tool for airway evaluation. Different sonographic parameters have been used to predict difficult and complicated intubations, with increased soft tissue depths being correlated with difficulty in intubations. It was demonstrated in the study of Wojtczak that a shorter hyomental distance ratio of 1.01–1.02 in morbidly obese patients can predict difficult laryngoscopy with high sensitivity. This measures the distance between the hyoid bone and mandibular mentum from the neutral position to the hyperextended neck position. Patients intubated easily were found to have a hyomental distance ratio ranging from 1.14 ± 0.02.

On the other hand, based on the study of Adhikary, the sonographic measurements of anterior neck soft tissue were greater in the difficult laryngoscopy group compared to the easy laryngoscopy group at the level of the hyoid bone with a value of 1.69 cm vs. 1.37 cm, respectively. A measurement of 2.8 cm at the thyrohyoid membrane level completely separated the patients with difficult and easy laryngoscopies. No statistically significant differences were found in the ultrasound measurements of the anterior neck soft tissue at other levels or at the base of the tongue between the difficult and non-difficult laryngoscopy groups. No significant correlation was also noted between thyromental distance and sonographic measurements. Pinto et al. in a recent study found similar findings using anterior neck thickness at the level of the thyrohyoid membrane.

Prediction of difficult intubation through measurement of the anterior neck shows favorable results, but many of these studies are preliminary observations and are limited to a small number of samples. More randomized controlled trial studies with bigger samples and level one evidence are needed before this method can be properly applied for conventional screening.

15.3.4 Prediction of Endotracheal Tube Size

The selection of the right endotracheal tube size is of much significance, especially in neonates and very young children, since an ETT that is too large can cause damage to the mucosa. Injury of the upper airway may result such as ulceration, ischemia, scar formation, and the possibility of an eventual subglottic stenosis. On the other hand, intubation of very young pediatric patients with an ETT that is too small may result in inadequate ventilation, anesthetic gas leakage, poor accuracy of end-tidal gas monitoring, risk of aspiration and gas pollution in the operating room. Predictive measurements for the right ETT size have been based on patient weight and height, but these systems are unreliable and inadequate.

There is a developing awareness in the capability of ultrasound to determine the correct ETT size which can be done through ultrasound measurement of the subglottic diameter. This method is more accurate in comparison to the age-based and height-based formula in calculating the correct ETT size (Fig. 15.8). The ultrasound has the

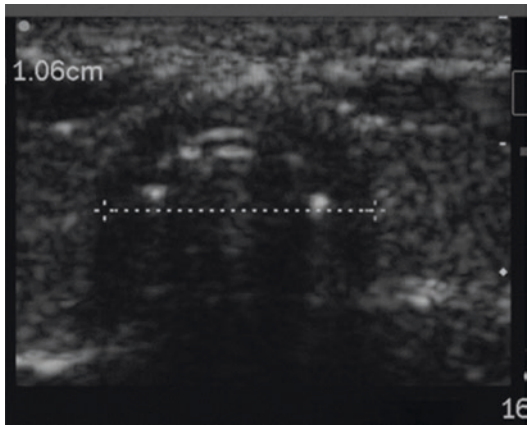

Fig. 15.8 Ultrasonographic image of subglottic diameter measurement. (Adapted from Shibasaki [5])

capacity to determine accurately up to 98% of cuffed ETT size and 96% of uncuffed ETT size. Age- and height-based formula, on the other hand, can only predict up to 35% for cuffed and 60% for uncuffed endotracheal tube according to a study by Shibasaki.

15.3.5 Prediction of Postextubation Stridor

Laryngeal edema may transpire in 2–15% of patients after extubation and can present as respiratory distress and stridor. Stridor is defined as the presence of a high-pitched inspiratory wheeze localized in either the trachea or the larynx. The clinical presentation is respiratory distress which requires medical attention and management. With such a clinical manifestation, there is a high probability of patients developing morbidity and mortality. What is strange is that there is no better technique that can predict patients who may develop postextubation stridor and laryngeal edema.

The cuff leak test, as demonstrated by Miller and Cole, refers to the presence or absence of an audible air leak when the sealing balloon cuff of the endotracheal tube is deflated. The authors were able to show that it can be a marker of laryngotracheal edema and postextubation stridor in high-risk patients. It has been investigated however that the cuff lick test is unreliable including its clinical application.

Ultrasound measurement of air column width at the level of the vocal cords has the potential to predict postextubation stridor. The laryngeal air column width is defined as the width of air passing through the VC as determined by ultrasound. Ding et al. compared the air-column width difference between postdeflation air column width from predeflation air column width. The study showed that the mean air-column difference was significantly lower among those who developed stridor, when compared with those who did not. The air column width during balloon cuff deflation was significantly lower in patients who developed stridor.

Venkategowda also did a study where he measured the air column ratio to predict postextubation stridor. The results showed that a ratio of 0.8 or less may be helpful in predicting postextubation stridor. On the other hand, the study of Sutherasan suggested that air column width difference of less than 1.6 mm may be considered in foretelling postextubation stridor.

The cut-off value to determine the possible occurrence of postextubation stridor may differ significantly among different types of population. With the results that are very inconsistent, the use of ultrasound to predict postextubation stridor requires further studies to be performed and with a bigger sample size.

15.4 Conclusion

Upper airway ultrasound is a handy, convenient, and useful tool that can be incorporated in the armamentarium of anesthesiologists, emergency room physicians, and internists in the screening of the airway. Its vast functionality calls for the incorporation of airway ultrasound as a routine practice in airway assessment.

References

1. Osman A, Meng Sum K, Shaik FA. Focused airway ultrasound: an armamentarium in future airway management. J Emerg Crit Care Med. 2019;3(31):1–10.
2. Osman A, Meng SK. Role of upper airway ultrasound in airway management. J Intensive Care. 2016;4:52.
3. Anusha C, Kundra P. Ultrasound imaging of the airway and its applications. Airway. 2018;1:17–24.
4. Gottlieb M, Dallas Holladay D, Burns K, et al. Ultrasound for airway management: an evidence-based review for the emergency clinician. Am J Emerg Med. 2019;38(5):1007–13.
5. Shibasaki M, Nakajima Y, Ishii S, et al. Prediction of pediatric endotracheal tube size by ultrasonography. Anesthesiology. 2010;113:819–24.

Echocardiographic Evaluation of Shock

16

Habiba Hemamid

16.1 Introduction

Circulatory shock is life-threatening, characterized by acute end-organ hypoperfusion. Management of this condition is the mainstay job of the intensivist. It relies on the diagnosis of the cause of the shock, the identification of the haemodynamic profile to provide an optimal management [1].

It has been shown that clinical evaluation is unable to estimate haemodynamic parameters like cardiac output [2] and accordingly incapable of resolving the circulatory compromise. Also, it is now well documented that early recognition, classification and profiling of the shock improve patient outcomes [3] and that underlie the importance of using monitoring tools [4].

Recently, echocardiography has acquired a central position in the management of critically ill patients. An international survey in intensive care patients with the coronavirus disease (COVID-19) was conducted. in this study [5]; echocardiography was reported to be widely used (was ranked one) to assess cardiac function, cardiac output, fluid responsiveness and pulmonary oedema. Moreover, the ultrasounds were recommended by all societies [6, 7].

Fig. 16.1 Echocardiographic image obtained to measure different parameters during the prone position ventilation in mechanically ventilated patients with severe acute respiratory syndrome coronavirus

In the same period, recent study has reported that echocardiographic images can be obtained to measure different parameters during the prone position ventilation in mechanically ventilated patients with severe acute respiratory syndrome coronavirus (Fig. 16.1) [8].

After the Covid pandemic 2019, echocardiography will universally become integral for the monitoring and management of the haemodynamically unstable patient.

In this chapter, we will outline how to use transthoracic echocardiography in shock states, focusing on haemodynamic monitoring assessment.

H. Hemamid (✉)
Medical Faculty, Intensive Care Unit, Critical Care Department, University Hospital of Sadna Mohamed Abdennour, University of Elbaz, Sétif, Algeria

© The Author(s), under exclusive license to Springer Nature Switzerland AG 2024

N. Bouarroudj et al. (eds.), *POCUS in Critical Care, Anesthesia and Emergency Medicine*,
https://doi.org/10.1007/978-3-031-43721-2_16

16.1.1 Value of Echocardiography in Shock State

In shock state, many components may be affected whether it be contractility, systemic vascular resistance, preload and afterload. Clinical evaluation is often unable to estimate these parameters and cannot reliably indicate whether the cardiac output is low or high [2]. Distinguishing between these altered components is extremely challenging and should be recognized because these can be prone to error and a worse management that may lead to organ dysfunction and poor outcome; that is why the use of monitoring evaluation is mandatory in the shocked patient. A plethora of tools were available and it was difficult to choose [9], but recently, bedside echocardiography has obtained wide acceptance and was adopted in lieu of the other invasive tools traditionally used to be in the first line, such as pulmonary artery catheter, to understand the cause of haemodynamic instability of shock [10, 11]. This approach offers the strong utility to provide valuable information with obvious qualitative evaluation, extremely adapted for the critical setting [12]. Echocardiography should be mandatory in shock. In the guidelines endorsed by the various societies, echocardiography is recommended as the first line in shock states and septic shock [3, 13].

This non-invasive technique is ideally suited to provide visual and real-time information on cardiac morphology and function which can be performed easily by the intensivist at the bedside. Indeed, the early use of echocardiography is an excellent choice for rapid diagnosis of mechanical causes of shock. It can resolve a diagnostic problem in a few minutes and excludes other causes. Moreover, this non-invasive technique offers also a large haemodynamic evaluation and more comprehension of clinical disorder. Serial assessment allows the diagnosis of uncommon acute conditions that may result in inadequate management and remain inaccessible to blind monitoring tools. Finally, the accurate results provided by echocardiography are crucial in guiding patient management [14, 15].

Owing to its low cost, durability, safety and capability for shared use for multiple critically ill patients, transthoracic echocardiography is increasingly available and recommended in resource-limited settings [16]. Indeed, this ultrasound technique is easy to integrate with other point-of-care ultrasound approaches, such as lung or abdominal echography.

Therefore, it should be kept in mind that the utility of echocardiography is strictly related to examiner competence; this implies good image acquisition, image interpretation and a cognitive base [17]. An inexperienced clinician may cause damage to patients and worsen the prognosis if therapeutic decisions are established on erroneous echocardiographic constatations and incorrect diagnostics.

In this chapter, we will show how integrate~~ing~~ this tool in different steps of assessment and management of circulatory shock.

16.1.2 When and How to Use Echocardiography in Shock

Circulatory shock is a common problem in critically ill patients. In the early hours of shock, echocardiography should be performed as soon as possible to confirm the cause of shock and rule out other etiologies of shock that require urgent treatments such as cardiac tamponade or pulmonary embolism. Echocardiography is also able to immediately identify the cause of haemodynamic instability whether it be distributive, hypovolaemic, cardiogenic or obstructive. Rapid diagnosis and intervention may avoid prolonged hypotension and prevent circulatory deterioration and eventually can improve patients' outcomes.

This technique is used to be carried out by the intensivist himself in a short time at the bedside; there is no necessity for the transportation of unstable patient to the consultant cardiologists while their interpretation is, in some sort, different and inadequate for the clinical scenario.

In ICU, when echocardiography is carried out on a critical patient with cardiopulmonary compromise, metabolic disorder and under high levels of circulating catecholamines, putting the clinician in echocardiography examination stress, the echocardiographic findings should be inte-

grated immediately for urgent diagnostic decision, including the clinical context, patients' medical history and other available data. Indeed, all prior treatments should be known and considered, particularly mechanical ventilation parameters in ventilated patients; that is why requiring competence in cognitive base is extremely important in critical echocardiography.

It is important to note that in the emergency and the intensive care unit, for haemodynamically unstable patients, it is not always easy to obtain the appropriate position to perform a classic echocardiographic evaluation such as left lateral approach, which may provide the best acoustic windows. The intensivist should be patient when the patient is difficult to study and, in some cases, the only window that can produce an acceptable image is the subcostal approach. The latter window may be affected by a surgical wound. Therefore, transoesophageal echocardiography is more effective in this purpose.

Clinical relevance of echocardiographic results should carefully be examined in patients with circulatory failure; accordingly, the intensivist assumes the responsibility of image acquisition and interpretation. If in doubt, it is logical to call for an expert in advanced echocardiography or consultant cardiologist for greater diagnostic accuracy.

Early critical echocardiography is based on qualitative evaluation by visual inspection based on two-dimensional imaging, using initially limited number of views, without any measurement to avoid time consumption, while the main objective is to answer rapidly some key clinical questions, in this condition, transthoracic echocardiography is the preferred modality to initiate cardiac and haemodynamic evaluation for immediate therapeutic management.

However, in many critically ill patients, cardiac visualization may be inadequate due to poor acoustic windows because of obesity, supine position and mechanical ventilation which makes interpretation difficult. In these patients, transoesophageal echocardiography (TEE) can provide high-quality images, especially for the posterior heart owing to its proximity to the oesophagus. Furthermore, for some specific indications, TEE is extremely helpful for the diagnosis of suspected aortic dissection, endocarditis, prosthetic valve dysfunction and intracardiac shunts. At last, the oesophageal probe could be left in place for continuous haemodynamic monitoring.

It is well established currently that echocardiography diagnostic capacity is better than other invasive techniques for many reasons. Conference consensus on monitoring during shock [3] emphasizes the initiation of basic monitoring such as echocardiography that should be completed by a another one after in case of unexplained hypotension.

In shock, if the source of haemodynamic instability is unclear in the initial evaluation, ultrasound can provide a complete evaluation to highlight more the haemodynamic status of circulatory failure [18].

Echocardiography is important not only for the early phase of haemodynamic instability but also as a monitoring device. It can be performed serially at the bedside to check the clinical evolution, therapeutic effect of fluid bolus, catecholamines' infusion, thrombolysis and the consequences of mechanical ventilation to achieve haemodynamic stabilization of patient.

16.2 Mechanisms of Shock

Circulatory shock is a common emergency in critically ill patients; rapid intervention is mandatory to prevent prolonged hypotension that may lead to organ dysfunction and poor prognosis. Immediate diagnosis and correct management may avoid this worse evolution.

In this chapter, we will describe the utility of echocardiography in detecting cardiac morphological abnormalities and establish the appropriate initial profile of shock.

16.2.1 Obvious Cardiac Abnormalities

It has been reported that transthoracic echocardiography is the only exam that is easy to perform in the early and rapid diagnosis of the

cardiac abnormalities which determine shock [3, 19].

In this indication, it is unrivalled against other scanning and blind monitoring devices in terms of speed and diagnostic accuracy. It should be known that the more the patient is unstable, the more echocardiographic findings are caricatured which facilitate their recognition. Pericardial fluid is relatively easy to identify, and tamponade can be detected by any intensivist whatever his skill; it manifests itself as a swinging heart. Acute pulmonary core (CAP) is usually easy to recognize; PE is suspected with markedly dilated RV. Echocardiography is the diagnostic procedure of choice for suspected mechanical complication of acute myocardial infarction (Fig. 16.2). Echocardiography is highly specific for acute valvular regurgitation that requires more expertise. TEE should be performed then for more comprehension [20]. In this situation, it should reveal if there is participation or not of these abnormalities in the constitution of the haemodynamic instability of shock. And as documented by a relevant study [21] in case of negative finding, echocardiography is well positioned to exclude a cardiac source of shock.

And lastly, it is assumed that no other blind device allows easy and rapid detection of so many cardiac abnormalities and acute disorders. After this step, when the examiner, even a beginner, puts his probe on the thorax, a global idea will be obtained through his haemodynamic profile, which can be hyper, hypo or normokinetic.

16.2.2 Hyperkinetic State

Hyperkinetic profile is the most relevant haemodynamic profile in shock state and typically manifested in septic shock. It is associated with profound instability and poor outcomes in critically ill patients [22]. This usually occurs at the first stage of septic or severe vasodilatory shock, indicated by small, tachycardic and high contractile ventricles, it can be recognized by simple eyeball evaluation or eyeball measurement of some cardiac cycles, which provide a reliable ejection fraction.

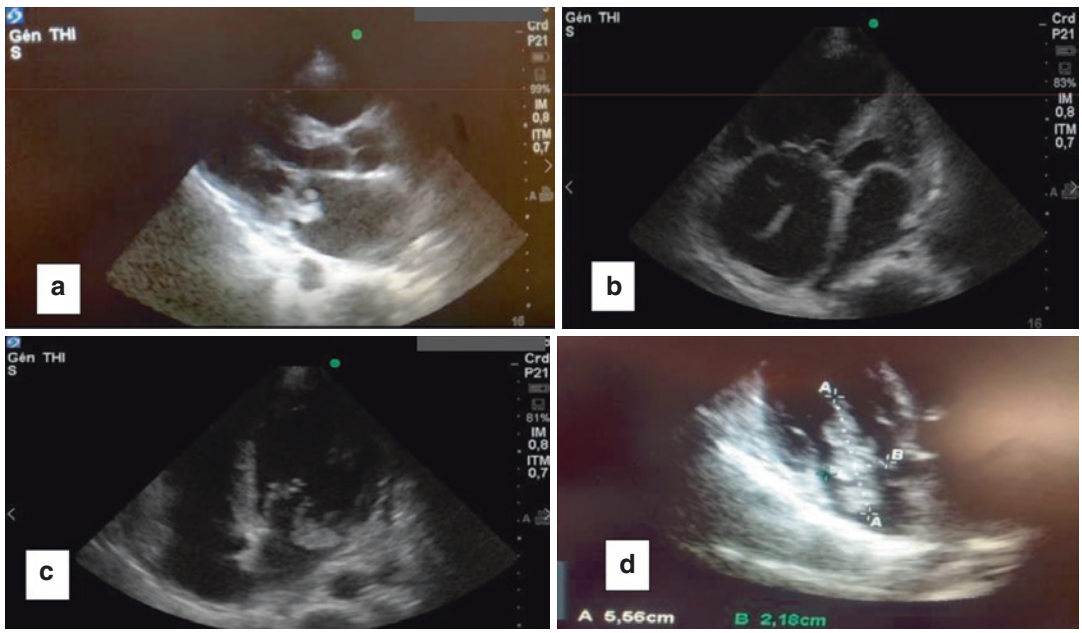

Fig. 16.2 Obvious cardiac abnormalities observed in shock: (**a** and **b**) RV dilatation with thrombosis material in the right ventricle; (**c** and **d**) vegetation on the mitral valve

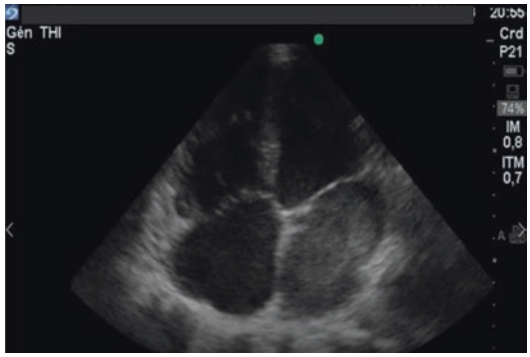

Fig. 16.3 Right and left dilatation cavities

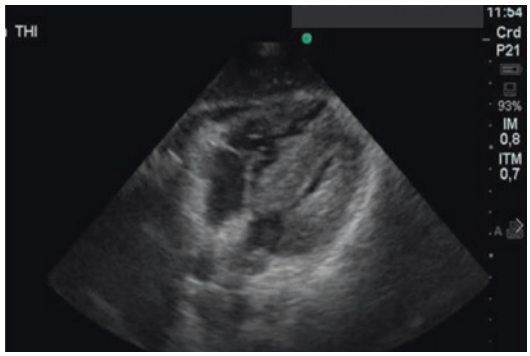

Fig. 16.4 Collapse of LV or "kissing heart"

In hyperkinetic profile, measuring left ventricle (LV) end-diastolic dimension is crucial to distinguish hypovolaemia from vasoplegia as follows: (1) hypovolaemia-associated hypercontractile heart chambers and decreased LV end-diastolic dimension with end-systolic collapse of LV or "kissing heart" (Fig. 16.3). (2) Vasoplegia appears with normal LV end-diastolic dimension and hypercontractile cavities [23]. In both situations, echocardiography shows small dimensions of vena cava with evident respiratory collapse.

16.2.3 Hypokinetic State

The contractile dysfunction can be classified as hypokinetic, akinetic or dyskinetic. Important dilatation of LV is easy to be eyeballed and appears obvious in comparison with normal size of LV (Fig. 16.4). Severe systolic dysfunction manifests on visual technique with little change in cavity area of the LV and minimal wall thickening during cardiac cycle. Many studies have shown that qualitative evaluation is reliable to estimate ejection fraction over complicated measurements [12].

Systolic wall motion abnormalities may be the main mechanism of shock and then should be systematically detected by eyeball echocardiography, especially in the short-axis view; then it is preferred to combine several measurements of ejection fraction.

Regional wall motion abnormalities indicate usually an ischaemic heart disease. Alternatively, it may be manifested in septic shock [24]. The association of circulatory shock signs with pulmonary oedema indicate then the presence of LV failure.

Hypokinetic state may be most frequently related to a complicated myocardial infarction or acute myocarditis or decompensated heart failure. Septic cardiomyopathy is also a relevant cause observed in such profile [24].

Echocardiography is also necessary for depicting chronic heart disease and its implementation in the constitution of haemodynamic instability and should be taken into account when deciding on the appropriate diagnostic.

16.2.4 Normokinetic State

In some cases, the LV may appear nondilated with preserved systolic function within haemodynamic scenario of instability, where one of the main pitfalls is to miss relevant systolic dysfunction. Indeed, normokinetic profile may be encountered in resuscitated septic shock with septic cardiomyopathy or in patients who receive catecholamines and volume resuscitation in the first stage of septic shock. Beta-blocker treatment can also mask the hyperdynamism. For this reason, it is mandatory to include the clinical context and current treatment because this may influence dynamic variables and changes the haemodynamic scenario.

16.3 Haemodynamic Profile of Shock

If the initial evaluation does not depict the problem or if shock persists after initial resuscitation, we should reassess the clinical scenario with a profound haemodynamic analysis. The assessment of haemodynamic status via a comprehensive approach using echocardiography is the key aspect for guiding the correct management of unstable patients with shock.

The evaluation of haemodynamic status relays on cardiac function assessment, cardiac output estimation, vasoplegia and fluid requirement.

In fact, the traditional classification of shocks is obsolete, and the new paradigms have demonstrated that one type of shock may spill over several impaired haemodynamic components. Sepsis can induce myocardial dysfunction in up to 60% of patients [24], myocardial infarction may be manifested with vasoplegia profile in around 80% [25]. Hypovolaemia, traumatic shock can present in different aspects. These situations can be prone to error, an inadequate management and result in a fatal outcome.

On the basis of this consideration, blind haemodynamic assessment is unable to solve the complexity of haemodynamic status with only pressures and volumes estimations. In contrast, echocardiography examination can depict mechanisms of instability that are not clinically suspected such as outflow tract obstruction (LVOTO) and acute valvular regurgitation.

Moreover, changes in haemodynamic must be serially assessed because several clusters can develop at any stage of sepsis and be associated with one. These clusters have been identified by statistical approaches based on echocardiographic and clinical parameters [26].

An original study [27] showed that echocardiographic monitoring in critically patients with septic shock can identify cardiovascular phenotypes based on cardiac dysfunction, hyperkinesia and fluid responsiveness, that are potentially important to guide fluid administration, vasopressor and inotropic therapy.

16.3.1 Left Ventricular Systolic Function

Accurate assessment of left systolic function is an essential aspect of haemodynamic evaluation. It is well known today that qualitative evaluation for global assessment of LV can be sufficient and can be also obtained by visual examination alone [12]. This approach may thus assess segmental wall motion, which is reproducible and less time-consuming compared with measurement of ejection fraction as an overall index of LV systolic function. Several methods are used to study left ventricular systolic function using two-dimensional approaches, from the simplest to the hardest, but they are not routinely used due to their scant additional value for practical application in critical setting and relay on best visualization of LV endocardial border. Nevertheless, qualitative evaluation requires skill and experience of examiner. Other methods are not frequently used such as S wave, mitral annular motion, dp/dt and MAPSE for mitral annulus plane. Recent advances in technology allow to follow and quantify cardiac muscle wall motion by global longitudinal strain speckle tracking [28].

Echocardiographic evaluation offers significant help on the characterization of the type of cardiac dysfunction, the degree of its severity and early detection.

Circulatory shock, combined with pulmonary venous congestion signs, suggests usually cardiogenic shock. The common cause is the LV systolic dysfunction secondary to extended acute myocardial infarction.

Echocardiography is a valuable tool that can provide information about ventricular loading which can be estimated by measuring the transmitral flow (E/A ratio) and the velocity of mitral annulus with tissue doppler imaging (E/E′). Other parameters could be useful in some cases such as Pulmonary venous flow, left atrial volume. Nevertheless, combining E/A with E/E′ is a non-invasive surrogate parameter for Pulmonary artery occlusion pressure (PAOP) that can be used in case of ARDS diagnosis. Overall and to be practical, when E/E′ <6, PAOP is probably

normal, while E/E′ >15 its indicative of high pressure. Between the two values, the grey zone of uncertainty is wide and, in this situation, the other parameters are helpful [29].

Increased LV diastolic dysfunction, in conjunction with decreased ejections parameters, indicates also LV failure. Indeed, in cardiogenic shock, echocardiography can identify the cause such as left or right systolic dysfunction, severe valvular pathology, endocarditis and aortic dissection. Current guidelines recommend performing routine echocardiography in the management of cardiogenic shock [30].

16.3.2 Cardiac Output Assessment

Cardiac output may be calculated and not measured discontinuously by echocardiography [31] using the pulsed doppler(pw) across the left ventricular outflow tract (LVOT) of aortic valve from an apical 5 chamber view, allowing measure of the aortic velocity time integral (***VTI***). Aortic annulus diameter should be also measured at the base of the aortic valves from parasternal long axis window. Thus, cardiac output may be computed as follows:

$$Qc = \left(\frac{\pi D^2}{4} \right) \times VTI \times HR$$

D is aortic annulus diameter and ***HR*** is heart rate.

Nowadays, it is well documented that this technique is as valid and reliable as the classic right heart catheterization [32].

However, there is a confusion about the use and the utility of the absolute value of cardiac output in circulatory shock because cardiac output is an adaptative parameter, and we should assess whether cardiac output is adjusted to metabolic needs.

Furthermore, ITV measurement reflects more directly stroke volume than cardiac output due to changes in heart rate and errors in measuring aortic annulus diameter. Accordingly, respiratory variation of VTI or response to fluid bolus are more relevant than stroke volume or cardiac output, that is why it is recommended recently as dynamic index in predicting fluid responsiveness and to perform mini-fluid challenge [33].

Indeed, in the ICU, it is very important to measure VTI because this may help to categorize the patient's shock profile after correction of hypovolaemia. In this condition, VTI is normal between 14 and 20 cm, low value <14 cm indicates decreased stroke volume due to hypovolaemia or cardiac failure. High values >20 cm, after correction of hypovolaemia, suggest vasoplegia.

Some precautions must be taken and respected in order to avoid incorrect VTI measurement. Overall, 3–5 cardiac cycles should be averaged, but in case of irregular rhythm such as atrial fibrillation, more cycles >10 need to be averaged. Aortic stenosis and aortic regurgitation can affect considerably VTI measurement. Alignment of doppler beam must be parallel to the aortic flow.

16.3.3 Fluid Requirement

In circulatory shock, hypovolaemia is the main common mechanism of instability and should be routinely looked for and corrected. Volume status evaluation is the cornerstone of haemodynamic exploration since hypovolaemia may worsen tissue hypoperfusion and affect microcirculation. Similarly, it is well shown that excessive fluid therapy is an independent risk factor of death and associated with multiorgan oedema that leads to organ dysfunction [34].

Accordingly, assessment of volume status and fluids needs are the key to adequate fluid resuscitation in order to improve stroke volume and then blood pressure.

It is extremely important to distinguish volume status concept from volume dependence. The latter means if we can predict the effect of fluid infusion on stroke volume, often called fluid responsiveness.

On the basis of this point of view, several markers have been developed and it is well established that static markers can estimate cardiac preload and are unable to predict the response of cardiac output to fluid bolus, except for extreme values [35].

In case of pronounced hypovolaemia, such as the first hours of septic shock, usually there is no need to assess fluid dependence. These markers

may manifest echocardiographically by kissing heart, small and vena cava collapse, decreased End-diastolic left ventricular (EDLV) diameter.

Nevertheless, after initial resuscitation and if we are uncertain, estimation of fluid needs requires dynamic indices that are based on the principle of changes in loading condition of heart induced by mechanical ventilation, in which respiratory variation in stroke volume may occur.

These dynamic indices may be achieved in ventilated patients by transthoracic echocardiography via respiratory variation of vena cava or VTI [36].

Vena cava variation and VTI variation are calculated as follow:

$$\Delta IVC = IVCmax - IVCmin \div \left(IVCmax + IVCmin\right) \div 2$$

$$\Delta VTI = VTImax - VTImin \div \left(VTImax + VTImin\right) \div 2$$

The threshold values are 12% for vena cava and 20% for VTI.

In case of spontaneous breathing, arrythmia and low volume tidal with mechanical ventilation, passive leg raising (PLR) is adapted for this purpose [35]. PLR is used as a fluid dependence challenge index and the main advantage of PLR is that it is a reversible test, allowing transfer of about 300 ml of blood towards the heart, resulting in increased cardiac output or VTI. The diagnostic threshold is increase in VTI >10%.

Therefore, mini fluid challenge is easy to perform and also valid whatever the ventilatory conditions and may be used where the other indices cannot be performed [35]. The diagnostic threshold is 10% [37].

Combining lung ultrasound enhances the relevance of fluid responsiveness indices. In fact, absence of B-lines strengthens fluid dependence and allows safe fluids administration [38].

16.3.4 Vasoplegia

Currently, increasing amount of evidence is emerging showing a strong association with vasoplegia and worse outcomes [39]; systemic vascular resistance can be assessed by the value of diastolic arterial pressure, but echocardiography offers great help in early detection of vasoplegia, which may be calculated using the equation:

$$SVR = \left(MAP - RAP\right) \div Qc$$

SVR is systemic vascular resistances, MAP is mean arterial pressure, RAP is right atrial pressure, Qc is cardiac output.

In the initial evaluation, calculation of systemic vascular resistances can reassure the distributive profile of shock and can appreciate the degree of vasoplegia severity that may indicate immediate vasopressor treatment before fluid bolus administration. Further, in same clinic scenarios of shock, multiple components can be associated and should be revealed to achieve the optimization management such as the situation in the second profile manifested with vasoplegia in cardiogenic shock [40–42].

The other arm, the value of ITV, is very contributive to this purpose; a higher value if ITV >2O cm after fluid therapy indicates the distributive profile of shock and a very high value is sign of hyperdynamic state.

By the evolution of shock, management therapy cannot be assessed by systemic vascular resistance calculation such as the other monitoring devices.

16.3.5 Right Ventricular Function

In circulatory failure, right ventricular (RV) dysfunction can provoke haemodynamic instability and, similarly to the LV evaluation, both RV systolic and diastolic function may be assessed. Despite irregular shape of RV, diastolic dysfunction is assessed through RV size; either by eyeball examination or by RV/LV end-diastolic area ratio measurement on a four-chamber view. RV/LV >0.6 indicates moderate dilatation. RV/LV >1 signals severe dilatation and should look for a paradoxical septal motion realizing D shape letter on parasternal short axis, defining acute cor pulmonale (Fig. 16.5). The most frequent causes are pulmonary embolism, RV infarction, ARDS and right septic cardiomyopathy.

Longitudinal systolic RV function is commonly estimated using tricuspid annular plan systolic excursion (TAPSE) and S wave by tissue doppler of tricuspid annulus; other methods are less used at bedside critical care.

Combining several parameters is interesting, especially in ARDS to assess more the impact of ventilation strategy on RV.

At the least, an algorithm is proposed to the intensivist using echocardiography to identify the mechanism of shock in step-by-step assessment considering cardiac abnormalities and the value of ITV for the haemodynamic evaluation.

The diagnostic process consists of two steps: (1) to detect the cardiac causal abnormalities such as pericardial tamponade, pulmonary embolism, dysfunction wall motion…, (2) to recognize haemodynamic profile if no cardiac abnormalities were observed through the measurement of ITV, allowing an individualized therapy (Fig. 16.6).

Because it is difficult to combine all situations, some associations can be observed which are much less frequent in the critical setting and have been ignored in this algorithm to avoid complexity.

Fig. 16.5 Severe acute cor pulmonale "**D sign**"

16.4 Haemodynamic Monitoring Using Repeated Echocardiography

The haemodynamic profile can change at any time either due to the progression of the shock or due to the effect of therapeutic interventions. Indeed, haemodynamic deterioration can occur at any stage of pathological process such as dynamic obstruction of the left ventricular outflow tract (LVOTO) resulting from combined anatomical, haemodynamic and therapeutic conditions. This problem can only be depicted by echocardiography and requires specific treatment depending on the underlying factor.

In septic shock, systolic dysfunction can manifest after increasing of LV afterload and must be recognized in order to adapt therapeutic strategy.

For this purpose, serial evaluation is necessary for guiding the continuous management of unstable patients at the bedside.

Bedside echocardiography is increasingly being incorporated in daily practice as an extension of standard haemodynamic monitoring.

There are now a number of reports that show a significant benefit of serial bedside assessment in terms of diagnosis, therapeutic impact [43, 44] and outcome; a randomized controlled clinical trial compared the use of continuous haemodynamic monitoring by TEE with usual care in

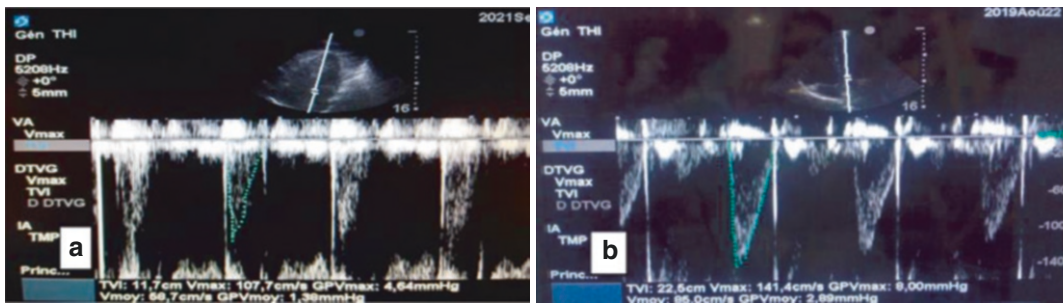

Fig. 16.6 Proposed diagnostic algorithm for shocked patients using bedside echocardiography

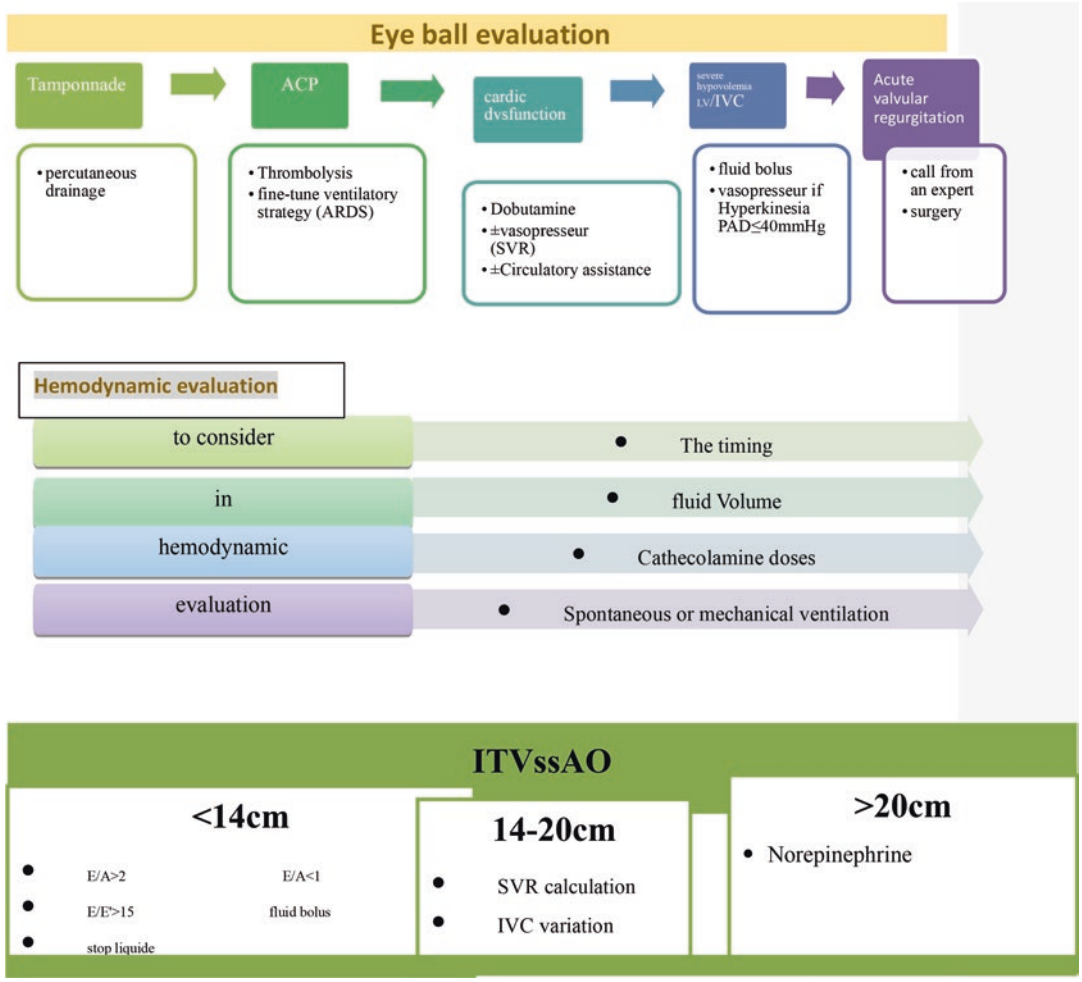

Fig. 16.7 Simple eye ball evaluation or eye ball measurement of VTI variation. (**a**) Fluid independence. (**b**) Fluid dependence

shocked patient. In this new study, the TEE group showed a significant reduction in haemodynamic instability in the first 72 h [45].

In cardiogenic shock, echocardiography is necessary; for the repeated evaluation of cardiac output [46], echo allows us to obtain serially qualitative finding and quantitative estimation in order to assess filling pressure, fluid responsiveness in critically ill patients. Moreover, from the simple examination of cardiac cycles, rapid eyeball measurement can provide decision (Fig. 16.7).

It should be kept in mind, during repetition echocardiography, the examiner should perform all views in regular sequence and afterwards focuses on particular views for specific findings or monitoring to follow their evolution.

However, repeated clinical examination remains also mandatory for the assessment of hypoperfusion signs (mottling, cold extremities, mental confusion and urine output) which is essential to achieve the optimal management of shocked patients.

16.5 Management of Shock

Echocardiography is a useful device not only for haemodynamic assessment but also as a guide for management optimization.

16.5.1 Therapeutic Impact

Since echocardiography can be repeated during the evolution of clinical conditions, modification in terms of treatments can consistently concern fluids, vasopressor, inotropic agents and other therapies that can be defined as having therapeutic impact; the latter has been well studied and it is significantly important in critically ill patients with circulatory failure according to studies [43]. This impact is more relevant in the first hours when the haemodynamic disorder is more marked; accordingly, it is directly correlated to the impaired haemodynamic components, thereafter, according to the clinical evolution, serial examination can generate a diagnostic impact which will be immediately followed by a therapeutic impact.

16.5.2 Assessment of Efficacy and Tolerance Therapy

Despite the virtues of diagnostic and therapeutic impact, haemodynamic resuscitation may be poorly tolerated and should be then assessed. Excessive of vasopressor or inotropic doses can occur LVOTO and no blind monitoring technique can depict it. The same consideration is done for fluid administration where echocardiography is the preferred tool to confirm its efficacy and the passage to the preload independence through a plethora of indices that can be combined in litigious situations.

In some cases, when instability reappears after perfect haemodynamic stabilization, worse effects of ventilator setting should be suspected in mechanically ventilated patients, thus echocardiography allows to regularly reassess the RV function and fine-tune ventilatory strategy []. Furthermore, this tool is the cornerstone of management of patient treated with mechanical support systems such as extra-corporeal membrane oxygenation (ECMO) [47].

However, prognosis impact of echocardiography is not yet clear as for the other monitoring techniques and needs more prospective studies specifically designed for this purpose.

16.6 Limitation of Echocardiography

Owing to its excellent profile in terms of safety, accuracy, simplicity and mobility, echocardiography has some limitations that have to be mentioned.

First of all, the main limitation of echocardiography is the environment of its use where the patient may present in several circumstances, with some positions, mechanical ventilation, surgical wound, therapeutic support and metabolic conditions that can influence the haemodynamic status.

Then, bad echogenicity and difficulties to obtain adequate views should be considered in up to 25%. It is the result of anatomical and technical factors, and the subcostal window is often the only saving window for the intensivist.

But the most important barrier to a more widespread adoption of this tool today is the lack of training and proficiency that can lead to inappropriate use of this technology. For this reason, it appears that structured training and certification in critical echocardiography are absolutely indispensable and urgent. Indeed, continuing investments in research and development of advanced imaging modalities and an expansion of clinical applications should be given to guarantee its widespread implementation and optimal use in emergency setting.

Also, the echocardiographic measurements are discontinuous, thus unable to detect its short-time changes. Accordingly, in cases of instability and refractory shock, the diagnosis and management of shock should be completed by an advanced monitoring tool and, in this condition, it is recommended to use a number of techniques rather than using only one [3, 19]. In addition, this device cannot assess the microcirculation which is currently considered the pivot of the monitoring and the resuscitation of circulatory shock.

Finally, if the utility of this non-invasive tool in the diagnosis and haemodynamic evaluation in circulatory shock is well shown, its impact on patient outcomes is still inconclusive; current studies do not yet indicate a beneficial effect on patient outcomes.

Nowadays, it is difficult to define monitoring effectiveness and for best clinical outcomes, the optimal path should be haemodynamic monitoring coupled to an optimized patient care algorithm.

16.7 Conclusion

Echocardiography has a shared utility in the emergency setting, as it aids the intensivist in reaching a diagnosis and establishing management therapy.

Including patient history and clinical symptoms within the summary of echocardiographic findings allows a differentiated haemodynamic evaluation and can help to guide an individualized and optimal cardiovascular strategy. Its unique advantage is that this tool is in the hands of the intensivist at point-of-care for immediate, goal directed, detailed and serial use.

This can only be achieved through adequate training and maintenance of competence via certification process. Future research should focus on the development of monitoring technology of echocardiography.

References

1. Vincent JL, De Backer D. Circulatory shock. N Engl J Med. 2013;369(18):1726–34.
2. Hiemstra B, Koster G, Wiersema R, Hummel YM, van der Harst P, Snieder H, et al. The diagnostic accuracy of clinical examination for estimating cardiac index in critically ill patients: the simple intensive care studies—I. Intensive Care Med. 2019;45:190–200.
3. Cecconi M, De Backer D, Antonelli M, Beale R, Bakker J, Hofer C, et al. Consensus on circulatory shock and hemodynamic monitoring. Task force of the European Society of Intensive Care Medicine. Intensive Care Med. 2014;40:1795–815.
4. De Backer D, Vieillard-Baron A. Clinical examination: a trigger but not a substitute for hemodynamic evaluation. Intensive Care Med. 2019;45(2):269–71.
5. Hussain A, Via G, Melniker L, Goffi A, Tavazzi G, Neri L, et al. Multi-organ point-of-care ultrasound for COVID-19 (PoCUS4COVID): international expert consensus. Crit Care. 2020;24(1):1–18.
6. Michard F, Malbrain ML, Martin GS, Fumeaux T, Lobo S, Gonzalez F, et al. Haemodynamic monitoring and management in COVID-19 intensive care patients: an international survey. Anaesthesia Crit Care Pain Med. 2020;39(5):563–9.
7. Phua J, Weng L, Ling L, Egi M, Lim CM, Divatia JV, et al. Intensive care management of coronavirus disease 2019 (COVID-19): challenges and recommendations. Lancet Respir Med. 2020;8(5):506–17.
8. García-Cruz E, Manzur-Sandoval D, Gopar-Nieto R, Murillo-Ochoa AL, Bejarano-Alva G, Rojas-Velasco G, et al. Transthoracic echocardiography during prone position ventilation: lessons from the COVID-19 pandemic. J Am Coll Emerg Phys Open. 2020;1(5):730–6.
9. Vincent JL, Rhodes A, Perel A, Martin GS, Rocca GD, Vallet B, et al. Clinical review: update on hemodynamic monitoring-a consensus of 16. Crit Care. 2011;15(4):1–8.
10. De Backer D, Bakker J, Cecconi M, Hajjar L, Liu DW, Lobo S, et al. Alternatives to the Swan–Ganz catheter. Intensive Care Med. 2018;44:730–41.
11. Vieillard-Baron A, Millington SJ, Sanfilippo F, Chew M, Diaz-Gomez J, McLean A, et al. A decade of progress in critical care echocardiography: a narrative review. Intensive Care Med. 2019;45:770–88.
12. Vieillard-Baron A, Charron C, Chergui K, Peyrouset O, Jardin F. Bedside echocardiographic evaluation of hemodynamics in sepsis: is a qualitative evaluation sufficient? Intensive Care Med. 2006;32:1547–52.
13. Rhodes A, Evans LE, Alhazzani W, Levy MM, Antonelli M, Ferrer R, et al. Surviving sepsis campaign: international guidelines for management of sepsis and septic shock: 2016. Intensive Care Med. 2017;43:304–77.
14. McLean A. Echocardiography in management of the shocked patient. Ultrasound Med Biol. 2019;45:S12.
15. De Backer D, Giglioli S. Echocardiographic approach to shock. J Emerg Crit Care Med. 2019;3:35–40.
16. Huson MA, Kaminstein D, Kahn D, Belard S, Ganesh P, Kandoole-Kabwere V, et al. Cardiac ultrasound in resource-limited settings (CURLS): towards a wider use of basic echo applications in Africa. Ultrasound J. 2019;11(1):1–10.
17. Mayo PH, Chew M, Douflé G, Mekontso-Dessap A, Narasimhan M, Vieillard-Baron A. Machines that save lives in the intensive care unit: the ultrasonography machine. Intensive Care Med. 2022;48(10):1429–38.
18. Vignon P, Merz TM, Vieillard-Baron A. Ten reasons for performing hemodynamic monitoring using transesophageal echocardiography. Intensive Care Med. 2017;43:1048–51.
19. Teboul JL, Saugel B, Cecconi M, De Backer D, Hofer CK, Monnet X, et al. Less invasive hemodynamic monitoring in critically ill patients. Intensive Care Med. 2016;42:1350–9.
20. Hlaing M, He J, Haglund N, Takayama H, Flynn BC. Impact of a monoplane hemodynamic TEE (hTEE) monitoring device on decision making in a heterogeneous hemodynamically unstable intensive care unit population: a prospective, observational study. J Cardiothorac Vasc Anesth. 2018;32(3):1308–13.

21. Joseph MX, Disney PJ, Da Costa R, Hutchison SJ. Transthoracic echocardiography to identify or exclude cardiac cause of shock. Chest. 2004;126:1592–7.
22. Micek ST, McEvoy C, McKenzie M, Hampton N, Doherty JA, Kollef MH. Fluid balance and cardiac function in septic shock as predictors of hospital mortality. Crit Care. 2013;17(5):1–9.
23. Bouchez S, Wouters PF. Echocardiography in the intensive care unit. Curr Anesthesiol Rep. 2019;9:360–7.
24. Boissier F, Razazi K, Seemann A, Bedet A, Thille AW, de Prost N, et al. Left ventricular systolic dysfunction during septic shock: the role of loading conditions. Intensive Care Med. 2017;43:633–42.
25. Van Diepen S, Katz JN, Albert NM, Henry TD, Jacobs AK, Kapur NK, et al. Contemporary management of cardiogenic shock: a scientific statement from the American Heart Association. Circulation. 2017;136(16):e232–68.
26. Daulasim A, Vieillard-Baron A, Geri G. Hemodynamic clinical phenotyping in septic shock. Curr Opin Crit Care. 2021;27(3):290–7.
27. Geri G, Vignon P, Aubry A, Fedou AL, Charron C, Silva S, et al. Cardiovascular clusters in septic shock combining clinical and echocardiographic parameters: a post hoc analysis. Intensive Care Med. 2019;45:657–67.
28. Sanfilippo F, Corredor C, Fletcher N, Tritapepe L, Lorini FL, Arcadipane A, et al. Left ventricular systolic function evaluated by strain echocardiography and relationship with mortality in patients with severe sepsis or septic shock: a systematic review and meta-analysis. Crit Care. 2018;22(1):1–12.
29. Nagueh SF, Smiseth OA, Appleton CP, Byrd BF, Dokainish H, Edvardsen T, et al. Recommendations for the evaluation of left ventricular diastolic function by echocardiography: an update from the American Society of Echocardiography and the European Association of Cardiovascular Imaging. Eur J Echocardiogr. 2016;17(12):1321–60.
30. Levy B, Bastien O, Bendjelid K, Cariou A, Chouihed T, Combes A, et al. Experts' recommendations for the management of adult patients with cardiogenic shock. Ann Intensive Care. 2015;5:1–10.
31. Blanco P, Aguiar FM, Blaivas M. Rapid ultrasound in shock (RUSH) velocity-time integral: a proposal to expand the RUSH protocol. J Ultrasound Med. 2015;34(9):1691–700.
32. Mercado P, Maizel J, Beyls C, Titeca-Beauport D, Joris M, Kontar L, et al. Transthoracic echocardiography: an accurate and precise method for estimating cardiac output in the critically ill patient. Crit Care. 2017;21:1–8.
33. Cholley B. Echocardiography in the intensive care unit: beyond "eyeballing". A plea for the broader use of the aortic velocity–time integral measurement. Intensive Care Med. 2019;45(6):898–901.
34. Malbrain ML, Van Regenmortel N, Saugel B, De Tavernier B, Van Gaal PJ, Joannes-Boyau O, et al. Principles of fluid management and stewardship in septic shock: it is time to consider the four D's and the four phases of fluid therapy. Ann Intensive Care. 2018;8(1):1–16.
35. Monnet X, Shi R, Teboul JL. Prediction of fluid responsiveness. What's new? Ann Intensive Care. 2022;12(1):1–16.
36. Pang Q, Hendrickx J, Liu HL, Poelaert J. Contemporary perioperative haemodynamic monitoring. Anaesthesiol Intensive Ther. 2019;51(2):147–58.
37. Muller L, Toumi M, Bousquet PJ, Riu-Poulenc B, Louart G, Candela D, et al. An increase in aortic blood flow after an infusion of 100 ml colloid over 1 minute can predict fluid responsiveness: the mini-fluid challenge study. J Am Soc Anesthesiol. 2011;115(3):541–7.
38. Mojoli F, Bouhemad B, Mongodi S, Lichtenstein D. Lung ultrasound for critically ill patients. Am J Respir Crit Care Med. 2019;199(6):701–14.
39. Lambden S, Creagh-Brown BC, Hunt J, Summers C, Forni LG. Definitions and pathophysiology of vasoplegic shock. Crit Care. 2018;22(1):1–8.
40. Hochman JS. Cardiogenic shock complicating acute myocardial infarction: expanding the paradigm. Circulation. 2003;107(24):2998–3002.
41. Mohebi R, Liu Y, van Kimmenade R, Gaggin HK, Murphy SP, Januzzi JL Jr. Inflammation across universal definition of heart failure stages: the CASABLANCA study. Eur J Heart Fail. 2023;25(2):152–60.
42. Squiccimarro E, Labriola C, Malvindi PG, Margari V, Guida P, Visicchio G, et al. Prevalence and clinical impact of systemic inflammatory reaction after cardiac surgery. J Cardiothorac Vasc Anesth. 2019;33(6):1682–90.
43. Vieillard-Baron A, Slama M, Mayo P, Charron C, Amiel JB, Esterez C, et al. A pilot study on safety and clinical utility of a single-use 72-hour indwelling transesophageal echocardiography probe. Intensive Care Med. 2013;39:629–35.
44. Alsaddique A, Royse AG, Royse CF, Mobeirek A, El Shaer F, AlBackr H, et al. Repeated monitoring with transthoracic echocardiography and lung ultrasound after cardiac surgery: feasibility and impact on diagnosis. J Cardiothorac Vasc Anesth. 2016;30(2):406–12.
45. Merz TM, Cioccari L, Frey PM, Bloch A, Berger D, Zante B, et al. Continual hemodynamic monitoring with a single-use transesophageal echocardiography probe in critically ill patients with shock: a randomized controlled clinical trial. Intensive Care Med. 2019;45:1093–102.
46. Chinen D, Fujino M, Anzai T, Kitakaze M, Goto Y, Ishihara M, et al. Left ventricular outflow tract velocity time integral correlates with low cardiac output syndrome in patients with acute decompensated heart failure. Eur Heart J. 2013;34(suppl_1):4249.
47. Bouchez S, Van Belleghem Y, De Somer F, De Pauw M, Stroobandt R, Wouters P. Haemodynamic management of patients with left ventricular assist devices using echocardiography: the essentials. Eur Heart J Cardiovasc Imaging. 2019;20(4):373–82.

Transcranial Doppler Sonography

17

Lamine Abdennour, Alice Jacquens, and Vincent Degos

17.1 Introduction

Transcranial Doppler (TCD) is currently a simple, non-invasive, inexpensive, and easily repeatable examination performed at the patient's bedside. It has become an essential diagnostic tool in the management of brain-damaged patients [1]. It is essential in assessing the state of their cerebral perfusion. It also allows to follow and to adapt the therapies. However, it requires two levels of competence depending on certain pathologies and their specificities.

The first level is the basic level required in trauma emergencies (Neurofast) to search for cerebral hypoperfusion secondary to intracranial hypertension.

The second, higher level, requires a higher degree of competence resulting from regular practice in a specialized environment. This concerns, for example, the search for vascular anomalies, such as cerebral arterial vasospasm in the case of subarachnoid haemorrhage, or retrograde circulation of an artery of the polygon of Willis in the case of dissection of a cervical artery destined for the brain.

The learning curve of basic level is in favour of a fast acquisition of the technique with a relatively low number of examinations (6–8 examinations) and in a short time (2–4 days). At the end of a short training cycle, the recognition of the middle cerebral artery and the measurement of its velocities, as well as the measurement of the pulsatility index are acquired. These are the basic data that should be collected in any brain-injured person without any specialization.

This chapter is exclusively devoted to transcranial ultrasound and colour-coded B-mode imaging coupled with pulsed Doppler. In addition to being able to identify anatomical structures and vessels, this technique offers the possibility of adjusting the insonation angle and aligning it with the artery and thus approaching real velocities as closely as possible.

17.2 The Main Acoustic Windows

17.2.1 Transtemporal Window (Picture 17.1)

This is the most important, most accessible and most used window. It is located above the zygomatic arch at mid-distance between the corner of the eye and the tragus of the ear. It allows access to the middle cerebral artery (MCA), the anterior cerebral artery (ACA), the internal carotid artery (ICA) in its terminal portion, the posterior

L. Abdennour (✉) · A. Jacquens · V. Degos
Neuro-Réanimation Chirurgicale, Département d'Anesthésie-Réanimation, Groupe Hospitalier Pitié-Salpêtrière, APHP-Sorbonne Université, Paris, France
e-mail: lamine.abdennour@aphp.fr

© The Author(s), under exclusive license to Springer Nature Switzerland AG 2024

N. Bouarroudj et al. (eds.), *POCUS in Critical Care, Anesthesia and Emergency Medicine*,
https://doi.org/10.1007/978-3-031-43721-2_17

Picture 17.1 Zygomatic arch (yellow arrow) probe on the temporal bone window

Picture 17.2 Transforaminal window

cerebral artery (PCA), the posterior communicating artery (PCoA) and the distal portion of the basilar trunk (BA).

17.2.2 Transforaminal Window (Picture 17.2)

This is the suboccipital route. With the patient in lateral decubitus, the head flexed forward, the probe is placed between the occiput and the cervical spine, slightly tilted and oriented towards the root of the nose. A small up and down movement of the probe allows to see the vertebral arteries, the basilar trunk, the postero-inferior cerebellar arteries (PICA), the antero-inferior cerebellar arteries (AICA), the superior cerebellar arteries (SCA) and sometimes the posterior cerebral arteries and exceptionally the anterior spinal artery (SAA). For intubated and ventilated patients in supine position, the probe can be positioned laterally between the occiput and the cervical spine. It is not necessary to lateralize the head. However, it is sometimes necessary to use a slight flexion of the head.

Picture 17.3 Transorbital window

17.2.3 Transorbital Window (Picture 17.3)

The probe is placed directly on the eyelid above the eyeball. The Doppler program must be switched to trans-orbital mode to reduce the power of emission and thus reduce the risk of ocular and retinal damage. This window allows access to the ophthalmic artery (OA) and the carotid siphon (CS) and sometimes to the anterior cerebral artery (ACA).

17.2.4 Submandibular Window (Picture 17.4)

The submandibular window allows access to the internal carotid artery (ICA) before it passes into the endocranium. The basilar trunk (BT) can be seen through this window, but this requires a very high level of expertise.

Picture 17.4 Submandibular window

17.3 Anatomical Landmarks

Anatomical landmarks in two-dimensional ultrasound are essential to guide the search for arteries. Their recognition is the guarantee of a good mastery of the tool. Once these landmarks have been identified, the use of colour Doppler allows direct visualization of the arteries. Vascular research from the outset by using colour is an obstacle to rigorous learning.

Anatomical landmarks by trans-temporal approach are easily identified (Fig. 17.1).

They are:

- Small wing of the sphenoid
- Sylvian fissure
- Cerebral peduncles

By placing the probe above the zygomatic arch, once the peduncles have been visualized, as well as the sylvian fissure, by printing a slight downward movement on the probe, a hyperechoic structure corresponding to the small wing of the sphenoid is seen (Fig. 17.2).

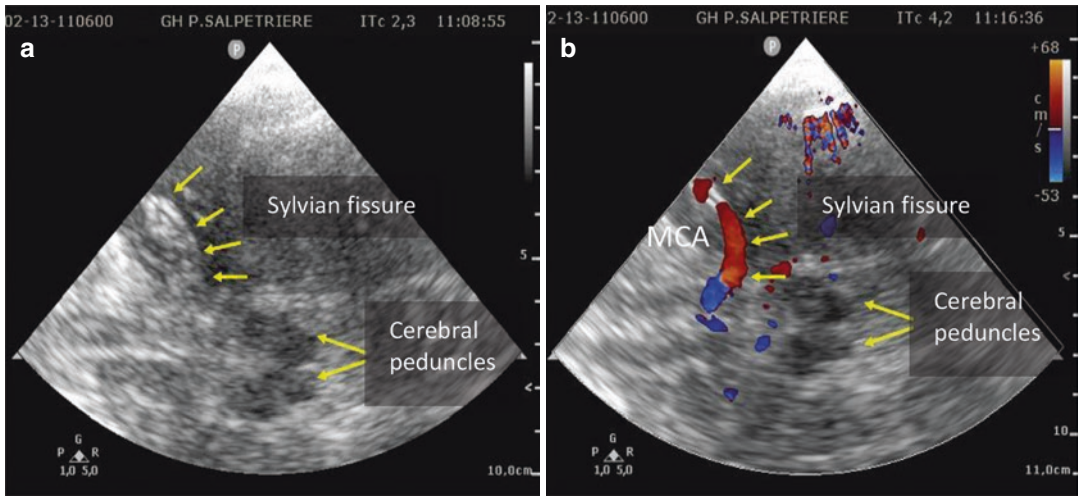

Fig. 17.1 (**a**) Transcranial ultrasound anatomic landmarks. (**b**) MCA middle cerebral arterym. *ACA* anterior cerebral artery

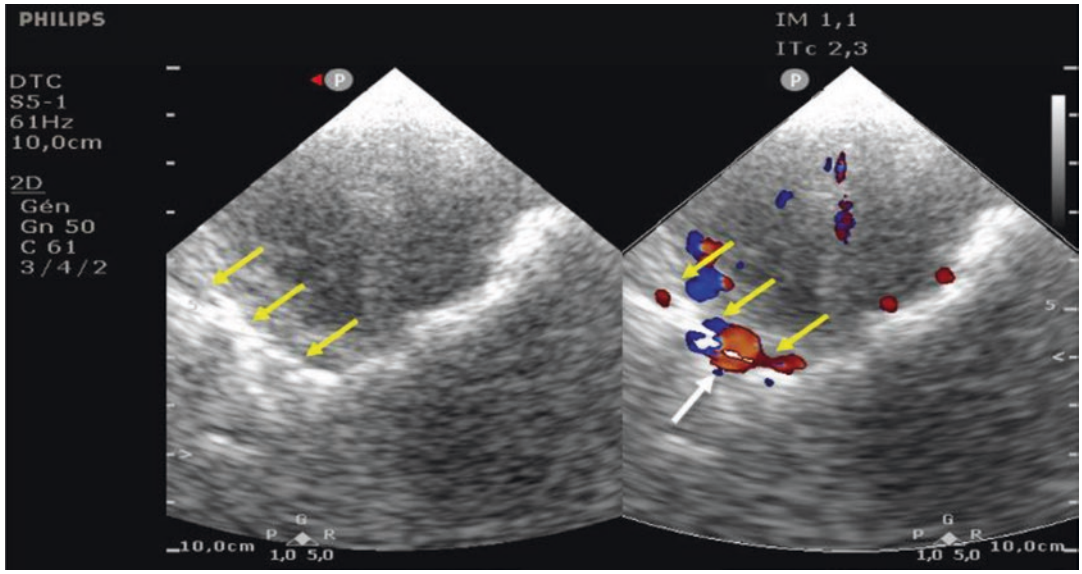

Fig. 17.2 Lesser wing of the sphenoid (yellow arrows), internal carotid artery ICA (white arrow)

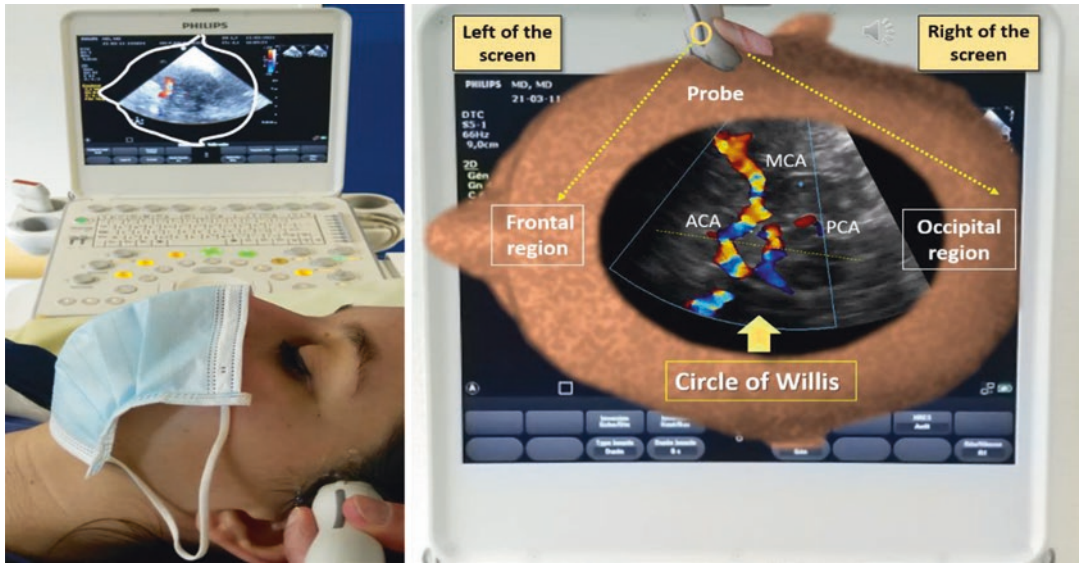

Fig. 17.3 Projection of the image of arteries on the screen

It is from this bony structure that the internal carotid artery enters the skull (Figs. 17.3 and 17.4).

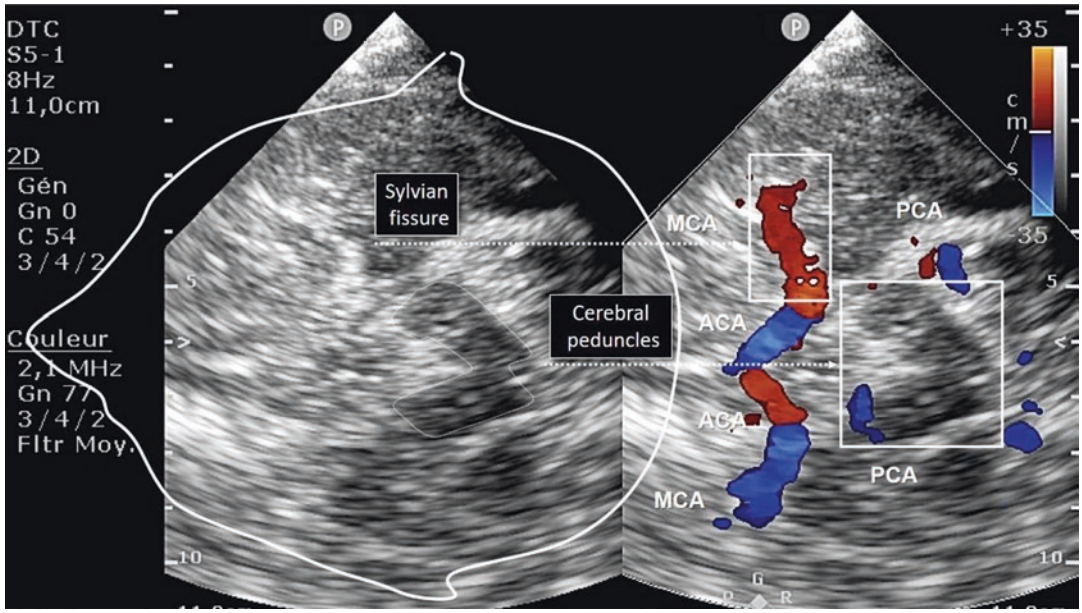

Fig. 17.4 (**a**) Landmarks without arteries; (**b**) Landmarks with arteries

17.4 The Main Cerebral Arteries

17.4.1 Carotid Circulation

17.4.1.1 Internal Carotid Artery: (ICA)

It is visualized by transtemporal approach. After locating the cerebral peduncles, the probe is slightly tilted towards the base of the skull to find the small wing of the sphenoid. This bony structure has a hyperechoic appearance on two-dimensional ultrasound. The use of colour Doppler allows visualization of the terminal portion of the internal carotid artery (ICA). In pulsed Doppler, it has a positive envelope with average velocities around 40 cm/s (Fig. 17.5).

17.4.1.2 Middle Cerebral Artery: MCA

The middle cerebral artery or sylvian artery arises from the division of the internal carotid artery into two arteries: the middle cerebral artery and the anterior cerebral artery. It is exclusively visible by trans-temporal approach (Fig. 17.6).

It has an "S" shape and follows the sylvian scissure. It is the most important artery in transcranial Doppler sonography (TCD) and the most accessible to non-experts. The learning of TCDT, starts with the recognition and measurement of the MCA velocities. Usually, the M1 and M2 segments are the most studied. In pulsed Doppler, its flow is positive with average velocities around 50–60 cm/s. The small insonation angle between the artery and the ultrasound waves allows reliable measurement of velocities without angle correction or with minimal correction.

17.4.1.3 Anterior Cerebral Artery: ACA

Like the MCA, the anterior cerebral artery (ACA) arises from the division of the ICA. Its A1 segment flows forward in the direction of the frontal lobe (Fig. 17.7).

It stops at the anterior communicating artery (ACoA) that bridges the two ACAs. The A1 segments and the ACoA constitute the anterior part of the circle of Willis. At the level of these arteries, the direction of flow can be reversed. This is the segment accessible in E-TCD and whose velocities are close to those of the ICA. There are anatomical variants with a single A1 segment and agenesis or hypoplasia of the contralateral segment. The A2 segment ipsilateral to the agenesis is taken over by the contralateral artery through the ACoA. Sometimes, it is the ACoA that is absent. The circle of Willis is then incomplete with the

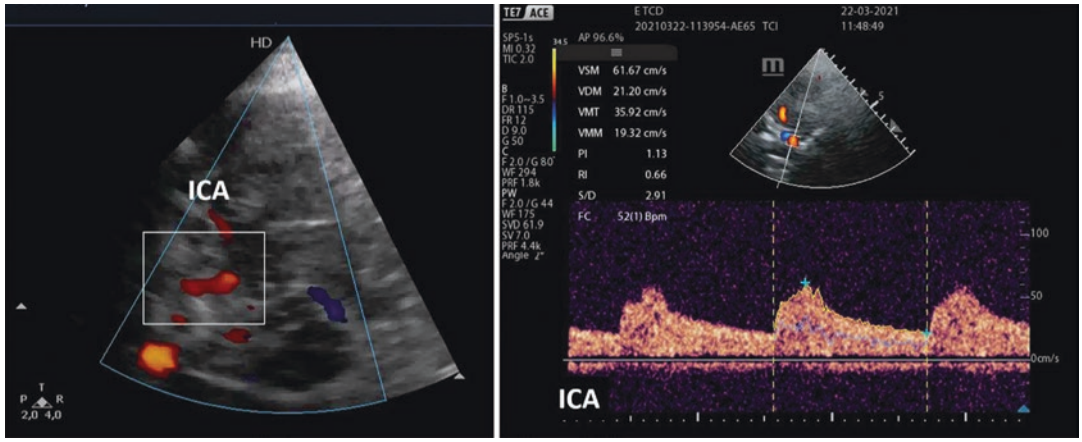

Fig. 17.5 *ICA* internal carotid artery

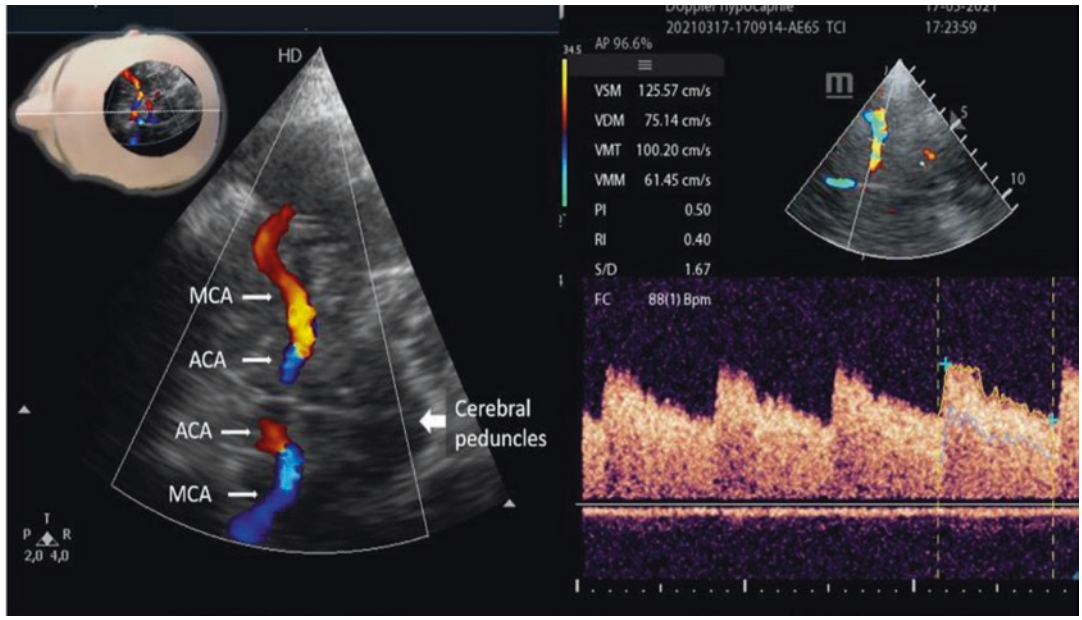

Fig. 17.6 *MCA* middle cerebral artery, *ACA* anterior cerebral artery

consequence that compensation between the two ACAs is impossible in case of carotid lesion. The ACA are explored from the temporal window.

17.4.1.4 Posterior Communicating Artery: PComA

The posterior communicating artery (PComA) arises from the internal carotid artery and joins the homolateral posterior cerebral artery. The PComA bridges the carotid and vertebro-basilar circulation. The PComA and the pre-communicating arterial segments of the posterior cerebral arteries (PCA) completes the circle of Willis. As a reminder, there is one ACoA and two PComAs (Fig. 17.8).

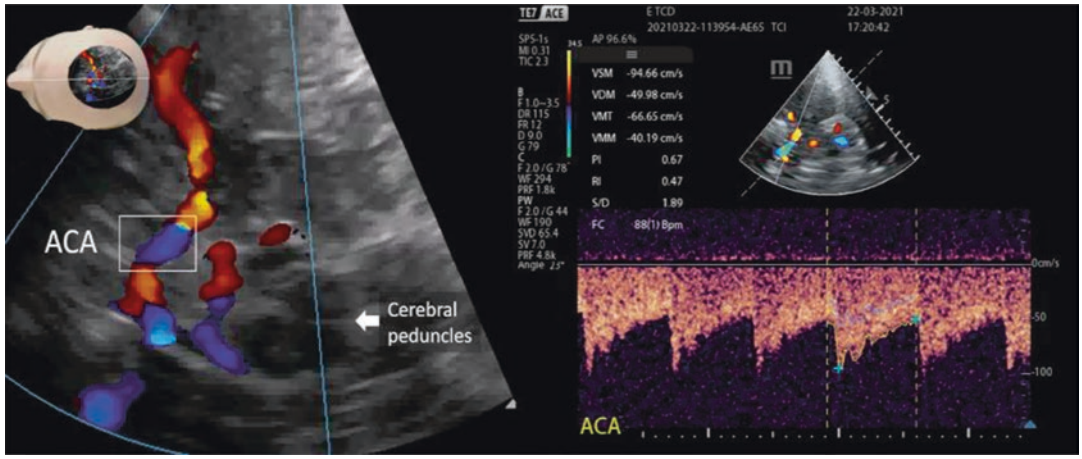

Fig. 17.7 *ACA* anterior cerebral artery

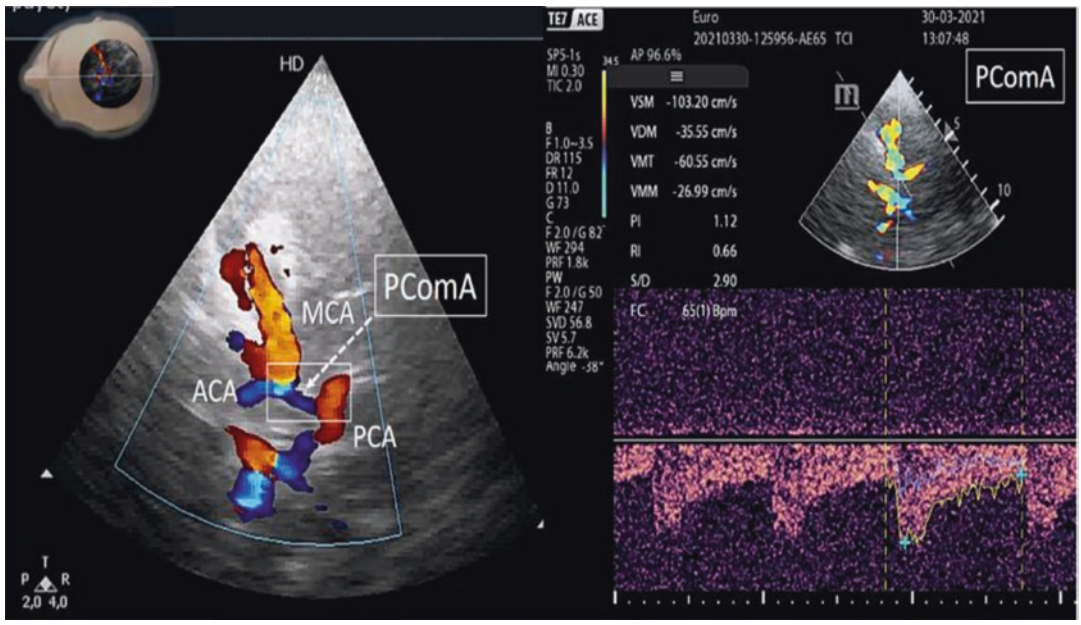

Fig. 17.8 *PComA* Posterior communicating artery, *ACA* anterior cerebral artery, *MCA* middle cerebral artery, *PCA* posterior cerebral artery

17.4.2 Posterior Circulation (Vertebro-basilar Circulation)

17.4.2.1 Posterior Cerebral Artery: PCA

The terminal portion of the basilar trunk (BA) divides into two posterior cerebral arteries (PCA). They communicate with the carotid circulation through the two PComA.

By transtemporal approach, the homolateral PCA, on its proximal portion, has a positive Doppler flow. When arcing around the cerebral peduncle, it initially has a positive flow that becomes negative (leaks the probe).

PCAs can sometimes be visualized transforaminal when they are in a favourable plane (Fig. 17.9).

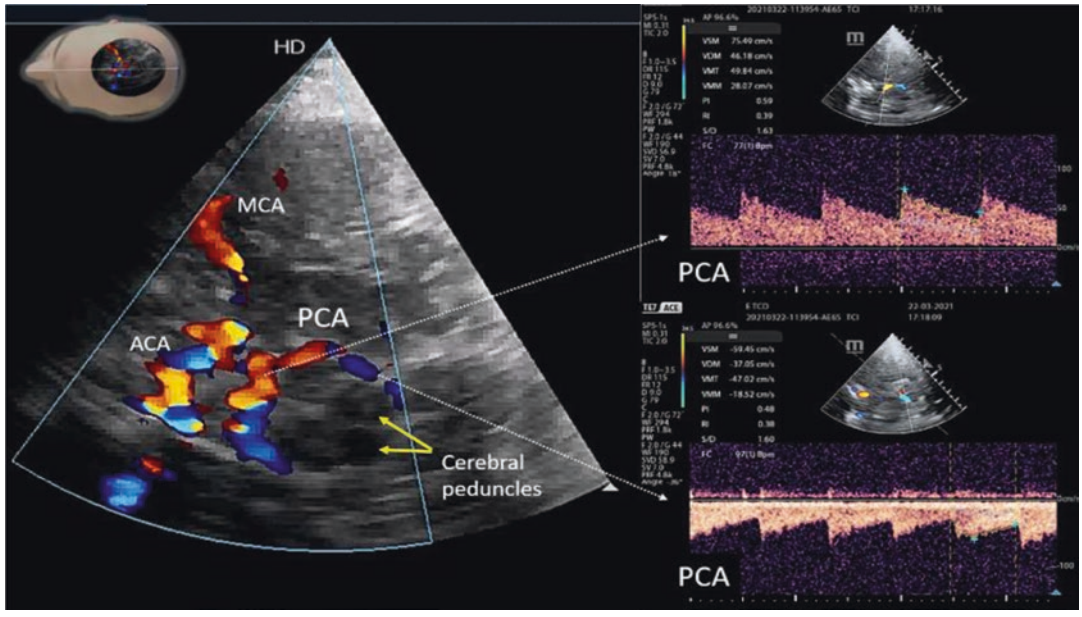

Fig. 17.9 *PCA* posterior cerebral artery, *ACA* anterior cerebral artery, *MCA* middle cerebral artery

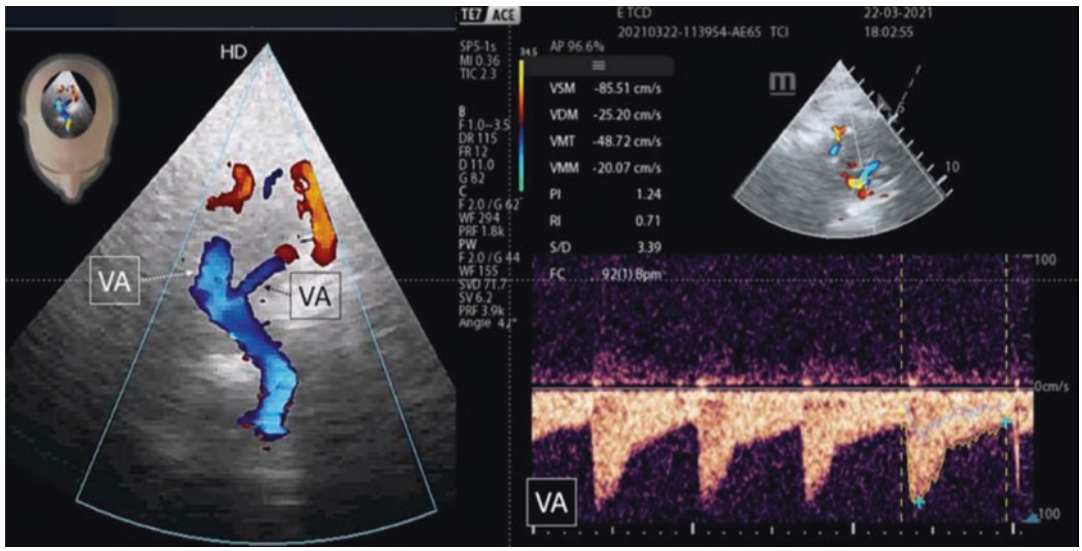

Fig. 17.10 *VA* vertebral artery

17.4.2.2 Vertebral Artery: VA

The vertebral arteries are visualized by transforaminal approach. This is their V4 segment which is endocranial. Two arteries arise from this segment: The posterior cerebellar artery (PICA) and a vascular branch that joins the one coming from the contralateral VA to form the anterior spinal artery. It is not uncommon to find a dominant vertebral artery and sometimes the absence of one of the two vertebral arteries. This is an anatomical variant in which the vertebral artery ends in PICA (Fig. 17.10).

The vertebral arteries have a negative flow on pulsed Doppler.

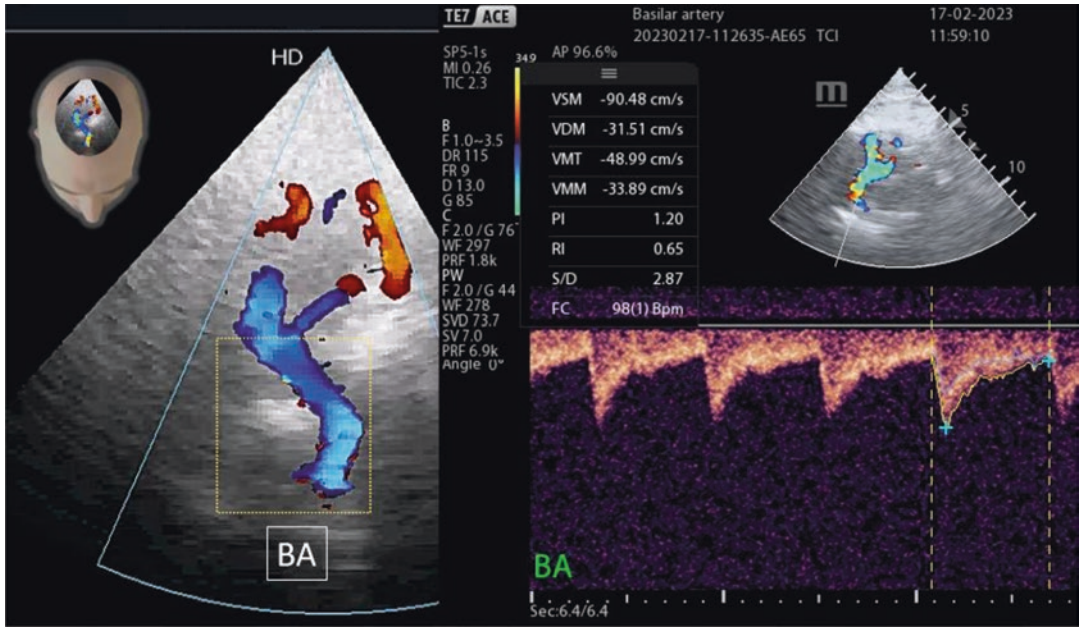

Fig. 17.11 *BA* basilar artery

17.4.2.3 Basilar Artery: BA

The basilar trunk is formed by the fusion of the two vertebral arteries. Its flow is negative on Doppler. Anatomically, the BA is not always in the same plane as the vertebral arteries. In this case, to visualize it, by transforaminal approach, a small inclination of the probe is necessary by directing it towards the root of the nose (Fig. 17.11).

The velocities of the vertebro-basilar circulation are low compared to those of the carotid circulation. They are between 30 and 40 cm/s. This is due to the fact that this circulation provides only 20% of the cerebral blood flow (CBF).

17.4.2.4 Postero-inferior Cerebellar Artery: PICA

The PICA is the first cerebellar artery. It originates from the V4 segment of the vertebral artery (VA). It is not systematically searched but its exploration is essential after a subarachnoid haemorrhage (SAH) by rupture of a PICA aneurysm or any other aneurysm located on the vertebro-basilar circulation. In this situation, the search for arterial vasospasm, which is very frequent and likely to be complicated by ischaemia, is crucial between the 4th and 12th day following the SAH (Fig. 17.12).

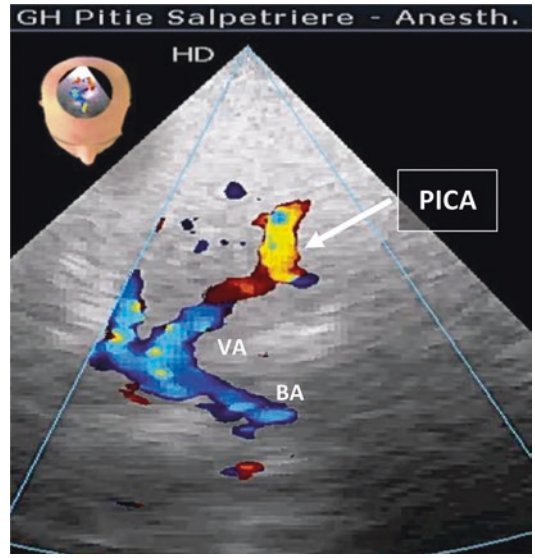

Fig. 17.12 *PICA* postero-inferior cerebellar artery, *VA* vertebral artery, *BA* basilar artery

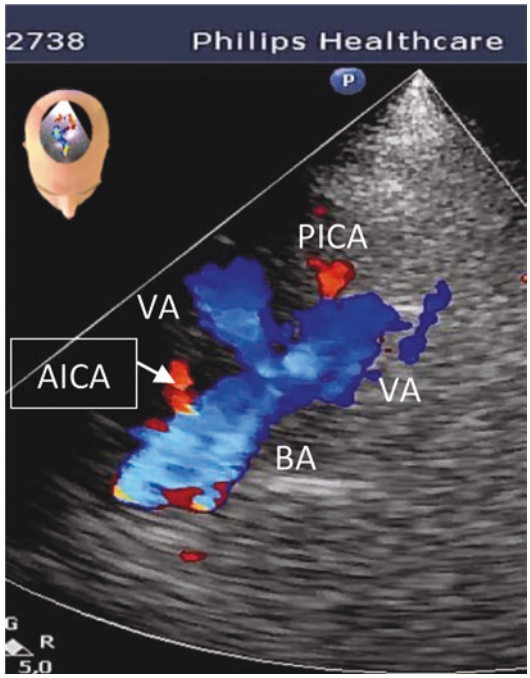

Fig. 17.13 *AICA* antero-inferior cerebellar artery, *VA* vertebral artery, *BA* basilar artery

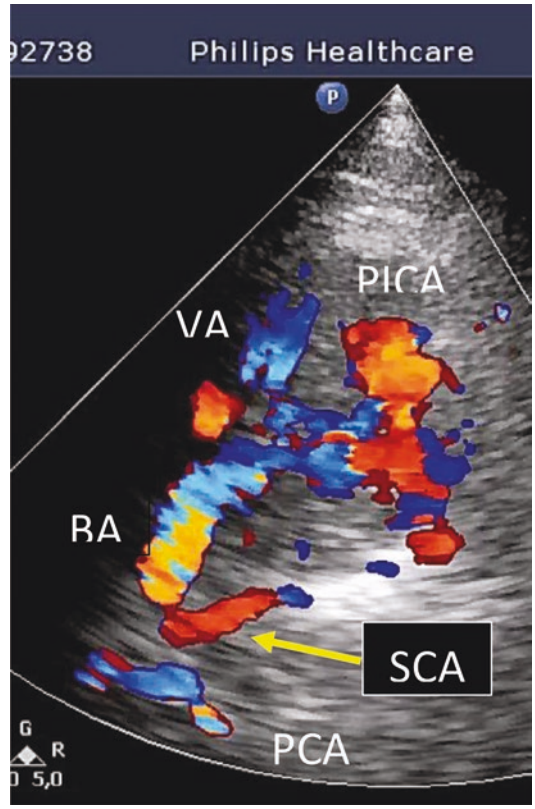

Fig. 17.14 *SCA* superior cerebellar artery, *BA* basilar artery, *PCA* posterior cerebellar artery, *VA* vertebral artery, *PICA* postero-inferior cerebellar artery

17.4.2.5 Antero-inferior Cerebellar Artery: AICA

The AICA usually arises from the initial basilar trunk portion and is not always easy to identify. Unlike PICAs, both AICAs arise on either side of the basilar trunk (BA) (Fig. 17.13).

17.4.2.6 Superior Cerebellar Artery: SCA

This is the third pair of cerebellar arteries. They arise just before the division of the basilar trunk into posterior cerebral arteries (Fig. 17.14).

17.4.3 The Characteristics of the Circle of Willis

The polygon of Willis, when complete, is made up of the A1 segment of the two ACA, the ACoA, the two PComA and the pre-communicating segment of the two ACP. Its role is essential because it very often makes it possible to compensate for the interruption of blood flow in one of the arteries that supplies it and that supplies certain cerebral territories. A reversal of the flow can then be observed, it allows to perfuse against the current the arteries depending on the one which is obstructed and to avoid most often the occurrence of an ischaemic stroke. Carotid dissection is the most common situation. This acute or chronic pathological situation will be detailed later (Fig. 17.15).

There are anatomic variants with an incomplete circle of Willis. These variants do not compensate for a cessation of flow in one of the arteries supplying it. The absence of an ACoA does not allow the contralateral ACA (A1) to supply the homolateral ACA (A2) and MCA of an internal carotid artery in the event of carotid dissection.

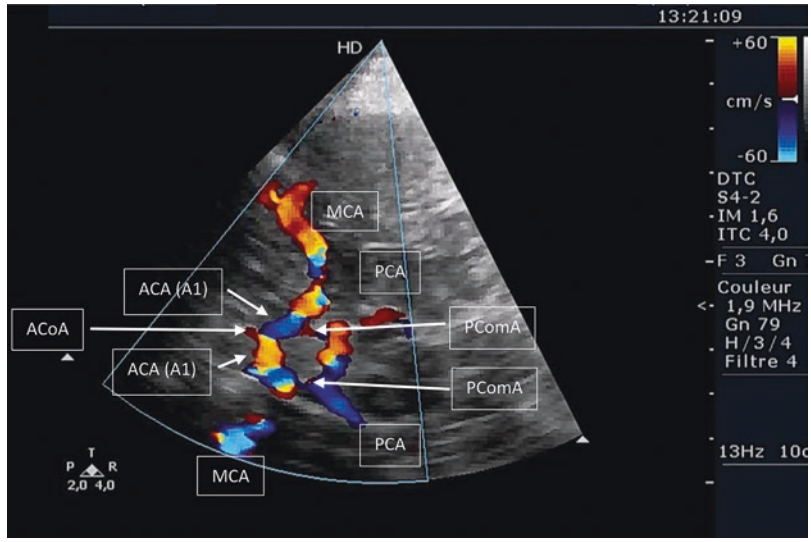

Fig. 17.15 Willis circle. *ACoA* anterior communicating artery, *ACA* anterior cerebral artery, *MCA* middle cerebral artery, *PCA* posterior cerebral artery, *PComA* posterior communicating artery. On colour E-TCD (Echo-transcranial Doppler) imaging, the two ACA branches can sometimes overlap or appear to merge, making the ACoA even less visible

17.5 Different Velocities Measurement and Index Calculation

The E-TCD measures the circulatory velocities of blood flow in the different proximal cerebral arteries (Table 17.1). From these velocities, indices are calculated that reflect the state of cerebral perfusion as well as that of vascular resistance.

Circulatory velocities expressed in centimetres per second do not correspond to cerebral blood flow (CBF). CBF measurement by DTC requires knowledge of the vascular diameter, which in clinical practice is currently not possible. However, apart from situations of vasospasm (vasospasm of SAH, inflammatory or infectious vasculitis), the velocities go in the same direction as the CBF. In contrast to extracranial arteries, the pulsatility of cerebral arteries is low because of near-laminar flow in these vessels under normal conditions. This is explained by the fact that the brain, a noble organ par excellence, is perfused continuously. Hence the need for a high diastolic velocity, in contrast to what is observed in musculocutaneous arteries. Changes in cerebral compliance, arterial diameter and/or haemodynamic conditions generate variations in the pulsatility of endocranial arteries assessed by three indices calculated from velocities. These are: (1) Pulsatility Index (PI); (2) Resistance index (RI); (3) Lindegaard index (LI).

Table 17.1 Normal arterial velocities

Artery	Systolic velocity cm/s	Diastolic velocity cm/s	Mean velocity cm/s
Internal carotid artery (ICA)	40–100	25–40	40–60
Middle cerebral artery (MCA)	90–130	40–60	55–70
Anterior cerebral artery (ACA)	70–110	30–50	50–60
Posterior cerebral artery (PCA)	40–80	20–40	40–50
Vertebral artery (VA)	40–80	20–40	30–40
Basilar artery (BA)	55–85	20–40	30–40

17.5.1 Normal Velocities

The use of colour Doppler in modern ultrasound devices simplifies the identification of arteries and allows for easier recognition of anatomical variations and pathological changes in blood flow. Overall, the passage emphasizes the impor-

tance of technology in improving the accuracy and ease of performing ultrasound imaging.

17.5.2 Pulsatility Index (Gosling Index): PI

The Pulsatility Index (PI) or Gosling index is a measure of the pulsatility of blood flow in the cerebral vessels and is widely used in clinical practice to evaluate intracranial pressure (ICP) and cerebral perfusion [2–4]. It is calculated as the difference between the systolic and diastolic velocities divided by the mean velocity of the MCA. The PI measurement is not affected by the insonation angle and is therefore a reliable index of cerebral perfusion.

An increase in PI above 1.3, accompanied by a diastolic velocity of less than 25 cm/s, is suggestive of cerebral hypoperfusion. This may be due to low blood pressure, insufficient cerebral perfusion pressure (CPP), hypocapnia or intracranial hypertension (ICH). On the other hand, a low PI is not always indicative of normal cerebral perfusion. In conditions such as vasospasm or extracranial arterial stenosis, the PI may be lower than normal despite compromised cerebral perfusion (Figs. 17.16 and 17.17).

$$\text{Pulsatility Index PI}\left(\text{Gosling index}\right) = \frac{\text{Systolic velocity} - \text{Diastolic velocity}}{\text{Mean velocity}} 0.9 \pm 0.20$$

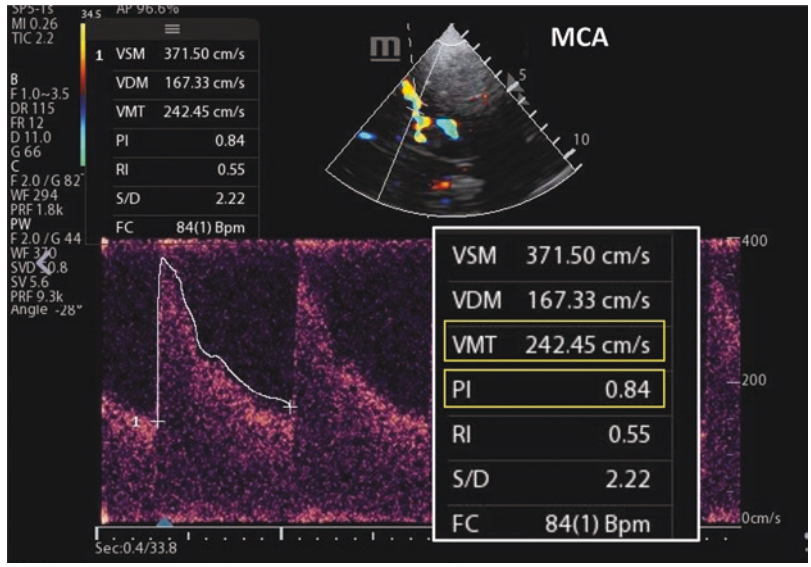

Fig. 17.16 Severe arterial vasospasm of MCA with high ischaemic risk but with a normal PI

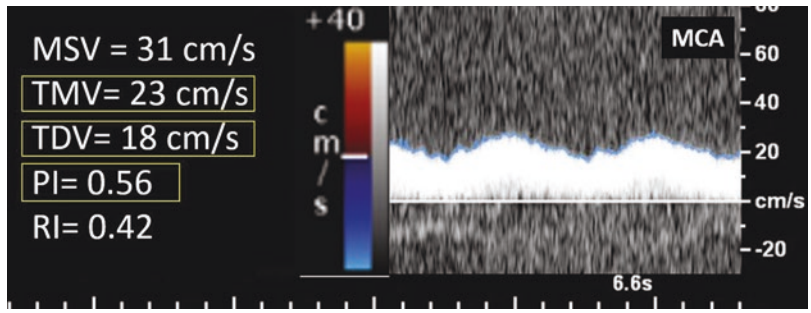

Fig. 17.17 TCD of MCA (middle cerebral artery) irrigated by ipsilateral ICA (internal carotid artery) site of dissection at its cervical portion

17.5.3 Resistance Index (Pourcelot Index): RI

It is an index used for the quantification of arterial stenoses. It is obtained by the difference between the systolic velocity and the diastolic velocity divided by the systolic velocity. It is less used by anaesthetists–resuscitators. In different studies, PI seems better than RI in the evaluation of ICP and cerebral perfusion in traumatic brain injury patients [5].

$$\text{Resistance Index}\left(\text{Pourcelot index}\right) = \frac{\text{Systolic velocity} - \text{Diastolic velocity}}{\text{Systolic velocity}} 0.5 \pm 0.08$$

17.5.4 Lindegaard or Aaslid Index (LI or AI): LI

This index is calculated when the average velocities of the ACM exceed 120 cm/s. It represents the ratio of the average velocity of the MCA to that of the ipsilateral ICA, measured at the cervical level. It helps to differentiate between vasospasm and hyperaemia. Indeed, a Lindegaard index of less than 3 would be in favour of hyperaemia, while a value above 3 would suggest vasospasm. Above 6, it not only confirms the vasospasm but also indicates its severe nature [6]. This index has been modified and adapted to the vertebro-basilar circulation with the ratio of the mean velocity of the basilar trunk to that of the extracranial vertebral artery. There is vasospasm when the modified Lindegaard index (ILm) is greater than 2. An ILm greater than 3 suggests severe vasospasm [7] (Fig. 17.18).

$$\text{Lindegaard index}\left(\text{Aaslid index}\right) = \frac{\text{MCA Mean velocity}}{\text{Ipsilateral cervical ICA Mean velocity}} < 3$$

$$\text{Modified Lindegaard index mLI} = \frac{\text{MCA Mean velocity}}{\text{Ipsilateral cervical ICA Mean velocity}} < 2$$

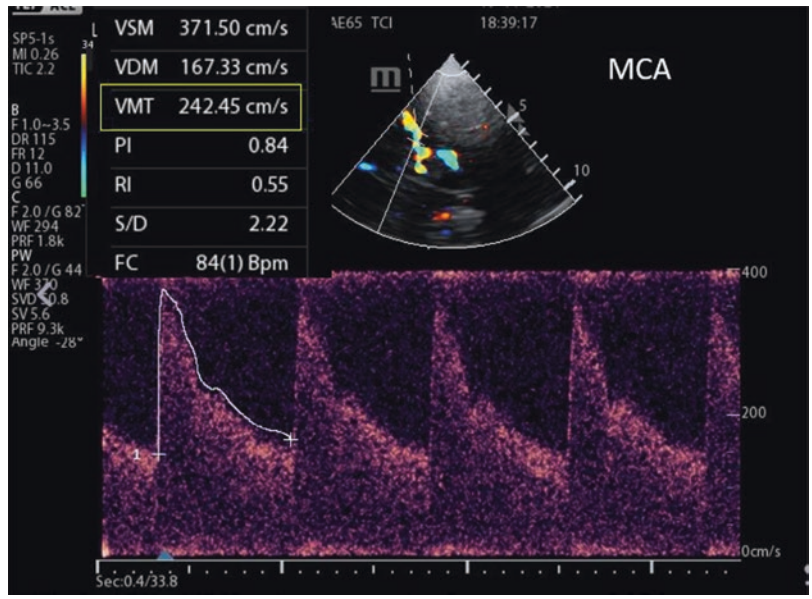

Fig. 17.18 MCA (middle cerebral artery) vasospasm

17.6 Exploration of Vascular Reactivity

17.6.1 Vascular Reactivity to Arterial Pressure: *Cerebral Pressure Autoregulation*

Pressure autoregulation [8, 9] is a specific physiological characteristic of cerebral circulation. Between 50 and 150 mmHg cerebral perfusion pressure (CPP), cerebral blood flow (CBP) remains constant (Fig. 17.19). This is the autoregulation plateau. On this plateau, the progressive increase in CPP is accompanied by an increase in cerebral vascular resistance (CVR) which ensures the constancy of the CBF. This increase in cerebral vascular resistance (CVR) leads to a decrease in cerebral blood volume (CBV) (Fig. 17.20). This property of cerebral circulation can be used to lower intracranial pressure in case of low compliance in brain-damaged patients. However, there are pathological situations where autoregulation is absent. In this case, an increase in blood pressure is accompanied by an increase in ICP. Autoregulation can be tested at the patient's bedside with E-TCD. The presence or absence of this makes it possible to adapt the treatments. In clinical practice, autoregulation is assessed by variations in ICP under the effect of the progressive increase in CPP by norepinephrine (Fig. 17.21). It can also be tested by compressing the cervical carotid artery for a few seconds, causing a collapse in velocities (low blood flow). The lifting of the compression is accompanied by a transient increase in the circulatory velocities measured at the level of the ipsilateral MCA, above from those measured before carotid compression, with a return to normal. This phenomenon of transient hyperaemia, accompanied by a return to pre-compression velocities, reflects normal vascular reactivity or autoregulation. The absence of this transient hyperaemia after lifting the compression is in favour of the absence of autoregulation.

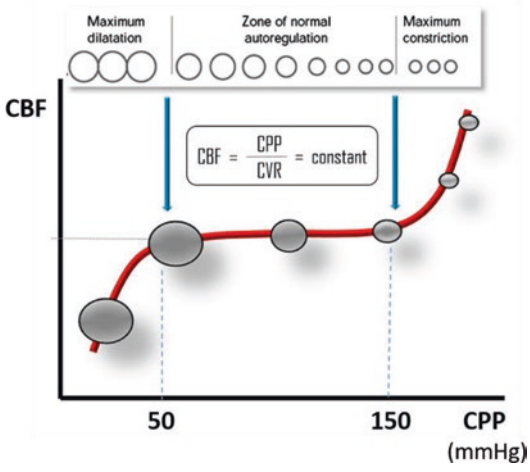

Fig. 17.19 Autoregulation plateau. Between 50 and 150 mmHg of PPC, the CBF remains constant due to an increase in CVR

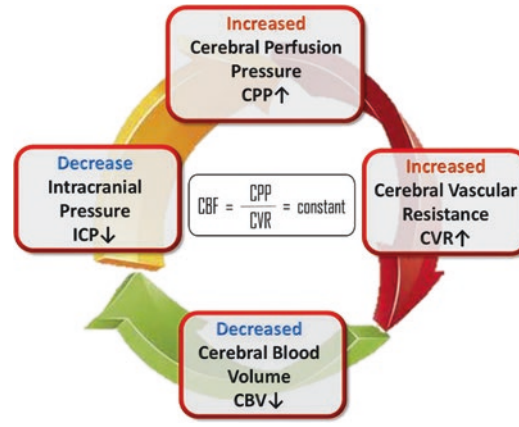

Fig. 17.20 Effects of increasing CPP on ICP, CVR and CBV

Authors have shown that autoregulation can be monitored continuously in patients on mechanical ventilation by using software which analyses simultaneously the relation between IPC and CPP. This relation is called PRx (Pressure reactivity index) [10]. The PRx is the slope of the linear regression line linking the ICP and the CPP. It varies between +1 and −1. The optimal PPC corresponds to the lowest PRx, i.e. which is close to −1.

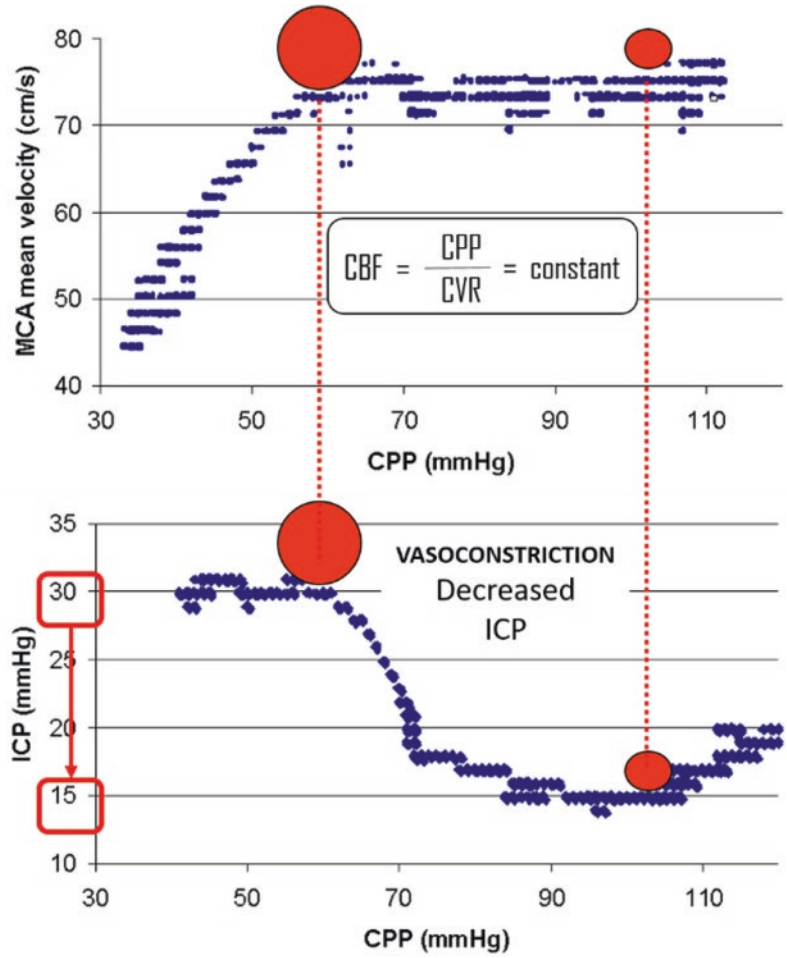

Fig. 17.21 Example of ICP drop in a patient with intracranial hypertension. The increase in the CPP beyond 50 mmHg does not modify the velocities at the TCD (plateau), whereas the ICP decreases

17.6.2 Cerebrovascular Reactivity to Au CO_2

Under physiological conditions, the variation of $PaCO_2$ leads to a variation of the RVC, but also of the CBF. Hypercapnia leads to an increase in VSC (vasodilation) as well as an increase in cerebral blood flow (CBF) [11, 12]. Conversely, hypocapnia leads to a decrease in VSC (vasoconstriction) and a decrease in DSC. Thus, hyperventilation in a patient with intracranial hypertension (ICH) leads to a reduction in ICP [13] by vasoconstriction secondary to a lowered $PaCO_2$ but also increases the risk of cerebral ischaemia by lowering CBF. The E-TCD makes it possible to objectify this drop in CBF with a slowdown in the average velocity of the MCA (Figs. 17.22 and 17.23).

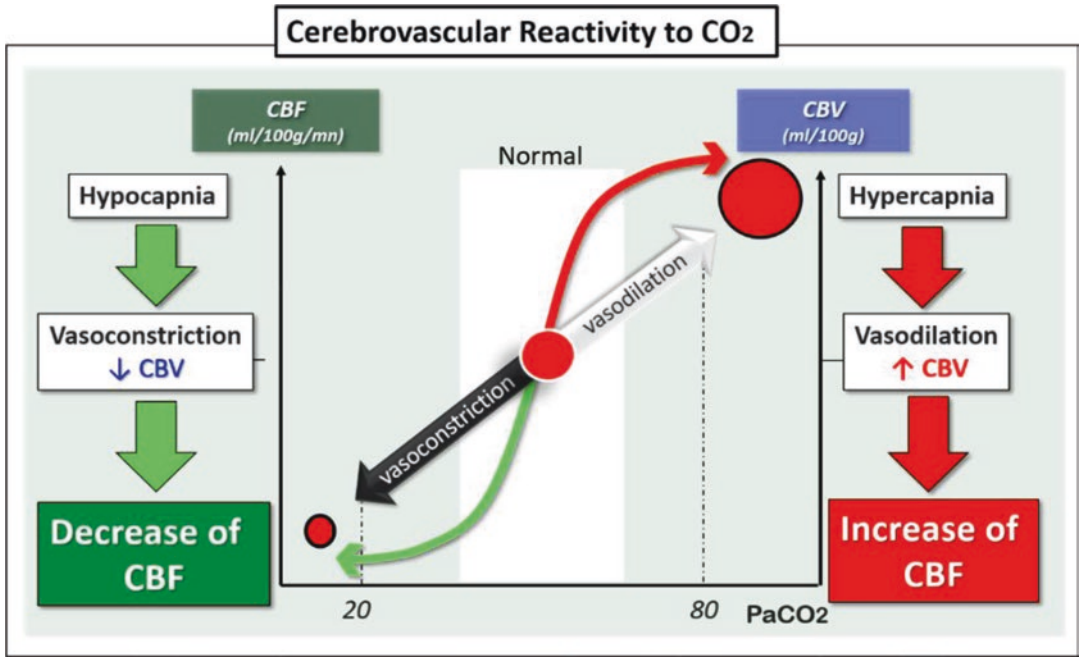

Fig. 17.22 Schematic representation of cerebrovascular reactivity. *CBV* cerebral blood volume, *CBF* cerebral blood flow

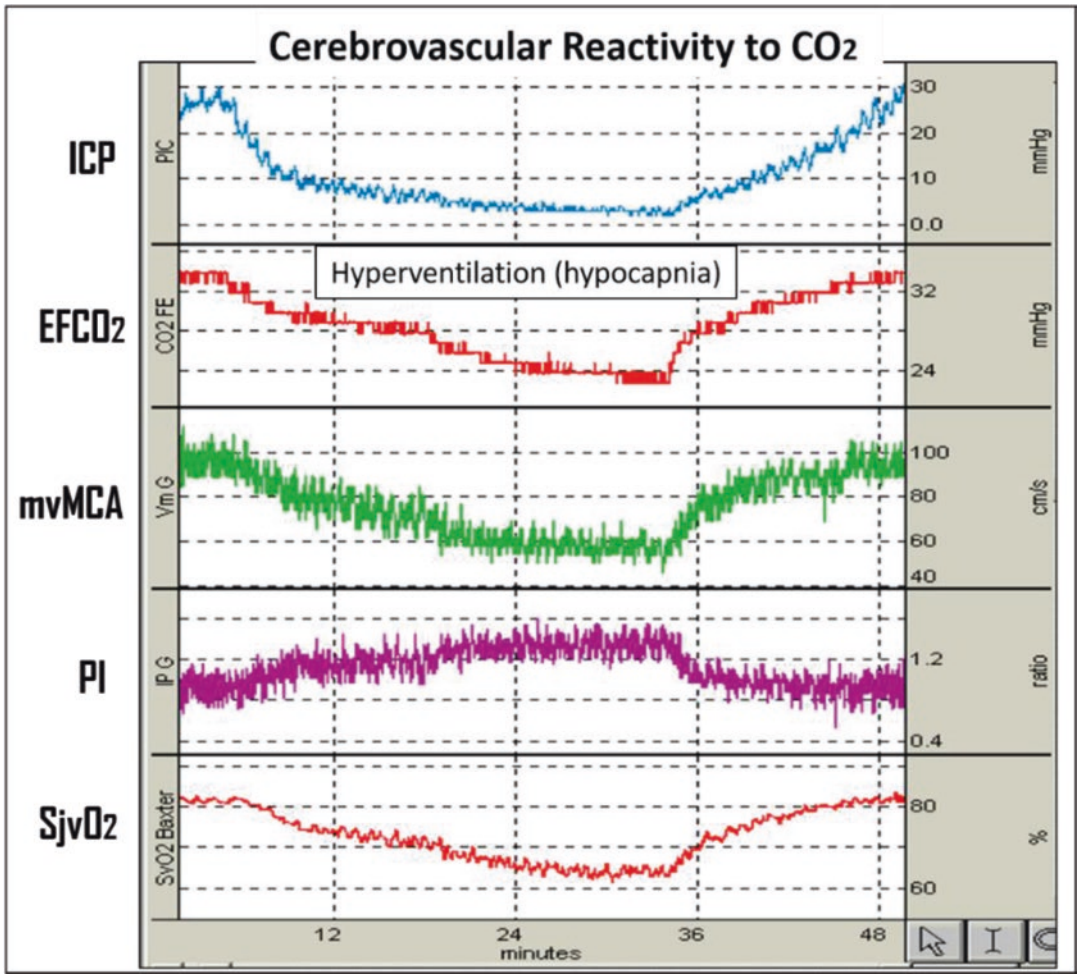

Fig. 17.23 Example of hyperventilation in a severe traumatic brain injury patient with intracranial hypertension. Hypocapnia induces a drop in ICP which is accompanied by a reduction in MCA velocities, an increase of PI and a drop in $SjvO_2$, in favour of CBF reduction

17.7 Pathological Situations

Different cerebrovascular pathological situations can be detected by TCD. This can allow the implementation of a treatment or its optimization and even justify the realization of imaging.

17.7.1 Hypoperfusion Situation

The alteration of the cerebral perfusion can be induced by an insufficient CPP, by a hypocapnia or an intracranial hypertension. In this situation, the TCD shows the increase in PI (>1.3) associated with à drop in diastolic velocity (<25 cm/s).

Studies, carried out mainly in mild to moderate cranial trauma patients, have shown a correlation between these values of PI and DV and an unfavourable evolution. In this situation, the E-TCD makes it possible to predict the evolution of patients as soon as they arrive at the hospital and identify those who require monitoring and rapid treatment [14, 15]. However, a normal PI does not rule out cerebral hypoperfusion.

Cerebral arterial vasospasm and arterial dissection at the level of the cervical vessels lead to a situation of ischaemia with normal PI (Figs. 17.16 and 17.17).

17.7.2 Hyperaemia and Hyperaemia Syndrome

In the brain-injured patient, impaired autoregulation can lead to intracranial hyperaemia and hypertension [16], which has a different therapeutic strategy from ischaemia. Carotid surgery, as well as the treatment of arteriovenous malformations, is frequently accompanied by hyperaemia. This is a normal situation and without consequence on the brain. On the other hand, the occurrence of a hyperaemia syndrome is often accompanied by cerebral oedema responsible for intracranial hypertension which may be poorly tolerated clinically. The Doppler velocities, in this case, are significantly accelerated with a well-defined envelope and a dense wave. This reflects a very large circulating globular mass contrary to what is observed in vasospasm. The Lindegaard or Aaslid index, described above, makes it possible to differentiate between hyperaemia and vasospasm, as will be seen later.

17.7.3 Vasospasm

Delayed cerebral ischaemia is very dreaded after subarachnoid haemorrhage. Cerebral arterial vasospasm is one of the main causes. It usually occurs between the 4th and 12th day following the haemorrhage. Its research by a daily realization of a transcranial Doppler must be systematic [17]. In the event of an increase in velocities at the level of the MCA above 120 cm/s, the Lindegaard index, also called Aaslid index, makes it possible to determine whether it is a vasospasm or a hyperaemia. A ratio greater than 3 suggests vasospasm (Fig. 17.24), while an index less than 3 suggests hyperaemia. This index is especially validated for the middle cerebral artery. It has also been applied to the vertebro-basilar circulation, when the average velocities of the basilar artery exceed 80 cm/s. In this case, the modified Lindegaard index (mLI) is the ratio between the average velocity of the basilar artery divided by the dominant vertebral artery at the cervical level. This ratio is considered in favour of a vasospasm when it is greater than 2.

17.7.4 Brain Death

The evolution towards a state of brain death secondary to a refractory ICH, results in the DTC by a collapse of the circulatory velocities. The systolic velocities of the MCA decrease sharply while its diastolic velocities reverse (Fig. 17.25). This is the “back-flow” or “reverse flow” which signals cerebral circulatory arrest. The persistence of a systolic speed before its complete disappearance corresponds to what is called angiographically “aspect of a dead tree.” In this case, vascular imaging shows opacification of the cerebral arteries with absence of cerebral venous network opacification.

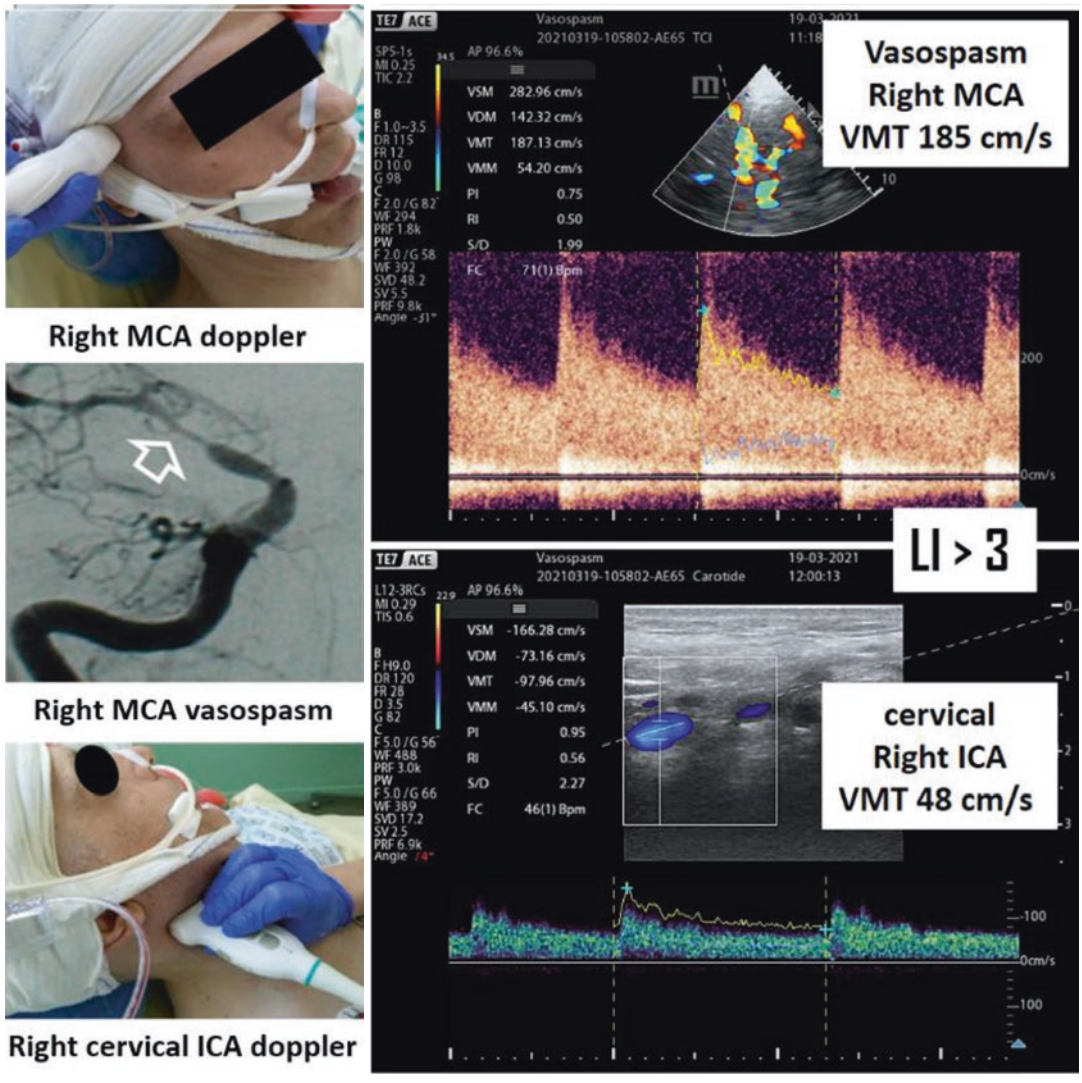

Fig. 17.24 *LI* Lindegaard index, *ICA* internal carotid artery, *MCA* middle cerebral artery

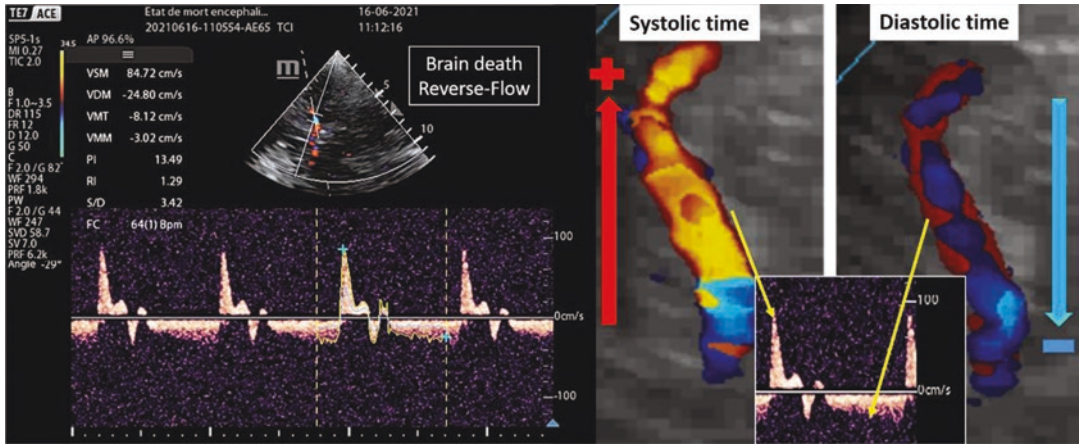

Fig. 17.25 E-TCD of brain death. Reverse diastolic flow. MCA velocities: Positive systolic velocity and negative diastolic velocity

17.8 Other Situations

17.8.1 Patent Foramen Ovale

The search for the patent foramen ovale (PFO) is usually done by echocardiography. The E-TCD is a tool capable of detecting the PFO [18] or an intrapulmonary shunt [19]. The research procedure is identical to that used in echocardiography. It consists of producing small bubbles by putting 1 mL of air in a syringe containing 9 mL of 0.9% sodium chloride or a colloid that is passed several times and recovered with a tap into an empty syringe. The millilitre of air disperses and forms an emulsion of very small bubbles. This "solution" is immediately injected intravenously. At the same time, the E-TCD examination, attached to the MCA, analyses the circulatory flow. The procedure is done without and with Valsalva manoeuvre. The appearance of high-intensity transient signals (HITS) which traverse the Doppler flow wave vertically indicates the existence of a PFO or an intrapulmonary shunt (Fig. 17.26).

17.8.2 Carotid Artery Dissection

Internal carotid dissection leads to a modification of the direction of the circulatory flow of certain arteries of the circle of Willis (Fig. 17.27). Indeed, a dissection of the ICA on a normal circle of Willis leads to a reversal of the direction of flow of the ipsilateral ACA, which becomes positive. Since the A1 segment of this artery is no longer supplied directly by the ICA, it is taken up in countercurrent by the contralateral ACA via the anterior communicating artery. On the E-TCD, in addition to the disappearance of the ICA, the ipsilateral ACA appears positive in continuity with the MCA. On the other hand, the posterior communicating artery returns forward, thus reversing its flow and becoming positive. It is supplied by the ipsilateral posterior cerebral artery (Fig. 17.28). Finally, the ophthalmic artery also reverses, its flow is negative because it is in countercurrent supplied by a branch of the external carotid artery. The change of this artery makes it possible to locate the level of the dissection which in this situation is located below the carotid siphon (Fig. 17.29).

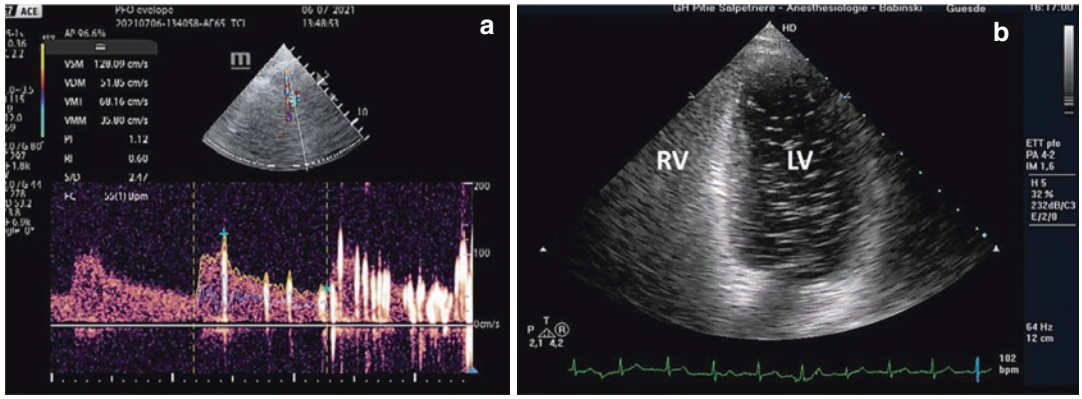

Fig. 17.26 (**a**) High-intensity transient signals; (**b**) *RV* right ventricle, *LV* left ventricle. Note the presence of bubbles in the right ventricle (normal), and the abnormal presence of bubbles in the left ventricle

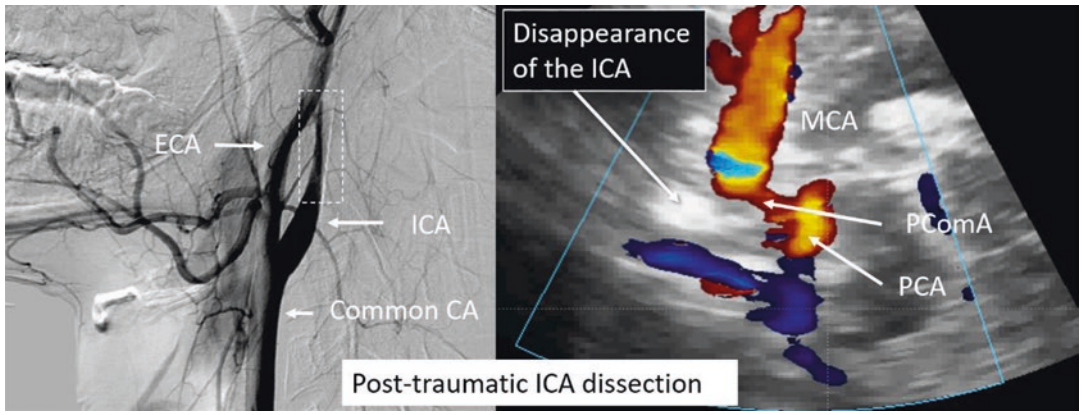

Fig. 17.27 Post-traumatic ICA dissection. *ECA* external carotid artery, *Common CA* common carotid artery

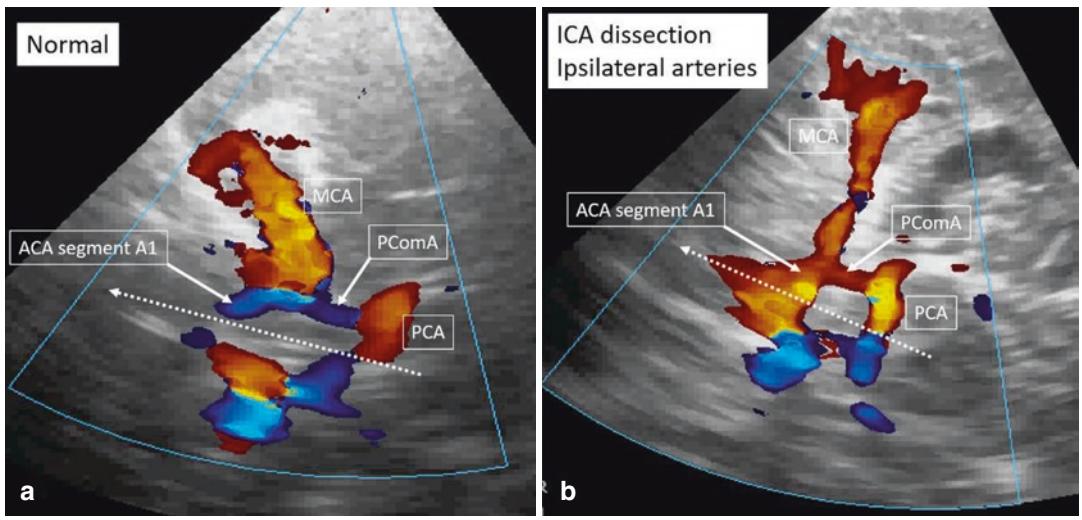

Fig. 17.28 (**a**) Normal circle of Willis. (**b**) Circle of Willis after traumatic CI dissection

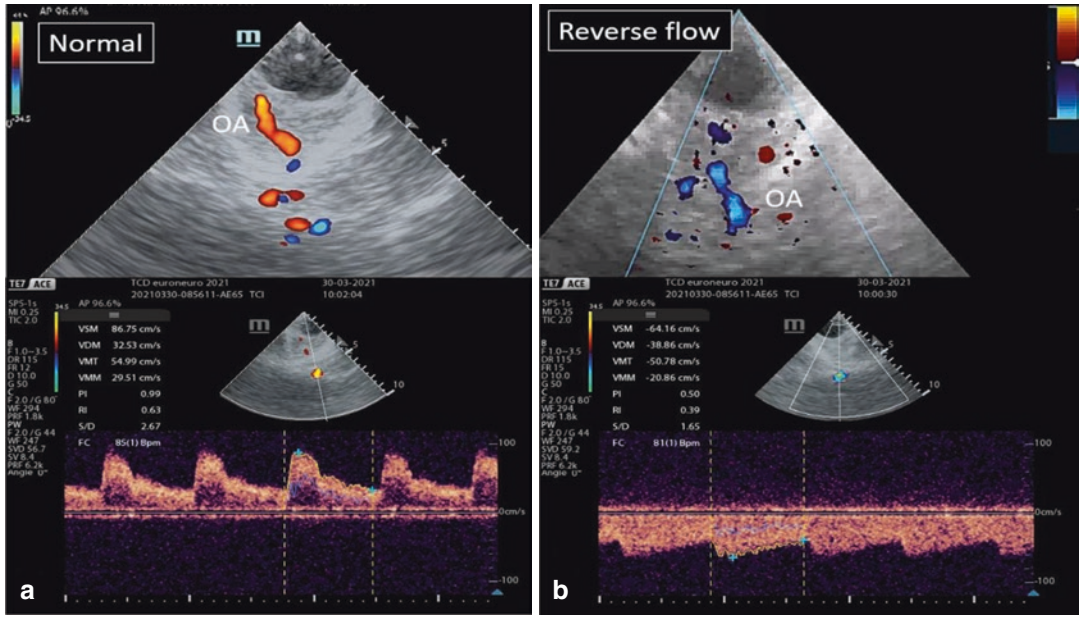

Fig. 17.29 (**a**) Normal flow of ophthalmic artery (OA). (**b**) Reverse flow after traumatic ICA dissection

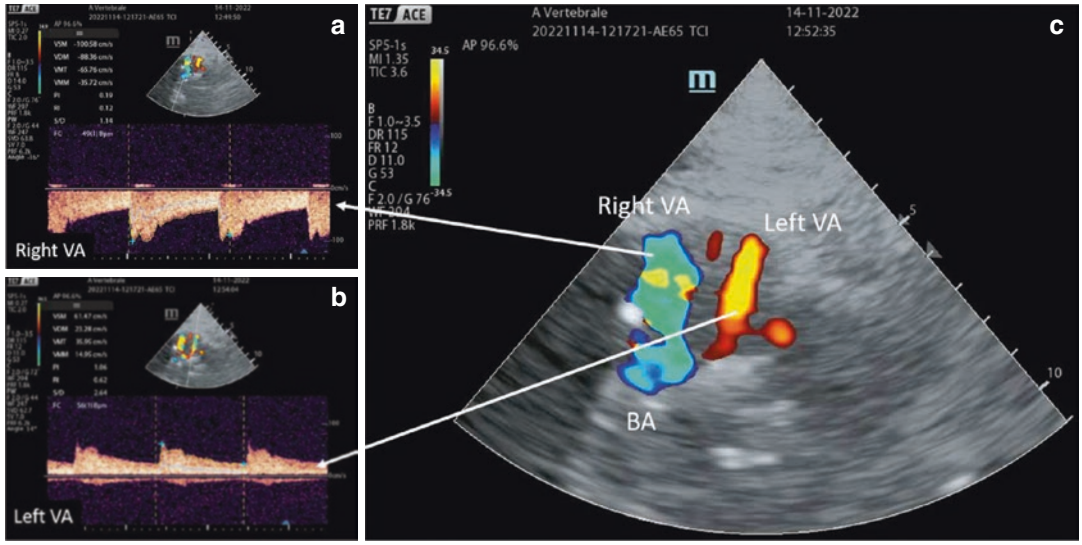

Fig. 17.30 (**a**) Right VA = normal flow (negative), (**b**) Left VA = reverse flow (positive) due to vertebral arterial dissection in the neck, (**c**) Colour Doppler of vertebral arteries

17.8.3 Vertebral Artery Dissection

Dissection of the cervical vertebral artery leads to an interruption of flow downstream of the artery. At the E-DTC, the V4 portion, which is intracranial, is perfused retrogradely by the contralateral vertebral artery which at the same time perfuses the basilar artery (Fig. 17.30).

17.8.4 Carotidcavernous Fistula

It is not uncommon for a craniofacial trauma to be complicated by a carotidcavernous fistula. Dissection of the carotid in its intracavernous segment causes communication between the internal carotid artery and the cavernous sinus. This results in a great turbulence of the flow at the level of the base of the skull within the E-DTC colour, a large vascular puddle formed of a mosaic of red and blue colours (Fig. 17.31). By scanning this area, it is possible to find the fistula (the hole between ICA and cavernous sinus) thanks to the flow which crosses it with high velocities (Fig. 17.32).

17.8.5 Venous Sinus Thrombosis

With experience, the sinus venous network of the brain becomes accessible. It is then possible to visualize venous thrombosis affecting in particular the transverse sinuses (Fig. 17.33), the confluence, or the sagittal sinus.

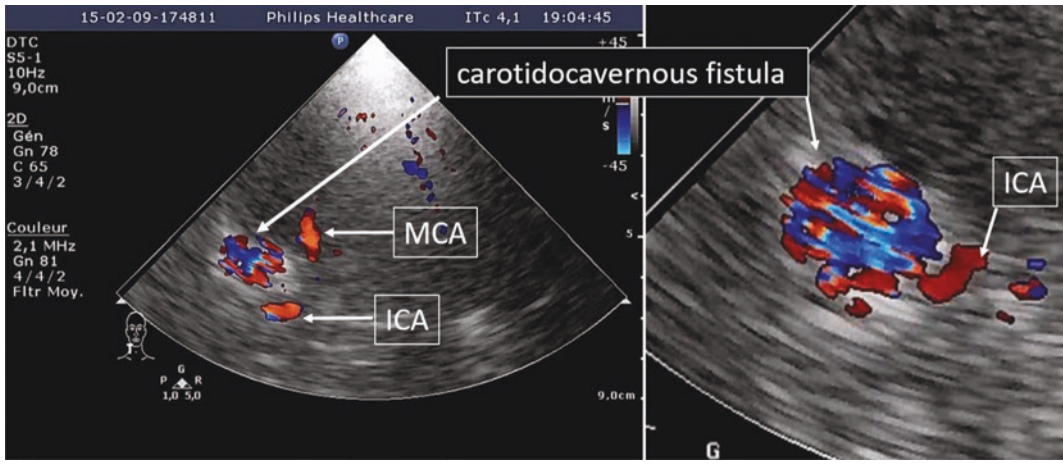

Fig. 17.31 Carotidocavernous fistula. *MCA* middle cerebral artery, *ICA* internal carotid artery

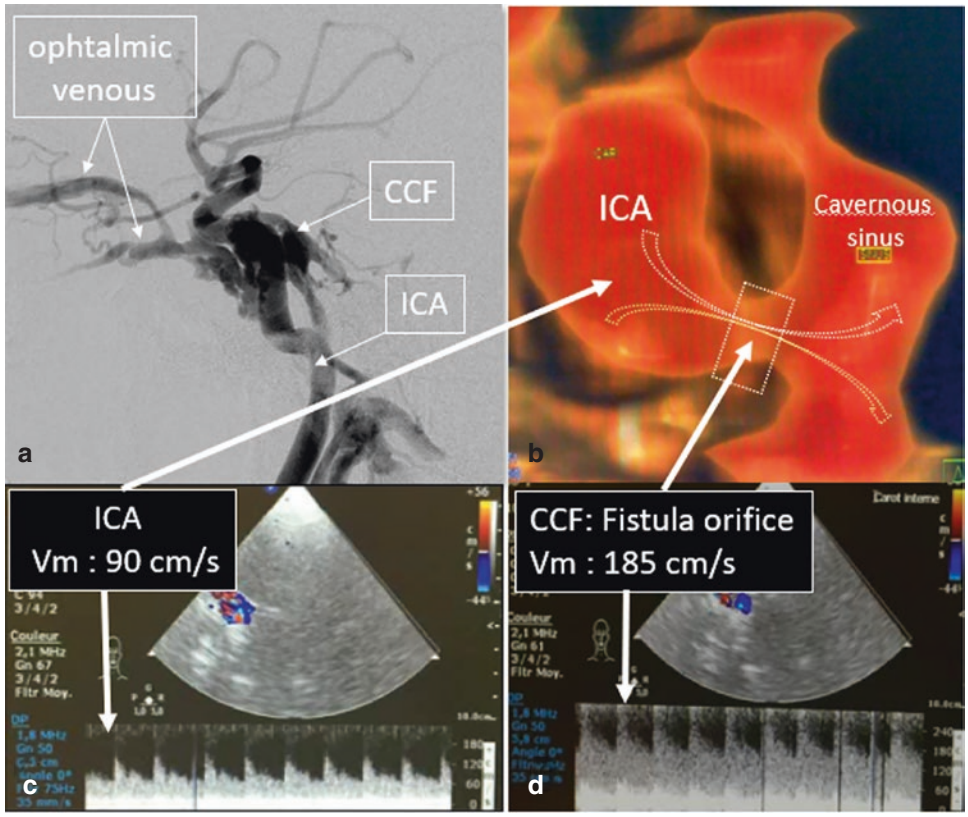

Fig. 17.32 (**a**) Angiography of carotidocavernous fistula (CCF). (**b**) Three-dimensional Angiography of CCF. (**c**) Vm: mean velocities in the ICA, the arrow shows the fistulous orifice on picture **b**. (**d**) Vm: mean velocities in the hole of the fistula (hole between ICA and cavernous sinus)

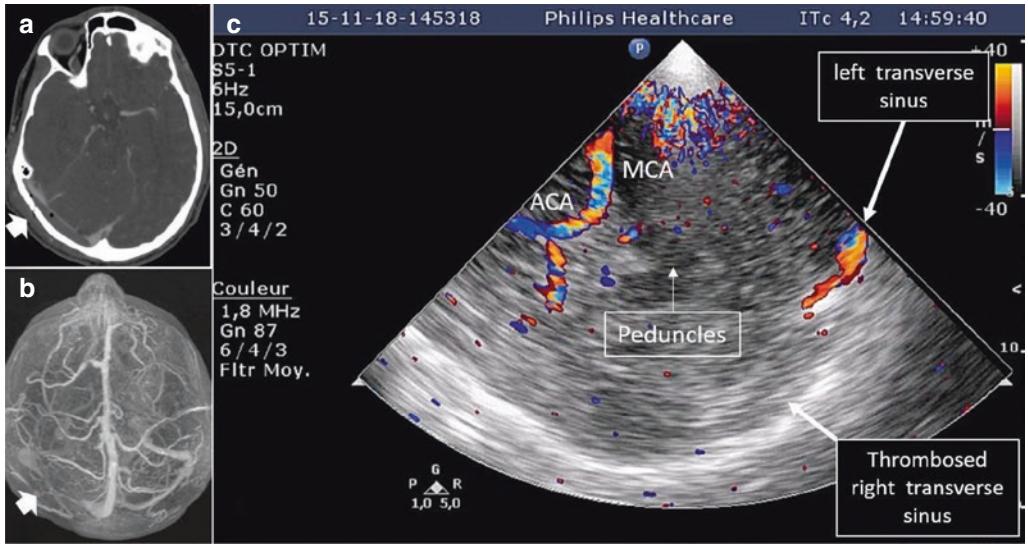

Fig. 17.33 (**a**) Fracture next to the right transverse sinus with the presence of an air bubble. (**b**) Venous angiography which shows an absence of opacification of the right transverse sinus. (**c**) Absence of the right transverse sinus on the colour TCD

17.9 Conclusions

E-DTC is the simplest and most useful tool in neuro-resuscitation today. Mastering this exam does not take much time. In addition, it provides information that helps to determine the haemodynamic status of the brain and to adapt therapies and judge the advisability of possibly resorting to other monitoring tools, most often invasive. The E-DTC does not make it possible to dispense with the monitoring of intracranial hypertension.

References

1. Lau VI, Arntfield RT. Point-of-care transcranial Doppler by intensivists. Crit Ultrasound J. 2017;9(1):21.
2. Bellner J, Romner B, Reinstrup P, Kristiansson KA, Ryding E, Brandt L. Transcranial Doppler sonography pulsatility index (PI) reflects intracranial pressure (ICP). Surg Neurol. 2004;62(1):45–51.
3. de Riva N, Budohoski KP, Smielewski P, Kasprowicz M, Zweifel C, Steiner LA, et al. Transcranial Doppler Pulsatility Index: what it is and what it isn't. Neurocrit Care. 2012;17(1):58–66.
4. Czosnyka M, Czosnyka Z, Smielewski P. Pressure reactivity index: journey through the past 20 years. Acta Neurochir. 2017;159(11):2063–5.
5. Kaloria N, Panda NB, Bhagat H, Kaloria N, Soni SL, Chauhan R, et al. Pulsatility index reflects intracranial pressure better than resistive index in patients with clinical features of intracranial hypertension. J Neurosci Rural Pract. 2020;11(1):144–50.
6. Aaslid R, Huber P, Nornes H. Evaluation of cerebrovascular spasm with transcranial Doppler ultrasound. J Neurosurg. 1984;60(1):37–41.
7. Sviri GE, Ghodke B, Britz GW, Douville CM, Haynor DR, Mesiwala AH, et al. Transcranial Doppler grading criteria for basilar artery vasospasm. Neurosurgery. 2006;59(2):360–6.
8. Meng L, Gelb AW. Regulation of cerebral autoregulation by carbon dioxide. Anesthesiology. 2015;122(1):196–205.
9. Drummond JC. Blood pressure and the brain: how low can you go? Anesth Analg. 2019;128(4):759–71.
10. Pochard J, Vigué B, Dubreuil G, Rodrigues A, Descorps-Déclère A, Duranteau J. Comparison of pressure reactivity index and mean velocity index to evaluate cerebrovascular reactivity during induced arterial blood pressure variations in severe brain injury. Neurocrit Care. 2021;34(3):974–82.
11. McDonnell MN, Berry NM, Cutting MA, Keage HA, Buckley JD, Howe PRC. Transcranial Doppler ultrasound to assess cerebrovascular reactivity: reliability, reproducibility and effect of posture. PeerJ. 2013;1:e65.
12. Reinstrup P, Ryding E, Asgeirsson B, Hesselgard K, Unden J, Romner B. Cerebral blood flow and transcranial Doppler sonography measurements of CO2-reactivity in acute traumatic brain injured patients. Neurocrit Care. 2014;20(1):54–9.
13. Godoy DA, Rovegno M, Lazaridis C, Badenes R. The effects of arterial CO2 on the injured brain: two faces of the same coin. J Crit Care. 2021;61:207–15.
14. Ract C, Le Moigno S, Bruder N, Vigué B. Transcranial Doppler ultrasound goal-directed therapy for the early management of severe traumatic brain injury. Intensive Care Med. 2007;33(4):645–51.
15. Bouzat P, Francony G, Declety P, Genty C, Kaddour A, Bessou P, et al. Transcranial Doppler to screen on admission patients with mild to moderate traumatic brain injury. Neurosurgery. 2011;68(6):1603–10.
16. Muttaqin Z, Uozumi T, Kuwabara S, Arita K, Kurisu K, Ohba S, et al. Hyperaemia prior to acute cerebral swelling in severe head injuries: the role of transcranial doppler monitoring. Acta Neurochir. 1993;123(1–2):76–81.
17. Aaslid R. Transcranial Doppler assessment of cerebral vasospasm. Eur J Ultrasound. 2002;16(1–2):3–10.
18. Van der Giessen H, Wilson LC, Coffey S, Whalley GA. Review: detection of patient foramen ovale using transcranial Doppler or standard echocardiography. Australas J Ultrasound Med. 2020;23(4):210–9.
19. de Havenon A, Moore A, Sultan-Qurraie A, Majersik JJ, Stoddard G, Tirschwell D. Ischemic stroke patients with active malignancy or extracardiac shunts are more likely to have a right-to-left shunt found by TCD than echocardiogram. Transl Stroke Res. 2015;6(5):361–4.

Renal Ultrasound

18

Nurul Shaliza Shamsudin,
Muhammad Faiz Baherin, and Nurul Liana Roslan

18.1 Introduction

Point-of-care ultrasound (POCUS) has made ground-breaking changes in patient care. Physicians from various disciplines have extensively used it to complement clinical assessment for a more accurate and rapid evaluation of an illness. POCUS provides a real-time image acquisition that will give profound insight into clinical disease.

Renal POCUS has emerged as one of the most valuable tools in diagnosing certain conditions in the last decade. It is non-invasive and radiation-free, and renal POCUS can be performed quickly at the bedside for accurate diagnosis. It has been widely used in the emergency department (ED), critical care unit, and wards.

The accuracy of renal POCUS as an adjunct in clinical assessment has been validated in many studies. For instance, a prospective observational study by Nepal, Dachsel, and Smallwood revealed that physicians with training in the POCUS curriculum could identify the presence or absence of hydronephrosis with a sensitivity of 90%, specificity of 100%, positive predictive value of 100%, and a 99% negative predictive value [1]. POCUS is an excellent alternative to formal renal ultrasound.

Furthermore, in another study by Pathan et al. on the accuracy of emergency physician (EP) to grade hydronephrosis, consensus between EP and CT scans demonstrated a specificity of 94.6% for the detection of moderate or severe hydronephrosis [2].

POCUS is now the bedside tool of choice in evaluating patient's possible urinary system-related complaints, which may reveal renal stones, hydronephrosis, cysts, mass, and abscess. It is also performed to assess patients with acute kidney injury and as part of hemodynamic assessment during fluid resuscitation and optimization in the ED and critical care unit.

18.2 Sonoanatomy of the Kidney

The urinary tract system comprises the kidneys, ureters, bladder, and urethra. The kidneys are retroperitoneal organs and are located on the posterior abdominal wall. An adult kidney's mean average pole-to-pole length is 10–13 cm, and the left kidney is generally slightly longer than the right [3].

Each kidney consists of the outer cortex and the inner medulla, which contain 6–8 renal pyra-

N. S. Shamsudin
Emergency and Trauma Department, Hospital Sultan Idris Shah, Serdang, Selangor, Malaysia

M. F. Baherin
Emergency and Trauma Department, Hospital Tuanku Ja'afar, Seremban, Negeri Sembilan, Malaysia

N. L. Roslan (✉)
Emergency and Trauma Department, Hospital Kuala Lumpur, Kuala Lumpur, Malaysia

© The Author(s), under exclusive license to Springer Nature Switzerland AG 2024

N. Bouarroudj et al. (eds.), *POCUS in Critical Care, Anesthesia and Emergency Medicine*,
https://doi.org/10.1007/978-3-031-43721-2_18

mids and surrounding columns of cortical tissue. It also consists of the renal sinus, which includes the renal pelvis, calyces, renal vessels, nerves, lymphatics, and perirenal fat (Figs. 18.1 and 18.2). The renal complex is surrounded by a fascial layer called Gerota's fascia.

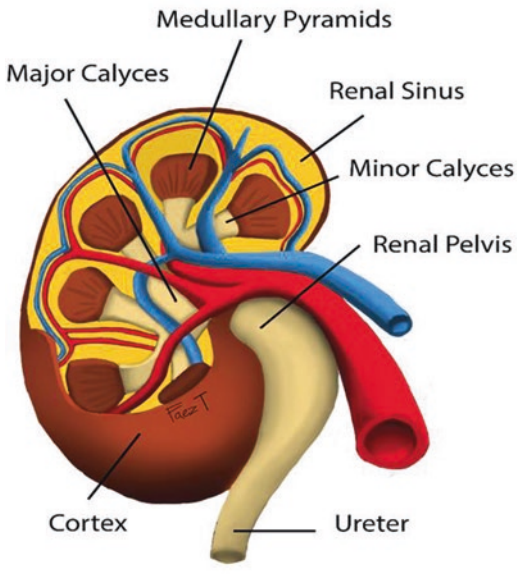

Fig. 18.1 Key renal structure

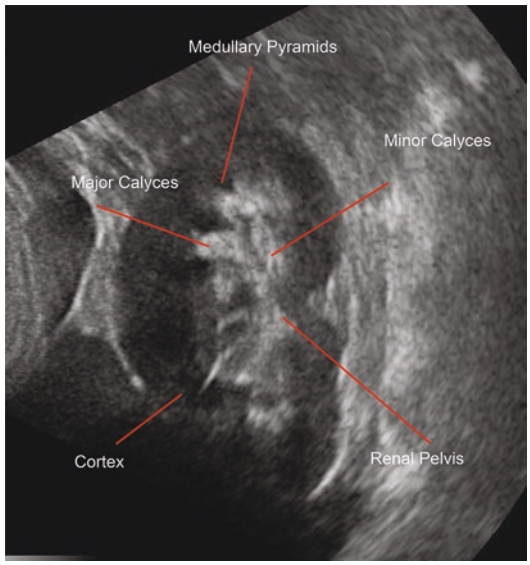

Fig. 18.2 Sonoanatomy of right kidney

18.3 Clinical Indications

Patients with possible urinary system-related problems may come with various complaints. They may present with hematuria, abdominal and back pain, dysuria, oliguria, and incontinence. Renal POCUS is a safe and rapid method to evaluate these presenting symptoms.

Renal POCUS can screen common pathologies related to the urinary system, such as renal calculi, mass, abscess, and hydronephrosis. Although ureteral stones may be difficult to visualize using POCUS, history and clinical assessment of renal colic with POCUS findings of hydronephrosis can confirm the diagnosis [4]. Diagnosis of nephrolithiasis by POCUS has a specificity of 70% and 75% using gold standard CT examination [5], and being radiation-free, decreases cumulative radiation exposure [6].

Renal POCUS can be adapted to the treatment pathway of renal colic. POCUS may help in the treatment direction as it can distinguish small and large calculi. Studies reveal that patients with mild hydronephrosis renal POCUS are less expected to have large calculi or require urologic intervention [7]. Patients with moderate to severe hydronephrosis are likely to have calculi of >5 mm in size [8].

In patients with abdominal and back pain and dysuria with signs and symptoms of infection such as chill, rigors, and fever, renal POCUS may help identify renal abscess. We may see a well-defined hypoechoic area within the cortex area or the corticomedullary parenchyma. In patients with suspected post-renal obstruction, ultrasound can measure bladder volume to evaluate post-void residual urine [9].

Renal POCUS has an essential role in hemodynamic assessment as well. By measuring renal arterial flow, we can look at the renal resistive index (RI) using Doppler mode. High RI in kidneys is associated with renal dysfunction and more adverse cardiovascular events. Venous congestion can also be assessed by measuring renal venous flow. Renal venous congestion status is beneficial in guiding fluid therapy in critically ill patients.

18.4 Preparation, Equipment, and Scanning Techniques

18.4.1 Patient and Machine Positioning

The most ergonomic way to perform renal ultrasound is to stand at the patient's right side and hold the probe with the right hand. The left hand manages the ultrasound controls. Ideally, the renal ultrasound is performed with the patient in the supine position. Decubitus, prone, and upright position may provide better ultrasound images of the kidneys as kidney is sometimes obscured by the bowel gas. Preferably, the exam is performed with either normal respiration or breath hold which allows the kidney to move inferiorly for better visualization [10].

18.4.2 Transducer Selection and Machine Setting

In the adult patient, a low frequency curvilinear 2–5 MHz probe is typically used, but ribs' shadows may obscure the ultrasound view. Ultrasound images from a curvilinear transducer will have higher resolution and may show greater details. A phased array 3.5–5 MHz probe with small footprint maybe used and allow easier navigation between the ribs (Fig. 18.3). A linear transducer with higher frequencies may be necessary to evaluate the children. The abdominal and renal preset is used for renal ultrasound examination. A depth of 15–20 cm is selected as starting depth that is suffice for most patients and can be adjusted as needed. Sonographic evaluation of the renal anatomy is easily performed using B-mode. Color or Power Doppler imaging can be used for evaluation of renal blood flow and identification of the vessels within the renal parenchyma (Fig. 18.4).

18.4.3 Scanning Technique

The kidneys and bladder are examined in longitudinal and transverse planes which is in accordance with American Institute of Ultrasound in Medicine (AIUM) practice guidelines [11]. When performing renal ultrasound, the kidneys specifically the cortex and renal pelvis, as well as perirenal regions should be assessed for abnormalities. The sonographic evaluation of the bladder is necessary part of renal ultrasound for evaluation of hydroureteronephrosis to evaluate for the presence of obstruction, to evaluate the bladder lumen and wall abnormalities as well as measurement of bladder volume.

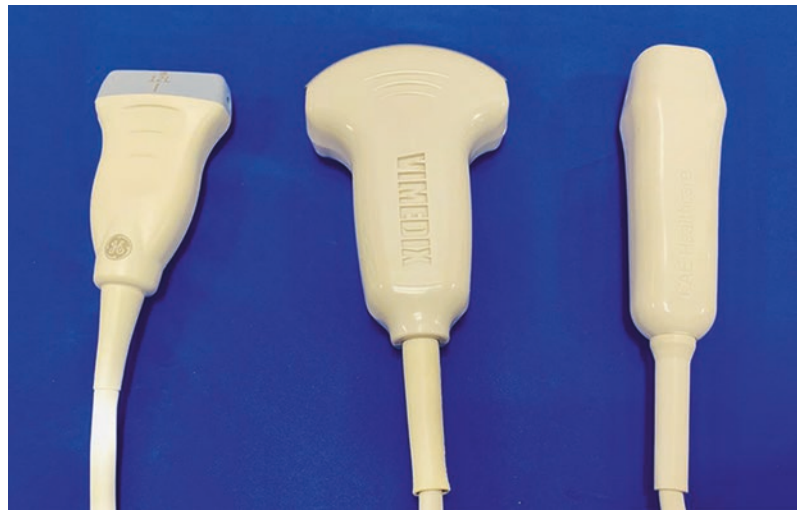

Fig. 18.3 Transducer selection for renal ultrasound

B Mode

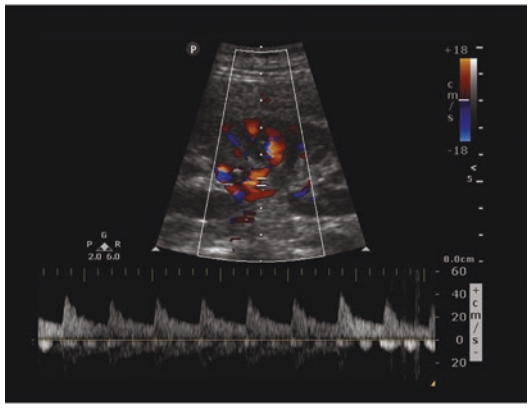

PW Doppler Mode

Fig. 18.4 Modes of renal ultrasound

18.5 Normal Sonographic Findings of Kidney, Ureter, and Bladder

Normal kidney and bladder on ultrasound will have the following characteristics [10]:

(a) Echogenic outer covering made up of Gerota's fascia and perinephric fat.
(b) Normal renal parenchyma is more hypoechoic when compared to the liver.
(c) The Renal cortex appears hypoechoic, saw-toothed ribbon deep to the margin of the cortex.
(d) Individual pyramids may or may not be visible as hypoechoic triangular structure within the medulla.
(e) The central renal sinus is hyperechoic which comprises the calyces, renal pelvis, and the major intrarenal vessels.
(f) Anechoic pockets or urine may be seen within calyces.
(g) The length of adult kidney is between 9 and 12 cm.
(h) The normal cortical thickness is generally >1 cm, which measures between renal surface and central hyperechoic renal sinus.
(i) Normal ureter is generally not well visualized on ultrasound, but when distended may appear as a tubular structure from the kidney.
(j) The bladder wall appears as an echogenic line with an anechoic cavity of fluid-filled bladder.
(k) Normal bladder has a thick, smooth muscular wall measuring 3–5 mm. Fluid filled bladder has a lesser wall thickness of 2–3 mm.
(l) Intermittent urethral flow jets can be observed near trigone area in patients with normal hydration.

18.5.1 Renal Ultrasound Landmark Summary

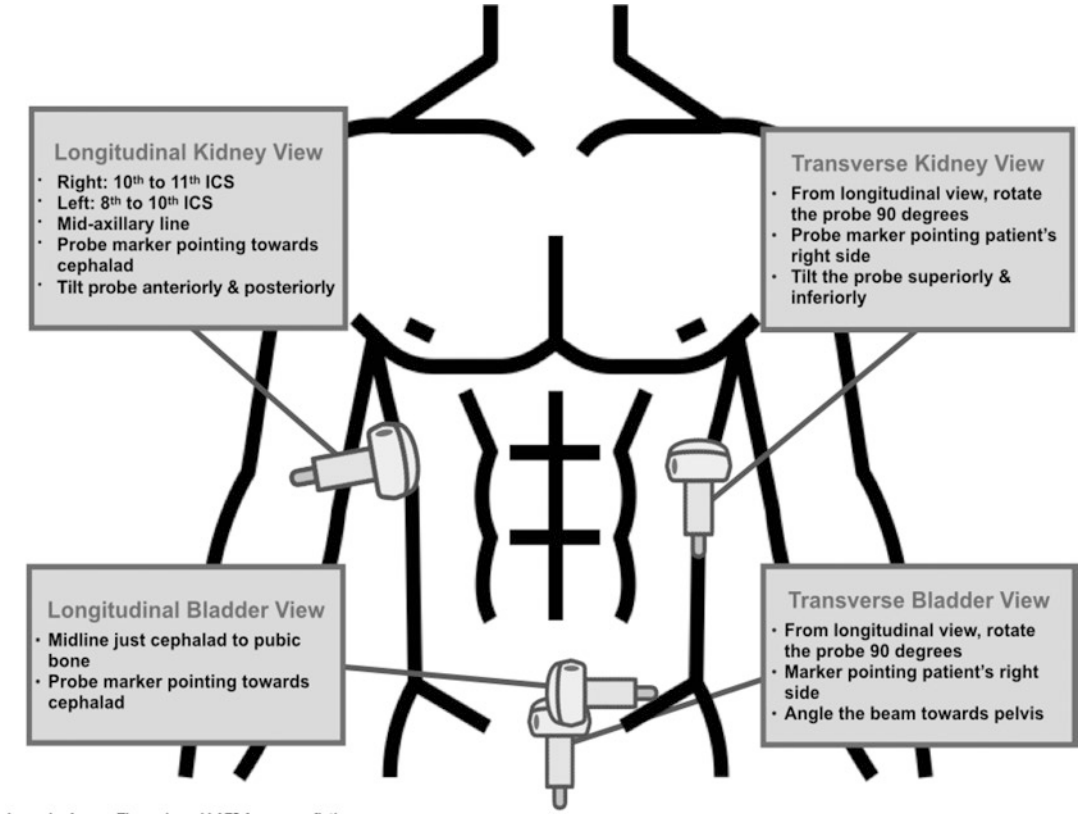
Longitudinal Kidney View
Right: 10th to 11th ICS
Left: 8th to 10th ICS
Mid-axillary line
Probe marker pointing towards cephalad
Tilt probe anteriorly & posteriorly
Transverse Kidney View
From longitudinal view, rotate the probe 90 degrees
Probe marker pointing patient's right side
Tilt the probe superiorly & inferiorly
Longitudinal Bladder View
Midline just cephalad to pubic bone
Probe marker pointing towards cephalad
Transverse Bladder View
From longitudinal view, rotate the probe 90 degrees
Marker pointing patient's right side
Angle the beam towards pelvis
Icons by Anggre Tionanda and LAFS from www.flaticon.com

18.5.1.1 Right Longitudinal Kidney View

The right kidney is easily visualized given its proximity to the liver, which serves an excellent acoustic window. The right kidney is examined with the patient in a supine position or left lateral decubitus position, which allows the clinician to access the posterior aspect of the right flank. Place the transducer at the right 10th to 11th intercostal space in the mid-axillary line with the transducer indicator directed towards the patient's head/cephalad. Once the image is obtained, slide the transducer superiorly/inferiorly, and gently tilt anteriorly/posteriorly to assess the entire right kidney. Visualize the ***Liver, Renal Cortex, Medullary Pyramids, Renal Pelvis, Renal Sinus, Minor Calyces***. Note that in the longitudinal view, the kidneys are football shaped. A normal size of an adult kidney is around 10–11 cm and the right kidney is often slightly longer than left kidney [12].

Tip: Rotate the transducer 10–20° counterclockwise to get in between the rib spaces to obtain the best image of the kidney in its maximal length. It also may be necessary to ask patient for deep inspiration and briefly hold the breath, which moves the right kidney inferiorly to a subcostal window.

The operator may use the color Doppler imaging for an advanced ultrasound technique, which can be used to detect the low flow states and differentiates the vasculatures from the dilated collecting systems (Figs. 18.5, 18.6, and 18.7).

Fig. 18.5 Transducer position for right longitudinal kidney view

Fig. 18.6 Longitudinal view of the normal right kidney. This longitudinal view of the right kidney demonstrates the white perinephric fat surrounding the hypoechoic renal cortex. In the center is the renal sinus which is a hyperechoic structure comprising the calyces, renal pelvis, and the major intrarenal vessels

18.5.1.2 Right Transverse Kidney View

From the longitudinal view, center the right kidney on the screen, and then rotate the transducer 90° counter-clockwise so that the transducer indicator is directed towards the patient's right. Once in the transverse plane, gently tilt the

Fig. 18.7 Normal right kidney with color Doppler. The color Doppler imaging demonstrates the blood flow in the renal arteries and veins which are enhanced with color. It is important to remember that red and blue indicate the blood flow direction, not the oxygenation status of the blood

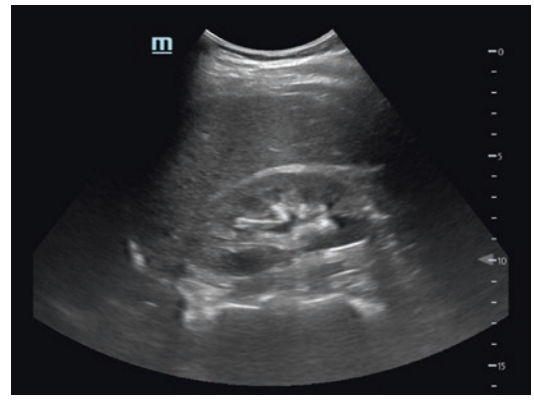

Fig. 18.8 Transducer position for right transverse kidney view

transducer superiorly and inferiorly to assess the entire kidney to visualize the ***Renal Cortex, Medullary Pyramid, Renal Pelvis, Renal Hilum***. Color Doppler imaging is useful to demonstrate flow in the renal artery and vein at the level of renal hilum as well as flow in the intrarenal vasculature. Note that in the transverse view, the kidneys appear C-shaped (Figs. 18.8 and 18.9).

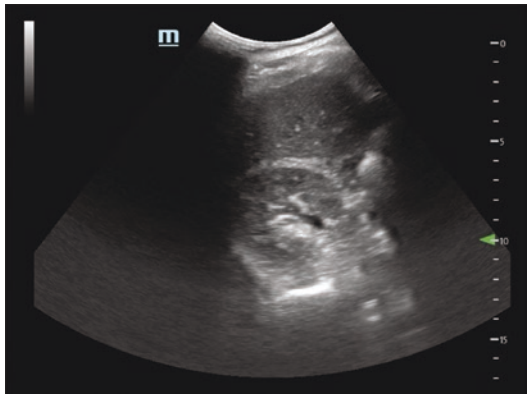

Fig. 18.9 Transverse view of the normal right kidney. In this view, the renal cortex, medullary pyramids, and renal pelvis as well as renal hilum can be visualized. The operator can adjust the angle of the transducer to maximize the window between the ribs

18.5.1.3 Left Longitudinal Kidney View

Unlike the right kidney, the left kidney lies slightly superior and posterior, absence of acoustic window provided by the liver and the interference from air in the stomach and intestine, leading to difficulty in obtaining the optimal view of the left kidney. The left kidney is best examined in right lateral decubitus position. Place the transducer at the left eighth to tenth intercostal space in the posterior axillary line with the probe indicator directed towards the patient's head/cephalad. Tilt the transducer superiorly and inferiorly or anteriorly and posteriorly to assess the entire kidney. Then slide the probe between the costal margin superiorly/inferiorly to visualize the left kidney. As with the right kidney, find the longest axis first before scanning the entire kidney. Visualize the same renal structures as in the right kidney (instead of the liver you will see the spleen). Always scan both kidneys for comparison (Figs. 18.10 and 18.11).

18.5.1.4 Left Transverse Kidney View

From the longitudinal view, rotate the probe 90° counter-clockwise so that the transducer indicator is directed towards the patient's right. Slowly tilt the transducer superiorly/inferiorly to assess the entire kidney. Visualize the same renal structures as the right kidney. This view is particularly

Fig. 18.10 Transducer position for the left longitudinal kidney view

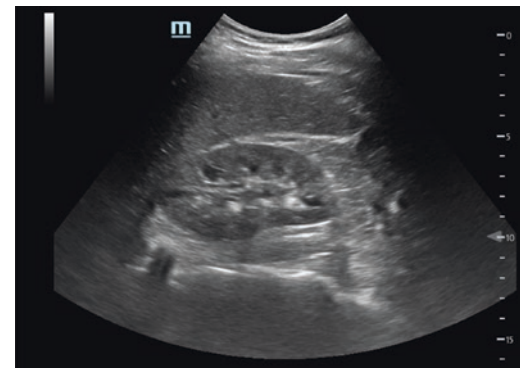

Fig. 18.11 Longitudinal view of normal left kidney. The same renal structures as in the right longitudinal view instead of liver you will see the spleen

helpful for imaging the inferior pole of the left kidney, which is often obscured by overlying gas within the descending colon (Figs. 18.12 and 18.13).

18.5.1.5 Longitudinal Bladder View

Bladder ultrasound is performed with the transducer in the suprapubic area with a moderately filled bladder for optimal scanning. The patient is best examined in the supine position. Place the transducer in the midline, just above the pubic symphysis so that the transducer indicator is

Fig. 18.12 Transducer position for the left transverse kidney view

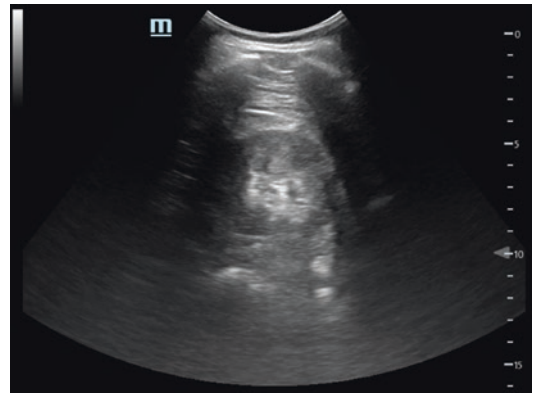

Fig. 18.13 Transverse view of normal left kidney. The same renal structures as in the right longitudinal view instead of liver you will see the spleen

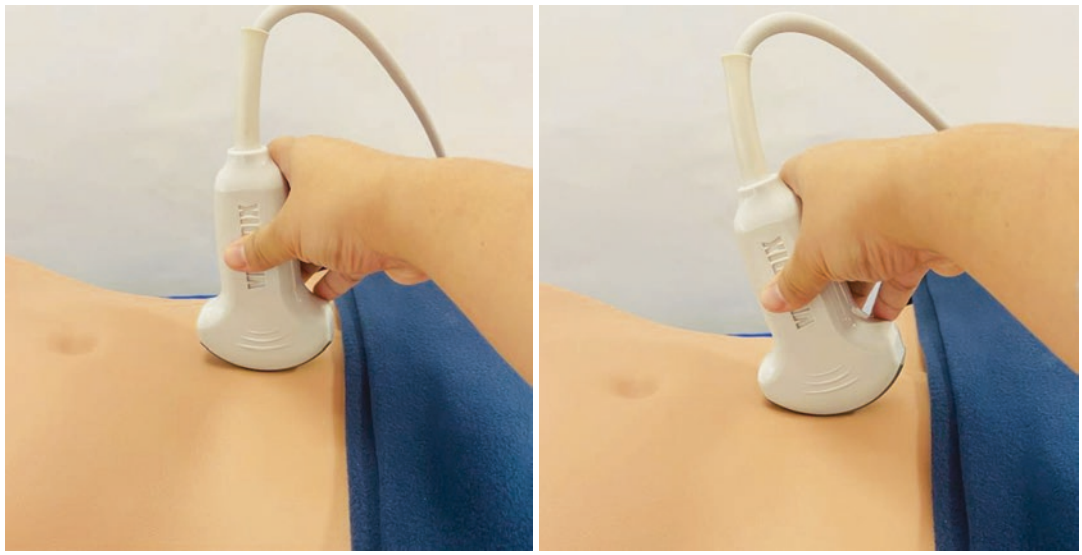

Fig. 18.14 Transducer position of the longitudinal view of the normal bladder

directed towards the patient's head/cephalad. If the bladder is not seen, angle the probe inferiorly towards the pelvic cavity. Gently tilt the transducer left and right to assess the entire bladder. Identify the ***Bladder, Bowel Gas, Uterus (females), Prostate (males), and Rectum*** (Figs. 18.14, 18.15, and 18.16).

18.5.1.6 Transverse Bladder View

From the longitudinal view, rotate the transducer 90° counter-clockwise so that the transducer indicator is directed towards the patient's right side. If the bladder is not seen, angle the probe inferiorly towards the pelvic cavity. Slowly tilt the transducer from superior to inferior to assess the entire bladder. Visualize the ***Bladder, Uterus (females), Prostate (males), and Rectum*** (Figs. 18.17 and 18.18).

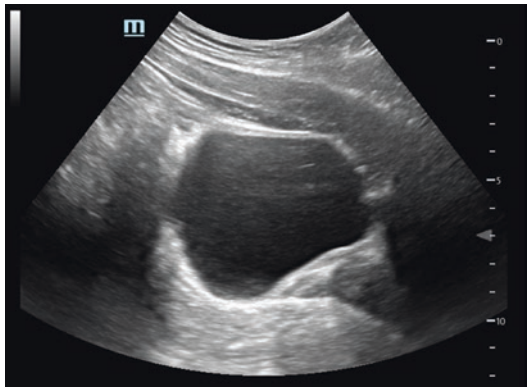

Fig. 18.15 Longitudinal view of the normal bladder (male). In this view, identify the anechoic bladder, prostate, and rectum

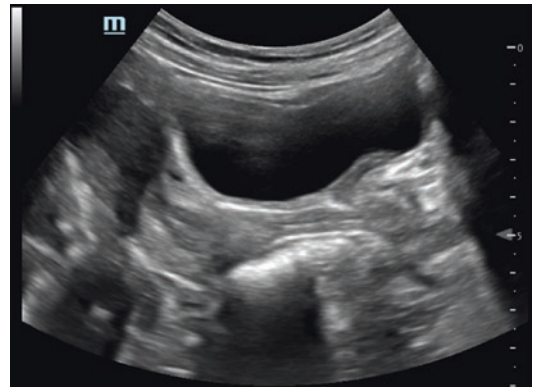

Fig. 18.16 Longitudinal view of the normal bladder (female). In this view, identify the anechoic bladder, uterus, and rectum

Fig. 18.17 Transducer position of the transverse view of the normal bladder

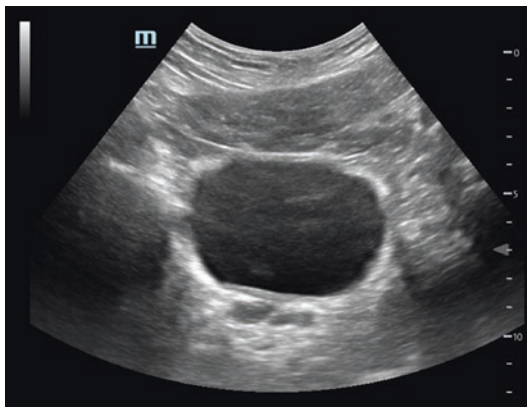

Fig. 18.18 Transverse view of the normal bladder (male). In this view, identify the anechoic bladder, prostate, and rectum

18.6 Renal Ultrasound Pathology

18.6.1 Hydronephrosis

One of the primary indications of a bedside renal ultrasound is evaluation for the presence of hydronephrosis. Hydronephrosis maybe present in an acute condition such as urinary obstruction from urinary retention, urolithiasis, retroperitoneal cancer, or a renal mass [13].

On ultrasound, hydronephrosis is seen as anechoic fluid-filled interconnected space with enhancement within the renal sinus. The degree of hydronephrosis seen in the ultrasound examination relates to the degree and extent of urinary

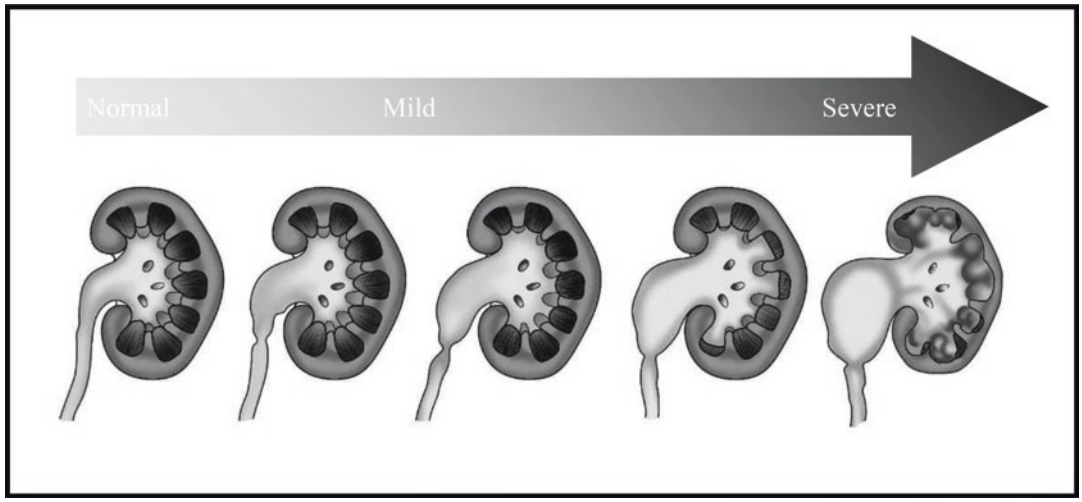

Fig. 18.19 Grades of hydronephrosis

obstruction. As the hydronephrosis increases in severity, there is an acute rise in intrarenal pressure, causing the dilatation of the renal pelvis and calyces first, while renal cortex remains unaffected. As obstruction continues, the renal cortex becomes compressed with progressive thinning of the medullary pyramids. Remember that the structures closest to the obstruction will be the first to be dilated. Therefore, the order of hydronephrosis depending on severity of urinary obstruction will be Renal Pelvis → Major Calyces → Minor Calyces → Renal Cortex (Fig. 18.19).

Hydronephrosis is typically categorized into mild, moderate, or severe. Mild hydronephrosis occurs when there is dilatation of the renal pelvis without dilatation of calyces. Moderate hydronephrosis causes dilatation of the renal pelvis and extends into the calyces. Mild cortical thinning may be seen. Severe hydronephrosis occurs when there is marked dilatation of the collecting systems resulting in renal cortical thinning. There will also be significant cortical atrophy and loss of the borders between the renal pelvis and calyces, which is sometimes called as "Bear Claw" sign (Figs. 18.20, 18.21, and 18.22).

Certain sonographic findings mimicking hydronephrosis that can present as false positives include extrarenal pelvis, parapelvic cysts, and polycystic renal disease. Extrarenal pelvis is an anatomical variant that where renal appears

Fig. 18.20 Mild hydronephrosis with proximal hydroureter

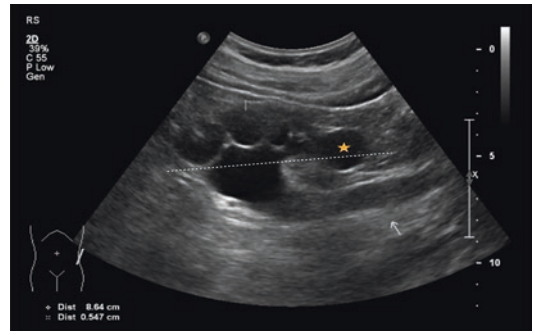

Fig. 18.21 Left kidney appears small, measures 8.6 cm in bipolar length with a cortical thickness of 0.5 cm. Dilatation of the left pelvicalyceal system with proximal hydroureter suggestive of moderate left hydronephrosis. No renal calculi seen. Renal cyst (star) seen at the lower pole of left kidney measuring 2.7 × 2.4 cm

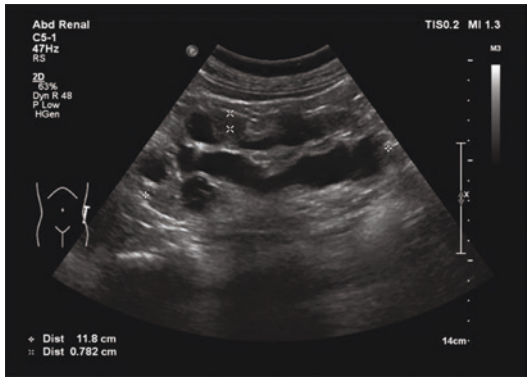

Fig. 18.22 The left kidney is slightly increased in echogenicity with reduced cortical thickness and preserved renal length (11.8 cm). Features of severe hydronephrosis of the left kidney can be well seen. This suggests left renal parenchymal disease with gross hydronephrosis

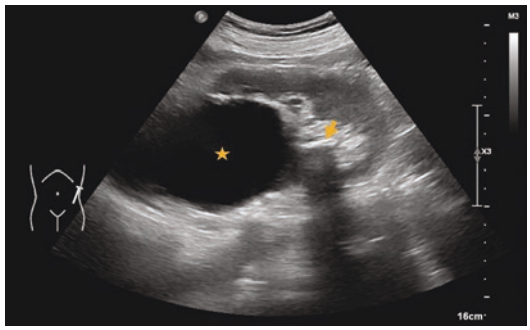

Fig. 18.23 Renal cortical cyst (star) measuring 10.8 × 7.4 cm at left upper pole with renal calculus (arrow) at lower pole of left kidney

hypoechoic mass adjacent to renal sinus without any dilatation of collecting system that may be confused with hydronephrosis [14]. Parapelvic cysts also can mimic hydronephrosis. It is a renal cyst that forms near the renal pelvis with anechoic or hypoechoic appearance on the ultrasound (Fig. 18.23). In contrast to hydronephrosis, parapelvic cysts are seen as "non-communicating" and renal sinus cystic masses and the shape is more spherical as opposed to irregular or cauliflower contour of hydronephrosis. A CT scan with contrast abdomen may be helpful to differentiate between these two conditions.

Renal ultrasound has modest diagnostic accuracy for diagnosis of kidney stones with a reported sensitivity of 70% and 75% when compared to the gold standard of CT examination [13]. There are various ultrasound findings that indicate the presence of kidney stones, depending on the size or location of the kidney stones on ultrasound. The most commonly described ultrasound findings for kidney stones include direct visualization of stone, hydronephrosis of the affected kidney, absence of ureteral jets, and twinkling artifacts.

18.6.2 Direct Visualization of Kidney Stone

Kidney stones maybe directly visualized on the ultrasound; however, most of kidney stones lie in the mid-ureter or ureterovesical junctions, which is difficult to directly visualize due to surrounding bowel gas. Kidney stones appear as hyperechoic structure with acoustic shadowing (Figs. 18.24 and 18.25). With ultrasound, larger stones >5 mm within the kidney can be differentiated, especially in the presence of hydronephrosis [15].

Fig. 18.24 The X-ray KUB of the patient showed opacities at the right renal fossa suggestive or right renal calculi

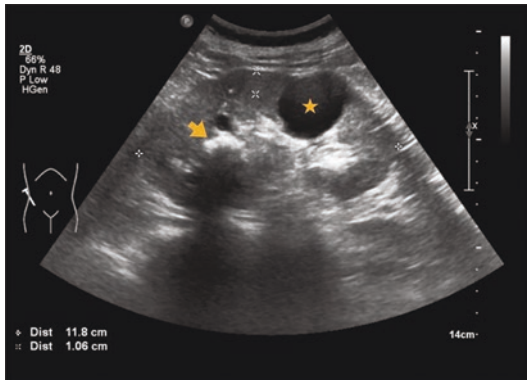

Fig. 18.25 The bedside ultrasound of the right kidney showed a normal size kidney (length 11.8 cm and cortical thickness of 1.0 cm) with normal echogenicity. The presence of hyperechoic calculi (arrow) with posterior acoustic shadowing at the upper pole confirmed right renal calculi. A simple renal cyst (star) also seen at mid-pole of the kidney measuring 3.6 × 3.8 × 3.9 cm

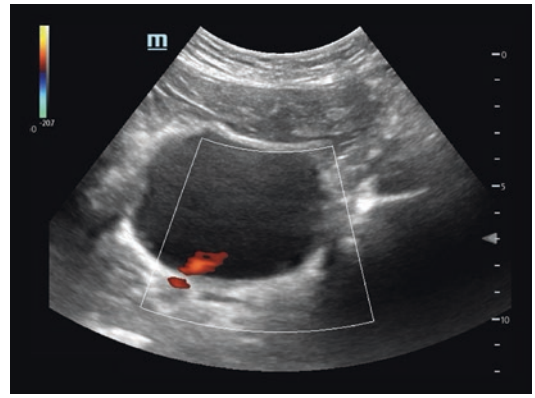

Fig. 18.26 Right urethral jets

18.6.3 Hydronephrosis of Affected Kidney

Because urethral stone can be difficult to visualize by ultrasound, an indirect finding of hydronephrosis is used to diagnose kidney stones when the clinical suspicion for renal colic is high. Increasing degree of hydronephrosis on ultrasound is associated with an increasing size of ureteral calculi. None or mild hydronephrosis on the renal ultrasound are more likely to have ureteral calculi <5 mm and less likely require urologic intervention, and those with moderate to severe hydronephrosis are likely to have >5 mm in size [8].

18.6.4 Absence of Ureteral Jets

Evaluation of ureteral jets flow by Doppler interrogation may be used to diagnose ureteral obstruction. The presence of ureteral jets flow indicates patency of upper urinary tract. While absence of a unilateral ureteral jets flow indicates obstruction due to stone is lodged within the ureter or ureterovesical junction. The bilateral absence of jets is less specific and may indicate a lack of difference in specific gravity between urine entering the bladder and urine in the bladder. To evaluate ureteral jet, perform the bladder scanning in the transverse view, then perform color Doppler imaging (Fig. 18.26).

18.6.5 Twinkling Artifact

The "Twinkling Artifact" is useful for early detection of ureteral stones, especially in the middle tract of the ureter. The artifact is located behind calcifications of ureteral calculi when color Doppler is applied. It appears as a multicolored high-intensity signal with or without an associated color comet-tail artifact. This leads to the "tail-like" appearance from numerous reverberation signals that the transducer is receiving. The diagnostic accuracy of Doppler twinkling artifact has a sensitivity and specificity of 90% and 100%, respectively, in detection of kidney stone at the ureterovesical junction [16] (Fig. 18.27).

18.6.6 Renal Cysts

Renal cysts are non-malignant, fluid-filled anechoic structures that are usually located in the renal parenchyma involving the cortex and medullary pyramids. It is an extremely common finding on ultrasound. Sonographic appearance of renal cyst includes round or oval in shape, an anechoic structure without internal echoes or solid elements, a well-defined interface between

the renal cyst and the adjacent renal parenchyma in all planes and orientations as well as an acoustic enhancement posterior to the cyst. Single or multiple renal cysts may be located everywhere in the kidney (Figs. 18.28 and 18.29).

18.6.7 Renal Masses

It is important to understand that not all hyperechoic lesions within the kidney are consistent with kidney stone. In contrast to kidney stone, a renal mass appears as a hyperechoic lesion without posterior acoustic shadowing. The majority of malignancies seen in the kidney are renal cell carcinoma (RCC) and angiomyolipoma (AML) [17]. RCC is the most common renal malignancy in adult with variable echogenicity in their sonographic appearance either isoechoic, hyperechoic, or hypoechoic compared to the adjacent parenchyma. Another common benign renal tumor seen in the kidney is AML. Although they are usually well demarcated, often unilateral and brightly echogenic on ultrasound, there is a significant overlap in their sonographic appearance with that of echogenic RCC. Both tumors may appear very similar in certain circumstances (Fig. 18.30).

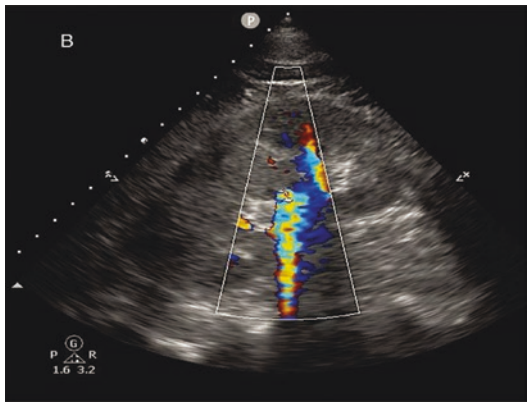

Fig. 18.27 Twinkling artifact seen behind the urethral calculi

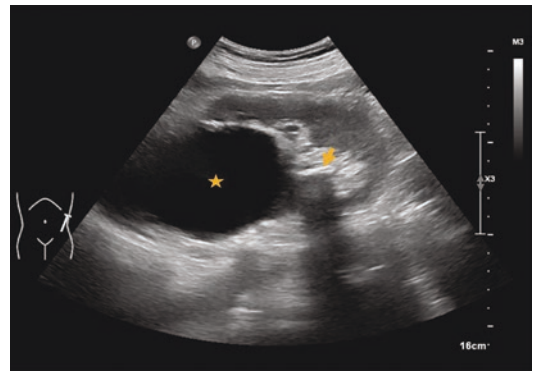

Fig. 18.28 Renal cortical cyst (star) measuring 10.8 × 7.4 cm at left upper pole with renal calculus (arrow) at lower pole of left kidney

Fig. 18.29 Bilateral polycystic kidney

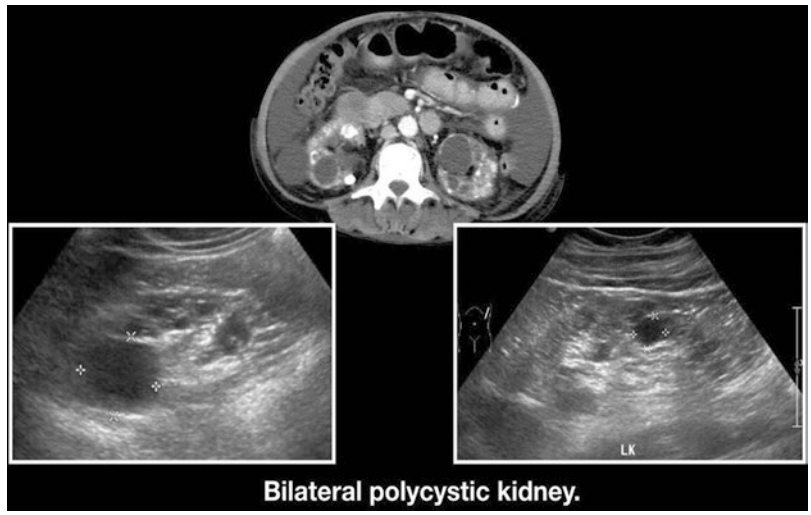

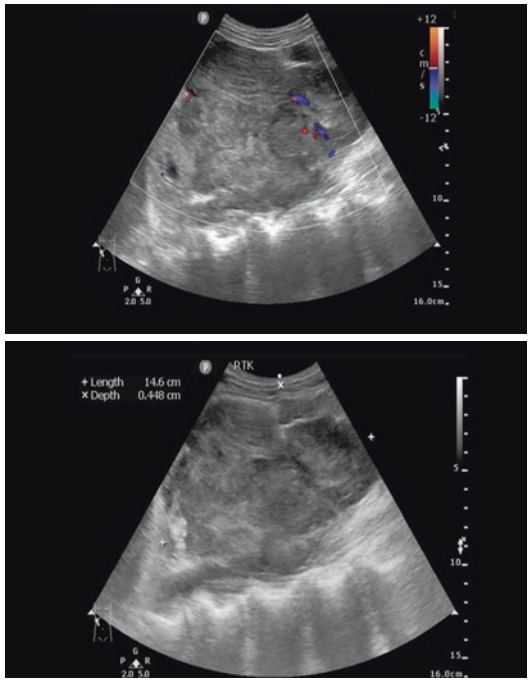

Fig. 18.30 The normal morphology of the right kidney is not visualized. There is a well-defined heterogenous hypo- to isoechoic renal mass seen at the right renal fossa region with an increase in vascularity within the mass evidenced by color Doppler. A CT renal 4 phase is required to rule out right renal mass malignancy

18.6.8 Urinary Tract Infection

Urinary tract infection (UTI) refers to any infection of the urinary tract, including the upper (kidneys and ureters) and lower (bladder and urethra); it is one of the most common infectious diseases [18]. Compared to lower urinary tract infections like cystitis, which are frequently diagnosed clinically, upper urinary tract infections, particularly kidney infections, are more challenging to diagnose as there aren't many radiological imaging modalities that can be used to diagnose them. Doppler techniques, contrast-enhanced ultrasonography (CEUS), and computed tomography (CT) may increase the diagnostic accuracy in cases of kidney infections, but they are not always available and carry risks such as radiation exposure, allergic reactions, and contrast-induced nephrotoxicity [19]. Point-of-care ultrasound (POCUS) is essential for determining the presence of renal infection and its complications, such as emphysematous pyelonephritis, renal abscess, and pyonephrosis, and directing the appropriate management [20, 21].

18.6.8.1 Acute Cystitis

Acute cystitis can be divided into complicated and uncomplicated lower urinary tract infections. Females are more likely to get a urinary tract infection due to their shorter, closer-to-the-anus urethras. Acute simple cystitis is diagnosed clinically in patients who exhibit symptoms such as frequent urination, dysuria, and/or urgency. In some patients, it could be associated with suprapubic discomfort or hematuria. Patients with pyuria and bacteriuria, fever, indicators of systemic illness, flank pain, and costovertebral tenderness that require further investigation are considered complicated [22]. The American Institute of Ultrasound in Medicine (AIUM) suggests performing an ultrasound examination to evaluate urinary tract pathology while searching for the source of fever and infection.

Sonographic features of cystitis:

- *Thickening and irregularities of the urinary bladder wall.* The normal thickness of the wall is 3–5 mm. The inner mucosal layer appears to have irregular, non-uniform thickening with an increased vascularity of the bladder wall due to the inflammatory reactions to the mucosal layer.
- *Presence of intraluminal debris (mobile echogenic particles)* (Fig. 18.31). The presence of bladder debris on ultrasound and urinalysis in the adult population was found to be associated with UTI, with a sensitivity and specificity for positive urine cultures of 52% and 86%, respectively (p 0.01) [23–25]. Interestingly, hydronephrosis or vesicoureteral reflux does not have any correlation with the presence of bladder debris and positive urine cultures [25].
- *Gas within the wall of the urinary bladder.* A dirty shadow or ring-down artifacts within the bladder wall suggest emphysematous cystitis, a rare cystitis complication.

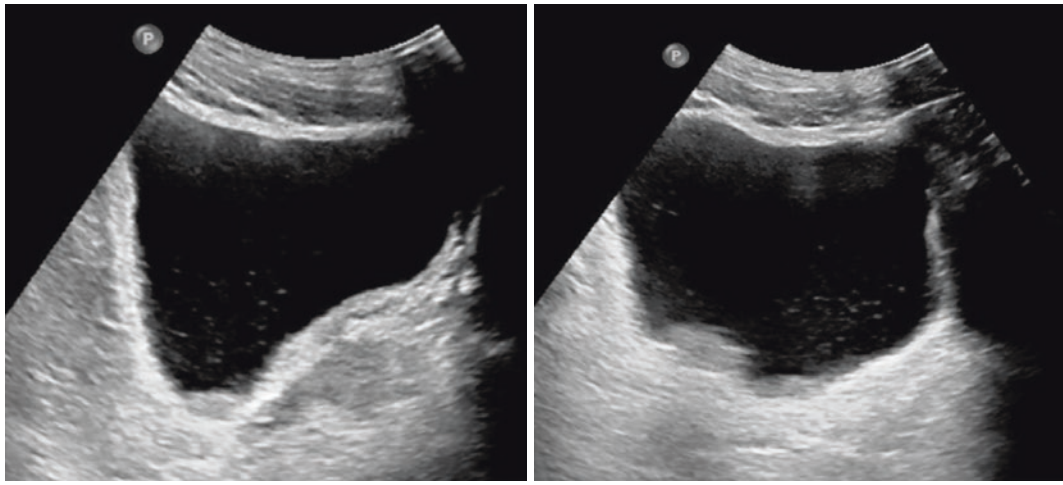

Fig. 18.31 The urinary bladder is distended with internal debris can be seen in longitudinal (left) and transverse axis (right)

18.6.8.2 Acute Pyelonephritis

Acute pyelonephritis is a consequence of an ascending urinary tract infection that affects the renal parenchyma and its collecting system. This route of infection is typically caused by gram-negative organisms, with *Escherichia coli* being the most prevalent. Patients with acute pyelonephritis typically exhibit flank pain, a high temperature, and dysuria in addition to bacteriuria and pyuria.

Sonographic features of acute pyelonephritis:

- *Enlargement of the kidney. The affected kidney may appear larger with a thicker renal pelvis due to the inflammatory responses and congestion. Renal enlargement is defined as an increase in kidney length of more than 15 cm, or the affected kidney being at least 1.5 cm longer than the unaffected kidney* [26, 27].
- *Abnormal echogenicity of the renal parenchyma with loss of corticomedullary differentiation. Focal or segmental hypoechoic regions (in edema) or hyperechoic regions (in hemorrhage) in the renal parenchyma can be observed in acute pyelonephritis. If the abnormalities are observed in one lobe, they are labelled as focal pyelonephritis; multifocal pyelonephritis occurs when they affect several kidney lobes* [28, 29].
- *Reduced areas of cortical vascularity due to corresponding tubular ischemia.*
- *Dilation of the renal pelvis and calyces due to the inhibition of ureteric peristaltic motion by the bacterial endotoxins, with or without appreciable obstruction* [21].
- *Thickening of the renal pelvis wall due to inflammation.*
- *Presence of debris, echogenic foci, or gas in the kidney (specificity of 100% and sensitivity of 62%)* [30].

Ultrasound is insensitive to detecting acute pyelonephritis changes; abnormalities are found in only one-fourth of cases [31]. It is operator-dependent, and findings might be limited by the patient's body habitus. Despite these drawbacks, it has been proven that POCUS is able to expedite appropriate treatment in 61% of patients with acute pyelonephritis. In 34.3% of patients, the use of POCUS led to the redirection of therapy, such as abscess drainage, stone removal, nephrostomy, and nephrectomy [32, 33]. Intriguingly, the combination of X-ray and POCUS is comparable to CT (56.6% vs. 58.8%) for identifying significant acute pyelonephritis findings.

18.6.8.3 Emphysematous Pyelitis and Emphysematous Pyelonephritis

Emphysematous pyelitis is a benign condition with a 20% mortality rate [34]. The presence of gas is confined to the renal excretory system, and the prognosis is remarkable, with rapid and complete recovery following medical treatment. The clinical manifestation of emphysematous pyelitis will often be non-specific, or similar to the clinical manifestation of acute pyelonephritis without complications. On the contrary, acute emphysematous pyelonephritis is a rare, life-threatening disease characterized by necrotized renal parenchyma and collecting system and typically caused by *E. coli* (70%), K. pneumonia, and P. Mirabilis. It has a mortality rate as high as 80% with antibiotics alone but may be reduced to 21.5% with antibiotics with surgery or percutaneous drainage [35, 36]. Patients with emphysematous pyelonephritis are severely ill, manifesting infective symptoms, disorientation, uncontrolled hyperglycemia, acidosis, dehydration, and electrolyte imbalance.

Sonographic features of acute emphysematous pyelonephritis include:

- *Enlarged affected kidney.*
- *Thickening of the renal pelvis.*
- *Coarse echoes within renal parenchyma or collecting.*
- *Posterior dirty acoustic shadowing is caused by reverberation artifacts from the gas.*
- *Ring-down artifacts from trapped air in the presence of fluid collection. This artifact needs to be differentiated from the comet tail artifact, as the latter has a triangular shape whose tip will dissipate with depth.*
- *Abscess formation in the renal parenchyma.*
- *±Gas in the perinephric or retroperitoneal space.*

Differentiating between emphysematous pyelitis and emphysematous pyelonephritis [34, 37] is important as the clinical management varies. The gas is limited to the collecting system in emphysematous pyelitis; hence, antibiotic therapy alone appears to be sufficient if there is no obstruction [29]. The presence of gas within the renal parenchyma, collecting system, or perinephric tissue necessitates drainage or nephrectomy in acute emphysematous pyelonephritis (Fig. 18.32).

18.6.8.4 Renal Abscess

Renal abscess is commonly caused by *Staphylococcus aureus, Escherichia coli, Klebsiella, and Proteus* [21] and is a complication of acute pyelonephritis. Patients at risk for renal abscess include those with inadequately controlled diabetes, renal tubular obstruction, intravenous drug abuse, or dialysis dependence. Patients typically present with vague symptoms, and up to 20% of those with renal abscesses have been reported to have a negative urinalysis [29].

Sonographic features of renal abscesses:

- *An enlarged kidney.*
- *In the early phase, there will be poor corticomedullary differentiation due to renal parenchymal edema. A fluid-filled hyperechoic to hypoechoic focal mass or cystic structure with an irregular wall can be observed in the late phase.*
- *Absence or lack of vascularity.*
- *Fluid-debris level.*
- *Reverberation artifact. The presence of gas-causing reverberation artifacts within a hypoechoic or cystic mass indicates the formation of an abscess* [29].
- *A perinephric or retroperitoneal collection can be seen when a kidney abscess ruptures.*

Ultrasound is a good tool for initial assessment to look for renal abscesses; however, the American College of Radiology's most recent recommendation continues to maintain CT as the preferred imaging study for patients with pyelonephritis who present with either a complex presentation or a failure to respond to antibiotics. The cornerstones of the treatment of renal abscesses are parenteral antibiotics and drainage (Figs. 18.33 and 18.34).

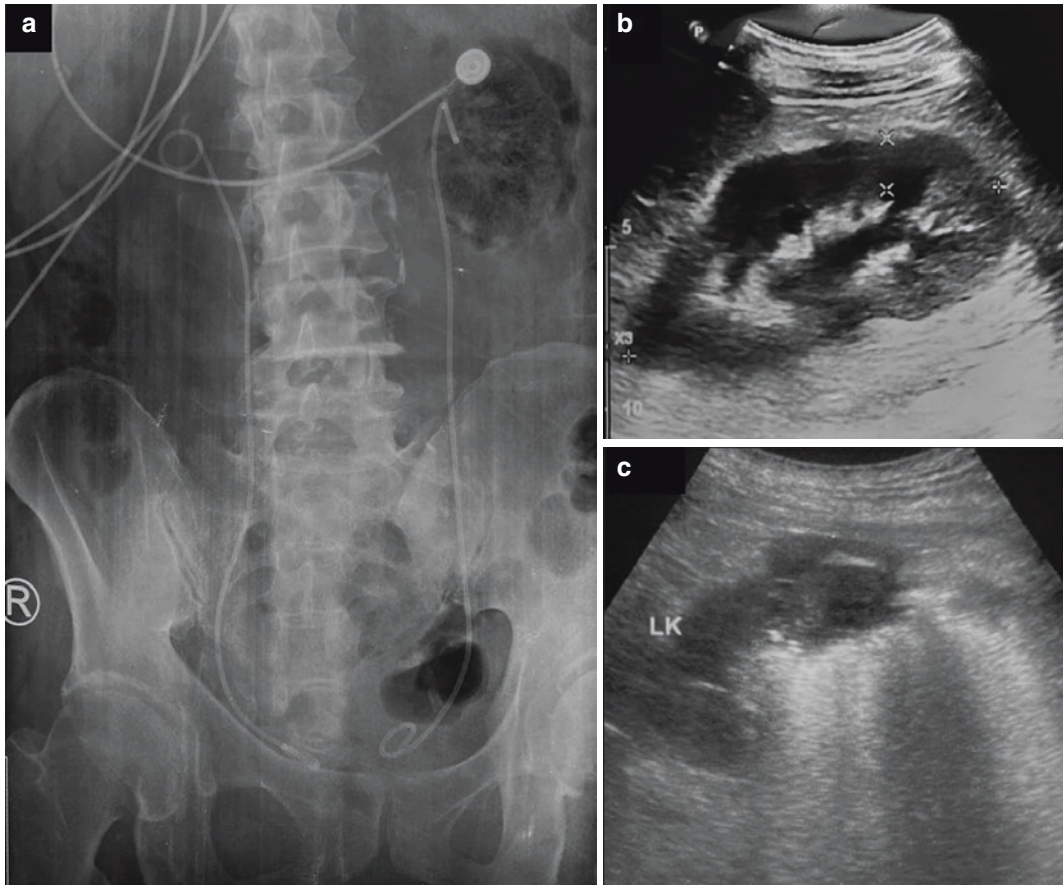

Fig. 18.32 The X-ray and ultrasound findings of the patient diagnosed with right hydronephrosis and emphysematous pyelonephritis of the left kidney. (**a**) The KUB X-ray after bilateral renal drainage showed mottled gas within the left renal fossa. (**b**) The right kidney has mild hydronephrosis with internal debris within the renal collecting system. (**c**) The left kidney is enlarged with reduced echogenicity. Multiple air can be seen within the renal parenchyma with posterior "dirty shadowing" artifacts. (**d**) A CT image of the patient's left kidney showed signs of acute emphysematous pyelonephritis: swollen left kidney, numerous air pockets (arrow), and destruction of normal renal parenchyma. Mild hydronephrosis is seen in the right kidney

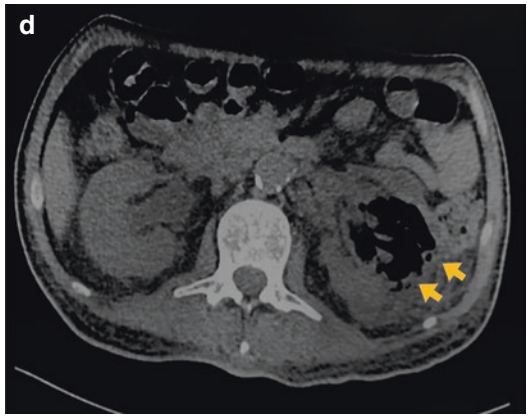

Fig. 18.32 (continued)

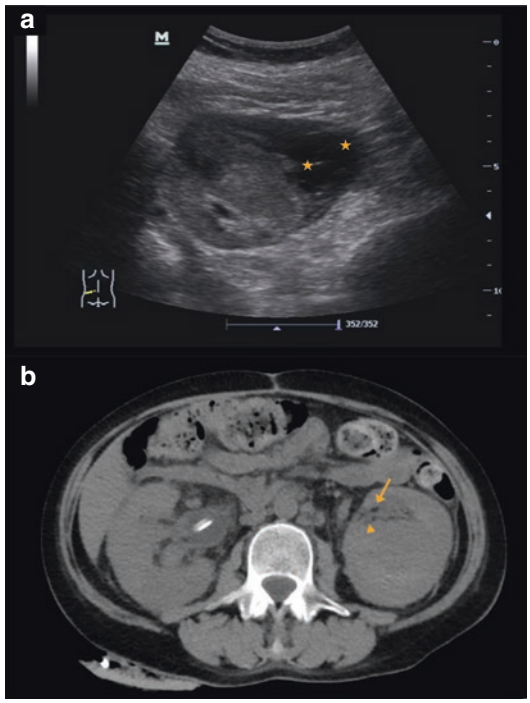

Fig. 18.33 Both of the images belong to a 36-year-old female with a history of bilateral hydronephrosis with urethral stricture. (**a**) Re-insertion of the left nephrostomy tube due to dislodgment was unsuccessful due to the non-dilated calyceal system. There are areas of hypodensity (star) noted in the subcapsular region of the left kidney. (**b**) CT scan shows a subcapsular fluid collection (arrowhead) with air locules (arrow) and minimal peri-renal and peri-ureteric fat stranding in the posterior aspect of the left kidney, consistent with an early left subcapsular abscess

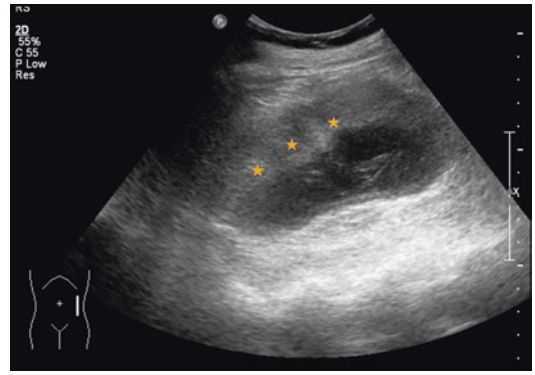

Fig. 18.34 Longitudinal ultrasound of the left kidney shows an ill-defined heterogeneous hypoechoic subcapsular collection (star) compressing the left kidney suggestive of possible left subcapsular renal abscess

18.7 Bladder Volume Calculation

Ultrasound is a non-invasive imaging technique that can be used to measure the urinary bladder volume since 1967. The procedure is simple and painless and does not involve any radiation exposure. The advancement of technology further allows calculation of bladder volume and evaluation of three-dimensional images of the bladder using portable bladder ultrasound devices.

More studies have been conducted to evaluate the best formulae and methods with a good accuracy to the actual urine volume. Most ultrasound machines have a function to automatically calculate volumes from the measurements used with the ultrasound calipers. However, if this function is not available, the volumes can also be calculated using an ellipsoid equation from the transverse and longitudinal view of the bladder ultrasound image [38, 39]. A study by Chang et al. (2021) introduced a novel method to calculate the bladder volume using a 3D ultrasound and a super-ellipse shape modification. They compared the differences and relationships among three parameters: actual urine volume, conventional ellipsoid method, and the new reconstruction model method. The study found that both methods are highly correlated with the actual volume, with a better mean percentage

error observed using the novel method. Although three-dimensional ultrasound has better accuracy (87–95%) in bladder volume estimation, it is rarely used as the 2D conventional ultrasound due to limited availability. Using the 2D conventional ellipsoid formula, a mean error value of 11.5–35% has been reported [40].

The prolate ellipsoid, double area, and double ellipsoid methods were evaluated during another prospective analysis of equations that accurately predict bladder capacity [41]. They observed that the overall difference between the approaches was significant ($p = 0.0007$) when compared to the actual bladder volume (mean urine volume of 228.3 mL) collected right after the scan. Despite having much lower values than the other two techniques (mean urine volumes of 230.1 mL and 236.9 mL, respectively), the prolate ellipsoid approach is recommended as the standard calculation method due to its practicality and user-friendliness [41].

The formula has multiple correction factors which follow a certain geometrical shape as the bladder's shape follows the contour of the pelvic structures. Bih and colleagues classified bladder's shape as triangular prism, cuboid, ellipsoid, and spherical. A cuboid shaped bladder appeared to be four-sided on both transverse and longitudinal scans with an approximately similar length of the edges. The ellipsoid bladder appeared to be round or elliptical on both transverse and longitudinal scans and the edges were approximately parallel in the upper or middle portion of the longitudinal scan. If the bladder appeared to be triangular or pear-shaped on the longitudinal scan, and had a distinct upper tip and flat bottom, the bladder is considered to have triangular prism shape. The most common shape is the ellipsoid, however, if the shape is indeterminate, correction coefficient of 0.72 can be used [40, 41]. Thickness of the bladder wall must not be included in the measurement of the bladder diameter to avoid overestimating bladder volume [40].

18.7.1 Steps to Perform Urinary Bladder Ultrasound

18.7.1.1 Preparation of the Patient

- Position the patient supine or propped up at 30–45°.
- If permissible, clamp or spigot the catheter prior to scanning to enable urine accumulation in the bladder and a better bladder window.
- Expose the patient's abdomen and the suprapubic region.

18.7.1.2 Ultrasound Machine, Transducer, and Setup

- Transducer: curvilinear probe or phased array probe.
- Exam preset: abdomen or renal.
- Machine positions: at the patient's shoulder and on the operator's ipsilateral side.

18.7.1.3 Scanning the Bladder

The urinary bladder will be scanned using a transabdominal approach.

The bladder's height should be measured along its longitudinal axis. Place the transducer superior to the pubic symphysis in the longitudinal axis, with the indicator of the transducer pointing towards the patient's head. From here, rock the transducer towards the pelvic cavity or the patient's lower limbs. Measure the craniocaudal height of the bladder.

Bladder's width and depth should be measured along its transverse axis. From the previous position, rotate the transducer 90° counterclockwise. The indicator should be facing towards the patient's right shoulder. By tilting the transducer in a transverse plane from superior to inferior, look for the greatest width and anterior-posterior depth (Fig. 18.35).

A normal urinary bladder has a thick, smooth, muscular wall measuring 3–5 mm; when the bladder is full, the wall thickness will reduce to 2–3 mm. A normal adult's urinary bladder can

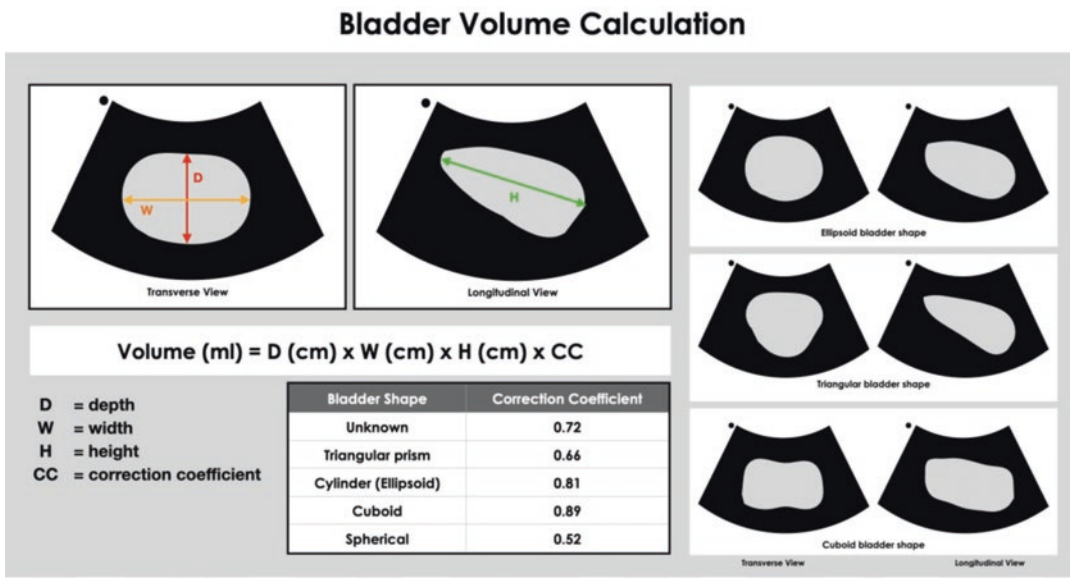

Fig. 18.35 The urinary bladder volume calculation depends on different bladder shapes. Two views are required for this purpose: the longitudinal and transverse view of the urinary bladder

hold around 300–500 mL. If the bladder volume is greater than this, it may indicate bladder outlet obstruction or other conditions that affect bladder emptying. The measurement of bladder wall thickness appears to be a helpful predictor of urinary bladder obstruction. A cutoff point of >5 mm is used to diagnose bladder outlet obstruction [42].

Acute urinary retention is a urologic emergency characterized by the sudden inability to urinate combined with suprapubic pain, bloating, urgency, distress, or, occasionally, mild incontinence. Chronic urinary retention, usually associated with non-neurogenic causes, is often asymptomatic. Normal post-void bladder volume is <50 mL in adult patients and <100 mL in those over 65 years old [43]. A post-void residual volume helps in the evaluation of many diseases, including but not limited to neurogenic bladder, cauda equina syndrome, urinary outlet obstruction, mechanical obstruction, medication-induced urinary retention, postoperative urinary retention, and urinary tract infections.

The current recommendations state that residual urine volume should be used to identify the presence or absence of urinary tract obstruction. There is no consensus regarding the definition for acute urinary retention; the American Urological Association recommends that chronic urinary retention be defined as PVR volume greater than 300 mL measured on two separate occasions and persisting for at least 6 months.

18.8 Renal Hemodynamics

18.8.1 Renal Venous Congestion

Patients with hemodynamic instability usually receive volume resuscitation to increase the cardiac output, blood pressure, and tissue perfusion. However, excess fluid will affect the kidney adversely, associated with increased mortality [44]. It increases the risk of tissue edema, causing higher interstitial pressure and eventually impairing kidney perfusion.

In all phases of fluid resuscitation, including resuscitation, optimization, stabilization, and evacuation phase, it is of utmost importance to determine patient volume adequacy, responsiveness, and tolerance. Apart from physical examination and non-invasive parameters, renal POCUS can help fine-tune fluid management where physicians can access the real-time response of the therapy.

A method using ultrasound Doppler to evaluate venous congestion was developed by looking at

the hepatic, portal, and renal venous waveforms. Venous excess ultrasound (VExUS) will give insight into each organ's venous congestion, possibly leading to compromised organ perfusion.

Renal VExUS is performed by identifying the interlobar vessels, and venous waveforms will be interpreted as normal, mildly abnormal, or severely abnormal patterns. They will be graded to determine the degree of venous congestion in the hepatic, portal, and renal circulation [45]. In critically ill patients, the variations in the venous patterns can guide fluid therapy, diuretic administration, or renal replacement therapy. A study of renal venous patterns found that elevated VExUS scores were associated with a higher risk of developing AKI, possibly due to a decrease in renal perfusion pressure [46].

To assess renal venous congestion, the kidney should be clearly viewed to assess the intrarenal vein, and color Doppler should be turned on to visualize the interlobar vessels. Pulse wave Doppler is placed at the area with the strongest signal and activated. Both arterial and venous flow can be seen in the same view, but Doppler tracing should be analyzed below the baseline to assess for venous congestion.

Below is a brief outline of how to interpret the venous Doppler tracings. Analyzing the Doppler tracing below the baseline will give an insight into renal venous congestion (Figs. 18.36, 18.37, and 18.38).

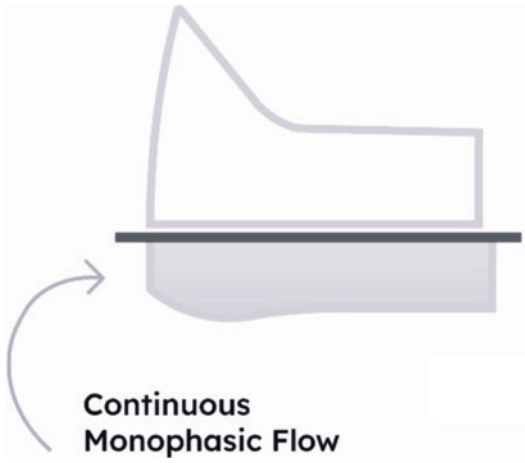

Fig. 18.36 Normal intrarenal vein Doppler pattern should reveal a continuous monophasic flow

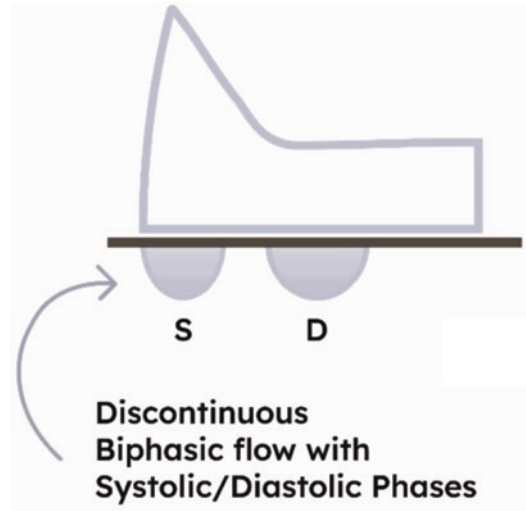

Fig. 18.37 In conditions with an increase in renal venous congestion, the systolic component of the wave will decrease with progression to a biphasic pattern

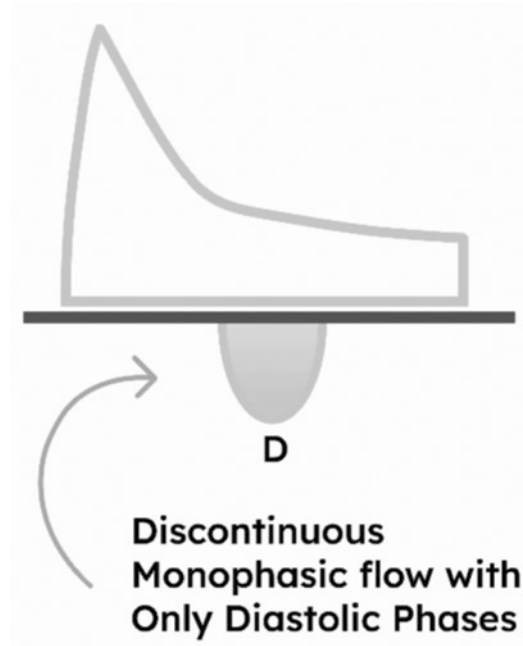

Fig. 18.38 Severe renal venous congestion will lead to monophasic diastolic flow (only with absence of systolic flow)

18.8.2 Renal Resistive Index (RI)

Renal resistive index (RI) measures the resistance of renal arterial flow to the kidney. Renal

artery blood flow occurs during systole and diastole in normal conditions. However, in certain situations, such as obstruction, inflammation, or transplant rejection, there will be a reduction in the renal artery during diastole. During this time, the resistive index is elevated. Reversed flow can occur through the renal artery in a more severe condition. The normal range of RI is 0.5–0.7, and elevation of this value is associated with a worse prognosis in patients with renal dysfunctions [47].

Some differential diagnoses for a high RI that should be considered include obstruction, acute tubular necrosis, pyelonephritis, severe hypotension, acute vascular event, and transplant rejection.

It is measured using this formula (Fig. 18.39):

Tips and Tricks

- Always look for the liver and spleen first! Compared to the right kidney, the left kidney's position is superior and more posterior than the right kidney. The left lateral decubitus position can be helpful for optimizing images.
- The fundus of the stomach frequently creates an odd shadow that resembles a soft tissue tumor. Therefore, it is beneficial to scan the kidney with the transducer positioned more posteriorly with the dorsal part of your hand touching the patient's bed or examination couch.
- Maximize your field of view when scanning the bladder. You may easily have missed the bladder wall hematoma.
- When performing bladder ultrasonography, it's important to keep in mind that the bladder is situated immediately posterior to the pubic bone and pubic symphysis. Your ultrasound transducer is probably too superiorly positioned if you can't acquire clear images.
- Remember to unclamp the urine drainage catheter and repeat the scan upon detection of hydronephrosis. A true hydronephrosis will persist after unclamping the drain. If the patient has hydronephrosis with an over-distended bladder, ultrasound examination should be repeated as well.
- Significant intestinal gas or scarring of the pelvic organs will obscure the ultrasound view. Consider repositioning the patient or repeating the examination after a few minutes.

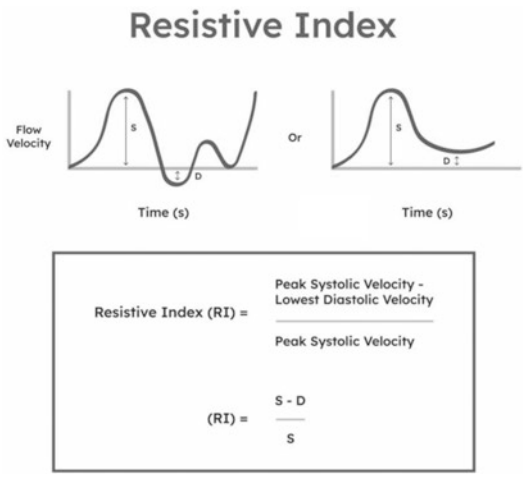

Fig. 18.39 Renal Resistive Index formula

Pitfalls

- A longer time is required to perform the US and it takes more effort from the operator to obtain the parameters (e.g., three bladder diameters) and calculate them. This necessitates training time to master the ability.
- In POCUS, calculating the bladder volume is less important than detecting the presence of urine or obstruction in the urinary tract.
- Remember the "Pseudo Kidney Sign?" There are several pathologies that can mimic a kidney, for example, colon carcinoma, inflammatory colitis, necrotizing enterocolitis, lymphoma, and in some cases even intussusception.
- It is important to be aware of physiological forms of hydronephrosis, for example, maternal hydronephrosis, which develops after 20 weeks of pregnancy. Additionally, patients with an over-distended bladder may also have dilated pelvicalyceal system of one or both kidneys.

- Doppler ultrasound frequently reveals increased blood flow in RCCs as a result of neovascularization and arteriovenous shunting. However, it is less sensitive to differentiate hypovascular tumors. Therefore, renal tumors without a Doppler signal that are not simple cysts should be further explored.

References

1. Nepal S, Dachsel M, Smallwood N. Point-of-care ultrasound rapidly and reliably diagnoses renal tract obstruction in patients admitted with acute kidney injury. Clin Med (Lond). 2020;20(6):541–4. https://doi.org/10.7861/clinmed.2019-0417. PMID: 33199317; PMCID: PMC7687308.
2. Pathan SA, Mitra B, Mirza S, Momin U, Ahmed Z, Andraous LG, Shukla D, Shariff MY, Makki MM, George TT, Khan SS, Thomas SH, Cameron PA. Emergency physician interpretation of point-of-care ultrasound for identifying and grading of Hydronephrosis in renal colic compared with consensus interpretation by emergency radiologists. Acad Emerg Med. 2018;25(10):1129–37. https://doi.org/10.1111/acem.13432. Epub 2018 May 28. PMID: 29663580.
3. Cheong B, Muthupillai R, Rubin MF, Flamm SD. Normal values for renal length and volume as measured by magnetic resonance imaging. Clin J Am Soc Nephrol. 2007;2(1):38–45. https://doi.org/10.2215/CJN.00930306. Epub 2006 Dec 6. PMID: 17699385.
4. Nicolau C, Claudon M, Derchi LE, Adam EJ, Nielsen MB, Mostbeck G, Owens CM, Nyhsen C, Yarmenitis S. Imaging patients with renal colic-consider ultrasound first. Insights Imaging. 2015;6(4):441–7. https://doi.org/10.1007/s13244-015-0396-y. Epub 2015 May 21. PMID: 25994497; PMCID: PMC4519809.
5. Wong C, Teitge B, Ross M, Young P, Robertson HL, Lang E. The accuracy and prognostic value of point-of-care ultrasound for nephrolithiasis in the emergency department: a systematic review and meta-analysis. Acad Emerg Med. 2018;25(6):684–98. https://doi.org/10.1111/acem.13388. Epub 2018 Mar 25. PMID: 29427476.
6. Smith-Bindman R, Aubin C, Bailitz J, Bengiamin RN, Camargo CA Jr, Corbo J, Dean AJ, Goldstein RB, Griffey RT, Jay GD, Kang TL, Kriesel DR, Ma OJ, Mallin M, Manson W, Melnikow J, Miglioretti DL, Miller SK, Mills LD, Miner JR, Moghadassi M, Noble VE, Press GM, Stoller ML, Valencia VE, Wang J, Wang RC, Cummings SR. Ultrasonography versus computed tomography for suspected nephrolithiasis. N Engl J Med. 2014;371(12):1100–10. https://doi.org/10.1056/NEJMoa1404446. PMID: 25229916.
7. Daniels B, Gross CP, Molinaro A, Singh D, Luty S, Jessey R, Moore CL. STONE PLUS: Evaluation of emergency department patients with suspected renal colic, using a clinical prediction tool combined with point-of-care limited ultrasonography. Ann Emerg Med. 2016;67(4):439–48. https://doi.org/10.1016/j.annemergmed.2015.10.020. Epub 2015 Dec 31. PMID: 26747219; PMCID: PMC5074842.
8. Goertz JK, Lotterman S. Can the degree of hydronephrosis on ultrasound predict kidney stone size? Am J Emerg Med. 2010;28(7):813–6. https://doi.org/10.1016/j.ajem.2009.06.028. Epub 2010 Jan 28. PMID: 20837260.
9. Chan H. Noninvasive bladder volume measurement. J Neurosci Nurs. 1993;25(5):309–12. https://doi.org/10.1097/01376517-199310000-00007. PMID: 8270812.
10. Hansen KL, Nielsen MB, Ewertsen C. Ultrasonography of the kidney: a pictorial review. Diagnostics (Basel). 2015;6(1):2. https://doi.org/10.3390/diagnostics6010002. PMID: 26838799; PMCID: PMC4808817.
11. American Institute of Ultrasound in Medicine. AIUM practice guideline for the performance of an ultrasound examination of the abdomen and/or retroperitoneum. J Ultrasound Med. 2008;27(2):319–26. https://doi.org/10.7863/jum.2008.27.2.319. PMID: 18204029.
12. Emamian SA, Nielsen MB, Pedersen JF, Ytte L. Sonographic evaluation of renal appearance in 665 adult volunteers. Correlation with age and obesity. Acta Radiol. 1993;34(5):482–5. PMID: 8369185.
13. Mostbeck GH, Zontsich T, Turetschek K. Ultrasound of the kidney: obstruction and medical diseases. Eur Radiol. 2001;11(10):1878–89. https://doi.org/10.1007/s003300101011. PMID: 11702120.
14. Koratala A, Bhattacharya D. Extrarenal pelvis mimicking hydronephrosis: a case for caution. Clin Case Rep. 2017;5(10):1720–1. https://doi.org/10.1002/ccr3.1143. PMID: 29026582; PMCID: PMC5628238.
15. Türk C, Petřík A, Sarica K, Seitz C, Skolarikos A, Straub M, Knoll T. EAU guidelines on diagnosis and conservative management of urolithiasis. Eur Urol. 2016;69(3):468–74. https://doi.org/10.1016/j.eururo.2015.07.040. Epub 2015 Aug 28. PMID: 26318710.
16. Ripollés T, Martínez-Pérez MJ, Vizuete J, Miralles S, Delgado F, Pastor-Navarro T. Sonographic diagnosis of symptomatic ureteral calculi: usefulness of the twinkling artifact. Abdom Imaging. 2013;38(4):863–9. https://doi.org/10.1007/s00261-012-9946-7. PMID: 23011549.
17. Forman HP, Middleton WD, Melson GL, McClennan BL. Hyperechoic renal cell carcinomas: increase in detection at US. Radiology. 1993;188(2):431–4. https://doi.org/10.1148/radiology.188.2.8327692. PMID: 8327692.
18. Bonkat G, Bartoletti R, Bruyère F, Cai T, Geerlings SE, Köves B, Schubert S, Pilatz A, Veeratterapillay

R, Wagenlehner F, Guidelines Associates: Devlies W, Horváth J, Mantica G, Mezei T, Pradere B, Guidelines Office: Smith EJ. EAU guidelines on urological infections. 2022.
19. Granata A, Floccari F, Insalaco M, Clementi A, Di Lullo L, D'Amelio A, Zamboli P, Logias F, Romano M, Fiorini F. L'ecografia nelle infezioni del rene [Ultrasound assessment in renal infections]. G Ital Nefrol. 2012;29 Suppl 57:S47–S57. Italian. PMID: 23229529.
20. Zulfiqar M, Ubilla CV, Nicola R, Menias CO. Imaging of renal infections and inflammatory disease. Radiol Clin North Am. 2020;58(5):909–23. https://doi.org/10.1016/j.rcl.2020.05.004. Epub 2020 Jul 14. PMID: 32792123.
21. Vourganti S, Agarwal PK, Bodner DR, Dogra VS. Ultrasonographic evaluation of renal infections. Radiol Clin North Am. 2006;44(6):763–75. https://doi.org/10.1016/j.rcl.2006.10.001. PMID: 17147985.
22. The AIUM practice parameter for the performance of an ultrasound examination of the abdomen and/or retroperitoneum. J Ultrasound Med. 2022;41(4):E1–E8. https://doi.org/10.1002/jum.15874. Epub 2021 Nov 18. PMID: 34792206.
23. Kanu GB, Chou YH. Ultrasonography of the urinary bladder. J Med Ultrasound. 2010;18(3):105–14. issn:0929-6441. https://www.sciencedirect.com/science/article/pii/S092964411060015X. https://doi.org/10.1016/S0929-6441(10)60015-X.
24. Fananapazir G, Golshani B, Chen LX, McGahan JP, de Mattos AM, Corwin MT. Bladder debris on ultrasound in the emergency department: correlation with urinalysis. Abdom Radiol (NY). 2018;43(9):2462–6. https://doi.org/10.1007/s00261-018-1513-4. PMID: 29470628.
25. Stevenson SM, Lau GA, Andolsek WC, Presson AP, Cartwright PC. Bladder debris on ultrasound as a predictor for positive urine culture in a pediatric population. J Pediatr Urol. 2018;14(3):254.e1–5. https://doi.org/10.1016/j.jpurol.2017.11.025. Epub 2018 Feb 3. PMID: 29456120.
26. Dinkel E, Orth S, Dittrich M, Schulte-Wissermann H. Renal sonography in the differentiation of upper from lower urinary tract infection. AJR Am J Roentgenol. 1986;146(4):775–80. https://doi.org/10.2214/ajr.146.4.775. PMID: 3513490.
27. Schaeffer AJ. Urinary tract infections. In: Gillenwater JY, Grayhack JT, Howards SS, Mitchell ME, editors. Adult and pediatric urology. 4th ed. Philadelphia: Lippincott Williams & Wilkins; 2002. p. 211–72.
28. Craig WD, Wagner BJ, Travis MD. Pyelonephritis: radiologic-pathologic review. Radiographics. 2008;28(1):255–77; quiz 327–8. PMID: 18203942. https://doi.org/10.1148/rg.281075171.
29. Lao H-W, Wu C-J. Ultrasound of renal infectious disease. J Med Ultrasound. 2008;16(2):113–22, issn:0929-6441. https:/www.sciencedirect.com/science/article/pii/S0929644108600120. https://doi.org/10.1016/S0929-6441(08)60012-0.
30. Jeffrey RB, Laing FC, Wing VW, Hoddick W. Sensitivity of sonography in pyonephrosis: a reevaluation. AJR Am J Roentgenol. 1985;144(1):71–3. https://doi.org/10.2214/ajr.144.1.71. PMID: 3880629.
31. Sim KC. Ultrasonography of acute flank pain: a focus on renal stones and acute pyelonephritis. Ultrasonography. 2018;37(4):345–54. https://doi.org/10.14366/usg.17051. Epub 2017 Nov 26. PMID: 29382187; PMCID: PMC6177687.
32. Chen KC, Hung SW, Seow VK, Chong CF, Wang TL, Li YC, Chang H. The role of emergency ultrasound for evaluating acute pyelonephritis in the ED. Am J Emerg Med. 2011;29(7):721–4. https://doi.org/10.1016/j.ajem.2010.01.047. Epub 2010 May 1. PMID: 20825875.
33. Cooper KL, Badalato GM, Rutman MP. Chapter 55. Infections of the urinary tract. In: Campbell-Walsh-Wein urology, 12th ed review. Philadelphia: Elsevier; 2020. p. 1129–1201.
34. Grayson DE, Abbott RM, Levy AD, Sherman PM. Emphysematous infections of the abdomen and pelvis: a pictorial review. Radiographics. 2002;22(3):543–61. https://doi.org/10.1148/radiographics.22.3.g02ma06543. PMID: 12006686.
35. Lu YC, Chiang BJ, Pong YH, Huang KH, Hsueh PR, Huang CY, Pu YS. Predictors of failure of conservative treatment among patients with emphysematous pyelonephritis. BMC Infect Dis. 2014;14:418. https://doi.org/10.1186/1471-2334-14-418. PMID: 25074590; PMCID: PMC4124134.
36. Somani BK, Nabi G, Thorpe P, Hussey J, Cook J, N'Dow J, ABACUS Research Group. Is percutaneous drainage the new gold standard in the management of emphysematous pyelonephritis? Evidence from a systematic review. J Urol. 2008;179(5):1844–9. https://doi.org/10.1016/j.juro.2008.01.019. Epub 2008 Mar 19. PMID: 18353396.
37. Huang JJ, Tseng CC. Emphysematous pyelonephritis: clinicoradiological classification, management, prognosis, and pathogenesis. Arch Intern Med. 2000;160(6):797–805. https://doi.org/10.1001/archinte.160.6.797. PMID: 10737279.
38. Choe JH, Lee JY, Lee KS. Accuracy and precision of a new portable ultrasound scanner, the BME-150A, in residual urine volume measurement: a comparison with the BladderScan BVI 3000. Int Urogynecol J Pelvic Floor Dysfunct. 2007;18(6):641–4. https://doi.org/10.1007/s00192-006-0219-2. Epub 2006 Nov 7. PMID: 17115233.
39. Cho MK, Noh EJ, Kim CH. Accuracy and precision of a new portable ultrasound scanner, the Biocon-700, in residual urine volume measurement. Int Urogynecol J. 2017;28(7):1057–61. https://doi.org/10.1007/s00192-016-3224-0. Epub 2016 Dec 10. PMID: 27942791.
40. Bih LI, Ho CC, Tsai SJ, Lai YC, Chow W. Bladder shape impact on the accuracy of ultrasonic estimation of bladder volume. Arch Phys Med Rehabil. 1998;79(12):1553–6. https://doi.org/10.1016/s0003-9993(98)90419-1. PMID: 9862299.

41. Hvarness H, Skjoldbye B, Jakobsen H. Urinary bladder volume measurements: comparison of three ultrasound calculation methods. Scand J Urol Nephrol. 2002;36(3):177–81. https://doi.org/10.1080/003655902320131839. PMID: 12201931.
42. Manieri C, Carter SS, Romano G, Trucchi A, Valenti M, Tubaro A. The diagnosis of bladder outlet obstruction in men by ultrasound measurement of bladder wall thickness. J Urol. 1998;159(3):761–5. PMID: 9474143.
43. Matsumoto M, Tsutaoka T, Yabunaka K, Handa M, Yoshida M, Nakagami G, Sanada H. Development and evaluation of automated ultrasonographic detection of bladder diameter for estimation of bladder urine volume. PLoS One. 2019;14(9):e0219916. https://doi.org/10.1371/journal.pone.0219916. PMID: 31487299; PMCID: PMC6728037.
44. Payen D, de Pont AC, Sakr Y, Spies C, Reinhart K, Vincent JL, Sepsis Occurrence in Acutely Ill Patients (SOAP) Investigators. A positive fluid balance is associated with a worse outcome in patients with acute renal failure. Crit Care. 2008;12(3):R74. https://doi.org/10.1186/cc6916. Epub 2008 Jun 4. PMID: 18533029; PMCID: PMC2481469.
45. Beaubien-Souligny W, Rola P, Haycock K, Bouchard J, Lamarche Y, Spiegel R, Denault AY. Quantifying systemic congestion with point-of-care ultrasound: development of the venous excess ultrasound grading system. Ultrasound J. 2020;12(1):16. https://doi.org/10.1186/s13089-020-00163-w. PMID: 32270297; PMCID: PMC7142196.
46. Bhardwaj V, Vikneswaran G, Rola P, Raju S, Bhat RS, Jayakumar A, Alva A. Combination of inferior vena cava diameter, hepatic venous flow, and portal vein pulsatility index: venous excess ultrasound score (VEXUS score) in predicting acute kidney injury in patients with cardiorenal syndrome: a prospective cohort study. Indian J Crit Care Med. 2020;24(9):783–9. https://doi.org/10.5005/jp-journals-10071-23570. PMID: 33132560; PMCID: PMC7584837.
47. Parolini C, Noce A, Staffolani E, Giarrizzo GF, Costanzi S, Splendiani G. Renal resistive index and long-term outcome in chronic nephropathies. Radiology. 2009;252(3):888–96. https://doi.org/10.1148/radiol.2523080351. Epub 2009 Jun 15. PMID: 19528356.

19 Obstetric and Gynaecological Ultrasound

Mohammad Fadhly Yahya,
Mohd Hafis Mohamed Sakan,
and Nor Hanisah Mohd Said

19.1 Introduction

Ultrasound is cost-effective, non-invasive and easily available in most centres that provide acute and critical care. It reduces time to diagnosis and is very useful in resource-limited settings [1].

Furthermore, ultrasound use poses no radiation risk to the growing fetus. This makes it a safe and valuable initial investigation modality for various acute obstetric and gynaecological conditions.

Point-of-care ultrasound (POCUS) is incorporated as part of an adjunct or an extension of clinical evaluation in the treatment strategy of time-sensitive critically ill conditions. It is performed to answer specific clinical questions that would help to determine the most appropriate course of action or intervention. It increases the providers confidence in managing these patients because of the ability to generate the relevant clinical information firsthand [2]. Over the years, POCUS has become the standard of care for diagnostic and therapeutic interventions in centres with developed medical systems. Due to its cost-effectiveness, availability and robust applications, the use of POCUS has spread fast among resource-limited countries since its introduction. In a recent survey performed, POCUS in obstetrics has been one of the top indications apart from cardiac and lungs in these countries [3].

As part of the management of patients with acute obstetric and gynaecological conditions, POCUS examination is used as an extension of physical assessment and the images are interpreted immediately, correlating to the patient symptoms and signs. It is used to answer specific questions and assist the treating physicians in various aspects such as interventional, diagnostic and screening, throughout the patients' care [4]. POCUS should not be used as a substitute for the more comprehensive imaging by the dedicated sonographer [2].

POCUS plays a very important role in the evaluation of shock. Ultrasound protocol such as the RUSH exam [5] simplified a three-step algorithm that rapidly assess both the physiological and anatomical derangements in shock patients, concurrent with shock management. In the absence of abdominal trauma, the identification of intraperitoneal free fluid in a shock patient of reproductive age should be considered a ruptured ectopic until proven otherwise. Equally, in an overtly shock patient, in the absence of intraperitoneal free fluid, a ruptured ectopic is unlikely to be the cause of haemodynamic instability. By integrating POCUS as part of multi-systemic clinical assessment, other types of shock will be evident: cardiogenic, obstructive or distributive.

This will be revealed when incorporating ultrasound protocols such as the RUSH exam, looking objectively at the pump, tank and pipes.

M. F. Yahya (✉) · M. H. M. Sakan
Emergency and Trauma Department, Melaka General Hospital, Melaka, Malaysia

N. H. M. Said
Hospital Pantai Ayer Keroh, Melaka, Malaysia

© The Author(s), under exclusive license to Springer Nature Switzerland AG 2024

N. Bouarroudj et al. (eds.), *POCUS in Critical Care, Anesthesia and Emergency Medicine*,
https://doi.org/10.1007/978-3-031-43721-2_19

During the assessment and treatment strategy of shock patients, the cornerstone of management is the identification of abnormal fluid collection during POCUS examination. Transabdominal ultrasound has been proven to be highly sensitive at detecting free fluids. In one study, fluid amount as low as 100 mL can already be detected by the examiners [6], and non-radiologists can perform bedside ultrasound equally well as the radiologists. POCUS examination also needs to identify the missing intrauterine gestational sac or the presence of tubal sac [4] to suggest an ectopic or extrauterine pregnancy. The finding of an intrauterine pregnancy (IUP) deemed ruptured ectopic unlikely.

POCUS is also useful when evaluating acute pelvic or lower abdominal pain among females in the emergency or acute care settings. It is a common presentation of vast differentials, with the causes that can originate from various different organ systems, namely gynaecological, gastrointestinal, urological, vascular and musculoskeletal. History, physical examination, the presence of associated symptoms and menstrual history often is able to narrow down the differentials. Considering the wide range of possible differential diagnoses, bedside ultrasound is the best initial imaging tool. In females of childbearing age, it is important to identify pregnancy early as ruptured ectopic pregnancy carries significant mortality.

Important differentials to consider when evaluating a female with lower abdominal pain are:

- Ectopic pregnancy
- Ruptured ovarian cyst
- Adnexal torsion
- Haemorrhagic cysts
- Pelvic inflammatory disease
- Tubo-ovarian abscess
- Dysmenorrhoea
- Endometriosis

Other clinically important non-gynaecological diagnoses to consider are:

- Ureteral obstruction
- Hydronephrosis
- Renal stones
- Pyelonephritis
- Appendicitis
- Diverticulitis

POCUS will be able to point to the right diagnosis, trigger the necessary referral and guide further investigations and imaging. In a broad population group, POCUS has benefited 27% of the treating physicians. POCUS also caused immediate change of treatment in a number of patients within the group studied [7].

POCUS is useful in the evaluation of patients presented with PV bleed. Ectopic pregnancy needs to be excluded early as PV bleeding is a common presenting symptom. It occurs in more than 75% of the cases in one study [8]. The presence of intrauterine pregnancy (IUP) (gestational sac + yolk sac and embryo) on ultrasound can safely exclude ectopic pregnancy. There are various causes of PV bleeding during pregnancy. Early pregnancy (<20 weeks) causes of PV bleeding include ruptured ectopic pregnancy, missed and incomplete abortion. During antenatal period of >20 weeks, PV bleeding can be caused by placenta abruption, placenta previa, uterine rupture and retained placenta.

Although studies evaluating the use of POCUS on safety and quality of care in obstetrics and gynaecology are still lacking, the widespread and ongoing use of POCUS as basic bedside imaging modality to aid in diagnosis and guide management of various acute obstetric and gynaecological conditions strongly implies that POCUS can improve outcomes [2].

19.2 Principles

Understanding the basic principles of ultrasound and its application in obstetric and gynaecological conditions is important to assist in image interpretation and making accurate diagnosis.

Ultrasound image is created when current is passed through the piezoelectric crystals within the transducer. The passing current contracts and expands these crystals creating waves of ultrasound beam that is projected to the various tissues within its direction of trajectory. Depending on the nature and biophysical properties of the tissues, these ultrasound waves or echoes are then reflected back to the transducer. The transducer then reconverts these waves into electrical currents, which is then analysed to construct an

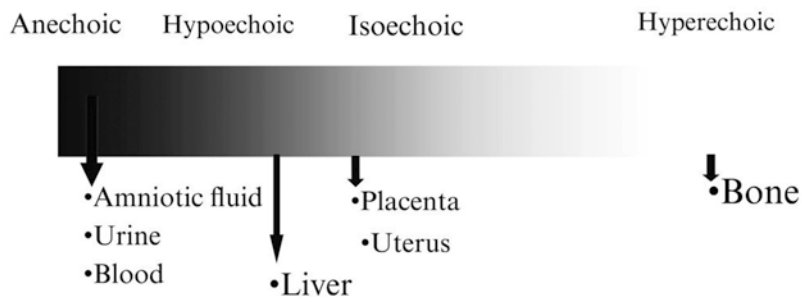

Fig. 19.1 The comparison of various ultrasonic echogenicity of different tissues

image [9]. Based on the different echo image displayed, we can have an understanding of the underlying anatomy and pathophysiology (Fig. 19.1).

Ultrasound is an excellent imaging modality to detect and identify cystic structures. In principle, simple cysts will appear as distinctive, well-defined, anechoic, spheroid structures with posterior acoustic enhancement [10]. The presence of debris or haemorrhage within the cysts will appear as internal echoes.

Various modes exist to display the properties of these reflected echoes. The most basic and commonly used is B-mode or Brightness mode. Each ultrasound beam produces a single line of image and when all lines are constructed together, they form a single frame. The frames are constructed at a fast rate of about 100 frames per second thus creating 'real-time' display [11]. This is commonly referred to as the two-dimensional or 2D-imaging. POCUS utilises B-mode in all the scenarios described in the subsequent topics in this chapter. B-mode is available in all basic ultrasound devices.

M-mode or motion mode traces motion within the tissues. M-mode can be used to determine fetal heart rate. Fetal viability is the term used to describe the identification of a fetal heartbeat, which is achieved most easily using ultrasound [12]. Identifying embryonic viability is one of the objectives when performing POCUS in early pregnancy, but most of the time, B-mode is sufficient to demonstrate fetal cardiac activity.

Doppler mode utilises the Doppler shift, i.e. the relative movement of the tissues to or from the transmitted ultrasound beam. The difference in the magnitude of the velocity change is what determines the frequency signals intensity. It is displayed in terms of spectral Doppler and colour Doppler. In colour Doppler, the image is superimposed on the B-mode image to better demonstrate its relationship with the surrounding tissues [11]. Flow direction and velocity can be determined using this mode. Doppler mode is used frequently to investigate flow inside blood vessels of various pelvic organs, including the placental circulation.

Understanding bio-effects of this technology is important to ensure its safety when subjected onto the dividing and proliferating cells of the growing fetus. Biological effects of ultrasound are in general based on the concern that thermal energy might be dissipated as a result from the ultrasonic propagation of energy [11]. Tissue temperature rises due to this heat absorption, albeit at a very small scale. A statement by International Society of Ultrasound in Obstetrics and Gynecology (ISUOG) supported the safety use of B-mode and M-mode for all stages of pregnancy [13]. The society also emphasised caution when using Doppler mode, especially when scrutinising a very small region of interest particularly adjacent to the bone due to the potentially significant temperature rise. If clinically indicated, ALARA principle (As Low As Reasonably Achievable) should be practised [14].

19.3 Normal Anatomy

19.3.1 Pelvic Cavity

The part of the abdomino-pelvic cavity that is bounded by the pelvic bones. It is funnel-shaped and spans from the iliac crest to the pelvic diaphragm inferiorly. The female pelvic cavity contains upper vagina, uterus, Fallopian tubes,

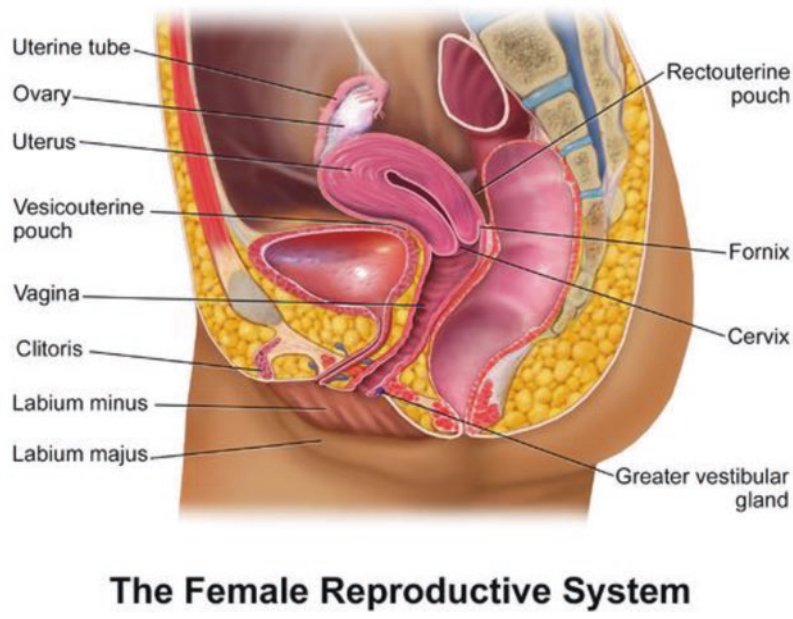

Fig. 19.2 The pelvic cavity. The relations of pelvic organs within the pelvic cavity. Note the potential spaces within the cavity, namely the vesicouterine and rectouterine pouch. (Imej: Blausen.com staff (2014). Medical gallery of Blausen Medical 2014. WikiJournal of Medicine 1(2). https://doi.org/10.15347/wjm/2014.010. issn:2002-4436. CC BY 3.0)

ovaries, intestinal tracts, urinary bladder, ureters and proximal urethra (Fig. 19.2). The peritoneum covering the female pelvic organs passes from the anterior abdominal wall onto the superior surface of the bladder, passes then posteriorly to cover the uterus and rectum. The deflection of this peritoneal lining at two areas of recesses within the pelvic cavity forms the cul-de-sacs [15].

19.3.2 Anterior Cul-de-Sac

Also called the vesicouterine pouch. The potential space between the bladder and anterior uterus. This space diminishes as the bladder is filled with urine.

19.3.3 Posterior Cul-de-Sac

Also termed the rectouterine pouch or Pouch of Douglas. This potential space is the most posterior and most dependent part of the female pelvic cavity.

Identifying these cul-de-sacs when performing POCUS is important as these are the potential spaces where free fluid will accumulate first due to their most dependent locations within the pelvic cavity.

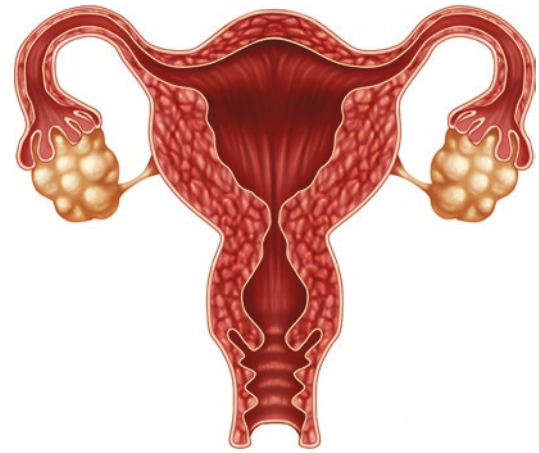

Fig. 19.3 The uterus and ovaries. The uterus is suspended at its axis by various pelvic ligaments. Note the positions of bilateral ovaries

19.3.4 Uterine Anatomy

19.3.4.1 Description

Uterus is a muscular hollow organ within the female pelvic cavity (Fig. 19.3). It is pear-shaped and its wall comprises three layers: Endometrium

(inner mucosal layer), myometrium (muscle layer) and serosa (outer membrane). Thickening of endometrium mucosal lining varies throughout menstrual phase.

19.3.4.2 Size

Varies depending on the pubertal stage. Nulliparous size: 7 cm length, 5 cm width and 5 cm in thickness. Slightly larger in multiparous. Uterine size decreases in postmenopausal.

19.3.5 Relations and Position

Typically located midline in the pelvic cavity. Situated between the bladder anteriorly and the rectum posteriorly. Variations exist whereby it might lie slightly lateral to the right or left from the midline. Uterus is suspended at its position and axis by the uterosacral/cardinal ligament complex, the round ligament (extension of the uterus) and the broad ligament [15]. These support structures are dynamic and flexible which allow some degree of mobility of the uterus and its variations in normal positions: anteverted, anteflex, retroverted, retroflex.

19.3.6 Ovarian Anatomy

Description: Ovaries are a pair of female reproductive organs where ova are produced. They are almond-shaped and contain numerous fluid-filled follicles. Ovaries received dual blood supplies: the ovarian artery (main supply) and branches of uterine artery.

Size: Ovary size varies depending on the age and phase of the menstrual cycle. It measures at 4 cm long, 3 cm wide and 2 cm in thickness. The ovaries decrease in size in postmenopausal due to atrophy.

Relations and position: Ovaries are located within the adnexa on both sides. Each ovary is suspended lateral and posterior to the uterus on both sides. It is attached to utero-ovarian ligament (attaches it to the uterus), the suspensory ligament (attaches it to pelvic wall) and the broad ligament (the mesovarium) [15].

19.4 Preparation, Equipment and Techniques

In general, two techniques are available for the routine scanning of obstetric and gynaecological ultrasound: Transabdominal (TAS) and transvaginal (TVS) scans. TAS is more easily performed, faster, readily available and less invasive compared to TVS.

TVS allows better visualisation of the endometrial contents and adnexal regions. In early pregnancy, TVS would provide better view of early intrauterine or extrauterine gestational sac [16]. However, TVS requires a different skillset, less appropriate is some patient groups (e.g. paediatrics) as it is more invasive and can only be performed by those who have the appropriate skills and credentials. Furthermore, transvaginal probes are not the general standard set of probes available in most emergency and ICU settings. TVS should also be deferred in some cases where there is obvious haemoperitoneum in the context of haemodynamic instability where ectopic pregnancy can readily be diagnosed transabdominally. TVS can also be deferred if there is clear IUP, ovaries are well-visualised with no mass and there is no intraperitoneal free fluid [16]. Therefore, only TAS will be discussed here.

19.4.1 Preparation

POCUS can be performed by individuals who have participated in continuous medical education and teachings in the use of diagnostic ultrasonography and have undergone trainings in point-of-care ultrasound. The individual should also be well-versed with the locally existing and appropriate care pathways upon discovery of suspicious or abnormal findings.

The patient lies supine, appropriately exposed for the examination and ideally with filled urinary bladder.

Fig. 19.4 The Curvilinear Transducer: low frequency of curvilinear probe is preferred for deeper tissues and structures. It also has the appropriate footprint for pelvic and transabdominal sonography

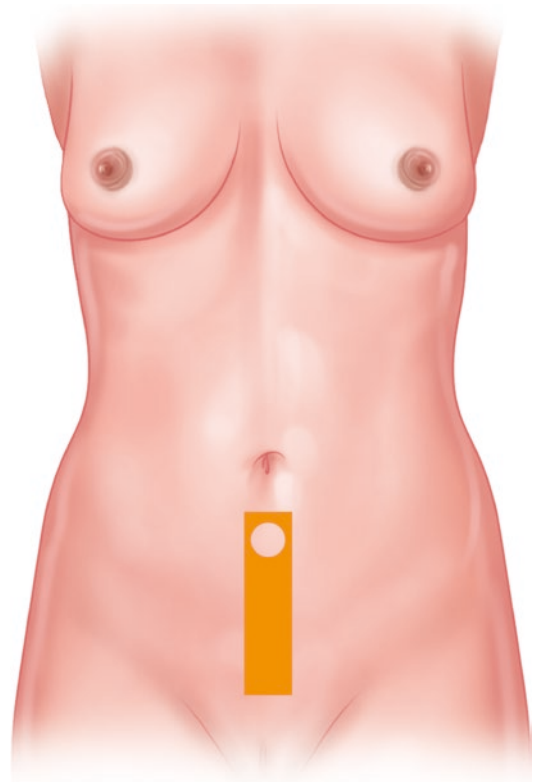

Fig. 19.5 Transabdominal sagittal plane

19.4.2 Equipment

- Transabdominal scan (TAS): An ultrasound machine with at least the capabilities of real-time, grey scale two-dimensional (2D) imaging.
- Transabdominal transducer (standard curvilinear 3–5 MHz) (Fig. 19.4).
- Adjustable acoustic power output controls with output display standards.
- Freeze frame and zoom capabilities.
- Preferably with electronic calipers and capacity to store images.
- Regular maintenance and servicing [12].

19.4.3 Technique

19.4.3.1 Sagittal Plane

Place transducer in sagittal plane just above the pubis symphysis (Fig. 19.5). Point marker to the patient's head. Start scanning with the probe transducer at the midline of the body to find the uterus at its long axis. In most cases, the body and fundus of the uterus will be visualised at this level. Look for the area between the bladder and uterus (anterior cul-de-sac) and the area between the bladder and bright rectum (posterior cul-de-sac). To improve visualisation, make small adjustments on the probe positions to appreciate the underneath structures better while keeping the uterus in the midline. Adjust the depth of the sector image to include the structures in question. Adjust the image Gain and TGC (Time Gain Compensation) to best differentiate these structures (Gain that is too high would amplify the noise. This would result in an image that is too bright and image differentiation would be lost).

19.4.3.2 Transverse Plane

From the sagittal plane, on the long axis of the uterus, rotate the probe 90°. Point marker to the patient's right (Fig. 19.6). The transducer is cur-

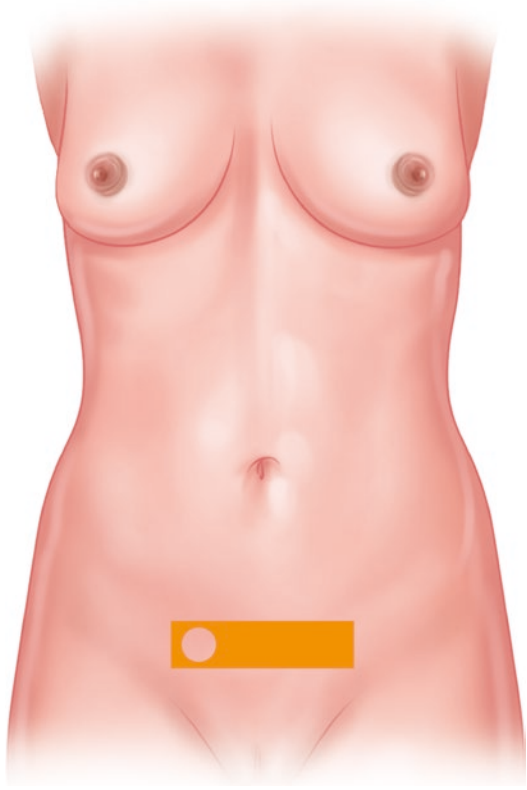

rently along the transverse plane over the patient's suprapubic region. Identify all the important pelvic structures, namely the uterus, bladder, the anterior and posterior cul-de-sacs and the ovaries. To visualise the ovaries and adnexa better, rock the probe along its long axis to the right or to the left. The adnexa and ovaries will appear immediately lateral to the uterus.

Fig. 19.6 Transabdominal transverse plane

19.5 Sonoanatomy

19.5.1 Transabdominal Sagittal Plane (Fig. 19.7)

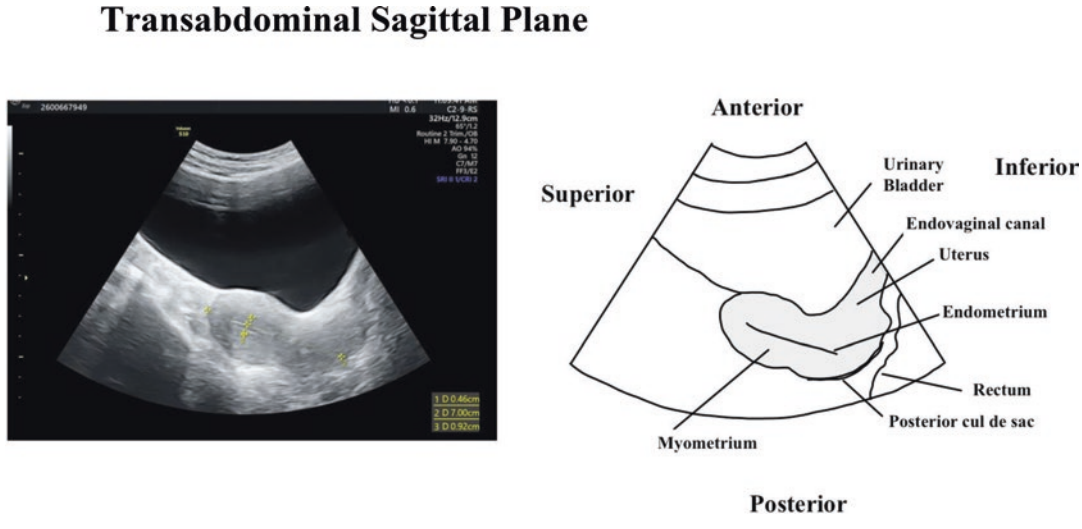

Fig. 19.7 Sonoanatomy of transabdominal sagittal plane

19.5.2 Transabdominal Transverse Plane (Figs. 19.8, 19.9, and 19.10)

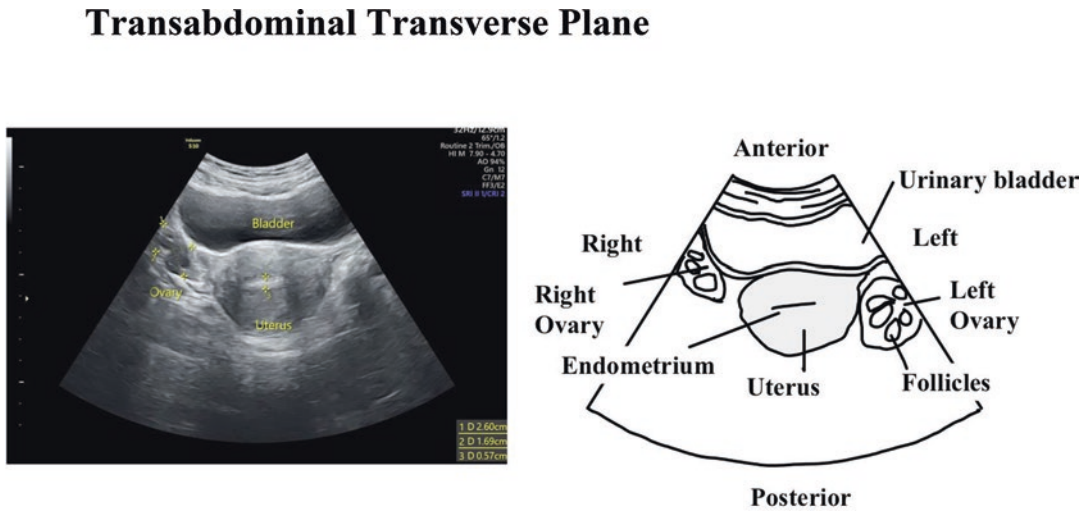

Fig. 19.8 Sonanatomy of transabdominal transverse plane

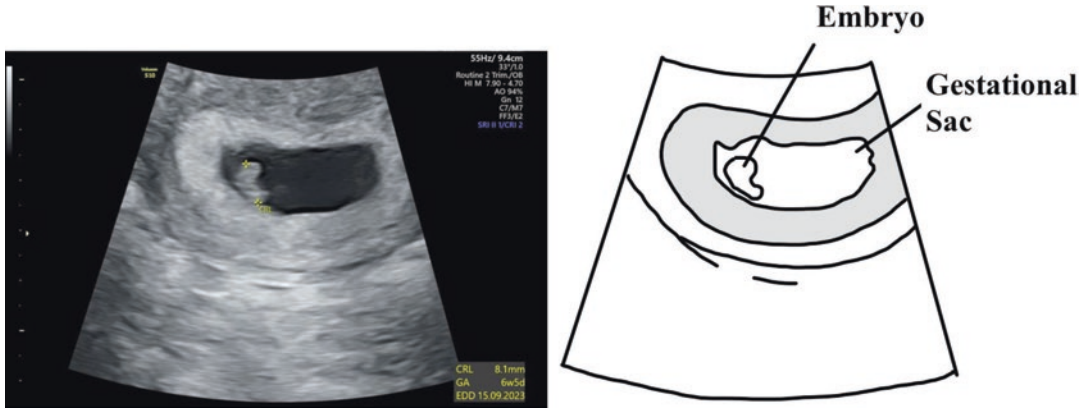

Fig. 19.9 Sonoanatomy of early pregnancy: embryo

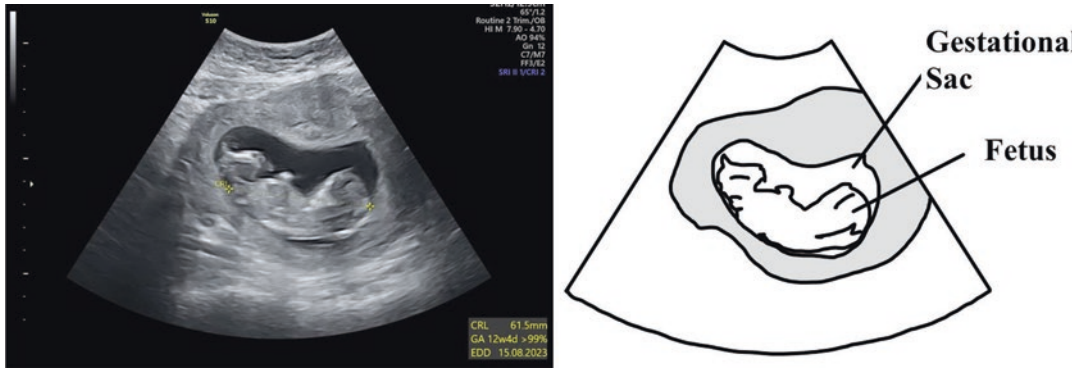

Fig. 19.10 Sonoanatomy of early pregnancy: fetus

19.6 POCUS in First Trimester Pregnancy Sonography of Important Pathology

19.6.1 Ectopic Pregnancy

Trace amounts of fluids in cul-de-sac might be normal in women of childbearing age. But in patient who is at risk, any amount of fluid within this cul-de-sac that is more than trace should be considered abnormal (Fig. 19.11).

In a woman with a positive pregnancy test, the most specific criteria for ectopic pregnancy is the identification of an extrauterine gestational sac that contains a yolk sac or an embryo, with or without cardiac activity (100% specific, 63% sensitivity). A less stringent criteria is the identification of complex adnexal mass with no intrauterine pregnancy (93–99.5% specificity, 21–84% sensitivity). The most lenient criteria: Free intraperitoneal fluid in cul-de-sac and an empty uterus (69% specificity, 63% sensitivity) [17].

More significantly, in a pregnant female, free fluid in hepatorenal recesses, i.e. Morrison's pouch view, is highly suggestive of operative intervention [18] (Fig. 19.12). This suggests that the additional ultrasound view at the Morrison's pouch may provide useful and immediate information regarding patient's disposition. In another study, the risk of ectopic pregnancy rose to 100% when volume of peritoneal fluid is judged to be moderate or large in amount [19] (Fig. 19.13).

The presence of echogenic free fluids (small suspended particles appeared as fleck of white and swirls with agitation or breathing) is suggestive of haemorrhagic in nature, hence a worrisome feature [16, 17]. It has positive predictive value of 86–93% in the diagnosis of ectopic pregnancy [16] (Fig. 19.14). Furthermore, over time, blood clot will form and could be seen surrounding the uterus, giving the uterus an appearance of ill-defined margins [17].

19.6.2 Molar Pregnancy

Molar pregnancy or hydatidiform mole is one of the commonest forms of gestational trophoblastic diseases, occurring in one of every 1000–2000 pregnancies [20]. Most patients present with vaginal bleed and examination revealed uterus that is larger than the expected gestational age. The chorionic villi are converted to a mass of clear vesicles and on ultrasound examination, this appears as a 'cluster of grapes' within the uterus. Other descriptions include 'Snowstorm appearance' [21] and 'Swiss-cheese pattern' (Fig. 19.15). These ultrasonic features represent solid collection of echoes with numerous anechoic spaces [20].

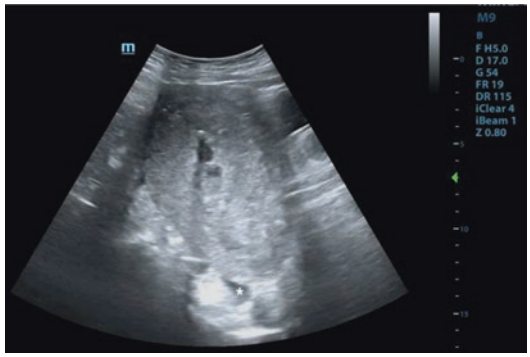

Fig. 19.11 Small amount of free fluid in rectovesical pouch, i.e. Pouch of Douglas (*)

Fig. 19.12 Free fluid in hepatorenal recesses, i.e. Morrison's Pouch (*) highly suggestive of moderate to large amount of free fluid and the need for operative intervention

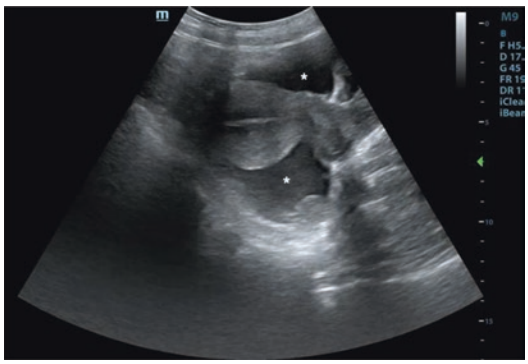

Fig. 19.13 Large amount of free fluids in pelvic cavity (*)

Fig. 19.14 Large amount of free fluid in pelvic cavity. Note the echogenic nature of the free fluid and the presence of clots (*)

Fig. 19.15 Transverse plane. Molar pregnancy. The enlarged uterus is filled with numerous vesicles of various sizes. No fetus is seen. (Courtesy of Dr. Norafidah Ahmad KPJ Sabah Specialist Hospital, Malaysia)

19.6.3 Missed/Incomplete Abortion

PV bleeding and abdominal pain in early pregnancy are the most common complaints upon presentation. Fetal viability is the most important question when performing POCUS. These features were shown to have 100% specificity of missed miscarriage/abortion:

- An initial US scan of an empty gestational sac when the Mean Sac Diameter (MSD) >25 mm.
- US scan of an embryo with no heart activity when CRL > 7 mm (Fig. 19.16).
- Beyond 70 days gestation, Mean Sac Diameter of >18 mm with no visible embryo [22].

19.6.3.1 Incomplete Abortion

In incomplete abortion, there is partial loss and incomplete passage of product of conception. Ultrasound would reveal a uterus with any endometrial thickness with the presence of heterogenous tissues with or without embryonic sac and a distorting midline endometrial echo [23] (the remaining product of conception) (Figs.19.17, 19.18, and 19.19).

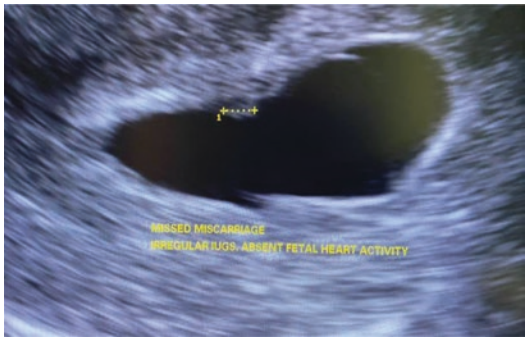

Fig. 19.16 Transverse plane. Missed abortion. Patient presented with PV bleeding during her early pregnancy. Ultrasound showed absent heart activity. CRL >7 mm. (Courtesy of Dr. Norafidah Ahmad KPJ Sabah Specialist Hospital, Malaysia)

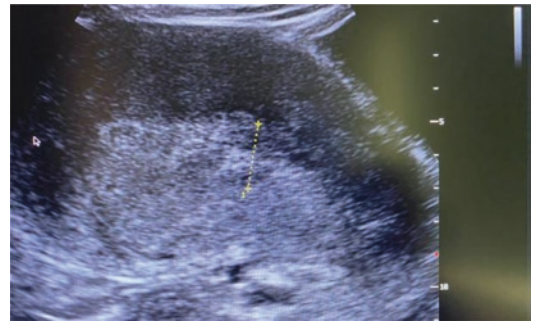

Fig. 19.17 Transverse plane. Incomplete abortion. Ultrasound shows focal mass of mixed echogenicity within the endometrium. (Courtesy of Dr. Norafidah Ahmad KPJ Sabah Specialist Hospital, Malaysia)

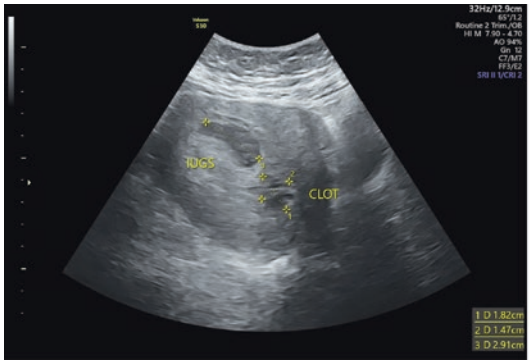

Figs. 19.18 and 19.19 Incomplete abortion. Patient presented with abdominal pain and PV bleed at 7 weeks of pregnancy. Ultrasound revealed irregular sac with heterogenous and thickened endometrium. There is also the presence of blood clot within endometrial cavity

19.7 POCUS in Antenatal (Second and Third Trimester Pregnancy) Sonography of Important Pathology

19.7.1 Placental Abruption (Abruptio Placentae)

It is described as the premature separation of the normally implanted placenta after the 20th week gestation and before the third stage of labour. Patient usually presents with PV bleed, shock and 'board-like' abdominal tone. Bleeding can sometimes be concealed, resulting in retroplacental haemorrhage and clot. It is potentially fatal due to exsanguination. Ultrasound features of placental abruption include a visible retroplacental haematoma of variable echogenicity (Fig. 19.20), intraplacental anechoic areas, separation and rounding of the placental edge. These are highly specific for placental abruption (96% specificity) but only seen in 11% of cases of placental abruption [24].

Ultrasound is not sensitive to detect this condition (24% Sensitivity) [24]. This is because haematoma is often isoechoic to the placenta, thus it can be mistakenly seen as focal thickening of the placenta. Furthermore, blood might have trickled down and escaped through the vagina resulting in external haemorrhage, clearing out the retroplacental blood. Hence, in most conditions, normal ultrasound does not rule out placental abruption.

19.7.2 Placenta Previa

Patient typically presents with painless vaginal bleed within the second half of pregnancy (>20 weeks gestation). In placenta previa, the maturing placenta covers the internal os (Grades III and IV) or lies very close to it (Grades I and II).

The position of the lower placental edge in relation with the internal os of the cervix is the defining feature. Placenta previa is suspected if the placenta appears to cover the cervix or within 2 cm from the edge of the cervix [25] (Figs. 19.21 and 19.22).

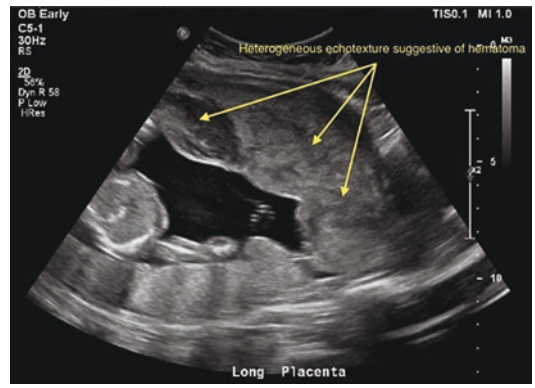

Fig. 19.20 Ultrasound showed anteriorly located heterogenous and hypoechoic mass suggestive of placental abruption. (Photo credit to Page N, Roloff K, Modi AP, et al. (2020). Management of placental abruption following blunt abdominal trauma. Cureus 12(9): e10337. https://doi.org/10.7759/cureus.10337)

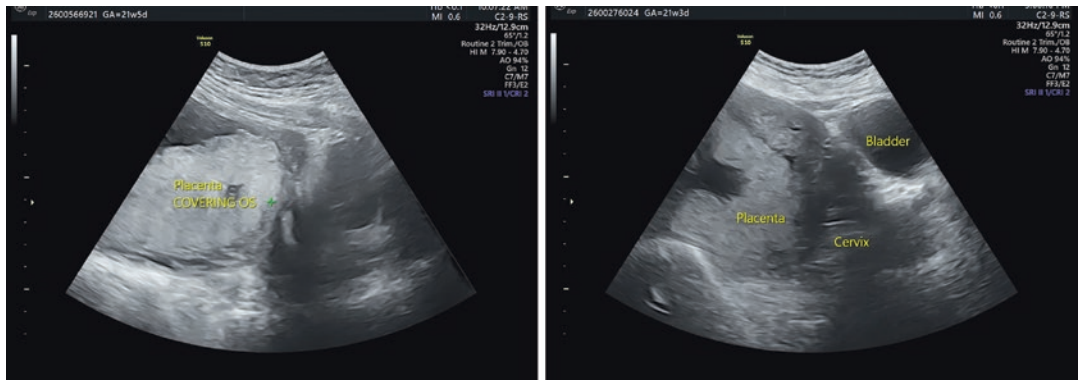

Figs. 19.21 and 19.22 Transabdominal ultrasound showing placenta completely covering the internal os of the cervix (*) in both patients

19.7.3 Uterine Rupture

A catastrophic event that is life-threatening for both mother and fetus. It is due to the disruption of the layers of uterus, including serosa, i.e. visceral peritoneum, after 28 weeks of gestation with or without the baby lying in the peritoneal cavity. There are no universal criteria for diagnosing uterine rupture as the clinical manifestations are highly variable and depend on the timing, extent of rupture and site of rupture. Suspect uterine rupture in a pregnant female who presents with abdominal pain, vaginal bleed with or without shock and loss of station of the fetal presenting part.

Point-of-care ultrasound would reveal indirect ultrasound findings such as intraperitoneal free fluids and extrauterine haematoma. Direct ultrasound findings include the identification of the protruding portion of the amniotic sac [26], thin wall with bulging of the fetal parts and visualisation of the ruptured portion of the uterus [27, 28] (Fig. 19.23).

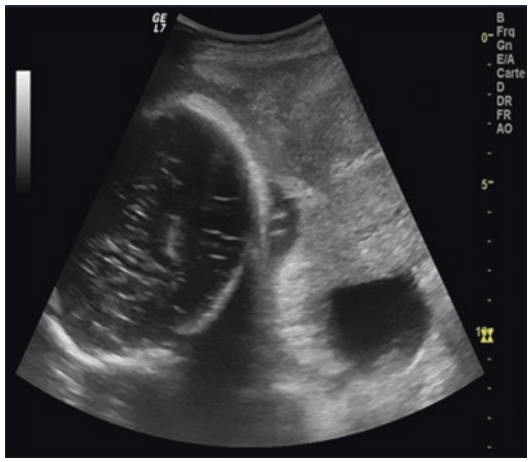

Fig. 19.23 Uterine rupture visualising the ruptured part of the uterus and fetal parts (fetal head) outside of uterus. (Photo credit to Guena M, Alapha F, Tiodjio S, Nganyou I, Houmtie C, Nana A. (2018) Non-laboring uterine rupture of an unscared uterus before term discover during obstetric ultrasound. Case Reports in Clinical Medicine, 7, 47–54. https://doi.org/10.4236/crcm.2018.71004. Creative Commons Attribution 4.0 International License. (CC BY 4.0))

19.7.4 Fetal Demise

Fetal death is the loss of fetus at any stage during the pregnancy [29]. Various terms exist and fetal death that occurs before the 20th week of gestation is commonly termed spontaneous abortion and those that occur after the 20th week are classified as fetal demise or stillbirth [30].

Fetal demise is often suggested by the reduced fetal movements and the inability to detect fetal heart tones on examination. It is diagnosed by visualisation of the absence of cardiac activity on bedside ultrasound.

19.7.5 Retained Placenta

Patient commonly presents with secondary postpartum haemorrhage. The retained product of conception may also become the foci of infection.

On ultrasound, the retained product of conception is suggested by the presence of heterogenous echogenic material within the endometrium representing a mass (Fig. 19.24) [31]. It is often accompanied by the presence of residual placental calcifications, appeared as focal areas of increased echogenicity [26].

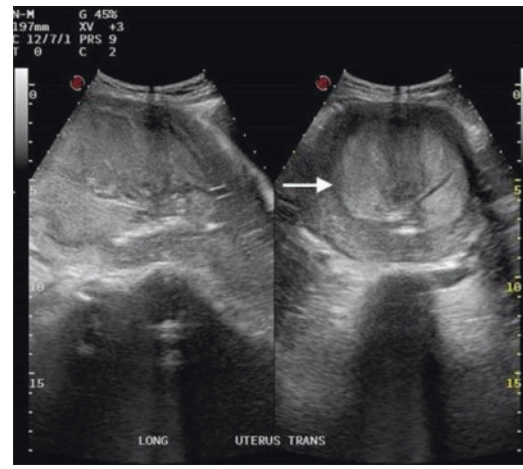

Fig. 19.24 Ultrasound showing endometrial mass (arrow) in a patient with retained placenta with postpartum fever

19.8 POCUS in the Non-Pregnant with Lower Abdominal Pain Sonography of Important Pathology

19.8.1 Ovarian Cysts Accident (Ruptured, Twisted, Haemorrhage)

Ovarian cyst is often described as any fluid collection surrounded by a thin wall within the ovary that exceeds 2.5–3 cm in measurement [32] (Figs. 19.25, 19.26, and 19.27). With ultrasound, ruptured cysts can be seen as cystic structures with irregular borders. It is often accompanied by free intraperitoneal fluid.

Haemorrhagic ovarian cyst occurs when a blood vessel breaks into an existing functional ovarian cyst causing stretching of the cyst capsule, resulting in severe lower abdominal pain. The blood forms into clot and spontaneously undergoes resorption over time [33], and this can be seen as an echogenic content with thin septations within the cyst (Figs. 19.28 and 19.29). Ultrasound image might vary depending on the stages of the haemorrhage and clot resorption. A ruptured haemorrhagic ovarian cyst might cause large intraperitoneal bleed which could be seen as free intraperitoneal fluid during POCUS examination.

Partial or complete twist or torsion of the ovarian pedicle can cause obstruction to venous and arterial blood flow. This condition is difficult to diagnose clinically as symptoms can be vague and non-specific.

High index of suspicion is required and POCUS might help. The twisted ovary will increase in size due to engorgement and oedematous changes. Ovaries greater than 4 cm is abnormally enlarged. Compare both sides of ovaries during scanning. The ovarian stroma is heterogenous in appearance due to the oedema and swelling. The follicles will be peripherally displaced within the ovary giving the appearance of a string of pearls (Fig. 19.30) [34]. Absence of blood flow on colour flow Doppler is a highly specific finding of torsion, but normal blood flow does not rule out torsion due to the ovarian dual blood supply (Fig. 19.31).

Due to the twisting of the pedicle and progressive swelling and enlargement, the ovary is often

Fig. 19.25 A 3.6 × 3cm Anechoic thick-wall cystic structure in left ovary suggestive of an ovarian cyst

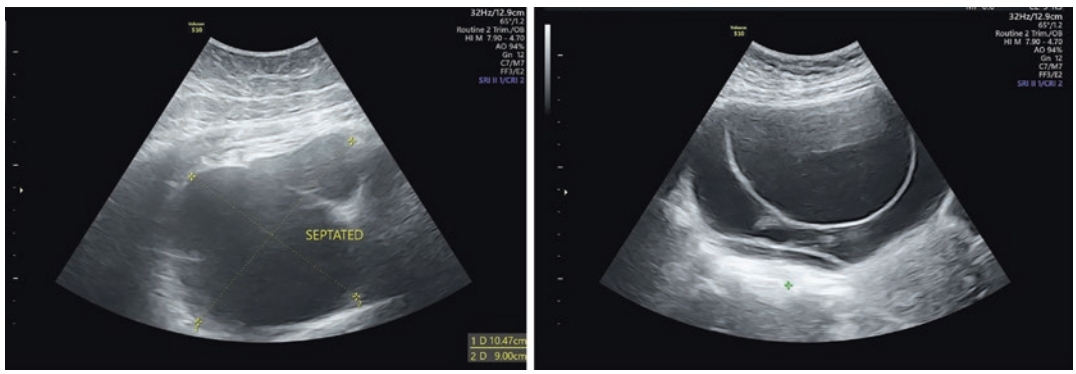

Figs. 19.26 and 19.27 Huge thin-walled, septated ovarian cyst measuring 10 × 9 cm in left ovary. Huge cysts are prone to rupture and haemorrhage. They can also twist at the ovarian pedicle causing ovarian torsion

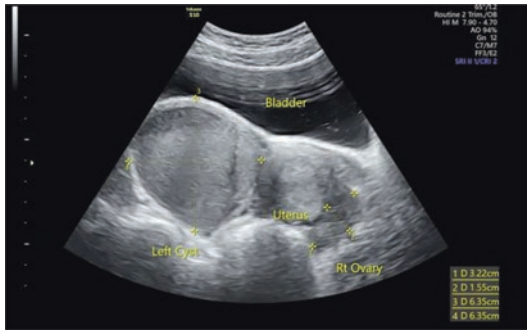

Fig. 19.28 Ultrasound image of a female presented with sudden onset of lower abdominal pain. Cystic structure with thin wall measuring 6.3 × 6.3 cm with ground glass echogenicity suggestive of haemorrhage and intracystic solid clot

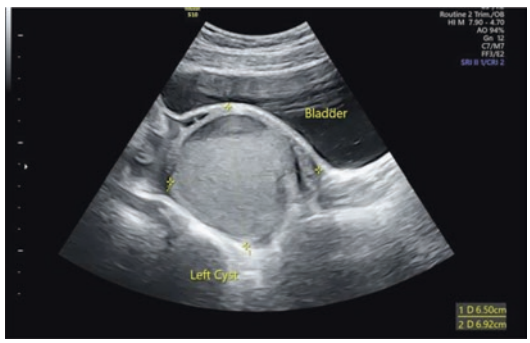

Fig. 19.29 Same patient. Notice the fluid-blood level within the cyst creating a fluid layer

Fig. 19.30 Sudden lower abdominal pain in a nulliparous female. Right ovary measuring >4 cm. Ovary is retracted towards midline and above the uterus. Note also the peripherally located follicles

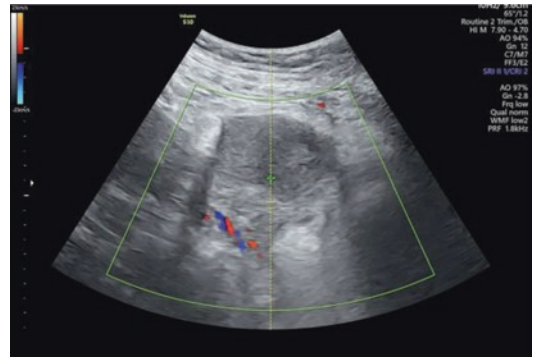

Fig. 19.31 On colour flow Doppler, note the absence of ovarian parenchymal blood flow. The blood flow terminates at the pedicle due to twisting at this level

relocated to the midline and retracted above the uterine fundus. Sometimes, the twisted ovary settles posteriorly within the cul-de-sac. There is also free fluid in the cul-de-sac.

In more than 70% of cases [35], there is often the presence of other pathology that predisposes the ovaries to twist, for example, dermoid cyst and large ovarian cyst. Actively look for these abnormalities during scanning and compare with the contralateral ovary. Ovarian hyperstimulation for infertility treatment might also predispose this condition as enlargement of the ovaries is expected following hyperstimulation.

19.8.2 Tubo-Ovarian Abscess

Tubo-ovarian abscess is a complication of pelvic inflammatory disease. There is unilateral or often bilateral complex cystic mass, with fluid-filled Fallopian tube (Fig. 19.32). Cross-sectional view of this tube might reveal ‘Cogwheel sign’ that indicates thickened endosalpingeal folds. This abscess can form a complex which is often located within the cul-de-sac (the Tubo-Ovarian Complex) [36]. There is also the presence of echogenic free fluids within the Pouch of Douglas.

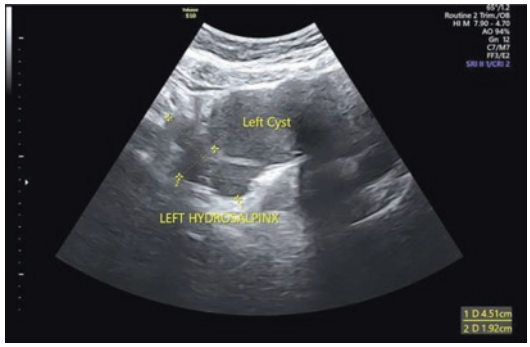

Fig. 19.32 Patient presented with suprapubic pain and sepsis. Note the thick tubal wall with incomplete septae within the tube, at cross-sectional view of the tube resembling 'Cogwheel sign'. The left cystic structure indicates an ovarian abscess. There is also fluid-filled dilation of the fallopian tube (Hydrosalpinx)

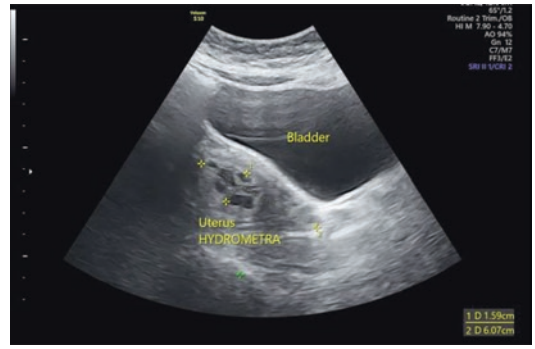

Fig. 19.34 Longitudinal ultrasound view of a female presented with fever and suprapubic pain. Ultrasound showed the presence of clear hypoechoic distension within the endometrial cavity suggestive of fluid collection (Hydrometra). The endometrial pipelle sampling from this lesion grew *E. coli and Klebsiella*

Fig. 19.33 Transverse pelvic view showed irregular mass of abnormal mixed echotexture within the right adnexa. Incomplete thick-walled septation within the mass. Features suggest an ovarian abscess

19.8.3 Pelvic Inflammatory Disease

The Fallopian tube wall appeared thickened usually >5 mm and commonly associated with the presence of incomplete septa within the structure (Fig. 19.33). The tube is usually dilated and filled with anechoic material suggestive of fluid collection (hydrosalpinx). There can be also the presence of echogenic fluid within the tube (pyosalpinx) suggestive of pus and cell debris. These fluids might also accumulate within the uterus, giving rise to hydrometra (Fig. 19.34).

Tips and Tricks

- Image optimisation: select the shallowest depth possible to visualise the area of interest. A scanning depth that is unnecessarily too deep will lose its optimum details on that particular area of interest. When the appropriately depth is selected, the echo from this area will be reflected back to the transducer at a shorter time, hence a higher number of frames rate can be achieved, giving a better image resolution. In general, the area on interest should cover about 3/4 of the depth of the sector image.
- If you feel that your scanning probe runs dry, add more gel. Plenty of gel is important as gel provides the 'conductive bridge' that improves the impedance matching between the probe and the abdominal surface. More waves can propagate through the tissue and less waves are reflected back. Don't forget to wipe the probe dry once you finish scanning.
- Adequately filled bladder can result in posterior enhancement artefact. This might reduce the resolution of the posterior structures. Adjust the Time Gain Compensation (TGC) of the deeper structure to improve the image.
- Adequately filled urinary bladder acts as an acoustic window for better sound wave pene-

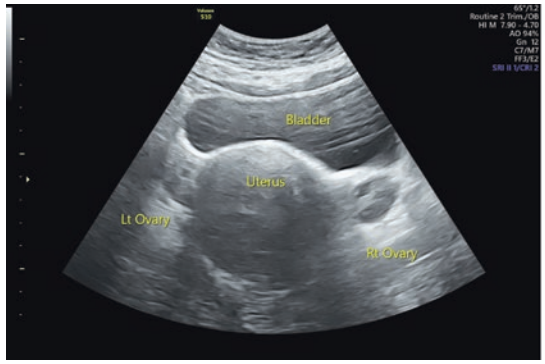

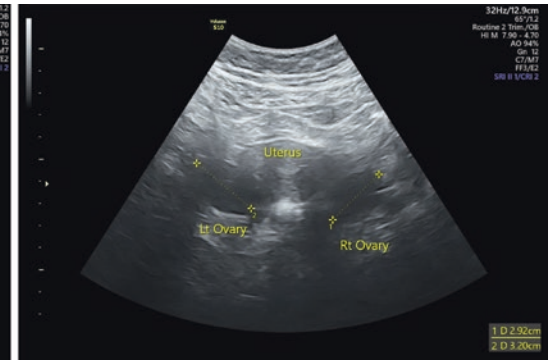

Figs. 19.35 and 19.36 Note the difference when scanning with full bladder (Fig. 19.35) vs empty bladder (Fig. 19.36). With full bladder, the posterior structures (uterus and ovaries) are better visualised

tration and improves visualisation of the underlying pelvic structures (Figs. 19.35 and 19.36). The filled bladder also displaces bowel loops that might be lying superiorly and causing artefacts. Equally important, overfilled bladder can overextend and pushes its dome superiorly into the false pelvis and pushes the pelvic organs out of the view. In this case, partially void the bladder if possible. The best urine volume is when the bladder dome is just at the same level of height as the uterus during scanning.

- At times, a good window can be achieved by adjusting patient positioning and respiratory technique. Put the buttock under the pillow just to elevate it slightly above the bed and let the patient rest comfortably. This manoeuvre would displace the bowel that might overlay the pelvic organs more superiorly towards the abdominal cavity. Making the patient hold her breath at end expiration during scanning might also have the same effect.
- When scanning on patients with lower abdominal pain, tensing of abdominal muscles might affect image quality. Have the patient well-relaxed before scanning, avoid vigorous pressure on the probe and good adequate analgesia are some of the good practices.
- Echogenic free fluid intraperitoneally is suggestive of haemorrhagic nature, especially in the setting of ectopic pregnancy. It appears as a fleck of white within the anechoic dark background of the free fluid. To appreciate this feature better, optimal adjustment of the gain control is required. One useful adjustment is to adjust the gain control and compare with the anechoic urine within the bladder. Adjust the gain slowly to a level that would introduce echo shadows within the urine of the bladder. The optimum gain is just below the level that would generate echo shadows within this urinary bladder.

References

1. Arnold MJ, Jonas CE, Carter RE. Point-of-care ultrasonography. Am Fam Physician. 2020;101(5):275–85. PMID: 32109031.
2. Jain V, O'Quinn C, Van den Hof M. Guideline no. 421: point of care ultrasound in obstetrics and gynaecology. J Obstet Gynaecol Can. 2021;43(9):1094–1099.e1. https://doi.org/10.1016/j.jogc.2021.07.003. Epub 2021 Jul 7. PMID: 34242823.
3. Shokoohi H, Raymond A, Fleming K, Scott J, Kerry V, Haile-Mariam T, Sayeed S, Boniface KS. Assessment of point-of-care ultrasound training for clinical educators in Malawi, Tanzania and Uganda. Ultrasound Med Biol. 2019;45(6):1351–7. https://doi.org/10.1016/j.ultrasmedbio.2019.01.019. Epub 2019 Mar 21. PMID: 30904246.
4. Recker F, Weber E, Strizek B, Gembruch U, Westerway SC, Dietrich CF. Point-of-care ultrasound in obstetrics and gynecology. Arch Gynecol Obstet. 2021;303(4):871–6. https://doi.org/10.1007/s00404-021-05972-5. Epub 2021 Feb 8. PMID: 33558990; PMCID: PMC7985120.
5. Perera P, Mailhot T, Riley D, Mandavia D. The RUSH exam: rapid ultrasound in SHock in the evaluation of the critically ill. Emerg Med Clin North Am. 2010;28(1):29–56, vii. PMID: 19945597. https://doi.org/10.1016/j.emc.2009.09.010.

6. Von Kuenssberg JD, Stiller G, Wagner D. Sensitivity in detecting free intraperitoneal fluid with the pelvic views of the FAST exam. Am J Emerg Med. 2003;21(6):476–8. https://doi.org/10.1016/s0735-6757(03)00162-1. PMID: 14574655.
7. Weile J, Frederiksen CA, Laursen CB, et al. Point-of-care ultrasound induced changes in management of unselected patients in the emergency department—a prospective single-blinded observational trial. Scand J Trauma Resusc Emerg Med. 2020;28:47. https://doi.org/10.1186/s13049-020-00740-x.
8. Casanova BC, Sammel MD, Chittams J, Timbers K, Kulp JL, Barnhart KT. Prediction of outcome in women with symptomatic first-trimester pregnancy: focus on intrauterine rather than ectopic gestation. J Womens Health (Larchmt). 2009;18(2):195–200. https://doi.org/10.1089/jwh.2008.0896. PMID: 18991513; PMCID: PMC2945719.
9. Abuhamad A. Ultrasound in obstetric and gynecology. Open Access e-book. https://www.evms.edu/obstetrics_and_gynecology/ultrasound_in_obstetrics_and_gynecology/?utm_source=shorturl&utm_medium=shorturl&utm_campaign=ultrasoundbook
10. Yacoub JH, Clark JA, Paal EE, Manning MA. Approach to cystic lesions in the abdomen and pelvis, with radiologic-pathologic correlation. Radiographics. 2021;41(5):1368–86. https://doi.org/10.1148/rg.2021200207. PMID: 34469214; PMCID: PMC8415047.
11. WINFOCUS Ultrasound life support basic level 1 instructor course manual, WINFOCUS ASIA.
12. International Society of Ultrasound in Obstetrics and Gynecology, Bilardo CM, Chaoui R, Hyett JA, Kagan KO, Karim JN, Papageorghiou AT, Poon LC, Salomon LJ, Syngelaki A, Nicolaides KH. ISUOG practice guidelines (updated): performance of 11-14-week ultrasound scan. Ultrasound Obstet Gynecol. 2023;61(1):127–43. https://doi.org/10.1002/uog.26106. PMID: 36594739.
13. Abramowicz JS, Kossoff G, Marsal K, Ter Haar G. Safety statement, 2000 (reconfirmed 2003) International Society of Ultrasound in Obstetrics and Gynecology (ISUOG). https://doi.org/10.1002/uog.36.
14. American Institute of Ultrasound in Medicine (AIUM) official statement. Medical ultrasound safety, 4th ed. http://aium.s3.amazonaws.com/resourceLibrary/mus4.pdf.
15. Agur AMR. Grant's atlas of anatomy, international edition. 9th ed. Williams and Wilkins; 1991.
16. Levine D. Ectopic pregnancy. Radiology. 2007;245(2):385–97. https://doi.org/10.1148/radiol.2452061031. PMID: 17940301.
17. Frates MC, Laing FC. Sonographic evaluation of ectopic pregnancy: an update. AJR Am J Roentgenol. 1995;165(2):251–9. https://doi.org/10.2214/ajr.165.2.7618535. PMID: 7618535.
18. Moore C, Todd WM, O'Brien E, Lin H. Free fluid in Morison's pouch on bedside ultrasound predicts need for operative intervention in suspected ectopic pregnancy. Acad Emerg Med. 2007;14(8):755–8. https://doi.org/10.1197/j.aem.2007.04.010. Epub 2007 Jun 6. PMID: 17554008.
19. Russell SA, Filly RA, Damato N. Sonographic diagnosis of ectopic pregnancy with endovaginal probes: what really has changed? J Ultrasound Med. 1993;12(3):145–51. https://doi.org/10.7863/jum.1993.12.3.145. PMID: 8492377.
20. Green CL, Angtuaco TL, Shah HR, Parmley TH. Gestational trophoblastic disease: a spectrum of radiologic diagnosis. Radiographics. 1996;16(6):1371–84. https://doi.org/10.1148/radiographics.16.6.8946542. PMID: 8946542.
21. Abdi A, Stacy S, Mailhot T, Perera P. Ultrasound detection of a molar pregnancy in the emergency department. West J Emerg Med. 2013;14(2):121–2. https://doi.org/10.5811/westjem.2012.7.12994. PMID: 23599844; PMCID: PMC3628456.
22. Preisler J, Kopeika J, Ismail L, Vathanan V, Farren J, Abdallah Y, Battacharjee P, Van Holsbeke C, Bottomley C, Gould D, Johnson S, Stalder C, Van Calster B, Hamilton J, Timmerman D, Bourne T. Defining safe criteria to diagnose miscarriage: prospective observational multicentre study. BMJ. 2015;351:h4579. https://doi.org/10.1136/bmj.h4579. PMID: 26400869; PMCID: PMC4580727.
23. Jauniaux E, Johns J, Burton GJ. The role of ultrasound imaging in diagnosing and investigating early pregnancy failure. Ultrasound Obstet Gynecol. 2005;25(6):613–24. https://doi.org/10.1002/uog.1892. PMID: 15861413.
24. Glantz C, Purnell L. Clinical utility of sonography in the diagnosis and treatment of placental abruption. J Ultrasound Med. 2002;21(8):837–40. https://doi.org/10.7863/jum.2002.21.8.837. PMID: 12164566.
25. Abu-Rustum RS. Placenta previa: practical approach to sonographic evaluation and management. Contemp OB/GYN J. 2019;64(11).
26. Kaakaji Y, Nghiem HV, Nodell C, Winter TC. Sonography of obstetric and gynecologic emergencies: part I, obstetric emergencies. AJR Am J Roentgenol. 2000;174(3):641–9. https://doi.org/10.2214/ajr.174.3.1740641. PMID: 10701602.
27. Al-Obaidi AD, Hashim AS, Salih S, Hashim HT. Spontaneous mid-trimester uterine rupture associated with fetal death in a young patient during COVID-19 pandemic: a case report. Clin Case Rep. 2022;10(12):e6802. https://doi.org/10.1002/ccr3.6802. PMID: 36590664; PMCID: PMC9794919.
28. Augustin G. Acute abdomen during pregnancy, 2nd ed. Springer; 2018.
29. MacDorman MF, Gregory EC. Fetal and perinatal mortality: United States, 2013. Natl Vital Stat Rep. 2015;64(8):1–24. PMID: 26222771.
30. Mattingly PJ. Evaluation of fetal death. https://emedicine.medscape.com/article/259165-overview.
31. AlMousa R, AlMuhaidib HR, Alanezi SM, Al Qahtani N. The rule of ultrasonography in the management of retained placenta. Cureus. 2021;13(1):e12696. https://

doi.org/10.7759/cureus.12696. PMID: 33614304; PMCID: PMC7883585.
32. Zafar N, Plavsic SK. Role of ultrasound in the evaluation of acute pelvic pain in nonpregnant reproductive age patients. Donald School J Ultrasound Obstet Gynecol. 2012;6:207. https://doi.org/10.5005/jp-journals-10009-1244.
33. Ștefan RA, Ștefan PA, Mihu CM, Csutak C, Melincovici CS, Crivii CB, Maluțan AM, Hîțu L, Lebovici A. Ultrasonography in the differentiation of endometriomas from hemorrhagic ovarian cysts: the role of texture analysis. J Pers Med. 2021;11:611. https://doi.org/10.3390/jpm11070611.
34. Strachowski LM, Choi HH, Shum DJ, Horrow MM. Pearls and pitfalls in imaging of pelvic adnexal torsion: seven tips to tell it's twisted. Radiographics. 2021;41(2):625–40. https://doi.org/10.1148/rg.2021200122. Erratum in: Radiographics. 2021 May-Jun;41(3):E97. PMID: 33646910.
35. Chang HC, Bhatt S, Dogra VS. Pearls and pitfalls in diagnosis of ovarian torsion. Radiographics. 2008;28(5):1355–68. https://doi.org/10.1148/rg.285075130. PMID: 18794312.
36. Munro KI, et al. Diagnosis and management of tubo-ovarian abscesses. Obstet Gynaecol. 2018;20:11–9.